



<https://theses.gla.ac.uk/>

Theses Digitisation:

<https://www.gla.ac.uk/myglasgow/research/enlighten/theses/digitisation/>

This is a digitised version of the original print thesis.

Copyright and moral rights for this work are retained by the author

A copy can be downloaded for personal non-commercial research or study,
without prior permission or charge

This work cannot be reproduced or quoted extensively from without first
obtaining permission in writing from the author

The content must not be changed in any way or sold commercially in any
format or medium without the formal permission of the author

When referring to this work, full bibliographic details including the author,
title, awarding institution and date of the thesis must be given

Enlighten: Theses

<https://theses.gla.ac.uk/>
research-enlighten@glasgow.ac.uk

The geochemistry of thermal aureoles at Cashel, Co. Galway and Comrie,
Perthshire.

by

Y. AHMED-SAID, D.E.S

A thesis submitted for the degree of Doctor of Philosophy at the University
of Glasgow.

Department of Geology
University of Glasgow
Scotland (U.K)

February 1988

ProQuest Number: 10997897

All rights reserved

INFORMATION TO ALL USERS

The quality of this reproduction is dependent upon the quality of the copy submitted.

In the unlikely event that the author did not send a complete manuscript and there are missing pages, these will be noted. Also, if material had to be removed, a note will indicate the deletion.



ProQuest 10997897

Published by ProQuest LLC (2018). Copyright of the Dissertation is held by the Author.

All rights reserved.

This work is protected against unauthorized copying under Title 17, United States Code
Microform Edition © ProQuest LLC.

ProQuest LLC.
789 East Eisenhower Parkway
P.O. Box 1346
Ann Arbor, MI 48106 – 1346

ABSTRACT

Detailed investigations of the Cashel-Lough Wheelaun and Comrie thermal aureoles show that similar intensive mineralogical changes have taken place in both aureoles irrespective of the intrusive and country rock types and the regional metamorphism experienced by the country rocks.

The chemistry in the two aureoles also generally shows similar trends although original sedimentary variations across the Aberfoyle slates severely affected the behaviour of most elements. In the Cashel thermal aureole, it is shown that the elements which are commonly enriched in acidic rocks viz : Si, K, Na, P, U, Rb, Ba, Th and to some extent Zr were removed from the envelope hornfelses, those commonly enriched in mafic rocks viz : Mg, Fe, Cr, Ni, and Co were enriched whereas those elements which are intermediate in character viz : Al, Ti, Ca, and Sr were both enriched and removed. Eu was removed much less significantly compared to the other REE thus giving increasing positive Eu anomalies as the degree of hornfelsing and partial melting rise. In the Comrie thermal aureole, the sedimentary variations mentioned above strongly affected the variation of elements during hornfelsing and partial melting of the Aberfoyle Slates, although the available evidence suggests similar trends to the Cashel thermal aureole.

Mineralogical, chemical and Sr isotope evidence show that the Cashel trondhjemite migmatite leucosomes were produced at degrees of partial melting of between 15 and 30% and their chemical compositions compare reasonably well with the melts derived from the metasediments as calculated using the strongly compatible elements Cr, Ni and Co. This conclusively indicates they were derived from the metasediments and so does the Cashel microgranite sill.

The Comrie leucosomes are dominantly late stage magmatic injections although the melts, which were probably near eutectic in composition in part, derive from the partially melted metasediments.

The elements as deduced from the Cashel, and probably also the Comrie and Cortlandt, New York aureoles, were fractionated into the melts in the following order :Si>K>Na>Ca>Mn>Al>Fe>Mg and Rb>Ba>Sr>Ga>Cr, Ni, Co. This calculated order of fractionation of elements, which is the opposite to magmatic crystallization, provides a unique picture on the mode of interaction of mantle derived magmas with the earth's crust and therefore gives clear explanation on how S-type granites and other crustally contaminated rock types are produced, especially as the melts derived from both the Cashel and Comrie hornfelses are S-type melts as defined by Chappell and White (1974)

Declaration

The material presented herein is the result of independent research by the author undertaken from January 1985 to February 1988 at the department of geology, University of Glasgow. Any published or unpublished results of other workers have been given full acknowledgement in the text.

I would like to thank my family and friends who have supported me throughout this journey. I am especially grateful to my mother and father for their constant love and encouragement. I also want to thank my friends who have been there for me through thick and thin. I am grateful to my friends who have been there for me through thick and thin.

I would like to thank my family and friends who have supported me throughout this journey. I am especially grateful to my mother and father for their constant love and encouragement. I also want to thank my friends who have been there for me through thick and thin. I am grateful to my friends who have been there for me through thick and thin.

I dedicate this thesis to my mother and father, brothers and sisters.

I would like to thank my family and friends who have supported me throughout this journey. I am especially grateful to my mother and father for their constant love and encouragement. I also want to thank my friends who have been there for me through thick and thin. I am grateful to my friends who have been there for me through thick and thin.

Acknowledgement

I wish to express my deep and sincere thanks to many people involved in bringing this thesis to fruition. Above all I wish to thank Professor Bernard E. Leake and Dr Collin M. Farrow for their invaluable help, advice and supervision over the last three years.

I am very grateful to Professor D. R. Bowes for his help to extend the research project to a Ph.D

Many people of the staff at the geology department , University of Glasgow also deserve my thanks and appreciation. these include Mr R. Morrison, G. Bruce, Jim, big Robert, Eddie, Jimmy for their unending help. D. MacClean is also thanked for producing high standard photographs.

I want to thank the staff of the SURRC, East Kilbride , for their assistance during my practical work . First and foremost, I would like to thank Dr A.B MacKenzie for his help on fission track analysis and Dr John E. Whitley for neutron activation analysis.

Thanks also go to Dr N. Walsh, J.Barker, A. Warren at the Royal Holloway and Bedford College, Egham , for their assistance for REE analyses.

^{BDW}
Dr Yardley, of Leeds University is specially thanked for his expert advice on the application of some thermometers and barometers.

^P
Dr Harvey, is also specially thanked for his "very last minute!" analysis of 4 restite-leucosome pairs for trace elements.

I am grateful to the "Minister de L'Enseignement superieur" in Algeria and the Algerian Embassy for their continuous support and sponsorship during my stay in Britain.

I am also deeply touched by the family care of Mrs Leake and family. I will always remember "WELCOME HOME"during my last christmas visit.

Finally, to my mother and father, brothers and sisters I express my deep respect for giving me the chance to do this thesis. For your endless love and understanding, I thank you above all.

^v
Mrs Haughton "Lisa" edited the final script to the highest standards for which she is sincerely thanked.

TABLE OF CONTENTS

Page number

Abstract

Table of contents

List of figures

List of plates

List of tables

Acknowledgement

CHAPTER ONE INTRODUCTION

1.1	Introduction	1
1.2	Aims of the study	2
1.3	Geological history and setting of the two studied areas	2
1.3.1	Cashel-Lough Wheelaun intrusion, Connemara, Ireland	2
1.3.2	Carn Chois intrusion, Perthshire, Scotland	5

CHAPTER TWO ANALYTICAL METHODS

2.1	Fission track analysis	8
2.1.1	Fission phenomena	8
2.1.2	Working principles	9
2.1.3	Methodology	10
2.2	Neutron activation analysis	13
2.2.1	Principles of γ spectroscopy	13
2.2.2	Method of determination of Th and U	15
2.2.3	Methodology	16
2.2.4	Reliability of the data	19
2.2.4.1	Precision	19
2.2.4.2	Accuracy	20
2.3	Inductively coupled plasma (ICP) spectrometry	21
2.3.1	Principles and practice of ICP	21
2.3.2	Sample preparation for REE analysis	22
2.3.3	REE analyses	23
2.4	X-ray fluorescence	24
2.4.1	Principles	24

2.4.2	Methodology	25
2.5	Comparison between INAA, ICP and XRF	26

CASHEL-LOUGH WHEELAUN INTRUSION, IRELAND

CHAPTER THREE CONDITIONS OF METAMORPHISM IN THE CASHEL-LOUGH WHEELAUN INTRUSION

3.1	Introduction	29
3.2	Mineralogical model	29
3.2.1	Geothermometry	30
3.2.2	Results	31
3.2.3	Errors	33
3.2.4	Field relationships	33
3.2.5	Effects of impurities	34
3.3	Physical model	38
3.3.1	Introduction	38
3.3.2	Temperature at the contact	39
3.3.3	Temperatures at different distances from the contact	42
3.4	Discussion	43
3.5	Geobarometry	45
3.5.1	Garnet-aluminosilicate quartz-plagioclase geobarometry	45
3.5.1.1	Results	46
3.5.2	Garnet-cordierite-sillimanite-quartz geobarometry	47
3.5.3	Discussion	48
3.6	General conclusions	48

CHAPTER FOUR MINERALOGY

4.1	Field description of the Cashel-Lough Wheelaun thermal aureole	60
4.2	Mineralogy	62
4.2.1	Nomenclature	62
4.2.2	Mineralogy of the unhornfelsed rocks	62
4.2.3	Mineralogical changes	65
4.2.4	Changes in the mineral chemistry	70

4.3	Field relationships	74
4.4	Summary and conclusions	75

CHAPTER FIVE CHEMISTRY

5.1	Introduction	108
5.2	General chemistry of the unhornfelsed rocks	108
5.2.1	Major and trace elements	108
5.2.2	Rare earth elements(REE)	110
5.3	Chemical changes	111
5.3.1	Fractionation of the major elements	112
5.3.2	Fractionation of the trace elements	114
5.3.3	Fractionation of the REE	116
5.4	Calculation of the absolute composition of the melts	118
5.4.1	Results	120
5.5	Partial melts and the Cashel microgranite sill	124
5.6	Discussion	126
5.7	Conclusions	128

CHAPTER SIX MIGMATITES

6.1	Introduction	156
6.2	Field description of the migmatite leucosomes	157
6.3	Mineralogy	158
6.4	Chemistry	159
6.4.1	Geochemistry of the major elements	160
6.4.2	Geochemistry of the trace elements	161
6.4.3	Rare earth elements	162
6.5	Factors affecting the final composition of the migmatites	163
6.5.1	Wall rock reactions	163
6.5.2	Xenoliths and xenocrysts	164
6.5.3	Fractional crystallization	165
6.6	Absolute chemical composition of the migmatites	165
6.6.1	Results	167
6.7	Comparison of the chemical composition of the migmatite leucosomes with those derived from experimental and theoretical studies	168

6.8	Rb-Sr isotopes	171
6.9	Summary and conclusions	173

CHAPTER SEVEN U AND TH

7.1	Introduction	195
7.2	Results of fission track analysis	195
7.2.1	Whole rock U distribution	195
7.2.2	Individual minerals	197
7.2.3	U in the Cashel microgranite sill and migmatite leucosomes	202
7.2.4	Field relationships	202
7.3	Results of U and Th analyses using INAA	204
7.3.1	Field relationships	205
7.3.2	U-Zr, U-P and U-K relationships	206
7.3.3	Th-Zr, Th-P and Th-K relationships	207
7.4	U and Th partitioning between the restites and leucosomes	207
7.5	Likely mechanisms of U and Th transport	209
7.6	Summary and discussion	210

COMRIE INTRUSION, PERTHSHIRE

CHAPTER EIGHT MINERALOGY

8.1	Field description of the Comrie thermal aureole	233
8.2	Mineralogy of the regional slates	233
8.3	Mineralogical changes	234
8.4	Changes in the mineral chemistry	239
8.5	Metamorphic thermal zones	240
8.6	Conditions of metamorphism	240
8.7	summary	242

CHAPTER NINE CHEMISTRY & ORIGIN OF THE LEUCOSOMES

9.1	Introduction	260
9.2	General chemistry of the unhornfelsed slates	260
9.2.1	Major and trace elements	260

9.2.2	REE	261
9.3	Chemical changes	262
9.3.1	Fractionation of the major elements	262
9.3.2	Fractionation of the trace elements	264
9.3.3	Fractionation of the REE	265
9.3.4	Discussion	266
9.4	The behaviour of U and Th in the Comrie aureole	269
9.4.1	Spatial distribution of U	269
9.4.2	Chemistry	270
9.4.2.1	Field relationships	271
9.4.2.2	Relationships of U and Th with K, Zr, P and Ca	271
9.4.2.3	Discussion	272
9.5	Possible origin of the pink-orange bands	273
9.5.1	Mineralogy	273
9.5.2	Chemistry	274
9.5.3	Conclusions	275
9.6	Summary of the chemistry of the Comrie aureole	275
	DISCUSSION AND CONCLUSIONS	306-9
	REFERENCES	310-27
	<u>APPENDICES</u>	
	Appendix 1 Equations used in geothermometry and geobarometry	328-31
	appendix 2 Modal analyses	332-7
	Appendix 3 Major and trace data.(REE included)	338-65

LIST OF TABLES

Table number	Page number
<u>CHAPTER ONE</u>	
2.1 Precision of INAA data	19,20
2.2 detection limits of XRF	26,6
<u>CHAPTER THREE</u>	
3.1 Mole fractions of Fe, Mg, Mn, Ca, Ti and Al ⁺⁶ of garnet, biotite and cordierite.	49,50
3.2 X _{Mn+Ca} , X _{Ti+Al+6} , K _D values and the calculated temperatures	51
3.3 Temperatures obtained using the corrections of Hodges and Spear (1982) and Indares and Martignole (1985).	52
3.4 Calculated pressures	53
<u>CHAPTER FOUR</u>	
4.1 Summary statistics of modal analyses.	77
4.2 Summary statistics of biotite, garnet and plagioclase analyses.	78
4.3 Mean biotite analyses.	79-85
4.4 Mean garnet analyses.	86-90
4.5 Cordierite analyses.	91
4.6 Spinel analyses.	91
4.7 Mean plagioclase analyses.	92-7
<u>CHAPTER FIVE</u>	
5.1 Comparison of Connemara pelites with various shale compositions.	130
5.2 Summary statistics of the REE data.	131
5.3 Summary statistics of the major and trace data.	132
5.4 Calculated degrees of partial melting and compositions of the melts derived from 10 hornfelses and 9 xenoliths.	133-5
5.5 Calculated order of fractionation of major and trace elements in the Cashel thermal aureole.	136-7
5.6 Comparison of the calculated melts compositions derived from the	

metasediments with the composition of the Cashel microgranite sill.	138-40
---	--------

CHAPTER SIX

6.1 Comparison of the Cashel migmatite leucosomes with migmatites from eastern Connemara.	175-6
6.2 REE in the Cashel migmatites.	177
6.3 Calculated degrees of partial melting and compositions of the melts derived from the Cashel formation pelites. The composition of the Cashel migmatite leucosomes is also given for comparison.	178-9
6.4 Molecular A/CNK ratios, normative corundum and normative Qz:Ab:Or ratios of the migmatites. Green's (1976) experimental starting glass and results are also given for comparison with the Cashel country rocks, migmatites, microgranite sill and northern unmigmatized pelites.	180-1
6.5 Rb-Sr composition and isotopic data of the migmatites.	172

CHAPTER SEVEN

7.1 Characteristics of zircon.	213
7.2 U contents of apatite and biotite.	214
7.3 U, Th, K and their relative ratios data.	215-7
7.4 Summary statistics of U, Th and Th/U ratios. The partition coefficients of U and Th between the restites and leucosomes are also given.	218

CHAPTER EIGHT (COMRIE AUREOLE)

8.1 Summary statistics of modal analyses.	243
8.2 Mean biotite, garnet, cordierite, orthopyroxene, spinel, plagioclase and K-feldspar analyses.	244-51

CHAPTER NINE

9.1 Summary statistics of the major and trace data.	278-9
9.2 Summary statistics of the REE data.	280
9.3 predicted contents of Ti, Mg, Cr, Co and Ni of the parent rocks	

of the contact hornfels.	267
9.4 Summary statistics of U, Th and their relative ratios.	281
9.4.A Quantitative estimation of U in apatite	282
9.5 U, Th, K and their relative ratios data.	283-4
9.6 Molecular A/CNK ratios, normative corundum and normative Qz:Ab:Or ratios of the Comrie leucosomes and a granodiorite.	284

LIST OF FIGURES

<u>Figure number</u>	<u>Page number</u>
<u>CHAPTER ONE</u>	
1.1 Geological sketch map of Connemara showing the regional metamorphic zones.	7
<u>CHAPTER TWO</u>	
2.1-5 Scatter diagrams of Ba(XRF) vs Ba(ICP), La(XRF) vs La(ICP), Ce(XRF) vs Ce(ICP), Th(XRF) vs Th(INAA), U(XRF) vs U(INAA).	28
<u>CHAPTER THREE</u>	
3.1 Plot of $\ln K$ versus $10^4/T(^{\circ}\text{C})$ for 3 garnet-biotite thermometers.	55
3.1.A Geological sketch map showing the temperatures derived from garnet-biotite thermometry and the metamorphic subdivisions.	56
3.2-7 Plots of X_{Ti} , $X_{\text{Al}^{+6}}$, $X_{\text{Ti}+\text{Al}^{+6}}$, $X_{\text{Ca}+\text{Mn}}$, X_{Mn} , X_{Ca} , versus K_D	57
3.8-9 plots of $T(^{\circ}\text{C})$ versus distance from the contact of the intrusion.	58
3.10 results of the Newton and Haselton (1981), Wells and Richardson (1980), Holdaway and Lee (1977), Ghent (1976) and Thompson (1976) of the garnet-sillimanite-quartz-plagioclase and garnet-cordierite-sillimanite-quartz calibrations plotted on a P-T grid.	59
3.11 Plot of $P(\text{kb})$ vs $T(^{\circ}\text{C})$ showing the slope of the Newton and Haselton (1981) calibration and the slopes of the samples used in geobarometry	59.
<u>CHAPTER FOUR</u>	
4.1 Geological sketch map of the Cashel district showing sample locations.	61
4.1.1 Sketch map showing the metamorphic subdivisions.	61'
4.2-3 Mineralogical cross-sections EE' and FF.'	99
4.4-5 Mineralogical cross sections CC' and AA'.	100

4.6-7	Traverses DD' and BB' showing the changes in the composition of biotite.	101
4.8-9	Traverses DD' and BB' showing the changes in the composition of garnet.	102
4.10-1	Typical zoning in garnets from the country and hornfelsed rocks.	103
4.12	Plot of An-Ab-Or showing the composition of plagioclase.	104
4.13	Traverse BB' showing the changes in the composition of plagioclase.	104
4.14-5	Tridimensional maps of modal analyses of garnet.	105
4.16-8	Tridimensional maps of modal analyses of cordierite and plagioclase	106
4.19-21	Tridimensional maps of modal analyses of quartz and biotite	107

CHAPTER FIVE

5.1-6	Plots of Al_2O_3 vs Fe_{tot} , TiO_2 vs Fe_{tot} , TiO_2 vs Al_2O_3 , Ga vs Al_2O_3 , Al_2O_3 vs U, Al_2O_3 vs Th.	143
5.7-12	Plots of Ni vs Fe_{tot} , Ga vs TiO_2 , Cr vs TiO_2 , Zr vs TiO_2 , Sr vs TiO_2 , Sr vs CaO.	144
5.13-8	Plots of Sr vs Na_2O , Rb vs K_2O , Ba vs K_2O , K_2O vs TiO_2 , Rb vs TiO_2 , Ba vs TiO_2 .	145
5.19-20	Plots of Rb vs $CaO+Na_2O$, Ba vs $CaO+Na_2O$.	146
5.21	REE distribution patterns in the unhornfelsed pelites.	146
5.22-3	Plots of CaO vs Na_2O , P_2O_5 vs CaO.	147
5.24-5	Plots of Zr vs TiO_2 , Niggli al vs Niggli fm.	148
5.26	Plot of K_2O vs Rb.	149
5.27	REE distribution patterns in the hornfelses.	149
5.28-9	REE distribution patterns in the xenoliths and metagabbros.	150
5.30	Comparison of REE distribution patterns in the unhornfelsed pelites, hornfelses and pelitic xenoliths.	151
5.31(A-D)	Plots of Lu vs Zr, Lu vs P_2O_5 , Eu vs Sr, Eu vs CaO.	152
5.32-3	Plots of Na_2O vs K_2O , A/CNK vs SiO_2	153
5.34(A-H)	Harker type diagrams of TiO_2 , Al_2O_3 , Fe_2O_3 , MgO, CaO, Na_2O , K_2O and MnO.	154

5.35-6a	PLots of order of fractionation of major and trace elements in magmas versus calculated order of fractionation of the same elements in the Cashel aureole.	155
---------	--	-----

CHAPTER Six

6..1	Plots of Ab:An:Or for plagioclase from the pelitic restites and migmatite leucosomes.	184
6.2-6	Harker type diagrams of Al_2O_3 , TiO_2 , Fe_{tot} , K_2O and Na_2O .	185
6.7-12	Plots of Na_2O vs CaO , P_2O_5 vs CaO , TiO_2 vs K_2O , Ba vs K_2O , Rb vs K_2O , Sr vs CaO .	186
6.13-8	PLots of Ga vs Al_2O_3 , Y vs P_2O_5 , La vs Ce , Ce vs Y , Ce vs K_2O , Cr vs TiO_2 .	187
6.19	REE distribution patterns in 3 Cashel pelitic restite-leucosome pairs.	188
6.20-4	PLots of MgO vs Al_2O_3 , MgO vs TiO_2 , Fe_{tot} vs TiO_2 , fe_{tot} vs MgO , Fe_{tot} vs Al_2O_3 .	189
6.25	Normative Qz:Ab:Or ratios of the Cashel migmatites and microgranite sill.	190
6.26	PLot of $(^{87}Sr/^{86}Sr)_p$ vs $(^{87}Rb/^{86}Sr)$ for the Cashel migmatites	191
6.27	Plot of $(^{87}Sr/^{86}Sr)_p$ vs $(^{87}Rb/^{86}Sr)$ for the Cashel formation pelites, migmatite leucosomes and granite sill.	191
6.28	PLot of $(^{87}Sr$ vs $^{86}Sr)_p$ vs $(^{87}Rb/^{86}Sr)$ for the Cashel formation pelites, migmatite leucosomes, granite sill, quartz diorite and K-feldspar gneisses.	192

CHAPTER SEVEN

7.1	Plot of vol% zircon versus distance from intrusion	220
7.2-7	Plots of Th vs U , Zr vs U , P_2O_5 vs U , K_2O vs U , Zr vs Th , P_2O_5 vs Th for the metasediments.	221
7.8-13	Plots of K_2O vs Th , P_2O_5 vs U , Zr vs U , K_2O vs U , K_2O vs Th , Zr vs Th for the migmatite leucosomes.	222
7.14	Plot of mole percent dissolved U^{+6} species vs pH in the Wind River Formation.	223

7.15	Plot of $w(\text{Fe}^{3+}/(\text{Fe}^{3+}+\text{Fe}^{2+}))$ vs U.	223
7.16-7	Plots of CO_2 and H_2O vs U; CO_2 and H_2O vs Th	224
7.18-20	Tridimensional maps of U and Th	225

CHAPTER EIGHT (COMRIE AUREOLE)

8.1	Geological sketch map of the Comrie area showing sample locations.	253
8.1A	Sketch map showing the metamorphic thermal zones.	253'
8.2-3	Mineralogical cross sections AA' and BB'.	254
8.4	Mineralogical cross section CC'.	255
8.5	Traverse BB' showing the changes in the composition of biotite.	255
8.6	Traverse AA' showing the changes in the composition of cordierite.	256
8.7	Plot of $\text{Na}_2\text{O}-\text{K}_2\text{O}-\text{CaO}$ showing the composition of plagioclase and K-feldspar.	256
8.8	Plot of P (GPa) vs T ($^{\circ}\text{C}$)	257

CHAPTER NINE

9.1-6	Plots of Rb vs K_2O , Ba vs K_2O , Rb vs $\text{CaO}+\text{Na}_2\text{O}$, Ba vs $\text{CaO}+\text{Na}_2\text{O}$, Sr vs CaO , Na_2O vs CaO .	287
9.7-12	Plots of FeO vs TiO_2 , Fe_2O_3 vs TiO_2 , Cr vs TiO_2 , K_2O vs Niggli al-alk, Rb vs Niggli al-alk, Ce vs Niggli al-alk.	288
9.13-7	Plots of Ba vs Niggli al-alk, Ga vs Niggli al-alk, Y vs Niggli al-alk, Zn vs Niggli al-alk, fe_{tot} vs al-alk.	289
9.18	REE distribution patterns in the unhornfelses slates	290
9.19	Niggli al vs Niggli fm.	290
9.20-1	REE distribution patterns in the intermediate and contact hornfelses.	291
9.22	Comparison of REE distribution patterns in the country slates and hornfelses.	292
9.23-8	Plots of Lu vs Zr, Yb vs Zr, Lu vs P_2O_5 , Yb vs P_2O_5 , Eu vs CaO , Eu vs Sr.	293
9.29-34	Plots of U vs Th, P_2O_5 , Zr, K_2O and CaO ; Th vs K_2O	294
9.35-8	Plots of Th vs P_2O_5 , Zr and CaO ; U vs w.	295
9.39	Plot of A/CNK vs SiO_2 .	295

9.40	Normative Qz:Ab:Or ratios of the Comrie leucosomes and intrusive rocks.	296
9.41	REE distribution patterns in two leucosomes and one granodiorite from the Comrie aureole.	296
9.42-7	Harker type diagrams of Al ₂ O ₃ , MgO, TiO ₂ , CaO, Fe _{tot} and K ₂ O.	297
9.48-53	Harker type diagrams of Na ₂ O, P ₂ O ₅ , Co, Ni, Cr and Rb	298
9.54-5	Harker type diagram of Zr and Ba	299

LIST OF PLATES

plate number	page number
-----------------	----------------

CHAPTER SIX

6.1-2	Migmatite leucosomes from the Cashel aureole	194
-------	--	-----

CHAPTER SEVEN

7.1'-2'	Typical whole rock U distribution patterns.	227
7.3'	U at the garnet-biotite boundaries.	228
7.4'	U in sericitized biotite.	228
7.5'	U in zircon within pinitized cordierite.	229
7.6'	U in veins of secondary epidote.	229
7.7'	U in apatite.	230
7.8'	U in zircon within a sericitized garnet poikiloblast.	230
7.9	U in a deep brown grain of zircon.	231
7.10	U in an intermediate crystal of zircon .	231
7.11	U in a pink crystal of zircon.	231
7.12	Spontaneous fission tracks in apatite.	231
7.13	Spontaneous fission tracks in pink zircon.	232

CHAPTER EIGHT (COMRIE AUREOLE)

8.1	Typical banding pattern in a Comrie contact hornfels.	259
8.2	Veins of orthopyroxene from the inner Comrie aureole.	259
8.3	Replacement of biotite by orthopyroxene in the Comrie aureole.	259

CHAPTER NINE

9.1'-2'	Typical whole rock U distribution patterns.	301
9.3-3'	U in crystals of zircon from the country rocks and hornfelses.	302
9.4-4'	U in apatites from the country rocks and a granodiorite.	303
9.5	Typical granophyric texture from the Comrie leucosomes	304
9.6	Typical graphic texture from the Comrie leucosomes.	304
9.7	Water-rich pipes from the magma cross cutting the restites.	304
9.8	Water-rich "sub-solidus" alterations at the restite leucosomecontact	304
9.9	Relict of slate and xenocrystic orthopyroxene inside a leucosome.	305

CHAPTER ONE : INTRODUCTION

1.1 Introduction

Thermal aureoles offer the opportunity of studying reaction sequences at constant pressure, the extent of heat transfer and whether chemical mobility changed the chemistry of the country rocks. Two thermal aureoles, those of Cashel-Lough Wheelaun, Connemara, Ireland and Comrie, Perthshire, Scotland were investigated to assess the mineralogical and chemical changes accompanying hornfelsing. These two contrasting aureoles were chosen because previous studies had established extensive mineralogical changes and the aureoles occur around different intrusive rocks in different country rocks experiencing different grades of metamorphism.

The basic and ultrabasic Cashel-Lough Wheelaun intrusion (Leake, 1958a; Leake and Skirrow, 1960; Leake, 1970) was emplaced into Dalradian pelitic and semi-pelitic rocks already experiencing amphibolite facies metamorphism. Most of the work was carried out in the vicinity of Cashel Hill because of the good exposure which allowed detailed investigations of the hornfelses, pelitic xenoliths, and partial melts. The contact between the igneous complex and the metasediments is complex and with the associated quartz diorite to granite gneisses extends over 40km in an E-W direction causing significant regional hornfelsing and partial melting. This "mid-crustal" gabbro-country rock interaction provides good evidence about how mantle-derived magma and crustal rocks interact and is clearly relevant to the mechanisms producing S-type granites and other crust-contaminated rocks.

The Carn Chois intrusive rocks are compositionally variable (from aplite to diorite) and were intruded into rocks (Ben Ledi Grits and Aberfoyle Slates) experiencing a much lower grade of metamorphism than those in Ireland (chlorite zone metamorphism). All investigations were restricted to the changes suffered by the Aberfoyle Slates because of the great sedimentary variations within the Ben Ledi Grits (Tilley, 1924a). Although the heat derived from the intrusion caused distinct thermal zones, important mineralogical and chemical changes and partial melting (Chapters 9-10), the chemical interaction between the Carn Chois intrusion and adjacent country

rocks is much less significant than in the Cashel thermal aureole.

1.2 Aims of the study

- Assess the mineralogical and chemical changes which take place in thermal aureoles.

- Investigate the possible origin of the leucosomes from both studied areas and assess the behaviour of elements during partial melting of metasedimentary rocks.

- Extend the available evidence to discuss the origin of S-type granites and other crust-contaminated rocks.

1.3 Geological history and setting of the two studied areas

1.3.1 Cashel-Lough Wheelaun intrusion, Ireland

The Cashel district of Connemara, Co. Galway in western Ireland, is within the 6-inch (1:10560) sheet Co. Galway 51 and one inch (1:63360) sheet 94. The area, principally described by Leake and coworkers, is fairly flat with an average elevation of 60m with the highest point being the Cashel Hill summit, 312m high. The exposure is fairly good on the sides of the small hills but not in the more flat lying peat bog covered areas.

Connemara is a SW extension in Ireland of Dalradian metasediments and associated igneous bodies which occupy most of the Highlands of Scotland, (Kilburn *et al.* 1965). The Dalradian rocks of Connemara, similar to those in the Scottish Highlands, underwent a series of polyphase deformations, metamorphisms and igneous activity during the early Caledonian or Grampian Orogeny during late Cambrian and Ordovician time.

The geological history of Connemara has been outlined by Moorbath *et al.* (1968). It begins with the deposition of a series of Dalradian sediments followed by the intrusion of early dolerite sills and dykes and folding (F1). The sediments were then regionally metamorphosed to staurolite-garnet grade (M1). A basic and ultrabasic magma was subsequently intruded into these sediments causing intense hornfelsing (M2) during continuing regional metamorphism (M3) and folding (F2) which therefore metamorphosed, folded and disrupted the syntectonic intrusive rocks themselves. Following intrusive quartz diorite, trondhjemite and granite gneiss, the early basic and ultrabasic

rocks were agmatized and injected by acidic gneiss (Leake 1969). The igneous episode was concluded with the injection of K-feldspar granite gneisses which are very well developed within and to the east of the Cashel district and these crystallized during to slightly after tight E-W folding (F3) accompanied by metamorphism (M4). These F3 folds caused a series of folds in north and south Connemara including the Cashel syncline. Further E-W folding (F4) and metamorphism (M5) subsequently formed the Connemara antiform and bent the (F3) axial planes within the Cashel area.

The geochemistry of the area has been subjected to various investigations; Leake (1970), Senior and Leake (1978) on the unhornfelsed pelites, Leake and Skirrow (1960), Evans (1964), Leake (1970) on the hornfelses, Leake (1958a, 1970) on the basic and ultrabasic rocks, Jagger (1985) on the basic and ultrabasic rocks, gneisses and hornfelses, Evans and Leake (1960), Leake (1972) on the striped amphibolites. This continuous work has led to an important understanding of the behaviour of the major and some of the trace elements in the various geological formations.

The basic and ultrabasic rocks. The first modern account of the basic and ultrabasic rocks was that of Wager (1932) followed by a summary of the geology of Connemara in 1939. In the Cashel area apart from the brief notes on the basic rocks and gneisses given by Callaway (1887) and Cronshaw (1923) the area remained unstudied until a full account of the Cashel-Lough Wheelaun intrusion was given by Leake (1958a).

The geochronological order as well as the origin of the basic and ultrabasic rocks have been the subject of considerable study e.g. Wager (1939), Rothstein (1964), Morton (1964), Leake (1964). After reviewing the available information, Leake (1970) stated "there seems to be no reasonable doubt that all the basic and ultrabasic rocks belong to the same magma series". Such a conclusion is supported by the abnormally calcic plagioclase and the spacial association with the quartz-diorite gneiss of these intrusions.

Quartz-diorite and K-feldspar gneisses. Since the early work of Callaway (1887) and Cronshaw (1923) on the Lettershina Hill gneisses, no

further detailed studies appeared until a description of the quartz-diorite gneisses of the Roundstone was published by Wager (1932, 1939). Those of the Cashel area remained undescribed until a full account was given by Leake (1969).

The origin of the gneisses has been discussed by many workers e.g. Leggo et al. (1966), Leake (1969), Keeling (1981). But the general consensus is that they were formed as the final differentiation products of the basic magma.

The metasedimentary rocks. The metasediments of Connemara, composed mainly of quartzites, pelites and semi-pelites, marbles and pebble beds with subordinate amphibolite, calc-silicate rocks, boulder beds and psammites, belong to the Dalradian supergroup and extend E-W for over 50km along strike in central parts of Connemara, being bounded to the north by a series of Ordovician and Silurian sediments and to the south by the igneous complex of gabbros and gneisses.

Different aspects of the geology of the metasedimentary rocks from Connemara have been investigated by many workers, among others Leake (1958b), Cruse and Leake (1968), Badley (1976), Yardley (1976), Tanner and Shackleton (1979). This extensive work led to a better understanding of both the geology and geochemistry of the metasediments. The first formal stratigraphy was published by Badley (1976). Tanner and Shackleton (1979), Leake et al.(1981) refined the available information and published regional geological maps of Connemara.

Metamorphism in Connemara. Generally the degree of metamorphism increases southward reaching its peak along the belt of the basic and ultrabasic and associated orthogneisses. This indicates that an abnormally high heat flow must have accompanied this major igneous emplacement.. Treloar (1985) has estimated the temperature gradient near the igneous complex and the highest temperatures of between 750°C and 900°C and this will be discussed in Chapter 3.

Most of the Connemara schists were regionally metamorphosed to amphibolite facies. The regional metamorphic zones have been summarized by Leake et al. (1981) and Barber and Yardley (1985) and strike broadly E-W

across Connemara (figure. 1.1). In the north a staurolite zone characterized by staurolite-muscovite-biotite-garnet-plagioclase-quartz gives way southward to a sillimanite zone but staurolite and sillimanite coexist over a broad region until staurolite and often garnet disappear southward. The presence of muscovite or K-feldspar subdivides the sillimanite zone further into sillimanite-muscovite and sillimanite K-feldspar zones. The latter overlaps with the migmatite zone which occurs in the south adjacent to the igneous complex and in it the pelites show signs of partial melting with migmatite leucosome development. The typical assemblage in the migmatite zone, to which the study area belongs (figure. 1.1), is biotite-sillimanite-quartz-plagioclase \pm garnet \pm K-feldspar \pm opaque but in the hornfelses immediately adjacent to the igneous complex garnet-biotite-cordierite-quartz-plagioclase \pm opaque \pm sillimanite is the most diagnostic assemblage. Garnet is not common and generally does not coexist with cordierite in the migmatite zone but it does in the hornfelses except in the most desilicated rocks (Leake and Skirrow 1960; also Chapter 4).

1.3.2. Carn Chois intrusion, Perthshire, Scotland

The Comrie thermal aureole, Perthshire, Scotland lies immediately to the N-W of the Highland Boundary Fault near Comrie village. The intrusion, the Carn Chois granodiorite, belongs to the newer granites of Caledonian age, 390-435 Ma (Brown, 1983). The intrusion is variable in terms of mineralogy and chemistry and consists mainly of diorite, granodiorite, pegmatite and aplite. This intrusive complex was intruded into two upper Dalradian formations, namely the Ben Ledi Grits and Aberfoyle Slates causing distinct thermal metamorphic zones (see figure. 8.1a).

Within the slates with which the present account deals, the exposure is fairly good and continuous sampling of a nearly complete section towards the intrusion has been possible (see figure. 8.1).

The first mention of contact metamorphism in the Comrie area was by Nicol (1863) where he noted the hardening and recrystallization of the slates as the contact of the intrusion is approached. The area was mapped by the British Geological Survey on the 6-inch scale and the results appeared in the 1-inch map published in 1888. The nature of the intrusive rocks appeared in

a paper published by Wyllie and Scott (1913). The most detailed research undertaken on the Comrie aureole so far was that published by Tilley (1924a) who also gave major element analyses of four hornfelses (3 Ben Ledi Grits, 1 Aberfoyle slate). Otherwise the geochemistry of the rocks from the aureole remained unstudied until the present work. Moreover, the present work has defined the contact position on the southern side much more precisely and small revisions of the geological map made.

Tilley (1924a) showed that the Ben Ledi Grits are turbidites which show progressive thermal metamorphism. The incipient induration of the rocks is quickly followed by the production of small biotites at a distance of 500m which then increase both in size and number as the contact is approached. By the appearance of prismatic andalusite and cordierite about 256m from the contact the rocks have become completely recrystallized. Cordierite is followed in the innermost parts of the aureole by magnetite, spinel, corundum, orthopyroxene and occasionally prismatic sillimanite. Tilley (1924a) attributed the silica-poor nature of the contact rocks to local metasomatism which depleted the country rocks in SiO_2 . However, it is probable that local partial melting, though not significant (see Chapter 9) took place in the contact areas because as seen in the Cashel-Lough Wheelaun intrusion, partial melting would produce silica-rich granitic liquid and the unmelted residue would correspondingly be depleted in silica but enriched in Al, Mg, Fe and Ti (*i.e.* abundant magnetite, corundum, spinel, orthopyroxene).

Tilley (1924a) also showed that the first sign of thermal alteration in the Aberfoyle slates was about 410m from the contact with the hardening of the slates and development of minute spots on the cleavage surfaces. This zone of spotted slates is immediately followed by the appearance of small flakes of biotite at about 265m. Cordierite enters the mineral assemblages about 137m followed by magnetite, spinel, corundum and orthopyroxene.

The thermal effects of the Carn Chois granodiorite are overprinted upon low grade regional metamorphism associated with the development of a penetrative cleavage in the pelitic rocks. The regional metamorphism belongs to the chlorite zone of the progressive metamorphic sequence described by Barrow (1912).

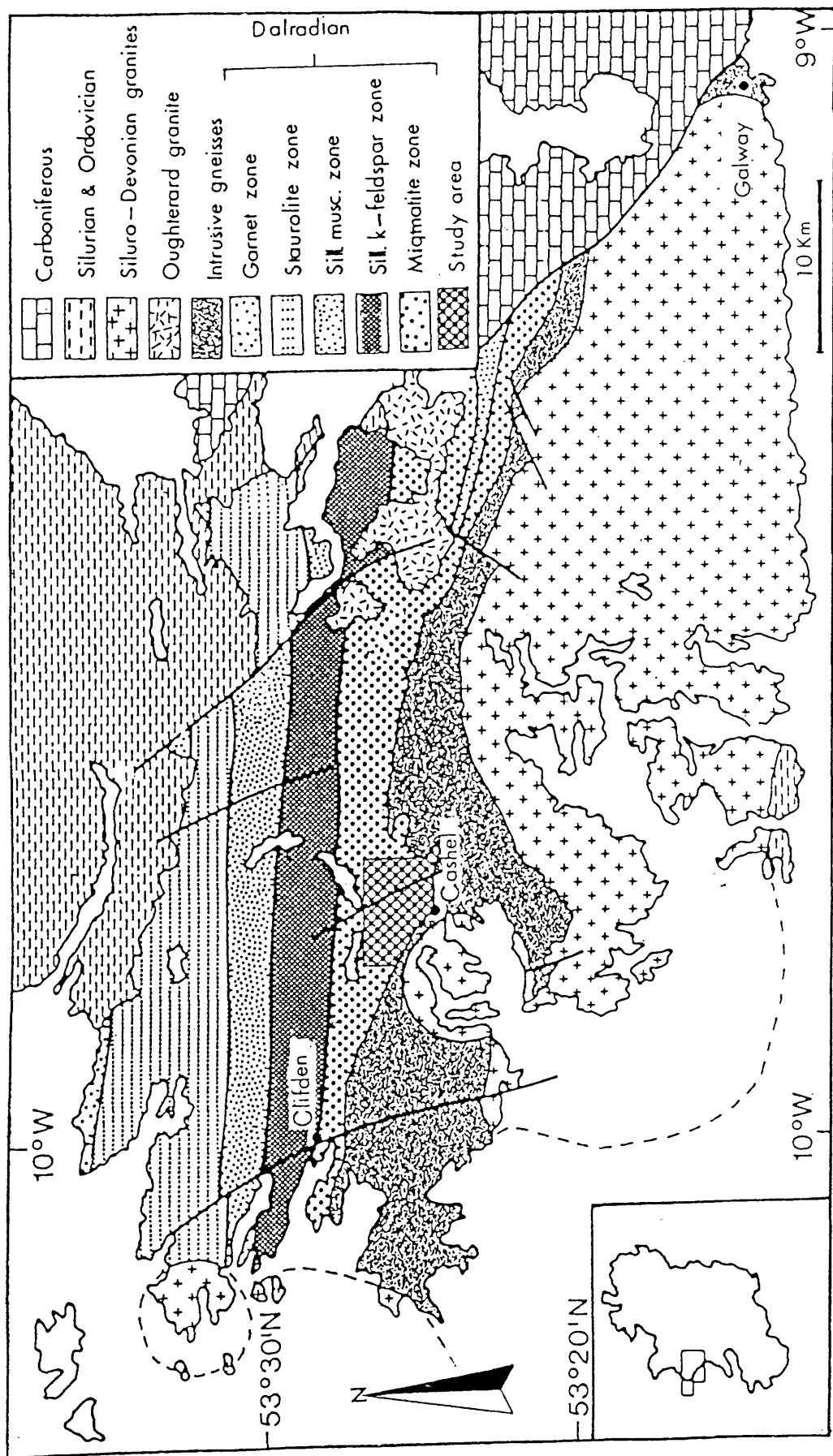


Fig.1.1 Geological sketch map of Connemara showing the metamorphic zones ; from Barber & Yardley 1985 and the location of the study area

CHAPTER TWO : ANALYTICAL METHODS

Four analytical techniques, X-ray fluorescence (XRF), inductively coupled plasma (ICP) spectrometry and fission track (FT) and instrumental neutron activation analyses(INAA) with conventional "wet chemical" methods for FeO, H₂O and CO₂, have been used throughout this work. Fission track analysis was mostly qualitative and has been used to investigate the distribution of U in the rock samples. Instrumental neutron activation analysis was used to quantify U and Th contents of the samples whereas inductively coupled plasma and X-ray fluorescence were used to derive the rare earth element (REE) and the major and many trace element contents respectively. La, Ce and Ba can be determined using ICP and XRF techniques without major interferences and therefore comparison between the two analytical methods is made. Similarly, U and Th of 108 rock samples were determined using XRF and INAA and the results are also compared in subsection 2.5.

2.1 Fission track analysis

The fission track analysis technique, developed in the mid 1960's by Fleischer et al. (1965 a-c), is a very useful method for measuring the average U and Th contents of geological samples and for investigating their spatial distribution by micromapping in polished rock sections and individual minerals. Fission track analysis has been used to study the geochemistry of U and/or Th in various rock types and minerals (e.g., Kleeman and Lovering 1967a; Komarov et al. 1967; Komarov and Skorovodkin 1969; Wollenberg 1972; Grauert et al. 1974) and has been extensively used in dating (e.g. Wagner 1968; Paupeau 1981; Storzer and Wagner 1982; Hurford and Green 1982,1983; Hurford et al. 1984 ; Das 1985). In the present study, fission track analysis is used to investigate the evolution of U in the Cashel-Lough Wheelaun (Ireland) and Comrie (Scotland) thermal aureoles. In this section, an outline of the fission phenomenon is first given followed by detailed descriptions of the principles and methodology of the technique.

2.1.1 Fission phenomena

Nuclear fission is a decay mode in which heavy nuclei break up into two or

more lighter nuclei and several neutrons with the liberation of some energy. There are two main types of fission namely : spontaneous and induced fission .

In the naturally occurring spontaneous fission of some unstable elements, the fragmentation of the heavy nucleus into two positively charged fragments is in fact hindered by a Coulomb barrier or "fission barrier" and fission is therefore regarded as a barrier penetration problem. The height of the barrier is the difference between the Coulomb energy of the two fragments when they are just touching and the energy released by the fission process. For U and elements in its region of the periodic table, both these quantities have values near 200 MeV and therefore the fission barrier is rather low thus allowing spontaneous fission to occur.

Induced fission comes about when enough energy is supplied by bombarding particles for the fission barrier to be surmounted. The bombarding particles are usually neutrons which are classified on the basis of energy as thermal, epithermal or fast. Thermal neutrons have energies of small fractions of eV (at temperatures of about 20°C the energy is about 0.025 eV or less), Friedlander et al. (1981). Epithermal neutrons are of somewhat higher energies, up to 1 KeV while neutrons with kinetic energies of several thousand electron volts or more are called fast neutrons.

2.1.2 Working principles

Some factors of importance in the application of fission phenomena to earth sciences are outlined below.

1- ^{238}U readily undergoes spontaneous fission with a half life of 10^{16} years which is more than a million times longer than the half-life of its alpha-decay of 4.47×10^9 years. ^{235}U , ^{234}U and ^{232}Th also exhibit spontaneous fission but at much slower rates than ^{238}U and therefore can be neglected .

2- ^{238}U and ^{232}Th undergo fission when irradiated by epithermal and fast neutrons.

3- ^{235}U undergoes fission most readily when irradiated by thermal neutrons.

4- The energy threshold of induced fission of ^{238}U and ^{232}Th is about 0.9 MeV whereas that of ^{235}U is ≤ 0.025 eV, Wollenberg (1972). Therefore

thermal irradiation causes only ^{235}U to fission while epithermal irradiations cause the fission of both ^{238}U and ^{232}Th .

A fission track is defined as the damage zone formed as a fission particle passes through a detector (generally a good insulating solid such as mica, plastic or glass) or a crystal. The particles formed at the time of fission of U and Th are highly charged nuclei that disrupt the electron balance of the atoms in the detector or crystal along their paths. As these nuclei pass, they leave zones of positive charges in their wakes causing the positively charged ions in the crystals to be repelled from each other and to be forced into the crystal structure thus forming the fission tracks. In polymer detectors, new chain ends and other chemically reactive sites are formed as a result of the ionizing character of the nuclei and consequently the fission tracks or trails are produced.

In their normal state, the fission tracks are too small to be seen except with an electron microscope but by choosing the proper chemical etchants, the damage zones can be enlarged and made visible through an optical microscope. This is discussed below.

2.1.3 Methodology

The preparative procedures for fission track studies were performed in four steps namely : sample preparation, irradiation, etching and analysis.

Slices of rock samples were mounted on microscope glass slides and reduced to $30\mu\text{m}$ thickness. Because smooth rock surfaces are required for FT analyses, Fleischer *et al.* (1975), the rock mounts were subsequently polished using $6\mu\text{m}$ and $1\mu\text{m}$ diamond paste respectively. The possibility that resistate minerals such as zircon and apatite, which are known to contain appreciable amounts of radioactive elements, may fill the fractures in the rock sections during the lapping and polishing processes was accounted for by continuously changing the water abrasive mixture and cleaning the rock slides in fresh petroleum ether in an ultrasonic cleaner for 20 minutes before irradiations. A set of reference axes was drawn on both ends of the slides then each slide was covered with an equal size piece of polycarbonate plastic (1mm thick "tuffac", Peter Plastic Ltd. Glasgow, U.K.). Before the reference axes were precisely drawn onto the plastics, both the slides and plastics were taped

together firmly. This way the fission tracks of U produced in the external detectors can accurately be matched with the mineral distribution in the rock sections simply by down focussing.

The method just described, though simple and attractive, can be misleading especially in fine grained rocks. The reference axes are drawn only with the naked eye and therefore serious mistakes during the matching processes can easily be made since the tracks are only visible under the microscope. Moreover, the rock-forming minerals can have significantly different hardnesses (micas compared to zircon, feldspars and quartz for instance) or more often, some minerals are included in others such as zircon in micas, feldspars and cordierite and hence there is a strong possibility that some U-bearing minerals cannot be at the contact with the detectors during irradiations. Furthermore, the fission track distribution patterns over zircons in thin sections are always star-like whereas those over zircon as monomineral mounts usually reflect the actual shape and size of the crystals. This indicates that zircons in the whole rock sections were not perfectly in contact with the detectors probably because the rock constituents have significantly different hardnesses. The evidence therefore suggests that mineral separation is necessary for more reliable micromapping of U in geological rocks. In the present work, the highly dense, star-like fission tracks produced by zircons were helpfully used for more precise matching while fission track studies of single minerals minimize the effects of different hardness of the rock constituents.

The preparations of individual minerals for fission track analyses were performed in the following way. To avoid breaking the mineral constituents of the rocks, their grain sizes were first measured in thin sections then the rocks were crushed accordingly. Individual minerals were subsequently obtained using magnetic separation, heavy liquid and hand picking techniques. An average of 10 grains of each mineral type from each sample were mounted individually on probe slides (4.7 x 2.1 cm) using thin drops of epoxy resin. The grain mounts were subsequently uncovered using self-adhesive silicon carbide paper discs (400 and 600 grits), polished by machine (6 μ m and 1 μ m diamond paste were used respectively) and placed face downwards on polycarbonate plastic detectors. Zircons intended for spontaneous fission

track investigations were mounted on small pieces (2 x 4 cm) of teflon as described by Gleadow et al. (1976). When the mineral mounts are intended for quantitative estimation of U, an accurately weighed piece of Specpure Fe wire (99.5% purity) was attached to each slide to monitor the neutron flux. A standard glass containing 0.823 ppm of U was also irradiated with the samples.

Irradiations to induce the fission of ^{235}U were performed in the thermal column of the UTR 300 reactor of the Scottish Universities Research and Reactor Centre (SURRC) for six hours at a position nominally corresponding to a neutron fluence of about $6 \times 10^{15} \text{ n cm}^{-2} \text{ s}^{-1}$ (MacKenzie, pers. com.). At this position, the neutron flux is well thermalized hence giving negligible fission of ^{232}Th , Toole (1985). Analytical problems did not allow fission track micromapping of Th to be carried out. An accelerator would solve the problem but it was not available for this study.

After irradiations, the samples were transferred to an isotope store and left to cool for about four weeks to allow the decay of short lived activation products and so that the samples became radiogenically safe to handle. The detectors were subsequently removed from the rock slides behind Pb shielding and cleaned with soft tissues ready for etching.

The chemical etchants, which are usually strong acids or bases attack both the damaged and undamaged zones of the detector or crystal but the rate of etching is greater in the damaged zones, Fleischer et al. (1975). The time factor is therefore very important to achieve an optimum track size for a given track density because excessive time results in a continuous track fading (shallower first, deeper second) while short etching time strongly affects the etching efficiency. In this study, spontaneous fission tracks of ^{238}U in apatite were revealed by immersing the polished grain mounts in 7% HNO_3 at room temperature for 20 seconds. Those in zircon were exposed using 1:1 NaOH and KOH at a fixed temperature of 250°C , Gleadow et al. (1976). The etching time varied between five and ten hours.

Induced fission tracks recorded on the polycarbonate plastic were etched in freshly prepared 6N NaOH at 40°C for about 35-45 minutes, Fleischer et al. (1975).

The mode of distributions of U in the rock slides and monominerals was

investigated under an optical microscope. The contents of U in apatite and biotite were calculated using the equation given below :

$$\frac{[U]_s}{[U]_{std}} = \frac{(\text{track density})_s}{(\text{track density})_{std}} \times \frac{(c)_{std}}{(c)_s} \quad 2.1$$

where [U] = concentration of U

s = sample

std = standard

c = count rate of the flux monitor in counts per second

2.2 Neutron activation analysis

Instrumental neutron activation analysis (INAA) was used to quantify the concentration of U and Th in the rock samples. In this technique sub-samples of 0.2g and standards for the relevant elements are exposed to a flux of neutrons in a nuclear reactor. Neutron capture by the constituent atoms produces radioactive species and the decay of radioactive products gives rise to emission of γ -radiation which can be detected and counted by γ -ray detectors. Comparison of the photopeak count rates of the sample with that of the standard for any element allows its concentration in the sample to be calculated. In this study, epithermal neutron activation analysis was used instead of thermal activation because it is not possible to determine U purely by γ -spectroscopy after thermal neutron activation due to severe interferences, Brunfelt and Steinnes (1969). However, the high advantage factor (*i.e.* the Cd ratio of the interfering nuclide divided by the Cd ratio of the nuclide under investigation) for ^{239}Np compared to the major activities, enables the determination of U with very good precision and accuracy, Brunfelt and Steinnes (1969) (see subsections 2.2.4.1-2 below).

2.2.1 Principles of γ -spectroscopy

The principles and methods of γ -spectroscopy are given in Adams and Dams (1970) and Friedlander *et al.* (1981). The more important aspects of

particular relevance to this work are summarized below.

To describe the detection of γ -radiation it is important to understand the interaction of the γ -radiation with matter. This involves interaction with electrons with two possible processes namely : photoelectric effect and Compton scattering. The photoelectric effect is a process by which a γ -photon transfers all of its energy to a bound electron in an atom or a molecule and the absorption of the γ -photon energy (E_γ) causes ejection of the electron as a photoelectron. The total absorption of the E_γ can only occur for a bound electron because the nucleus is essential in conserving momentum. The energy in the photoelectric effect is conserved according to the equation :

$$E_\gamma = E_C + E_b \quad 2.2$$

where E_γ = γ -photon energy
 E_C = energy of photoelectron
 E_b = binding energy of electron

Compton scattering is an interaction between γ -photon and an electron which can be either bound or free. In this process, the electron absorbs only parts of the photon energy leaving the scattered γ -photon of reduced energy. Again the energy in this process is conserved in the process according to the equation:

$$E_\gamma = E_{\gamma_1} + E_C + E_b \quad 2.3$$

where E_{γ_1} = energy of the scattered γ -photon
 E_γ , E_C and E_b as in 2.2

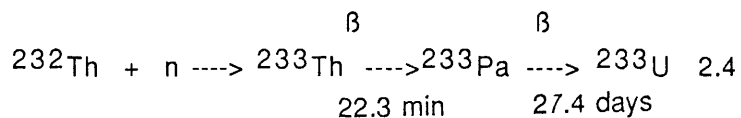
The ejection of the electrons in both the photoelectric and Compton scattering processes results in ionization. The photoelectric effect produces well resolved photopeaks which can be used for γ -spectroscopy, while the Compton effect produces a non-specific count rate at lower energies (which can hinder the determination of lower energy γ -emitters).

In this study , a high resolution (1.8 KeV at 663 KeV) Ge(Li) detector of 25 cm³ active volume was used for U and Th determinations while an 80cm³ detector of 2.0 KeV at 663 KeV was used for the flux monitors. The operation of the detectors is based upon collection of the charge produced as electron-

hole pairs by the interaction of γ -photons with the Ge(Li) detectors. To collect the charge, a voltage of 4000-5000 volts is applied to the detectors by a high voltage supply. Since the size of the charge pulse is proportional to the radiation energy, measurement of the different pulses produced gives a measure of the energies of the γ -photons interacting with the detectors. The amplitude of the voltage pulses are converted to digital signals by analogue-digital converters (ADC's) and stored in multichannel analysers. The channel contents are displayed as spectra on an oscilloscope and analysed by an EG&G Ortec data acquisition and analysis system containing 4 x 4096 channel analysers.

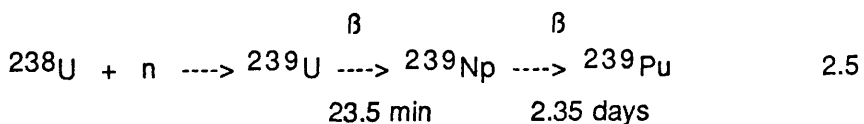
2.2.2 Method of determination of Th and U

The Th concentrations were determined from the induced ^{233}Pa activity according to the following reaction :



The activity of ^{233}Pa was determined using the γ -photopeak at 311.9 KeV which has an intensity of 36%, Friendlander *et al.* (1981) and free from interferences. However, the only species that can be identified from the γ -energy tables, Wakat (1971), as possibly interfering with ^{233}Pa photopeak at 311.9 KeV is the weak (0.89% intensity) 309.6 KeV γ -ray of ^{160}Tb ($t_{1/2}=72.1 \text{ d}$). If such interference exists, it is always below 1%, MacKenzie *et al.* (1986) and therefore can be regarded as insignificant.

U contents of the rock samples were derived from the activity of ^{239}Np using the γ -photopeaks at 277.5 KeV, 228.2 KeV and 210 KeV according to the reaction :



^{239}Np has a half life of 2.35 days and major photopeak intensities of 14.1%, 10.7% and 3.4% at 277.5 KeV, 228.2 KeV and 210 KeV respectively, Friendlander *et al.* (1981). The 210 photopeak has the lowest intensity, the highest total error and it is not detected in many samples. The 228 KeV photopeak gives high values and there is a possibility that it interferes with the 229 KeV γ -ray of ^{182}Ta . However, the 278 KeV photopeak has the highest intensity, the lowest total error and it is free from interferences, Brunfelt and Steinnes (1969). Consequently, the U content of the analysed rock samples is taken at the 278 KeV γ -ray.

2.2.3 Methodology

INAA is performed in four steps namely : preparation, irradiation, counting and calculations.

The preparative procedures consist of crushing the the rock samples to fine powders (the 250 mesh fraction was taken), then about 0.2g sub-samples are wrapped in Al-foil. Pieces of Specpure Fe wires (about 2 cm long and 99.5 purity) for monitoring the neutron fluence are accurately weighed and attached to each sample. An average of 10 samples, one standard and the corresponding flux monitors are packed together in an Al-foil and wrapped in a $\bar{\text{C}}\text{d}$ -sheet in order to minimize activation by thermal neutrons. Three materials were used as standards, a SURRC standard, international atomic energy agency (IAEA) standard and U and Th standard solutions. The SURRC standard (RC 1388), an apatite-rich syenite, has been characterized at the SURRC for U (24.7 ppm) and Th (107.7 ppm) and was used routinely with all samples. "soil-5" is a certified reference material provided by the IAEA. This standard has been used to characterize U and Th concentrations in the samples and in RC1388. The third standard consists of two atomic absorption standard solutions (AASS) each containing 1000 ppm of U and Th. Small quantities are taken from each solution and diluted to 100 ppm to reduce the radioactive hazards and minimize the dead time.

The irradiations of the samples were performed in the core of the reactor for six hours at a full power of 300 KW which provides a thermal neutron flux of about $3.8 \times 10^{12} \text{ n cm}^{-2} \text{ s}^{-1}$ with a Cd ratio of 4.6 (Whitley, pers. com.). However the samples could experience different neutron fluences

during irradiation depending on their position within the stack. This was corrected for by assuming that the specific activity induced in the Fe wires attached to each sample is proportional to the neutron fluence experienced by the sample and consequently was taken into account during the calculations. At the end of irradiations, the samples were left to cool in an isotope store for three days to allow the decay of excess short-lived nuclides (e.g. ^{24}Na , ^{28}Al , ^{42}K) before they were unwrapped behind Pb shieldings and transferred to polythene containers ready to count.

The counting technique requires two important factors to be considered at all times namely : the dead time and background radiation. The analyser requires a finite time to process any individual pulse and during this time no other pulses can be accepted and hence the instrument is said to be dead. To compensate for this, the analyser counts for the real time which is the sum of live time *i.e.* preset time and dead time. However, no serious uncertainties can be introduced to the measurements if the dead time is kept below 10% and this criterion was applied to all samples. The Ge(Li) is very sensitive so that small background radiations can introduce serious errors during counting. The main contributors to background radiations are either cosmic radiations and/or radioactive sources in the counting laboratory. The former cannot be totally excluded but it is probably not very important while several measures were taken to minimize the latter. The detectors are situated as far as possible from areas of high activity such as the reactor area, isotope stores and hot chemistry facilities. Moreover, only the sample being counted is left in the laboratory and the following sample to be counted is transported in two inch thick Pb containers after the counting time of the previous sample is completed.

The counting time of the samples varied quite considerably from a minimum of one hour up to 13 hours depending on the concentration of U and Th in the samples. The pelitic restites usually gave total errors below 10% after 60 minutes counting time while the migmatitic leucosomes and the pelitic xenoliths gave errors of between 10% and 20% despite being counted overnight and this is probably because of their very low U and Th contents.

The counting rate (R) at the end of the irradiation of a sample that contains (m) grams of the isotope of atomic weight (w) to be assayed is given by the

equation written below, Friedlander et al. (1981).

$$R = \frac{m}{W} N \phi \sigma \Sigma (1 - e^{-\lambda t}) \quad 2.6$$

where N = Avogadro's number

ϕ = neutron flux

σ = probability of the reaction

Σ = efficiency of the detector

λ = decay constant of the nuclide measured

t = irradiation time

In view of the difficulties of accurately determining some of these parameters, analyses are usually performed by comparing the activities induced in samples and standards which are subjected to identical irradiation and counting conditions. The amount (M) of an element (i) in the samples is then given by the following equation :

$$M(i) \text{ in sample} = \frac{M(i) \text{ in standard} \times C \text{ from sample}}{C \text{ from standard}} \quad 2.7$$

where C = counting rate at specified common time

$M(i)$ = amount of element (i)

All calculations were performed using the SURRC computer facilities. The spectra were stored in the EG&G Ortec data acquisition system(DAAS). The photopeaks were identified and count rate calculated by the program gamma-2 and the final results obtained using the SURRC programme NAA, Harris (1982).

2.2.4 Reliability of the data

The advantages of epithermal neutron activation as a multi-element method of analysis have been discussed by Brunfelt and Steinnes (1969). In this section, an attempt is made to characterize the precision and accuracy of the method for both U and Th.

2.2.4.1 Precision

Like in all nuclear counting, the precision of epithermal neutron activation is dependent on counting statistics, counting geometry and weighing errors. In this study the precision is calculated in two ways, by analyzing one sample eight times, and eight samples twice each sample and the results are given below :

TABLE 2.1 Precision of INAA

	U(ppm) 1σ	Th(ppm) 1σ
Y 50 1	3.45 ± 0.02	17.87 ± 0.03
2	3.45 ± 0.02	17.65 ± 0.03
3	3.68 ± 0.03	19.77 ± 0.01
4	3.22 ± 0.02	17.14 ± 0.01
5	3.33 ± 0.02	17.94 ± 0.01
6	3.36 ± 0.03	17.02 ± 0.02
7	3.24 ± 0.03	18.04 ± 0.02
8	3.30 ± 0.03	17.76 ± 0.02
Y 7 1	3.12 ± 0.02	20.25 ± 0.03
2	2.94 ± 0.03	18.49 ± 0.03
Y10 1	2.92 ± 0.02	11.55 ± 0.02
2	3.05 ± 0.02	12.33 ± 0.02
Y17 1	1.45 ± 0.06	11.54 ± 0.05
2	1.51 ± 0.07	10.94 ± 0.06
Y20 1	1.70 ± 0.03	10.44 ± 0.03
2	1.77 ± 0.04	11.82 ± 0.03
Y43L 1	0.13 ± 0.03	0.23 ± 0.04
Y43L 2	0.15 ± 0.03	0.34 ± 0.03
Y50 1	3.45 ± 0.02	17.87 ± 0.03
2	3.45 ± 0.02	17.65 ± 0.03
Y53 1	1.55 ± 0.02	14.63 ± 0.03
2	1.72 ± 0.03	15.52 ± 0.03
Y54 1	1.54 ± 0.03	10.08 ± 0.03
2	1.55 ± 0.03	10.12 ± 2.94

Each sample was counted on the contact of the 25 cm³ detector for 60 minutes except Y 43L (a migmatite leucosome) which was counted for 13 hours.

The precision calculated from the sample Y50 is 4.11% for U and 4.40% for Th while the average precisions from the eight samples is 2.73% for U and 5.64% for Th. These values are very good and prove that epithermal NAA is a precise method for determining U and Th. The slight variations sometimes recorded are probably related to the heterogeneous distributions of U and Th-bearing minerals particularly zircon and apatite, counting geometry and statistics and sample weighing.

2.2.4.2 Accuracy

Ultimate accuracy depends on the reliability of the amounts of the required elements in standards. An in-house SURRC (Glen Dessary syenite - apatite-rich, RC1388) was used as a routine standard and the reliability of U and Th concentrations in this material are considered below.

a) Uranium

Previous results for U obtained by isotope dilution mass spectrometry (Van Breeman *et al.*, 1979) which is recognized as providing an accuracy of better than $\pm 1\%$, were 24.8, 24.8 and 24.6 ppm. These values were confirmed by obtaining the following results by epithermal NAA, with reference to the AASS : 24.67 and 24.43.

b) Thorium

Th was determined in RC 1388 by NAA with reference to soil-5 and the following results obtained : 104.2 ± 2.1 ppm and 111.2 ± 2.2 ppm producing a mean value of 107.7 ± 3.8 ppm which was used as the reference value with all analysed samples. This value was confirmed by the results obtained with reference to AAS solutions of 109.3 ± 2.0 ppm and 102.5 ± 1.4 ppm giving a mean value of 105.9 ± 3.4 ppm. It is clear that the accuracy is not as good as the precision of a single determination but it is better than $\pm 4\%$.

2.3 Inductively coupled plasma(ICP) spectrometry

ICP spectrometry, a solution method of analysis, consists of dissolving about 0.5g of rock samples using conventional acid digestion techniques and introduction of the rock solutions into the ICP unit for analysis. The efficiency of ICP for major and trace element analyses is very well documented (e.g. Walsh, 1980, 1982, 1985; Walsh and Howie, 1980; Walsh *et al.*, 1981). In this study, rare earth elements (REE) in 30 samples were determined using this technique following the procedure described by Walsh *et al.* (1981).

2.3.1 Principles and practice of ICP

The principles and practice of ICP spectrometry, a summary of which is given below, have recently been discussed by Walsh and Howie (1986).

Once a sample is in solution the first step of analysis is introduction into the ICP torch. This is done by pumping the solution into the "nubilizer" where it is converted to an aerosol by the flow of Argon. The efficiency of most ICP nubilizer/spray chamber systems is very low, typically only 1-2 % of the solution entering finally reaches the ICP flame and the remainder drains away to waste (Walsh and Howie 1986).

From the nubilizer /spray chamber, the aerosol enters the ICP torch itself. The ICP is contained within a two (or possibly more) turn coil which carries a high frequency current. When the high frequency current flows in the coil it generates a rapidly varying magnetic field within it. When charged particles (for example, an ionized gas containing the analytical solution) flow through the field, cutting the magnetic lines of force, then ohmic heating results generating the ICP flame. The inductive heating effect maintains the ICP flame at temperatures of 6000°K and up to 10,000°K at its hottest point. This high temperature gives the technique its greatest assets, namely its relative freedom from interferences and complete atomization of the solution being analysed. More importantly, many atoms are converted to ions thus giving a wide choice of sensitive spectral lines especially for the refractory elements such as REE.

The principle of ICP analysis is that when the light emitted by the ICP source is focussed into the spectrometer (simultaneous or sequential), the

diffraction grating resolves the light into its component wavelengths which fall on a series of light sensitive photomultiplier tubes located at precise wavelengths in the diffracted light spectrum. The light signals generate a mV signal in the photomultiplier and this electric signal is normally fed to a capacitor and then to a digital voltmeter. There should be a straight line relationship between this electrical signal and the concentration of the element being measured. Almost all ICP systems have dedicated computers which when calibrated with the appropriate standard solutions, read out the results directly as concentrations.

Normal analytical practice would therefore consist of first preparing a series of standard solutions which would cover the range of concentrations anticipated for the elements to be measured. The standard solutions would then be run first on the ICP system and then the signal level of each element is stored as a calibration line in the computer system. After calibration, unknowns can be run and concentration equivalents from the signals obtained calculated.

The advantages and disadvantages of ICP spectrometry are not discussed here but can be found in Walsh and Howie (1986).

2.3.2 Sample preparation for REE analysis

The procedures for REE determinations consist of three steps namely; sample dissolution, REE separation and analysis.

Acid digestion of samples was performed in groups of eight (six samples, one standard and one blank). 0.5g powdered rock is weighed accurately into a platinum crucible, 5ml of HClO_4 and 15 ml $\text{HF}(40\%)$ added and the solution digested to incipient dryness on a sand bath. The cake is left to cool and then dissolved in 20ml warm 25% HCl , filtered and washed with distilled water through Whatman N^o 42 filter paper. The precipitate is ignited to 800°C in an Ag crucible (30 minutes under 300°C and another 30 minutes under 800°C), fused for 30 minutes with 0.5-0.7g NaOH and after cooling dissolved in a total of 15-20ml $\text{HCl}(25\%)$ and finally added to the filtrated portion and made to 100ml with distilled water. Magnetite- and garnet-rich samples did not fuse well in NaOH and therefore fusion with LiBiO_2 was used instead. In this procedure, the precipitate is ignited to 800°C in a platinum crucible,

fused in 1-2g LiBiO_2 for 30 minutes on a Bunsen burner while the mixture is continuously swirled. The cake is then dissolved in three to four successive 5ml amounts of about 10% HCl stirring with a magnetic bead. Again the solution is added to the filtered portion and made up to 100ml.

REE are separated using chromatographic glass columns loaded with clean resin (Dowex AG 50W-X8, 200-400 mesh from Bio Rad Laboratories). The resin (12cm settled length) is then washed with 600ml of 4N HCl and rinsed with 450ml of 1.7N HCl. The samples are then loaded onto the columns and washed with 450ml of 1.7N HCl to remove the major and most trace elements. The REE which are held on the resin together with all Ba and some Sr, Zr and Hf are eluted with 600ml of 4N HCl. The solutions are filtered through Whatman N^o5 filter paper to remove any resin particles, evaporated to about 15ml, transferred to 50ml beakers and taken down to dryness. The REE are subsequently redissolved in 5ml of 10% HNO_3 and pumped into the ICP source unit.

2.3.3 REE analysis

REE were determined at the Royal Holloway and Bedford College (RHBC), Egham, U.K. using a Philips PV8490 ICP source unit and PV8050 emission spectrometer.

Three standard types were used, REE composition standard, interfering element standards and drift standards.

The REE composition standard solution contains 10ppm(La,Nd,Y); 2ppm(Pr,Gd,Sm); 1ppm(Eu,Dy,Ho,Er,Yb,Lu). This solution, which is a calibration standard, is analysed after distilled water to define the lowest and highest intensity of the electric signal respectively.

Seven standard solutions [20ppm(Ce_2O), 100ppm(Fe,Ba,Ca), 50ppm(Sr, Zr), 10ppm(Nd)] were analysed to account for possible interference of the REE with these elements. Small corrections were carried out for the following elements.

Ca for La	Zr for Ho
Ba for Nd	Nd for Er,Pr,Sm
Sr for Ce,Pr	Ce for Pr

Fortunately, Eu, which is very important in most REE interpretations does not interfere with any element .

The drift standards (KC10-14) are granites characterized in the RHBC for REE contents. The results obtained for these standards are quite similar to the accepted values so that only small drift calculations were performed.

Spectral lines of the REE, the precision and accuracy of ICP spectrometry are not included here but have been discussed by Walsh et al. (1981).

2.4 X-ray fluorescence

The principles and practice of X-ray fluorescence are well documented (e.g. Norrich and Chappell,1967; Jenkins and De Vries,1967), and the application to the determination of major-and trace-elements in geological material have been discussed (Leake et al.,1969; Harvey et al.,1973). This technique has been used in the present work to quantify the major and trace element contents in the samples.

2.4.1 Principles

On bombarding a sample with a source of X-rays, the atoms present in the sample will scatter some, and absorb the remaining photons. Photons absorbed by an atom in the sample will give rise to characteristic X-ray emission of that element. The characteristic X-ray photons produced by this X-ray bombardment of an element is known as X-ray fluorescence. The intensity of the characteristic fluorescent radiation for a given intensity of source X-rays is not completely linear in relation to the element concentration due to various absorbance effects by the sample matrix. These effects which depend essentially on the thickness of the substance, its density and its absorption coefficient are corrected for and the concentration of elements can be estimated.

The detection of an element in X-ray fluorescence emerges from the application of Braggs equation ($n = 2d \sin\theta$). For a given value of the angle, θ may be predicted if a crystal having a known atomic spacing (d) is used. Since the X-ray radiation for every element has known fixed wavelengths then the value of θ can be calculated for any element. Thus, the fluorescent radiation emitted by a rock sample may be investigated to find whether an

element is present and if so in what concentration.

2.4.2 Methodology

Rock analyses were carried out in the Geology Department, University of Glasgow, U.K. using a Philips PW1450/20 automatic X-ray fluorescence spectrometer equipped with a 60 position sample changer and on-line superBrain microcomputer for data processing. The computer programme used was written by Dr C.M. Farrow of the Geology Department.

The major elements are analysed from fused glass discs prepared according to the method of Harvey *et al.* (1973) while for the trace elements, pressed pellets are used (Leake *et al.* 1969). FeO is analysed by titration and H₂O and CO₂ are determined simultaneously using the method of Riley (1958).

The detection limits of X-ray fluorescence for major and some trace elements are given below :

Table 2.2 Detection limits of XRF

	<u>Major elements</u>		<u>Trace elements</u>	
	detection limits(wt%)	accuracy (wt%)	detection limits(ppm)	
SiO ₂	0.086	0.46	Cr	1.9
TiO ₂	0.018	0.11	Ni	4.8
Al ₂ O ₃	0.087	0.36	Co	3.2
Fe ₂ O ₃	0.045	0.10	Ga	2.4
MnO	0.012	0.008	Sr	1.5
MgO	0.165	0.13	Zr	2.7
CaO	0.006	0.17	Rb	1.7
Na ₂ O	0.155	0.26	Zn	1.8
K ₂ O	0.002	0.09	Cu	4.4
P ₂ O ₅	0.018	0.02	Pb	11.6

2.5 Comparison between INAA, ICP and XRF

Comparisons between different analytical techniques are always subjective and often designed to prove the superiority of one particular method. Moreover, conclusions usually depend on the material used and the range of elements sought. 28 rock samples were analysed for La, Ce and Ba using both ICP and XRF techniques. XRF was also used along with INAA to quantify U and Th contents in 108 samples and therefore comparison between these methods is made.

The results obtained using XRF are plotted in Figures 2.1-5 against those obtained by ICP and INAA respectively. Simple least square linear regression analyses were computed for each element, and the best fitting straight lines are also shown in Figures 2.1-4.

Expressing the results in the form of straight line equations i.e. $x = am + c$ the results yield :

La	: XRF = 0.96 ICP - 4.7	(0-150ppm)
Ce	: XRF = 0.85 ICP + 3.8	(0- 200ppm)
Ba	: XRF = 1.03 ICP + 12.6	(0-2000ppm)
Th	: XRF = 0.87 INAA + 2.04	(0-30ppm)

It is clear that the overall agreement between the XRF and ICP techniques is good although ICP more often yields higher values than XRF for the REE La and Ce. While the two methods generally yield somewhat similar values for Th, XRF is clearly significantly less sensitive than INAA for U determinations and therefore the least square calculations were not computed and the best fitting straight line not shown.

Generally there are many factors affecting the accuracy and precision of XRF on the one hand and ICP and INAA on the other. These include the accuracy of the reference values for the standards used during the calibrations, possible interference of elements, incomplete dissolution of the rocks during chemical separation in the case of ICP, the effects of the counting statistics and geometry in INAA, heterogeneity and weight (0.5g in ICP, 0.2 g in INAA, 6g in XRF) of the samples. It is clear on the basis of the above factors that no significant systematic differences exist between XRF and ICP for the elements

concerned. However, XRF is not a reliable method for U analyses but can be used for Th determinations with reasonable confidence.

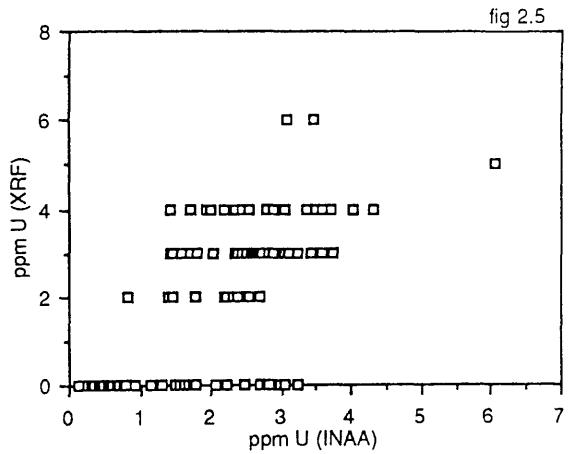
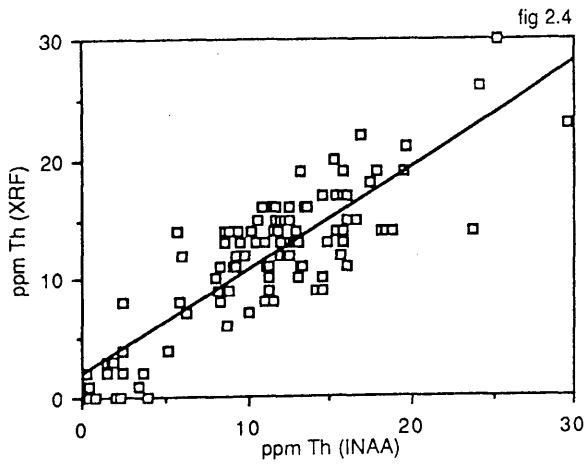
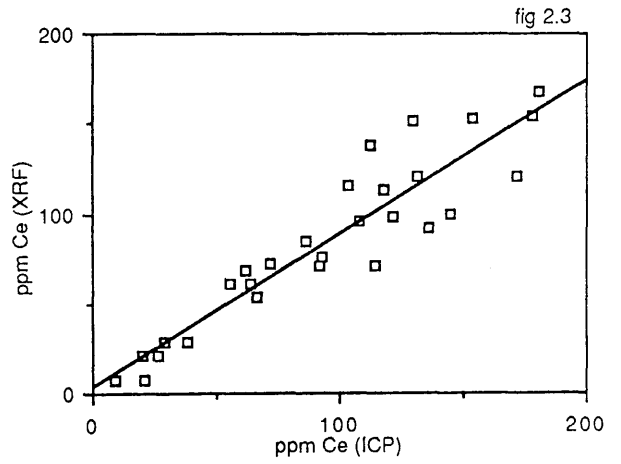
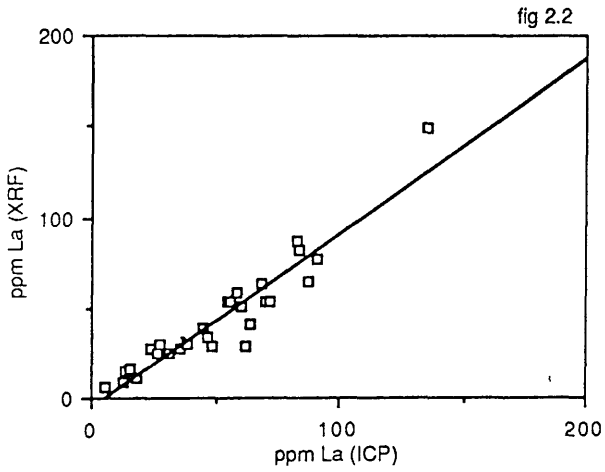
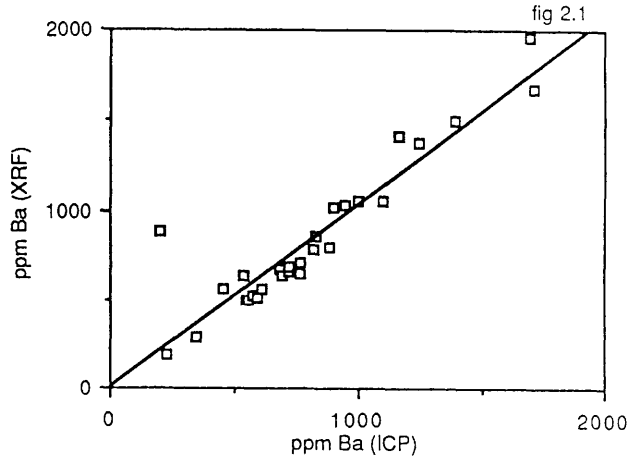
fig 2.1 plot of Ba (XRF) versus Ba (ICP)

fig 2.2 plot of La (XRF) versus La (ICP)

fig 2.3 plot of Ce (XRF) versus Ce (ICP)

fig 2.4 plot of Th (XRF) versus Th (INAA)

fig 2.5 plot of U (XRF) versus U (INAA)



**THE CASHEL-LOUGH WHEELAUN INTRUSION, CO.
GALWAY, IRELAND**

CHAPTER THREE : CONDITIONS OF METAMORPHISM

3.1 Introduction

The past thermal gradient in the Cashel thermal aureole is quantified using two independent models namely: mineralogical and physical models. The mineralogical model which has also been used to quantify the pressures is based upon the partitioning of elements between a pair of coexisting phases. Five different calibrations have been used in geothermometry and two in geobarometry and comparison between these calibrations is made. The physical model is based on the Fourier's general differential equation which covers all possible variables affecting the thermal history of two bodies having different temperatures and in contact with each other. The model has been first applied to geological problems by Lovering in 1935 and then subsequently in 1936 and 1955. It was elaborated by Carslaw and Jaeger (1947,1959) and Jaeger (1957,1959). In contrast to the physical model which remained unchanged since its elaboration, there is still considerable debate concerning the accuracy of the mineralogical model and efforts are still being made to produce more consistent calibrations; therefore this model is studied in more detail. The equations used in geothermometry and geobarometry are given in appendix one.

The aim of the study is to define the P-T conditions under which the minerals crystallized in the Cashel aureole.

3.2 Mineralogical model

The distribution of elements between a pair of coexisting phases is a function of temperature, pressure and composition of the phases and again the compositional effect depends on the thermodynamic properties of the respective phases, Kretz (1961). The partitioning of elements between minerals, particularly Fe^{+2} and Mg between garnet and other minerals such as biotite, cordierite, anorthite, amphibole, pyroxene, has been extensively investigated (e.g. Kretz 1959, Frost 1962, Phinney 1963, Albee 1965, Saxena 1969, Sen and Chakraborty 1968, Lyons and Morse 1970). Despite this considerable work, it is only in the last decade that the results were successfully calibrated as quantitative geothermometers and geobarometers. A critical component in the calibrations is the equilibrium constant K_D which is

related to the standard free energy (Gibb's energy) ΔG^0 according to the equation given below and which provides the basis of temperature and pressure calculations.

$$\Delta G^0 = - R T(^{\circ}\text{K}) \ln K_D$$

where R = gas constant (1.987 cal mole⁻¹ degree⁻¹)

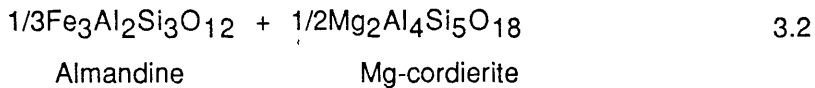
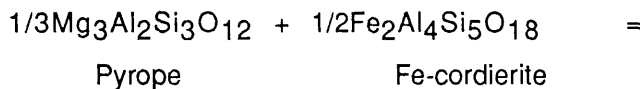
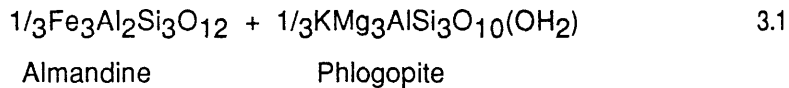
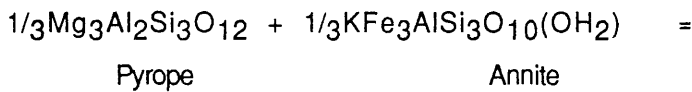
T = temperature in degree Kelvin (^oK)

In geothermometry, chemically zoned minerals must be used with caution, Tracy *et al.* (1976), Yardley (1977c). In this study all phases used in the P-T calculations are essentially homogeneous except along the garnet rims (0-200 μ) where the Mg content always decreases but Fe and/or Mn increase. Because this chapter is aimed at establishing the peak metamorphic conditions reached within the aureole and zoning in garnets is believed to be of retrogressive origin (Chapter 4), only the mean core garnet compositions have been used as these are likely to preserve the highest original temperatures. Biotite and cordierite can also affect the P-T estimates if their present compositions are significantly different from the original compositions because of continuing cation exchange reactions during cooling with other Fe-Mg phases. The mineral chemistries, discussed in Chapter 4, show that biotites from the matrix are always unzoned and those inside garnet and cordierite which show possible re-equilibrations during cooling were excluded from the P-T calculations. Cordierite is almost always completely pinitized and because only 2 analyses were possible no conclusive interpretations can be made, but Treloar (1981) noted that cordierite cores are homogeneous and therefore most of the calculated temperatures and pressures are likely to represent the peak metamorphic conditions.

3.2.1 Geothermometry

The partitioning of Fe⁺² and Mg between coexisting garnet, biotite and cordierite is temperature dependent and it has been calibrated to produce 3 two phase exchange reaction geothermometers. Thompson (1976), Holdaway and Lee (1977) produced 2 empirical calibrations of the garnet-biotite and garnet-cordierite thermometers and Ferry and Spear (1978) published the

only experimentally determined calibration of the first thermometer. The two cation exchange reactions are given below and are potentially useful thermometers for two reasons. Firstly, no fluid phase is involved in both reactions and therefore the activity of volatile components such as H₂O and CO₂ is not important. Secondly, the reactions have very small Δv [(0.019 cal/bar (Ferry and Spear, 1978 for reaction 3.1) and (0.0303 cal/bar (Holdaway and Lee, 1977 for reaction 3.2))] and thus are only slightly pressure dependent.



The empirical calibration of Thompson (1976) is based upon natural coexisting garnet cores and biotite analyses. By using independently determined temperatures from the studied rocks Thompson (1976, p429) produced a $\ln K_D$ versus $10^4/T$ plot. This calibration is heavily weighted at the low temperature end but only extrapolated by best fit techniques to higher temperature regions; hence any small error at the low temperature end will be magnified at higher temperatures.

The calibration of Holdaway and Lee (1977) is primarily founded on the previous calibration, but because the low temperature end of Thompson's calibration is mostly based on the work of Osberg (1971), Holdaway and Lee consider that the temperatures obtained by Osberg are too low and their calibration takes account of this.

The experimentally determined calibration of Ferry and Spear (1978) is based upon the partitioning of Fe-Mg between pure end-members of reaction 3.1 and it has been produced at 2.07 Kb at temperatures of between 550° and 800°C.

The Ferry and Spear calibration assumes that Fe⁺² and Mg mix ideally in both garnet and biotite and therefore neglects the effects of possible octahedral substitution of Ca and Mn in garnets and Al⁺⁶, Ti and Fe⁺³ in biotites, hence giving geologically unreasonable temperatures (Hodges and Spear 1982; Pigage and Greenwood 1982; Indares and Martignole 1985). The empirical calibrations are also subject to the same criticism except that being based on natural mineral assemblages these substitutions may have been intrinsically taken into account. In this study the 3 original calibrations are first used as they appeared in the literature and then the corrections suggested by Hodges and Spear (1982, equation 9) and Indares and Martignole (1985, equations 18 and 19) are applied to Thompson's and/or Ferry and Spear's calibrations. Comparisons between the results are then drawn, the effects of impurities on the K_D are investigated and finally a discussion is given.

3.2.2 Results

The mean composition of biotites, garnet cores and cordierite, presented in Tables 4.3-5, have been used to calculate garnet-biotite and garnet-cordierite temperatures. The formulae used to calculate the mole fractions of phase components, given in Tables 3.1 and 3.2, are those suggested by Hodges and Spear (1982, p1127).

19 garnet-biotite pairs and 1 garnet-cordierite pair have been analysed and indicate temperatures of between 670° and 1081°C depending upon which calibration is used (Table 3.2). The experimental calibration of Ferry and Spear (1978) consistently yields higher temperatures than both the empirical calibrations of Thompson (1976) and Holdaway and Lee (1977), with the latter always yielding the lowest temperatures. However, the difference is more pronounced at higher temperatures especially between the experimental calibration on the one hand and the empirical calibrations on the other; hence the largest difference between the three calibrations is found in the sample Y16 in which the highest temperature is recorded with the least

difference in Y23 in which the lowest temperature is obtained. This trend is expected because all the calibrations are based on relatively low temperatures ($\leq 800^{\circ}\text{C}$) and the slope of $\ln K_D$ versus $T(^{\circ}\text{K})$ of the Ferry and Spear (1978) calibration is markedly different from both Thompson's and Holdaway and Lee's calibrations shown in Figure 3.1. From this figure it can be seen that the temperatures derived from the 3 calibrations would yield very similar temperatures between 525°C and 600°C , but the Ferry and Spear calibration would constantly yield higher temperatures above 600°C followed by Thompson's then Holdaway and Lee's calibrations. However, the empirical calibrations do not vary significantly from each other but since the calibration of Thompson (1976) is likely to be more reasonable at higher temperatures, (Indares and Martignole, 1985), it will form the basis for future discussion.

In sample Y17 the calibration of Thompson (1976) and Holdaway and Lee (1977) for the temperature dependent Fe-Mg exchange between coexisting garnet and cordierite yield lower temperatures than the corresponding garnet-biotite calibrations (Table 3.2). However the difference is only 21°C and 11°C between the two thermometers respectively and because zoning in cordierite is uncertain, it is not clear whether the temperatures obtained represent a minimum or a maximum.

3.2.3 Errors

The errors (\pm) illustrated in Table 3.2 for the calibration of Thompson (1976) are calculated from the extreme Fe-Mg of individual garnet and biotite analyses within the same sample and should not be confused with the real errors of the calibrations which are in the order of $\pm 50^{\circ}\text{C}$. They were calculated using K_D max which involves the Fe-richest garnet and Mg-richest biotite and K_D min which is the opposite. This way not only shows the spread of the data but also any inherent error in the microprobe technique is accounted for.

3.2.4 Field relationships

Although two complete traverses for P-T calculations were attempted, only discontinuous analyses were possible because of the alteration of biotite

and/or absence of garnet. The results obtained in this study together with those derived by Treloar (1985) are recorded on a simplified geological map in Figure 3.1a. The metamorphic subdivisions discussed in Chapter 5 are also presented.

Along the eastern traverse, an abnormally high temperature of between 800° and 940°C is constantly recorded in the vicinity of the Cashel Hill intrusion, but it drops off abruptly to a plateau of between 670° and 766°C in less than 200m from the contact, thus indicating a steep thermal gradient. Along the western traverse, the highest temperature of 811°C is recorded in Y55, the nearest sample to the Cashel basic sill, with the temperatures decreasing northward.

Within the contact zone, the temperatures recorded are always higher than 790°C except in three samples, Y23, Y65 and Y70 from which temperatures of 670°, 695° and 735°C are obtained respectively. Y23 is an intermediate hornfels but the other two samples are contact hornfelses by most criteria (see Chapter. 4 for the definition of terms) and these temperatures appear to be unreasonably low. The three samples were collected where migmatitic leucosomes are excellently exposed, with Y65 and Y70 being restite-leucosome pairs, and consequently some down temperature re-equilibration between these migmatite leucosomes and biotite compositions has probably taken place. This is likely to have occurred because some biotite recrystallization especially at the boundaries between the leucosomes and the restites has been noted (Barber and Yardley 1985, Chapter 6).

In the rocks which have only been regionally metamorphosed, the temperatures are always below 800°C with the average of the four analysed rocks being $759 \pm 34^\circ\text{C}$. This value is in excellent agreement with temperatures from similar rocks from eastern Connemara derived by Barber and Yardley (1985) and it probably represents the peak regional metamorphic temperature.

3.2.5 The effects of impurities.

The effects of octahedral substitution of Mn and Ca in garnets and Ti, Fe⁺³ and Al⁺⁶ on the K_D have been theoretically studied by Dallmeyer (1974). In biotite, octahedral substitution of Ti, Fe⁺³, and Al⁺⁶ for Fe⁺² and Mg

increases the positive charges in the octahedral layer. This excess positive charge is accommodated in two ways (Foster, 1960): first, through increased tetrahedral substitution of Al and Si to provide less positive charge on the tetrahedral layer. Second, by having unoccupied octahedral positions thus producing negative charges in the octahedral layer. Both mechanisms of charge compensation frequently occur in biotites (Dallmeyer, 1974). Substitution of Al 0.47\AA for Si 0.34\AA (all ionic radii are taken from Whittaker and Muntus, 1970) enlarges the tetrahedral layer. In contrast, substitution of Ti (0.69\AA), Fe^{+3} (0.73\AA) and Al^{+6} (0.61\AA) for Fe^{+2} (0.86\AA) and Mg (0.80\AA) in the octahedral positions, together with an increase of vacant octahedral sites, serves to reduce the dimensions of the octahedral layer. In order to reduce this structural mismatch, the slightly larger Fe^{+2} would be preferred for Mg in the biotite octahedral layer. Therefore at a constant temperature, increasing octahedral Ti, Fe^{+3} and Al^{+6} substitutions would decrease the $K_D^{\text{gt-bio}}_{\text{Fe-Mg}}$ and result in an overestimation of the temperature. In garnet, any octahedral substitution of the larger Ca (1.08\AA) and Mn (0.91\AA) cations for Fe^{+2} and Mg should produce structural expansions within the garnet structure and therefore Fe^{+2} would be preferentially incorporated in the octahedral sites to increase the overall cell size and thereby minimize local intercrystalline strains (Dallmeyer 1974, p202). Consequently, $K_D^{\text{gt-bio}}_{\text{Fe-Mg}}$ will increase with increasing Ca and Mn substitutions, hence giving low temperatures.

The study aureole probably forms a rare place where the effects of Mn and Ca substitution in garnet and Ti in biotite can easily be tested because significant changes in the content of these elements occurred gradually in the same rocks and within a small area (see Chapter 4). For this purpose, a series of scatter diagrams have been plotted and the corresponding correlation coefficients calculated and reported on each plot in Figures 3.2-7.

When $X_{\text{Mn}}^{\text{gt}}$ and $X_{\text{Ca}}^{\text{gt}}$ are considered together, it is apparent from Figure 3.5 that a fairly good positive correlation exists between the K_D and $X_{\text{Mn+Ca}}^{\text{gt}}$, hence indicating that both elements affect the K_D . If $X_{\text{Mn}}^{\text{gt}}$ and $X_{\text{Ca}}^{\text{gt}}$ are considered individually (Figures 3.6-7), it is apparent that $X_{\text{Mn}}^{\text{gt}}$

and the K_D exhibit a fairly good positive correlation with the correlation coefficient being 0.516. X_{Ca}^{gt} also exhibits a broad positive but poor correlation with the K_D . The correlation coefficients between the K_D and X_{Ti}^{bio} and X_{Ca}^{gt} are the same (0.290) thus suggesting that Ca and Ti have very similar effects on the K_D . The sample Y9 has the highest X_{Mn}^{gt} of 0.130 but plots individually on Figure 3.6 because it has a low K_D (3.05). If this sample is excluded, the correlation coefficient between X_{Mn}^{gt} and the K_D becomes 0.697 thus indicating that the effects of Mn on the K_D are more pronounced in spessartine-poor garnets than in spessartine-rich ones. This conclusion contradicts that reached by Yardley *et al.* (1980, p389) that while X_{Mn}^{gt} does affect the K_D , the effects only become detectable for garnets unusually rich in spessartine. However, because most garnets studied in this thesis were crystallized under much higher temperatures than those investigated by Yardley *et al.* (1980), it seems that some relationship exists between the grade of metamorphism and the effects of Mn on the K_D with this being more significant at the Mn-poor end at high grades and at the Mn-rich end at moderate and low grades.

In biotite, there is a positive but weak correlation between the K_D and X_{Ti}^{bio} (Figure 3.2) but there does not appear to be any correlation between the X_{Al+6}^{bio} and the K_D with the correlation coefficients being 0.290 and 0.08 respectively. When plotted together, the K_D and X_{Ti+Al}^{bio+6} exhibit a positive but again very weak correlation and the correlation coefficient is only 0.165. Consequently the effects of X_{Ti} on the K_D , although they are not very significant, are much more pronounced than those of X_{Al+6} .

The influence of X_{Mn}^{gt} , X_{Ca}^{gt} and X_{Ti}^{bio} on the K_D have just been discussed and proved to affect the K_D thereby affecting the temperatures derived using garnet-biotite thermometry. More recently, Hodges and Spear (1982), and Indares and Martignole (1985) produced modified calibrations of the Ferry and Spear calibration which account for Ti and Al substitutions in biotite and/or Mn and Ca in garnet. The former calibration accounts for the composition-activity relationships in garnets only and it has been applied to both the calibrations of Thompson (1976) and Ferry and Spear (1978) whereas the latter accounts for the effects of non ideality in both garnet and

biotite but is applicable to Ferry and Spear's calibration only. The temperatures derived from both corrections are given in Table 3.3 and the difference between the modified and original calibrations are also given in parentheses in Table 3.3. Three observations of particular importance emerge from the correction of Hodges and Spear(1982). First, at temperatures below 850°C and 810°C for the calibrations of Ferry and Spear (1978) and Thompson (1976) respectively there is but only a slight increase in the temperatures derived using the modified calibration and the lower the temperature recorded in the samples the greater the difference. Second, at temperatures above the limits just stated the case is reversed and the temperatures obtained are either the same as those of the uncorrected form or lower. Third, the largest increase is not recorded in Y5' and Y9 which are the Mn-richest garnet bearing rocks. These observations are slightly more noticeable in the calibration of Ferry and Spear (1978) than in Thompson's (1976) although the general patterns are maintained in both calibrations. At high metamorphic grades the correction of Hodges and Spear (1982) does not give any significant changes compared to the original calibrations but it is probably effective at low grades. The fact that the largest increase is not recorded in the Mn-richest garnet bearing samples indicates that substitutional compensation of Ti and Al⁺⁶ in biotite against Mn in garnet had occurred (i.e. the effects of Ti and Al⁺⁶ in biotite on the temperature estimates are stronger than those of Mn and Ca in garnet). The two equations of Indares and Martignole (1985) sometimes yield significantly different temperatures depending on the Mn and Ca contents of garnet, hence the largest difference of 62°C is recorded in Y9 which is the Mn-richest garnet bearing sample but the same values are obtained from Y17 containing the Mn-poorest but the Ca-richest garnet, Table3.3. Because equation 19 takes account of both Ca and Mn substitutions in garnet and is based on the more recent thermochemical data of Ganguly and Saxena (1984) it is used for further discussion. Table 3.3 shows three important features. Firstly, the temperatures derived from the correction of Indares and Martignole (1985) are almost always significantly lower than those obtained using the original calibration of Ferry and Spear (1978). Secondly, The largest and smallest differences are recorded in Y9 and Y72 which are the Mn-richest garnet and

Ti-richest biotite-bearing samples respectively. Thirdly, in Y23 where the lowest temperature is obtained, the case is reversed and the temperature derived from the modified calibration is higher than that derived from the original one. The second and third points are probably the most important ones because they show that at high grades the effects of Ti and Al⁺⁶ in biotite are the source error in the calibration of Ferry and Spear (1978) and therefore define the lower limit at which the the correction should be applied. Table 3.3 shows that there are two limits at which the two corrections of Hodges and Spear (1982) and Indares and Martignole (1985) oppose their fundamental aims thus defining the maximum and minimum temperature limit at which they should be applied respectively.

3.3 Physical model

3.3.1 Introduction

The mathematical theory of heat conduction in solids is due to J.B.J. Fourier (1768-1830). Its principle emerges from the fact that when different parts of a solid body or two bodies are at different temperatures, heat flows from the hotter to the colder portions by a process of electronic and atomic energy transfer known as "conduction". The rate at which heat will be transferred depends particularly upon the thermal conductivities, densities and specific heats of the substances.

The Fourier's general differential equation can be written as :

$$\frac{\partial T}{\partial t} = k \left(\frac{\partial^2 T}{\partial x^2} + \frac{\partial^2 T}{\partial y^2} + \frac{\partial^2 T}{\partial z^2} \right) \quad 3.3$$

where T = temperature

t = time

$\partial T/\partial i$ = thermal gradient (i=x, y, z)

k = thermal diffusivity (k=K/c_pd)

K = thermal conductivity

C_p = specific heat

d = density

In applying the heat conduction theory to geological problems, the number of variables is so large that the Fourier's differential equation becomes mathematically unsolvable and therefore simplifying assumptions are necessary and have been made by Lovering (1935, 1936,) and Jaeger (1957,1959). Those assumptions which are relevant to the present study are given below.

1 - The country rock is initially at a constant temperature (T_0) and at a time, $t=0$, a magma of a definite thickness or diameter (D) extending indefinitely in the perpendicular direction is suddenly intruded into it, thus neglecting any possible pre-heating of the country rock prior to intrusion.

2 - The magma has a definite crystallizing point which for simplicity is taken as the liquidus temperature (T_m) and it is intruded at this temperature. The latent heat of fusion of the magma is taken as $L=100 \text{ calg}^{-1}$.

3 - The country rock has thermal conductivity (K_0), density (d_0), specific heat (c_{p0}), diffusivity (k_0) and the solidified magma has corresponding values K_1 , d_1 , c_{p1} and k_1 and are assumed to be independent of the temperature.

4 - The effects of transport of heat by volatiles and convection in the magma are not accounted for and cooling is assumed to be by conduction only.

3.3.2 Temperature at the contact

When a magma is intruded into country rocks, the temperature at the contact rises to a certain value (T_c) which is given by the equation, Jaeger (1959) :

$$T_c = \frac{\sigma T_m}{\sigma + \text{erf } \lambda} \quad 3.4$$

$$\text{where } \sigma = K_1 k_0^{1/2} / K_0 k_1^{1/2}$$

λ is the root of :

$$\lambda(\sigma + \text{erf } \lambda)e^{\lambda^2} = C_{p1} T_m / L \Pi^{1/2}$$

$$\text{erf } \lambda = 2 / \int_0^\lambda e^{-\zeta^2} d\zeta$$

The Cashel Hill envelope is described in Chapter 4 and consists dominantly of semi-pelites and pelites with some psammites and striped amphibolites. Because no physical constants are available for these rocks, the temperatures at the contact and at different points from it will be estimated from the available data for quartzites and shales and then the average temperature will be roughly estimated by mixing different proportions of these two components.

Two values of T_m are considered, 1200°C and 1000°C as these are likely to represent the liquidus temperature of the basic magma. The contact temperatures (T_c) are given below and were calculated using the following constants given in c.g.s and calorie, Jaeger (1959) [(Gabbro, $K_1=0.0043$, $c_{p1} = 0.25$, $k_1 = 0.008$); (Shales, $K_0 = 0.0019$, $k_0 = 0.004$), (quartzites $K_0 = 0.0128$, $k_0 = 0.031$)] and assuming the initial temperature of the country rock, $T_0 = 0$. The value of 500°C which probably represents the true T_0 , Yardley *et al.* (1987) is added to T_c .

T_m	T_0	<u>Shales</u>	<u>Quartzite</u>
		T_c	T_c
1200°C	0°C	890°C	595°C
	500°C	1390 °C	1095°C
1000°C	0°C	751°C	515°C
	500°C	1251°C	1015°C

If the assumption that 50% pure quartzites and 50% pure shales are mixed to produce the semi pelites, pelites and psammites present in the area then the temperature at the contact would be half that calculated for pure quartzites and shales, thus at T_m values of 1200° and 1000°C the temperatures at the contact are 1242° and 1133°C respectively. These values are higher than T_m itself which is extremely unlikely. There are many factors which can cause such a trend: the country rocks were initially at low temperature ($\approx 100^\circ\text{C}$); the influence of volatiles on heat transfer; the rate of crystallization of the magma; the water content of the country rocks and the magma. The assumption that the country rocks were initially at 100°C yields $T_c = 990^\circ\text{C}$ which falls within the range of temperatures derived from the

mineralogical model (Table 3.2). However, this assumption is unlikely because the geochronological order of the various formations in Connemara is well established, Leake *et al.* (1981), and the rocks were probably at about 500°C when the magma was intruded, Yardley *et al.* (1987).

The non-applicability of Jaeger's model to the Cashel aureole probably arises from the effects of volatiles on heat transfer. Leake (1970, p121) noted that the crystallization of spinel, forsterite-rich olivine and enstatite-rich orthopyroxene followed by basic bytownite or anorthite in the Connemara basic and ultrabasic intrusions deviate from the more usual gabbro assemblage of augite and labradorite and this was attributed to high water vapour pressure of about 5kb thus suggesting that the heat was not transferred by conduction only and consequently invalidating Jaeger's model. Moreover, the country rocks near the intrusion suffered significant dehydration and partial melting (Leake and Skirrow 1960, Evans 1964, present work) and it seems that the effects of the outgoing mobilized material (including any fluids) from the partially melted metasediments work against the effects of the latent heat and volatiles of the crystallizing magma. In the calculations given below, it has been assumed that these effects are equal and hence cancel each other. For semi-infinite country rock and intrusion in contact with each other, the temperature at the contact is given by :

$$\frac{T_c - T_m}{T_o - T_m} = \frac{b_o}{b_o + b_1} \quad 3.5$$

where $b_o = K_o/k_o$

$b_1 = K_1/k_1$

Thus

	<u>shales</u>	<u>quartzites</u>	
T_m	T_o	T_c	T_c
1200°C	500°C	930°C	778°C
1000°C	500°C	808°C	669°C

By mixing 60% shales and 40% quartzites, T_c becomes 870°C and 764 °C at T_m values of 1200°C and 1000°C respectively. The T_c value of 870°C agrees excellently with temperatures derived from garnet-biotite

thermometry using the calibration of Thompson (1976), Table 3.2.

3.3.3 Temperatures at different distances from the contact

The maximum temperature (T_x) reached at any point (x) in the envelope is a function of T_c , size of intrusion, thermal properties of the rocks and time (t) and it can be obtained by:

$$\frac{T_x}{T^*} = \text{erf } c \frac{X_i}{2(k_0 t)^{1/2}} \quad 3.6$$

$$\text{where } T^* = T_c - T_0$$

t = Time after intrusion

However, because the temperature at the contact also changes with time, new T_c should be calculated at any specific time by using the equation for calculating the depth of penetration (D'); (i.e. the distance from the surface of the intrusion where the temperature change is 1% change of surface temperature change). D' is given by :

$$D' = 4 (k_1 t)^{1/2} \quad 3.7$$

hence for the Cashel hill intrusion where $D = 1800\text{m}$ (i.e. $D' = 900\text{m}$) the time t is equal to 1585 years. Therefore, if $T_m = 1200^\circ\text{C}$ then the temperature at the surface of the intrusion will change by 12°C every 1585 years and consequently new T_c is generated within this time. The evolution of T_c and T_x in time and space for times from 0 to 50,000 years and distances up to 1000m from the contact are plotted in Figure 3.8 for pure shales ($T_c=930^\circ\text{C}$; $T_m=1200^\circ\text{C}$). The evolution of four points (100m, 200m, 400m, 600m) in the country rocks with time up to 20,000 years is shown in Figure 3.9. There are two important facts which are relevant to the present work. First, at a distance of 200m from the contact, the minimum temperature should be about 790°C and therefore the values 690°C , 695°C , 735°C obtained from the samples Y23, Y65 and Y70 respectively and which

occur within this distance are too low and indicate different re-equilibration during cooling. Second, if the assumption that the heat within the aureole was derived from the Cashel Hill intrusion only then at any distance greater than 430m from the contact, the temperature must be less than 700°C (Figure 3.8). This contradicts the average of $759 \pm 32^\circ\text{C}$ derived from garnet-biotite geothermometry for rocks occurring at greater distance than 430m. The only tenable explanation is that the country rocks are underlain by sheets of basic rocks occurring at different depths and which generated some heat to raise the country rock temperature to about 750°C. This is consistent with the fact that minor basic bodies have been mapped north of the main Cashel Hill intrusion.

3.4 Discussion

In the vicinity of the Cashel Hill intrusion, the thermal effects of the basic and ultrabasic magma completely overprint the regional metamorphism but the temperatures fall off abruptly to below 750°C in less than 200m from the contact, thus indicating a steep thermal gradient. However this sharp drop of the temperature in a short distance as confirmed by the physical model must have partly resulted from down temperature re-equilibration during cooling and consequently the steep thermal gradient is only apparent.

Bohlen and Essen (1980) questioned the validity of using the garnet-biotite thermometer in high grade pelitic rocks and whether it records small temperature changes ($\sim 50^\circ\text{C}$). However, the fact that the highest temperatures are always recorded adjacent to the ultrabasic rocks, the very good agreement between the mineralogical and physical model for the contact temperatures, the predictability of their decrease northward especially in the unhornfelsed rocks and the narrow difference between temperatures obtained using garnet-cordierite and garnet-biotite geothermometers (one sample only) all increase the degree of confidence in the presented results; although some low temperature re-equilibration has probably modified some of the results.

The effects of increased substitution of Ti and Al^{+6} in biotite and Mn and Ca in garnet on the $K_D^{\text{gt-bio}}_{\text{Fe-Mg}}$ have been discussed and only Mn and Ca in garnets and Ti in biotites affect the K_D . The correction for Mn and Ca

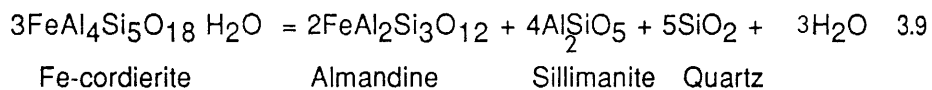
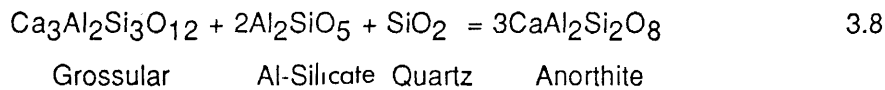
substitutions in garnets as suggested by Hodges and Spear (1982) has been applied to all samples and proved to give only negligible differences relative to the uncorrected calibration of Ferry and Spear (1978). The reason for this is probably because at higher metamorphic grades the garnet compositions tend to become more uniform and therefore the assumption of ideal or non ideal mixing in garnets does not change the results significantly although the inaccuracy of the Margules parameters can also be an alternative cause. At temperatures above 700°C, the correction of Indares and Martignole (1985) yields about 100°C lower than the temperatures derived from the original calibration of Ferry and Spear (1978) hence reflecting the strong effects of high Ti and Al concentrations in biotites on the temperature estimates. This big difference is expected especially as the $X_{\text{Ti+Al}+6}^{\text{bio}}$ is almost always higher than 0.15 which is the upper limit that Ferry and Spear (1978) suggested for the use of their calibration without corrections. Below 700°C, the case is reversed and the temperatures are higher using the corrected calibration than the original one and therefore this value is regarded as the temperature above and below which Ti and Al⁶ substitutions in biotite and Mn in garnets become significant and consequently define the upper and lower limits for the use of the corrections of Hodges and Spear (1982) and Indares and Martignole (1985) respectively. Whether the temperatures obtained using the latter correction are reliable cannot be tested but in view of the widespread partial melting of the rocks, many values are too low. In conclusion neither of the corrections discussed is satisfactory although that of Indares and Martignole (1985) is more promising if Margules parameters are better defined.

The equation suggested by Jaeger (1959), has been used to calculate the temperature at the contact but gave unacceptably high values which are higher than the liquidus temperature of the basic magma itself and this is attributed to the effects of volatiles on the conduction of heat from the magma into the surrounding country rocks. However, when assuming that the effects of volatile components and latent heat of the solidifying magma equal those of the fluid derived from the melting of the metasediments, the temperatures determined show excellent agreements with those derived from the calibration of Thompson (1976) using garnet-biotite geothermometry, hence suggesting

that dehydration and partial melting of the country rocks and volatiles of the magma have strong effects on the conduction of heat but they generally tend to work against each other. These effects must be encountered ^{for} prior to any application of the physical model to geological problems.

3.5 Geobarometry

Two pressure-sensitive mineral assemblages are common in the study area and have been used to quantify the pressures reached by the rocks within the aureole. The equilibrium relations are given below :



3.5. Garnet-aluminosilicate-quartz-plagioclase geobarometry

Based on early assumptions, such that of Miyashiro (1953), Sturt (1962), Kepezkinskas (1973), that the partitioning of Ca between garnet and plagioclase coexisting with quartz and aluminosilicate is pressure sensitive, Ghent (1976) published the first calibration of reaction 3.3. This early work was followed by others including Ghent *et al.* (1979), Newton and Haselton (1981) and Hodges and Spear (1982).

Ghent (1976) produced three calibrations depending upon which aluminosilicate phase is present in the rocks but they were subsequently criticized for treating both garnet and plagioclase as ideal solutions (*i.e.* the activity of grossular in garnet and anorthite in plagioclase are assumed equal to their mole fractions). Although Ghent *et al.* (1979) attempted to account for the activity-composition relationships in their calibration no significant improvements were made because these relationships were not well understood. However the work of Orville (1972) showed that the activities of the plagioclase components are larger than their mole fractions at 700°C and 2kb and consequently would result in an overestimate of the pressures if the effects of non-ideality are not accounted for. Ganguly and Kennedy (1974)

and Ganguly and Saxena (1984) proved that the activity of grossular at small concentrations can be significantly larger than its mole fractions hence underestimating the pressures if ideal mixing in garnets is assumed. More recently, Newton and Haselton (1981) published a calibration formulated from a number of investigations concerning the activity-composition relationships of garnet and plagioclase and using recent thermochemical data of Goldsmith (1980) of the end-members of reaction 3.8. Both the calibrations of Ghent (1976) and Newton and Haselton (1981) have been applied to ^{the} study aureole in an attempt to reveal the effects of the activity-composition relationships on the pressure estimates.

3.5.1.1 Results

12 samples have been used to quantify the pressure terms in the Cashel thermal aureole and the results are given in Table 3.4. All the pressures were calculated from the mean garnet and plagioclase core analyses except in two samples, Y13 and Y20, in which the core and rim analyses were used separately. Table 3.4 shows that the calibration of Ghent (1976) constantly yields about 1.2kb higher than the calibration of Newton and Haselton (1981) thus reflecting the significance of the activity-composition relationships on the pressure estimates. However, despite these systematic differences between the two calibrations it is encouraging to note that all samples fall well within the sillimanite stability field for both Holdaway (1971) and Richardson *et al.* (1969) aluminosilicate phase diagrams, Figure 3.10. The calibration of Newton and Haselton (1981) only is considered further as it accounts for non ideality of Ca in both garnet and plagioclase. The \pm values shown in Table 3.4 for this calibration are computed from the maximum and minimum temperatures obtained from the calibration of Thompson (1976) within individual samples.

The pressure varies from 3.7kb to 6.6kb, the highest values being always recorded about 50m from the contact thus apparently suggesting greater burial depths of the contact zone compared to the other zones. However, if this explanation is true then it is expected that on a P-T diagram, the contact samples and those occurring far away from the contact plot at two different angles with the slope of the calibration. Figure 3.11 shows that this is not the

case and all samples plot randomly and are parallel to each other and only form a small angle with the slope of the calibration indicating a strong pressure dependent on the temperature. Therefore the differences recorded are geologically insignificant and the low pressures obtained in the outer envelope are probably the result of down temperature re-equilibration during cooling. This interpretation does not exclude the possibility that the contact samples were metamorphosed at higher pressures but it indicates that the values obtained are doubtful although the presence of andalusite in some of the contact samples disfavours the high pressures recorded. Sample Y 55 plots distinct from the other samples by forming the largest angle ($\approx 37^\circ\text{C}$) with the slope of the calibration and hence the pressure of $4.05 \pm 0.02 \text{ kb}$ is geologically more significant.

In samples Y13 and Y20, the pressures obtained are always higher in the rims compared to the cores. In Y13 K-feldspar is present and the high pressure recorded from the rims is probably the result of cation exchange reactions on cooling between K-feldspar and plagioclase with Na preferentially retained in plagioclase. In Y20 K-feldspar is absent but the sample contains 23.7% muscovite and because this was probably formed from the breakdown of K-feldspar (Chapter 4) the explanation given for Y13 holds for Y20.

3.5.2 Garnet-cordierite-sillimanite-quartz geobarometry

Owing to extensive pinitization of cordierite, only one sample (Y17) was available for pressure calculations and therefore this geobarometer is not detailed. The calibrations of Thompson (1976), Holdaway and Lee (1977) and Wells and Richardson (1980) have been applied to this sample and the results obtained are in very good agreement with each other and fall within the field stability of sillimanite of both Holdaway (1971) and Richardson *et al.* (1968) aluminosilicate phase diagrams (Figure 3.10). The pressures derived using this barometer are always lower than those calculated from the garnet-plagioclase barometer (Table 3.4) but since only one sample has been analysed, it is not clear whether this trend is systematically maintained or not.

3.5.3 Discussion

The pressures derived from the calibration of Newton and Haselton (1981) average 4.8 ± 1.1 kb which is likely to represent the peak metamorphic pressures. However, in the sample Y17, a difference of about 1.6 kb is recorded between garnet-plagioclase and garnet-cordierite barometers thus indicating considerable differences between different geobarometers.

3.6 General conclusions

The rocks occurring in the immediate contact with the basic rocks have probably experienced temperatures in excess of 850°C and pressures of about 4.8 ± 1.1 kb.

The thermal gradient at different distances from the contact is difficult to define because of down temperature re-equilibration of minerals during cooling and the possibility that the whole envelope is underlain by a sheet of basic rocks or a series of minor basic bodies similar to those which outcrop north of Cashel Hill.

The empirical corrections of Hodges and Spear (1982) and Indares and Martignole (1985) for the garnet-biotite geothermometer are valid only for the range of temperatures for which they are formulated. The application of these corrections to the Cashel thermal aureole where significant elemental substitutions have taken place suggests that 700°C is probably the limit below and above which the two calibrations are to be used respectively.

The calibration of Thompson (1976) for garnet-biotite geothermometry agrees well with temperatures derived from the physical model and therefore is suggested for use at high grades without any corrections.

The combination of the mineralogical and physical models to study the evolution of thermal aureoles is more informative and preferred than one model but the effects of volatile transport on the heat transfer pattern are difficult to quantify but were probably significant.

Table 3.1 Mole fractions of Fe, Mg, Mn, Ca, Ti and Al⁺⁶ in garnet, biotite and cordierite.

Sample number	<u>Garnet</u>				<u>Biotite</u>			
	X _{Fe}	X _{Mg}	X _{Mn}	X _{Ca}	X _{Fe}	X _{Mg}	X _{Ti}	X _{Al+6}
Y4	0.793	0.130	0.050	0.025	0.507	0.273	0.078	0.142
Y5'	0.739	0.115	0.111	0.033	0.495	0.290	0.075	0.140
Y9	0.690	0.144	0.136	0.027	0.498	0.317	0.065	0.118
Y10	0.764	0.136	0.073	0.025	0.482	0.318	0.087	0.112
Y13	0.715	0.512	0.090	0.037	0.434	0.338	0.068	0.158
Y16	0.739	0.196	0.029	0.033	0.507	0.298	0.065	0.130
Y17	0.650	0.287	0.018	0.044	0.379	0.500	0.057	0.063
Y19	0.734	0.200	0.029	0.036	0.468	0.324	0.068	0.138
Y20	0.757	0.194	0.015	0.032	0.482	0.319	0.056	0.141
Y23	0.773	0.143	0.040	0.043	0.447	0.359	0.065	0.128
Y42	0.719	0.158	0.080	0.041	0.449	0.389	0.061	0.099
Y49	0.757	0.153	0.060	0.028	0.499	0.315	0.072	0.160
Y50	0.760	0.166	0.034	0.038	0.490	0.323	0.048	0.137
Y53	0.775	0.143	0.043	0.036	0.480	0.329	0.050	0.139
Y55	0.747	0.180	0.047	0.023	0.467	0.330	0.078	0.124
Y65	0.782	0.122	0.051	0.043	0.473	0.296	0.090	0.140
Y70	0.702	0.165	0.091	0.040	0.429	0.360	0.083	0.125
Y72	0.804	0.158	0.012	0.024	0.481	0.289	0.093	0.135
Y79	0.783	0.148	0.043	0.025	0.512	0.294	0.055	0.137

Cordierite

(Y17)

X_{Fe} X_{Mg}
0.280 0.768

formulae used to calculate the mole fractions of phase components (number of ions were used) are given below:

Table 3.1 Continued

Garnet

$$X_{Fe} = Fe / (Fe + Mg + Mn + Ca)$$

$$X_{Mg} = Mg / (Fe + Mg + Mn + Ca)$$

$$X_{Mn} = Mn / (Fe + Mg + Mn + Ca)$$

$$X_{Ca} = Ca / (Fe + Mg + Mn + Ca)$$

$$X_{Mn+Ca} = (Mn+Ca) / (Fe+Mg+Mn+Ca)$$

Biotite

$$X_{Fe} = Fe / (Fe + Mg + Ti + Al^{+6})$$

$$X_{Mg} = Mg / (Fe + Mg + Ti + Al^{+6})$$

$$X_{Ti} = Ti / (Fe + Mg + Ti + Al^{+6})$$

$$X_{Al^{+6}} = Al^{+6} / (Fe + Mg + Ti + Al^{+6})$$

$$X_{Ti+Al^{+6}} = (Ti+Al^{+6}) / (Fe+Mg+Ti+Al^{+6})$$

	0.100	0.200	0.300	0.400	0.500	0.600	0.700
0.100	0.100	0.196	0.288	0.375	0.457	0.534	0.606
0.200	0.196	0.200	0.292	0.375	0.450	0.521	0.588
0.300	0.288	0.292	0.300	0.375	0.440	0.505	0.564
0.400	0.375	0.375	0.375	0.375	0.425	0.475	0.525
0.500	0.457	0.450	0.440	0.425	0.425	0.450	0.475
0.600	0.534	0.521	0.505	0.475	0.450	0.450	0.450
0.700	0.606	0.588	0.564	0.525	0.475	0.425	0.375

(garnet cordierite geothermometer) 782
 (1976)
 and Lee (1977)
 and Spear (1978)

Table 3.2 X_{Mn+Ca}^{gt} , $X_{Ti+Al+6}^{bio}$, K_D values and the temperature estimates in °C obtained using garnet-biotite geothermometers (uncorrected form).

Sample number	X_{Mn+Ca}^{gt}	$X_{Ti+Al+6}^{bio}$	Range of K_D	Average K_D	Average T(°C)	H&L	F&S
Y4	0.075	0.220	3.45-3.17	3.284	766±16	724	811
Y5'	0.145	0.216	1 gt only	3.764	717 ---	682	741
Y9	0.165	0.184	3.12-2.86	3.050	794±16	747	853
Y10	0.099	0.199	3.95-3.60	3.706	722±17	687	748
Y13	0.127	0.226	3.99-3.58	3.663	726±18	690	754
Y16	0.063	0.196	2.34-2.04	2.216	940±35	865	1081
Y17	0.062	0.121	3.11-2.87	2.987	803±18	757	865
Y19	0.065	0.207	2.97-2.11	2.540	873±80	811	973
Y20	0.048	0.198	2.76-2.46	2.582	866±26	805	962
Y23	0.083	0.194	4.44-4.24	3.341	670±7	643	676
Y42	0.123	0.161	4.40-3.42	3.942	701±42	669	719
Y49	0.089	0.187	3.35-2.68	3.123	785±45	740	839
Y50	0.072	0.187	3.26-2.87	3.018	799±25	751	859
Y53	0.080	0.190	3.83-3.43	3.715	721±19	686	747
Y55	0.071	0.202	3.08-2.78	2.932	810±16	760	877
Y65	0.095	0.231	4.15-3.77	4.011	695±16	664	711
Y70	0.132	0.209	4.01-3.58	3.570	735±30	698	767
Y72	0.037	0.228	3.36-2.81	3.050	794±35	747	853
Y79	0.068	0.193	3.47-2.71	3.030	797±49	749	857
Y17 (garnet-cordierite geothermometer)					782	- - -	746

T = Thompson (1976)

H&L = Holdaway and Lee (1977)

F&S = Ferry and Spear (1978)

Table 3.3 Temperatures in °C obtained using the corrections of Hodges and Spear (1982, equation 9) and Indares and Martignole (1985, equations 18 and 19).

Sample number	T		F&S		I&M (19)		I&M (18)	
	Hodges and Spear							
Y4	768	(+2)	812	(+1)	662	(-149)	672	(-139)
Y5'	719	(+2)	743	(+2)	657	(-84)	620	(-121)
Y9	796	(+2)	853	(0)	804	(-49)	735	(-118)
Y10	724	(+2)	750	(+2)	620	(-128)	607	(-141)
Y13	728	(+2)	756	(+2)	663	(-91)	642	(-112)
Y16	939	(-1)*	1076	(-5)*	921	(-160)	938	(-143)
Y17	804	(+1)	864	(-1)*	775	(-90)	775	(-90)
Y19	872	(-1)*	969	(-4)*	817	(-156)	837	(-136)
Y20	866	(-1)*	960	(-2)*	816	(-146)	848	(-114)
Y23	674	(+4)	681	(+5)	690	(+14)*	695	(+19)*
Y42	704	(+3)	722	(+3)	661	(-58)	631	(-88)
Y49	787	(+2)	840	(+1)	701	(-138)	706	(-133)
Y50	800	(+1)	859	(0)	764	(-95)	824	(-35)
Y53	723	(+2)	749	(+2)	661	(-86)	667	(-92)
Y55	811	(+1)	877	(0)	723	(-154)	730	(-147)
Y65	698	(+3)	714	(+2)	569	(-142)	575	(-136)
Y70	737	(+2)	769	(+2)	663	(-104)	635	(-132)
Y72	795	(+1)	853	(0)	641	(-212)	682	(-171)
Y79	798	(+1)	857	(0)	744	(-113)	753	(-104)

I&M = Indares and Martignole (1985)

F&S = Ferry and Spear (1978)

T = Thompson (1976)

} using equation 9 of Hodges and Spear (1982)

Table 3.4 The pressure estimates in bars derived from the calibration of Ghent (1976) and Newton and Haselton (1981).

Sample number	Plagioclase X_{Ca}	Garnet X_{Ca}	G	N&H
Y4	0.294	0.025	5500	4253±266
Y10	0.283	0.025	5058	3767±271
Y13	0.373	0.037	5648	4341±279
	rim 0.401		5317	4061±270
	core 0.334		6154	4815±292
Y16	0.410	0.033	7618	6693±495
Y17	0.436	0.044	6860	6243±267
Y19	0.430	0.036	6910	5980±116
Y20	rim 0.399	0.032	6589	5613±369
	core 0.188		10510	9185±478
Y49	0.302	0.028	6166	4978±700
Y53	0.396	0.036	5178	3891±284
Y55	0.322	0.023	5109	4050±223
Y72	0.315	0.024	5354	4227±509
Y79	0.265	0.025	6442	5589±789

N&H = Newton and Haselton (1981)

G = Ghent (1976)

Pressures derived from garnet-cordierite barometry for the sample Y17:

- Wells and Richardson (1981) = 4635 bars
- Holdaway and Lee (1977) = 4409 bars
- Thompson (1976) = 4369 bars

KEY TO FIGURES 3.1 - 11

Figure 3.1 Plot of $\ln K$ versus $10^4/T(^{\circ}K)$.

$$K = \frac{X_{Fe}^{gt} \cdot X_{Mg}^{bio}}{X_{Mg}^{gt} \cdot X_{Fe}^{bio}}$$

F & S = Ferry and Spear (1978)

H & L = Holdaway and Lee (1977)

T = Thompson (1976)

Figure 3.1A Geological sketch map of the Cashel area showing the temperatures in $^{\circ}C$ (derived using garnet-biotite geothermometers) and the metamorphic subdivisions.

Figures 3.2-4 Plots of $K_D^{Fe-Mg}_{gt-bio}$ versus X_{Ti}^{bio} , X_{Al+6}^{bio} and $X_{Ti+Al+6}^{bio}$ respectively.

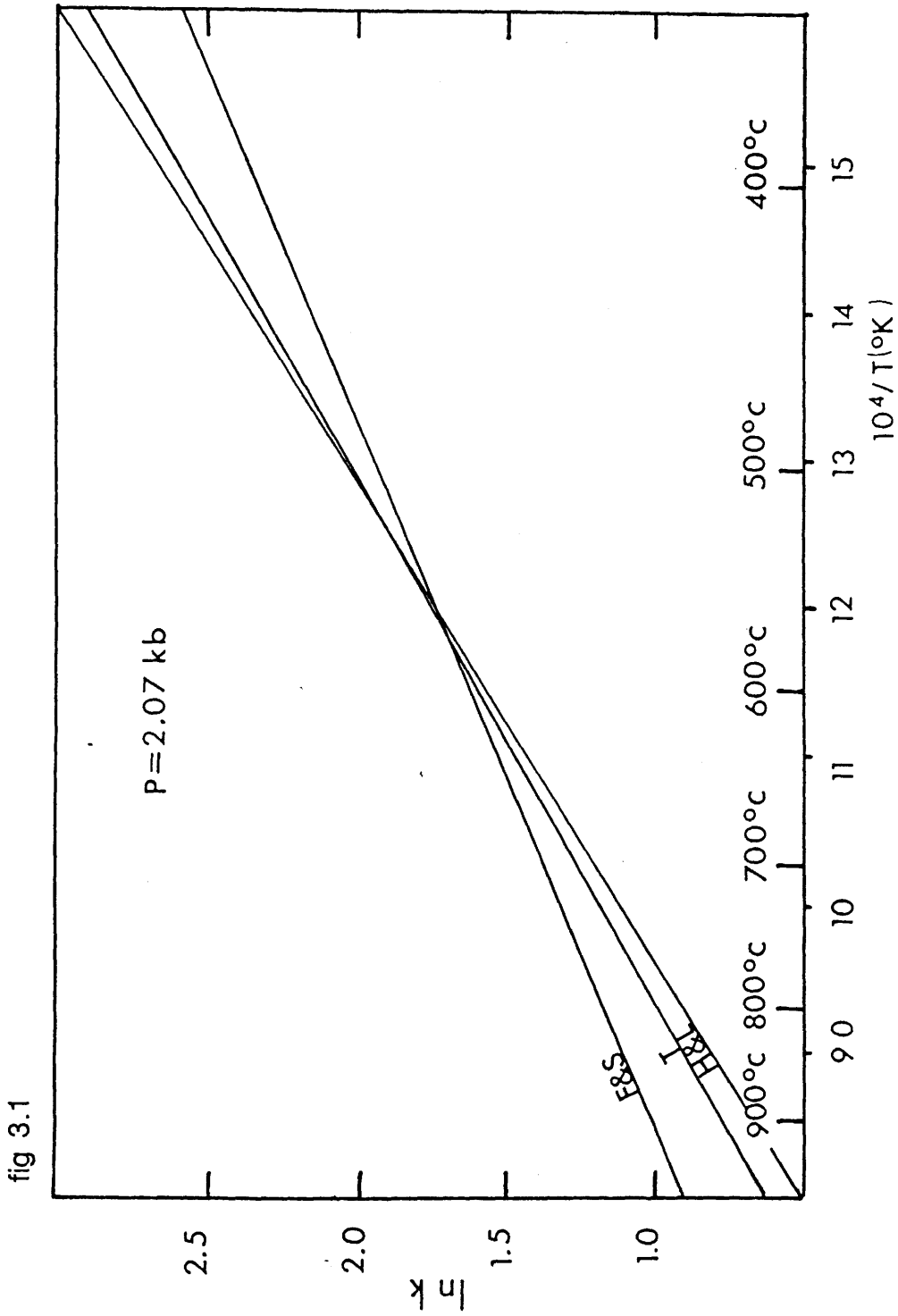
Figures 3.5-7 Plots of $K_D^{Fe-Mg}_{gt-bio}$ versus X_{Mn+Ca}^{gt} , X_{Ca}^{gt} and X_{Mn}^{gt} respectively.

Figure 3.8 Plot showing the evolution of temperatures in the Cashel-Lough Wheelaun aureole. A to F represent the time in years after intrusion.

Figure 3.9 Plot showing the evolution in time of T_c and 4 points in the envelope hornfelses (100m, 200m, 400m, and 600m).

Figure 3.10 Results of the Ghent (1976) and Newton and Haselton (1981) calibrations of the garnet-sillimanite-quartz-plagioclase geobarometer. The calibrations of Thompson (1976), Holdaway and Lee (1977) and Wells and Richardson (1980) of the garnet-cordierite-sillimanite-quartz calibrations for sample Y17 are also shown. H, aluminosilicate phase diagram of Holdaway (1971); R et al., aluminosilicate phase diagram of Richardson et al. (1969). Direction of arrows are pressures derived from cores to rims.

Figure 3.11 Plot of $P(K_b)$ versus $T^{\circ}C$. The slope of Newton and Haselton (1981) calibration is also shown. Continuous lines are hornfelses; discontinuous lines are regional pelites.



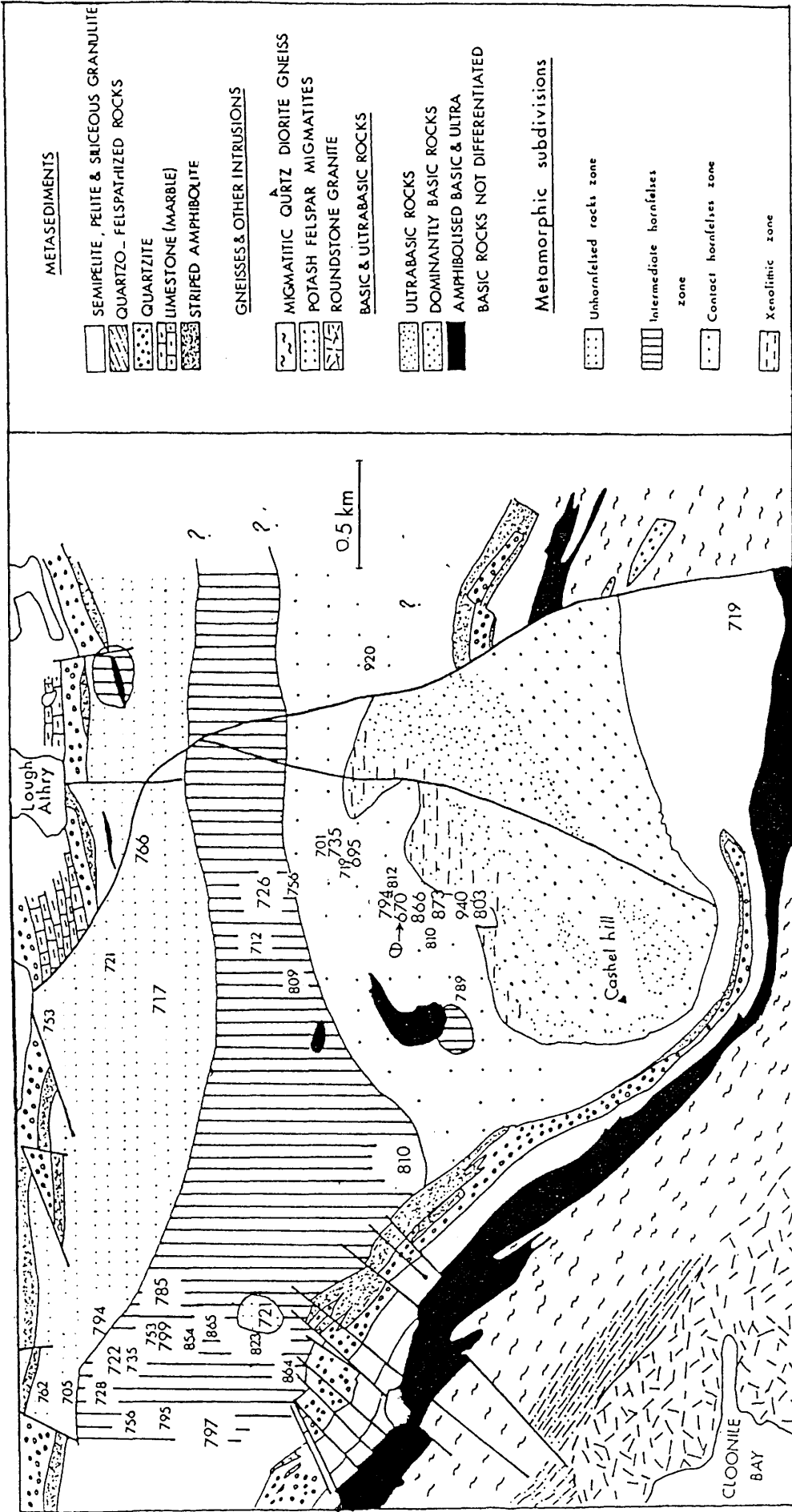


figure 3.1.A : geological sketch map of the Cashel area (after Leake,1970) showing temperatures in °C derived from garnet-biotite thermometry and the metamorphic subdivisions discussed in chapter 4. The small numbers are temperatures taken from Treloar (1985)

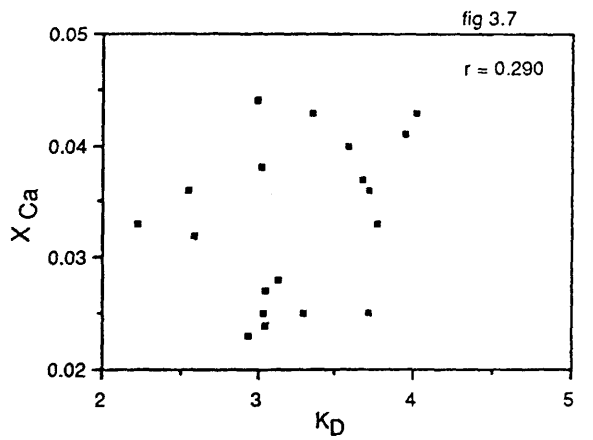
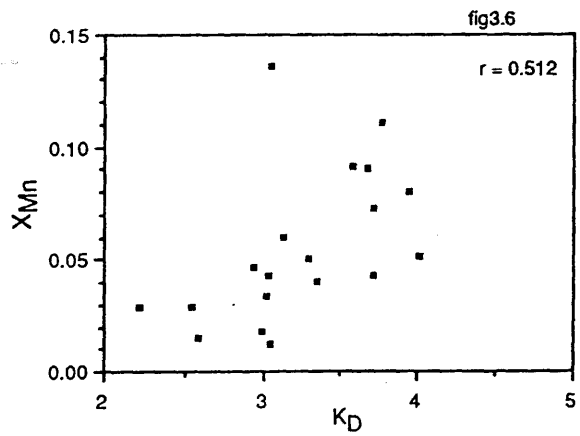
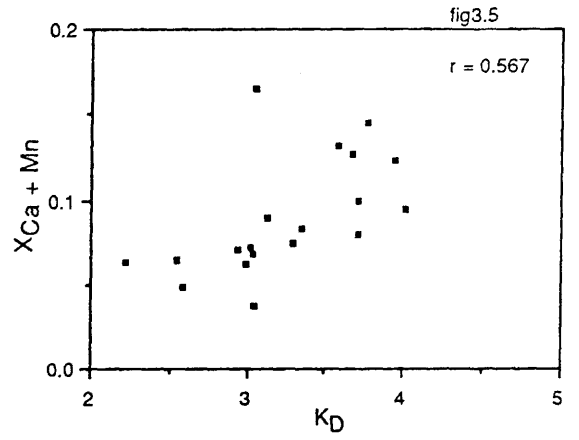
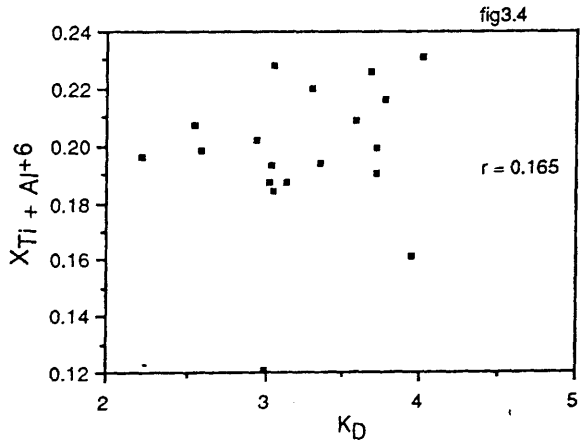
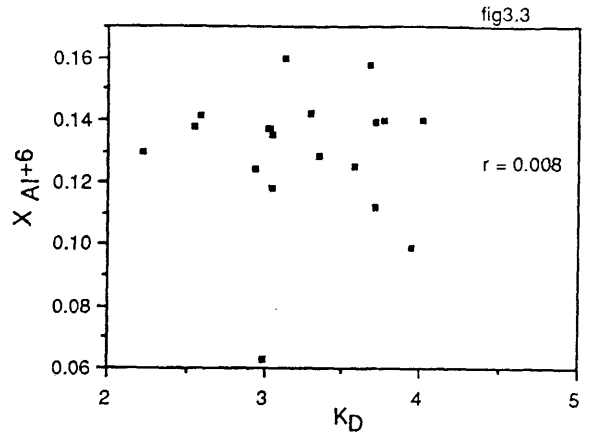
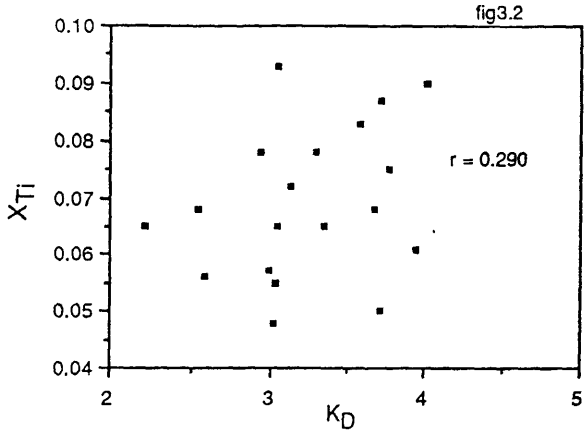


fig 3.8

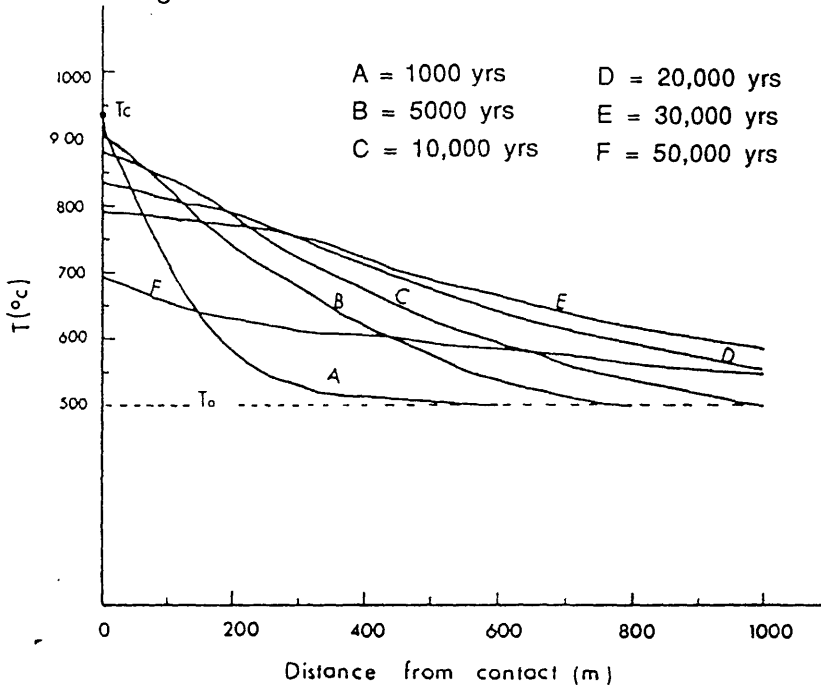


fig 3.9

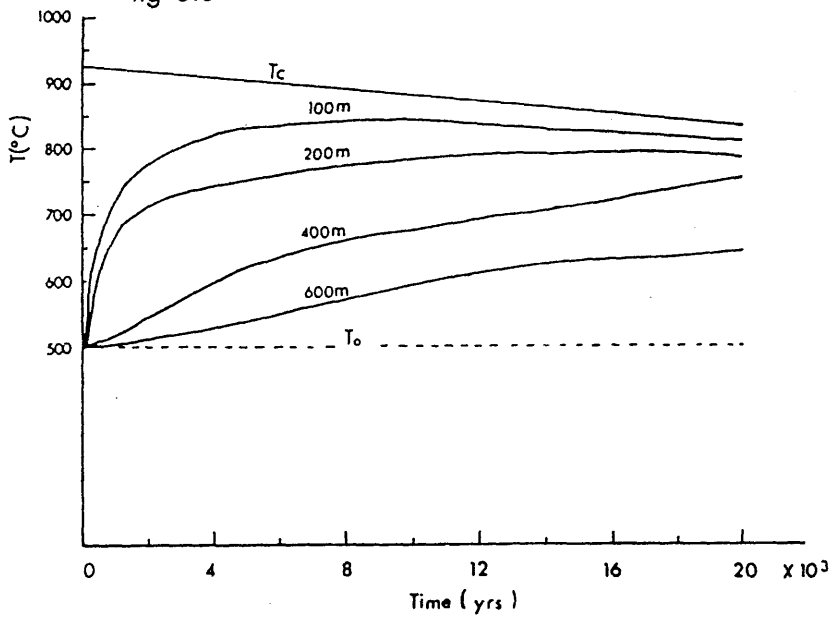


fig 3.10

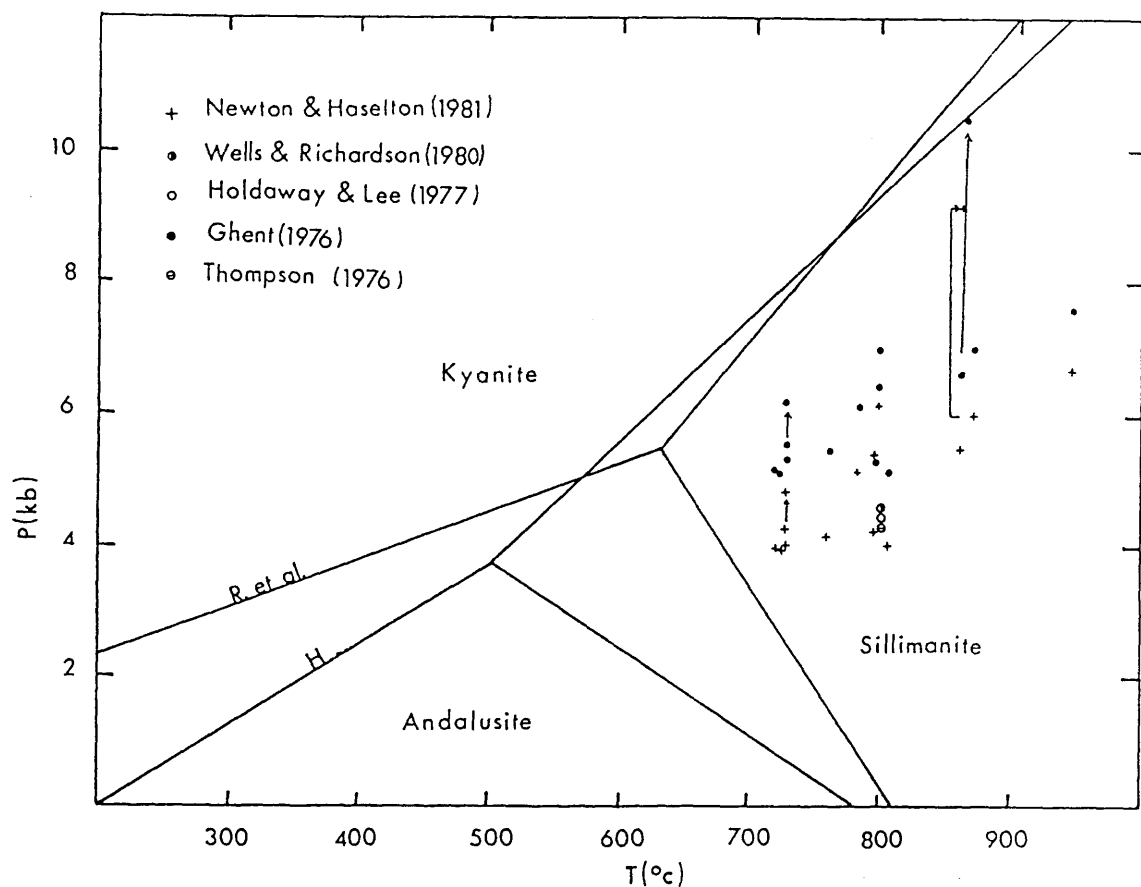
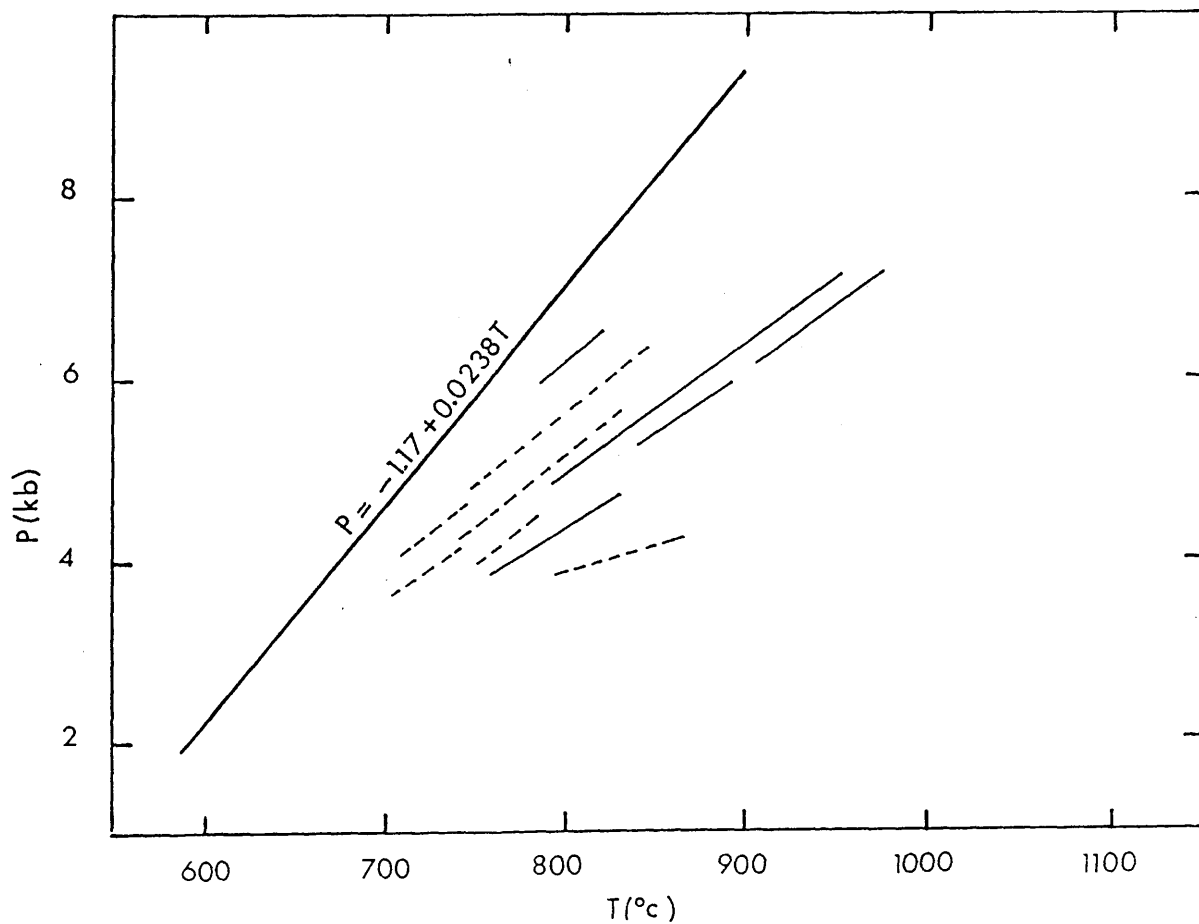


fig 3.11



CHAPTER FOUR : MINERALOGY

4.1 Field description of the Cashel-Lough Wheelaun thermal aureole

The envelope of the Cashel-Lough Wheelaun intrusion consists essentially of a thick series of pelites and semi-pelites with only subordinate psammites (siliceous granulites and quartzites), calc-silicate layers (marbles) and amphibolites. The quartz-rich semi-pelites and psammites, apart from a hardening of the rock and rare cordierite development, generally lack significant thermal metamorphic changes, (Leake and Skirrow 1960; present work). The calc-silicates and amphibolites occur only as sporadic layers embedded within the pelites and semi-pelites (Figure 4.1). Therefore, neither the quartz-rich semi-pelites and psammites nor the calc-silicate rocks and amphibolites are considered in the present study.

The thermal aureole extends up to 1300m from the contact and the northern side, adjacent to the ultrabasic side of the intrusion, shows the greatest degree of hornfelsing with the metasediments having been strongly mobilized. These mobilized hornfelses are characterized by their lack of schistosity, the existence of disoriented slabs of siliceous granulites and occasionally ultrabasic rocks. They are absent from the southern side of the intrusion probably because they were tectonically squeezed out between the extremely tight Cashel anticline and the Cashel-Lough Wheelaun intrusion during the southerly movement of the Cashel body, Leake (1970).

Although the rocks occurring in the close proximity of the intrusion, especially those within 50m, have been strongly hornfelsed, the most altered rocks occur as xenoliths. These, principally crowded within the ultrabasic masses, are composed of pelites, semi-pelites, quartzites and ultrabasic fragments. The pelitic xenoliths consist essentially of two types namely: strongly metasomatized pelitic discs typically 2 x 0.3cm and larger pelitic xenoliths frequently 12 x 5cm in size but up to at least 1.0 x 0.5m. Leake and Skirrow (1960) reported sheets of country rocks inside the intrusion up to a few hundred metres in length. Both types of xenoliths are rusty-coloured, most widespread along the margins of the intrusion and have similar mineralogical compositions except that the discs, believed to be strongly melted pelitic xenoliths (Leake and Skirrow 1960) contain much less biotite

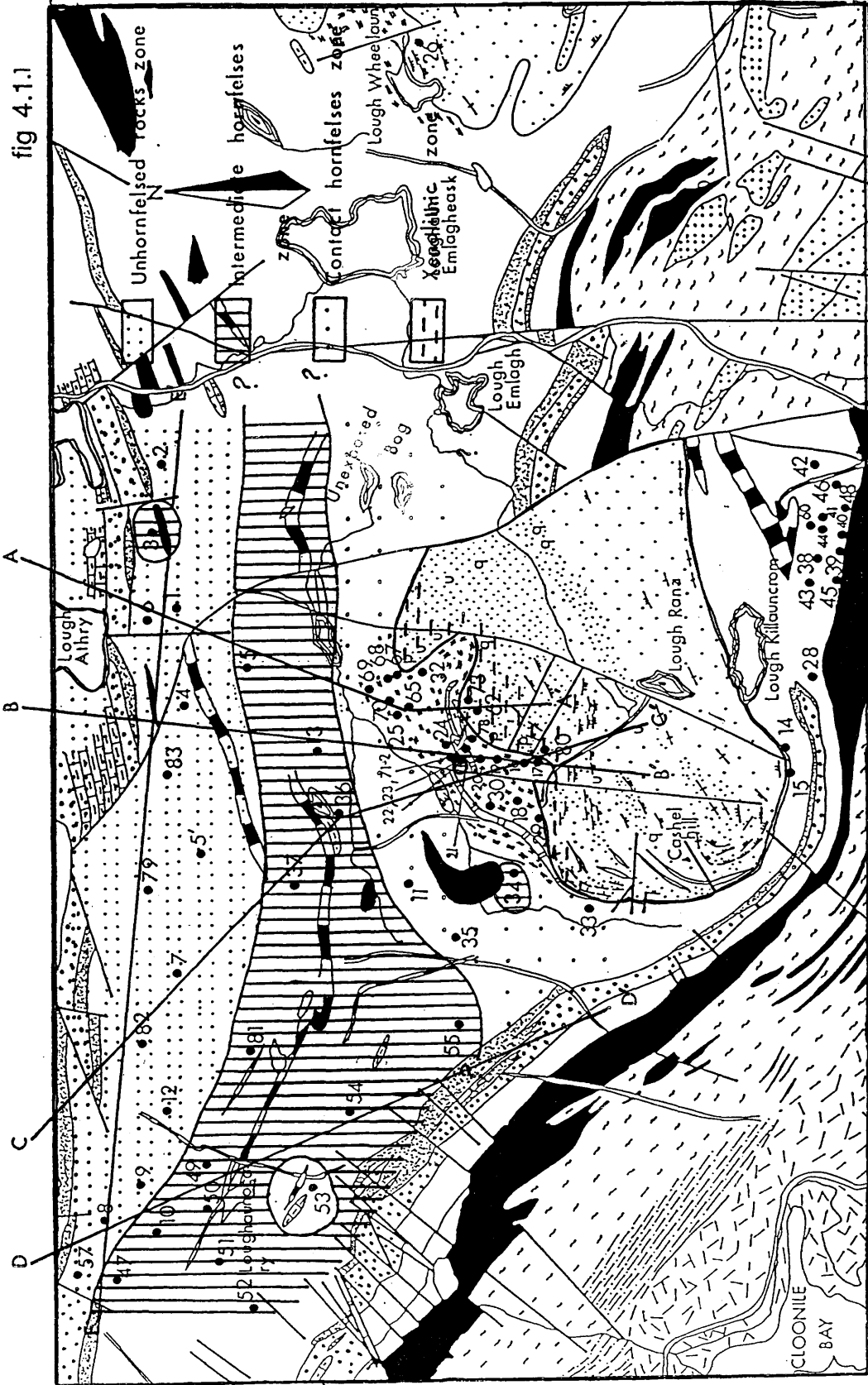


fig 4.1 : Geological sketch map of the Cashel district (after Leake, 1970) showing sample locations



fig 4.1 : Geological sketch map of the Cashel district (after Leake, 1970) showing sample locations

and cordierite and more magnetite, spinel and corundum than the sheets of the country rocks.

The largest xenoliths seen often show fritted boundaries with the ultrabasic hosts and sometimes preserve the original schistosity especially in the innermost parts whereas the original fabric is significantly overprinted in the pelitic discs and small xenoliths.

Read (1923, 1924, 1931, 1935, 1966) working on thermal aureoles in Aberdeenshire (Haddo House, Huntly, Arnage, Inch) all of which show very similar metamorphic conditions to the studied aureole, also noted that the largest xenoliths generally lack notable thermal changes compared to the small ones. This suggests that the thermal capacity of the larger xenoliths prevents the temperatures rising to a level necessary for substantial melting.

4.2 Mineralogy

4.2.1 Nomenclature

As a mineralogical and geochemical framework, the metasediments are classified into four groups namely : regional pelites, intermediate and contact hornfelses and xenoliths. The regional or unhornfelses rocks are defined as those rocks which have only been regionally metamorphosed and hence are free from hornfels minerals *viz.*: cordierite, prismatic sillimanite, spinel, corundum and orthopyroxene. The rocks which contain any of these minerals are termed hornfelses. Those containing less than 20% cordierite and lacking prismatic sillimanite, spinel, corundum and orthopyroxene are intermediate hornfelses while the contact hornfelses contain one or more of prismatic sillimanite, spinel, corundum and/or more than 20% cordierite. The fourth group is easily distinguished and consists of pelitic xenoliths which are essentially magnetite, spinel, corundum and orthopyroxene-bearing rocks.

4.2.2 Mineralogy of the unhornfelses pelites

The unhornfelses pelites are composed of about 42% biotite, 26% plagioclase, 18% quartz, 4% fibrolite, 2% garnet, 0.38% opaque and very rare orthoclase and tourmaline (Table 4.1). Apatite and zircon are invariably present as accessories but in some samples make up to 1.2 and 0.8 volume percent respectively. Secondary sericite, chlorite and muscovite are

ubiquitous minerals but prehnite and calcite are very rare. Biotite (0.40 x 0.10 mm average flake size) is often variably chloritized and sericitized. When fresh, it is usually brown and red-brown although some rare red and brown-blackish flakes are also occasionally present. Biotite is rich in zircon inclusions with large (average diameter 0.06 mm but up to 0.12 mm) pleochroic haloes. Apatite is sometimes included in biotite but the pleochroic haloes around it are much smaller and less conspicuous compared to those around zircon. This is probably because zircon always holds much larger concentrations of U and Th compared to apatite (Chapter 7) thus giving greater radiation damage.

Plagioclase (0.30mm average diameter) is generally partly sericitized, abundantly polysynthetic twinned with only rare Carlsbad-albite and pericline twinning, and apart from some rare sporadic zircon and apatite inclusions it is virtually inclusion-free. Plagioclase ranges in composition from An₂₇ to An₃₉ (three samples only) and the results obtained using microprobe analyses agree within $\pm 5\%$ with the determinations of plagioclase compositions using extinction angles (estimation made from three samples, four determinations in each case). Plagioclase is generally unzoned but some slight normal and reversed zoning occurs.

Quartz is also abundant (Table 4.1) and occurs as either euhedral to subhedral grains (0.25mm average diameter) and non-uniformly distributed throughout the rocks or else as large, up to 2mm, subhedral porphyroblasts which are either isolated or more frequently tend to form thin veins. This latter quartz is similar to that in the migmatite leucosomes occurring about 100-150m from the contact with the basic and ultrabasic intrusion and thus is believed to represent the mobilized and/or melted out silica affected by the migmatization processes, Leake *et al.* (1981), Barber (1985)

Fibrolitic sillimanite occurs as mats and felts, faserkeisel and sporadic single needles. The mats and felts and faserkeisel are by far the most abundant, most widespread and can reach up to 1.2mm and 2.3mm in thickness and diameter respectively. They are usually replacing biotite but also intergrowing with it, quartz and plagioclase. Small needles (0.01mm average length) are also widespread and occur in biotite, plagioclase and poikiloblastic garnet and unlike the mats and felts which are often parallel to the schistosity,

the small needles grow in all directions. Prismatic sillimanite was specifically searched for but not found, hence agreeing with Leake (pers. com.) that prismatic sillimanite is absent from rocks which have only been regionally metamorphosed.

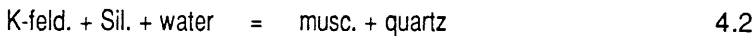
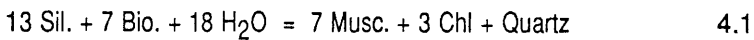
Garnet usually occurs as fresh isolated grains although some poikiloblasts show signs of chloritization and/or sericitization especially along the fractures and grain boundaries. Garnets average 2mm in diameter but reach up to 5cm and are strongly fractured and full of quartz, biotite, sillimanite and zircon inclusions. Rare small subhedral garnets are also recorded and are often unfractured and virtually inclusion-free.

Opaque minerals (0.11mm average diameter) consist of magnetite, ilmenite, pyrite and chalcopyrite. Magnetite and ilmenite are in close spatial association with biotite, garnet and occasionally sillimanite and often tend to replace biotite either by coating its boundaries or growing along its cleavages. In garnet, magnetite is more euhedral than in biotite and it is found as inclusions only. Pyrite and chalcopyrite are always spatially related to each other and occur as sporadic grains which are often less associated with the ferromagnesian minerals than with quartz and plagioclase.

K-feldspar is absent from most unhornfelsed pelites, a pattern confirmed by cobaltonitrite staining of the rock thin sections and microprobe analyses. However, in Y53 and Y83, both of which are unhornfelsed rocks, K-feldspar is present and it is often altered to muscovite and sericite. In both samples, K-feldspar is always either associated with the porphyroblastic quartzes or more often concentrated at the boundaries between the pelitic restites and the quartzo-feldspathic veins. This textural evidence suggests that K-feldspar was crystallized by partial melting of the pelites which are K-feldspar-free (Chapter 6). The veins were always avoided during the preparation of powders for chemical analyses, though some microscopic veins and/or isolated grains might have been included. Nevertheless, biotite, sericite and muscovite are the major K-bearing phases present in the rocks.

Sericite, chlorite, muscovite and prehnite are believed to be secondary minerals because their presence depends solely on the degree of alteration of the rocks and they are totally absent from fresh samples. Sericite is often present and it is usually replacing plagioclase, biotite, garnet and also

fibrolite. Chlorite is also ubiquitous and unlike prehnite which overgrows biotite only, chlorite replaces biotite, garnet and sillimanite. Muscovite occurs as large plates 2 x 0.90mm but averages 0.90 x 0.18mm. In all studied unhornfelsed rocks, it is always below 0.2% in amount except in 2 samples, Y53 and Y83, in which it reaches 22.4% and 24.8% respectively. Muscovite is usually intergrown with biotite and replaced K-feldspar where present thus suggesting the following reactions :



Generally the rocks occurring in the vicinity of the basic rocks contain more muscovite than the unhornfelsed rocks (except Y53 and Y83) which suggests that muscovite is a mineral formed by low temperature hydrothermal alterations.

Andalusite is recorded in three samples only (Y19, Y71 and Y42). The first two samples are strongly hornfelsed rocks and occur near the contact on the northern side of the Cashel Hill intrusion but Y42 comes from the southern side. Leake and Skirrow (1960, p30) recorded andalusite on the southern side only and concluded that lower temperature prevailed in the south compared to the north. This does not appear to be the case and the presence of andalusite in the north and south suggests that the temperature was the same on both sides and probably everywhere around the intrusion.

4.2.3 Mineralogical changes

The mineralogical changes caused by the heat derived from the intrusive magma are summarized by studying three N-S sections (AA', CC', FF') and compared with an E-W one (EE') through the unhornfelsed rocks (Figure 4.2). The mineralogical sections, all of which are shown on a cellophane sheet in Figure 4.1.1, were obtained using the modal percentages. Because of the relatively large number of rocks point counted, the number of counts per slide was limited to 500 with the results being presented in Appendix 2 and summarized in Table 4.1. The standard deviation for 500 counts at 95%

confidence is about $\pm 4.5\%$, $\pm 4\%$, $\pm 3\%$, $\pm 2\%$ for volume percentages of 50%, 28%, 12% and 5% respectively (Van Der Plas and Tobi 1965).

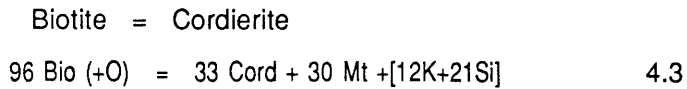
The effects of some small basic and ultrabasic masses, widespread throughout the study area, on the surrounding metasediments have not been taken into consideration but they are probably not very significant compared to the main basic and ultrabasic complexes.

In this section, the hornfels minerals are first described in order of appearance (*i.e.* increasing degree of hornfelsing) followed by a description of the changes suffered by the primary minerals. The changes in the mineral chemistry are established, then the field relationships are discussed, and finally some preliminary conclusions are attempted.

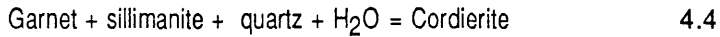
Figures 4.3-5 all show that cordierite is the first mineral to appear, followed as the contact is approached by prismatic sillimanite, spinel and corundum with orthopyroxene only in the most desilicated xenoliths. The appearance and increase of these minerals is accompanied by a pronounced rise in the magnetite content with quartz, biotite, garnet and to some extent sillimanite and possibly plagioclase gradually diminishing to their lowest values, or disappearing completely, in the pelitic xenoliths.

Cordierite is recorded first at a distance of 1300m from the contact of the intrusion. It appears as small to medium (0.7mm average diameter), irregularly-shaped grains, then increases rapidly in size, (up to 3cm but averages 2mm in diameter), and in abundance, (up to 80%), in the rocks occurring about 50-70m from the contact resulting in a coarse granoblastic texture. Cordierite has quartz, biotite, sillimanite and zircon inclusions and it is commonly completely altered to a fine-grained aggregate of pinitite and white micas. When fresh cordierite is present, it occasionally shows lamellar and/or sector twinning and is always confined to the cores of the extensively pinitized grains. These fresh cores are small and it was not possible for cordierite to be analysed for any possible zoning. The average of two core analyses from sample Y17 is given in Table 4.5 and both show that cordierite is Mg-rich, in agreement with the chemical analyses given by Evans and Leake (1970) and Trearor (1981). Despite the large grain size of the zircon inclusions in cordierite the pleochroic haloes around it are less developed and smaller in size than those around zircons in biotite. This is probably because

zircon in biotite holds larger amounts of U than zircon in cordierite (Chapter 7). Figures 4.3-5 reveal that the appearance and increase of cordierite is generally accompanied by an antipathetic decrease in the biotite content. Microscopically cordierite replaces biotite which suggests the following reaction (Leake and Skirrow 1960).

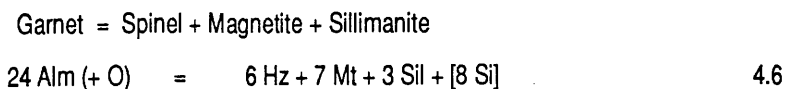
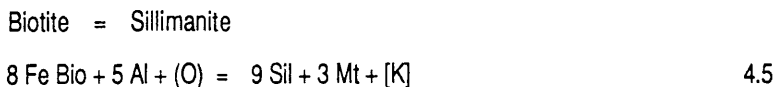


Sometimes, garnets are embayed by cordierite indicating that the latter has replaced the former according to the reaction :



Cordierite finally decreases in the most altered pelitic discs and xenoliths.

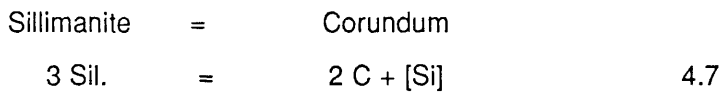
Prismatic sillimanite (1mm average length), recorded at a distance of 90-120m from the contact, is usually associated with fibrolite, biotite, cordierite and garnet. Those prisms occurring within the fibrolitic mats and felts are the most abundant of all and are usually parallel to the schistosity planes. Those in biotite are usually also parallel to the schistosity of the rocks but in garnet and cordierite they often form at an angle of about 15-20° (rarely 25-30°) with the schistosity planes. Prismatic sillimanite was probably formed in 3 ways namely : as recrystallized fibrolite, by replacing biotite and from the breakdown of garnet. The probable reactions are given below (Leake and Skirrow 1960) :



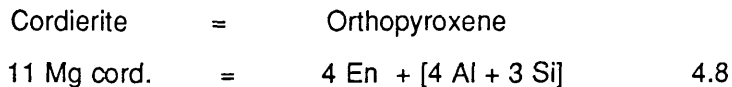
Spinel appears first as small (0.03mm average diameter) green droplets in garnet and occasionally in cordierite, often associated with magnetite. Since

its appearance, 80-100m from the contact, spinel remains low in grain size and abundance until in the xenoliths where it becomes remarkably coarser (0.6mm average diameter), more euhedral and can reach up to 6% (Figures 4.4-5). In fact, because spinel in the xenoliths is almost always magnetite coated and/or it is growing inside magnetite as numerous small grains, its modal percentage is probably underestimated while that of magnetite is overestimated. The spinel is a pleonaste (Table 5.6), but its composition tends towards hercynite. The Fe^{+2}/Mg ratio ranges from 1.05 to 0.741, hence indicating considerable substitution of Fe^{+2} for Mg. Trace elements Co and Cr are usually present but Ni has not been detected.

Corundum is recorded about a metre from the contact or in the xenoliths only. It occurs as euhedral crystals 0.23mm average grain size but sometimes it is as large as 0.6mm and it is usually associated with cordierite and magnetite. In Y17, a sample immediately adjoining the contact, corundum is fresher than in the xenoliths where it is often altered to diaspore. Corundum was possibly formed according to the following reaction :



Orthopyroxene (0.18mm average diameter) is restricted to the xenoliths only and occurs as euhedral crystals, mostly fresh and invariably set in cordierite. This indicates that orthopyroxene was probably formed from the breakdown of cordierite according to the reaction :



Magnetite occurs as euhedral to subhedral and elongated crystals in the unhornfelsed rocks. As the contact of the intrusion is approached, especially within about 60m from the contact, the magnetite coating of biotites increases noticeably and garnets sometimes become up to three quarters full of large (up to 0.80mm in diameter) magnetite. This observation, the above mentioned distance within which spinel appears (i.e. 80-100m) and the beginning of

garnet instability in the immediate contact followed by its disappearance in the xenoliths all suggest that magnetite and also spinel and prismatic sillimanite have grown from the breakdown of garnet following the reaction given above as 4.6

In the xenoliths, the magnetite content increases sharply reaching up to 38 times higher than in the unhornfelsed rocks. This dramatic increase in magnetite and also in spinel results in a radical change in the texture of the rocks. The perfectly schistose texture prominent in the regional pelites which had by the appearance and increase of cordierite subsequently become granoblastic and coarser in the contact samples, is overprinted by a curious "cellular" network in the xenoliths. The cellular network is the result of the partial replacement of cordierite by magnetite, spinel and occasionally corundum with the unreplaced parts being left as irregular "patches or islands". These were subsequently converted into pinite and sericite. Rare inclusions of rutile in magnetite have also been noted.

Biotite is reduced drastically in amount, from 42% in the average regional pelites, through 39% and 22% in the less hornfelsed and contact samples respectively, to 14% in the xenoliths (Table 4.1). This dramatic decrease in the biotite content is caused by its replacement by sillimanite, cordierite and garnet. Where biotite is unreplaced it has often been recrystallized into large, red biotite flakes although the regional flake shape and size are sometimes preserved even within a few metres from the contact. In the xenoliths relict biotite has been extensively replaced by large (0.80 x 0.55mm average size) poikiloblastic plates of strongly red biotite and the unrecrystallized relicts are very thin and mostly magnetite coated.

The colour of biotite generally changes, from red-brown in the unhornfelsed rocks through a much redder shade in the hornfelses occurring about 60-100m from the contact to deep red, pale or black-oak in the rocks occurring in the innermost aureole and in the xenoliths. These changes in the colour of biotite are common in thermal aureoles (Chapter 8) and have long been attributed to an increase in Ti and the Fe/Mg ratio (e.g. Tilley 1924 ; Leake and Skirrow 1960). However the results of microprobe analyses of 23 rock samples ranging from unhornfelsed rocks through to pelitic xenoliths within the intrusion show that the Fe/Mg ratio decreases as biotites become redder.

Because the Ti contents change within relatively large limits, red and red-brown biotites were analysed within the same rock samples (Y13 and Y72). The results were decisive in that red biotites always have higher Ti and X_{Mg} (ions $Mg/(Fe+Mg)$) than the red-brown ones.

With rising temperature, garnet increases noticeably in grain size, up to 5cm in diameter and in abundance, up to 37% but averages 7% only in the contact samples (Table 4.1). This increase in the garnet content is often accompanied by a rise in the biotite, magnetite and sillimanite inclusions but in contrast, quartz which is usually surrounding garnets or included inside them in the regional or less hornfelsed rocks generally diminishes. This quartz diminution is irregular and many poikiloblastic garnets, even those occurring about 20m from the ultrabasic masses are still rich in quartz inclusions. These rocks were not tectonically moved to their present place relatively late because they contain prismatic sillimanite and more than 20% cordierite. Therefore, the term "gradually" used by Leake and Skirrow (1960) to describe the way quartz inclusions in garnets diminish in the hornfelses is incorrect. Within 10m or so from the contact, garnets become unstable and they are replaced by cordierite, magnetite, prismatic sillimanite and spinel. In the most desilicated pelitic discs and xenoliths garnet is totally absent.

Quartz decreases as the contact is approached but the large porphyroblasts become abundant and form nubulitic patches and /or veins with albitic plagioclase and little K-feldspar. The detailed composition and possible origins of these migmatitic leucosomes are discussed in Chapter 6. Quartz is practically absent from the most altered pelitic xenoliths.

The effects of the heat on plagioclase are not clear because it is often badly altered to sericite.

4.2.4 Changes in the mineral chemistry

Microprobe analyses include 23 samples for biotite, 16 for garnet and 18 for plagioclase. The number of minerals analysed per slide and the number of spots per mineral were set to between 3 and 6 depending on the variability of the results, the changing of the mineral chemistry and the aim of the analyses. The analysed rocks include unhornfelsed pelites, intermediate and contact

hornfels and xenoliths.

Biotite analyses from four unhornfelsed rocks, eight intermediate hornfels, nine contact hornfels and three xenoliths are presented in Table 4.3 and summarized in Table 4.2 for direct comparison. To visualize the changes, two traverses, one towards the main Cashel Hill intrusion (BB') and the other towards the basic sheet running E-W to the west of the Cashel Hill (DD'), are presented in Figures 4.6-7. They were chosen because they have continuous distances (i.e. from 1380m from the contact to -10m).

Outside the aureole, biotites are always unzoned and have a Ti content below 4 wt%. The X_{Mg} (number of ions of Mg/(Mg+Fe)) values between samples are very small and do not vary noticeably from the average value of 0.367. In the hornfels biotites remain unzoned but the Mg content increases as the contact is approached reaching its highest value of 0.718 in the pelitic xenolith Y80 (Figure 4.7). This rise in Mg is accompanied by a parallel decrease in the Fe content hence giving higher X_{Mg} in the more hornfelsed rocks. Biotite inside garnet from Y72 gave higher X_{Mg} than the matrix biotites but another flake within the same garnet gave lower X_{Mg} suggesting different re-equilibration between garnet and biotite during cooling and hence the biotites included in the garnet were not considered in the T-P calculations. As would be expected, the Mg-richest biotite in the hornfels (the xenoliths are garnet free) occur in Y17, about a metre from the contact, with the Mg-richest garnet.

Garnets are always almandine-rich and the average garnet composition from four unhornfelsed rocks is Alm₇₅ Pyr₁₃ Spess₉ Gross₃ (Tables 4.2, 4.5). These values are significantly different from those published by Barber and Yardley (1985) of Alm₈₀ Pyr₁₅ Spess₂ Gross₃. Although almandine is always lower in the present analysed rocks than that reported by Barber and Yardley (1985) and grossularite is almost the same, the spessartine and pyrope contents vary quite considerably. Their values fall well between garnets from the intermediate and contact hornfels and therefore cannot be looked at as a typical Cashel formation garnet composition. Because the four samples analyzed in the present work are free from hornfels minerals, the garnet composition given above is likely to represent the typical garnet composition of the Cashel formation.

As expected, garnets underwent significant changes in the thermally affected rocks and these changes can be seen from Table 4.2 and Figures 4.8-9, being the same traverses as with the biotite (*i.e.* BB', DD'). Clearly the early and most significant changes are exhibited by Mg and Mn. Mg increases progressively as the contact is approached reaching its highest values within about 40m or so from the contact but Mn declines to its lowest values within the same distance. This is expected especially as the rocks occurring in the inner aureole suffered much higher temperatures than those in the outer envelope. Fe does not seem to have been significantly affected until about a metre from the contact where it drops to its lowest values thus giving the highest X_{Mg} of 0.306. Ca does not show any clear trend although a slight enrichment in Y17 can be noted (Figure 4.9). These changes are not always regular as can be seen from Table 4.2 where the almandine content remains unchanged and it decreases only by 2% in the innermost part of the aureole. In contrast, pyrope increases but spessartine decreases from 13% and 9% in the unhornfelsed rocks through 15% and 6% in the less hornfelsed pelites to 18% and 4% in the contact hornfelses respectively. The case of grossularite is less conspicuous but an increase, but only slightly, is recorded in the more thermally affected rocks.

Zoning in metamorphic garnets most commonly involves the major cations Fe, Mg, Mn and Ca which occupy the large eight coordinated sites within the garnet structure (Meagher, 1982). There are four main interpretative models which have been proposed to explain zoning in garnets :

1- Preferential fractionation and/or segregation of ions during growth of garnets ; Atherton (1968); Hollister (1966); Leake (1967).

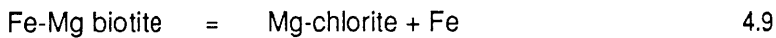
2- Volume and/or intergranular diffusion of ions ; Anderson and Buckley (1973); Loomis (1978, 1978a); Yardley (1977c).

3- Changing P-T conditions, Tracy *et al.* (1976).

4- Retrograde metamorphism, Grant and Weiblen (1971).

Garnets from the unhornfelsed and/or slightly hornfelsed rocks are essentially unzoned and only exhibit zoning in their outermost (100-150 μ) rims where the Mg content decreases, Mn increases but Fe and Ca remain unchanged (Figure 4.10). This non-bell-shaped zoning in garnets is common in high grade metamorphic terranes, (*e.g.* Grant and Weiblen 1971)

and it is probably the result of retrograde metamorphism. Although similar zoning is also recorded in Y42, about 50m from the contact, the most widespread type of zoning in the contact hornfelses is the Fe enrichment at the rims ($\approx 200\mu$) matched by a decrease in the Mg content but Mn and Ca remain essentially unchanged (Figure 4.1.1). The zoning of garnets in the contact hornfelses cannot be primary because under the high temperature prevailed near the contact (Chapter 3), higher Mg is expected near the intrusion whereas the opposite is found and consequently such zoning is believed to be of retrogressive origin. The reason for the regional rocks and contact hornfelses exhibiting different types of zoning is either because the four unhornfelled rocks studied are not representative or garnets have reacted retrogressively with cordierite resulting in Fe being retained in garnets and Mg transferred to cordierite. Treloor (1981, p183), working on the same pelites noted an increase in the X_{Mg} (ions $Mg/(Fe+Mg)$) at the rims^{of cordierite}, hence suggesting retrogressive rim reactions had taken place. Because the garnet rims are resorbed and sometimes converted to chlorite the following reactions are an alternative explanation :



In conclusion, zoning in garnets from the Cashel aureole is best explained by retrogressive metamorphism.

The plagioclase composition in four unhornfelled rocks, 12 hornfelses and three xenoliths (table 4.7) are summarized in table 4.2 and plotted on a An-Ab-Or diagram in Figure 4.12. The most significant changes in the plagioclase composition is the pronounced increase in the An content from An₂₈ in the regionally hornfelled pelites, through An₃₀ and An₃₆ in the intermediate and contact hornfelses respectively to An₇₄ in the xenoliths (figure 4.13). Plagioclase from the xenolith Y80 has an anorthite content of 87% (basic bytownite), which is of the same composition as the ultrabasic rocks. This indicates that an equilibrium between the magma and xenoliths was reached and, as predicted by Bowen (1928), some An-rich plagioclase crystallized in the xenoliths.

4.3 Field relationships

The classification of the rocks and mineralogical changes described in subsections 4.2.2-3 respectively were first established from the rock thin sections without any field considerations. Unexpectedly, when matched with the sample location map, four metamorphic subdivisions could be traced quite cleanly. These, obvious only on the northern side of the intrusion for reasons already stated, are shown in Figure 3.1a and plotted on a clear cellophane sheet in Figure 4.1.1 for comparison with garnet-biotite geothermometry and easy matching with the sampling map. Except for four samples, Y 3, Y23, Y34 and Y53, all samples falling in any zone obey the conditions given in subsection 4.2.1. Y3 does not follow the rule simply because it was collected near a basic sill (Figure 4.1).

The new metamorphic subdivisions are broad and true only within relatively large scale because there are great variations within the same zones. The spatial variations of quartz, plagioclase, biotite, garnet and cordierite are shown through tri-dimensional maps constructed by precisely recording the location of the samples using the X and Y coordinates and taking the "Z axis" as the modal analyses of minerals (Figures 4.14-21). Two viewing positions, one roughly from Lough Emlagh and the other from Loughaunocary were chosen for biotite, garnet and cordierite. Clearly all the maps presented show that the mineralogical changes described exhibit significant variations, although the general trends are excellently seen.

The variations can be attributed to tectonic and/or physical reasons. Based on field evidence, Leake and Skirrow (1960, p26) interpreted the mineralogical variations as the result of folding during and after the emplacement of the Cashel intrusion and concluded that much of the material adjoining the ultrabasic rocks has moved to its present position late in the intrusion's history. A complementary interpretation, also given by the same authors, is the presence of other small basic intrusions in the district and because their effects sometimes overlap with those of the main intrusion, such variations are thought to be likely. From field evidence and the results of Chapter 3, these interpretations are almost certainly true and explain most of the observed facts.

The physical reasons, considered here as a complementary, not an

alternative explanation, to the proposed interpretation, can be inferred from Chapter 3, subsection 3.3. First, if the country rocks are assumed to range from pure quartzite to pure shales, then considerable differences between their thermal conductivities and diffusivities exist (see Chapter 3, subsection 3.3). Clearly while most of the heat is badly diffused into the metasediments (*i.e.* absorbed by the pelites), the psammites and quartz-rich semi-pelites are much better conductors and diffuse the heat more easily into the surrounding rocks. Because these rocks are spatially irregular relative to each other, the conduction and diffusion of heat must have been irregular and consequently similar rocks could have experienced different amounts of heat and hence produce different proportions of hornfels minerals. Second, it has been shown in Chapter 3, subsection 3.3.3, that the country rocks are possibly underlain by basic sheets which generated some heat to raise the regional temperature to about 750°C. Consequently, varying depths of these basic sheets coupled with the spatial irregularities of rocks having significantly different thermal properties can cause such variations.

4.4 Summary and conclusions

The thermal aureole around the Cashel-Lough Wheelaun intrusion extends up to 1.3km in the surrounding metasediments. This large radius of the aureole, though it is primarily associated with the high heat derived from the basic and ultrabasic complex, is probably due to the presence of basic sheets below the metasediments and the relatively large heat conductivity and diffusivity of the psammites and quartz-rich semi-pelites.

The established mineralogical changes which agree closely with those of Leake and Skirrow (1960) show that cordierite appears at a distance of 1300m followed by prismatic sillimanite (90-120m), spinel (80-100m), corundum (\approx 1m) and orthopyroxene in the xenoliths only. The field variations of the mineralogical changes are attributed to two main factors :

1- Tectonic factors; deduced from field evidence and due to contemporaneous and late folding relative to the emplacement of the intrusion.

2- Physical factors; resulting from differences in the thermal properties of the country rocks, especially heat conductivities and diffusivities of the pelites, semi-pelites and psammites and the spatial irregularity of these rocks

relative to each other.

Secondary phenomena, such as sericitization, chloritization, saussurization, affected the individual mineral chemistries and sometimes completely overprinted the original shape of the minerals, making their identification uncertain. These secondary alterations had some bad effects on the modal analyses and will affect the overall chemistry of the rocks

The content of quartz is often obscured by the migmatization of the pelites and will probably obscure the behaviour of silica in the aureole.

Despite the above mentioned complications, four metamorphic subdivisions could be traced quite cleanly and only four samples out of a total of 64 disobey the given conditions.

100	2.15	32.17
100	2.37	
100	1.87	0.17
100	0	0.30
100	0.24	0
100	0.04	0.11
100	0.53	25.10
100	0.77	1.54
100	1.01	0.34
100		0.30

Table 4.1 Summary statistics of modal analyses of 64 rocks point counted. They are grouped into 4 groups according to the degree of hornfelsing.

	Unhornfelsed rocks (13 samples)		Intermediate hornfelses (17 samples)		Contact hornfelses (31 samples)		Xenoliths (3 samples)	
	Mean	S	Mean	S	Mean	S	Mean	S
	Quartz	18.63	8.23	16.12	7.59	9.45	6.82	T
Plagioclase	26.03	9.83	19.32	9.52	8.46	9.41	1.54	0.75
Biotite	42.31	7.75	39.91	11.01	22.30	12.09	14.6	6.89
Garnet	1.81	1.24	2.72	2.80	6.94	7.49	0	0
Sillimanite	4.11	4.24	2.51	3.36	4.50	9.40	T	-
Cordierite	0	0	6.82	6.18	30.94	18.81	9.87	1.63
Opaque	0.40	0.40	1.02	0.87	2.05	2.50	32.13	9.86
Spinel	0	0	0	0	T	-	2.87	2.36
Corundum	0	0	0	0	0.32	1.80	0.47	0.33
Orthopyroxene	0	0	0	0	0	0	0.200	0.16
Zircon*	0.20	0.24	0.17	0.22	0.15	0.24	0	0
Apatite*	0.36	0.39	0.24	0.49	0.04	0.11	0	0
Sericite	2.40	2.21	6.05	5.12	6.68	8.23	26.06	6.54
Chlorite	0.20	0.37	2.17	4.28	5.42	9.85	1.54	2.16
Muscovite	3.60	8.52	2.38	5.32	1.99	4.81	0.54	0.37
Tourmaline	0	-	0	-	0	-	9.56	11.01

T = trace

Table 4.2 Summary statistics of biotite, garnet and plagioclase analyses classified according to the degree of hornfelsing. Only the number of ions of interest are averaged. S = standard deviation.

Biotite analyses

	4 unhornfelsed rocks		8 intermediate hornfelses		9 contact hornfelses		3 xenoliths	
	Mean	S	Mean	S	Mean	S	Mean	S
Fe	2.790	0.07	2.647	0.15	2.528	0.23	1.664	0.21
Mg	1.620	0.07	1.855	0.10	2.038	0.44	3.432	0.22
Ti	0.395	0.05	0.393	0.06	0.391	0.08	0.372	0.03
XMg	0.367	0.01	0.410	0.03	0.443	0.07	0.673	0.04

Garnet analyses

	4 unhornfelsed rocks		6 intermediate hornfelses		8 contact hornfelses	
	Mean	S	Mean	S	Mean	S
Fe	4.583	0.277	4.612	0.107	4.501	0.289
Mg	0.820	0.076	0.952	0.087	1.134	0.281
Mn	0.521	0.240	0.353	0.119	0.250	0.171
Ca	0.169	0.020	0.201	0.044	0.227	0.038
XMg	0.152	0.015	0.171	0.014	0.200	0.046

Garnet end-members

Alm	75.21	75.38	73.64
Pyr	13.45	15.56	18.55
Spess	8.55	5.76	4.09
Gross	2.77	3.28	3.71

Plagioclase analyses

	4 unhornfelsed rocks		6 intermediate hornfelses		6 contact hornfelses		2 xenoliths	
	Mean	S	Mean	S	Mean	S	Mean	S
Ca	1.074	0.30	1.177	0.16	1.409	0.37	2.962	0.53
Na	2.679	0.24	2.625	0.11	2.413	0.31	1.022	0.48
K	0.030	0.01	0.052	0.01	0.026	0.02	0.001	0.01

Plagioclase end-members

An	28.36	30.53	36.65	74.21
Ab	70.74	68.11	62.75	25.60
Or	0.009	0.013	0.007	0.002

Table 4.3 continued

	Y80	
	Mean	S
Major elements (oxide wt%)		
SiO ₂	35.87	0.31
TiO ₂	3.15	0.18
Al ₂ O ₃	17.14	0.24
FeO	11.71	0.22
MgO	16.75	0.23
MnO	0.06	0.09
CaO	0.05	0.07
Na ₂ O	0.47	0.10
K ₂ O	8.85	0.21
Total	94.05	
Number of ions per formula unit computed on the basis of 22 oxygens		
Si	5.33	0.023
Al+4	2.67	0.023
Al+6	0.337	
Ti	0.354	0.021
Fe	1.458	0.028
Mg	3.716	0.048
Mn	-	-
Ca	-	-
Na	0.317	0.029
K	1.679	0.037
Total	15.681	
Ions	<u>Mg</u>	0.718
	Fe+Mg	

Table 4.4 Mean garnet analyses

	Y4		Y5'		Y9		Y10	
	Mean	S	Mean	S	Mean	S	Mean	S
Major elements (oxide wt%)								
SiO ₂	36.84	0.13	37.14	0.09	37.25	0.15	37.16	0.18
Al ₂ O ₃	20.86	0.22	21.03	0.17	20.99	0.05	21.26	0.02
FeO	36.11	0.23	33.88	0.53	31.511	0.47	35.16	0.35
MgO	3.34	0.05	2.95	0.30	3.79	0.19	3.53	0.15
MnO	2.28	0.10	5.06	0.74	6.207	0.24	3.33	0.22
CaO	0.90	0.04	1.16	0.06	0.977	0.00	0.92	0.09
Total	100.33		101.22		100.72		101.36	
Number of ions per formula unit computed on the basis of 24 oxygens								
Si	5.95	0.008	5.95	0.001	5.95	0.004	5.94	0.026
Al	3.97	0.026	3.97	0.278	3.89	0.120	4.00	0.004
Fe	4.864	0.032	4.54	0.075	4.157	0.120	4.694	0.051
Mg	0.800	0.014	0.706	0.072	0.870	0.049	0.840	0.035
Mn	0.310	0.014	0.687	0.100	0.824	0.040	0.450	0.032
Ca	0.154	0.009	0.203	0.013	0.167	0.004	0.157	0.012
Total	16.048		16.056		15.848		16.081	
Ions <u>Mg</u>	0.141		0.134		0.173		0.152	
Fe+Mg								
End-member proportions (mol%)								
Alm	79.37		73.98		69.07		76.43	
Pyr	13.05		11.50		14.45		13.67	
Spess	5.05		11.19		13.69		7.32	
Gross	2.51		3.30		2.77		2.55	
Total	99.98		99.97		99.98		99.97	

Table 4.4 continued

	Y13		Y16		Y17		Y19	
	Mean	S	Mean	S	Mean	S	Mean	S
Major elements (oxide wt%)								
SiO ₂	37.12	0.20	37.68	0.06	38.45	0.22	37.38	0.13
Al ₂ O ₃	21.24	0.06	21.33	0.09	21.60	0.09	21.05	0.20
FeO	32.732	0.35	34.45	0.20	30.67	0.43	34.26	0.09
MgO	3.93	0.13	5.15	0.21	7.62	0.07	4.92	0.10
MnO	4.11	0.34	1.38	0.06	0.88	0.27	1.43	0.09
CaO	1.34	0.03	1.22	0.05	1.65	0.08	1.35	0.18
Total	100.47		101.21		100.87		100.39	
Number of ions per formula unit computed on the basis of 24 oxygens								
Si	5.92	0.012	5.94	0.016	5.96	0.020	5.96	0.020
Al	3.98	0.012	3.96	0.018	3.94	0.004	3.94	0.028
Fe	4.407	0.016	4.547	0.032	3.980	0.065	4.560	0.021
Mg	0.937	0.028	1.210	0.053	1.757	0.012	1.244	0.082
Mn	0.554	0.049	0.184	0.009	0.114	0.033	0.180	0.008
Ca	0.227	0.004	0.204	0.009	0.270	0.014	0.227	0.030
Total	16.025		16.045		16.021		16.111	
Ions Mg	0.175		0.210		0.306		0.214	
Fe+Mg								
End-member proportions (mol %)								
Alm	71.95		73.99		65.02		73.41	
Pyr	15.29		19.69		28.70		20.02	
Spess	9.04		2.99		1.86		2.90	
Gross	3.70		3.31		4.41		3.65	
Total	99.98		99.98		99.99		99.98	

Table 4.4 continued

	Y20		Y23		Y42		Y49	
	Mean	S	Mean	S	Mean	S	Mean	S
Major elements (oxide wt%)								
SiO ₂	37.41	0.09	37.17	0.13	37.65	0.19	37.60	0.09
Al ₂ O ₃	21.25	0.01	21.28	0.20	21.28	0.05	21.17	0.11
FeO	34.86	0.10	35.55	0.26	33.65	0.14	34.95	0.09
MgO	5.03	0.16	3.70	0.05	4.17	0.33	4.01	0.33
MnO	0.75	0.09	1.80	0.08	3.74	0.32	2.78	0.35
CaO	1.21	0.10	1.59	0.02	1.55	0.02	1.06	0.02
Total	100.51		11.09		102.04		101.57	

Number of ions per formula unit computed on the basis of 24 oxygens

Si	5.93	0.008	5.92	0.020	5.93	0.047	5.95	0.009
Al	3.98	0.004	4.00	0.021	3.95	0.020	3.95	0.008
Fe	4.620	0.016	4.737	0.036	4.436	0.018	4.620	0.080
Mg	1.187	0.044	0.877	0.009	0.976	0.075	0.936	0.070
Mn	0.094	0.016	0.247	0.009	0.500	0.045	0.370	0.050
Ca	0.20	0.016	0.267	0.004	0.256	0.047	0.176	0.004
Total	16.011		16.048		16.048		16.002	

Ions <u>Mg</u>	0.205		0.156		0.180		0.168	
Fe+Mg								

End member proportions (mol%)

Alm	75.72		77.30		71.91		75.71	
Pyr	19.45		14.31		15.82		15.33	
Spess	1.54		4.03		8.10		6.06	
Gross	3.27		4.35		4.15		2.88	
Total	99.98		99.99		99.98		99.98	

Table 4.4 continued

	Y50		Y53		Y55		Y65	
	Mean	S	Mean	S	Mean	S	Mean	S
Major elements (oxide wt%)								
SiO ₂	37.41	0.13	37.31	0.07	37.52	0.07	37.29	0.18
Al ₂ O ₃	21.15	0.09	21.15	0.12	21.32	0.19	21.16	0.20
FeO	34.95	0.80	35.82	0.10	34.65	0.42	35.61	0.12
MgO	4.31	0.00	3.75	0.13	4.68	0.09	3.14	0.08
MnO	1.60	0.01	1.98	0.28	2.20	0.13	2.34	0.04
CaO	1.39	0.05	1.32	0.03	0.88	0.03	1.57	0.06
Total	100.81		101.33		101.25		101.11	
Number of ions per formula unit computed on the basis of 24 oxygens								
Si	5.95	0.021	5.93	0.012	5.94	0.016	5.95	0.032
Al	3.96	0.020	3.97	0.014	3.98	0.021	3.98	0.028
Fe	4.650	0.028	4.763	0.004	4.563	0.028	4.760	0.014
Mg	1.020	0.000	0.886	0.030	1.103	0.030	0.746	0.020
Mn	0.210	0.008	0.266	0.038	0.290	0.016	0.313	0.004
CaO	0.233	0.009	0.223	0.004	0.146	0.004	0.266	0.009
Total	16.023		16.038		16.022		16.015	
Ions <u>Mg</u>	0.179		0.157		0.195		0.135	
Fe+Mg								
End member proportions (mol%)								
Alm	76.09		77.47		74.77		78.22	
Pyr	16.68		14.41		18.07		12.25	
Spess	3.43		4.32		4.75		5.14	
Gross	3.80		3.62		2.39		4.37	
Total	100.0		99.82		99.98		99.98	

Table 4.4 continued

	Y70		Y72		Y79	
	Mean	S	Mean	S	Mean	S
Major elements (oxide wt%)						
SiO ₂	37.77	0.33	37.24	0.11	37.39	0.25
Al ₂ O ₃	21.26	0.19	21.08	0.07	21.05	0.11
FeO	33.36	0.31	37.06	0.32	36.27	1.20
MgO	4.17	0.23	4.08	0.14	3.80	0.32
MnO	4.11	0.23	0.59	0.11	1.98	0.25
CaO	1.45	0.04	0.86	0.11	0.91	0.04
Total	102.12		100.91		101.40	

Number of ions per formula unit computed on the basis of 24 oxygens

Si	5.94	0.009	5.94	0.004	5.95	0.008
Al	3.94	0.004	3.96	0.012	3.96	0.028
Fe	4.166	0.224	4.942	0.036	4.780	0.035
Mg	0.980	0.048	0.973	0.032	0.906	0.075
Mn	0.543	0.036	0.076	0.016	0.263	0.032
Ca	0.243	0.004	0.150	0.016	0.153	0.047
Total	15.812		16.042		16.012	

Ions Mg 0.190 0.164 0.159
 Fe+Mg

End member proportions (mol%)

Alm	70.22	80.47	78.33
Pyr	16.52	15.84	14.84
Spess	9.15	1.23	4.31
Gross	4.09	2.44	2.50
Total	99.98	99.98	99.98

Table 4.5 Cordierite analyses

	Y17
SiO ₂	48.15
Al ₂ O ₃	32.49
FeO	6.53
MgO	9.45
Total	96.62

Number of ions calculated on the basis of 18 oxygens

Si	4.99
Al	3.97
Fe	0.57
Mg	1.46

Number of ions $\frac{Mg}{Fe+Mg} = 0.719$

Table 4.6 Spinel analyses

	Y80(1 only)	Y80(1 only)	Y62(1 only)
SiO ₂	-	-	-
TiO ₂	-	-	-
Al ₂ O ₃	59.539	55.639	59.206
Fe _{tot}	27.963	33.776	29.765
MgO	12.602	12.950	10.447
MnO	0.323	0.17	0.328
Total	100.42	102.53	99.74

Number of ions per formula unit computed on the basis of 32 oxygens

Si	-	-	-	-
Ti	-	-	-	-
Al	14.957	13.89	15.993	15.156
Fe ⁺³	1.044	2.103		0.845
Fe ⁺²	3.939	3.881		4.559
Mg	4.002	4.088	7.999	3.380
Mn	0.058	0.030		0.060
<u>Mg</u>	1.016	1.054		0.741
Fe ⁺²				

16.001 } 16.001
 7.999 } 7.999

Table 4.7 Mean plagioclase analyses

	Y4		Y8		Y10		Y13	
	Mean	S	Mean	S	Mean	S	Mean	S
Major elements (wt%)								
SiO ₂	60.24	0.38	60.77	0.47	60.52	0.29	58.30	0.71
Al ₂ O ₃	23.98	0.15	24.04	0.10	24.08	0.21	25.62	0.42
FeO	-	-	-	-	0.02	0.05	-	-
CaO	5.77	0.17	5.70	0.13	5.63	0.12	7.49	0.58
Na ₂ O	7.52	0.15	7.36	0.10	7.64	0.16	6.76	0.30
K ₂ O	0.21	0.04	0.22	0.05	0.33	0.04	0.27	0.01
Total	97.72		98.09		98.22		98.44	
Number of ions per formula unit computed on the basis of 32 oxygens								
Si	10.92	0.036	10.95	0.020	10.91	0.043	10.56	0.106
Al	5.12	0.037	5.11	0.013	5.12	0.040	5.47	0.104
Fe	-	-	-	-	-	-	-	-
Ca	1.120	0.032	1.097	0.032	1.085	0.023	1.453	0.117
Na	2.640	0.052	2.575	0.015	2.670	0.051	2.373	0.103
K	0.05	0.010	0.047	0.013	0.074	0.010	0.063	0.004
End member proportions (mol%)								
An	29.40		29.50		28.33		37.36	
Ab	69.29		69.23		69.73		61.01	
Or	1.3		1.26		1.93		1.61	

Table 4.7 continued

	Y13		Y16		Y17		Y19		
	core	rim 1	rim 2	Mean	S	Mean	S	Mean	S
Major elements (wt%)									
SiO ₂	57.84	57.84	59.32	57.81	0.36	57.00	0.39	57.09	0.26
Al ₂ O ₃	25.98	26.26	25.02	25.80	0.40	29.09	0.45	26.14	0.08
FeO	-	-	-	0.05	0.05	0.14	0.10	0.06	0.06
CaO	8.02	7.86	6.68	8.13	0.32	8.65	0.39	8.45	0.14
Na ₂ O	6.44	6.08	7.18	6.28	0.23	6.09	0.17	6.04	0.14
K ₂ O	0.26	0.43	0.27	0.27	0.11	0.30	0.21	0.20	0.04
Total	98.54	98.47	98.47	98.34		98.27		97.98	
Number of ions per formula unit computed on the basis of 32 oxygens									
Si	10.48	10.48	10.71	10.46	0.064	10.39	0.082	10.4	0.017
Al	5.55	5.67	5.32	5.56	0.062	5.60	0.088	5.61	0.029
Fe						0.02	0.014	-	-
Ca	1.560	1.541	1.291	1.575	0.061	1.687	0.073	1.647	0.031
Na	2.260	2.160	2.510	2.200	0.078	2.154	0.062	2.132	0.049
K	0.061	0.100	0.060	0.060	0.023	0.024	0.012	0.045	0.008
End member proportions (mol%)									
An	40.19	40.54	33.43	41.07		43.64		43.07	
Ab	58.23	56.82	65.00	57.36		55.73		55.75	
Or	1.57	2.63	1.55	1.56		0.006		0.01	

Table 4.7 continued

	Y20 (zoning)			Y45		S	Y49	
	core 1	rim 1	core 2	rim 2	Mean		Mean	S
Major elements (wt %)								
SiO ₂	57.29	63.07	57.81	58.83	63.86	0.18	60.46	0.17
Al ₂ O ₃	26.12	23.12	25.66	24.24	21.82	0.00	24.24	0.12
FeO	0.14		0	0.25	0.11	0.02	0.09	0.08
CaO	8.24	3.87	8.11	7.08	2.95	0.00	6.05	0.16
Na ₂ O	6.85	9.06	6.56	7.05	8.67	0.38	7.62	0.22
K ₂ O	0	0.18	0	0	0.04	0.04	0.07	0.04
Total	98.64	99.30	98.15	97.45	97.45		98.53	
Number of ions per formula unit computed on the basis of 32 oxygens								
Si	10.39	11.20	10.50	10.63	11.46	0.005	10.86	0.014
Al	5.58	4.85	5.49	5.37	4.61	0.01	5.13	0.021
Fe	0.02			0.03	0.01	0.010	0.01	0.010
Ca	1.601	0.73	1.580	1.370	0.565	0.005	1.160	0.029
Na	2.410	3.11	2.310	2.460	3.100	0.040	2.658	0.064
K	0	0.04	0	0	0.005	0.005	0.014	0.008
End member proportions								
An	39.91	18.81	40.61	35.77	15.39		30.27	
Ab	60.00	80.15	59.38	64.22	84.46		69.36	
Or	0.09	0.010	0.001	0.001	0.001		0.004	

Table 4.7 continued

	Y51		Y53		Y53 1 analysis (Ca richest)		Y54	
	Mean	S	Mean	S			Mean	S
Major elements (wt%)								
SiO ₂	61.35	0.43	63.71	0.20	57.46		60.90	0.76
Al ₂ O ₃	23.65	0.13	22.08	0.22	26.06		23.70	0.28
FeO	0.02	0.03	0.17	0.04	0.10		-	-
CaO	5.22	0.26	3.13	0.22	8.06		5.29	0.45
Na ₂ O	7.84	0.25	8.93	0.16	6.65		7.66	0.32
K ₂ O	0.27	0.03	0.09	0.08	0.17		0.26	0.08
Total	98.35		98.11		98.50		97.81	
Number of ions per formula unit computed on the basis of 32 oxygens								
Si	11.03	0.041	11.4	0.050	10.42		1.00	0.089
Al	5.00	0.043	4.66	0.040	5.57		5.05	0.082
Fe	-	-	0.024	0.004	0.01		-	-
Ca	1.005	0.057	0.597	0.044	1.56		1.025	0.091
Na	2.737	0.079	3.097	0.049	2.34		2.682	0.102
K	0.060	0.007	0.017	0.017	0.04		0.055	0.020
End member proportions (mol %)								
An	26.43		16.08		39.59		27.24	
Ab	71.98		83.45		59.39		71.29	
Or	0.015		0.005		0.01		0.02	

Table 4.7 continued

	Y55		Y72		Y73		Y73 (more calcic)
	Mean	S	Mean	S	Mean	S	
Major elements (oxide %)							
SiO ₂	60.47	0.34	59.378	0.61	52.39	0.02	48.98
Al ₂ O ₃	23.93	0.30	24.42	0.47	29.32	0.36	30.85
FeO	0.04	0.03	-	-	0.10	0.10	0.16
CaO	5.87	0.22	6.25	0.32	12.33	0.08	14.79
Na ₂ O	7.50	0.07	7.37	0.31	4.21	0.04	2.83
K ₂ O	0.24	0.04	0.22	0.03	0.09	0.09	0.0
Total	98.05		98.04		98.44		97.61
Number of ions per formula unit computed on the basis of 32 oxygens							
Si	10.92	0.061	10.71	0.164	9.63	0.060	9.15
Al	5.09	0.654	5.20	0.105	6.35	0.070	6.79
Fe	-	-	-	-	0.015	0.015	0.02
Ca	1.334	0.045	1.210	0.065	2.425	0.015	2.96
Na	2.630	0.024	2.584	0.104	1.505	0.015	1.02
K	0.047	0.012	0.048	0.007	0.02	0.02	0
End member proportions							
An	33.25		31.49		61.39		74.37
Ab	65.56		67.25		38.10		25.62
Or	0.01		0.01		0.005		0.01

Table 4.7 continued

	Y79		Y80	
	Mean	S	Mean	s
Major elements (oxide %)				
SiO ₂	61.78	0.58	45.74	0.01
Al ₂ O ₃	23.87	0.34	33.69	0.43
FeO	0.10	0.08	0.25	0.005
CaO	5.32	0.52	17.55	0.27
Na ₂ O	7.92	0.14	1.50	0.08
K ₂ O	0.09	0.03	0	0
Total	99.08		98.73	

Number of ions per formula unit computed on the basis of 32 oxygens

Si	11.01	0.092	8.51	0.045
Al	5.03	0.084	7.39	0.055
Fe	0.01	0.012	0.04	0
Ca	0.997	0.091	3.50	0.04
Na	2.744	0.044	0.54	0.03
K	0.017	0.004	0	0

End member (mol %)

An	26.53	86.66
Ab	73.0	13.36
Or	0.50	0

KEY TO FIGURES 4.2-21

Figure 4.2 Mineralogical cross section (EE')

Figure 4.3 Mineralogical cross section (FF')

Figure 4.4 Mineralogical cross section (CC')

Figure 4.5 Mineralogical cross section (AA')

Figure 4.6 Traverse DD' showing the changes in the composition of biotite

Figure 4.7 Traverse BB' showing the changes in the composition of biotite

Figure 4.8 Traverse DD' showing the changes in the composition of garnet

Figure 4.9 Traverse BB' showing the changes in the composition of garnet

Figure 4.10 Typical zoning patterns of garnets from the unhornfelsed rocks

Figure 4.11 Typical zoning patterns of garnets from the hornfelses

Figure 4.12 Composition of plagioclase represented on An-Ab-Or diagram

Figure 4.13 Traverse BB' showing the changes in the composition of plagioclase

Figures 4.14-21 Tridimensional maps of modal analysis of garnet, cordierite plagioclase, quartz and biotite respectively.

fig 4.2

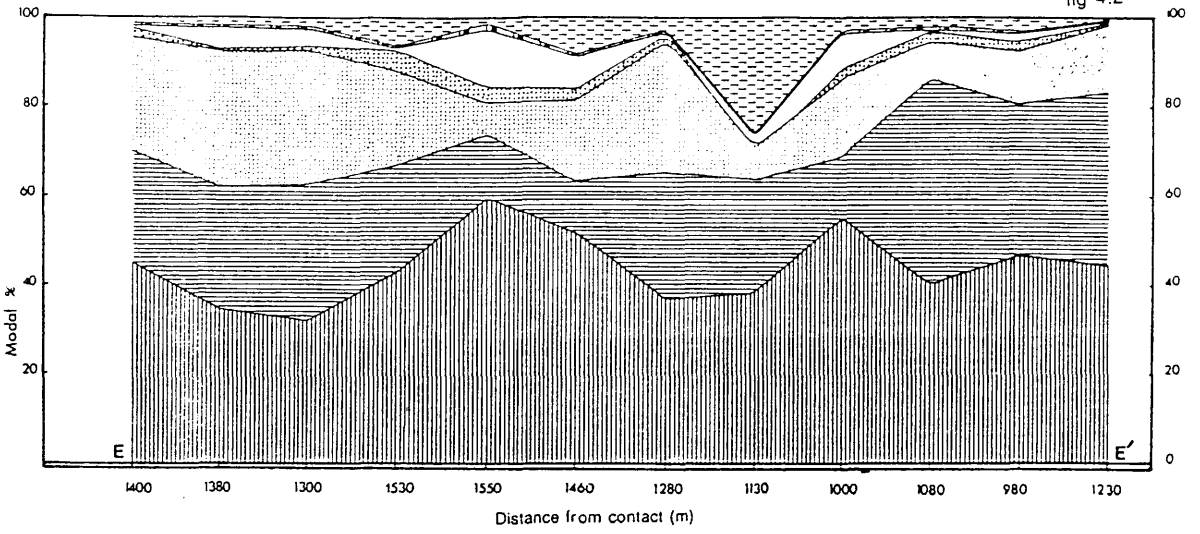

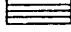
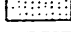
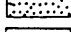
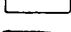
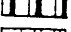
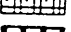

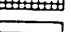
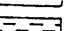



fig 4.3

Key

-  Biotite
-  Plagioclase
-  Quartz
-  Garnet
-  Sillimanite
-  Opaque
-  Cordierite
-  Spinel
-  Corundum
-  Orthopyroxene
-  Secondary minerals

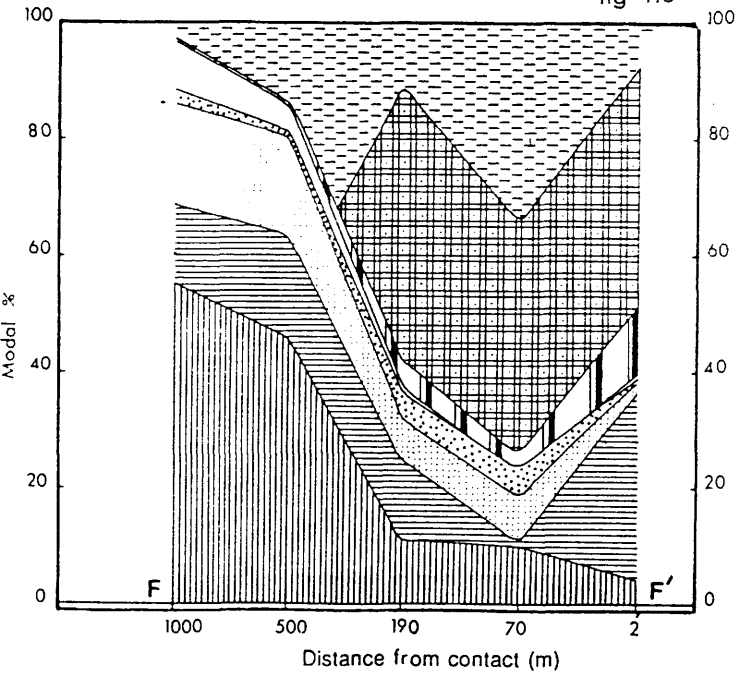


fig 4.4

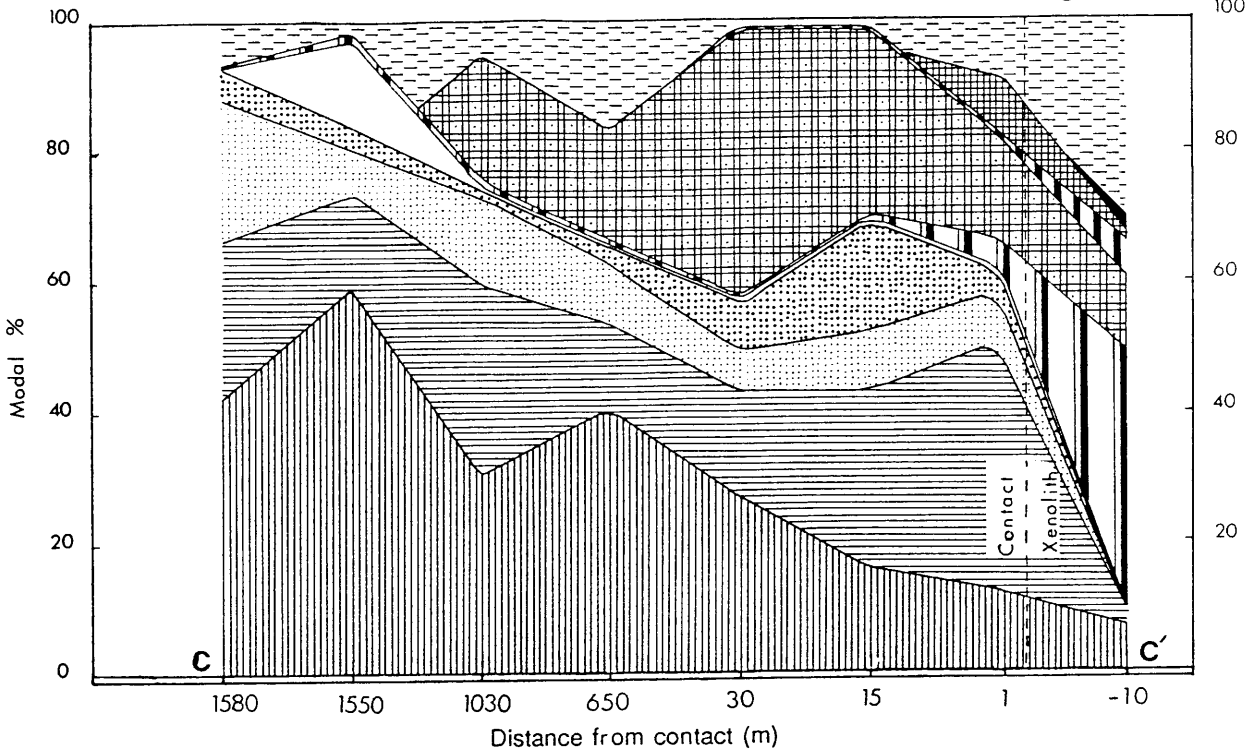


fig 4.5

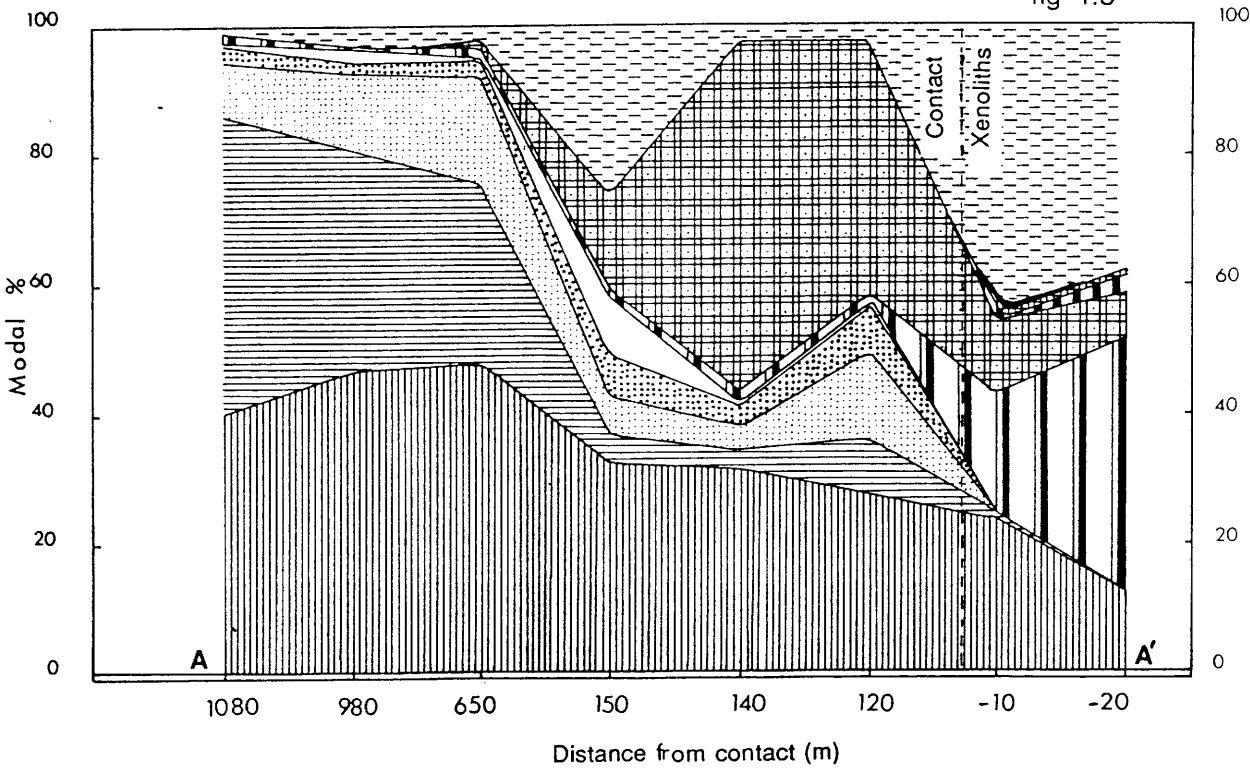


fig 4.6

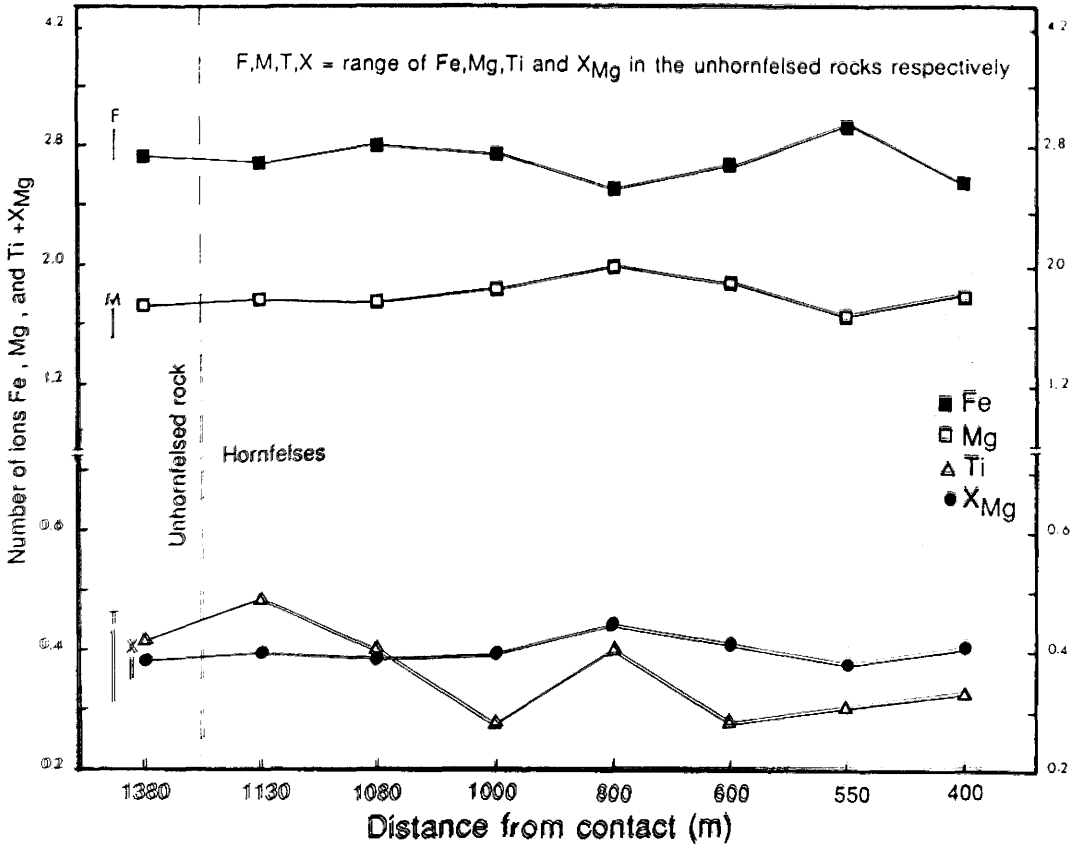


fig 4.7

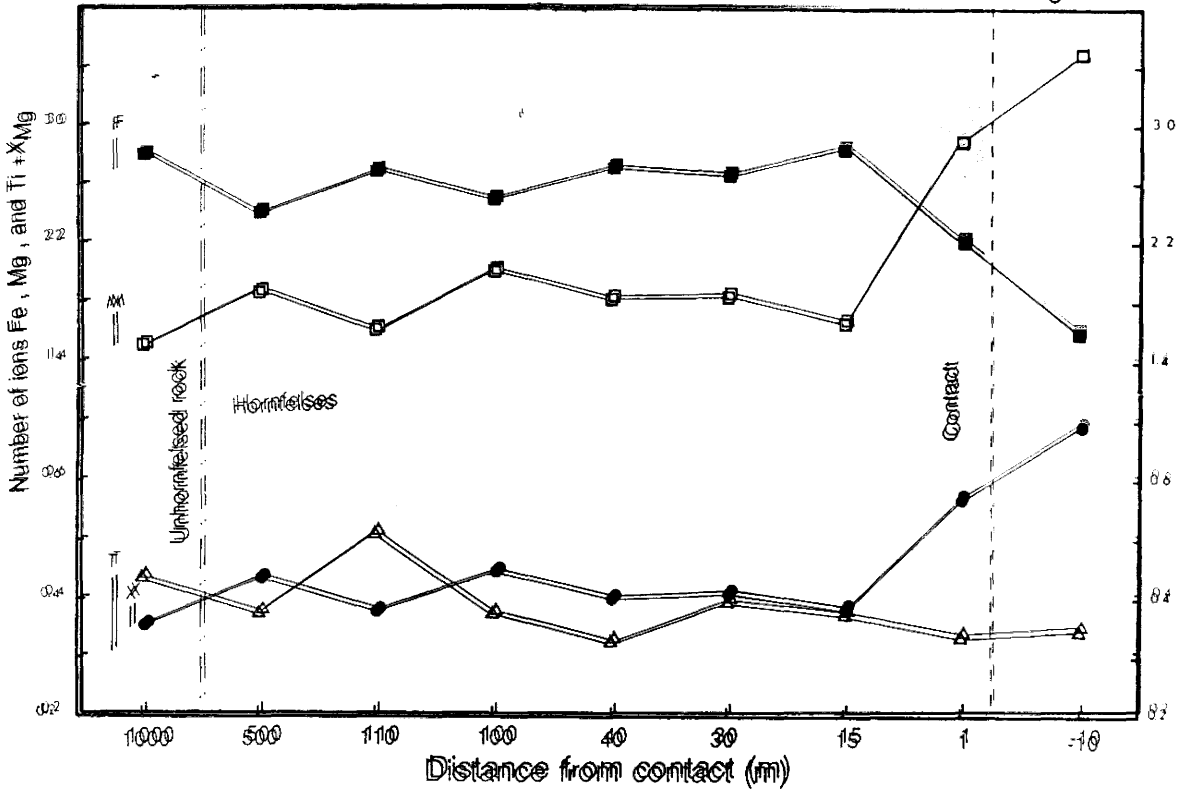


fig4.8

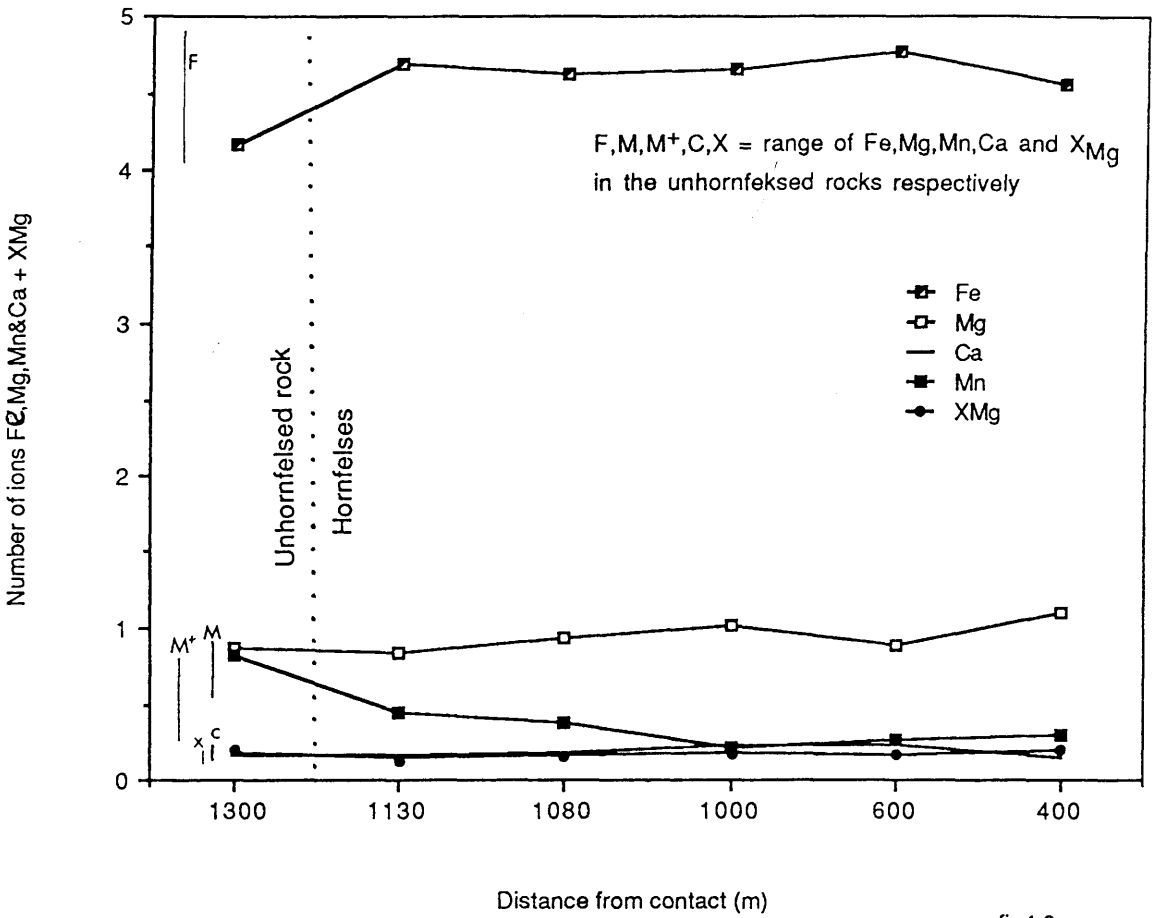


fig4.9

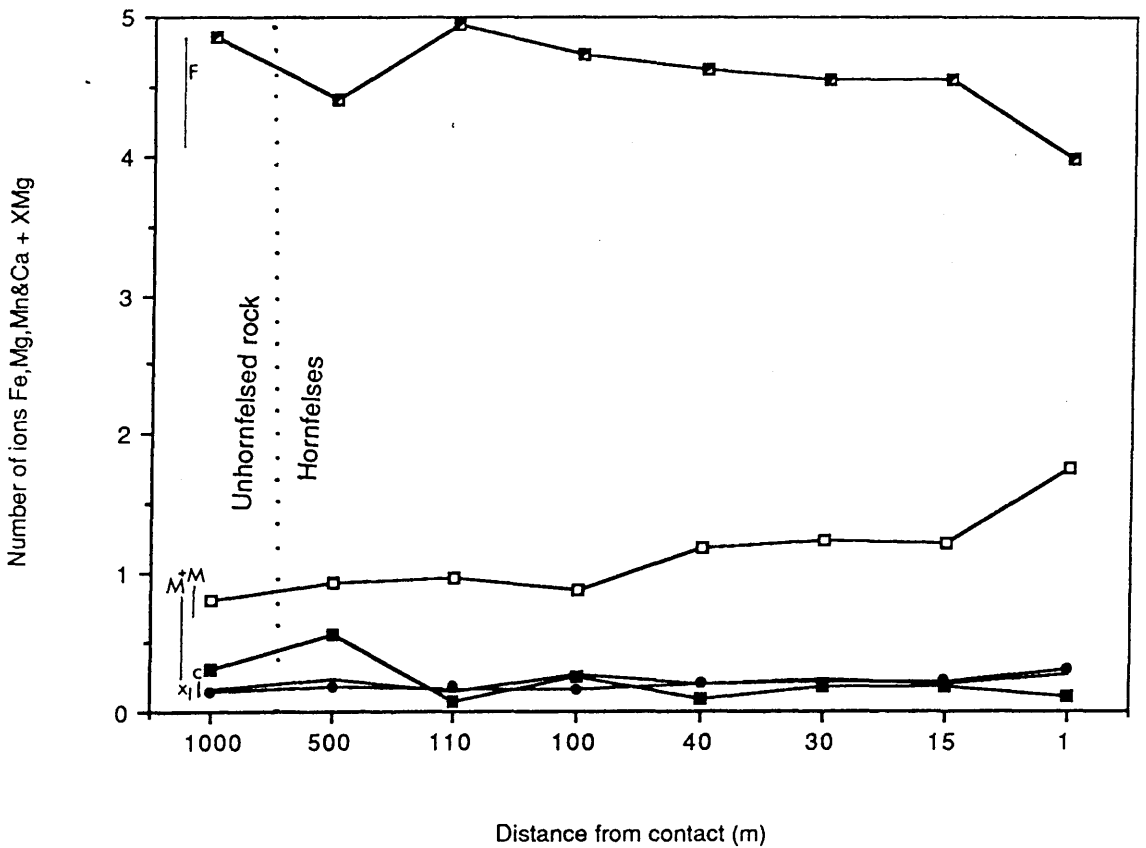


fig 4.10

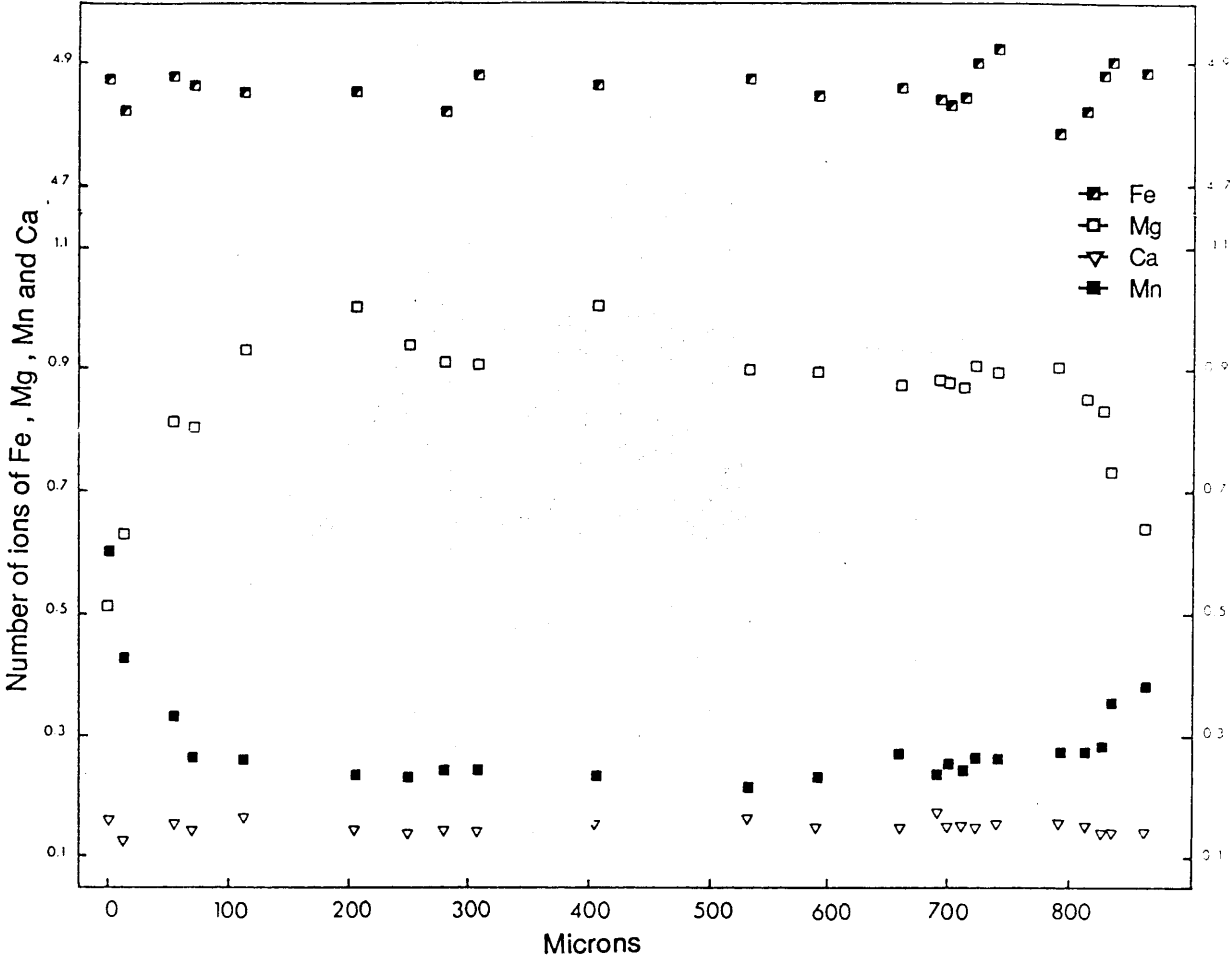


fig 4.11

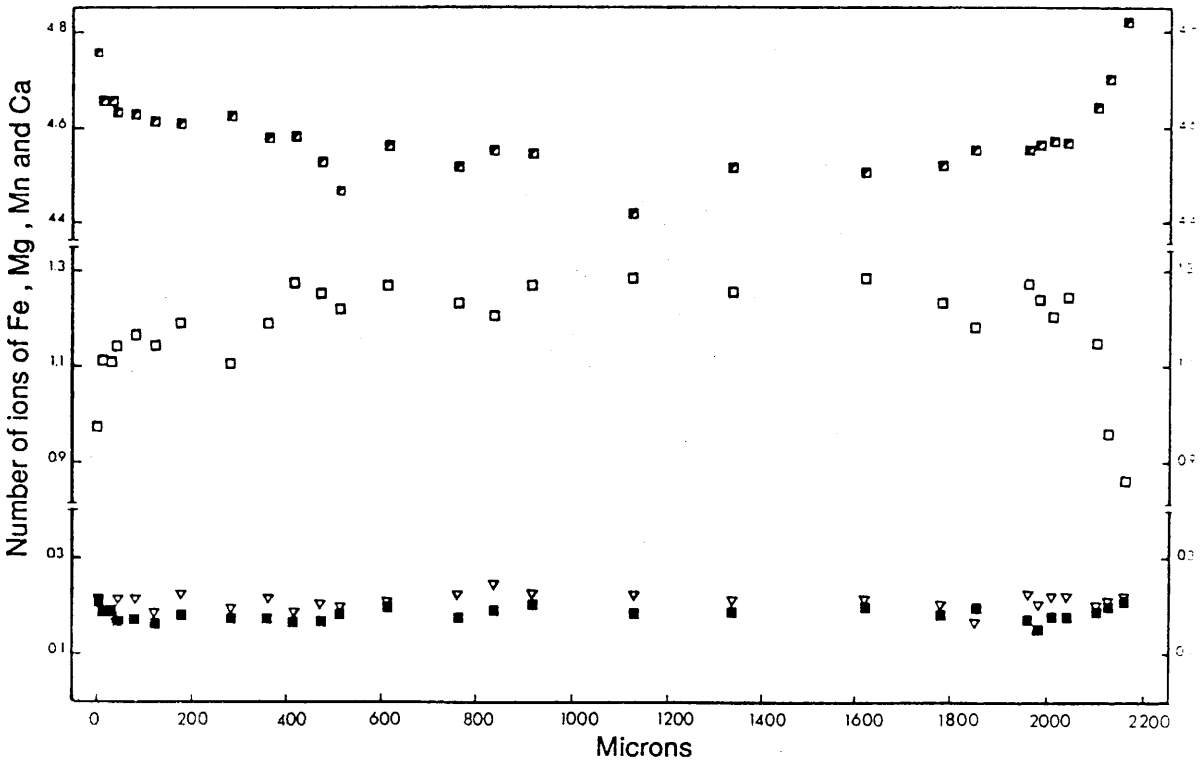


fig 4.12

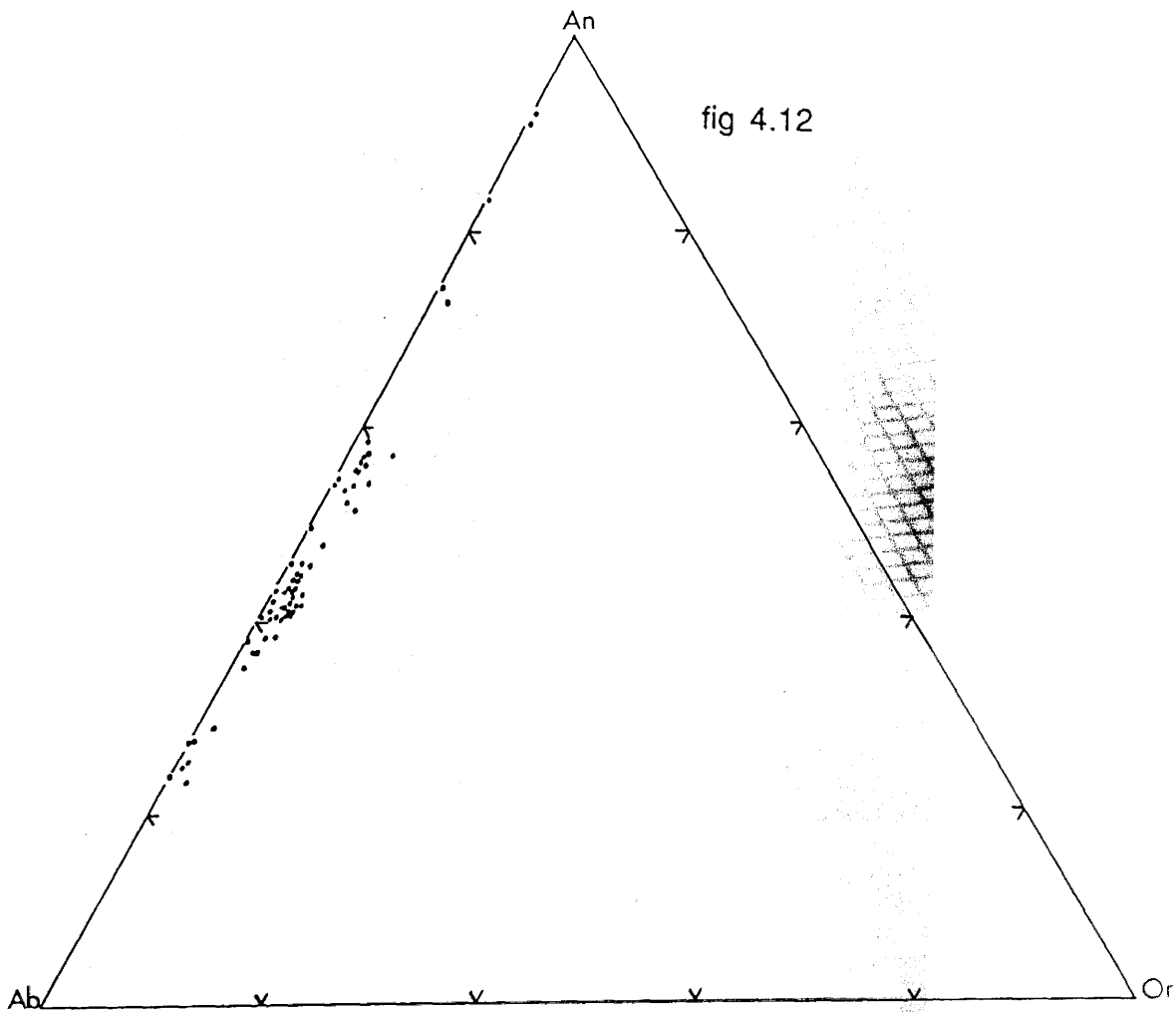


fig 4.13

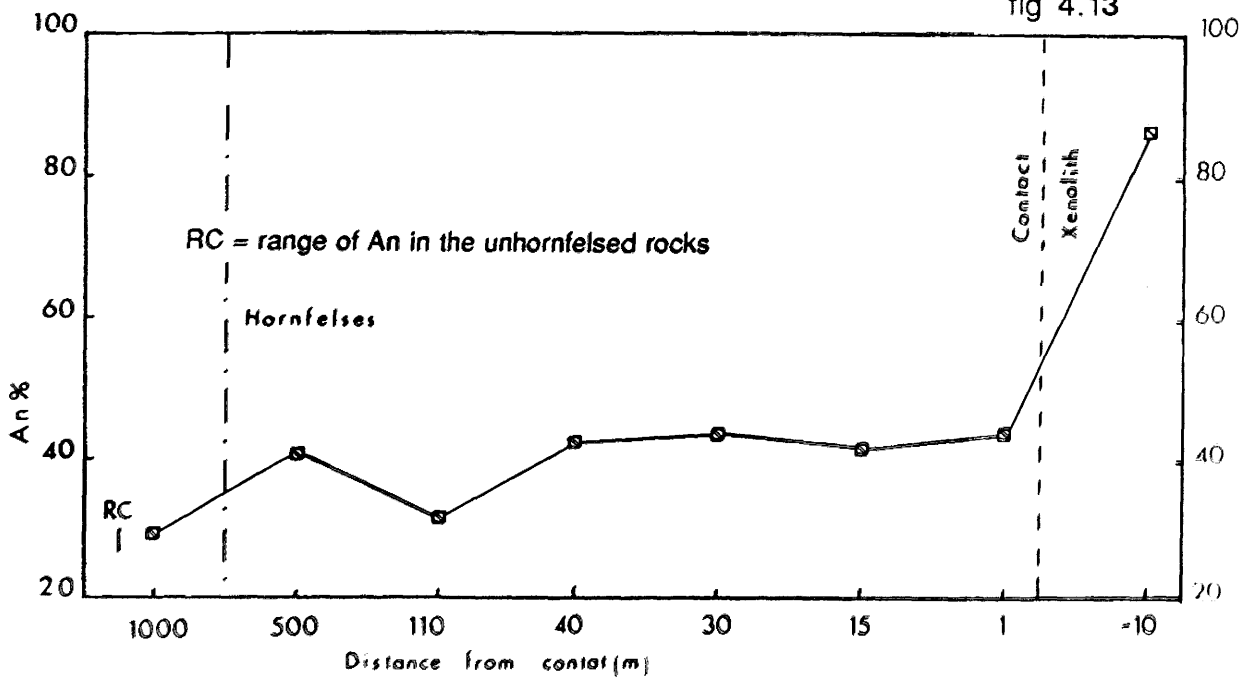


fig 4.14

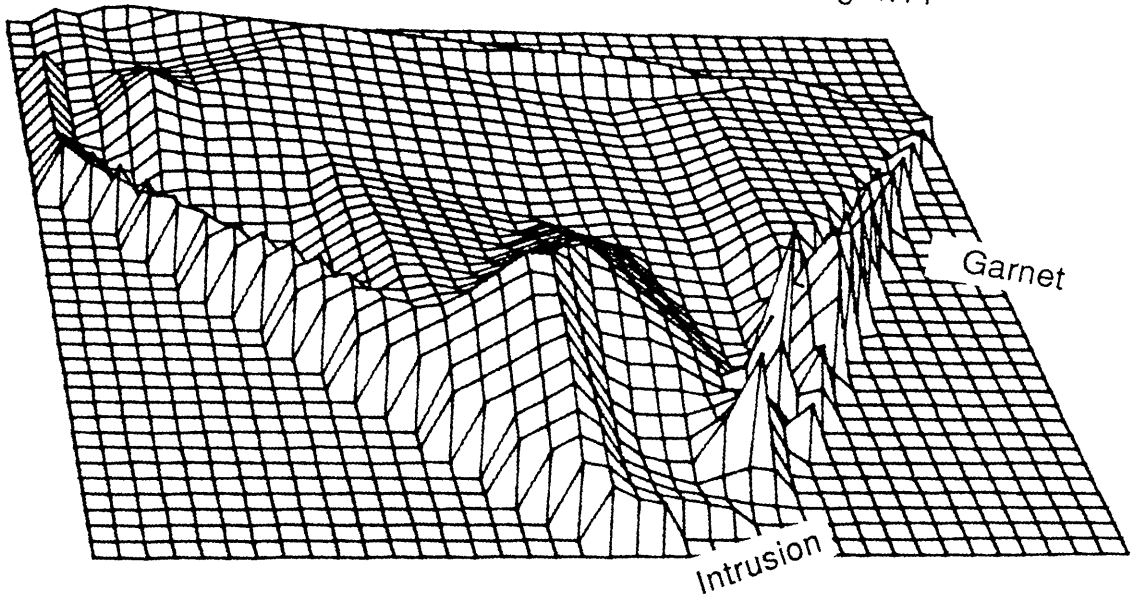
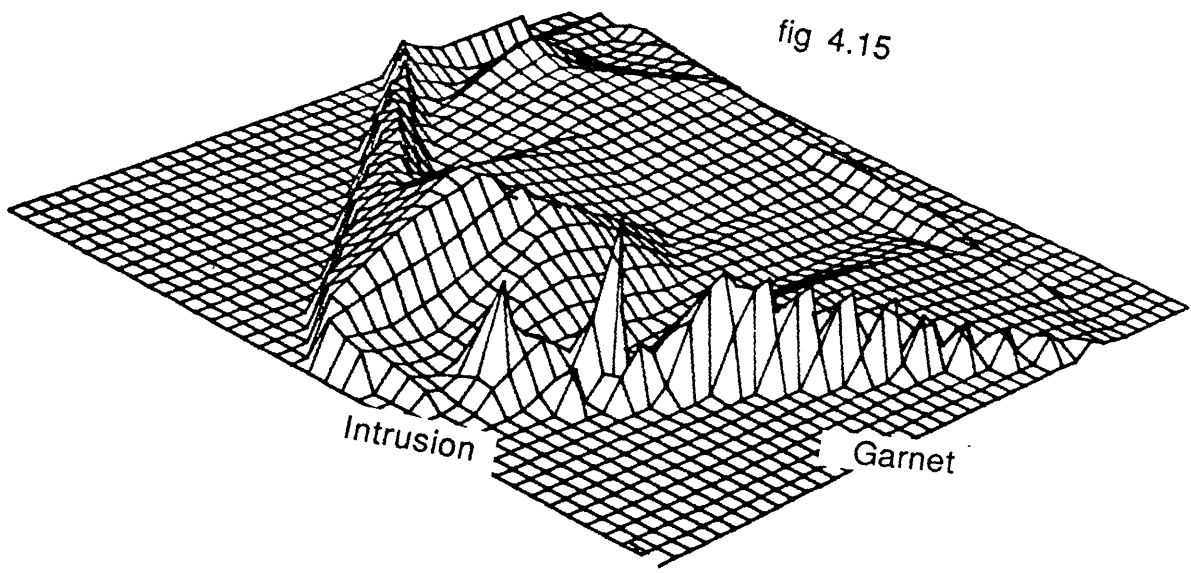
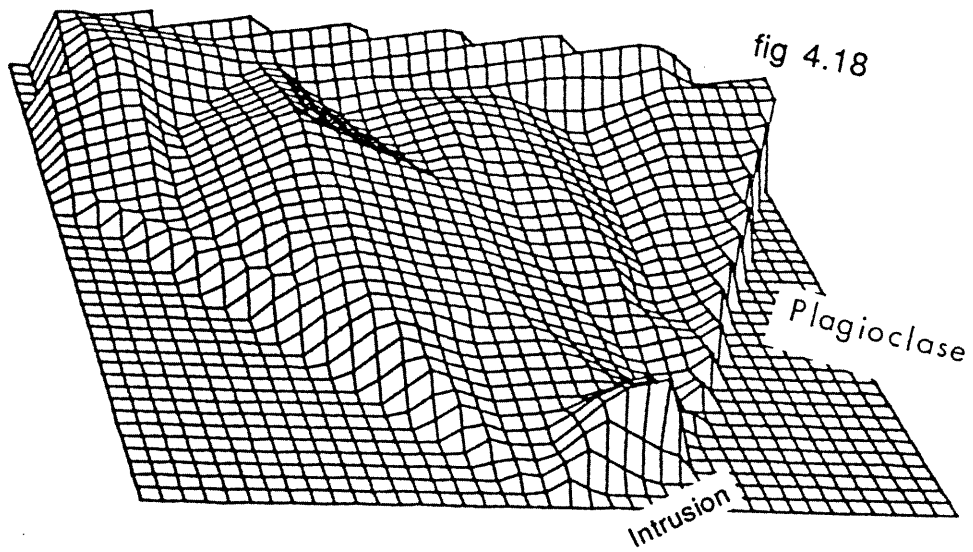
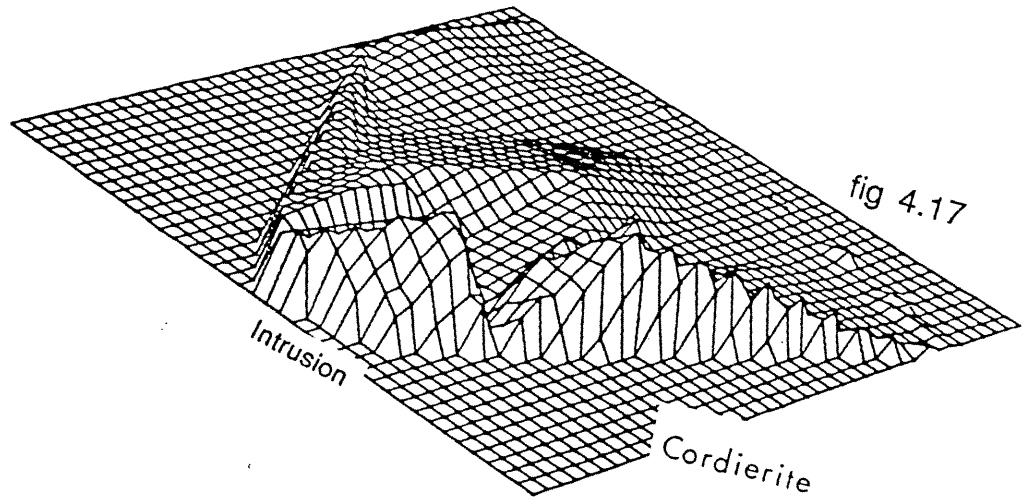
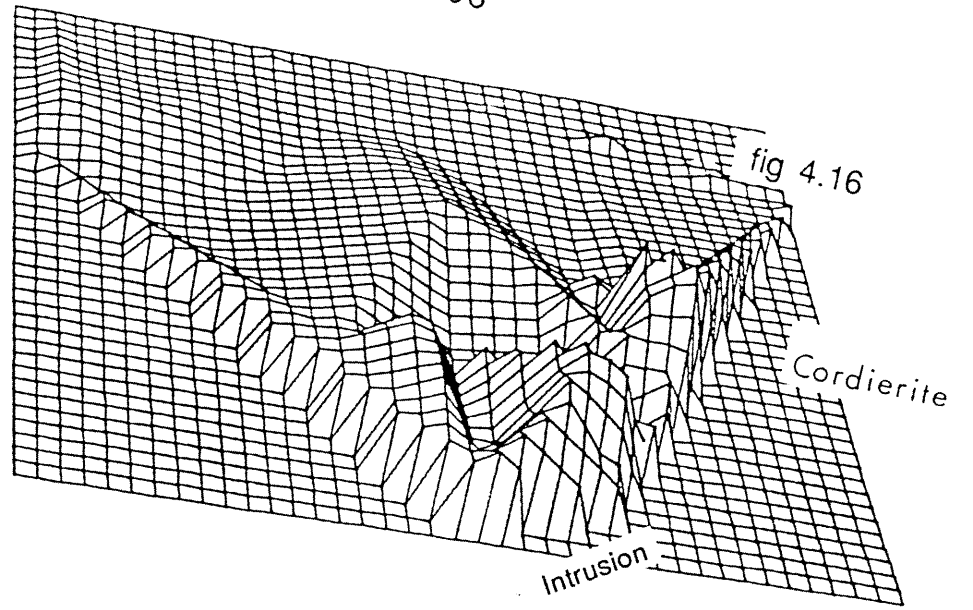
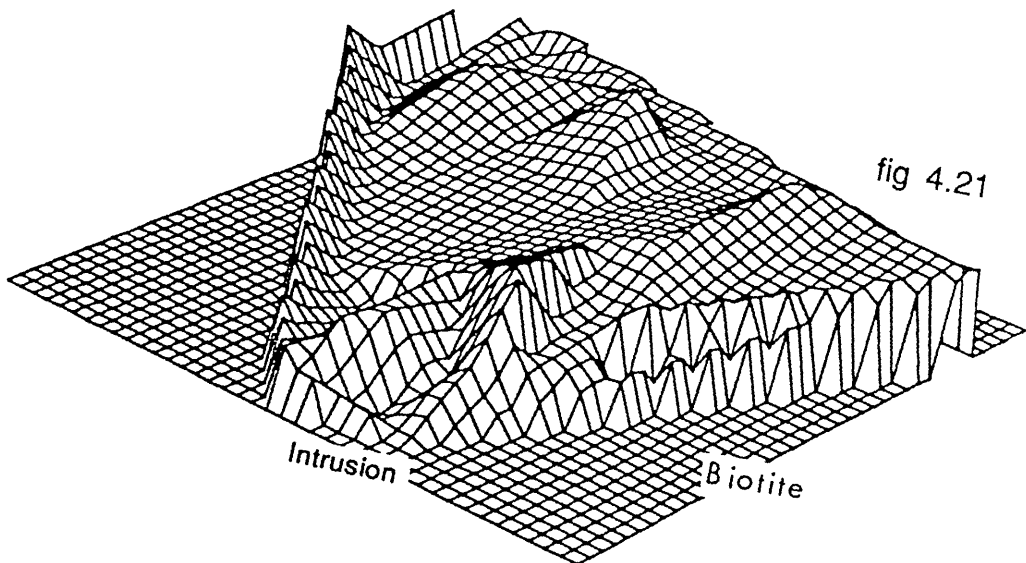
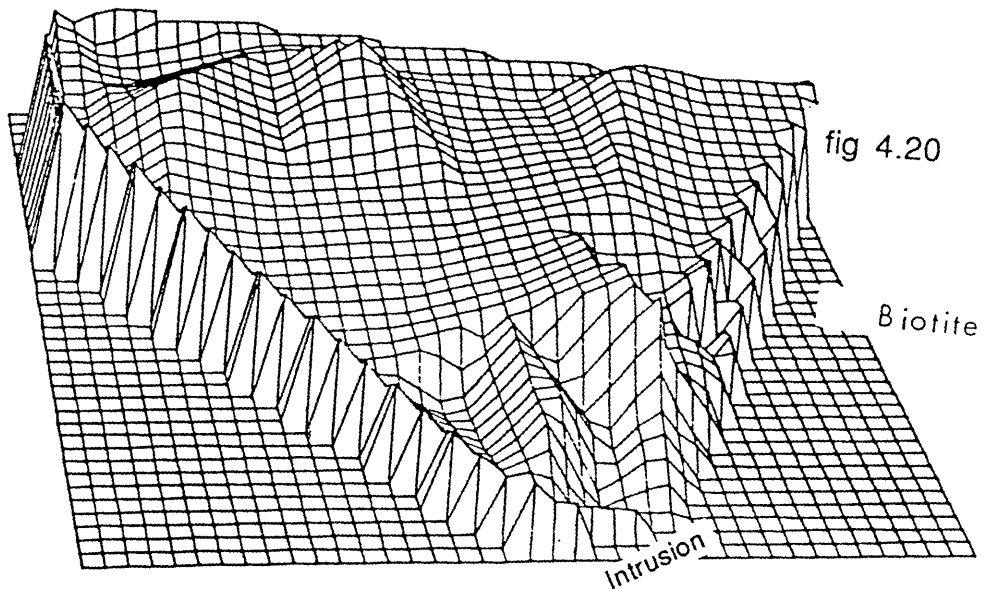
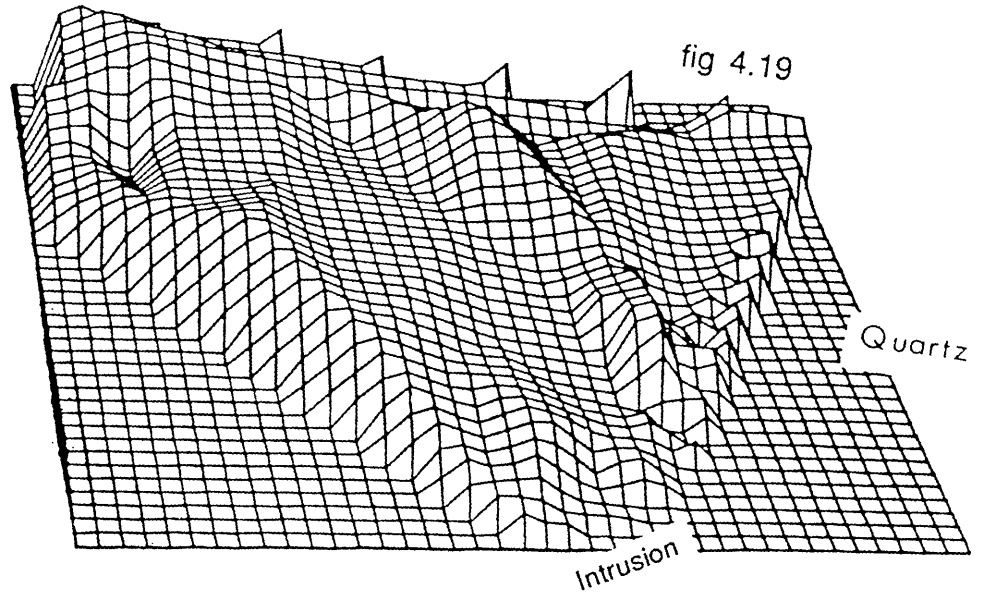


fig 4.15







CHAPTER FIVE : CHEMISTRY

5.1 Introduction

The T.P conditions under which the behaviour of elements is studied have been discussed in Chapter Three and are probably about (700-900)^oC and 4.8 ± 1.1kb; although the influence of retrogressive changes on the T.P estimates is sometimes significant. The mineralogy described in Chapter Four showed that significant but irregular changes occurred as a result of the hornfelsing of the metasediments. In addition, migmatization of the pelites and secondary retrogressive -especially hydrothermal- effects have influenced the chemistry of the rocks and will be pointed out when they have been detected. The general chemistry of the unhornfelled rocks is first outlined followed by detailed studies of the chemical changes suffered by the hornfelses and pelitic xenoliths. The absolute chemical composition of the melted-out material is then calculated and the chemical changes are evaluated in terms of the available evidence in the literature on the relative compatible-incompatible nature of the elements concerned.

5.2 General chemistry of the unhornfelled rocks

The results of 13 unhornfelled pelite analyses are given together with four analyses for rare earth elements (REE) in Appendix 3 and summarized in Tables 5.1-2. The major and trace elements, excluding U and Th which are detailed in Chapter Seven, are compared in Table 5.1 with the average of 35 southern Connemara pelites given in Senior and Leake (1978) and with other shale and pelite compositions from the literature whereas the REE are treated separately and compared to various shale compositions in Table 5.2

5.2.1 Major and trace elements

The chemistry of the Connemara pelites has been discussed by Leake (1958a), Evans (1964) and Senior and Leake (1978). Leake (1958, p294) has shown that the pelitic schists (excluding the quartz-rich semi-pelites) are rather poor in silica but richer or have normal alumina and total iron than many pelites described in the literature. In contrast, Evans (1964, p130) revealed that related to the silica-poor nature of the pelites, generally higher levels of trace element abundances are usually recorded compared to many

pelites and shales. However, the pelites analysed in this work are higher in SiO_2 , but lower in Al_2O_3 and Fe_{tot} (as Fe_2O_3) respectively than the seven pelites reported by Leake (1958a, p284) but their major contents agree with the average of 35 southern pelites given in Senior and Leake (1978) (Table 5.1). The wt% SiO_2 from the 13 analysed rocks ranges from 51.06% to 63.49% thus suggesting that some of the samples are possibly semi-pelites and the high SiO_2 but low Al_2O_3 and Fe_{tot} recorded in the present samples relative to those reported by Leake (1958a) are therefore the result of sampling. Nevertheless, the average wt% SiO_2 and Al_2O_3 of the Connemara pelites (13 from this work, 35 from Senior and Leake 1978 and 7 from Leake, 1958a) tend to be lower and higher in silica and alumina respectively than the average of many shales given in Taylor and McLennan (1985, p28), (Table 5.1) hence agreeing with Leake (1958a).

The content of trace elements is more variable and sometimes the average of individual elements such as Ba and Rb is more similar to the mean shales of Turekian and Wedepohl (1961) than to the average of the seven southern pelite analyses given in Evans (1964, p130). Significant differences, especially for Rb, Ni, Pb and Cu also exist between the average of 35 southern pelites published by Senior and Leake (1978) and the average of the 13 pelites analysed in this work (Table 5.1); although it is encouraging to note that the average of most elements falls within the standard deviations given by Senior and Leake for individual elements. The Connemara pelites are consistently higher in Ba, Zr, Ga, Zn, and Pb than shales published by Turekian and Wedepohl (1961), Krauskopf (1967) and Taylor and McLennan (1985), indicating that the Connemara pelites were originally rich in some trace elements.

Senior and Leake (1978) noted that in the Connemara schists Al_2O_3 , TiO_2 and Fe_{tot} exhibit positive correlations with each other as well as with some trace elements such as Ni, Cr, Co, Ga and they interpreted these relationships as being diagnostic of the presence of clay mineral components in the original sediments. Therefore, the degree to which elements correlate with TiO_2 , Al_2O_3 and Fe_{tot} (elements not significantly affected by metasomatism) would indicate which trace elements were dominantly added in clay minerals. Figures 5.1-10, despite some rare scattered points, show positive correlations between

Al₂O₃, Fe_{tot} and TiO₂ as well as Al₂O₃ with Ga, Th, U (only the results obtained in this work are shown for U and Th); Fe_{tot} with Ni and TiO₂ with Co, Cr, and Zr indicating that much of the trace elements were originally controlled by clay and sheet mineral content of the sediments. However, Sr does not correlate with TiO₂, Al₂O₃ and Fe_{tot} (only Sr versus TiO₂ is shown in Figure 5.11) but exhibits good positive correlation with both CaO and Na₂O (Figures 5.12-13) indicating that Sr was substantially added with detrital feldspar especially as the CaO/Na₂O ratio of the pelites is always below 1.2 thus excluding Ca and Sr having been added in carbonates. Both Rb and Ba exhibit very good positive correlation with K₂O but all exhibit very weak correlations with TiO₂ (Figures 5.14-18). Ba and Rb were not dominantly added with detrital feldspar as both elements do not correlate well with CaO+Na₂O, (Figures 5.19-20) and K-feldspar is not abundant in the pelites. It has been shown in Chapter Four that biotites (probably crystallized from clay minerals) are rich in Ti and therefore positive correlation between Ti and K and eventually Rb and Ba is expected but not found, and this trend is probably caused by some K being held in secondary sericite, muscovite, prehnite and calcite.

5.2.2 Rare earth elements(REE)

The REE contents were obtained from four country rocks using inductively coupled plasma (ICP) technique as described by Walsh *et al.* (1981) and have been normalized to the corresponding elements in chondrites given by Taylor and McLennan 1985, (Appendix 3). The advantage of normalization is that any variation between REE of odd and even atomic number is eliminated and the extent of any fractionation among various REE in the specimens is discernible because there is considered to have been no fractionation between the light REE (LREE) and heavy REE (HREE) in the chondrites. The normalized REE are indicated as REE*. The degree of fractionation between the LREE and HREE is usually estimated by calculating the ratios of chondrite normalized La (the lightest REE) to chondrite normalized Lu (the heaviest REE) and it is written as (La/Lu)_{CN}. Eu sometimes lies away from the trend of the other REE on a chondrite normalized diagram and this departure is known as the Eu anomaly. It is positive for Eu/Eu* > 1 and negative for Eu/Eu* < 1 and is calculated by

assuming a straight line REE pattern in the region Sm-Eu-Gd; i.e. $\text{Eu}/\text{Eu}^* = \text{Eu}_N / [(\text{Sm}_N)(\text{Gd}_N)]^{1/2}$.

The REE, given in Appendix 3, are compared in Table 5.2 with values for Post Archean Australian shales (PAAS) (Nance and Taylor 1976); North America metamorphic shales composite (NAMSC) (Haskin *et al.* 1968) and European shales composite (ESC) (Haskin and Haskin 1966). The striking feature is the remarkable REE enrichment of the Connemara pelites compared to PAAS, NAMSC and ESC with the total REE(ΣREE) being 315, 183, 172 and 204 respectively. However, the average Eu/Eu^* ratio of the pelites is very similar to that of the various shales (Table 5.2) thus suggesting that the pelites are still preserving the original sedimentary signature and indicating that the REE enrichment is probably a sedimentary feature of the pelites. The slightly high $(\text{La}/\text{Lu})_{\text{CN}}$ ratio indicates that the pelites are enriched in LREE relative to HREE thus giving slightly steep distribution patterns (Figure 5.21). The four unhornfelsed pelites have negative Eu anomalies with Eu/Eu^* ratios always below unity. Sample Y82 has the highest Eu/Eu^* ratio of 0.94 and this slight enrichment in Eu relative to the other samples is probably caused by the presence of inseparable migmatite leucosomes.

5.3 Chemical changes

The fractionation of the major and some trace elements including REE in the hornfelses and pelitic xenoliths is discussed below in the light of the mineralogical changes described in Chapter Four and in relation to the compatible-incompatible nature of the elements as deduced from magmatic and experimental evidence. In order to increase the sample size and therefore minimize the effects of sampling, the average in major elements of 34 southern pelites (27 from Senior and Leake, 1978 and 7 from Leake, 1958a; 11 contact hornfelses and 3 xenoliths from Leake and Skirrow, 1960) were included in the calculations. The trace elements from the previous work were not considered on account that the influence of analytical precisions and accuracies is believed to be significant; for instance, Zr has not been detected in 11 samples published by Senior and Leake (1978), Ba is not detected in two xenoliths analysed by Evans (1964) and also the 13 pelites tend to be lower in Ni and to some extent Rb than most of the previous published data (Figures 5.7,

5.14). The absolute composition of the melts derived from the hornfelses and xenoliths are calculated using Cr, Ni and Co and the order of fractionation of elements into the melts is estimated and also compared to the order of fractionation of elements in magmas.

5.3.1 Fractionation of the major elements

The average wt% SiO₂, given in Table 5.3, shows that the contact samples are only 6wt% lower than the regional pelites and then only if the standard deviations are ignored. This trend is probably caused by the sampling being complicated by quartz segregations, veins, porphyroblasts and lenses which are present in the hornfelses (Chapter 4). Further complications also arise from the fact that many of the hornfelses e.g. Y14, Y22, Y24, Y25, Y34 are probably semi-pelites because they have Si:Ti ≥ 65 compared to the pelites which have Si:Ti ratios ≤ 65 . In the xenoliths, SiO₂ finally drops off to its lowest value of 19.95 ± 9.51 wt% which should be compared to 54.9 ± 5.62 wt% in the country rocks.

Both Na and K clearly tend towards zero in some xenoliths as biotite and feldspar were broken down and released the removed alkalis. This is consistent with Niggli alk which declines from 15.23 in the unhornfelled rocks to 2.99 in the pelitic xenoliths (Table 5.3).

The average wt% CaO of 1.93 ± 1.07 in the unhornfelled rocks changes insignificantly down to values of 1.51 ± 0.52 and 1.34 ± 1.33 in the intermediate and contact hornfelses respectively before rising to an average of 2.84 ± 3.39 in the xenoliths. The better positive correlation between CaO-Na₂O than between CaO-P₂O₅ (Figures 5.22-23) indicate that Ca is being lost with Na in the melting out of plagioclase, the melts being therefore higher in Na/Ca than the solid residue as is well established from the Ab-An liquid-solid equilibrium diagram, (Bowen, 1928). As a result, the anorthite content of plagioclase increases from An₂₈ in the unhornfelled rocks through An₃₆ in the contact hornfelses to An₇₄ in the xenoliths. Clearly some plagioclase entered the melts and the calculations performed in subsection 5.4 support this suggestion. The abnormally high wt% CaO in the xenoliths Y 73, Y80 of 8.72 and 8.18 respectively is a marked reversal of the progressive loss of Na and Ca and is almost certainly due to addition of a plagioclase (bytownite) forming-

material from the basic magma, a view confirmed by the similarity of the plagioclase in the xenoliths to that in the basic rocks both as regards composition (An_{80-90}) and twinning (Carlsbad-albite twins). Sample Y69 is abnormally rich in Ca because of the abundance of secondary prehnite which extensively replaces biotite.

P_2O_5 falls from an average of $0.19 \pm 0.11\text{wt}\%$ in the parent country rocks to 0.04 ± 0.01 in the xenoliths indicating strong fractionation of P into the melts.

Mn does not show any clear trend but if the standard deviations are ignored lower averages are recorded in the xenoliths compared to the country rocks which suggests that some Mn, if any, has entered the outgoing melts.

Having remained almost unchanged in the intermediate hornfelses compared to the country rocks, Ti tends to increase, but only insignificantly in the contact samples followed by a more important rise in some xenoliths (Table 5.3, Figure 5.24). However, other xenoliths such as Y80 and Y62 have Ti concentrations lower than most of the hornfelses and country rocks suggesting that some Ti has left the crystal phases and this is supported by the calculations given in subsection 5.4. There is an increasing positive correlation between Ti and Zr as the contact is approached but it tends to disappear in some xenoliths which are low in Zr and high in Ti compared to the country rocks and non-xenolithic hornfelses (Figure 5.24). This suggests that zircon strongly melted out of the xenoliths but much of Ti was held in rutile, magnetite, and spinel which must have had higher melting points than zircon. Rutile, magnetite and spinel have melting points of 1825°C , 1494°C and 2135°C respectively (Deer *et al.*, 1966) while that of zircon is rather ambiguous and varies from as low as 1650°C (Deer *et al.*, 1982) up to 2190°C , (Johnstone, 1954). As with all minerals however, zircon will melt much below its pure melting point when mixed with other minerals, and therefore the evidence from the literature favours this conclusion.

Al, Mg and Fe_{tot} increase progressively in the envelope hornfelses to concentrations in the xenoliths up to five times higher than in the country rocks for Fe_{tot} and two times for Al and Mg. This remarkable increase is probably caused by the systematic melting out, or breakdown and removal of quartz and feldspar and the breakdown of biotite and cordierite to magnetite,

spinel, corundum and orthopyroxene in the xenoliths (Chapter 4). This removes Si, Al, alkalis and Ca and leaves behind Fe, Mg and relatively increased Al. Fe^{+3} rises more rapidly than Fe^{+2} as the degree of hornfelsing rises giving increasing oxidation ratios $w(\text{mole } Fe^{+3}/(Fe^{+3}+Fe^{+2}))$ as the contact of the intrusion is approached indicating that oxidizing conditions prevailed during the hornfelsing of the metasediments.

When plotted against each other, Niggli al decreases as Niggli fm increases (Figure 5.25) and this would be the result if Fe and Mg were added to the hornfelses, Al was subtracted from them or both processes had occurred. However, except for the slight enrichment in the envelope hornfelses, mg maintains similar values both in the country rocks and pelitic xenoliths (Table 5.3) and therefore Fe and Mg were not appreciably added to or subtracted from the xenoliths and the negative correlation between al and fm is probably because Al was removed from the hornfelses with Si, K and other incompatible elements which thereby enriched the xenoliths in residual Fe and Mg (Leake and Skirrow 1960). Because Al was removed in smaller proportions than it was present in the original pelites, the proportions of Al remaining in the residual hornfelses increased markedly despite some removal of Al. The melts compositions derived from the contact hornfelses and pelitic xenoliths obtained in subsection 5.4 show that Al was indeed removed and at more advanced stages small amounts of Fe and Mg also entered the melts.

5.3.2 Fractionation of the trace elements

Rb changes insignificantly in the envelope hornfelses then drops off in the xenoliths to an average three times lower than in the country rocks (Table 5.3). The Rb-K coherence is so good that the two elements plot linearly against each other (Figure 5.26). The $Rb \times 10^{-4} : K$ ratio does not vary significantly from an average of 0.00332 throughout the aureole although the hornfelses and xenoliths tend to be lower compared to the regional rocks thus agreeing with magmatic crystallization where the Rb:K ratio increases in a sequence mafic to acidic rocks (Wedepohl, 1978).

The average Ba also varies little in the envelope hornfelses but declines to its lowest values in the xenoliths (Table 5.3). The ratio $Ba \times 10^{-4} : K$ in the country rocks (0.02556), which differs little from that of the intermediate

hornfels (0.02413), rises to values of 0.03022 and 0.06429 in the contact hornfels and xenoliths respectively.

Likewise, Zr shows no significant change until the xenoliths in which it decreases to an average of 120 ± 44 ppm compared to 272 ± 47 ppm in the unhornfelsed pelites. This is consistent with the general behaviour of Zr in magmas where it increases with increasing magmatic differentiation, (Wedepohl, 1978). However, in granitic rocks, the trends of Zr vary depending on the type of parent magma; for calc-alkaline granites Zr decreases with increasing differentiation whereas the opposite occurs for alkaline granites. Thus in terms of Zr, the melts extracted from the xenoliths would be alkaline in character.

The mean values of Sr decrease from 242 ± 64 ppm in the unhornfelsed rocks to 154 ± 90 ppm in the contact hornfels then rise to an average of 596 ± 386 ppm in the xenoliths (Table 5.3). The ratio $Sr \times 10^{-4} : Ca$ increases from 0.01527 in the regional pelites through 0.01756 in the intermediate hornfels to 0.03263 in the contact hornfels but falls back to 0.02496 in the xenoliths. This suggests that the Sr:Ca ratio was lower in the outgoing liquid than in the residual plagioclase. This trend exhibited by the Sr:Ca ratio is not compared to magmatic differentiations because in the literature both increase and decrease of the Sr:Ca ratio with increasing magmatic differentiation are reported, (e.g. Turekian and Kulp, 1956; Wedepohl, 1978). Based on Sr and Nd isotopes, Jagger (1985) showed that some Sr has probably moved out of the Cashel intrusion into the pelitic xenoliths and the metasediments immediately adjacent to the contact and therefore, the high Sr:Ca ratios recorded in the xenoliths and some contact hornfels, e.g. Y33, Y39 is possibly related to this contamination.

Ga shows no significant changes in the envelope hornfels but in the xenoliths it rises to an average two times higher than in the country rocks (Table 5.3). Because Ga frequently substitutes for Al in plagioclase (Wedepohl, 1978), the addition of Al from the magma as shown earlier was probably accompanied by small amounts of Ga.

Ni is enriched in femic minerals and increases steadily from an average of

48 ± 11ppm in the unhornfelsed rocks to 173 ± 60ppm in the pelitic xenoliths (Table 5.3). The calculations performed in subsection 5.4 (using Cr) show that even at a degree of partial melting of 71% i.e. Cr=388ppm, Ni does not enter the melts which confirms that it is held firmly in high melting point minerals such as orthopyroxene, magnetite and ilmenite.

Co does not change significantly in the envelope hornfelses but in the xenoliths it rises sharply to an average of 101 ± 28ppm which should be compared to 23 ± 7ppm in the country rocks. As with Ni, Co remains in the crystal fraction (magnetite, spinel, orthopyroxene) even at a degree of partial melting of 71%.

Cr shows similar trends to both Ni and Co by increasing from an average of 109 ± 12ppm in the country rocks to 388 ± 158ppm in the xenoliths thus indicating a strong preference for the crystal phases over the fluid phase as confirmed by the calculations of the material melted out of the hornfelses and xenoliths given in Tables 5.4-5. At higher degrees of partial melting, Cr enters the melt first followed by Co and Ni respectively.

Cu and Zn increase from 29 ± 19 and 115 ± 20ppm in the unhornfelsed rocks to 85 ± 29 and 575 ± 286 in the xenoliths respectively but in contrast Pb is 5 times lower in the xenoliths than in the country rocks (Table 5.3). The presence of chalcopyrite in the rocks (Chapter 4) indicates that Cu and probably also Zn are coming in but not Pb. Since S has not been determined these elements are not considered further.

5.3.3 Fractionation of the REE

The REE from six hornfelses, two xenoliths, one xenolithic and one non-xenolithic metagabbro are given in Appendix 3 and plotted in figures 5.27-29. The average and range of individual elements from the hornfelses and xenoliths are compared with those from the four unhornfelsed rocks in Table 5.2 and Figure 5.30 respectively.

In the Cashel thermal aureole, the REE exhibit three main intriguing features namely : a decline in the total REE and increase in the $(La/Lu)_{CN}$ and Eu/Eu^* ratios. The total REE decreases markedly from 315 ± 38 in the regionally metamorphosed rocks through 216 ± 27 in the envelope hornfelses to 67.5 ± 9 in the pelitic xenoliths (Table 5.2). However the loss of the HREE

is swifter and more pronounced than the LREE thus giving steep REE distribution patterns and an exceptionally high $(La/Lu)_{CN}$ ratio of 65.6 ± 17.22 in the xenoliths (Table 5.2; Figure 5.28). HREE are often enriched in zircon, apatite, garnet, orthopyroxene e.g. McCarty and Kable (1978); Henderson (1984); Taylor and McLennan (1985); Ward (1987). In the regional pelites and hornfelses, garnet, zircon and apatite are often present but the HREE were probably related to detrital zircon and apatite in the original sediments because both Zr and P_2O_5 exhibit good positive correlations with Lu (Figure 5.31(A,B)). Rocks with similar proportions of garnets e.g. Y19 (7.46%) and Y69 (6.40%) yield considerably different distribution patterns (Figure 5.27) thus suggesting insignificant influence of garnet on the HREE as would be expected if zircon and apatite were the main controls. In the xenoliths, the $(La/Lu)_{CN}$ ratio rises up to 82.8 indicating strong partitioning of the HREE into the melt probably because of the melting of zircon and apatite, which indicates that the HREE were not significantly accommodated in orthopyroxene after they were released from zircon and apatite.

Sample Y 69 has a remarkably high $(La/Lu)_{CN}$ ratio despite being rich in pink zircons which suggests that metamorphic recrystallization of brown zircons not only released U into the melts (Chapter 7) but probably also HREE. The concave shaped distribution pattern exhibited by some hornfelses in Figure 5.27 possibly reflects different proportions of pink and deep brown zircons.

The Eu/Eu^* ratio changes gradually from consistently less than unity in the unhornfelled rocks through both more and less than unity in the hornfelses to well above unity in the pelitic xenoliths thus indicating continuous enrichment of Eu relative to the other REE as the degree of hornfelsing rises. Eu exhibits positive correlations with both Ca and Sr except in the four samples which show $Eu/Eu^* > 1$ (two contact samples and two xenoliths) (Figure 5.31(C,D)) suggesting that some of Eu^{+2} was converted to Eu^{+3} although the presence of a significant positive Eu anomaly in these samples indicates that most of Eu must have been in the divalent state. Because the ratio of Eu^{+2}/Eu^{+3} depends on the temperature, oxygen fugacity and composition of the melts (e.g. Morris and Haskin 1974; Drake 1975) and because these factors are not accurately known the ratio has not been calculated but must be very high. The positive Eu anomaly in the xenoliths cannot have originated

from the basic magma for three reasons : first, the abnormally high Ca and eventually Sr are always accompanied by very low Eu contents thus excluding significant Eu addition in magmatic plagioclase. Second, the REE contents, distribution patterns and Eu anomalies of the xenolithic and non-xenolithic metagabbros are similar to each other (Figure 5.29) but are markedly different from those of the pelitic xenoliths. This excludes the transfer of significant amounts of Eu from the magma to the xenoliths because if this did occur then the xenolithic and non-xenolithic metagabbros would reflect this by exhibiting significantly different sizes of Eu anomaly and probably also different REE distribution patterns. Third, the two pelitic restite-leucosome pairs Y68, Y69 both have $Eu/Eu^* > 1$ but are remote from the basic rocks (Figure 4.1). The only tenable explanation is that a granitic melt has left the xenoliths and some contact hornfelses which thereby became depleted in REE but enriched in Eu relative to the other REE. The calculations performed in subsection 5.4 show that the material removed from the xenoliths always has a negative Eu anomaly which supports this explanation.

Positive Eu anomalies in the lower crust of the earth and in sedimentary xenoliths within igneous bodies are common (e.g. Rogers 1977; Drury 1978) and have been interpreted by Taylor and McLennan (1985) as being residual in character thus supporting the above interpretation.

The large positive Er anomaly recorded in the pelitic xenolith Y62 is rather puzzling because the two xenoliths analysed (Y80, Y62) have similar mineralogies except that Y62 contains abundant tourmaline (25%) and therefore the anomaly is probably attributable to this mineral.

5.4 Calculation of the absolute composition of the removed melts

From their known compatible geochemistry, the femic elements such as Cr, Ni, Co, V, Ti, Fe, and Mg do not significantly enter early formed melts until very high temperatures are attained (e.g. Evans 1964, Wedepohl 1978) and therefore these elements can be used to ascertain the composition of melts derived from rocks suffered partial melting assuming, as an approximation, that none of these elements enter the melts initially. In this study, Cr, Ni and Co have been used to quantify the compositions of the melted out material from the contact hornfelses and pelitic xenoliths and comparisons between these

compositions are made. The mean 47 unhornfelsed rocks (13 from this work; 27 from Senior and Leake 1978; 7 from Leake 1958) is used in the calculations as a representative composition of the original pelites and semi-pelites prior to the hornfelsing processes for major elements but only the mean trace elements of the 13 samples analysed in this work are considered. Although this reduces the sample size it is preferable to adding the average of the 35 and 7 southern pelites published by Senior and Leake (1978) and Evans (1964) respectively in view of differences in their trace element contents especially Ni and Zr and which are probably due to differing analytical precisions and accuracies.

The calculations are performed in two steps : estimation of the degree of partial melting (P) and the compositions of the melts (M). The degree of partial melting is calculated by subtracting the mean of any femic element in the hornfelses or xenoliths from that in the country rocks and then dividing by its mean in the hornfelses or xenoliths. For instance the mean Cr in the regional pelites is 109 ppm, therefore a hornfels with 200 ppm has lost 45.2% of its original composition and a hornfels with 300 ppm has retained only 36.5% of its original composition and so forth. The melts compositions are estimated by assuming the composition of the unhornfelsed rocks equals the composition of the hornfelses or xenoliths plus that of the melts derived therefrom and therefore a simple mass-balance equation can be formulated :

If

$$i = \text{concentration of element } i$$

and

$$P = \text{degree of partial melting expressed as fraction of one}$$

then,

$$i_{\text{unhornfelsed rocks}} = i_M P + (1-P) i_{\text{hornfelses or xenoliths}} \quad 5.1$$

and hence

$$i_M = \frac{i_{\text{unhornfelsed rocks}} - (1-P) i_{\text{hornfelses or xenoliths}}}{P} \quad 5.2$$

Therefore if the degree of partial melting (P) and the concentration of any

element i in the regional pelites and hornfelses or xenoliths are known the compositions of the outgoing melts can be calculated and more importantly the order of fractionation of elements into the melts can be determined by simply varying the degrees of partial melting (see Table 5.5).

5.4.1 Results

The compositions of the liquid derived from the average of ten hornfelses and nine xenoliths (six from this work and three from Leake and Skirrow, 1960) are given in Table 5.4. Ten hornfelses; Y16-9, Y29, Y33, Y67, Y68, Y71, Y72 were chosen out of the 45 contact samples because they all occur near the contact of the intrusion, although the presence of inseparable quartzo-feldspathic veins and lenses and the abundance of secondarily pinitized cordierite, which always contains about 7% K_2O , indicates that Si and K must have been higher in the melts than it appears in the calculations.

The calculated degrees of partial melting expressed in percentages and the composition, CIPW norms, K_2O/Na_2O and mole $(Al_2O_3/(CaO+Na_2O+K_2O))$ ratios (hereafter called A/CNK) of the melts are presented in Table 5.4. From this table it can be seen that the hornfelses suffered partial melting between 33 % and 40% indicating that the xenolithic stages were probably reached after the country rocks had lost between 30% and 40% of their initial compositions. It is very interesting to note that the three elements yield similar melt compositions particularly those derived from the xenoliths (Table 5.4). The CIPW norms indicate that the melts are granitic in character and consist of almost equal proportions of normative quartz, normative orthoclase and normative (albite+anorthite).

Based on mineralogical and chemical criteria, Chappell and White (1974) classified granitic rocks into two types, I- and S-type granites. Those hornblende-bearing granites with normative diopside, low K_2O/Na_2O , metaluminous in the sense of Clarke (1981), *i.e.* A/CNK <1.0, high Fe^{+3}/Fe^{+2} and having accessory sphene and magnetite are termed I-type granites. In contrast, S-type granites are predominantly biotite and muscovite bearing rocks and having, normative corundum, high K_2O/Na_2O , peraluminous *i.e.* A/CNK >1.0, low Fe^{+3}/Fe^{+2} and accessory monazite, ilmenite, garnet and cordierite. From Table 5.4 it can be seen that the melts

derived from the metasediments (both the contact hornfels and xenoliths) have $A/CNK \geq 1.0$ (Figure 5.33) and normative corundum. The Fe^{+3}/Fe^{+2} is not numerically assessed but the sharp rise of Fe^{+3} relative to Fe^{+2} in the xenoliths indicates that the ratio Fe^{+3}/Fe^{+2} in the melts derived therefrom must have been very low. If Fe_{tot} is included in the calculations as Fe^{+2} , then accessory ilmenite would appear in the CIPW norms instead of rutile. Laouar (1987) showed that the ratio $K_2O:Na_2O$ shows the most fundamental chemical difference between S- and I-type granites of the Connemara granitic rocks. When the $K_2O:Na_2O$ ratios of the calculated melts are compared with values derived from the Galway and Oughterard granites and the Cashel microgranite sill, the calculated melts have very comparable $K_2O:Na_2O$ ratios with those of the Cashel microgranite sill which is an S-type granite, (Laouar 1987), but have significantly lower values than those of the Galway granite which is an I-type granite (Figure 5.32). The evidence therefore indicates that the granitic melts derived from the metasediments particularly from the xenoliths are S-type granites thus confirming the growing consensus that S-type granites are rocks produced by anatexis of metapelitic crustal material (*e.g.* Chappell and White 1974; Hine *et al.* 1978; White and Chappell 1977,1983)

From its known strongly compatible geochemistry, Cr is probably the most informative element and therefore has been used to study the detailed fractionation of the major and trace elements with the results of the calculations being shown in Table 5.5 and portrayed in terms of Harker-type diagrams in Figure 5.34 (A-H). In these diagrams, the wt% of the principal oxides of each analysed rock are plotted against the wt% of SiO_2 with the assumption being that silica percentage represents the stage of magmatic evolution that has been reached. However, the "sum effects" should be taken into account before reading petrogenetic significance into these diagrams (Chayes 1964). The sum-effects result from the fact that the major oxides taken together make up almost 100% of a rock analysis and since wt% SiO_2 is by far the most abundant constituent of most rocks, at least some negative correlations with SiO_2 are therefore expected among the other oxides irrespective of petrogenetic considerations. These effects are not noticeable in Figure 5.34 probably because only very few points are shown although the steep slope of Al_2O_3 versus SiO_2 may be due to these effects. When the melts

derived from the xenoliths and those calculated at various degrees of partial melting from Table 5.5 are plotted on Harker-type diagrams, it is clear from Figure 5.34 that TiO_2 , Al_2O_3 , MgO and to some extent Fe_{tot} decrease while the alkalis increase with increasing SiO_2 . At early stages of partial melting, high concentrations of SiO_2 were accompanied by low values of Mn but Mn increases with SiO_2 as partial melting rises.

The trends discussed above are in excellent agreement with magmatic fractional crystallization and therefore suggest that fractional melting of the metasediments was probably the most operative mechanism. Further support for this suggestion is discussed below.

Table 5.5 shows that the major elements were fractionated into the melts in the following order : $\text{Si} > \text{K} > \text{Na} > \text{Mn} > \text{Ca} > \text{Al} > \text{Mg} > \text{Fe}$ (P and TiO_2 are treated with the trace elements). If small amounts of Ca are subtracted from the average xenoliths to account for Ca coming in anorthitic plagioclase (probably added from the magma) and in secondary tourmaline (25% in the xenolith Y62), Ca would have entered the melt just after Na. The high values of Fe in the xenoliths (*i.e.* low concentrations in the melts) are due to Fe_2O_3 rather than to FeO ($\text{Fe}^{3+}/\text{Fe}^{2+} = 0.43$ in the country rocks compared to 0.93 in the xenoliths) which indicates that Fe (dominantly as Fe^{2+}) must have entered the melts much earlier than it appears in Table 5.5, probably with or just after TiO_2 . Therefore the final sequence becomes : $\text{Si} > \text{K} > \text{Na} > \text{Ca} > \text{Mn} > \text{Al} > \text{Fe} > \text{Mg}$.

The trace elements were fractionated in the outgoing fluid in the following way : $\text{Rb} > \text{Zr} > \text{Ba} > \text{P} > \text{Ti} > \text{Sr} > \text{Ga} > \text{Cr}, \text{Ni}, \text{Co}$.

Since the pioneer research of Bowen (*e.g.* Bowen 1928; Bowen *et al* 1935) followed by Tuttle and Bowen (1958), the order of crystallization of mafic and salic minerals in cooling magmas is known to be from Mg-rich to Fe-rich and from Ca-rich to Na- and K-rich respectively. This order coupled with the distribution coefficients of elements suggest the following fractional order (basic-->acidic) : $\text{Mg} > \text{Fe} > \text{Mn} > \text{Al} > \text{Ca} > \text{Na} > \text{K} > \text{Si}$. The position of Al is rather arbitrary and has been arranged before Ca because it is essential in forming plagioclase. It should be noted however that the mineral stability (or instability) is the major control on elements in magmas and not vice versa.

The trace elements are related to stability in mineral species versus

stability in magmas (i.e. compatibility is not absolute but related to the minerals crystallizing). The order of fractionation of the trace elements is therefore deduced from their relative degree of compatibility. Elements which have low distribution coefficients (<1) for common crystallizing minerals during extended stages of magmatic fractionation are termed incompatible elements as they are not incorporated in the crystals and the opposite is true for compatible elements. The distribution coefficients of elements have been reviewed by Irvine (1978) and summarized by Henderson (1982). As pointed out by Henderson (1982), the available distribution coefficients, usually derived from mineral-matrix pairs, sometimes show a wide scatter of results of any one element in a particular mineral pair. These variations are due to the dependence of the coefficients on T , P and the major element composition but also to analytical errors (Irving 1978). The order of fractionation of the trace elements is therefore, $Ni > Co > Cr > Ti > Zr > P > Sr > Ga > Ba > Rb$. Again the classification of Ga is arbitrary because no partition coefficients for this element could be found, although its tendency to be concentrated in feldspars and to some extent in micas and iron oxides justifies its position in the sequence. Moreover, Ga is impoverished in both Ca- and Na-rich plagioclase (Wedepohl 1978), suggesting that it is possibly incorporated in plagioclase after Sr.

The calculated order of fractionation of elements in the Cashel thermal aureole is compared to their order of fractionation in magmas in Figures 35-36. From Figure 5.35, it is clear that for the major elements, the only difference between magmatic and calculated order of fractionation resides in Al and Mn. In the calculations Al enters the melts after Mn but the early entry of K, Na and Ca compared to Mn and the tendency of these elements to form plagioclase indicates that these elements must have been accompanied by some Al and consequently a very good agreement between magmatic and calculated order of fractionation is suggested. The case of trace elements is more complex with Ti, P and Zr showing large disagreements (Figure 5.36). The reason for this is attributed to the small number of samples taken to represent the original south Connemara pelites (only 13 samples for trace elements), the gross inaccuracy of the calculations due to the large standard deviation of many trace elements and the poor definition of some partition coefficients, e.g. Zr. In magmas however, zircon, apatite and ilmenite and sphene can crystallize

before, with or after Mg-olivine and Ca-plagioclase (Read and Watson 1962) and therefore their order of fractionation in magmas is not fixed. If Zr, P and Ti are not considered assuming that they crystallize as accessory zircon, apatite and ilmenite and/or sphene respectively, the remaining trace elements show the same order of fractionation as in magmas (Figure 5.36a). The evidence therefore suggests that in the Cashel aureole, the elements fractionated into the melts in inverse order to their separation during magmatic crystallization indicating that fractional melting of the metasediments took place.

The order of fractionation of the REE into the melts is very difficult to define on account of the HREE being strongly controlled by the accessory minerals, the few samples analysed and the gross inaccuracy of the calculations for the trace elements. Despite these complications it is very interesting to note that the calculated compositions of the melts derived from the xenoliths always have *negative Eu anomalies* which strongly supports the *enrichment of Eu in the restites and xenoliths as being residual in character*. The Eu/Eu^* ratio rises insignificantly with increasing degree of partial melting then it tends to stop at higher temperatures (Table 5.5) indicating that Eu would be dominantly enriched in the residual fractions compared to the liquid. The low Eu/Eu^* ratio in the melts indicates lower oxidizing conditions in the outgoing liquid compared to the xenoliths.

5.5 Partial melts and the Cashel microgranite sill

In the foregoing sections, it has been shown that the emplacement of the Cashel-Lough Wheelaun intrusion caused intense hornfelsing, mobilization and partial melting of the metasediments. The calculations performed in subsection 5.4 showed that the composition of the material left in the metasediments was granitic in composition and agrees well with S-type granites as defined by Chappell and White (1974). The question which arises is where have these granitic melts migrated to?

Leake (1970) proposed that the microcline-rich microgranite sill, traceable along the northern edge of Cashel Hill part of the intrusion (Figure 5.1) represents the segregation of liquid derived from the partially melted metasediments along a curved surface of decollement during the southerly displacement of the Cashel body. The sill, which extends for over a kilometer in

a northeasterly direction, varies in width from a few metres to over ten metres and it is displaced in places by subsequent faulting. Leake (1970) also favourably compared the major elements of the granitic sill with the average composition of the melts derived from four pelitic xenoliths calculated by Leake and Skirrow (1960) and Evans (1964). In these calculations, the representative composition of the country rocks was derived from the average of seven samples only. Moreover, Leake (1970) compared the composition of the material melted out of four xenoliths with one granitic sill analysis only and therefore the effects of the sample size on the calculations must have been significant.

In the present study, the average of 47 country rocks is taken to represent the south Connemara pelites and the melt compositions are derived from the average of nine pelitic xenoliths and compared to seven granitic sill analyses. The major elements recalculated to 100% on a water-free basis, the CIPW norms and the trace elements, including REE, of the granitic sill and calculated melts are compared in Table 5.6. Clearly, the results are enigmatic in that the microgranite and melts have almost the same compositions even in their trace element contents. Particularly different is the systematically lower Sr contents in the calculated melts compared to the microgranite sill and this is almost certainly due to the addition of Sr in plagioclase from the magma to the xenoliths which has not been taken into account in the calculations. Cr is higher in the microgranite compared to the melts derived using Ni and Cr because it has been assumed that none of these elements enter the melt which is clearly not perfectly correct although the substantially low contents of Cr, Co and Ni in the microgranite sill do not significantly affect the assumption that these elements remain in the crystal phases.

REE in the melts, calculated using Cr only, are significantly different from those of the microgranite sill probably because of the small number of samples analysed and the inaccuracy of the calculations. However, it is very interesting to note that the granite sill has a negative Eu anomaly as predicted from the calculations (Table 5.6) hence supporting the interpretation that the sill represents the melts derived from the contact hornfels and pelitic xenoliths.

As expected, the CIPW norms of the microgranite sill and calculated melts show very good agreement with each other. The melts and so the microgranite

sill can be seen to consist of very similar proportions of normative quartz, normative orthoclase and normative plagioclase (albite+anorthite) with small amounts of normative corundum, hypersthene and apatite, consistent with the mineralogy of the microgranite sill which is composed of approximately equal proportions of euhedral quartz, euhedral^{to}subhedral plagioclase and microcline with small quantities of chloritized biotite and accessory apatite, zircon, allanite, muscovite, ilmenite rarely sphene.

The A/CNK and $K_2O:Na_2O$ ratios of the calculated melts also agree very well with those of the granitic sill (Table 5.6) and both agree with S-type granites. The sample analysed by Leake (1970) seems different from the other samples by having relatively lower normative quartz, higher normative hypersthene, normative sphene instead of corundum and significantly low A/CNK (Table 5.6).

In summary, the chemistry and mineralogy as deduced from the CIPW norms of the material melted out of the xenoliths and those of the Cashel granite sill agree excellently with each other but more importantly all agree with S-type granites as defined by Chappell and White (1974), consistent with conclusions deduced from S isotope studies (Laouar 1987). Consequently, no reasonable doubt remains that the Cashel microgranite sill represents the segregated material derived from the melting of the Cashel metasediments thus supporting Leake (1970).

5.6 Discussion

The behaviour of the major and trace elements in the Cashel Hill aureole is significantly affected by retrograde reactions and migmatization of the pelites. Despite these complications the chemical changes described above show a number of interesting features. With increasing degree of hornfelsing, the elements Si, K, Na, Ca, P, and to a lesser extent Mn were removed from the envelope hornfelses and xenoliths in varying amounts but in contrast Fe and Mg were significantly enriched in them. Al and Ti were both removed and enriched and at very high degrees of partial melting, small amounts of Fe and Mg have also left the crystal fractions.

The major and trace elements were probably strongly controlled by the mineralogy because both the mineralogical and chemical changes are consistent with the melting of an essentially granitic magma, i.e. quartz, K-feldspar and

sodic plagioclase as shown by the norms in Table 5.4. Although badly modified by late sericitization of plagioclase, garnet and biotite and pinitization of cordierite, K decreases dramatically in the xenoliths as the result of the partial decomposition of biotite to sillimanite, cordierite and garnet without forming K-feldspar presumably because K-feldspar was unstable. Na and Ca also decrease as the contact of the intrusion is approached but Ca generally enters the liquid phase in small amounts at the beginning and in increasing amounts at higher temperatures, consistent with the fractional solution of sodic and then more calcic plagioclase. The losses of Si, K, Na and Ca must have been accompanied by Al to form (K-Na-Ca) feldspars. However Al is both removed and enriched, because it is removed in smaller proportions than it occurs in the country rocks and therefore increases in the residue while being removed because much more silica is removed than Al_2O_3 (Table 5.5). Ti rises in some xenoliths but declines in others and perhaps this variable behaviour of Ti is related to ilmenite stability. However, Table 5.5 shows that Ti enters the melts almost as early as Al suggesting that small amounts of Ti probably left the system during the early decomposition of biotite.

The relative increase of Fe and Mg is attributed to the losses of the silic elements, although above 50% partial melting both elements enter the outgoing liquid and this is possibly caused by the decomposition of Mg-biotite, cordierite and ilmenite although much Fe and Mg is left in spinel, magnetite and orthopyroxene.

The significant losses of the major elements Si, K, Na, Ca, Mn, P and Al were accompanied by Rb, Ba, Zr, Sr and to some extent Ga. Sr and Ga left the crystal fractions at degrees of partial melting of between 56% and 63% and it is very interesting to note that they were both fractionated into the melts after Ca and Al respectively (Table 5.5).

The femic elements Cr, Ni and Co are between three and four times higher in the xenoliths than in the country rocks and are retained in spinel, magnetite, ilmenite and orthopyroxene. The three elements remain in the crystal fractions even at a degree of partial melting of 71%.

The order of fractionation of elements into the melts has been calculated and compared to the order of fractionation of elements concerned in magmas as deduced from the literature and experimental evidence. It has been found that

the major elements and most of the trace elements fractionated into the melts opposite to their behaviour in natural magmas and therefore fractional melting of the metasediments is suggested as the dominant process of melting of the country rocks, consistent with conclusions reached from Harker-type diagrams.

The granitic melts derived from the metasediments agree excellently with S-type granites as defined by Chappell and White (1974). More interestingly, the composition of the melts calculated using Cr, Ni and Co and the composition of the Cashel microgranite sill show excellent agreement with each other even in their trace element contents (REE not included) and both (i.e. the microgranite and melts), agree with S-type granites, consistent with conclusions reached from S isotopes (Laouar 1987). These similarities indicate that the microgranite represents the material melted out of the metasediments, a conclusion supported by the high $^{87}\text{Sr}/^{86}\text{Sr}$ of the granitic sill, Jagger (1985).

All REE fractionated into the melt but at variable relative proportions. Their order of fractionation is difficult to define for reasons already mentioned but the combination of the calculated melts coupled with their behaviour in the hornfelses and xenoliths suggest the following remarks : At early stages of partial melting the LREE(La-Nd) entered the melts accompanied by small amounts of Sm, Eu, Gd, MREE (Dy-Er) and HREE (Yb-Lu). The significant loss of HREE is possibly related to the beginning of metamorphic recrystallization of detrital brown zircons and melting of apatite (Chapter 7). At more advanced stages, LREE were still enriched in the melts but Sm and Gd were fractionated into the liquid in significant amounts compared to Eu giving positive Eu anomalies. At the xenolithic stage, the melting of zircon and apatite resulted in a dramatic loss of MREE and HREE from the crystal fractions but some LREE were possibly retained in Mg-rich and/or relict biotites thus giving very high $(\text{La}/\text{Lu})_{\text{CN}}$ ratios.

5.7 Conclusions

During the hornfelsing of the metasediments around the Cashel-Lough Wheelaun intrusion, major and trace elements behaved in very systematic ways. Those elements which are commonly enriched in basic rocks viz.: Fe, Mg, Cr, Ni and Co largely remained in the crystal fractions while those elements commonly enriched in acidic rocks viz.: Si, K, Na, P, Rb, Ba and to some extent Zr were fractionated into the melts. Those elements which are intermediate in character viz.: Al, Ti, Ca, Ga and Sr are both enriched and removed. More importantly, the melt compositions extracted from the contact hornfels and pelitic xenoliths show that most of the major elements were fractionated into the liquid according to the composition of granitic melts which agree with that of the Cashel microgranite and both agree with S-type granites; thus indicating that the granitic sill probably represents the material left the partially melted metasediments.

The major and trace elements studied coupled with the Rb:K, Ba:K and Sr:Ca ratios agree excellently with the fractionation of elements in magmas and hence support the fractional melting model of the metasediments proposed by Evans (1964).

REE were removed from the hornfels and xenoliths in considerably different amounts. Eu entered the melts in small amounts compared to Sm and Gd and probably also to the other REE thus giving positive Eu anomalies in the more partially melted rocks. The major control of accessory minerals on the HREE strongly affected their behaviour during partial melting of the metasediments severely restricting comparisons of REE in the aureole with magmatic differentiation.

Table 5.1 Comparison of the Cashel Formation pelites with various shale compositions.

	U	S	S&L	S	C	K	T&M
Major elements(wt%)							
SiO ₂	56.55	4.24	54.32	5.95	60.15	61.6	62.8
TiO ₂	1.21	0.21	1.31	0.39	0.26	1.0	1.0
Al ₂ O ₃	19.19	2.51	19.85	3.44	16.45	18.3	18.9
Fe ₂ O ₃	1.25	0.63	2.55	1.31	4.04	- - -	- - -
FeO	7.30	1.21	6.79	3.01	2.9	7.4	6.5
MnO	0.15	0.04	0.24	0.17	- - -	0.13	0.11
MgO	2.75	0.58	3.52	1.07	2.32	2.7	2.2
CaO	1.84	0.88	1.93	1.15	1.41	4.2	1.3
Na ₂ O	2.86	0.90	2.01	0.76	1.10	1.1	1.2
K ₂ O	3.50	1.35	3.92	1.19	3.6	3.4	3.7
P ₂ O ₅	0.19	0.11	0.21	0.11	0.15	0.22	0.16
	U	S	S&L	S	T&W	K	T&M
Trace elements(ppm)							
Rb	117	39	187	67	140	140	160
Ba	891	404	1242	719	580	580	650
Zr	272	46	289	86	160	200	210
Sr	242	64	264	164	300	450	200
Ga	27	5	30	6	19	19	20
Ni	48	11	87	31	68	95	55
Co	24	7	30	9	19	20	23
Cr	109	12	97	45	90	100	110
Pb	23	11	55	30	- - -	20	20
Zn	115	19	174	60	- - -	80	85
Cu	29	19	67	89	- - -	57	50

U = average of 13 unhornfelsed pelites analysed in this work

S&L = average of 35 pelites from senior and Leake (1978)

T&M = average of 23 pelites from Taylor and McLennan (1985)

C = average of 50 Palaeozoic pelites from Clarke (1924)

K = representative continental crust analyses taken from Krauskopf (1967).

T&W = data taken from Turekian and Wedepohl (1961)

S = standard deviations

--- = not determined

Table 5.2 Summary statistics of the REE in the Connemara pelites and hornfelses. REE contents of some shales from the literature are also given.

	U	S	H	S	X	S	XG	NZG
La	66.53	15.04	49.07	17.37	18.78	4.93	26.11	32.16
Ce	130.91	30.14	91.86	25.66	29.59	8.47	61.23	73.65
Pr	16.12	4.16	10.92	3.85	3.02	0.85	7.79	9.17
Nd	61.51	12.83	40.90	17.03	11.74	3.42	35.36	41.93
Sm	10.38	2.33	6.21	2.90	1.44	0.44	6.26	7.77
Eu	2.11	0.25	1.52	0.56	0.77	0.13	1.21	1.91
Gd	8.77	2.07	5.04	2.39	1.04	0.36	5.07	6.39
Dy	7.54	1.66	4.03	2.12	0.49	0.11	3.51	4.63
Hb	1.73	0.40	0.91	0.50	0.09	0.02	0.74	1.04
Er	4.86	1.17	2.61	1.36	0.39	0	2.08	2.73
Yb	4.23	0.99	2.57	1.14	0.21	0.02	1.48	2.10
Lu	0.61	0.14	0.41	0.16	0.03	0	0.21	0.30

Σ REE	315.30	38.31	216.05	27.14	67.59	9.12	151.05	183.78
Eu/Eu*	0.71	0.17	1.13	0.73	2.02	0.30	0.65	0.82
(La/Lu)CN	11.24	0.82	12.64	1.62	65.59	17.22	12.91	11.13

	PAAS	NAMSC	ESC	
La	38	34	41.1	U = average of 4 unhornfelses pelites
Ce	80	73.8	81.3	H = average of 6 hornfelses
Pr	8.9	8.2	10.4	X = average of 2 pelitic xenoliths
Nd	32	35	40.1	XG = 1 xenolithic metagabbro (J2 = Jagger 1985)
Sm	5.6	6.05	7.3	NXG = 1 non-xenolithic metagabbro (GJ009 Jenkin)
Eu	1.1	1.51	1.52	PAAS = Post Archean Australian shales
Gd	4.7	5.70	6.03	NAMSC = North America metamorphic shales composite
Dy	4.4	- - -	---	ESC = European shales composite
Hb	1.0	1.12	1.20	
Er	2.9	3.30	3.55	
Yb	2.8	2.71	3.29	
Lu	0.43	0.41	0.58	

Σ REE	183	171.9	204
Eu/Eu*	0.66	0.78	0.70
(La/Lu)CN	9.17	8.60	7.35

Table 5.3 Summary statistics of the major and trace elements in the Connemara pelites and hornfelses. (S = standard deviation)

	U	S	I	S	C	S	X	S
SiO ₂	54.90	5.62	55.87	5.47	48.84	7.85	19.95	9.51
TiO ₂	1.28	0.36	1.15	0.38	1.55	0.56	2.34	1.48
Al ₂ O ₃	19.69	3.34	19.08	2.61	22.72	5.14	35.08	9.43
Fe ₂ O ₃	2.19	1.30	1.58	0.44	2.49	1.61	12.10	5.25
FeO	6.92	2.67	7.06	1.45	9.03	2.65	13.60	4.16
MnO	0.22	0.16	0.16	0.07	0.17	0.07	0.17	0.06
MgO	3.31	1.03	3.29	0.61	4.19	1.39	7.14	2.07
CaO	1.93	1.07	1.51	0.52	1.34	1.33	2.84	3.39
Na ₂ O	2.24	0.92	2.50	1.00	1.33	0.72	1.06	1.00
K ₂ O	3.78	1.23	3.89	1.58	3.47	1.39	0.87	0.65
P ₂ O ₅	0.20	0.19	0.13	0.10	0.10	0.07	0.04	0.02
Rb	117	39	134	39	115	35	35	15
Ba	891	404	901	302	1057	375	680	20
Zr	272	46	236	69	259	85	120	43
Sr	242	64	203	64	154	89	596	386
Ga	27	5	27	4	33	8	74	20
Ni	48	11	57	13	72	22	173	59
Co	23	7	23	8	33	10	101	28
Cr	109	11	125	21	151	52	388	158
Pb	23	11	23	9	16	8	4.84	3
Zn	115	20	134	25	157	45	575	286
Cu	29	19	34	30	73	155	85	28
Rbx10 ⁻⁴ :K								
	0.00348		0.00322		0.00317		0.00337	
Bax10 ⁻⁴ :K								
	0.02556		0.02413		0.03022		0.06450	
Srx10 ⁻⁴ :Ca								
	0.01527		0.01756		0.03263		0.02496	
Niggli mg	0.40		0.41		0.40		0.35	
Niggli alk	15.23		16.56		10.94		2.99	
Niggli w	0.25		0.18		0.21		0.46	

U = mean unhornfelses pelites (47 for major elements, 13 for trace elements)

I = mean intermediate hornfelses (17 for both trace and major elements)

C = mean contact hornfelses (45 for major elements, 34 for trace elements)

X = mean xenoliths (9 for major elements, 6 for trace elements)

Table 5.4 Calculated degrees of partial melting and compositions of the melts removed from 10 contact hornfelses and 9 xenoliths. CIPW norms, A/CNK, and K₂O/Na₂O ratios are also given.

	Cr(ppm)			Ni(ppm)			Co(ppm)								
	U	H	X	P(H)	P(X)	U	H	X	P(H)	P(X)	U	H	X	P(H)	P(X)
	109	162	388	33.5	71.9	48	80	173	40	42.2	23	36	101	35.1	77.2
Major elements (wt%).															
	M(H)					M(X)									
	U	C	X	Co	Ni	Cr	U	C	X	Co	Ni	Cr			
SiO ₂	56.70	51.96	20.63	65.47	63.81	66.11	67.34	70.5	7	70.77					
TiO ₂	1.33	1.47	2.42	1.07	1.12	1.05	1.01	0.91	0.90						
Al ₂ O ₃	20.33	22.00	36.28	17.24	17.82	17.03	15.62	14.21	14.02						
Fetot	9.59	12.59	28.14	4.05	5.08	3.63	4.12	2.46	2.34						
MnO	0.23	0.17	0.17	0.34	0.32	0.35	0.25	0.25	0.25						
MgO	3.42	4.33	7.39	1.74	2.06	1.61	2.25	1.89	1.87						
CaO	1.99	1.88	2.94	2.19	2.16	2.20	1.71	1.62	1.62						
Na ₂ O	2.31	2.01	1.09	2.86	2.76	2.90	2.67	2.78	2.80						
K ₂ O	3.90	3.49	0.90	4.66	4.52	4.72	4.78	5.05	5.07						
P ₂ O ₅	0.20	0.10	0.04	0.38	0.35	0.40	0.25	0.26	0.26						
Total	100	100	100	100	100	100	100	100	100						

contd

Table 5.4 continued

Trace elements (ppm)	M(H)			M(X)					
	U	C	X	Co	Ni	Cr	Co	Ni	Cr
Cr	109	164	388	7	28	0	23	1	0
Ni	48	80	173	0	0	0	8	0	0
Co	24	37	101	0	0	0	0	6	0
Ga	27	35	740	12	15	11	13	9	9
Sr	242	237	596	251	249	252	132	104	102
Zr	272	252	120	309	302	311	320	332	332
Ba	891	1047	658	603	657	581	964	982	983
Rb	117	103	35	143	138	145	143	149	150
CIPW norms									
Quartz				24.78	23.74	25.19	27.20	29.52	29.55
Orthoclase				27.54	26.71	27.89	28.25	29.84	29.96
Albite				24.19	23.35	24.53	22.59	23.52	23.69
Anorthite				8.38	8.43	8.330	6.85	6.34	6.34
Hypersthene				4.33	5.13	4.01	5.60	4.70	4.65
Apatite				0.88	0.81	0.93	0.58	0.60	0.60
Corundum				4.42	5.30	4.11	3.54	1.84	1.70
Rutile				1.07	1.12	1.05	1.01	0.91	0.90
A/CNK*				1.26	1.33	1.23	1.23	1.11	1.09
K ₂ O/Na ₂ O				1.63	1.64	1.63	1.79	1.82	1.81

contd

Table 5.4 continued

- U = mean unhornfelsed pelites (47 for major elements, 13 for trace elements)
 H = mean contact hornfelses (10 for both major and trace elements)
 X = mean xenoliths (9 for major elements, 6 for trace elements)
 P(H) = calculated degrees of partial melting using H and U (i.e. mean 13 pelites and 34 hornfelses)
 P(X) = calculated degrees of partial melting obtained using X and U (i.e. mean 13 pelites and 6 xenoliths)
 M(H) = composition of the melts extracted from 10 hornfelses calculated using P(H)
 M(X) = composition of the melts extracted from 9 xenoliths calculated using P(X)

The trace elements Co, Ni and Cr are quoted to show which element was used in the calculations.

Fe_{tot} as Fe₂O₃

A/CNK* = mole[Al₂O₃/(CaO + Na₂O + K₂O)]

Note that the CIPW norms, A/CNK, and K₂O/Na₂O ratios are calculated for the melts only.

Table 5.5 Fractionation of the major and some of the trace elements including the REE with increasing degrees of partial melting (calculated using Cr).

	U	X	P=0.27	P=0.45	P=0.56	P=0.63	P=0.69	P=0.71
Major elements (wt %)								
SiO ₂	56.70	20.63	91.38	87.99	84.06	76.87	73.67	70.77
TiO ₂	1.33	2.42	0	0	0.45	0.68	0.82	0.90
Al ₂ O ₃	20.33	36.28	0	0.72	4.22	10.81	12.83	14.12
Fetot	9.59	28.14	0	0	0	0	0.86	2.34
MnO	0.23	0.17	0.23	0.27	0.26	0.26	0.26	0.25
MgO	3.42	7.39	0	0	0.29	1.08	1.55	1.87
CaO	1.99	2.94	0	0.72	1.19	1.41	1.54	1.62
Na ₂ O	2.31	1.09	3.90	3.33	3.17	2.99	2.88	2.80
K ₂ O	3.90	0.90	7.12	6.62	6.05	5.60	5.32	5.07
P ₂ O ₅	0.20	0.04	0.37	0.35	0.32	0.30	0.27	0.26
Total	100	100	100	100	100	100	100	100
Trace elements (ppm)								
Cr	109	388	0	0	0	0	0	0
Ni	48	173	0	0	0	0	0	0
Co	23	101	0	0	0	0	0	0
Ga	27	74	0	0	0	0.81	6	9
Sr	242	596	0	0	0	38	80	102
Zr	272	120	685	457	391	360	342	332
Ba	891	658	1525	1174	1073	1026	998	983
Rb	117	35	340	217	181	165	155	150
REE (ppm)								
La	66.5	18.8	196.1	124.5	103.8	94.0	88.3	85.3
Ce	130.9	29.6	405.9	253.8	210.0	189.2	177.1	170.8
Pr	16.1	3.0	51.6	32.0	26.3	23.6	22.1	21.2
Nd	51.5	11.7	196.5	151.9	10.3	90.1	84.2	67.2
Sm	10.4	1.4	34.6	21.2	17.3	15.5	14.4	13.9
Eu	2.1	0.8	2.7	3.7	3.1	2.9	2.7	2.6
Gd	8.7	1.0	29.7	18.1	14.8	13.2	12.3	11.8
Dy	7.5	0.5	26.6	16.1	13.0	11.6	10.7	10.3
Hb	1.7	0.09	6.2	3.7	3.0	2.6	2.4	2.3
Er	4.8	0.4	20.0	10.3	8.3	7.4	6.9	6.6
Yb	4.2	0.2	15.1	9.1	7.3	6.5	6.0	5.8
Lu	0.6	0.03	2.2	1.3	1.0	0.9	0.8	0.8
Eu/Eu*	0.71	2.02	0.55	0.58	0.60	0.61	0.62	0.62
(La/Lu) _{CN}	11.24	65.59	9.33	9.86	10.16	10.38	10.53	10.67

Table 5.5 continued

P = degree of partial melting expressed as fraction of one.

U and X as in Table 5.4 except that the average of the REE was obtained from 4 unhornfelsed rocks and 2 xenoliths only.

Note that the calculated compositions are always from P = 0 to the degree of partial melting stated (i.e. P = 0 to P = 27, P = 0 to P = 45 and so on).

Sample	U	X	P	Other
1	1.00	1.00	0.00	
2	1.00	1.00	0.00	
3	1.00	1.00	0.00	
4	1.00	1.00	0.00	
5	1.00	1.00	0.00	
6	1.00	1.00	0.00	
7	1.00	1.00	0.00	
8	1.00	1.00	0.00	
9	1.00	1.00	0.00	
10	1.00	1.00	0.00	
11	1.00	1.00	0.00	
12	1.00	1.00	0.00	
13	1.00	1.00	0.00	
14	1.00	1.00	0.00	
15	1.00	1.00	0.00	
16	1.00	1.00	0.00	
17	1.00	1.00	0.00	
18	1.00	1.00	0.00	
19	1.00	1.00	0.00	
20	1.00	1.00	0.00	
21	1.00	1.00	0.00	
22	1.00	1.00	0.00	
23	1.00	1.00	0.00	
24	1.00	1.00	0.00	
25	1.00	1.00	0.00	
26	1.00	1.00	0.00	
27	1.00	1.00	0.00	
28	1.00	1.00	0.00	
29	1.00	1.00	0.00	
30	1.00	1.00	0.00	
31	1.00	1.00	0.00	
32	1.00	1.00	0.00	
33	1.00	1.00	0.00	
34	1.00	1.00	0.00	
35	1.00	1.00	0.00	
36	1.00	1.00	0.00	
37	1.00	1.00	0.00	
38	1.00	1.00	0.00	
39	1.00	1.00	0.00	
40	1.00	1.00	0.00	
41	1.00	1.00	0.00	
42	1.00	1.00	0.00	
43	1.00	1.00	0.00	
44	1.00	1.00	0.00	
45	1.00	1.00	0.00	
46	1.00	1.00	0.00	
47	1.00	1.00	0.00	
48	1.00	1.00	0.00	
49	1.00	1.00	0.00	
50	1.00	1.00	0.00	

Table 5.6 Comparison of the calculated composition of the melts derived from 9 xenoliths with 7 analyses of the Cashel microgranite sill.

Major elements (wt%)	M(X)									
	L	JM	JM	LR	LR	Y21	Y56	Co	Ni	Cr
SiO ₂	68.09	69.73	70.76	70.15	69.28	69.16	69.44	67.34	70.57	70.77
TiO ₂	0.59	0.60	0.59	0.55	0.60	0.63	0.60	1.01	0.91	0.90
Al ₂ O ₃	14.40	14.81	14.31	15.01	15.04	15.31	14.99	15.62	14.21	14.12
Fetot	3.03	2.94	3.89	2.89	2.95	2.97	3.00	4.12	2.46	2.34
MnO	0.20	1.30	1.27	0.03	0.03	0.03	0.04	0.25	0.25	0.25
MgO	2.43	1.30	1.27	1.27	1.44	1.50	1.45	2.25	1.89	1.87
CaO	2.12	1.50	1.38	1.35	2.32	1.91	2.47	1.71	1.62	1.62
Na ₂ O	3.21	2.74	2.54	3.36	3.01	3.04	2.88	2.67	2.78	2.80
K ₂ O	5.68	4.90	4.81	5.13	5.08	5.24	4.91	4.78	5.05	5.07
P ₂ O ₅	0.26	0.18	0.18	0.26	0.25	0.21	0.22	0.25	0.26	0.26
Total	100	100	100	100	100	100	100	100	100	100

Trace elements (ppm)	M(X)						
	Co	Ga	Sr	Zr	Ba	Rb	Cr
Cr	-	-	221	209	-	-	0
Ni	-	-	-	372	-	-	0
Co	-	-	-	825	-	-	0
Ga	-	-	-	157	-	-	9
Sr	-	208	223	209	-	-	104
Zr	-	-	359	372	-	-	332
Ba	-	-	820	825	-	-	982
Rb	-	149	141	157	-	-	149

contd

Table 5.6 continued

CIPW norms	M(X)									
	L	JM	JM	JM	LR	LR	Y21	Y56	Co	Ni
Quartz	20.41	30.39	33.23	26.91	25.91	25.68	27.06	27.20	29.52	29.55
Orthoclase	33.56	28.96	28.42	30.31	30.02	30.96	29.01	28.25	29.84	29.96
Albite	27.15	23.18	21.48	28.42	25.46	25.72	24.36	22.59	23.52	23.69
Anorthite	8.10	6.27	4.67	5.00	9.87	8.10	10.81	6.85	6.34	6.34
Hypersth.	6.02	3.23	3.16	3.16	3.58	3.73	3.61	5.60	4.70	4.65
Apatite	0.60	0.41	0.42	0.60	0.58	0.49	0.51	0.58	0.60	0.60
Corundum	0	2.70	2.84	2.10	0.97	1.67	0.97	3.54	1.84	1.70
Rutile	0.38	0.60	0.59	0.55	0.60	0.63	0.60	1.01	0.91	0.90
Sphene	0.50	0	0	0	0	0	0	0	0	0
A/CNK*	0.94	1.19	1.21	1.12	1.03	1.09	1.04	1.23	1.11	1.09
K ₂ O/Na ₂ O	1.58	1.79	1.89	1.53	1.69	1.72	1.71	1.79	1.82	1.81

contd

Table 5.6 continued

	Y21	M(X)1
La	45.61	85.33
Ce	99.05	170.80
Pr	10.80	21.27
Nd	45.04	67.17
Sm	7.08	13.90
Eu	1.52	2.63
Gd	5.22	11.81
Dy	2.86	10.31
Hb	0.58	2.37
Er	1.64	6.61
Yb	1.06	5.81
Lu	0.18	0.83
Eu/Eu*	0.76	0.62
(La/Lu)CN	26.33	10.67

L = one analysis given in Leake (1970)

JM = two analyses given in Jagger (1985)

LR = two analyses given in Laouar (1987)

Y = two analyses, this work

- = not determined

M(X) and A/CNK* as in Table 5.4

M(X)1 = composition of the melt derived from two pelitic xenoliths

Table 5.6 continued

	Y21	M(X)1
La	45.61	85.33
Ce	99.05	170.80
Pr	10.80	21.27
Nd	45.04	67.17
Sm	7.08	13.90
Eu	1.52	2.63
Gd	5.22	11.81
Dy	2.86	10.31
Hb	0.58	2.37
Er	1.64	6.61
Yb	1.06	5.81
Lu	0.18	0.83
Eu/Eu*	0.76	0.62
(La/Lu)CN	26.33	10.67

L = one analysis given in Leake (1970)

JM = two analyses given in Jagger (1985)

LR = two analyses given in Laouar (1987)

Y = two analyses, this work

- = not determined

M(X) and A/CNK* as in Table 5.4

M(X)1 = composition of the melt derived from two pelitic xenoliths

KEY TO FIGURES 5.1-36a

Figures 5.1-20 Scatter diagrams of the Connemara unhornfelses pelites

- Figure 5.1 Al_2O_3 vs Fetot
- Figure 5.2 TiO_2 vs Fetot
- Figure 5.3 TiO_2 vs Al_2O_3
- Figure 5.4 Ga vs Al_2O_3
- Figure 5.5 Al_2O_3 vs U
- Figure 5.6 Al_2O_3 vs Th
- Figure 5.7 Ni vs Fetot
- Figure 5.8 Co vs TiO_2
- Figure 5.9 Cr vs TiO_2
- Figure 5.10 Zr vs TiO_2
- Figure 5.11 Sr vs TiO_2
- Figure 5.12 Sr vs CaO
- Figure 5.13 Sr vs Na_2O
- Figure 5.14 Rb vs K_2O
- Figure 5.15 Ba vs K_2O
- Figure 5.16 K_2O vs TiO_2
- Figure 5.17 Rb vs TiO_2
- Figure 5.18 Ba vs TiO_2
- Figure 5.19 Rb vs $\text{CaO} + \text{Na}_2\text{O}$
- Figure 5.20 Ba vs $\text{CaO} + \text{Na}_2\text{O}$

Figure 5.21 REE distribution patterns in the unhornfelses pelites

Figure 5.22-6 Scatter diagrams of the regional pelites, hornfelses and pelitic xenoliths

- Figure 5.22 CaO vs Na_2O
- Figure 5.23 P_2O_5 vs CaO
- Figure 5.24 Zr vs TiO_2
- Figure 5.25 Niggli al vs Niggli fm
- Figure 5.26 K_2O vs Rb

Figure 5.27 REE distribution patterns in the hornfelses

Figure 5.28 REE distribution patterns in the pelitic xenoliths

Figure 5.29 REE distribution patterns in the metagabbros

Figure 5.30 Comparison of REE distribution patterns of the unhornfelsed pelites with hornfelses and pelitic xenoliths

Figure 5.31 (A-D) Scatter diagram of Lu versus Zr and P_2O_5 and Eu versus Sr and CaO in the analysed unhornfelsed pelites, hornfelses, pelitic xenoliths and migmatite leucosomes.

A: Lu vs Zr

B: Lu vs P_2O_5

C: Eu vs Sr

D: Eu vs CaO

Figure 5.32 Scatter diagram of Na_2O vs K_2O for the Galway, Oughterard granites, Cashel microgranite sill and calculated melts derived from 10 contact hornfelses and 9 pelitic xenoliths.

Figure 5.33 Mole A/CNK vs SiO_2 for the granites and melts stated above in Figure 5.32.

Figure 5.34 (A-H) Harker-type diagrams of TiO_2 , Al_2O_3 , MgO, CaO, Fe_2O_3 , MnO, Na_2O and K_2O respectively for the calculated melts.

Figure 5.35 Order of fractionation of the major elements in magmas versus calculated order of fractionation of the same elements in the Cashel thermal aureole.

Figure 5.36 Order of fractionation of trace elements in magmas versus calculated order of fractionation of the same elements in the Cashel thermal aureole.

Figure 5.36a The same as Figure 5.36 but excluding Ti, P and Zr.

fig 5.1

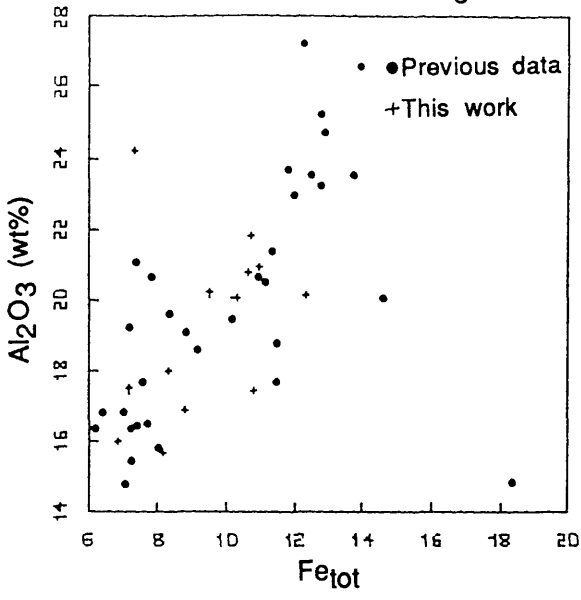


fig 5.2

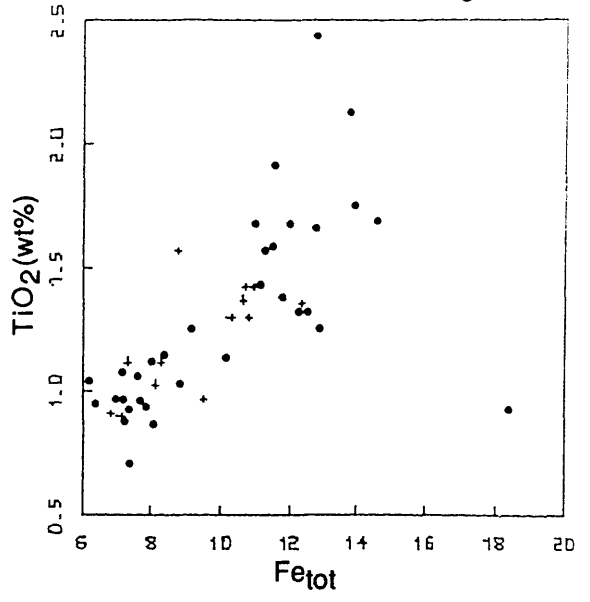


fig 5.3

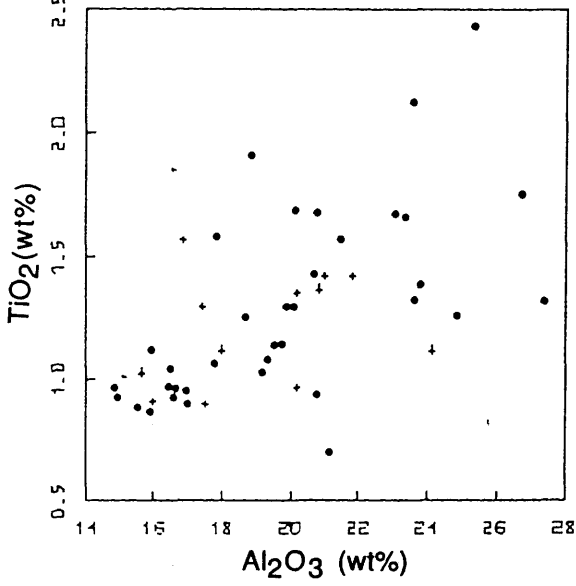


fig 5.4

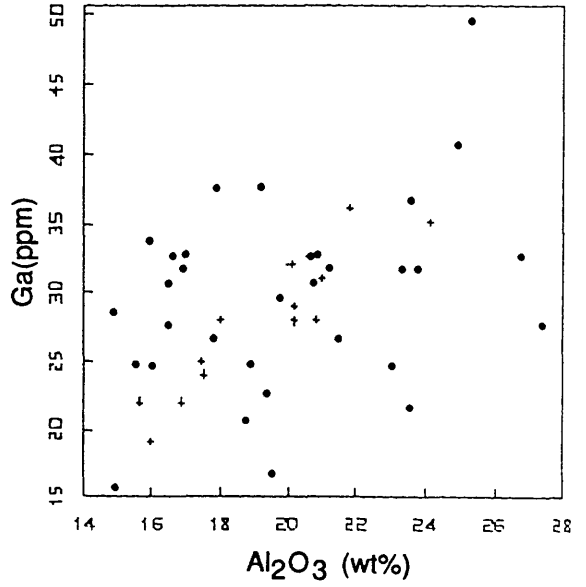


fig 5.5

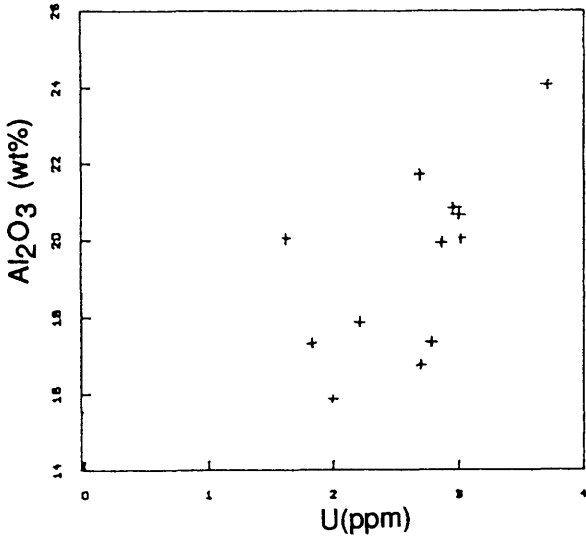


fig 5.6

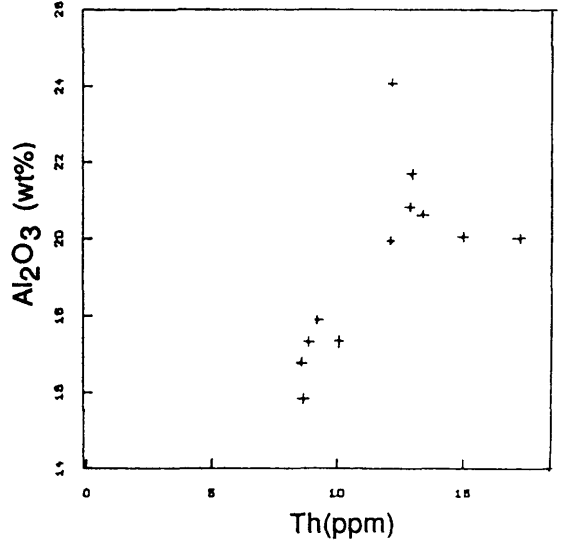


fig 5.7

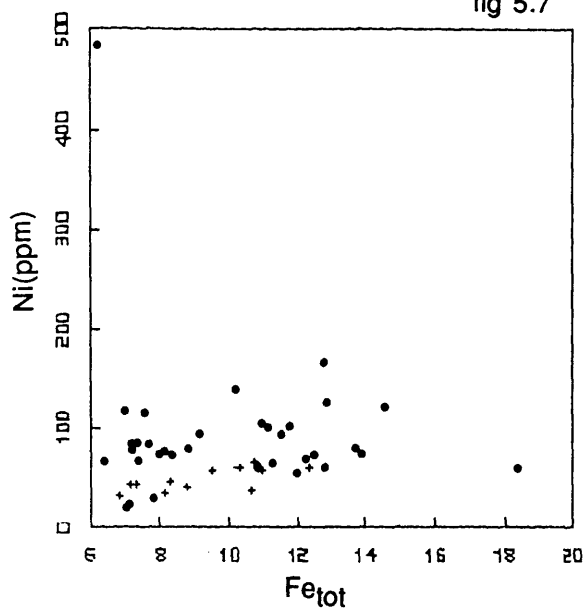


fig 5.8

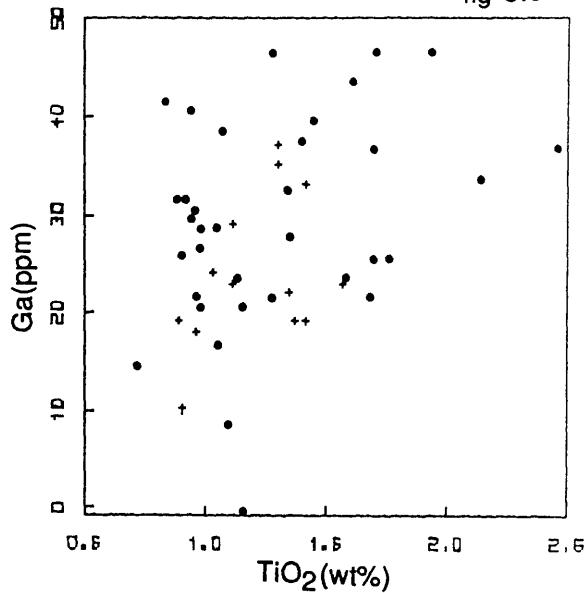


fig 5.9

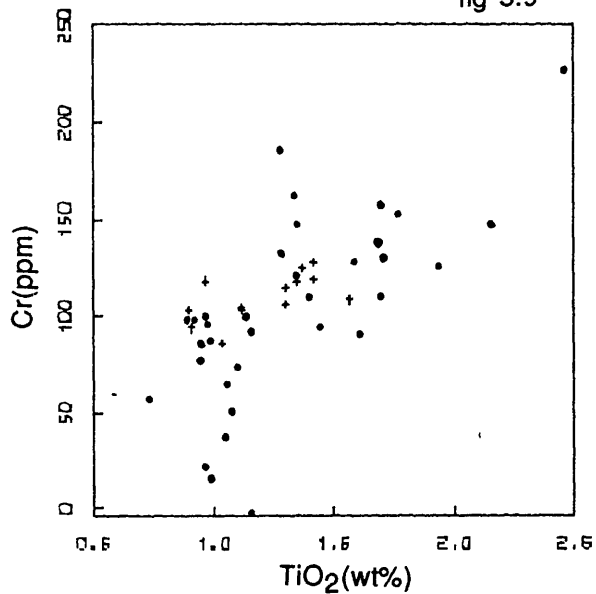


fig 5.10

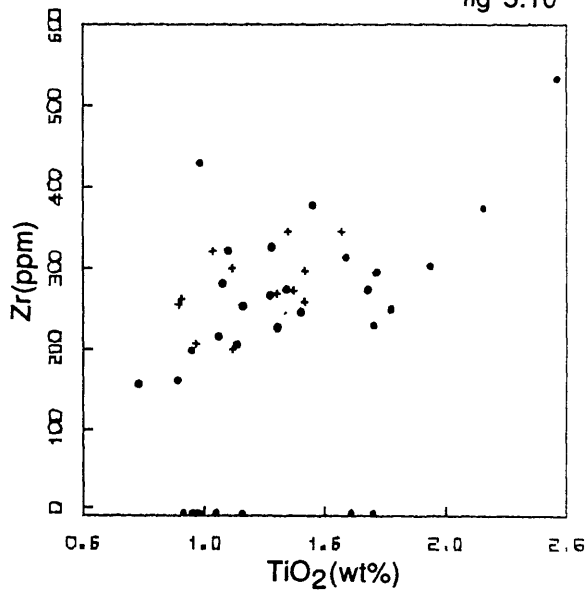


fig 5.11

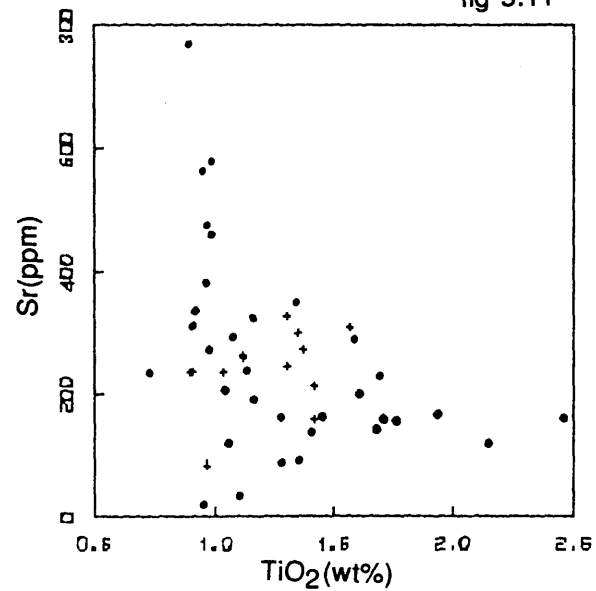


fig 5.12

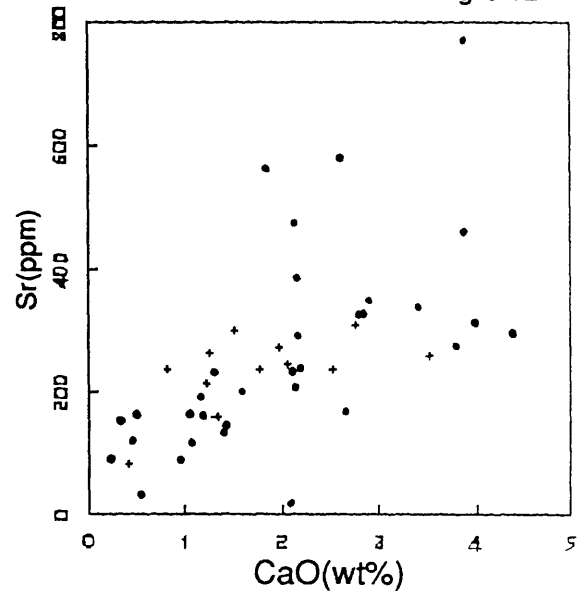


fig 5.13

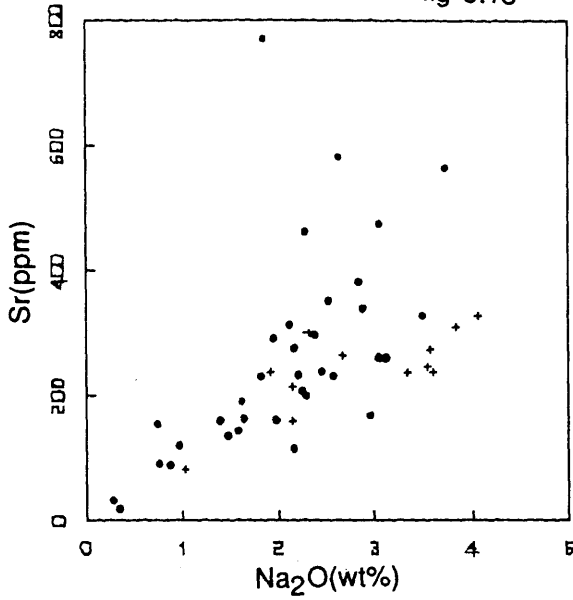


fig 5.14

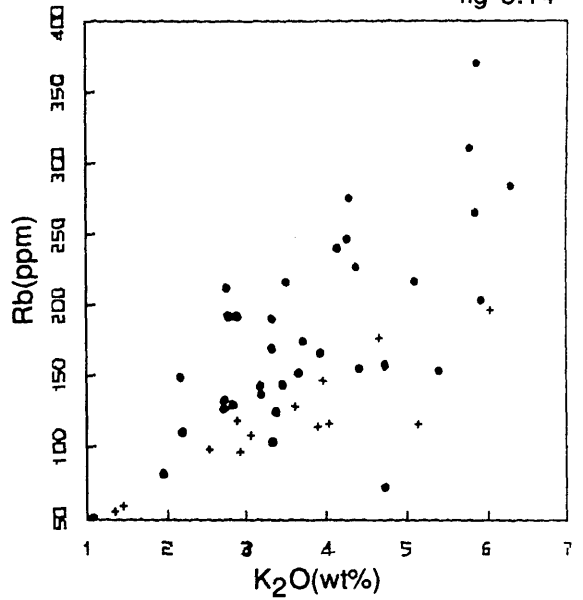


fig 5.15

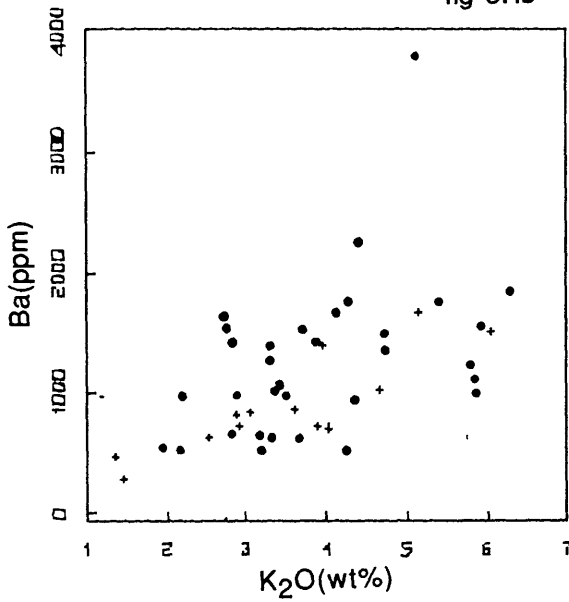


fig 5.16

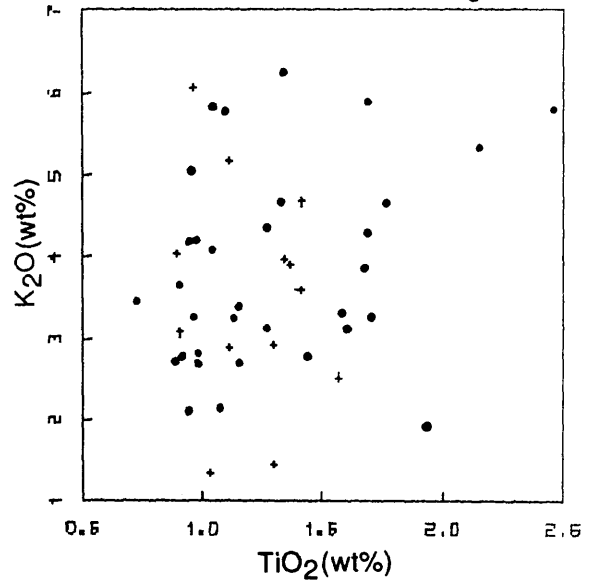


fig 5.17

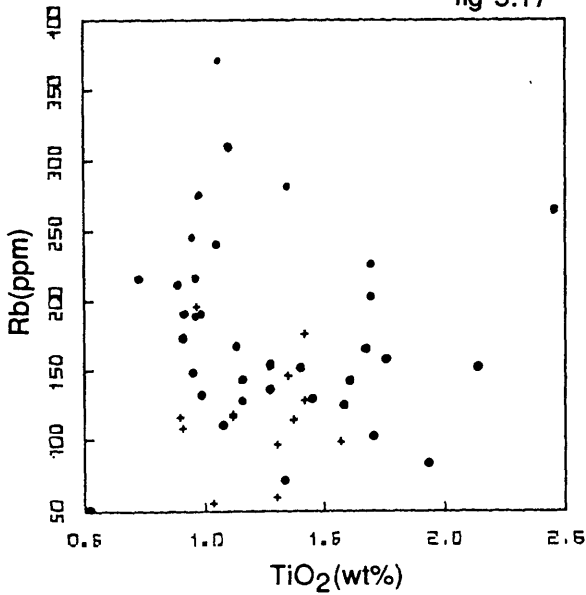


fig 5.18

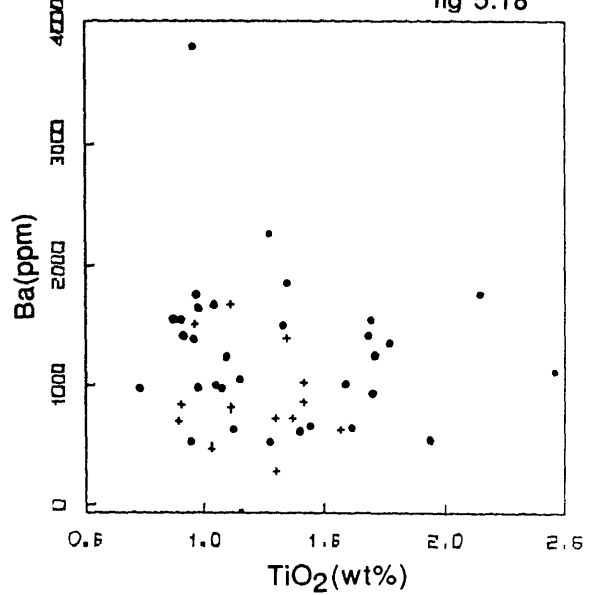


fig 5.19

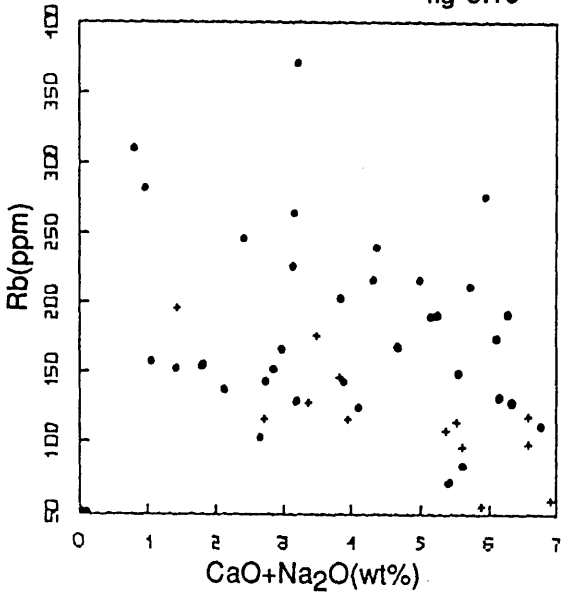


fig 5.20

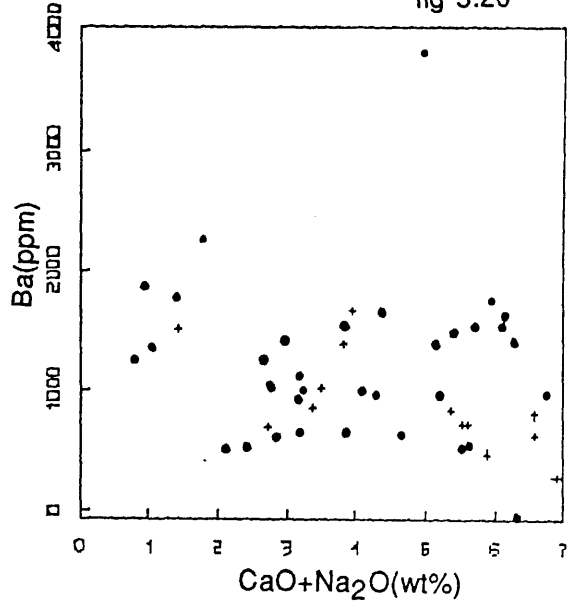


fig 5.21

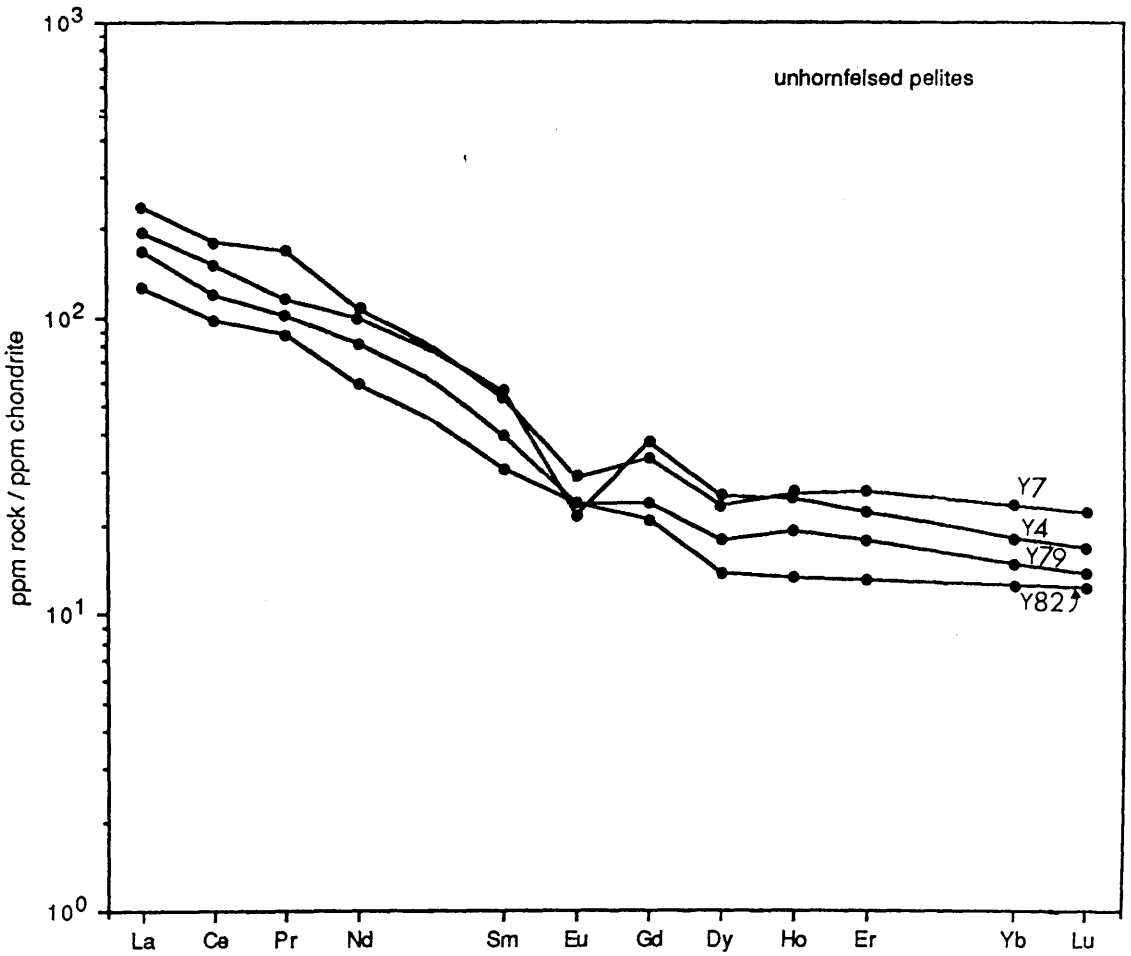


fig 5.22

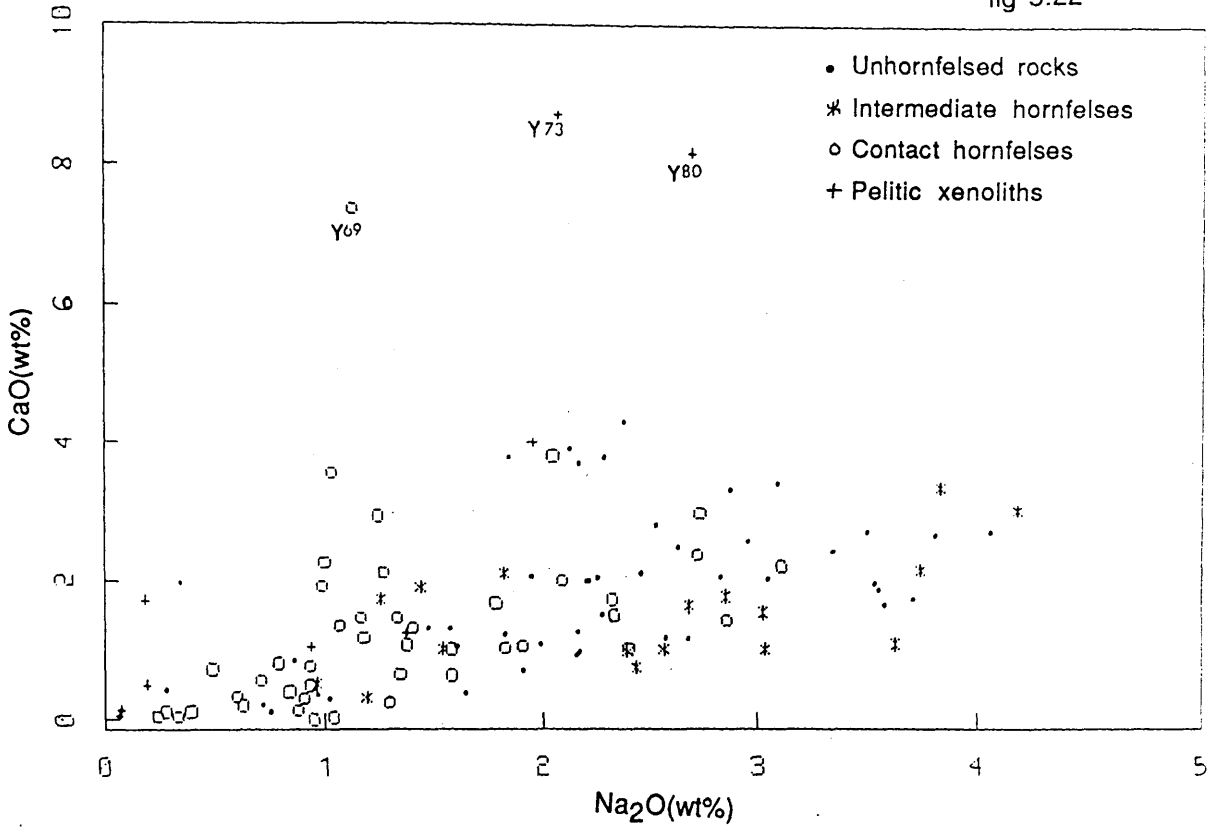


fig 5.23

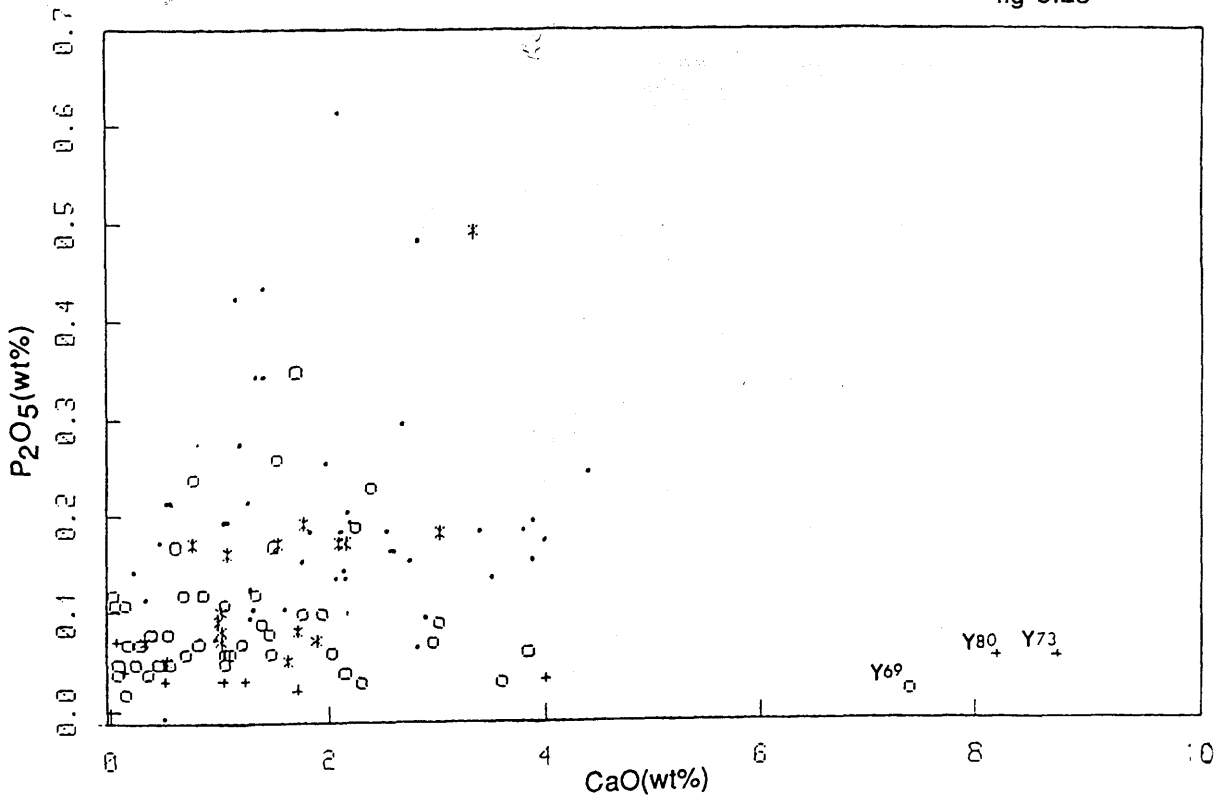


fig 5.24

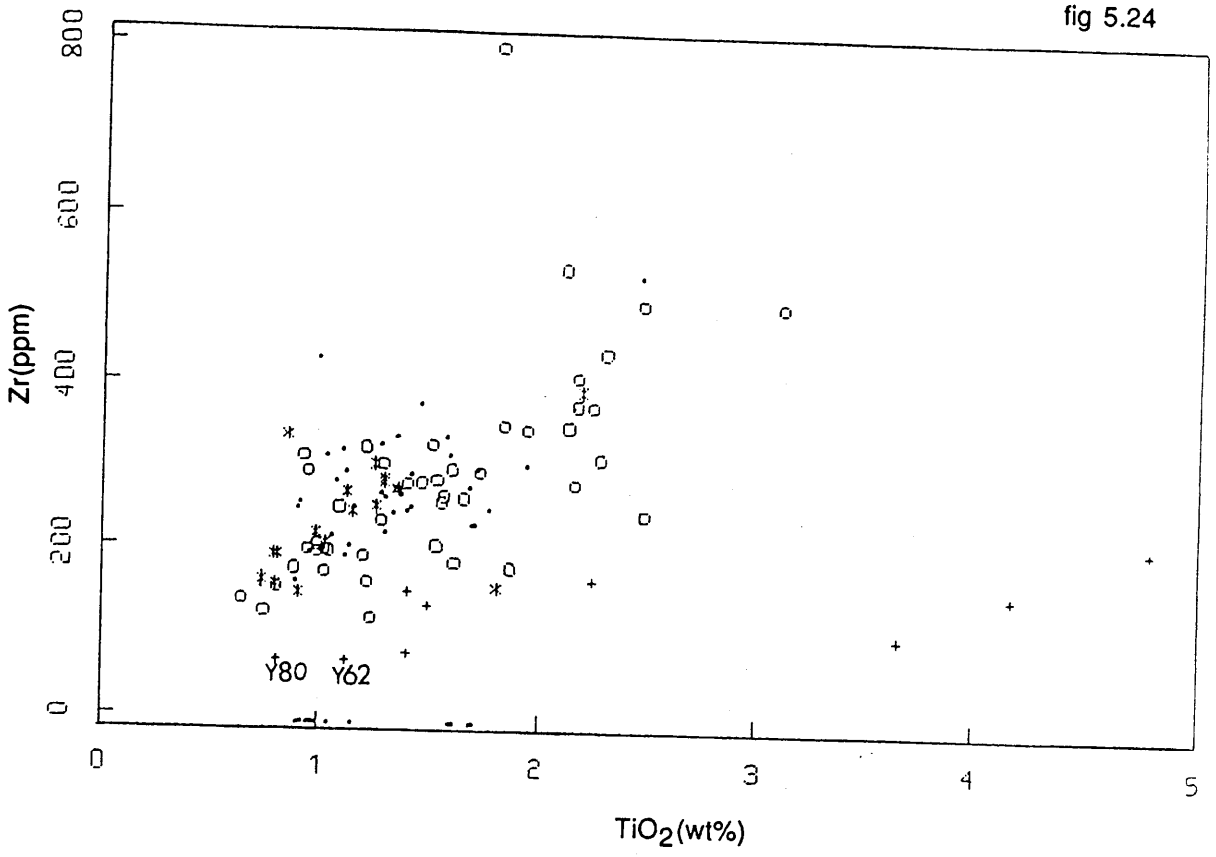


fig 5.25

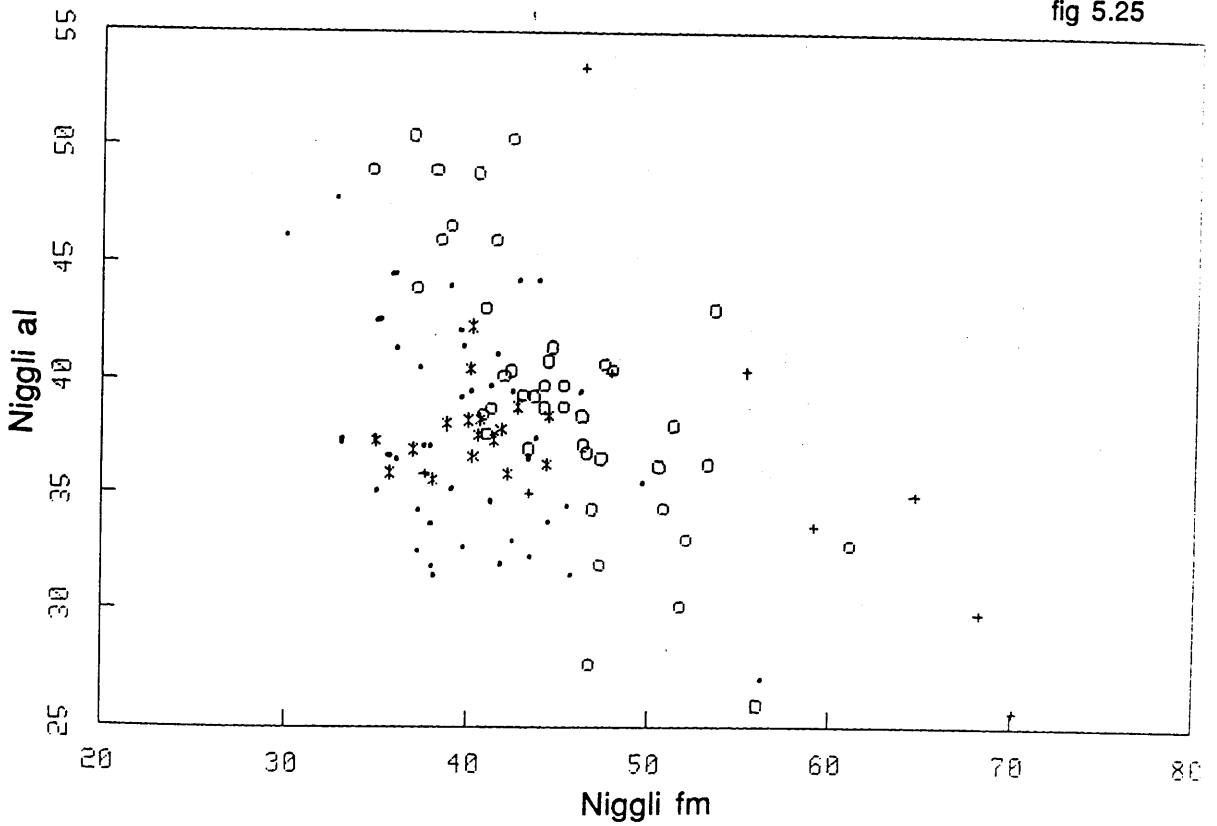


fig 5.26

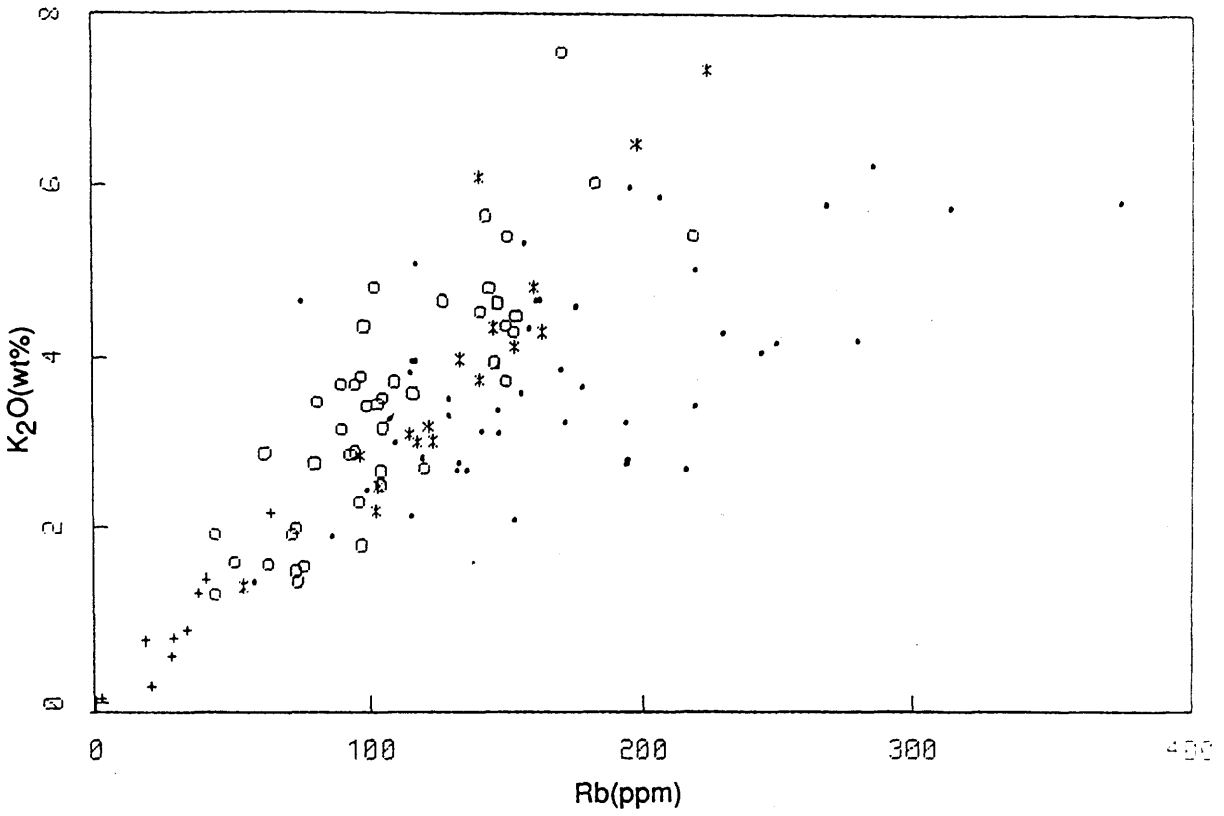


fig 5.27

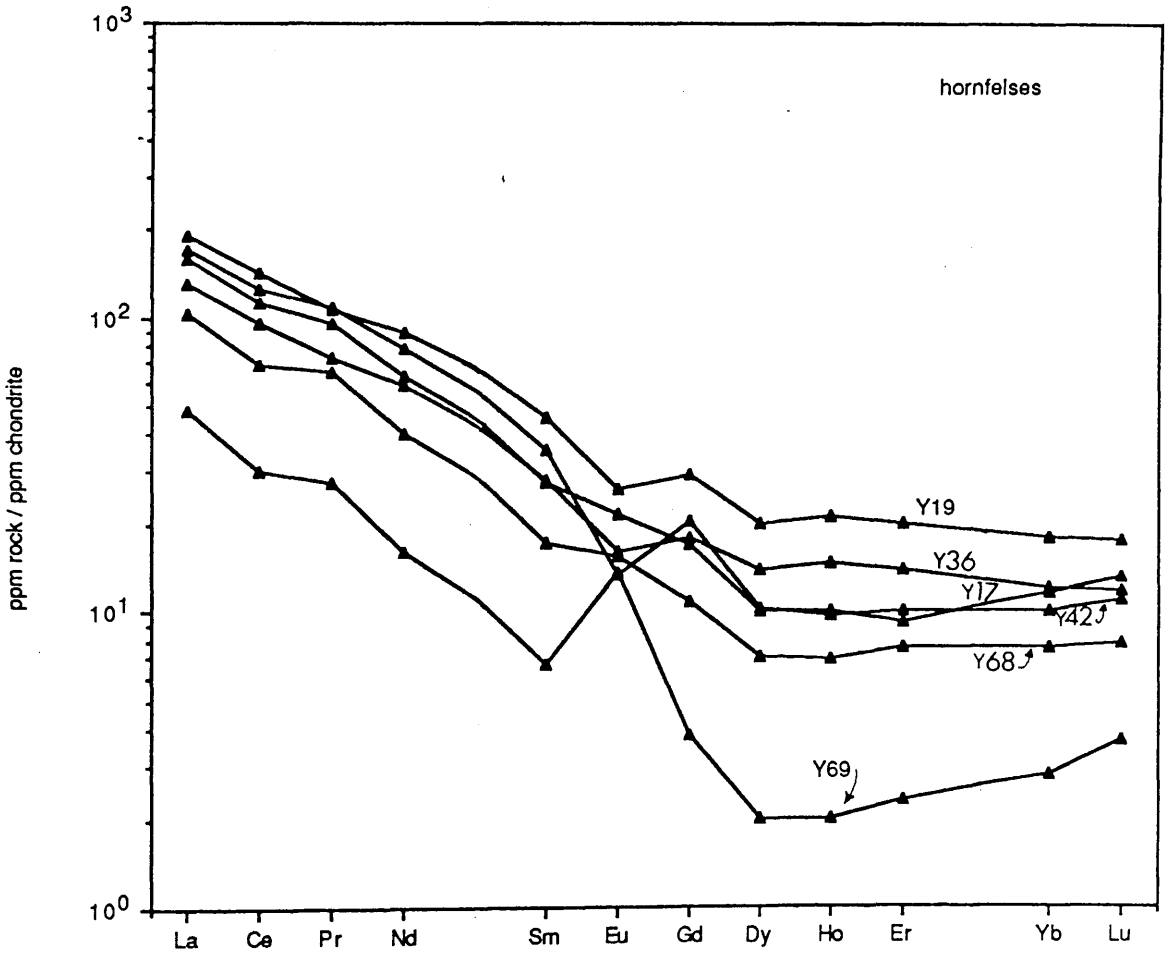


fig 5.28

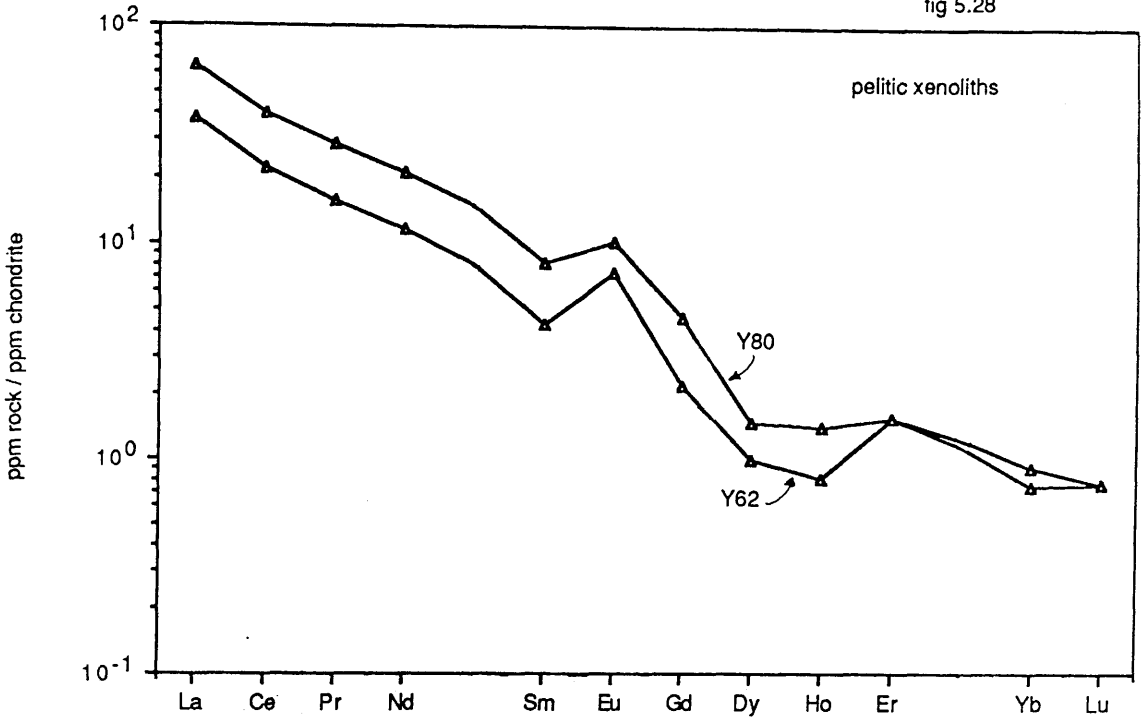


fig 5.29

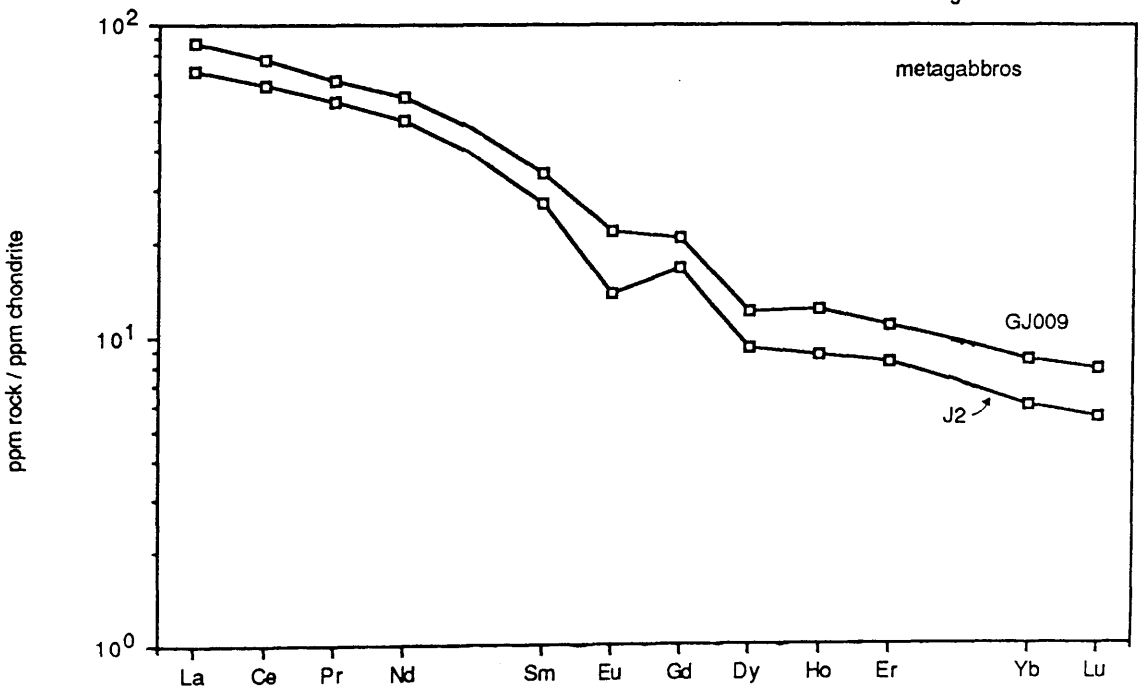


fig 5.30

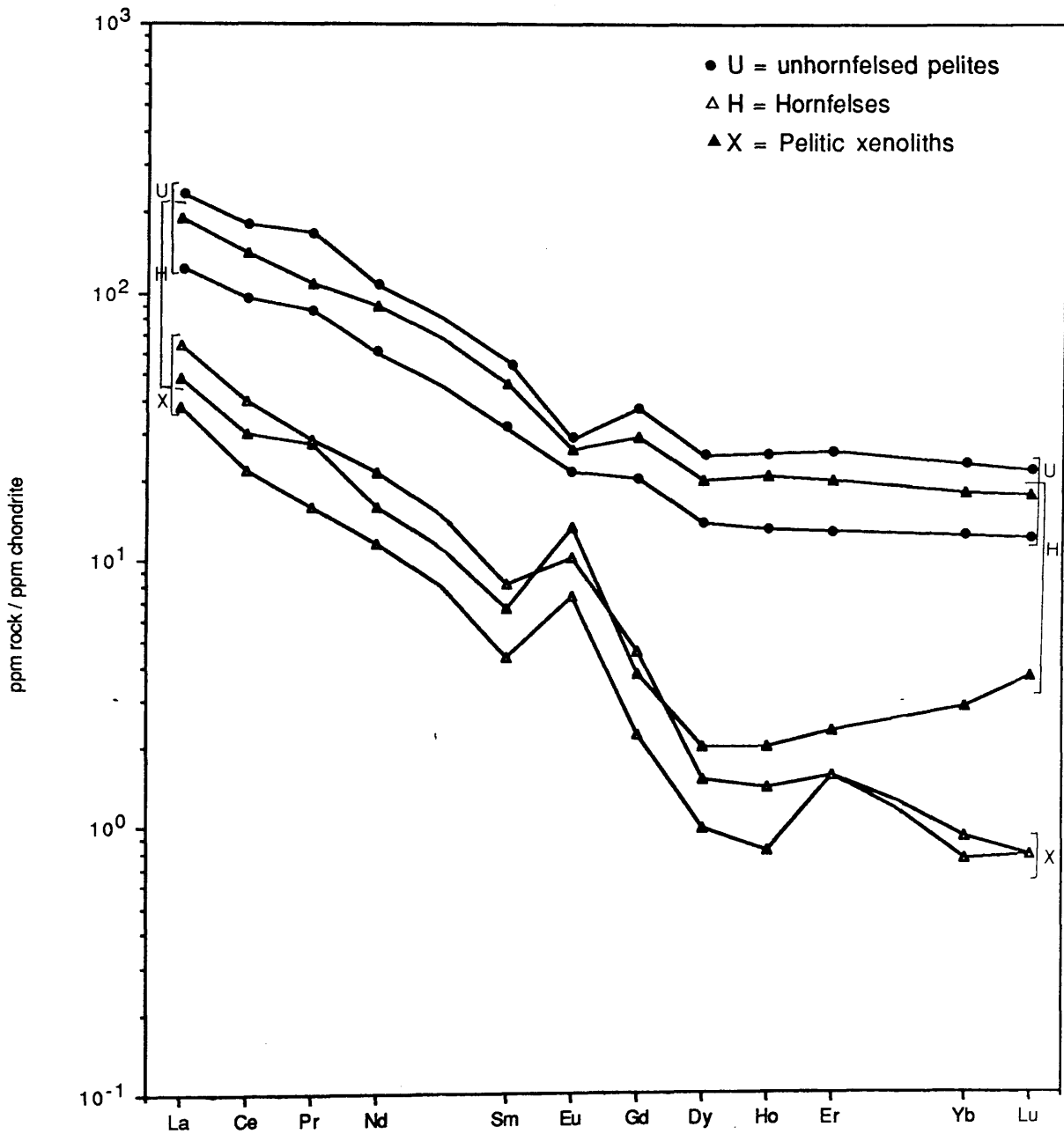


fig 5.31

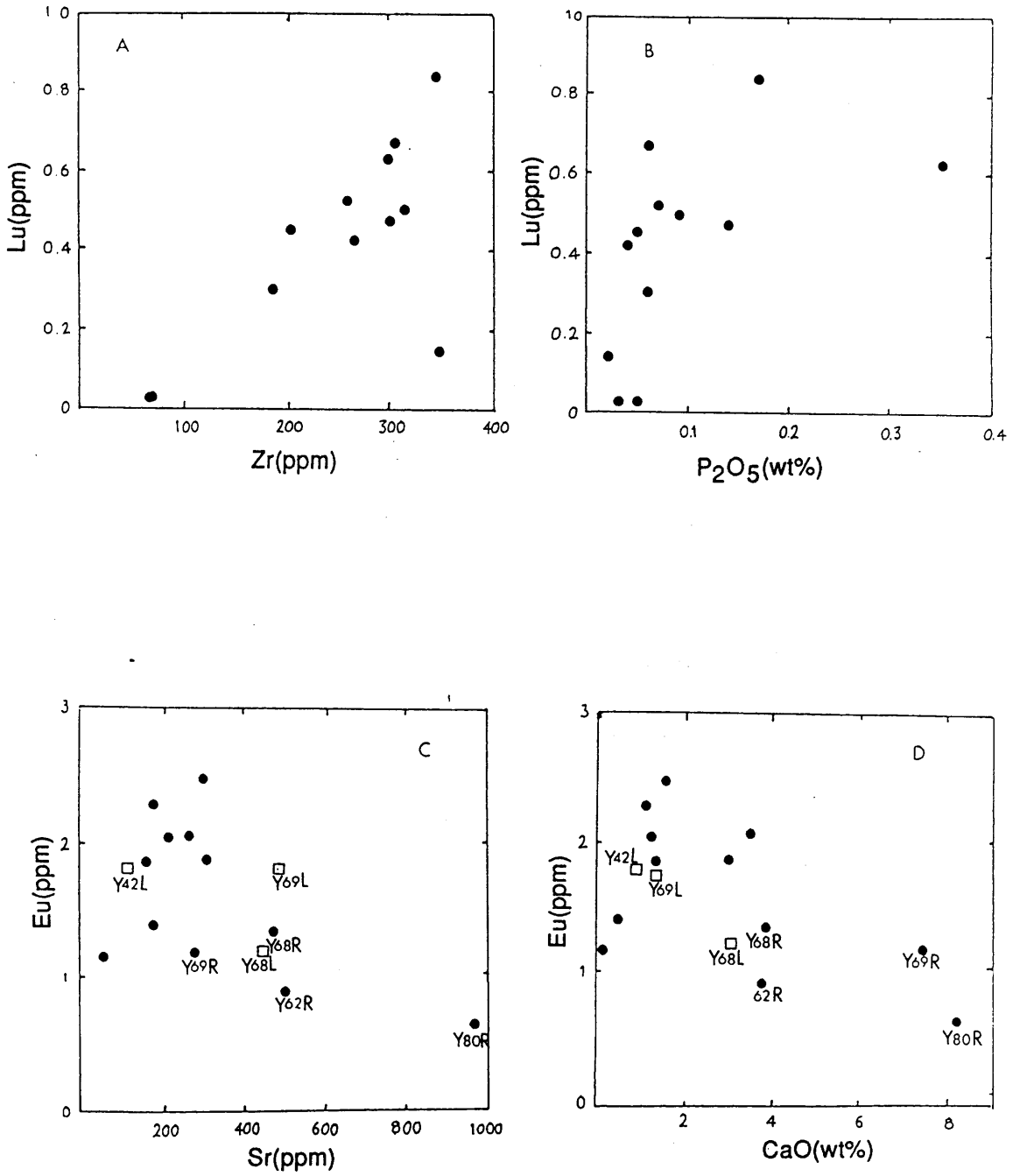


fig 5.32

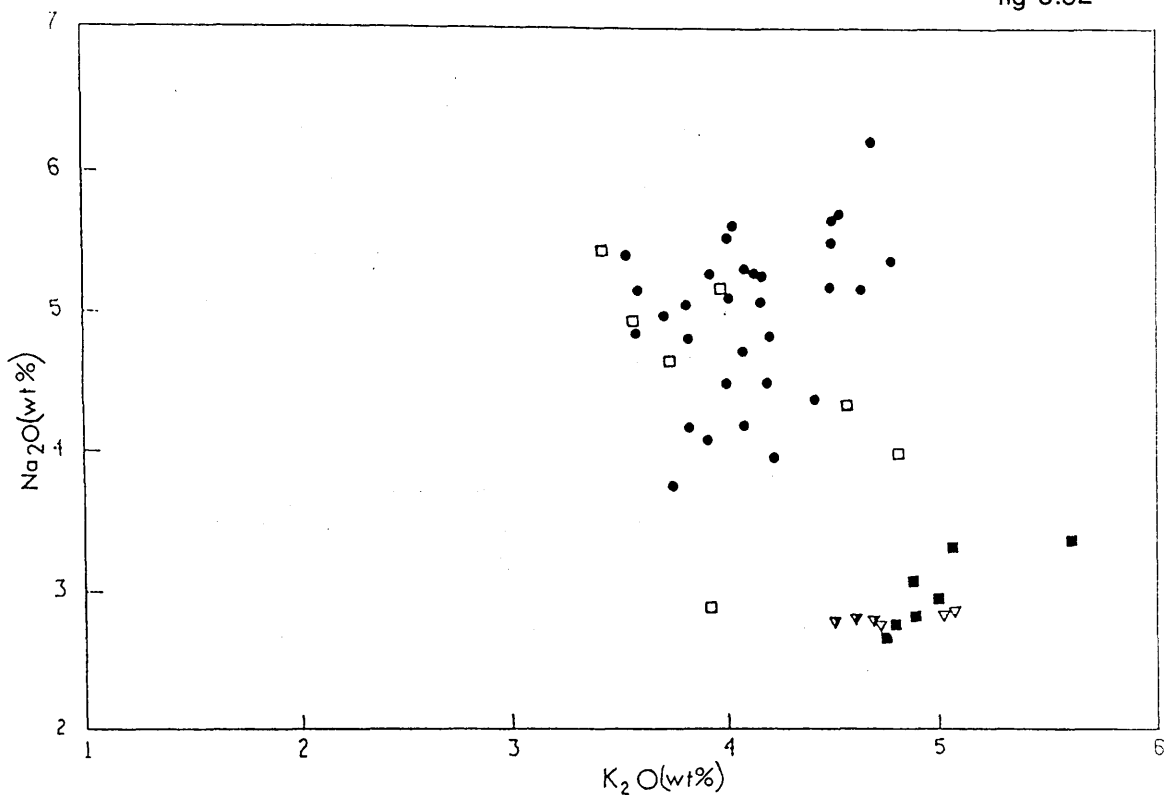


fig 5.33

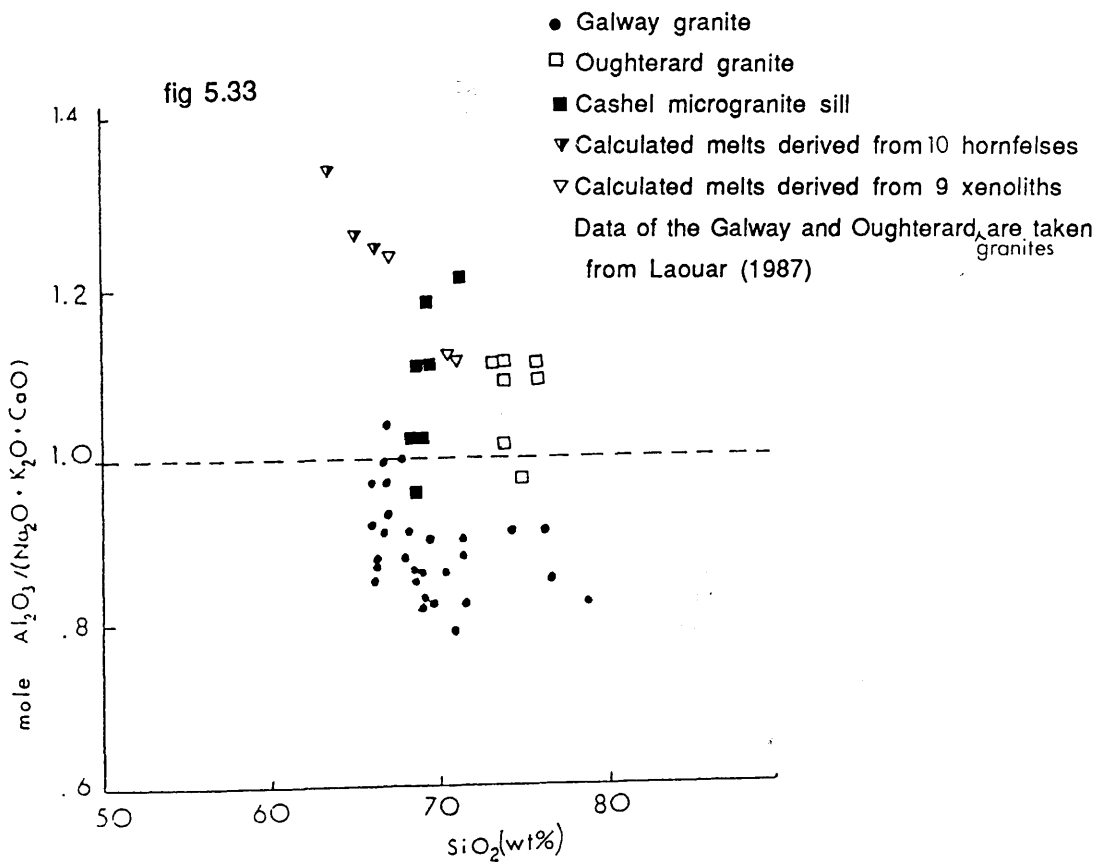
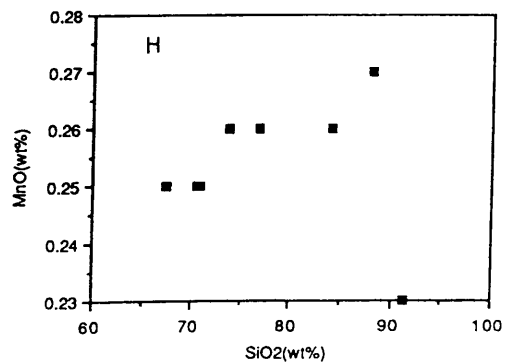
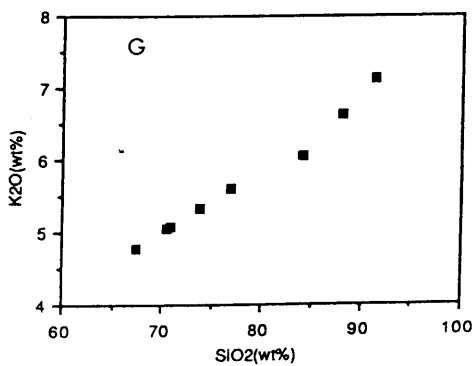
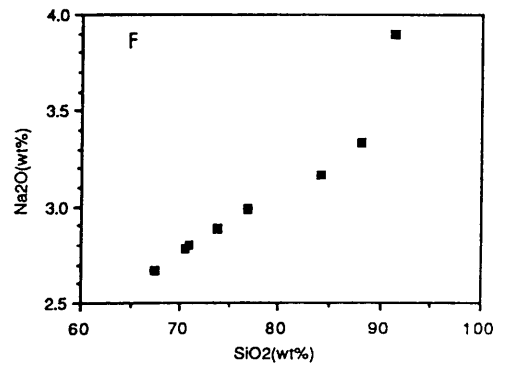
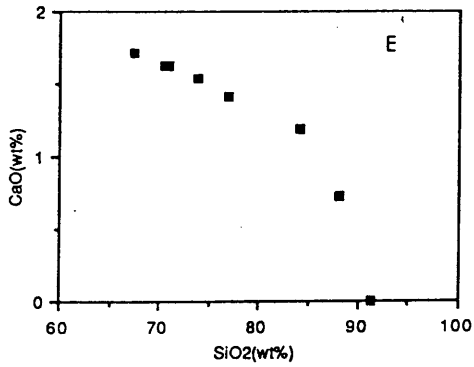
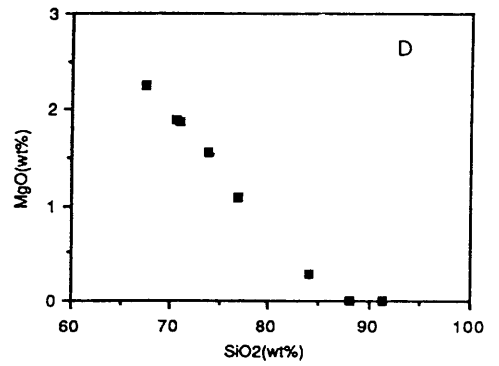
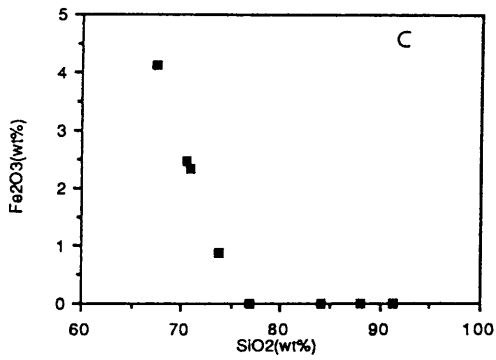
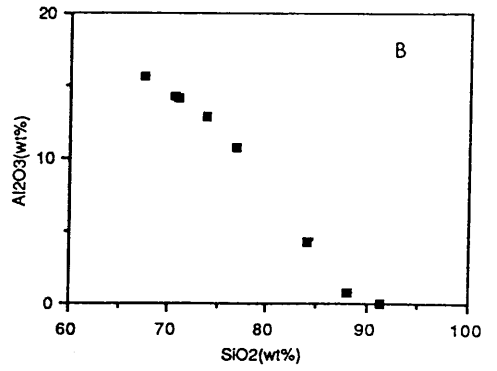
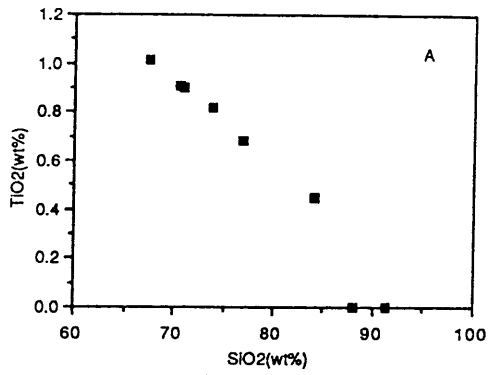
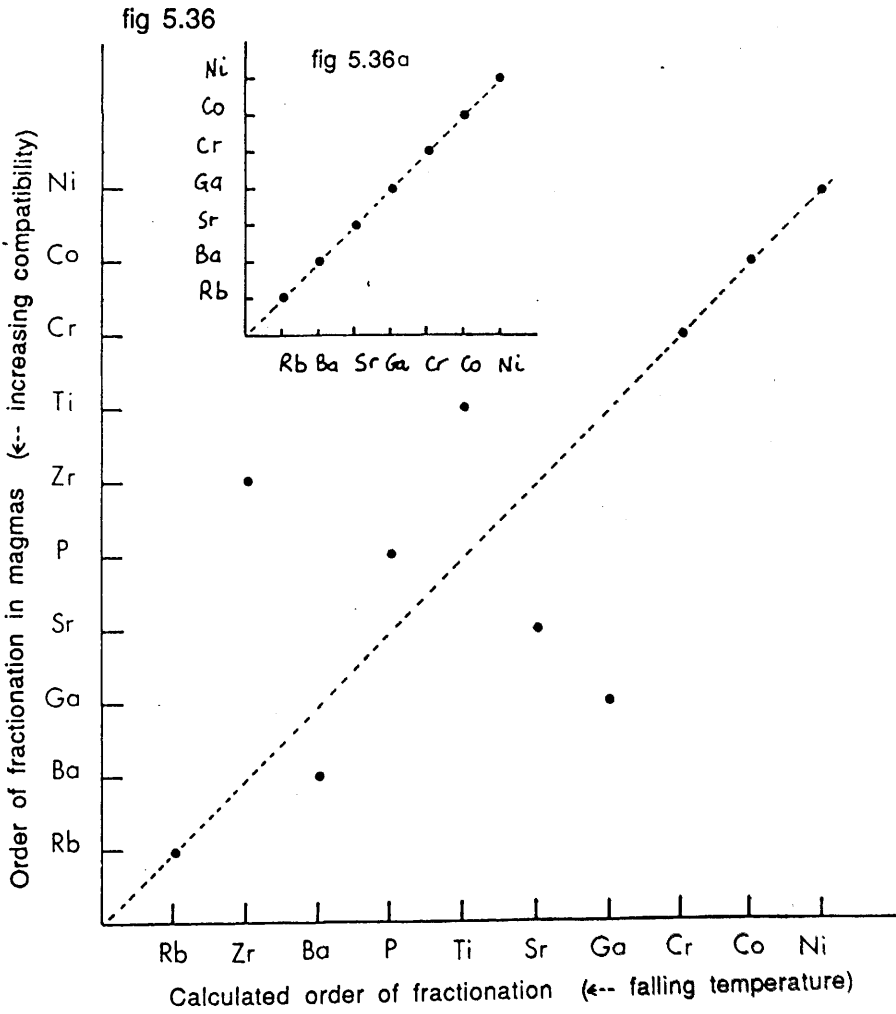
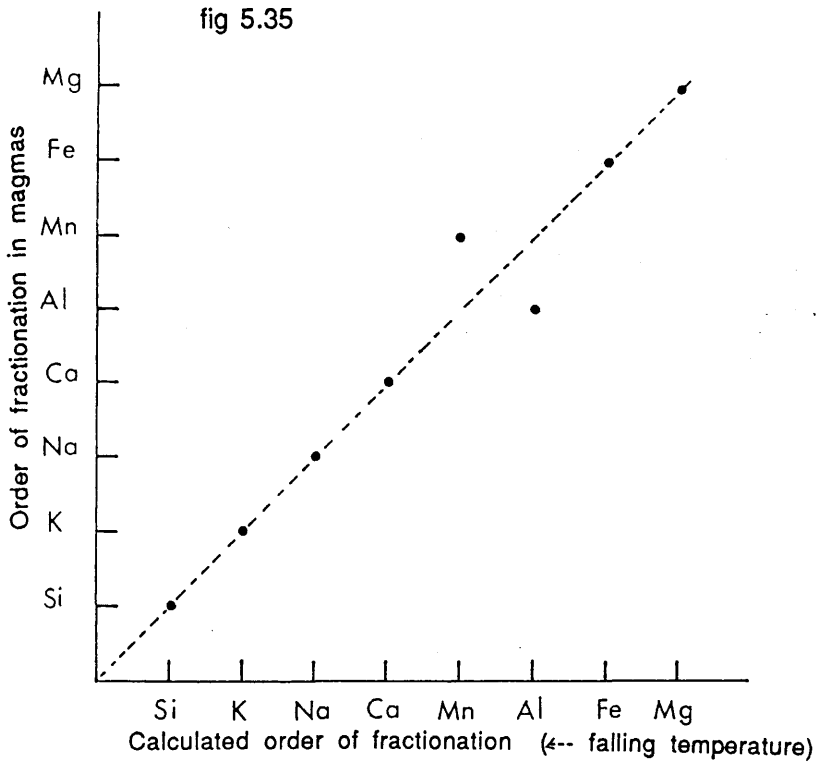


fig 5.34





CHAPTER SIX : ORIGIN OF THE CASHEL MIGMA TITE LEUCOSOMES

6.1 Introduction

In metamorphic terranes, high-grade metamorphic rocks are often spatially associated with migmatite leucosomes and considerable work has been carried out (e.g. Mehnert 1968, White 1966, Olsen 1977, Yardley 1978, Ashworth 1985) to study the processes by which these migmatites were produced. The general consensus now is that migmatites can be produced by four main mechanisms namely: igneous injections, anatexis, metamorphic segregations and metasomatism

Migmatites produced by igneous injections were described in the literature (e.g. Pitcher and Berger 1972). Typically, these types of migmatites display igneous textures and if the host rocks are at low temperature at the time of injection, contact metamorphic effects and possibly chilled margins can be produced. Significantly different isotopic signature between the host rocks and the igneous migmatites is to be expected and this feature is vital in distinguishing between anatectic and igneous origin for migmatites.

- Extensive work (e.g. Ashworth 1976, Kenah and Hollister 1983, Tracy and Robinson 1983) showed that anatexis has played a very important role in the genesis of many migmatite leucosomes. Migmatites produced by this mechanism do not exhibit "lit par lit" structures and the host rocks do not show chilled margins or contact effects. Distinctive mafic selvages (paleosomes or restites) are common and igneous texture can be produced (Mehnert 1968). Isotopically, the paleosomes and migmatites generated by anatexis should be identical and chemically, if closed systems are assumed, the sum of the leucosomes and melanosomes should equal the unmigmatized restites. However, if the system becomes open during the crystallization of the melt for instance, in the case of wall-rock reactions, the presence of xenoliths and/or xenocrysts, the migration of the melt etc; mass-balance equations which are usually used in the calculations become inapplicable and the sum leucosomes plus paleosomes can be significantly different from the original unmigmatized pelites.

Migmatite leucosomes generated in metamorphic segregations are common (e.g. Hedge 1972, Yardley 1975) and their formation involves transport of material through a pore fluid with the composition being often controlled by the host pelites. Yardley (1978) concluded that since only a small amount of fluid is present at any one time, extensive, closely spaced "lit par lit" leucosomes without any rotation of the enclosed host rocks may be recorded in the field although cross-cutting veins can also be developed. Since segregation leucosomes are internally derived in a closed system, the migmatites and paleosomes should be isotopically identical and chemically their sum should be equivalent to the original pelites.

Metasomatic leucosomes can exhibit both sharp and diffuse boundaries with the host rocks and sometimes develop "lit par lit" structures. If uncontaminated, these leucosomes are isotopically distinct from their adjacent paleosomes and chemically the sum of the leucosomes and paleosomes bear no relationships to that of the country rocks. Olsen (1984) performed mass-balance calculations on the Colorado Front Range migmatites and concluded that metasomatism was important in the generation of these rocks.

The purpose of this chapter is to investigate the genetic origin of the metasedimentary migmatites of the Cashel area. It should be noted that throughout this chapter the term migmatite leucosomes is used to denote the granitic portions that are spatially associated with the metasedimentary rocks and therefore should not be confused with the term granite or granitic which will be used in the sensu lato. The descriptive terminology of migmatites will be that of Mehnert (1968).

6.2 Field description of the migmatite leucosomes

The migmatites are generally parallel to the foliation of the rocks. They range in size from small blebs, a few centimeters long, up to veins 0.5-1.00m wide and 10-15m long. They are discontinuous, rich in mafic (dominantly biotite, garnet and sillimanite) selvages and often develop dark (biotite-rich) layers (paleosomes) at the restite-leucosome boundaries. Strömatic or layered, shlieren and nebulitic leucosomes are the dominant structures although veinitic structures are also frequent (Plates 6.1-2).

6.3 Mineralogy

The migmatites consist of quartz, feldspar and very rare orthoclase with the majority being quartz-rich. Biotite, garnet, sillimanite, zircon, apatite and secondary sericite, muscovite and occasionally prehnite are also often present. Some rare thin (≤ 1 mm) cross-cutting veins of pure quartz have been recorded.

Quartz (3.5mm average diameter) occurs as euhedral to subhedral crystals with only rare interstitial grains. Feldspars are always present and consist of euhedral to subhedral crystals (3mm average diameter) of normally zoned plagioclase which varies from typically fresh through to completely sericitized crystals. Fresh K-feldspars are very rare and when found, they are identified at the leucosome-paleosome interfaces. However, a phase which is always altered to sericite and muscovite is present in most migmatites and this phase is tentatively suggested to have been K-feldspar.

All the plagioclase analyses obtained from the migmatite leucosomes are plotted and compared to those from the pelitic restites in Figure 6.1. This Figure shows that the vast majority of plagioclase from the migmatites lie between An_0 and An_{40} . Particularly An-rich plagioclase (An_{77}) comes from the migmatite leucosome Y68L which also exhibits an igneous texture and its possible origin will be discussed later. Pure K-feldspars have not been analysed but K-rich plagioclase ($An_4Ab_{57}Or_{40}$) has been analysed.

Garnets in the migmatites are similar to those in the pelitic restites in that they are fractured, rich in quartz, sillimanite and biotite inclusions and both have the same chemical compositions. Therefore, both garnet and sillimanite are believed xenocrysts (i.e. derived from the restites). Much of the biotites are also thought to be xenocrysts because the biotite^{-sillimanite} intergrowth seen in the leucosomes is a common feature in the restites (Chapter 4). However, many large, strongly red biotite flakes are recorded particularly at the leucosome-restite interface and which are not intergrown with sillimanite. Some of these flakes are believed to have grown primarily with the minerals of the migmatites.

Andalusite is recorded in leucosome Y42L only and it is partly converted to white micas (shimmer aggregates). Andalusite is not replacing any pre-

existing Al_2SiO_5 phase and there is no textural evidence which suggests that it represents a primary growth in the migmatite leucosomes. The argument given by Barber (1985) and Barber and Yardley (1985) that andalusite has probably primarily grown from the melt because it is found in the leucosomes only is not valid because this mineral is found in both the migmatites and restites (Chapter 4).

Cordierite in the leucosomes examined is very rare and where found it occurs as small crystals usually partly pinitized. A cordierite phenocryst, Y42PC (4 x 2 cm) was separated from sample Y42 and chemically analysed (subsection 6.4). This phenocryst contains only very rare biotite inclusions but it is sillimanite-quartz- and zircon inclusions-free. These features contrast with those of cordierite in the restites suggesting that some cordierite in the migmatites may have grown from the melt.

Y38PM is a massive rock in which the migmatite leucosome and pelitic restite parts are not distinguishable but form a compact mass. Mineralogically, all the restite and leucosome mineral assemblages are found but clearly migmatization of the whole rock is very significant.

6.4 Chemistry

Eight migmatite leucosomes dominantly sampled from stromatic and schlieren outcrops, six from small veins, quartz-rich outcrops, one cordierite phenocryst (Y42PC) and one strongly migmatized rock (Y38PM) have been analysed in this work. The results are given in Appendix 3 and are statistically summarized and compared in Table 6.1 with 21 Cashel formation migmatite leucosomes from eastern Connemara (14 leucosomes associated with pelitic rocks, two with semi-pelitic rocks and five cordierite-rich migmatites), given in Barber (1985).

The eight migmatite leucosomes have somewhat higher SiO_2 , lower MgO and to some extent Fe_2O_3 and K_2O than the 14 migmatites from eastern Connemara. Most of the trace elements particularly Ce, Zr, Cr, Pb, La and Ni are also lower in the eight leucosomes compared to the 14 migmatites. However, despite some differences (e.g. Ce, Ni, Cr), generally a better agreement exists between the five cordierite-rich segregations and the two leucosomes associated with semi-pelitic rocks on the one hand and the eight

migmatites on the other. The six quartz-rich segregation leucosomes are clearly significantly higher in SiO_2 but lower in the remaining major and most of the trace elements than all the other types of leucosomes thus suggesting that they either represent metamorphic segregations or early mobilizates. This is examined later.

The differences noted above between the eight migmatites analysed in this work and those studied by Barber (1985) are probably the result of sampling but possibly also are related to the fact that the rocks from eastern Connemara have suffered higher partial melting compared to their equivalents in central Connemara. These two possibilities will be examined later. The similarities between the eight migmatites and the two leucosomes associated with semi-pelitic rocks do not imply that the migmatites analysed in this work were derived from semi-pelitic rocks because most of the restites have low Si:Ti ratios (≤ 65) compared to the semi-pelites which have Si:Ti ratios (≥ 65) (Chapter 5). The evidence therefore suggests that chemically similar migmatite leucosomes can be generated from different starting material and different leucosomes from identical material by melting under different conditions.

Samples Y38PM and Y42PC have particularly different chemistries from all the other migmatites though it is very interesting to note that Y38PM exhibits the same trends as the other migmatites. Particularly intriguing is the high K, Ba and Rb of the cordierite phenocryst. This is extensively pinitized and the high K, Rb and Ba are attributed to secondary muscovite or illite forming part of the pinite which is a composite aggregate of chlorite and mica.

6.4.1 Geochemistry of the major elements

The major element variation diagrams as shown in Figures 6.1-9 illustrate clearly that the migmatite leucosomes exhibit large variations in their element contents but it is important to note that all types of migmatites tend to form one continuous sequence. This suggests that they were all produced by one continuous mechanism and hence if the migmatite leucosomes were produced by anatexis as is probably the case (see later sections) then many of the quartz-rich segregation leucosomes probably represent an

incipient partial melting.

SiO_2 exhibits good negative correlation with Al_2O_3 , TiO_2 , Fe_{tot} (as Fe_2O_3), K_2O and Na_2O (Figures 6.2-6). However, some of the quartz-rich leucosomes are particularly rich in SiO_2 thus plotting separately from the remaining migmatites. The negative correlation between SiO_2 and K_2O and Na_2O is the opposite to what would be expected in magmatic differentiation and therefore excluding the migmatite leucosomes to have originated from late differentiate magmatic juices.

There is a positive correlation between CaO and Na_2O (Figure 6.7) but very poor correlation between CaO and P_2O_5 (Figure 6.8) indicating that much of Ca is coming in plagioclase.

The positive correlation between TiO_2 and K_2O (Figure 6.9) indicates that much of K is in biotite. The samples Y42L, Y43L, Y44L and Y40L tend to plot separately from the other migmatites probably because K is coming in K-feldspars but also in sericite and muscovite.

6.4.2 Geochemistry of the trace elements

The trace elements generally mirror the behaviour of their major equivalents in that the quartz-rich leucosomes are depleted in most of the trace elements compared to the other types of migmatites. As expected K_2O exhibits very good positive correlation with both Ba and Rb (Figures 6.10-11), CaO with Sr (Figure 6.12) and Al_2O_3 with Ga (Figure 6.13). P_2O_5 correlates positively with Y (Figure 6.14) indicating that much of Y is accommodated in apatite. Ce and La correlate positively with each other (Figure 6.15) but neither correlates with Y (only the Ce-Y diagram is shown in Figure 6.16). However, a positive but poor correlation exists between K_2O and Ce (Figure 6.17) suggesting that some Ce and La are held in biotite although some are possibly coming in K-feldspar where present.

Positive correlations exist between TiO_2 and Cr and Ni (only TiO_2 -Cr is shown in Figure 6.18) indicating that these elements are enriched in biotite, a mineral phase commonly observed in many migmatite leucosomes. Microprobe analyses showed that ilmenite and rutile are also present in the leucosomes suggesting that some Cr, Ni and Co are also held in these minerals.

6.4.3 Rare earth elements

Three migmatite leucosomes have been analysed for REE and the results are given in Table 6.2 and portrayed together with their equivalent pelitic restites in Figure 6.19.

The migmatites have lower REE contents than their adjacent pelitic restites and with the exception of Y68L the remaining two migmatites have steeper distribution patterns than their equivalent restites. Particularly intriguing are the positive Eu anomalies exhibited by all leucosomes with two restites (Y68R, Y69R) also exhibiting positive Eu anomalies.

In Chapter 5 it has been argued that the positive Eu anomalies exhibited by the strongly melted pelitic xenoliths are mainly due to removal of a granitic melt. Thus the Cashel granitic sill, which is believed to represent this melted material, exhibits a negative Eu anomaly. Therefore, if the three migmatite leucosomes are derived by partial melting from their equivalent restites, it is unlikely that both rock types (restites and leucosomes) exhibit positive Eu anomalies. The evidence as deduced from the mineralogy, chemistry, and Rb-Sr isotopes coupled with field observations indicates that the leucosomes were probably derived by anatexis and metamorphic segregation from the Cashel pelitic rocks (see below). Therefore the positive Eu anomalies suggest that either the leucosomes are particularly rich in xenocrystic plagioclase or more probably fractional crystallization was operative.

In partial melting where fractional crystallization was operative Eu would be preferentially incorporated in early crystallized phases with the succeeding fractions of partial melts being gradually depleted in Eu (McCarthy and Kable 1978). Therefore, if fractional crystallization occurred, a positive Eu anomaly can be produced and although fractional crystallization could not be proved from the samples studied, the REE suggest that this process took place. The poor correlation between Eu and Sr (see Figure 5.31) suggests that some of Eu was in the form Eu^{+3} thus excluding plagioclase being the main cause of the Eu enrichment. This indicates that crystallization of the melt took place under reducing conditions, a deduction supported by the low oxidation ratios of the migmatites. Other factors which may have affected the Eu anomaly include changing oxygen fugacity and melting temperature (Sun *et al.*

1974), changing melt composition (Fraser 1975), the presence of chloride and fluoride in the fluid phase during melting (Flynn and Bunham 1978) and metamorphic segregations before anatexis.

6.5 Factors affecting the final composition of the migmatites.

In the foregoing sections it has been shown that the migmatite leucosomes are chemically variable and this variability is likely to have been the result of many factors including different starting material (pelites and quartz-rich semi-pelites for instance) and differences in temperature and pressure within the migmatite zone.

The experimental work of Green (1976), discussed in subsection 6.6, clearly shows that a wide compositional range of granitic rocks can be produced from exactly the same starting material due to variations in the temperature and pressure. It has been shown in Chapter 3 that large variations in both temperature and pressure are recorded within the studied area and although much of the variations are attributed to temperature resetting on cooling, some of the variations are likely to have been primary, particularly as the pelites and semi-pelites have significantly different thermal conductivities and diffusivities (Chapter 4). Therefore some of the chemical variations are likely to have resulted from these primary P-T variations.

Other factors which can affect the final composition of the melt include wall-rock reactions, assimilation of xenoliths and/or xenocrysts and fractional crystallization. These factors are discussed below:

6.5.1 Wall-rock reactions

In the migmatite leucosomes examined there are no "exotic" minerals (*i.e.* minerals not associated with either the leucosomes or restites) suggesting that wall-rock reactions were probably not significant. However the large biotite flakes occurring at the leucosome-restite interface mentioned in subsection 6.3 were possibly formed by this process but if these biotites are truly the result of wall-rock reactions, the frequency of occurrences indicates that the process was too insignificant to have strong effects on the composition of the leucosomes.

6.5.2 Xenoliths and xenocrysts

In the field, pelitic xenoliths are frequently present in the strauatic, Shlieren and nebulitic migmatites but these xenoliths were excluded during sampling and crushing for chemical analyses. However, as shown in subsection 6.3, garnet, biotite, sillimanite and cordierite are also sometimes present. It has been argued that all garnet and sillimanite and some biotite and cordierite are xenocrysts and therefore have chemical effects on the composition of the migmatite leucosomes.

The effects of xenocrysts can be shown through a series of scatter diagrams because if there is only one xenocryst phase in a migmatite, the whole rock chemistry should lie along the straight line connecting the composition of the xenocryst-free migmatite with that of the xenocryst itself and hence the position of the whole rock analysis would indicate roughly the phases present and their percentages.

Since the most common xenocrystic phases present are garnet, biotite and cordierite, it is likely that these minerals influence the SiO_2 , Al_2O_3 , TiO_2 , Fe_{tot} and MgO of the migmatite leucosomes. The representative composition of these three phases as shown in Figures 6.20-24, are taken from the average of 25 biotite, 19 garnet and one cordierite analyses (Chapter 4). Figures 6.20-24 clearly show the strong effects of these xenocrysts especially on the leucosomes studied by Barber (1985) with the quartz-rich leucosomes being almost xenocryst-free. This indicates that the differences recorded between the migmatites from eastern and central Connemara are the result of sampling rather than differing regional P-T conditions.

In addition to the above mentioned xenocrysts, the experiments of Winkler and Breitbarth (1978) show that xenocrysts of both quartz and plagioclase can also be present in migmatites hence strongly affecting the Qz:Ab:Or ratios and therefore making them different from the experimental results summarized by Winkler (1979). Quartz and plagioclase cannot be easily distinguished from those crystallized from the melts based on textural evidence only; however, Figure 6.1 shows that many feldspar analyses from the migmatites and restites overlap with each other with plagioclase from Y68L being more Ca-rich than most pelitic restites. It is unfortunate that

plagioclase analyses from the restite Y68R could not be obtained due to its altered nature. The high Ca content of plagioclase from some migmatites suggests that some plagioclase may have been incorporated into the melts from the restites. Definite proof is lacking however.

6.5.3 Fractional crystallization

There is no textural evidence which suggests that fractional crystallization was operative nor could the effects of late-stages sub-solidus alterations be proved. However, the behaviour of the REE suggests that fractional crystallization was operative though it was probably not significant.

6.6 Absolute chemical composition of the migmatites

It has been shown above that the migmatite leucosomes exhibit large chemical variability and this is probably largely due to different initial composition as wall rock reactions, xenocrysts and fractional crystallization were probably insignificant. Therefore it is of interest to derive as accurately as possible the original composition of the melts produced by anatexis. The calculations can be performed easily provided that the original composition of the pelites which produced the melts and the degree of partial melting are known.

The original composition of the pelites which produced the Cashel migmatites remains unknown because no distinctive, quantitatively analyzable paleosomes are found. However the average of the 47 unhornfelsed pelites can be taken to represent the original composition of the Cashel pelites because none of these rocks contain hornfels minerals. 29 migmatite leucosomes (8 from this work and 21 from Barber 1985) are taken to represent the average Connemara migmatites but the average of the quartz-rich leucosomes is not included due to their significant chemical differences. The average of 54 northern unmigmatized pelites given in Barber (1985) was also used as the original composition of the pelites and therefore comparison between the two results is made.

The principles and methodology for calculating the degree(s) of partial melting and composition(s) of the melt(s) described in Chapter 5 are still valid except that because the migmatites are spatially associated with the

restites but not the granite sill, the composition of the migmatite leucosomes should be included in the formulation of the equations.

Thus if

P = degree of partial melting expressed as a fraction of one

i = concentration of element i

then

$$P = \frac{\text{mean femic element in restites} - \text{its mean in unhornfelsed pelites}}{\text{its mean in restites} - \text{its mean in migmatite leucosomes}} \quad 6.1$$

$$i \text{ leucosomes} = \frac{i \text{ in unhornfelsed rocks} - (1-P)i \text{ restites}}{P} \quad 6.2$$

It follows therefore from equation 6.1 that if xenocrysts are present in the leucosomes, then restite-migmatite wall reactions and fractional crystallization processes took place, they would have some effects on the calculated degrees of partial melting and eventually on the composition of the melts. Some of these effects are discussed briefly below :

The effects of fractional crystallization can only be significant if elements which readily enter the melt phase are used in the calculations but not strongly compatible elements such as Cr, Ni, Co as in the present study. For instance, if we assume 150ppm and 90ppm as the respective averages of Cr in the restite and unhornfelsed pelites and 10 ppm Cr in the average leucosomes, then the degree of partial melting would be 42.8%. If fractional crystallization took place and 50% of the melt was removed leaving only 5ppm of Cr in the leucosomes, the degree of partial melting becomes 41.4%. Assuming that when the 50% of the melt left it did not taken any Cr (i.e. Cr=15ppm in the leucosomes), the degree of partial melting becomes 44.5%. From this example, it is clear that fractional crystallization would not have significant effects on the calculations.

If the xenocrysts are femic elements-bearing minerals, then the effects on the calculations would be significant. In the present calculations, the minimum degree of partial melting has been computed by assuming 0ppm of Cr, Ni and Co in the migmatite leucosomes (minimum melt generated), and the

maximum by taking the actual concentration of these elements in the leucosomes in order to minimize the effects of xenocrysts.

6.6.1 Results

The degrees of partial melting as shown in Table 6.3 are clearly strongly dependent on the original composition of the pelites with lower degrees of partial melting being recorded when the average of the northern unmigmatized pelites is taken as the starting material. However, these differences are corrected for by calculating the possible melt compositions between the minimum (taken as 10%) and maximum (taken as 50%) computed degrees of partial melting.

The calculated melts of between 18% and 38% partial melting either if the starting material is taken as the Cashel unhornfelsed rock or the northern unmigmatized pelites agree well with the average migmatite leucosomes

within one standard deviation (Table 6.3). Particularly different is the higher Al_2O_3 and P_2O_5 but lower Na_2O , CaO and MnO in the melts derived using the unmigmatized pelites compared to the Cashel unhornfelsed rocks and these differences are probably due to the fact that the standard deviations have not been considered in the calculations.

It is unfortunate that the actual composition of the migmatite leucosomes cannot be used to decide which of the two formations is most likely to have been the starting material because of the possible effects of xenocrysts, wall-rock reactions and fractional crystallization. However if these effects are not considered, then the original composition that produced the migmatite leucosomes would have been roughly about (85-65)% Cashel unhornfelsed rocks plus (15-35)% northern unmigmatized pelites.

Table 6.3 also shows that at 10% melting, about 17 wt% Al_2O_3 enters the melt if the unmigmatized pelites are used as the starting material which is very unlikely. At such low degrees of partial melting, only small amounts of Al would have fractionated into the melt and although this suggests that the northern pelites were possibly Al-rich compared to their equivalents in the south, the high Al generated in the calculations is possibly because of the small sample size, the presence of unrepresentative samples and more importantly because of the inaccuracy of the calculations due to the use of the mean values

only

It can be concluded that the migmatite leucosomes were probably generated by partial melting from within the metasediments and the differences recorded at low degrees of partial melting are attributed to the starting material being not exactly known but it was probably between (85-65)% and (15-35)% of the present composition of the unhornfelsed and northern unmigmatized pelites respectively (*i.e.* within the standard deviations). It follows therefore that if the quartz-rich leucosomes were produced by partial melting then they should be chemically similar to those mobilizates calculated at low degrees of partial melting. Table 6.3 shows that 10% partial melting would produce a melt similar in composition to the average of the six leucosomes if (85-65)% of the unhornfelsed and (15-35)% unmigmatized pelites are mixed together as the starting composition. This indicates that these quartz-rich leucosomes were probably formed by incipient partial melting.

6.7 Comparison of the chemical composition of the migmatite leucosomes with those derived from experimental and theoretical studies

Despite the numerous theoretical and experimental studies undertaken to explain the granite genesis (*e.g.* Tuttle and Bowen 1958; Luth *et al.* 1964), only a few studies were carried out on naturally occurring metasedimentary rocks at the appropriate crustal P-T conditions. Such studies include the work of Green (1976) and Winkler (1976, 1979).

Granitic rocks formed by partial melting of metasedimentary rocks are termed S-type granites and their characteristic features have already been discussed (Chapter 5, subsection 5.4.1). The formation of these peraluminous granites has been discussed by a number of authors, among others, Tracy 1978; Abbot and Clarke 1979; Thompson and Tracy 1979; Clemens and Wall 1981 and Thompson 1982. From these studies it can be concluded that a wide variety of granitic compositions can be generated from pelitic rocks as a result of original differences in the mineralogy of the rocks, variations in both temperature and pressure and the compositions and amounts of the fluids present at the time of melting. The effects of HCl, F and B when present in the fluid phase during melting have been studied experimentally by

Manning (1981), Pichavant (1981) and Manning and Pichavant (1983) who showed that the presence of these components in the fluids lowers the solidus temperature significantly. From the experimental and theoretical studies undertaken, it is now understood that chemically variable granitic melts can be generated during anatexis of pelitic rocks and the melts need not correspond to the "minimum melt" compositions.

The A/CNK of the migmatite leucosomes studied in this work are given in Table 6.4 as are the CIPW normative corundum and Qz:Ab:Or ratios recalculated to 100. With the exception of sample Y69L, which is strongly trondhjemitic, all migmatite leucosomes collected from stratum, nebulitic and schlieren outcrops are peraluminous ($A/CNK \geq 1$). Out of the six quartz-rich leucosomes analysed only sample Y65L has A/CNK significantly lower than unity. This sample consists of abundant quartz and very rare plagioclase suggesting that it was produced by metamorphic segregations.

Green (1976) performed a series of experiments over a range of P-T conditions using a synthetic pelite glass as a starting material and it is this study which can be reliably used to compare the naturally occurring composition of the migmatites in Connemara with those produced experimentally. The composition of the starting material and the results of Green's experiments are compared in Table 6.4 with the compositions of Cashel unhornfelsed and northern unmigmatized pelites, migmatite leucosomes and the microgranite sill. Because the migmatites studied by Barber (1985) possibly contain more xenocrysts than those studied in this work, the average of the eight migmatites is first represented separately and then added to the 21 migmatites of Barber (1985) as a representative composition of the Connemara migmatites.

It is evident from Table 6.4 that the starting material used by Green (1976) is higher in SiO_2 but lower in TiO_2 , Al_2O_3 and Fe_{tot} and to some extent Na_2O than both the Cashel unhornfelsed and northern unmigmatized pelites although these differences are insignificant if the standard deviations are considered. Therefore it is not surprising if the compositions of the glasses produced in the experiments and those of the Connemara leucosomes exhibit slight differences.

The most applicable results of Green's experiments to the Cashel

migmatite leucosomes are those produced at 780°C and 4kb as these P-T conditions are similar to those which prevailed in the studied area (Chapter 3). It is clear from Table 6.4 that good agreement between the experimentally derived glass and the naturally occurring Cashel migmatite leucosomes can be postulated although there is a tendency for the glass to be richer in SiO₂ and K but lower in Na and Ti (Ti if only the eight leucosomes are considered). Green (1976 p.87) noted that the results of the experiments are consistently lower in Na than naturally occurring S-type granites from the New England batholith and attributed these differences to the pelites used in the experiments being lower in Na than those produced by the batholith, technical problems in analyzing Na and the fact that the pelites in the experiments may have suffered a higher degree of partial melting. The Cashel microgranite sill which was probably formed from highly melted rocks compared to the leucosomes (Chapter 5) is richer in both Na and K, lower in Si but has similar Ca values compared to the composition of the glass which suggests that the differences recorded between the experimentally determined glass and the naturally occurring Cashel microgranite sill and migmatite leucosomes are due to differing composition of the starting material, differing degrees of partial melting and P-T conditions, although the low Na in the glasses is probably the result of analytical problems in the experiments of Green (1976). However, the migmatite leucosomes are consistently lower in K compared to both the Cashel granite sill and the experimental glass because they contain only very little, if any, K-feldspar probably because it was unstable and was converted to sericite and muscovite.

Bearing the above complications in mind, the agreement between the Cashel migmatites and the experimentally derived glass is quite good.

Although as discussed above, a wide range of granitic composition can be generated by anatexis of pelitic rocks, Winkler (1979 p.332) summarized the Qz:Ab:Or ratios of many experimentally derived anatectic melts produced from a wide range of compositionally diverse metasedimentary rocks. This anatectic field is shown in Figure 6.25 in which the Qz:Ab:Or ratios of the Cashel microgranite sill and migmatite leucosomes are also represented. It is clear that while most of the microgranite sill plots within Winkler's anatectic field, the leucosomes are far more variable in terms of their Qz:Ab:Or ratios

and only a few points plot within the field with the majority plotting in the Qz-rich side of the triangle particularly the quartz-rich leucosomes.

The migmatite leucosomes do not plot within the anatectic field not because this was produced at 2kb compared to about 4-6kb in the Cashel area (Chapter 3) because increasing the pressure would shift the field towards the Ab apex (direction of arrow in Figure 6.25). It seems likely that the actual composition of the migmatites does not totally represent the melt generated at the time of melting because of the effects discussed in subsection 6.4 or that two processes (metamorphic segregation and partial melting for instance) took place. The effects of xenocrystic biotite, garnet and cordierite have already been discussed and must have increased the quartz normative values. These effects cannot be estimated numerically because some biotite and cordierite are believed to have crystallized from the melt.

In metamorphic segregations, the composition of plagioclase of the restite and leucosome are the same or the leucosome may be about 5% more albitic than the restite (Misch 1968). It has been shown in Figure 6.1 that plagioclase from the leucosomes and restites sometimes overlap with each other suggesting that metamorphic segregations have possibly taken place, an assumption supported by the presence of veins of apatite in the restites (see Chapter 7). However, the presence of normative orthoclase and the dominantly Na-rich plagioclase of the leucosomes (i.e. low Ca/Na ratios in the migmatites) indicate that partial melting was very significant. It can be postulated therefore that the quartz enrichment shown in Figure 6.25 indicates that metamorphic segregations took place either before or with partial melting.

6.8 Rb-Sr isotopes

The primary aim of Rb-Sr isotope study is to estimate the isotopic composition of the migmatite leucosomes of the Cashel area and determine whether they are internally derived from within the Dalradian metasediments or alternatively whether they are genetically related to the granites or intrusive migmatites present in the area.

The concentrations of Rb and Sr and the Rb-Sr isotopic compositions of five samples including one pelitic restite-migmatite leucosome pair

(Y68R/L) are given below in Table 6.5 and plotted on a conventional present day $(^{87}\text{Sr}/^{86}\text{Sr})_p$ ratios diagrams in Figure 6.26.

Table 6.5 Rb-Sr isotopic composition of the migmatite leucosomes

Sample number	Rb(ppm)	Sr(ppm)	$^{87}\text{Rb}/^{86}\text{Sr}$	$(^{87}\text{Sr}/^{86}\text{Sr})_p$	$(^{87}\text{Sr}/^{86}\text{Sr})_{480}$
Y42L	118.5	153.5	2.241	0.73936 ± 6	0.724033
Y65L	15.84	48.06	0.9558	0.72851 ± 8	0.72197
Y68L	14.53	462.8	0.09091	0.71756 ± 6	0.71693
Y68R	103.1	482.3	0.6193	0.72166 ± 4	0.71742
Y69L	13.73	497.3	0.07997	0.71759 ± 10	0.71704

Clearly there is a large scatter of the results and the best-fit regression line to the five data points has a very high MSWD of 357 and is therefore meaningless in terms of chronological information. However, the tie line joining the pelitic restite Y68R to its migmatite leucosome Y68L defines a slope corresponding to a Caledonian age of 544 my which is higher than the average age of 442 ± 25 my obtained from seven pelitic restite-migmatite leucosome pairs from eastern Connemara (Barber 1985).

Based on 31 samples, Barber (1985) showed that the peak metamorphism in Connemara was reached at about 480 my, an age in good agreement with that determined for the basic rocks of 487 ± 3 my (Jagger 1985) and therefore the initial $^{87}\text{Sr}/^{86}\text{Sr}$ ratios of the analysed samples were calculated at this age (i.e. 480 my). The $(^{87}\text{Sr}/^{86}\text{Sr})_{480}$ of the migmatites from the Cashel area are very similar to those obtained from similar migmatites from eastern Connemara (range from 0.71576 to 0.72365, Barber 1985). Y68L has a high initial $(^{87}\text{Sr}/^{86}\text{Sr})_{480}$ of 0.71693 which is very similar to that of its pelitic restite of 0.71742 which indicates that this migmatite was derived therefrom.

Since the main aim of Rb-Sr isotope study is to establish whether the migmatite leucosomes were internally derived from within the metasediments, from the basic magma as late differentiates or else from the intrusive granites, Rb-Sr isotopes of the intrusive gneisses and granites

(sensu lato) which are likely to have been the source and/or contamination of the migmatites were plotted for clarity in Figures 6.27-8. The data shown include 31 pelitic restites (one from this work, 10 from Jagger 1985; 20 from Barber 1985); 14 migmatite leucosomes (four from this work, 10 from Barber 1985) and 2 granite sills, 11 quartz diorite gneisses and 22 K-feldspar gneisses (Jagger 1985). The isochrons of the Oughterard and Galway granites are re-plotted from Leggo et al. 1966.

It is clear from Figures 6.27-8 that the migmatite leucosomes and the Cashel microgranite sill have very similar $^{87}\text{Sr}/^{86}\text{Sr}$ values to those of the metasediments but plot distinct from the Oughterard and Galway granites and quartz-diorite and K-feldspar intrusive gneisses. This conclusively indicates that the migmatite leucosomes and microgranite sill have no genetic relationships with the intrusive granites and gneisses present in the area but were almost certainly internally derived from within the metasediments.

6.9 Summary and discussion

In the foregoing sections, it has been noted that in the studied area the migmatite leucosomes exhibit stromatic, schlieren and nebulitic structures with abundant small, quartz-rich veins. Chilled margins, "lit par lit" structures and contact effects were not recorded which indicates that the temperatures between the pelitic restites and migmatite leucosomes were not significantly different from each other.

Mineralogically, the migmatites are trondhjemitic, quartz-rich and contain abundant xenocrysts of biotite, garnet, cordierite, sillimanite and possibly plagioclase, although textural evidence suggests that some biotite and cordierite were crystallized from the melt.

Although plagioclase in migmatite Y68L is richer in Ca than most restites, it is usually richer in Na and K than plagioclase in the pelitic restites. This is what would be expected in partial melting because of the strong fractionation of K and Na into the melt relative to Ca.

Chemically, the composition of the migmatite leucosomes is rather variable particularly if the 21 migmatites given in Barber (1985) are included. This variability is likely to be the result of wall-rock reactions, presence of xenocrysts, variations in the P-T conditions and fractional crystallization as

suggested by the REE. Comparison of the melts compositions calculated using compatible elements Cr, Ni and Co with the actual compositions of the migmatites show that the leucosomes were probably formed between 15-40% partial melting which is consistent with field observations.

The wide spread of the migmatite compositions around the experimentally determined field of Winkler (1979) suggests that naturally occurring migmatites exhibit chemically larger compositional ranges than those produced in the laboratory although the excess of normative quartz is probably the result of metamorphic segregations, diffusion of silica which may have occurred before melting with the position of the veins being determined or during melting during which a steep SiO_2 gradient could have been produced. However the presence of normative Or is evidence that the quartz-rich leucosomes were not derived simply by segregation processes.

Sr isotopes show that the migmatites have a significantly different signature from that of the Galway and Oughterard granites and quartz-diorite and the K-feldspar intrusive gneisses. This conclusively demonstrates that they are not related to these intrusive rocks but were internally derived from the metasediments.

The evidence presented therefore indicates that anatexis played the most important role in the generation of the Cashel migmatite leucosomes although metamorphic segregations were probably also significant.

Table 6.1 Comparison of the Cashel migmatite leucosomes with migmatites from eastern Connemara.

Major elements (wt%)	Y		Y1		B		B1		Y38PM		Y42PC		B2	
	Mean	S	Mean	S	Mean	S	Mean	S	Mean	S	Mean	S	Mean	S
SiO ₂	71.31	2.88	87.42	4.71	65.24	5.65	68.42	3.58	50.81	42.23	70.31			
TiO ₂	0.25	0.16	0.11	0.11	0.79	0.40	0.51	0.15	1.65	0.02	0.35			
Al ₂ O ₃	15.16	1.46	6.18	2.75	16.60	2.55	15.95	1.06	21.93	29.78	14.90			
Fe ₂ O ₃	0.56	0.43	0.25	0.16	1.42	0.51	1.08	0.43	1.88	2.14	0.77			
FeO	1.60	0.91	0.72	0.48	3.64	1.55	3.30	1.20	9.09	6.24	1.84			
MnO	0.03	0.01	0.02	0	0.08	0.03	0.08	0.04	0.16	0.13	0.05			
MgO	0.82	0.61	0.24	0.27	1.51	0.49	1.66	0.80	3.41	5.90	0.74			
CaO	2.15	0.60	0.82	0.61	2.19	0.51	1.50	0.38	1.70	0.0	3.04			
Na ₂ O	3.67	1.78	1.39	1.00	3.31	0.71	2.81	0.37	1.71	0.36	4.80			
K ₂ O	1.66	0.88	1.01	0.38	2.24	0.64	2.25	0.34	3.46	7.65	1.18			
P ₂ O ₅	0.11	0.07	0.08	0.06	0.17	0.11	0.14	0.08	0.35	0.01	0.49			

Table 6.1 continued

Trace elements (ppm)	33	32	17	72	24	74	12	99	339	31
Rb	53	32	17	72	24	74	12	99	339	31
Ba	376	270	90	633	351	441	165	768	2480	281
La	15	8	4	38	16	39	12	40	0	20
Ce	19	19	6	81	29	80	23	99	0	46
Y	16	6	4	24	9	21	4	58	0	39
Zr	42	55	105	187	57	40	4	263	0	60
Sr	274	108	82	326	107	233	63	210	81	336
Ca	17	7	2	20	4	18	3	28	34	13
Ni	8	3	4	27	15	24	9	48	12	16
Co	3	2	3	-	-	-	-	32	23	-
Cr	6	5	7	62	28	47	23	26	9	23
Zn	49	42	15	73	27	58	17	121	131	33
Cu	12	14	18	38	60	41	21	42	6	6

Y = average of 8 migmatite leucosomes dominantly taken from strauatic and schlieren outcrops.

Y1 = average of 6 migmatite leucosomes dominantly taken from thin veins quartz-rich outcrops.

B = average 14 migmatite leucosomes from eastern Connemara given in Barber (1985).

B1 = average 5 cordierite-rich segregation leucosomes given in Barber (1985).

B2 = average 2 migmatite leucosomes associated with semi-pelites taken from Barber (1985).

S = standard deviations

- = not determined

Table 6.2 REE in the Cashel migmatite leucosomes

	Y42L	Y68L	Y69L
La	15.81	12.60	5.11
Ce	26.50	19.98	9.25
Pr	3.59	2.66	1.23
Nd	11.72	7.61	4.84
Sm	1.70	1.24	1.08
Eu	1.87	1.10	1.85
Gd	1.36	1.08	1.13
Dy	0.90	1.08	0.72
Hb	0.16	0.28	0.08
Er	0.56	0.86	0.34
Yb	0.47	0.88	0.13
Lu	0.08	0.14	0.02
Σ REE	64.72	49.51	25.78
Eu/Eu*	3.75	2.91	5.12
(La/Lu) _{CN}			
	20.69	9.62	26.76

Table 6.3 Calculated degrees of partial melting and composition of the melts derived from the Cashel metasediments.

	P1		P2		R.P	S	P.R	S	M.G	S	10%	20%	30%	40%	50%
	Min	Max	Min	Max											
Cr	24.3	31.2	8.9	9.2											
Ni	29.4	44.5	17.6	26.7											
Co	20.0	22.3													
SiO ₂	56.7	5.62	52.30	6.12	56.7	5.62	52.30	6.12	69.35	4.54	81.45	72.06	67.40	63.40	61.10
TiO ₂	1.33	0.36	1.68	0.48	1.33	0.36	1.68	0.48	0.56	0.31	0	0	0.52	0.80	0.98
Al ₂ O ₃	20.33	3.34	22.03	3.71	20.33	3.34	22.03	3.71	16.48	2.00	4.26	13.30	15.83	17.77	18.63
Fetot	9.59	3.30	12.40	2.78	9.59	3.30	12.40	2.78	4.39	1.97	0	0	3.05	5.39	6.78
MnO	0.23	0.16	0.16	0.06	0.23	0.16	0.16	0.06	0.06	0.02	0.72	0.50	0.39	0.33	0.30
MgO	3.42	1.03	3.88	0.90	3.42	1.03	3.88	0.90	1.31	0.60	0	1.55	2.36	2.73	2.96
CaO	1.99	1.07	1.54	0.95	1.99	1.07	1.54	0.95	2.16	0.65	5.10	3.72	3.06	2.66	2.44
Na ₂ O	2.31	0.92	1.88	0.75	2.31	0.92	1.88	0.75	3.49	1.07	5.24	3.96	3.34	2.96	2.74
K ₂ O	3.90	1.23	3.99	1.23	3.90	1.23	3.99	1.23	2.04	0.70	2.61	3.48	3.71	3.67	3.81
P ₂ O ₅	0.20	0.19	0.14	0.10	0.20	0.19	0.14	0.10	0.16	0.14	0.62	0.43	0.34	0.29	0.26
Total	100	100	100	100	100	100	100	100	100	100	100	100	100	100	100

contd

Table 6.3 continued

	U.P	S	P.R	QRL	S	10%	20%	30%	40%	50%
SiO ₂	56.39	3.89	52.30	88.91	4.71	78.83	71.51	65.93	62.53	60.56
TiO ₂	1.32	0.21	1.68	0.11	0.11	0	0	0.48	0.78	0.96
Al ₂ O ₃	21.81	2.73	22.03	6.28	2.75	16.77	20.57	21.29	21.49	21.54
Fetot	10.26	1.98	12.40	1.07	0.69	0	1.67	5.26	7.05	8.10
MnO	0.14	0.01	0.16	0.02	0.00	0	0.06	0.09	0.11	0.12
MgO	2.78	0.38	3.88	0.25	0.27	0	0	0.21	1.13	1.68
CaO	1.37	0.64	1.54	0.83	0.61	0	0.68	0.98	1.11	1.20
Na ₂ O	1.98	0.74	1.88	1.41	1.00	2.43	2.34	2.22	2.13	2.07
K ₂ O	3.68	0.76	3.99	1.03	0.38	0.76	2.40	2.96	3.21	3.37
P ₂ O ₅	0.27	0.11	0.14	0.09	0.06	1.21	0.77	0.58	0.46	0.40
Total	100	100	100	100	100	100	100	100	100	100

R.P = average of 47 regional (unhornfelsed) pelites

P.r = average of 104 pelitic restites (42 from Barber, 1985 and 62 hornfelses from this work)

U.P = average of 54 unmigmatized pelites from Barber (1985)

M.G = average of 29 migmatite leucosomes (21 from Barber, 1985 and 8 from this work)

P1 = degrees of partial melting calculated using R.P and P.R (only the average of 62 samples for Cr contents was taken in P.R).

P2 = degrees of partial melting calculated using U.P and P.R (only the average of 9 samples for Cr and 53 samples for Ni were taken in U.P)

QRL = average of 6 quartz-rich leucosomes

S = standard deviations (one sigma)

Percentages indicate degree of partial melting

- = not determined

Table 6.4 continued

- C = normative corundum
- 1 = pelitic glass of Green (1976), anhydrous
- 2 = results of Green at 4kb, 780°C, 124 hours, 5% water added
- 3 = results of Green at 10kb, 820°C, 95 hours, 5% water added
- 4 = results of Green at 10kb, 1040°C, 2.5 hours, 5% water added
- C.M = average of seven Cashel microgranite sill analyses
- M.L = average of the eight migmatite leucosomes collected from strauematic and schlieren outcrops
- R.P, U.P, M.G, S as in Table 6.3.

KEY TO FIGURES 6.1 - 28

Figure 6.1 Ab:An:Or diagrams showing the composition of plagioclase from the pelitic restites and migmatite leucosomes. The arrows indicate changing compositions from cores to rims.

Figures 6.2 - 18 Scatter diagrams of the migmatite leucosomes

Figure 6.2 Al_2O_3 vs SiO_2

Figure 6.3 TiO_2 vs SiO_2

Figure 6.4 Fe_{tot} vs SiO_2

Figure 6.5 K_2O vs SiO_2

Figure 6.6 Na_2O vs SiO_2

Figure 6.7 Na_2O vs CaO

Figure 6.8 P_2O_5 vs CaO

Figure 6.9 K_2O vs TiO_2

Figure 6.10 Ba vs K_2O

Figure 6.11 Rb vs K_2O

Figure 6.12 Sr vs CaO

Figure 6.13 Ga vs Al_2O_3

Figure 6.14 Y vs P_2O_5

Figure 6.15 La vs Ce

Figure 6.16 Ce vs Y

Figure 6.17 Ce vs K_2O

Figure 6.18 Cr vs TiO_2

Figure 6.19 REE distribution patterns in 3 pelitic restite-migmatite leucosome pairs from the Cashel aureole.

Figure 6.20 - 24 Scatter diagrams showing the effects of xenocrysts on the compositions of the Cashel migmatite leucosomes.

Figure 6.20 MgO vs Al_2O_3

Figure 6.21 MgO vs TiO_2

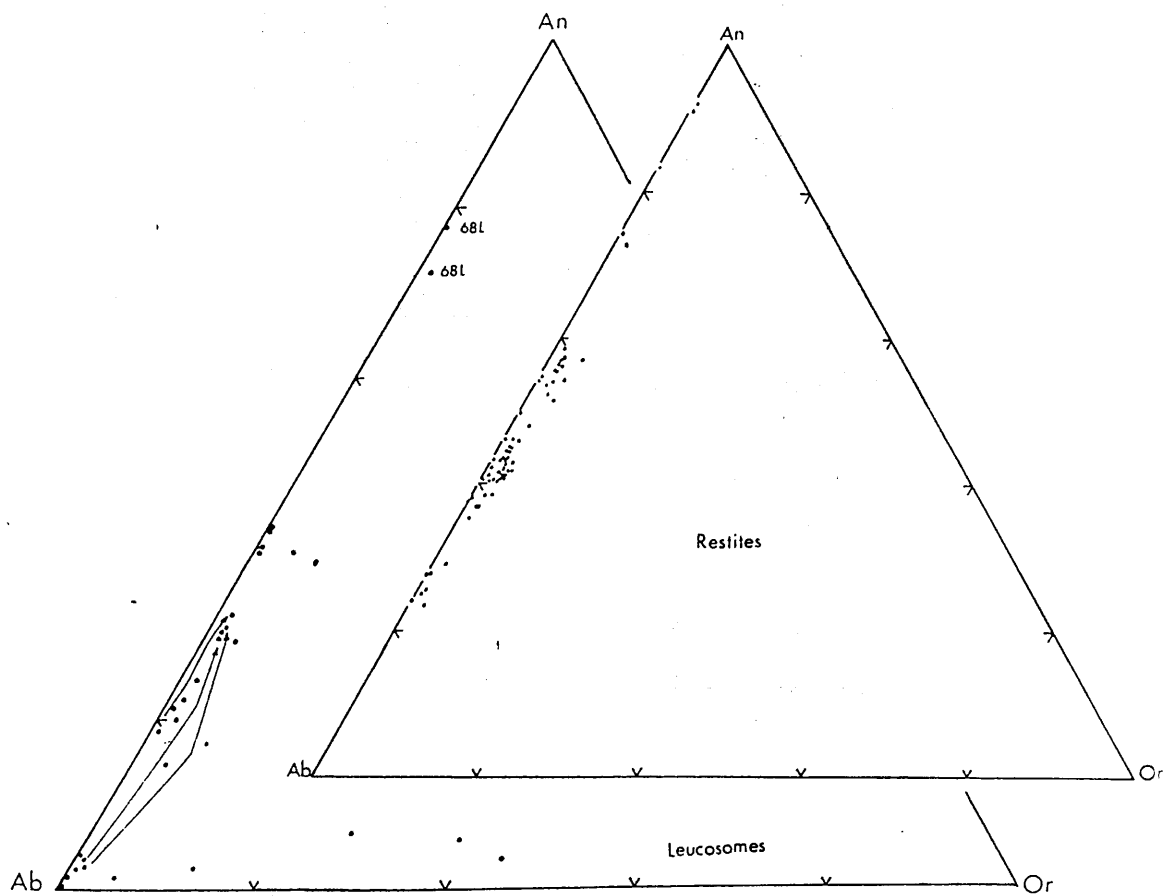
Figure 6.22 Fe_{tot} vs TiO_2

Figure 6.23 Fe_{tot} vs MgO

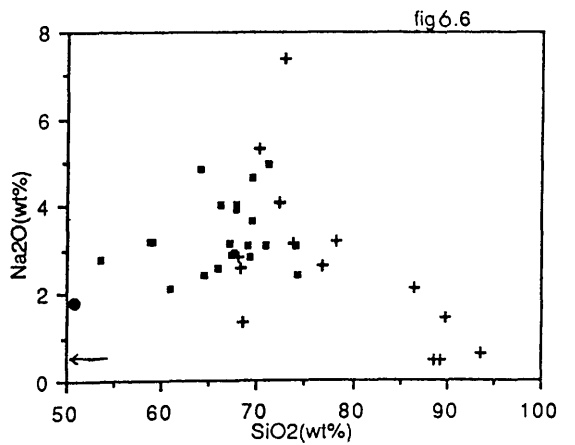
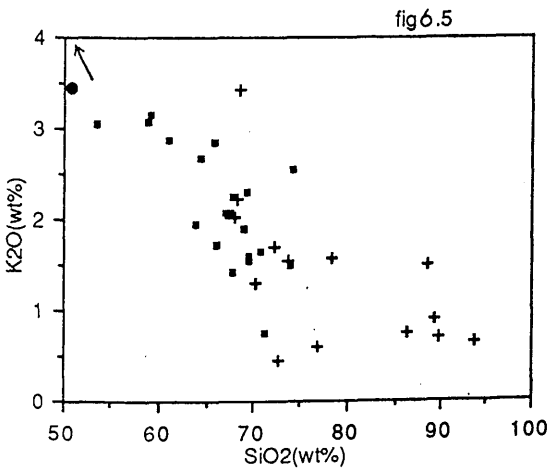
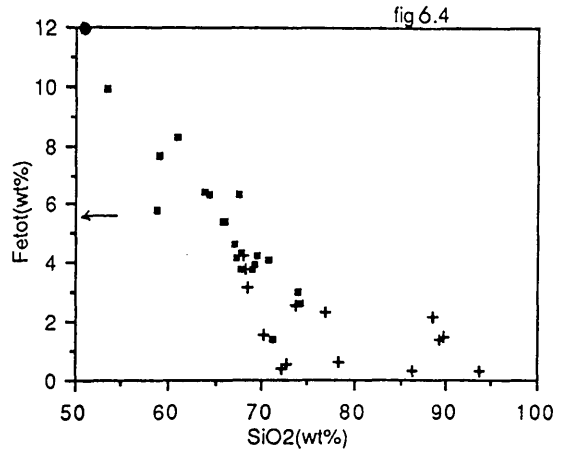
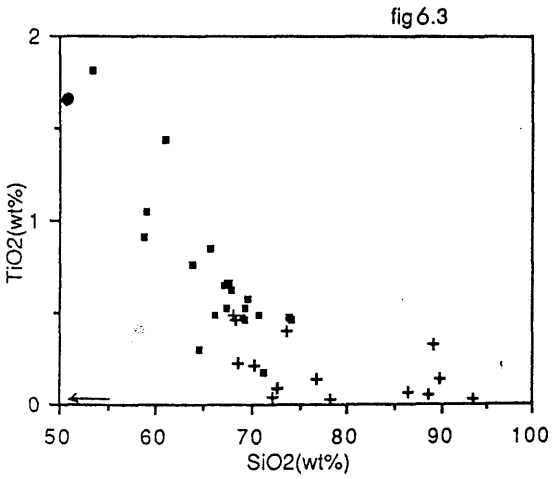
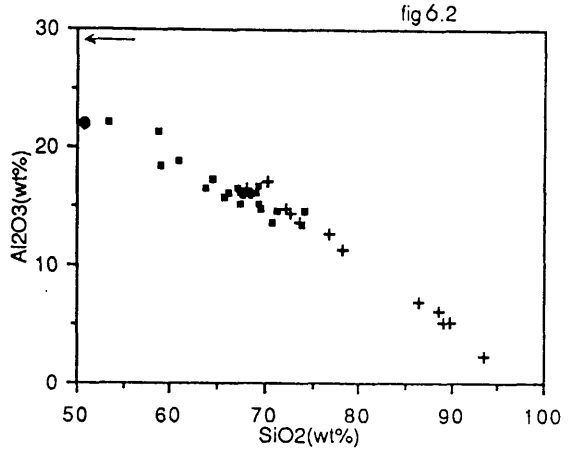
Figure 6.24 Fe_{tot} vs Al_2O_3

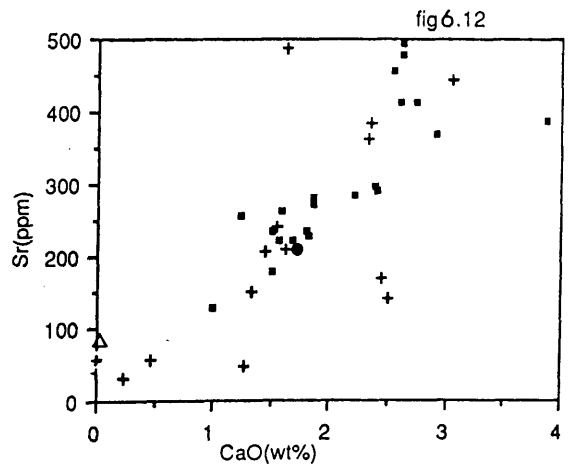
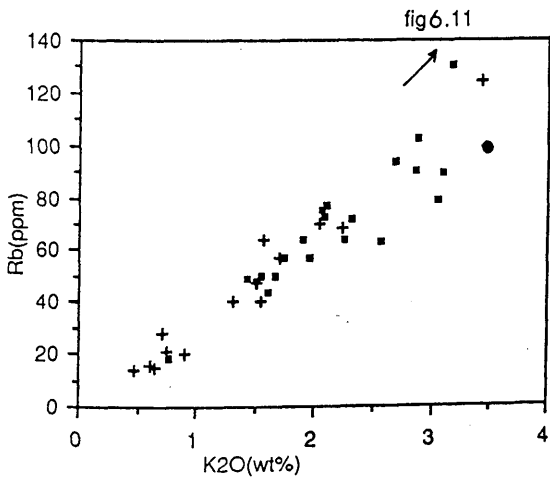
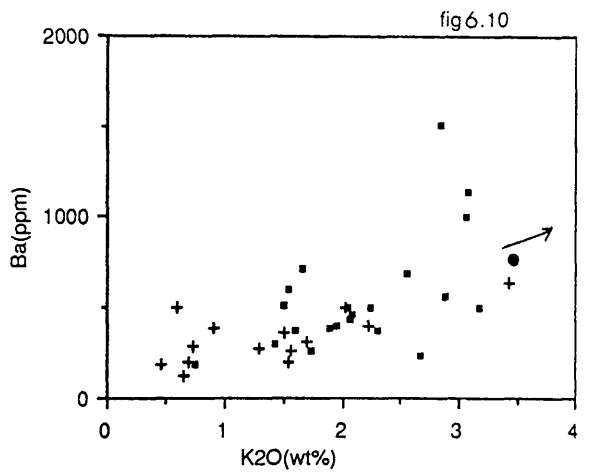
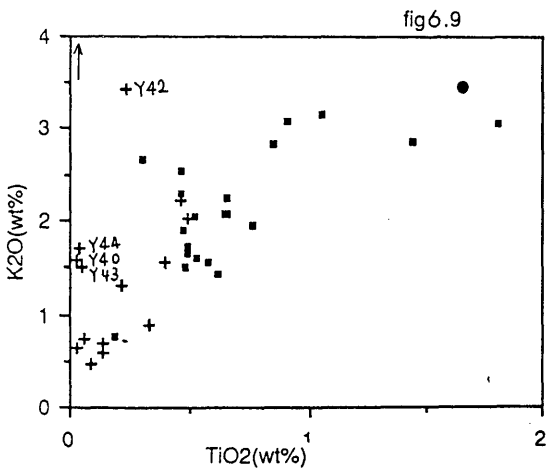
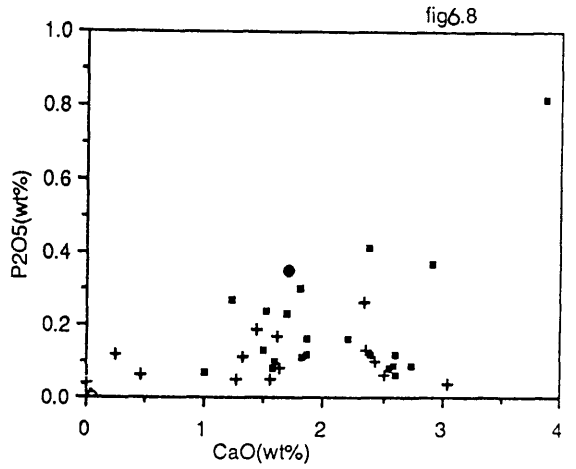
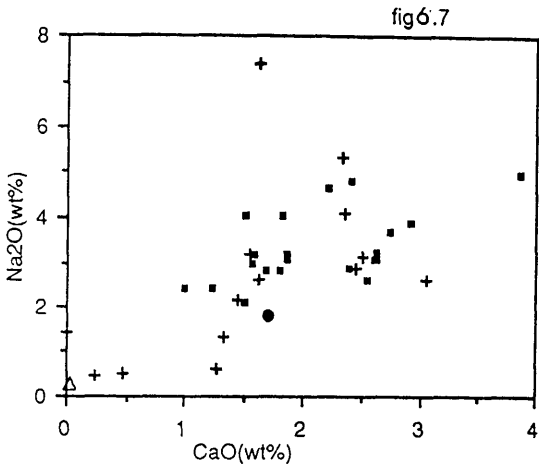
- Figure 6.25 Normative Qz:Ab:Or: ratios of the magmatite leucosomes, sample Y38PM and Cashel microgranite sill. The anatectic field of Winkler (1979) is also shown.
- Figure 6.26 $(^{87}\text{Sr}/^{86}\text{Sr})_p$ vs $(^{87}\text{Rb}/^{86}\text{Sr})$ for 4 migmatites and 1 restite analysed in this work.
- Figure 6.27 $(^{87}\text{Sr}/^{86}\text{Sr})_p$ vs $(^{87}\text{Rb}/^{86}\text{Sr})$ for the Cashel Formation metasediments, migmatite leucosomes and microgranite sill. The isochrons of the Oughterard and Galway granites are also shown.
- Figure 6.28 $(^{87}\text{Sr}/^{86}\text{Sr})_p$ vs $(^{87}\text{Rb}/^{86}\text{Sr})$ for the Cashel Formation metasediments, migmatite leucosomes, microgranite sill, K-feldspar and quartz diorite gneisses.

fig 6.1



- Migmatite leucosomes from eastern Connemara
- + Migmatite leucosomes from the Cashel area
- Sample Y38 PM
- △ Sample Y42PC (direction of arrow unless stated)
Fetot as Fe₂O₃





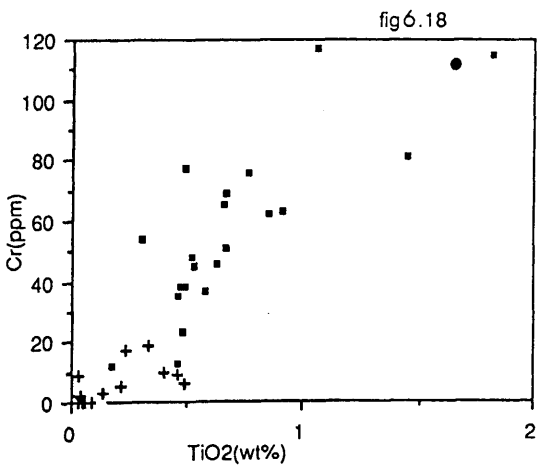
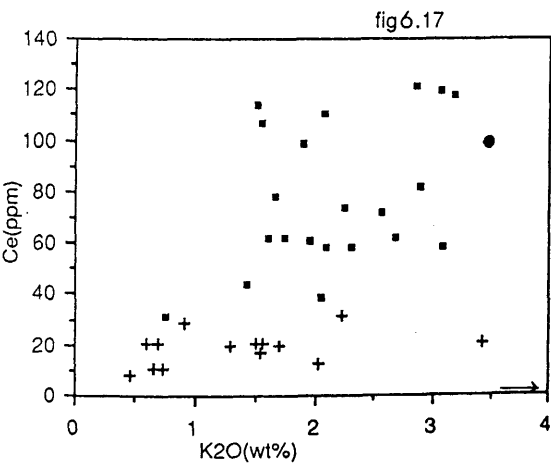
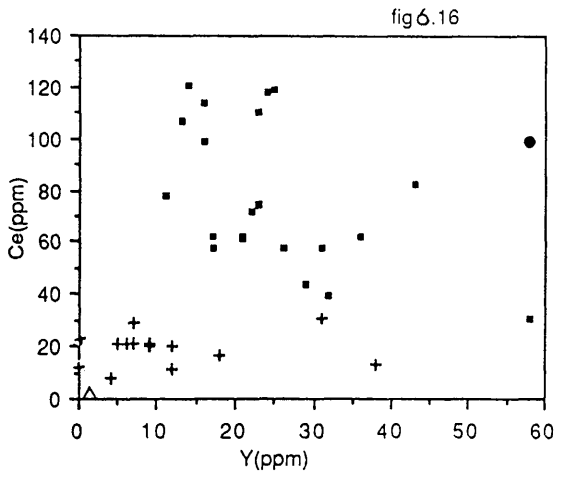
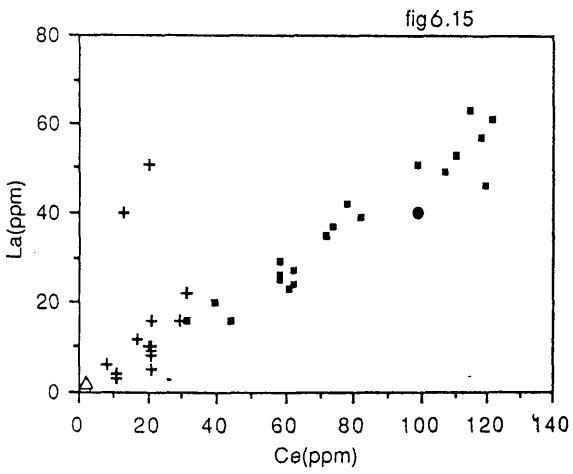
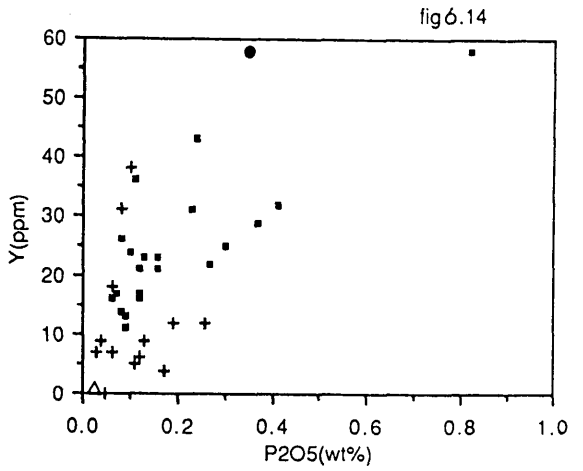
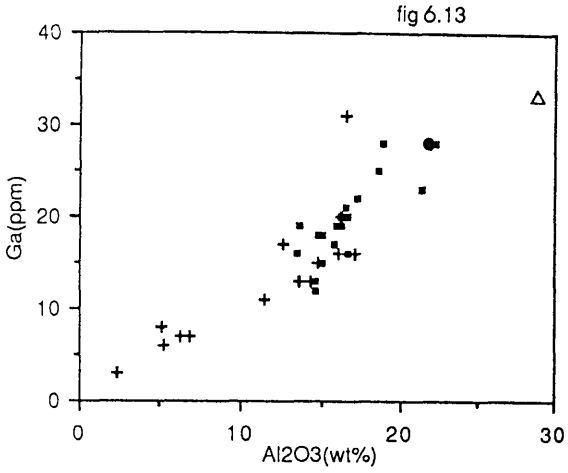
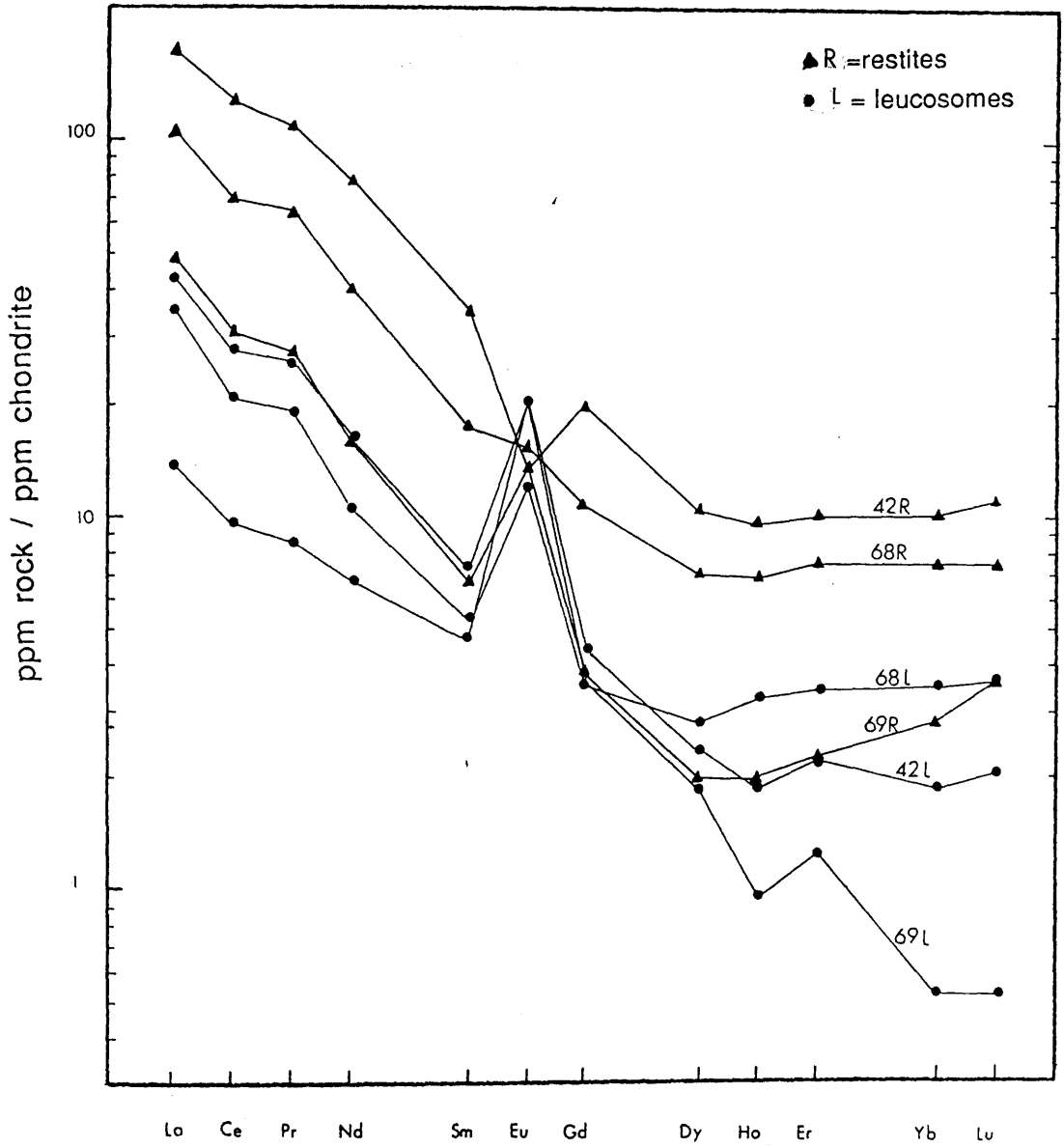


fig 6.19



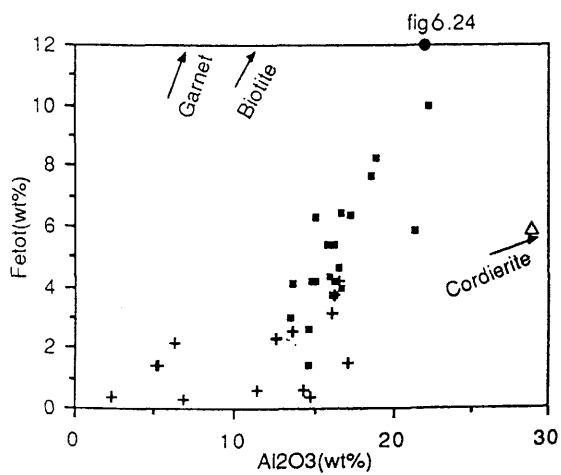
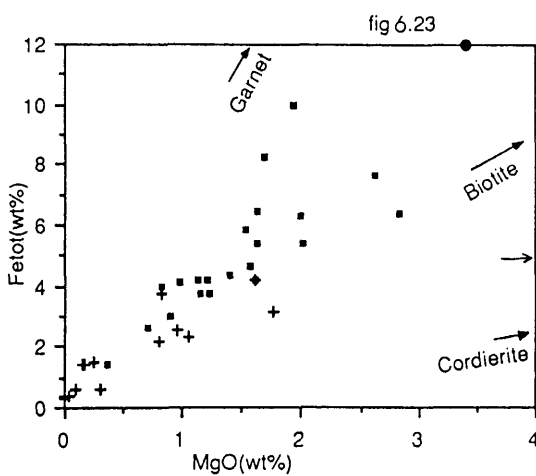
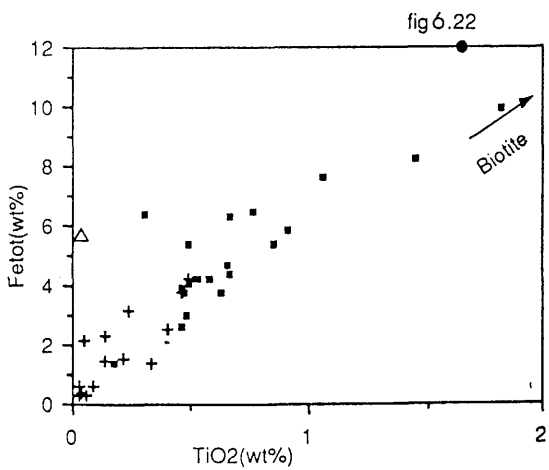
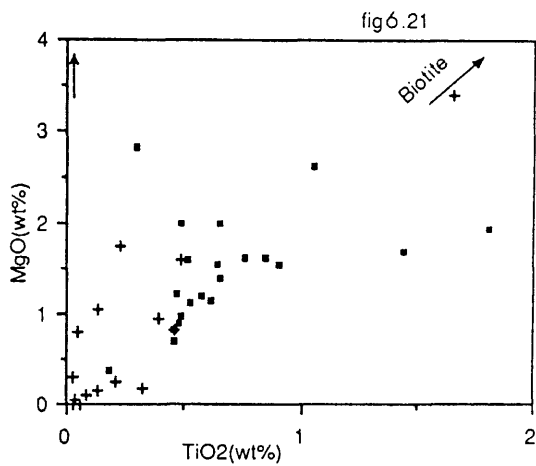
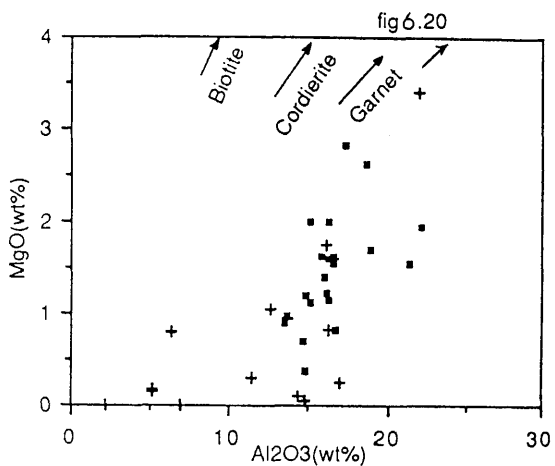
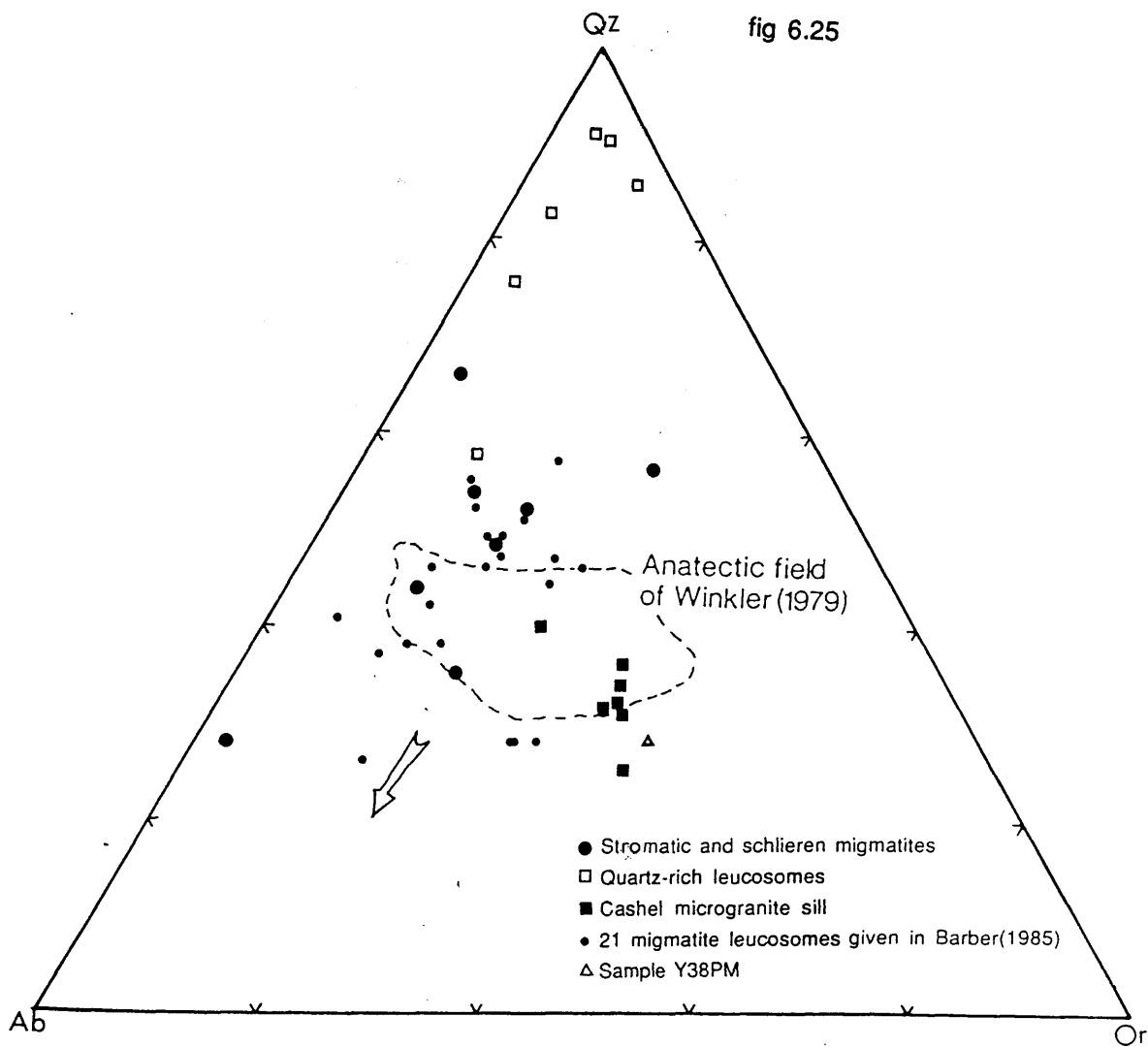


fig 6.25



UNIVERSITY OF TORONTO
 LIBRARY

fig 6.26

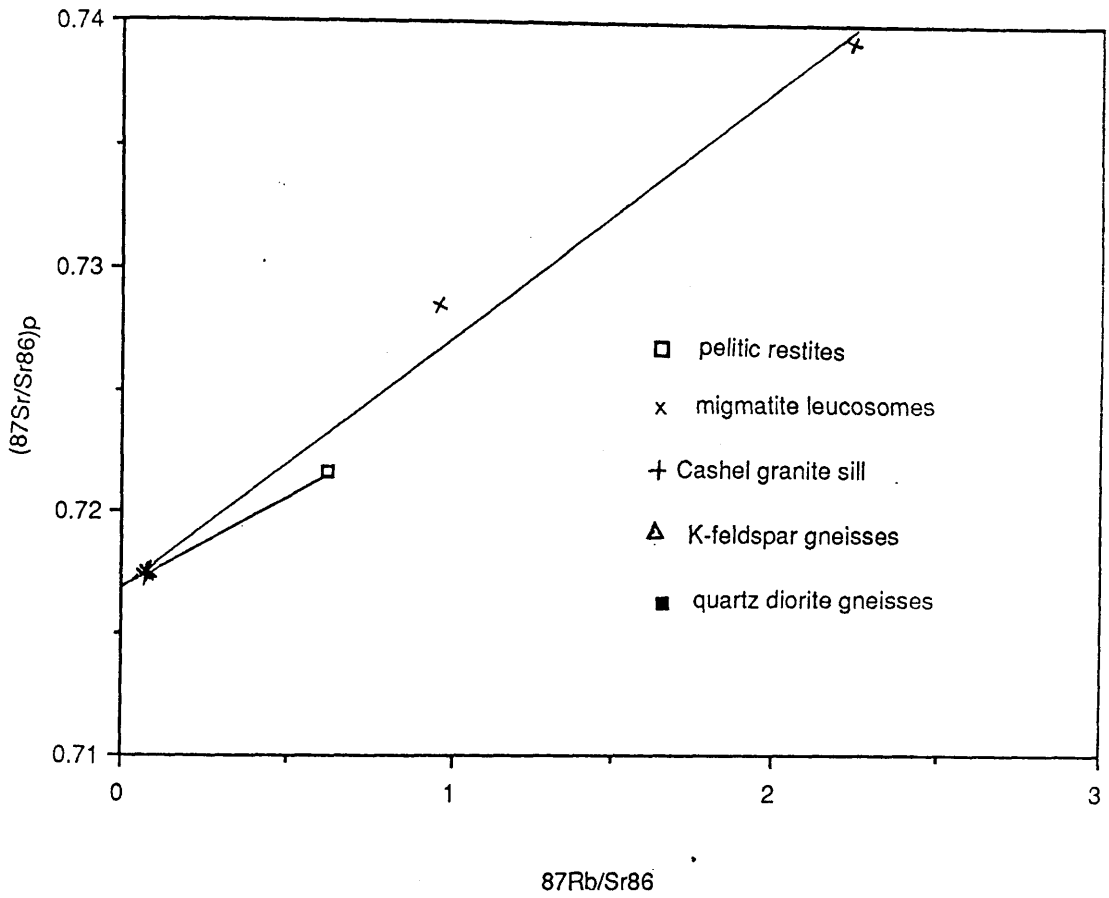


fig 6.27

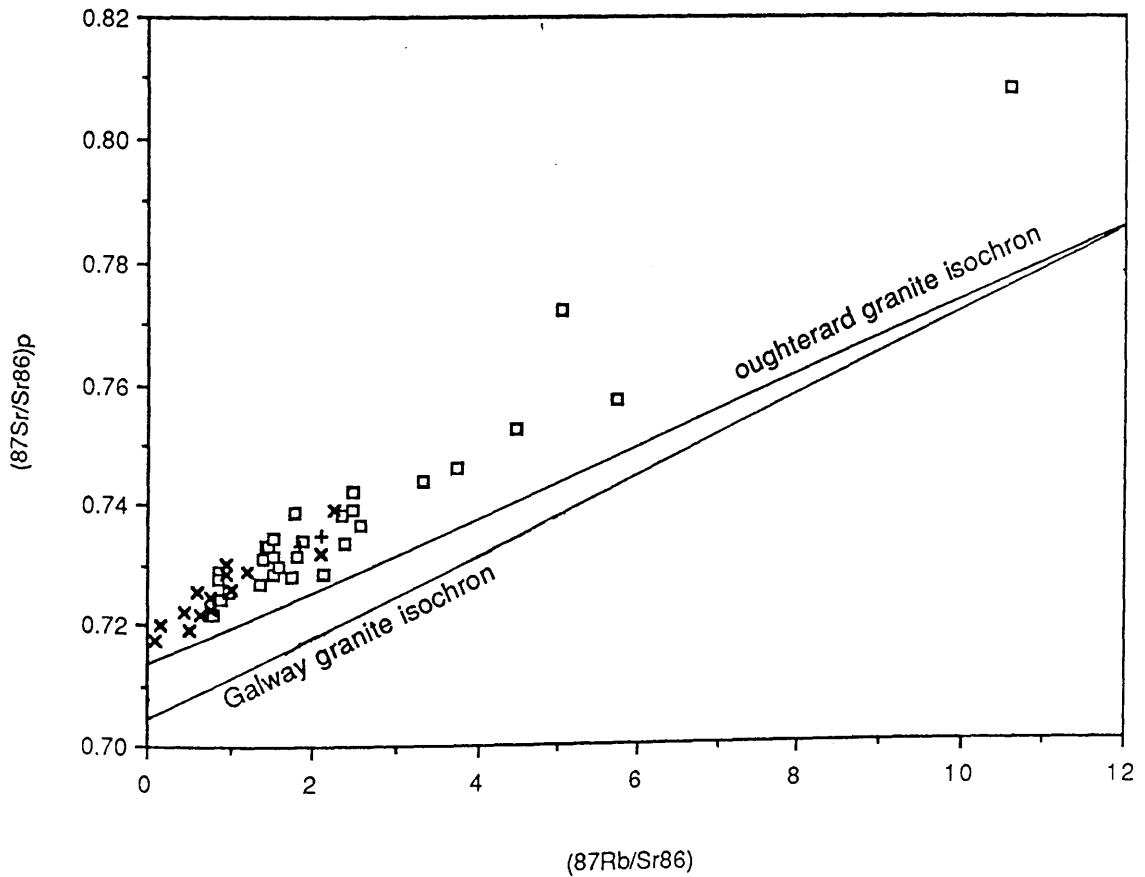
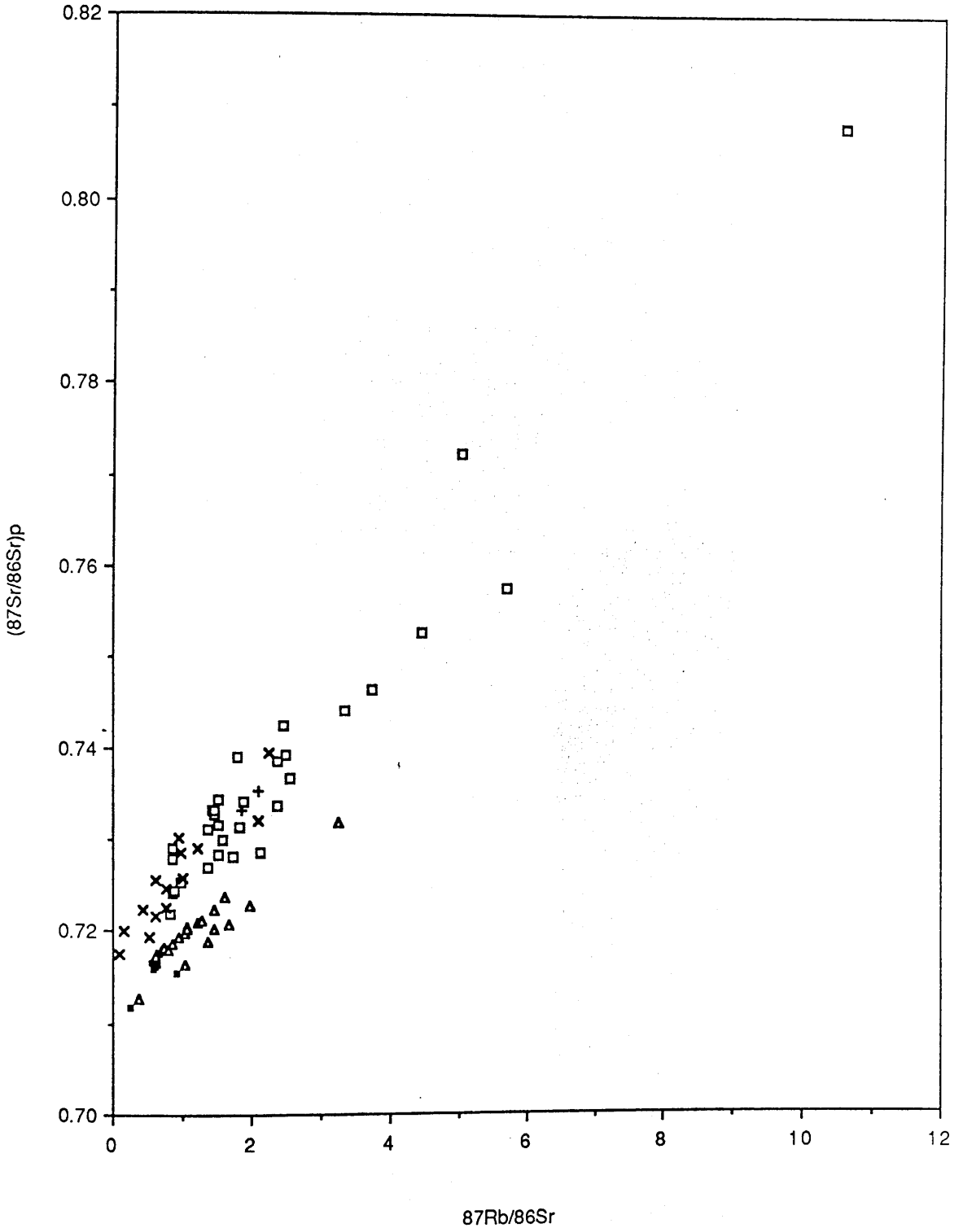


fig 6.28

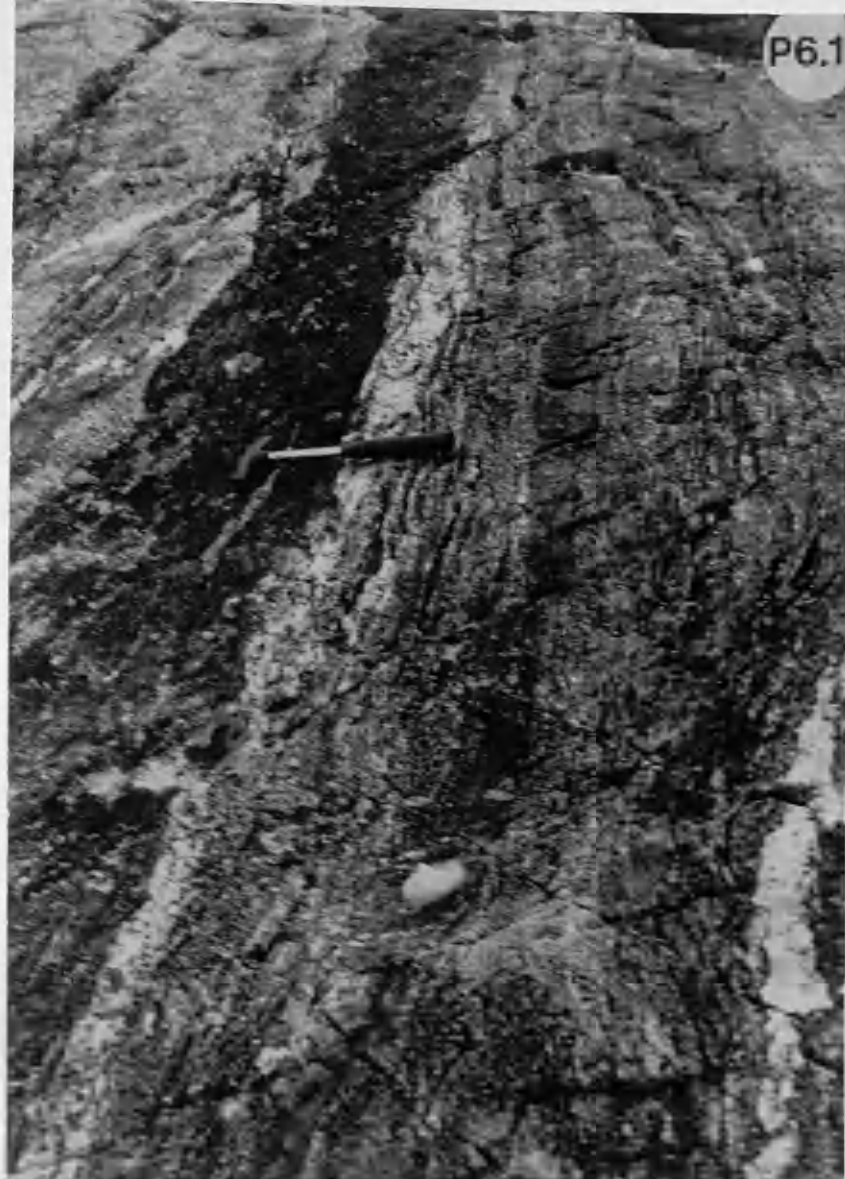


6.1 -2 Migmatite leucosomes from the Cashel aureole

6.1 StrOmatic "layered" migmatites from the southern side of Cashel Hill.

6.2 Small veins of leucosomes from the northen side of Cashel Hill.





U and Th

7.1 Introduction

The behaviour of the major and some trace elements in the Cashel thermal aureole including their behaviour during anatexis and metamorphic segregation have already been discussed in Chapter 6. In this chapter, the behaviour of U and Th is considered and their partition coefficients between the restites and migmatite leucosomes are also discussed

The fission track and instrumental neutron activation analyses, the principles and methodology of which are discussed in Chapter Two, were used throughout this study and are aimed at :

- 1- Investigating the spatial distribution of U in the Cashel metasediments.
- 2- Studying the evolution of U and Th with hornfelsing of the metasediments.
- 3- Investigating the distribution of U in individual minerals and when possible estimating its content.
- 4- Evaluating the relationships between the concentrations of U derived using instrumental neutron activation analysis and the variation in its spatial distribution with hornfelsing of the metasediments.

Rock samples 70 and 77 were successfully subjected to fission track and neutron activation analyses respectively for U but due to analytical problems no fission track mapping for the distribution of Th could be achieved. The rock types investigated include unhornfelsed pelites, hornfelses, pelitic xenoliths, migmatite leucosomes, Cashel microgranite sill. Some minerals including zircon, apatite and biotite have also been subjected to fission track analyses.

7.2 Results of fission track analysis

7.2.1 Whole rock U distribution

In the Cashel pelites U occupies a variety of sites including zircon, apatite, biotite, grain boundaries, alteration products, veins, along the schistosity planes and mineral fractures. Typical whole rock U distribution patterns are shown in Plates 7.1-8. The mode of distribution of U in zircon, apatite and biotite is not included here but is detailed in subsection 7.2.1.2

U located along the mineral boundaries is uncommon and seems to be more important only in those samples showing signs of hydrothermal alteration. It is revealed by scattered, less conspicuous single fission tracks particularly

over the sericitized and chloritized parts of biotite and garnet when in contact with each other (Plate 3). This type of U was possibly either released from garnet and/or biotite or hydrothermally added. The modes and conditions of occurrences of U in garnets have been investigated by Komarov *et al.* (1967) who noted that U occurs in the crystal structure of garnets, as uraniferous microscopic inclusions and as hypogene thin films. They also noted that the more calcic the garnets the higher the U contents. Therefore its position in the garnet structure is probably determined by the similarities of its ionic radius (0.97Å) to that of Ca^{+2} (0.99Å) *i.e.* in the eight fold coordination in respect to oxygen.

In the Cashel metasediments, garnets are almandine-rich and include only minor amounts of Ca (Chapter 4). Because U has too large an ionic radius compared to Fe^{+2} (0.74Å), almandine is expected to be extremely low in U and indeed the fission track analysis show that it is the case. Therefore U detected at the grain boundaries of garnets cannot have originated therefrom. Since biotites do contain U, it is very likely that some of it was released from biotites to the altered parts although its tendency to be more widespread in the more altered rocks suggests that the addition of some U via hydrothermal solutions is very probable.

In the altered minerals and alteration products, particularly in sericitized plagioclase, biotite and garnet, U is shown by scattered fission tracks which are sometimes relatively dense (Plate 4). The presence and density of the fission tracks are directly proportional to the degree of alteration of the rocks mainly sericitization and except biotite, all other fresh minerals do not produce any fission tracks at all, thus suggesting that U is not primary but probably secondarily added and/or redistributed.

U residing along mineral fractures is rare and detected in fractured garnets only. Individual garnets were separated from the same rocks showing this type of U distribution to test whether it is hypogene or related to other minerals included inside garnets. The final garnet grains were unfractured and virtually free from any foreign inclusions. The grains were then mounted on microprobe glasses, polished using 6 μ and 1 μ diamond paste respectively, cleaned in petroleum ether for 20 minute and irradiated under similar conditions to those of the thin sections. The results were decisive in that no

one single fission track could be seen over more than 200 garnets. The presence of U in the fractures is therefore related to the accessory minerals and/or it was secondarily added. The fission tracks over zircons are star-like that can readily be identified and indeed some of the U in fractured garnets is related to zircon (Plates 7.3,7.8). However, microprobe analyses show that sericite is also abundant in the fractures suggesting that some U is coming in this secondary mineral although hydrothermal addition of U is also possible.

U along the schistosity planes is revealed by single fission tracks which are sometimes quite dense. This type of U distribution is more frequent in the more schistose pelites and contributes substantially to the whole rock U contents and although much of it is located in sericite because the density of the fission tracks is higher in the more altered parts, some is likely to be adsorbed onto the surfaces of biotites. The single tracks sometimes developed over fibrolitic sillimanite along the schistosity planes are also attributed to sericite because U has too large an ionic radius to enter sillimanite and there is no indication of U-bearing sillimanite in the literature.

U in veins is rare and has been recorded in one sample only (Y14) which is strongly altered and reveals all the types of U distribution discussed so far. The density of fission tracks is between that of zircon and apatite over thin veins of secondary epidote which are cross-cutting the schistosity of the rock (Plate 7.6). Hydrogen isotope ratios of epidote and quartz from similar veins indicate a formation temperature of 300 ± 16 °C (Jenkin, pers. com.). δD values of epidotes from the studied area range from -30 to -10‰ and probably indicates that the fluids deposited these veins had similar δD values. Values this high can only be derived by having some component of sea water or equatorial meteoritic water within the fluid. Because the nearby Roundstone granite has also been affected by similar retrogressive events, the epidote veins were probably formed in a hydrothermal connective circulation system set up by the Roundstone granites and probably also the Galway granite (Jenkin, pers. com.).

7.2.2 Individual minerals

Fission track studies of individual minerals separated from the pelites show that U is exclusively restricted to zircon, apatite and biotite. Garnet,

quartz, feldspars and cordierite must therefore be very low in U .

Zircon is usually included in biotite but also in cordierite, garnet and plagioclase. It has great inhomogeneities in both U contents and distribution patterns. Such a behaviour led to more detailed studies including high power binocular microscope and intensified fission track analyses. More than 300 grains were hand picked at random from eight samples occurring at different distances from the Cashel hill intrusion for shape, colour, surface abrasion, overgrowth, and fission track studies with the results being shown in Table 7.1 and portrayed in Figure 7.1. The results of the fission track analysis are discussed at the end of the section.

The shape of zircons is very variable and ranges from completely rounded grains through to typically tetragonal crystals. Near the basic intrusion, zircons are larger in size, more euhedral and frequently show complex facetting. The colour also changes from dominantly deep brown in the unhornfelsed rocks through to mostly pink in the contact areas.

Brown zircons are small in size (often $\leq 90\mu\text{m}$), frequently rounded to subrounded and always show the typically pitted and abraded surfaces even in those grains picked from samples collected adjacent to the basic rocks (e.g. Y15 and Y17). These signs, which indicate mechanical abrasion during transport, can be considered as good evidence that no later overgrowth or resorption took place and therefore suggest a detrital origin for this group of zircons. This suggestion is supported by the dominance of brown zircons in the unhornfelsed rocks and their extremely high U contents (Plate 7.8). The rare brown but euhedral crystals occasionally recorded were possibly protected in other minerals during transport.

Pink zircons, however, are larger in size (often $\geq 60\mu\text{m}$), more euhedral, exhibit complex facetting, have intact, shining surfaces and have well preserved terminations on one end and sometimes on both ends. The remaining zircons examined are intermediate in colour, shape and U contents between deep brown and pink zircons.

The volume percentages of different zircon types obtained from eight samples were calculated from the total number of grains counted and this is better than taking the absolute number because duplicate separations from the same samples yielded variable numbers of grains possibly because of the

inhomogeneity of the rocks. The proportions of each type in six samples plotted at decreasing distance towards the intrusion are shown in Figure 7.1. Pink zircons increase noticeably as the degree of hornfelsing rises reaching their highest percentages near the contact of the intrusion but in contrast brown zircons diminish to their lowest values. This trend is possibly caused by recrystallization processes whereby most of brown zircons were recrystallized into intermediate and pink ones, a suggestion supported by the abnormally high temperature reached particularly near the basic rocks. This is discussed further below.

Generally there are three possible origins for pink zircons namely: detrital, recrystallized or newly crystallized zircons. The first possibility is unlikely because the more euhedral the crystals, the greater the size, which is opposite to that expected for detrital grains. Moreover, the proportions of pink zircons, their size and degree of refacetting increase systematically and markedly towards the intrusion and there is no evidence which suggests that those zircons occurring far away from the contact should be smaller in size, and anhedral with pitted surfaces compared to those near the contact. Furthermore, pink zircons cannot have been detrital grains overgrown by more euhedral, U-rich layers because for an overgrowth to have occurred then the cores should have similar fission track density and distribution patterns to those of brown zircons which is not the case (see below).

Pink zircons as metamorphic recrystallization of detrital ones is justified in many respects. The grain size and number of euhedral crystals increase towards the intrusion, consistent with the abnormally high temperature reached near the basic rocks. Moreover, the presence of intermediate zircons in colour, shape, U contents and the relative increase of pink zircons but decrease of brown ones is another support. This can be regarded as an argument to exclude the third possible origin because if the pink zircons are unrelated to the brown zircons then no field, morphological and U contents gradation between the two extreme groups should be found (see Plates 7.8-10). It is almost certain therefore that pink zircons are metamorphic recrystallization of detrital ones. However because some few pink zircons are also invariably present in the unhornfelsed rocks, it seems probable that recrystallization processes took place in the whole migmatite zone but more

significantly near the basic and ultrabasic complex. U-Pb dating of pink zircons should yield a recrystallization age which should be similar to that of the basic intrusion which is 487 ± 3 Ma (Jagger 1985).

The density of the fission tracks in zircons depends primarily on their colours, the deeper the colour the higher the density. Brown zircons exhibit the same fission track distribution patterns and accommodate large quantities of U which is homogeneously distributed throughout the whole grains (Plate 7.8). Pink zircons also exhibit very similar fission track density and distribution patterns among each other but significantly different from those of brown zircons. The pink crystals examined showed great inhomogeneities in the distribution of U but in most cases these inhomogeneities show a regular pattern, being dense at the rims, two ends and along fractures but scattered in the cores (Plate 7.10).

The fission tracks at the rims are sometimes dense so that the shape of the crystals can be drawn without matching with the actual zircons. Those produced along fractures are rare but when present are denser than those at the cores. At the two ends, the fission tracks are also dense but restricted to the more euhedral crystals. The tendency of U to be concentrated at the rims is of particular importance because of its high concentrations and regularity among the studied pink zircons. Three possible processes can cause such a pattern namely overgrowth of zircons by U-rich layers, recrystallization of detrital zircons with U gain by equilibration with the environment or supergene addition of U.

Overgrowth of zircons has already been excluded and therefore crystallization of new U-rich layers is very improbable.

The process of recrystallization with U gain by equilibration with the environment seems to have some support. While recrystallization of zircon has already been discussed, the availability of U in the environment is probably due to the replacement of U-bearing biotite by U-free cordierite, garnet and sillimanite and recrystallization of U-rich brown zircons into U-poor pink ones. The mechanism(s) of uptake of U by zircons is difficult to define reliably. Absorption of U by zircons through their external microfractures seems to be a special property of the fractured surfaces of the grains which allow the penetration of U through thin cracks (Grauert *et*

al.,1974). Although no microcracks were seen and U is not distributed along channels (Plate 7.10), an inward diffusion of U through the microcracks is regarded as most probable because the high density of the fission tracks can make the channels invisible.

If U along fractures and at the rims is supergene then spontaneous fission tracks would not appear along the margins and fractures. This is not the case and indeed spontaneous fission tracks are denser along fractures, at the two ends and to some extent at the rims, compared to the cores (see Plate 7.12) which indicates that U in zircons is primary.

In biotite U occupies three main sites namely: in zircon inclusions, adsorbed onto the flake surfaces and in the crystal lattices. In the crystal lattices, the presence of U is favoured by the large ionic radii positions available within biotites. U is revealed by single, uniformly distributed fission tracks indicating that U is homogeneously distributed within the flakes. The fission track densities from the 12 biotites analysed ranges from $0.76 \times 10^4 \text{ t cm}^{-2}$ to $3.25 \times 10^5 \text{ t cm}^{-2}$ giving a U concentration of between 0.09ppm and 3.25ppm which is significantly low compared to both zircon and apatite (Table 7.2).

A common feature which was noted in all studied samples is that not all biotites contain U and the reason for this will be considered later.

Apatites whatever their crystal shape, size and mounting positions always exhibit the same pattern of U distributions, being uniformly distributed throughout the whole crystals (Plates 7.7¹²). The fission track densities vary from $0.75 \times 10^6 \text{ t cm}^{-2}$ to $5.59 \times 10^6 \text{ t cm}^{-2}$ giving U contents of between 7.64ppm and up to 57.90ppm. This particular wide range coupled with relatively large U variations within the same samples (Table 7.2) suggest that recrystallization of apatite took place. Mineral separation of apatite did not give much information because the grains examined, either acicular or hexagonal, are colourless and do not show any signs of mechanical effects. However two acicular apatites were yellowish in colour unlike the remaining apatites and these may be detrital in origin; although the lower melting point of apatite compared to zircon suggests - by inference - that recrystallization of apatite is very probable.

7.2.3 U in the Cashel microgranite sill and migmatite leucosomes

In the Cashel microgranite sill, U occurs in zircon, apatite and sphene. Sphene is very rare and therefore no specific fission track studies were carried out on this mineral whereas both zircon and apatite exhibit the same pattern of distribution as those in the metasediments. The similarity of U distribution in zircons from the sill to that of intermediate and pink zircons from the pelites is of particular importance because it supports the interpretation that the granite sill represents the material melted from the metasediments rather than late differentiate of the basic magma. The major minerals are very low in U because no fission tracks were produced but where found they are very rare and always over sericitized minerals.

In the migmatite leucosomes, U is restricted to zircon and apatite and only very few single tracks are formed over sericitized plagioclase indicating that U is strongly controlled by the accessory minerals.

7.2.4 Field relationships

All types of zircon produced extremely high fission track densities that counting of the tracks is impracticable and consequently any changes in their U contents toward the intrusion could not be numerically evaluated. However, the recrystallization of U-rich brown zircon into U-poor (roughly 30-50% poorer) pink zircons near the basic intrusion and the substantial melting of this in the pelitic xenoliths indicate that significant amounts of U were lost from the pelites.

The contents of U in apatite exhibit large variations within the same samples (Table 7.2) and no changes toward the the contact of the intrusion could be obtained. However, the steady decrease of apatite as the degree of hornfelsing rises followed by a further drop in the pelitic xenoliths indicates that U in apatite must have left most of the contact hornfelses and pelitic xenoliths.

In biotites, U is more abundant in the regional pelites and their adjacent intermediate hornfelses than in the more desilicated contact hornfelses and it is practically absent in the xenoliths. The most significant loss of U from biotites is caused first by its replacement by U-free cordierite, garnet and sillimanite and second as a result of its recrystallization.

Biotite does not always produce fission tracks and sometimes even within the same samples some flakes contain U while others do not. There are four possible reasons which can cause such a trend namely: the biotites are not the same, some biotites were not at the contact of the detectors during irradiations, selective supergene addition or removal of U or a characteristic feature originally present in the sediments from which the biotites were crystallized.

Biotite analyses from 25 samples (Chapter 4) show that the only significant difference that can be detected is the higher Mg/Fe ratios in the contact samples and xenoliths compared to the regional pelites which have no bearing on U contents because neither does U substitute for Fe and Mg nor form solid solution with them thus excluding this possibility.

Although much of chloritized biotites were possibly not at the contact of the detectors during irradiations because of their altered nature, it is certain that it is not the only cause because separated biotites were at the contact but have not produced any tracks at all.

U is unlikely to be secondarily added because if it were, then the hydrogen isotope analyses of U-rich biotites should record some systematic changes. Analyses of U-bearing biotites from one sample containing apparently fresh biotites (Y4) and two samples containing apparently altered biotites (Y1 and Y50) and U-deficient biotites from two sample containing apparently fresh biotites (Y13, Y10) gave the following results :

<u>Fresh biotites</u>	δD	%yield (μMmg^{-1})
Y4	- 70.7	2.289
Y10	- 58.5	2.443
Y13	- 69.5	2.723
"(rerun)	- 68.8	3.161
<u>Altered biotites</u>		
Y1	- 54.8	3.788
"(rerun)	- 55.8	3.881
Y50	- 53.3	3.873
"(rerun)	- 53.5	4.033

It is clear that biotite from samples Y4 and Y10 are both fresh but the former contains U while the latter does not. The remaining biotites from the other samples are all chloritized to some extent but in contrast to biotites from Y1 and Y50 which contain U, those from Y13 do not contain any.

In Chapter Six it has been shown that like most trace elements, U was originally dominantly added with clay minerals from which biotite subsequently crystallized. The presence of U in biotite as discussed above coupled with the relatively comparable Th/U and Eu/Eu* ratios of the pelites with sedimentary shales indicate that the sedimentary signature is still preserved within the pelites. Therefore, it can be inferred that the biotites which are very low in U to produce fission tracks were possibly crystallized from U-poor clay fractions, or that U was lost during the early crystallization of biotites themselves.

7.3 Results of U and Th analyses using INAA

65 rock samples (11 unhornfelsed rock, 14 intermediate hornfelses, 25 contact hornfelses, five pelitic xenoliths, 11 migmatite leucosomes and one microgranite sill) have been analysed from the Cashel thermal aureole and the results are given in Table 7.3 together with six pelitic restite-migmatite leucosome pairs from eastern Connemara. Summary statistics of the rocks collected from within the aureole are given in Table 7.4 along with the partition coefficients of U and Th between the restites and leucosomes.

As shown in Table 7.4, the unhornfelsed rocks average 2.62 ± 0.5 ppm U, 10.80 ± 2.39 ppm Th and 4.25 ± 0.79 Th/U ratios. These values are somewhat similar to their equivalents in sedimentary shales (excluding black shales) of 3.7 ± 0.50 ppm U, 12.1 ± 1 ppm Th and 3.8 ± 1.1 Th/U ratios (Heier and Adams 1965), thus indicating that the sedimentary signature of the pelites was not significantly affected. However, unlike Th, U is slightly lower in the Cashel pelites than in common sedimentary shales consistent with the greater mobility during surface chemical weathering and leaching of U rather than Th under supergene conditions (Wedepohl 1978), although the high metamorphic grade reached by the Cashel pelites suggests that desorption of U from the mineral surfaces might also have occurred during regional metamorphic

recrystallization. An original depletion of U cannot be the alternative explanation because as shown in Chapter five the Connemara pelites are richer in most of the trace elements analysed than many shales described in the literature.

7. 3.1 Field relationships

U generally decreases as the contact of the basic intrusion is approached but Th remains unchanged until the xenolithic stage is reached where both elements finally drop off to their lowest values of 0.52 ± 0.13 ppm and 2.30 ± 0.83 ppm respectively (Table 7.4, see also Figures 7.18-20). As a result, the Th/U ratios tend to rise towards the contact, from 4.25 ± 0.79 in the regional pelites through 6.35 ± 2.21 ppm in the intermediate hornfelses to 8.65 ± 3.25 in the contact hornfelses. The ratio finally falls back to an average of 4.38 ± 0.87 in the pelitic xenoliths and this is probably due to the fact that the basic magma strongly suppressed the differences by homogenizing the contents of U and Th in the most desilicated rocks (see Figure 7.2). The rise in the Th/U ratio cannot be totally due to low temperature mobilization of U compared to Th because as shown by Stuckless and Nkomo (1978); Zielinski *et al.* (1981) and Stuckless *et al.* (1983) if low temperature and oxidizing mobilization of U had occurred, then the correlation between Th and U must be badly destroyed. The correlation coefficient between the two elements in the unhornfelled rocks is 0.69 indicating that while some but insignificant low temperature mobilization of U had occurred, the systematic increase of the Th/U ratio towards the intrusion is due to primary processes such as those discussed in subsection 7.2 (*i.e.* fractionation between the two elements). Sample Y24 is particularly rich in U (6.05ppm) compared to Th (9.42ppm) and this enrichment is related to the presence of veins of apatite indicating strong metamorphic segregations has taken place.

The behaviour of Th is very intriguing because despite the marked mineralogical and chemical changes described in Chapters 4-5, Th changes insignificantly throughout the aureole. Th cannot have been regionally added by metasomatism to the pelites because Senior and Leake now think that regional metasomatism did not take place and the differences reported by Senior and Leake (1978) between the northern and southern pelites are due to

comparing stratigraphically different pelites. Even the assumption that regional metasomatism took place does not explain the behaviour of Th because it is extremely unlikely that Th was added preferentially to the hornfelses but not to the unhornfelsed rocks especially as all the samples were collected from within a small area (see Figure 4.1). The alternative is that Th was redistributed within the newly formed mineral(s) or the ability of biotite to hold larger amounts of Th has increased with increasing temperature. The latter possibility seems improbable because if the capacity of biotite to accommodate larger amounts of Th has increased with increasing temperature then very high Th contents would be expected in the most desilicated rocks but Th is clearly tending toward zero in the pelitic xenoliths.

The good positive correlation between Th and K (Figure 7.8) suggests that Th is held in biotite but also in pinitized cordierite and possibly sericite. Pinitized cordierite seems to hold large amounts of Th because some samples poor in biotite and rich in cordierite contain high concentrations of Th. For instance, Y29 with 4.4% biotite and 41.8% pinitite contains 24.3ppm Th compared to the average of 10.80 ± 2.9 ppm in the biotite-rich regional pelites. This indicates that Th released from biotite was possibly held by the replacing mineral cordierite. It is unfortunate that due to analytical problems the fission track analysis of Th could not be achieved to test this hypothesis.

7.3.2 U-Zr, U-P and U-K relationships

As illustrated in Figures 7.3-5, U generally exhibits positive correlations with Zr, P_2O_5 and K_2O consistent with fission track mapping of U where this is held in zircon, apatite and biotite but also in K-bearing secondary minerals. It is also clear that a better correlation exists between U and K in the unhornfelsed pelites compared to both the hornfelses and xenoliths, better correlation between U-Zr and U-P in the hornfelses compared to the regional pelites but in the pelitic xenoliths only Zr exhibits positive correlation with U consistent with fission track analyses. In the unhornfelsed rocks U is dominantly in biotite but also in zircon and apatite but as the contact of the intrusion is approached, U-bearing biotites were replaced by U-free cordierite, garnet and sillimanite and desorped from the flake surfaces and much of the U was held in zircon and apatite but sometimes also in biotite. In

the xenoliths U is held only in zircons because the remnant biotites were recrystallized into U-free Mg-rich plates and apatite melted dramatically releasing U to the outgoing melts. However, some hornfelses (e.g. Y15) are rich in zircon but plot in the poor side of the diagram (Figure 7.3) and this trend is caused by U-rich brown zircons have been recrystallized into U-poor pink ones as revealed by the fission track work.

7.3.3 Th-Zr, Th-P and Th-K relationships

As expected, there is a good positive correlation between K and Th but there is only a very poor correlation between Th and Zr (Figures 7.6-8) indicating that Th is not significantly held in zircon but it is essentially coming in biotite, pinitized cordierite but possibly also in sericite and hence keeping similar Th/K ratios throughout the whole aureole. In most of the hornfelses, there is a tendency for Th to positively correlate -but poorly- with P and to some extent also Zr (Figures 7.6-7) and this possibly suggests that any Th released from biotite was uptaken by the -postulated- recrystallized apatite and zircon, thus maintaining similar values throughout the whole aureole.

7.4 U and Th partitioning between the restites and leucosomes

The geochemistry of U and Th in magmatic processes is reasonably well understood. U and Th are incompatible with distribution coefficients for major rock-forming minerals less than unity (Wedepohl, 1978). Both elements should therefore concentrate in residual liquids to high concentrations provided early crystallization of substantial amounts of accessory minerals such as zircon and monazite does not occur. However, because U is a mobile element in low temperature solutions under oxidizing conditions it can be separated from relatively insoluble Th resulting in high Th/U ratios compared to the commonly accepted Th/U ratios of 3.8 ± 1.1 ppm.

It follows therefore that both U and Th would fractionate preferentially into the melts compared to the pelitic restites, although the tendency of Th to be uptaken by cordierite and possibly apatite and zircon, the possible low temperature redistribution of U relative to Th, the presence of xenocrysts in the leucosomes, the control of high melting points (zircon and apatite)

particularly over U and possible fractional crystallization of the melt will strongly affect the calculated restite-leucosome partition coefficients.

As clear from Figures 7.18-20, the contents of both U and Th are very low where the pelites are strongly migmatized which indicates that both elements were fractionated into the melts. This therefore indicates that Th left the pelitic restites as a result of partial melting only whereas U was removed as a result of both partial melting and hornfelsing of the metasediments (*i.e.* recrystallization of the country rocks). Figure 7.19 is the same as Figure 7.18 except that sample Y24 which contains the highest U content is ignored to better show the variations of U in the field. Table 7.4 shows that the partition coefficients (*i.e.* U or Th in restites divided by U or Th in migmatites) are extremely variable and are all above unity. Partition coefficients calculated for U are usually lower than those of Th indicating stronger partitioning of U to the melt compared to Th. Half of the migmatite leucosomes from eastern Connemara yield Th partition coefficients higher than those of U and this is probably caused by the presence of Th-bearing xenocrystic biotites as shown by the generally positive but very poor correlation between Th and K (Figure 7.12).

In the migmatite leucosomes and Cashel microgranite sill U is strongly controlled by zircon and apatite (Figure 7.9-10) but there is no obvious relationship between U and K (Figure 7.11) indicating that U is not coming in biotite and K-feldspar when present. In the Cashel microgranite sill high contents of Zr are accompanied by very low concentration of U (direction of arrow in Figure 7.10) despite the fact that U resides in this mineral as revealed by the fission track analysis. This is probably because zircon belongs to the U-poor group (*i.e.* recrystallized U-poor pink zircon) and some U is also held in sphene and apatite.

Th exhibits positive correlation with both K and Zr (Figure 7.12-13) suggesting that Th is held in biotite but possibly also in pink zircons. However, two K-feldspar-rich samples from the Streamstown Formation migmatite leucosomes (JB567 and JB643) and one sample from the southern side of the Cashel Hill intrusion (Y42) are clearly rich in K but poor in U thus excluding Th being substantially held in K-feldspar. Similarly, sample JB643 is rich in Zr but poor in Th thus plotting separately from all the

remaining samples. If we assume that recrystallization of zircon also occurred in the Streamstown Formation pelites, then the low Th but high Zr contents suggests that zircon is brown in colour (i.e. detrital) which suggests that zircon can also occur as xenocrysts.

7.5 likely mechanisms of U and Th transport

The presence of U in zircon, apatite and in the crystal lattices of biotite suggests that much of U is in the tetravalent form (U^{+4}). However, the absence of stable U minerals such as uraninite ($(U_{1-x}^{+4} U_x^{+6})O_{2+x}$) and/or coffinite ($U(SiO_4)_{1-x}(OH)_{4x}$) coupled with the presence of secondary and/or hydrothermal U as shown by the fission track analysis indicate that low temperature redistribution of U occurred most probably as a result of oxidizing conditions and interaction of (water) fluid with U-bearing minerals. The mobility and transport of U at low temperatures is caused by oxidizing UO_2 ($+4U$) to UO_2^+ ($+5U$) and UO_2^{2+} ($+6U$) although the U^{+5} complex is much less stable than U^{+6} (Langmuir 1978).

The solubility of U in waters and/or fluids depends on a number of factors mainly temperature, H, Eh and CO_2 partial pressure (Langmuir 1978, Sergeyeva et al. 1972); climatic conditions; type and degree of fracturation of the host rocks; time of interaction between (water) fluid and the source of U (Lopatkina 1964, Szalay 1964, Szalay and Samsoni 1969, Boyle 1982). There are a number of uranyl complexes which enhance the solubility of U with the most effective being given below : $[UO_2F]^+$, $[UO_2Cl]^+$, $[UO_2NO_3]^+$, $[UO_2(SO_4)_2]^{-2}$, $[UO_2H_2PO_4]^+$, $[UO_2H_3PO_3]^{+2}$, $[UO_2(HPO_4)_2]^{-2}$, $[UO_2(CO_3)_2]^{-2}$, $[UO_2(CO_3)_3]^{-4}$. The relative stability of some uranyl complexes is shown in Figure 7.14.

No water or fluid inclusion analyses were carried out from the studied area but the presence of H_2O and CO_2 as the main fluid inclusion compositions in both the pelitic restites and related migmatitic veins in similar rocks from eastern Connemara as shown by Yardley et al. (1983) coupled with the presence of pyrite, chalcopyrite and secondary calcite suggest that hydroxy, carbonate, sulfate, and phosphate complexes were probably very important. Uranyl silicate complex $[UO_2SiO_2(OH)_3]^+$ was probably not significant because of the insolubility of silica under low temperature (Langmuir 1978).

At similar low temperature conditions, Th is relatively immobile mainly because the element requires high mobilization and migration energies, features that greatly restrict its migration in low temperature metamorphic fluids (Boyle 1982).

There is very little experimental work done on the behaviour of U and Th at high temperatures and pressures. Boyle (1982) suggests that at temperature of $(450-700)^{\circ}\text{C}$ and pressure $(3-12)\text{kb}$ of regional metamorphism and granitization both U and Th are readily transported in the aqueous environment probably as hydrous oxides or hydroxides of the type $[\text{Th}(\text{OH})_4]_n$ and $[\text{U}(\text{OH})_4]_n$ in a dense (water) fluid. In this respect the elements behave much like silica and alkalis because the presence of these probably induce Th and U to form highly mobile silicate complexes. Similarly, the availability of volatiles such as F, Cl, B, CO_2 and H_2O in the fluids probably has a marked effect in increasing the mobility of both U and Th under high temperature and pressure conditions as both elements form complexes of the form $[\text{ThF}_6]^{-2}$ and $[\text{UF}_6]^{-2}$.

In the studied area, the oxidation ratio w ($\text{mole Fe}^{+3}/(\text{Fe}^{+3} + \text{Fe}^{+2})$) exhibits a very poor negative correlation with U indicating that U was not lost from the hornfels and xenoliths as a result of increasing oxidizing conditions. Dehydration and decarbonation of the hornfels and xenoliths were badly obscured by late secondary alterations and therefore their H_2O and CO_2 contents cannot be used reliably to test which uranyl complexes were significant. Despite these complications the positive correlation between CO_2 and U and to some extent Th in the pelitic xenoliths and also between Th and H_2O in most of the hornfels (Figures 7.16-17) suggest that both U and Th were removed as carbonate and hydroxy complexes.

7.6 Summary and Discussion

In the unhornfelsed rocks U, Th and Th/U ratios average $2.62 \pm 0.50\text{ppm}$, $10.80 \pm 2.39\text{ppm}$ and $4.25 \pm 0.70\text{ppm}$ respectively. The average Th/U ratio is quite similar to the commonly accepted ratio of 3.8 ± 1.1 in common sedimentary shales (black shales excluded), although the tendency of the ratio to approach the upper limit suggests that some U was possibly lost -though not significantly- from the pelites especially as the average U in shales is $3.7 \pm$

0.5ppm. This suggestion is consistent with previous findings that rocks experiencing high grades of regional metamorphism have higher Th/U ratios relative to their lower grade equivalents due to the greater solubility of oxidized uranyl complex ions compared to Th (e.g. Heier and Adams 1965; Rich *et al.* 1977; Heier 1979), although the good positive correlation between Th and U in the unhornfelses rock coupled with the very poor correlation between U and the oxidation ratio suggest that secondary remobilization of U was insignificant.

Fission track analysis revealed that U is held in biotite (in the crystal lattices and adsorbed onto the flake surfaces), zircon and apatite but also along the grain boundaries, fractures, schistosity planes, veins and alteration products. Analytical problems severely restricted mapping of Th but the poor correlation between Zr, P₂O₅ and Th and the good correlation between Th and K suggest that most of the Th is in biotite and sericite.

U generally decreases as the contact of the basic intrusion is approached but Th remains almost unchanged until in the xenoliths where both U and Th finally tend towards zero. U was possibly extracted from the hornfelses and pelitic xenoliths through five possible mechanisms:

1- Recrystallization of minerals. This mechanism probably affected U in two ways; first recrystallization of U-rich brown zircon into U-poor pink ones and second replacement of U-bearing biotite by U-free cordierite, garnet and sillimanite and possibly also the recrystallization of biotite into large plates of Mg-rich biotites.

2- Changing texture. The coarsening of the texture is due to the appearance and increase of cordierite in the hornfelses which probably caused desorption of U from the mineral surfaces along the schistosity planes.

3- Melting of U main carriers. This is most pronounced in the pelitic xenoliths where melting of zircon, and apatite was very significant.

4- Partial melting with U preferentially fractionated into the melt.

5-Defluidization of the metasediments particularly dehydration and decarbonation of the rocks during melting.

It is difficult to identify reliably the processes which caused the loss of Th although recrystallization and melting of Th-bearing minerals are looked at as the most effective mechanisms.

From the above discussion it is clear that the partial melts derived from the hornfelses should have lower Th/U ratios than the melts derived from the pelitic xenoliths and indeed Table 7.4 shows that the migmatite leucosomes have significantly lower Th/U ratios than the Cashel granite sill which is believed to represent the melts derived from the most desilicated contact hornfelses and xenoliths. However, the very low U content of the granite sill is rather puzzling and it seems as if some U was fractionated to the melt but removed early before partial melting became significant or all U was lost to the melts but subsequent processes such as fractional crystallization or supergene alterations removed U but not Th.

The calculations performed in Chapter 5 showed that the predicted melts derived from the xenoliths and the actual composition of the granite sill agree excellently with each other and therefore excluding the possibility that the Yearly melts were significantly removed. The greater mobility of U relative to Th cannot be an alternative explanation because in the sill U is strongly controlled by the accessory zircon, apatite and sphene as revealed by the fission track analysis. Again fractional crystallization of the major rock-forming minerals must have had insignificant effects on U because these are extremely low in U. The remaining possibility is that much of the U fractionated into the melt was removed before the xenolithic stage was reached by combining with the volatiles available in the liquid particularly H_2O , CO_2 , F, N_2 and B. An alternative is that low melting point mobilizates which were quantitatively insignificant to affect the overall composition of the melts but rich in volatiles to induce the mobility of highly compatible elements such as U migrated from the main melts.

Table 7.1 : Characteristic of zircons

Sample number	total zircons counted	types of zircon	number of zircons counted	volume percent	morphology		
					E-S	R-S	R
Y5'	31	brown	20	64.5	1	19	0
		interm.	5	16.12	2	3	0
		pink	6	19.3	3	0	3
Y8	14	brown	10	71.42	3	7	0
		interm.	2	14.28	0	2	0
		pink	2	14.28	0	0	2
Y9	81	brown	27	33.34	13	14	0
		interm.	18	22.23	7	11	0
		pink	36	44.44	21	11	4
Y15	73	brown	12	16.43	3	8	1
		interm.	14	19.17	6	8	0
		pink	47	64.38	27	9	11
Y16	14	brown	3	21.42	0	3	0
		interm.	2	14.28	1	1	0
		pink	9	64.28	3	2	4
Y17	97	brown	11	11.34	2	9	0
		interm.	10	10.3	5	3	2
		pink	76	78.35	46	20	10
Y19	27	brown	2	7.4	0	2	0
		interm.	11	40.74	3	6	2
		pink	14	51.85	9	3	2
Y60	19	brown	2	10.52	0	2	0
		interm.	4	21.05	0	3	1
		pink	13	68.42	5	2	6

interm = intermedite in colour between brown and pink

E-S = euhedral to subhedral

R-S = rounded to subrounded

R = refacettted crystals

Table 7.2 : Quantitative estimation of U in apatite and biotite. The samples are listed from top to bottom in decreasing distance toward the contact.

Sample number	tracks counted	track density(tcm-1)	U(ppm)
<u>Apatite</u>			
Y10	75	0.75 . 10 ⁶	7.64
	219	1.80 "	18.35
	162	1.67 "	17.02
Y50	337	3.37 "	34.90
	359	3.59 "	37.18
	151	5.59 "	57.90
Y1	269	2.69 "	25.88
	123	1.23 "	11.85
	189	3.02 "	29.06
Y16	123	3.41 "	31.97
	134	2.09 "	19.59
	178	3.95 "	37.03
Y17	266	2.66 "	26.75
	179	1.77 "	18.04
	196	1.96 "	20.30
<u>Biotite</u>			
Y50	104	9.54 . 10 ⁴	1.13
	90	9.99 "	1.19
	13	0.76 "	0.09
	39	2.43 "	0.29
Y4	86	9.56 "	1.08
	198	19.51 "	2.21
	165	13.65 "	1.54
	73	8.12 "	0.92
Y1	276	2.30 . 10 ⁵	2.31
	29	0.35 "	0.35
	32	0.64 "	0.64
	293	3.25 "	3.27

Table 7.3 : U, Th, K and their relative ratios in the Cashel metasediments, migmatite leucosomes and microgranite sill.

Sample number	U(ppm)	Th(ppm)	K ₂ O(wt%)	Th/U	Th/K	U/K
Unhornfused pelites						
Y1	2.44±0.03	13.41±0.03	3.90	5.41	3.44	0.62
Y4	2.96±0.02	12.97±0.02	4.67	4.38	2.78	0.63
Y5'	2.71±0.02	8.68±0.02	2.52	3.20	3.45	1.07
Y6	2.88±0.02	12.24±0.02	1.46	4.25	8.38	1.97
Y7	3.03±0.02	13.37±0.03	3.96	5.73	4.38	0.76
Y8	2.80±0.02	10.14±0.04	4.03	3.62	2.51	0.70
Y9	2.01±0.03	8.73±0.03	3.07	4.34	2.84	0.65
Y57	1.58±0.03	5.71±0.30	1.35	3.61	4.23	1.17
Y79	2.70±0.03	13.05±0.02	3.60	4.84	3.62	0.56
Y82	2.23±0.02	9.28±0.02	2.89	4.16	3.21	0.77
Y83	3.50±0.02	11.25±0.02	5.15	3.21	2.19	0.70
Intermediate hornfelses						
Y10	3.05±0.02	12.33±0.02	3.00	4.04	4.11	1.02
Y13	2.82±0.02	16.00±0.02	6.07	5.67	2.63	0.46
Y23	2.60±0.02	19.40±0.01	7.34	7.46	2.64	0.35
Y25	1.31±0.03	11.31±0.02	4.34	8.63	2.66	0.31
Y34	1.14±0.06	14.31±0.03	3.97	12.55	3.60	0.29
Y36	1.69±0.03	12.00±0.02	6.46	7.10	1.86	0.26
Y47	3.06±0.03	13.16±0.02	3.73	4.30	3.53	0.82
Y49	2.78±0.03	11.59±0.03	2.99	4.17	3.87	0.93
Y50	3.45±0.02	17.78±0.03	4.12	5.15	4.31	0.83
Y51	1.70±0.03	12.47±0.02	4.81	7.33	2.59	0.35
Y52	2.82±0.02	14.53±0.02	3.08	5.15	4.72	0.91
Y54	1.54±0.03	10.10±0.03	2.83	6.55	3.57	0.54
Y55	1.69±0.04	11.25±0.02	2.18	6.67	5.16	0.77
Y81	2.99±0.04	12.52±0.04	1.32	4.18	9.48	2.26

contd

Table 7.3 : Continued

Sample number	U(ppm)	Th(ppm)	K ₂ O(wt%)	Th/U	Th/K	U/K
Contact hornfelses						
Y11	1.17±0.03	12.90±0.02	4.55	11.02	2.83	0.25
Y14	3.22±0.02	14.08±0.02	2.89	4.37	4.87	1.14
Y15	1.74±0.04	16.00±0.02	1.59	9.19	10.06	1.09
Y16	1.47±0.05	12.45±0.04	2.32	8.47	5.36	0.63
Y17	1.48±0.06	11.24±0.05	1.63	7.60	6.89	0.90
Y19	1.42±0.05	18.00±0.03	3.74	12.67	4.81	0.38
Y20	1.73±0.04	11.13±0.03	4.39	6.44	2.53	0.39
Y22	1.30±0.04	11.06±0.02	2.87	8.50	3.85	0.45
Y24	6.05±0.03	9.42±0.04	3.75	1.55	2.51	1.62
Y28	2.67±0.03	14.81±0.02	2.68	5.54	5.52	0.99
Y29	1.77±0.05	24.03±0.02	3.70	13.34	6.49	0.48
Y35	1.62±0.04	15.58±0.02	3.50	9.61	4.45	0.46
Y42	1.54±0.02	15.76±0.01	5.45	10.23	2.89	0.28
Y43	2.65±0.01	18.30±0.01	4.51	6.90	4.06	0.38
Y44	1.57±0.03	13.35±0.01	4.33	8.50	3.08	0.36
Y60	3.48±0.01	25.14±0.01	4.83	7.22	5.20	0.72
Y65	0.78±0.04	10.59±0.01	6.06	13.57	1.74	0.12
Y67	1.58±0.03	5.91±0.03	2.77	3.74	2.13	0.57
Y68	1.79±0.03	7.96±0.02	3.19	4.44	2.49	0.56
Y69	0.93±0.04	3.44±0.04	1.96	3.69	1.75	0.48
Y70	1.26±0.04	15.29±0.02	4.66	12.13	1.60	0.10
Y71	0.55±0.04	9.05±0.01	5.67	16.45	1.59	0.54
Y72	1.46±0.05	14.51±0.03	2.91	9.93	4.98	0.50
Y78	3.22±0.03	23.63±0.03	3.70	7.33	6.38	0.87
Pelitic xenoliths						
Y26	0.59±0.06	2.30±0.07	1.24	3.90	1.85	0.47
Y62	0.43±0.06	2.00±0.05	0.70	4.65	2.85	0.61
Y73	0.54±0.02	1.80±0.02	2.17	3.15	0.83	0.26
Y80	0.33±0.07	1.54±0.07	1.41	4.67	1.09	0.23
BEL1470	0.70±0.07	3.89±0.06	0.73	5.56	5.32	0.95

contd

Table 7.3 : Continued

Sample number	U(ppm)	Th(ppm)	K ₂ O(wt%)	Th/U	Th/K	U/K
Pelitic restites from eastern Connemara						
JB109	2.82±0.07	14.52±0.08	3.40	5.14	4.27	0.82
JB501	4.86±0.03	21.95±0.03	4.48	4.51	4.90	1.08
JB567**	6.80±0.03	30.60±0.04	5.32	4.50	5.75	1.28
JB571**	3.83±0.05	18.84±0.05	4.84	4.92	3.89	0.79
JB643**	6.34±0.04	19.41±0.05	5.61	3.06	3.46	1.13
JB646	3.28±0.04	16.50±0.03	3.73	5.03	4.42	0.88
Migmatite leucosomes						
Y42L	0.34±0.08	2.46±0.06	3.42	7.24	0.72	0.10
Y43L*	0.13±0.03	0.23±0.04	1.50	1.76	0.16	0.09
Y44L	0.77±0.03	0.45±0.20	1.70	0.58	0.26	0.45
Y60L*	0.25±0.09	2.39±0.06	0.70	9.56	3.41	0.35
Y65L*	0.13±0.07	0.80±0.07	0.65	6.15	1.23	0.20
Y68L	0.49±0.06	1.47±0.06	0.60	3.00	2.45	0.82
Y69L	0.67±0.02	0.39±0.07	0.46	0.58	0.84	1.45
Y71L	0.46±0.02	1.96±0.02	2.03	4.26	0.96	0.23
Y72L	0.81±0.02	3.65±0.02	1.55	4.50	2.35	0.53
Y78L	0.67±0.04	5.13±0.03	0.90	7.65	5.70	0.75
JB109L	2.23±0.10	13.92±0.09	3.05	6.24	4.46	0.73
JB501L	3.85±0.04	18.19±0.04	3.16	4.72	5.75	1.21
JB567L**	0.64±0.04	-	8.54	-	-	0.07
JB571L**	2.49±0.10	16.90±0.06	4.70	6.78	3.59	0.52
JB643L**	2.99±0.07	4.65±0.20	4.73	1.55	0.98	0.63
JB646L	1.50±0.15	6.07±0.012	1.43	4.05	4.24	1.05
Granite sill						
Y21	0.78±0.14	29.61±0.02	5.24	37.96	5.65	0.15

* = Quartz-rich leucosomes

**= Streamstown formation

JB = J. Barber

BEL = B.E. Leake

- = not detected

U/K and T/K = U, Th/K x 10⁴

Table 7.4 : Summary statistics for U, Th and their relative ratios. The partition coefficients between the pelitic restites and migmatite leucosomes are also given.

	U	Th	Th/U	Th/K x 10 ⁴	U/K x 10 ⁴
R	2.62	10.80	4.25	3.73	0.87
S	0.50	2.39	0.79	1.60	0.39
I	2.33	13.48	6.35	3.90	0.72
S	0.74	2.56	2.21	1.78	0.50
C	1.75	14.09	8.74	4.02	0.54
S	0.76	5.20	3.33	2.06	0.27
C'	1.93	13.90	8.44	3.96	0.59
S'	0.13	5.25	3.56	2.04	0.34
X	0.52	2.30	4.38	2.38	0.50
S	0.13	0.83	0.81	1.62	0.26

Partition coefficients(restite/migmatite)

	U	Th	<u>Key to table 7.4</u>
Y42L	4.53	6.40	
Y43L	20.38	79.56	R = average of 11 country pelites
Y44L	2.03	29.67	I = average of 14 intermediate hornfelses
Y60L	13.92	10.51	
Y65L	6.00	13.23	C = average of 24 contact hornfelses
Y68L	3.65	5.41	C' = C but excluding sample Y24
Y69L	1.38	8.82	X = average of 5 pelitic xenoliths
Y71L	1.19	4.61	S = standard deviation
Y72L	1.19	4.61	
Y78L	4.80	4.60	
JB109L	1.26	1.04	
JB501L	1.26	1.20	
JB567L	10.62	very high	
JB571L	2.12	4.17	
JB643L	2.19	2.71	
JB646L	1.53	1.11	

KEY TO FIGURES 7.1 - 7.20

Figure 7.1 Plot of vol% of zircon versus distance from the contact of the intrusions

Figures 7.2 - 8 Scatter diagrams for the metasediments

Figure 7.2 Th vs U

Figure 7.3 Zr vs U

Figure 7.4 P₂O₅ vs U

Figure 7.5 K₂O vs U

Figure 7.6 Zr vs Th

Figure 7.7 P₂O₅ vs Th

Figure 7.8 K₂O vs Th

Figures 7.9 - 13 Scatter diagrams for the migmatite leucosomes

Figure 7.9 P₂O₅ vs U

Figure 7.10 Zr vs U

Figure 7.11 K₂O vs U

Figure 7.12 K₂O vs Th

Figure 7.13 Zr vs Th

Figure 7.14 Distribution of uranyl complexes vs PH

Figure 7.15 w (Fe⁺³/(Fe⁺³+Fe⁺²)) vs U

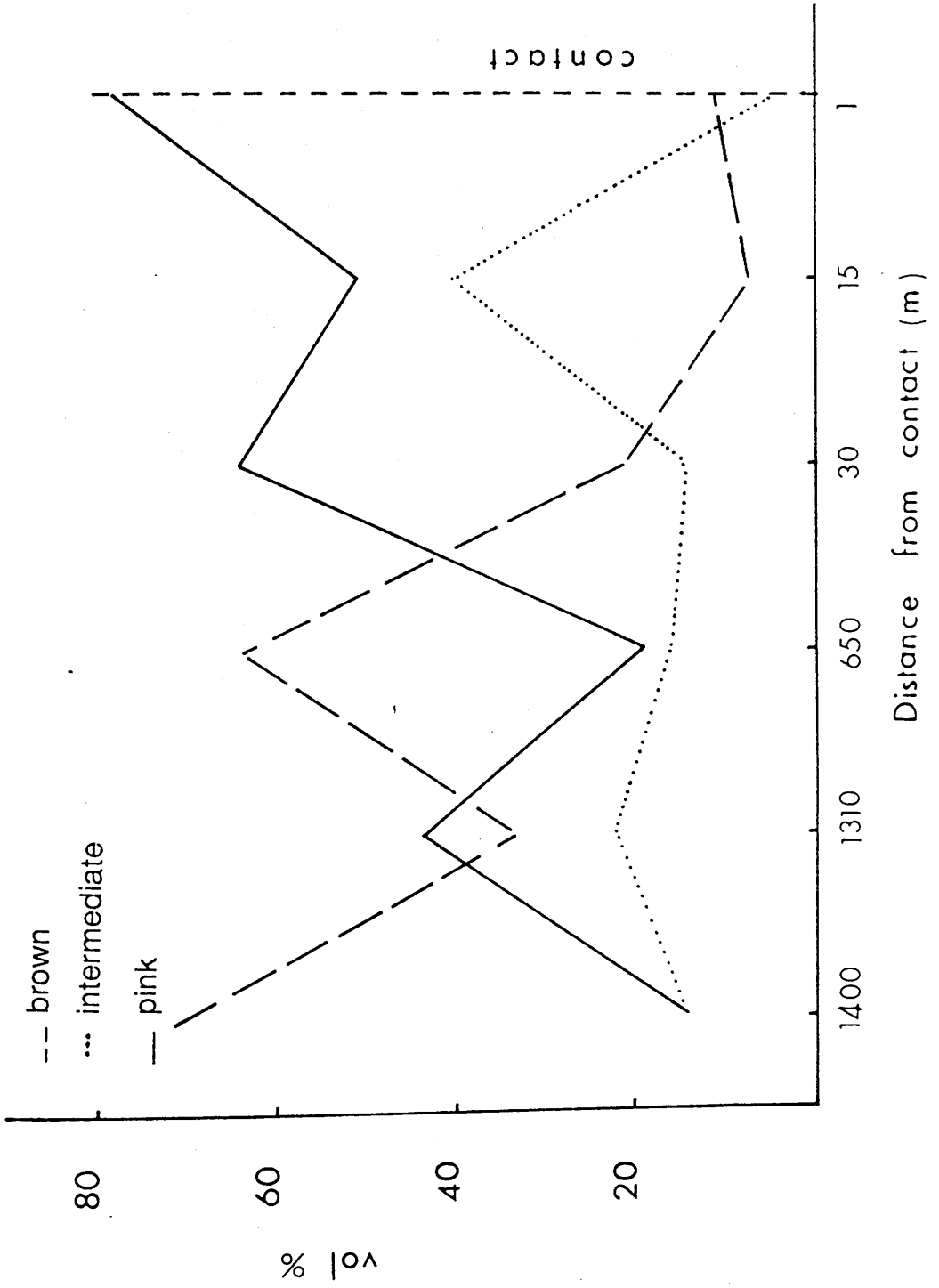
Figure 7.16 CO₂, H₂O vs U

Figure 7.17 CO₂, H₂O vs Th

Figure 7.18-19 Tridimensional maps of U

Figure 7.20 Tridimensional map of Th.

fig 7.1



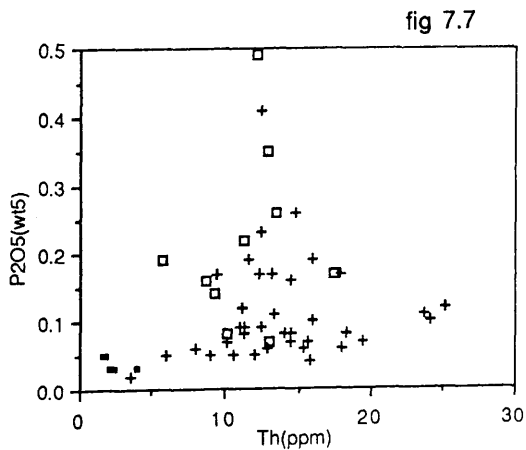
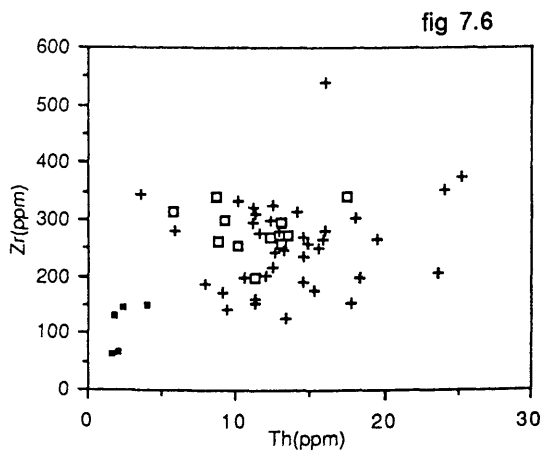
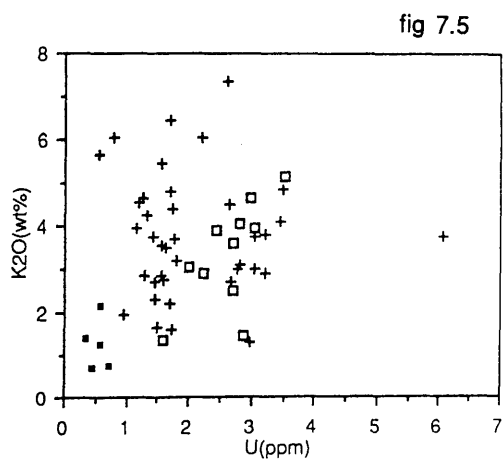
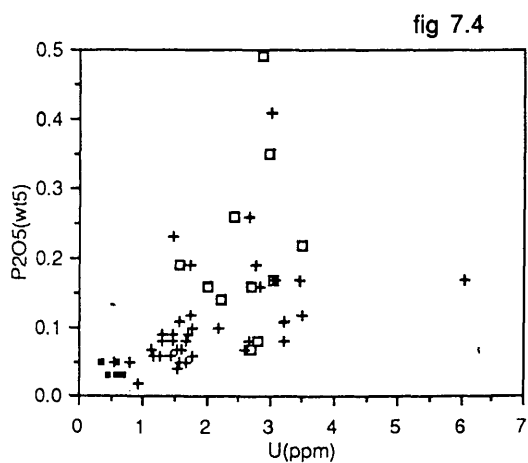
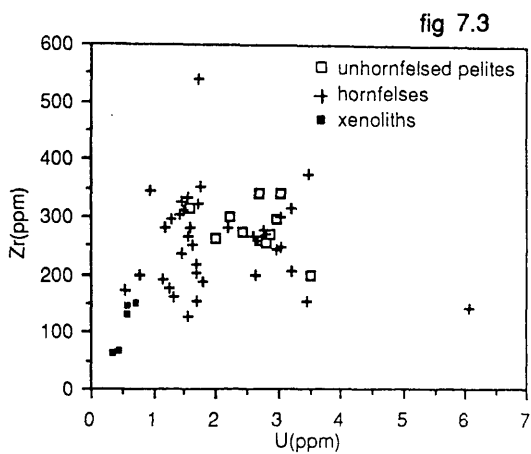
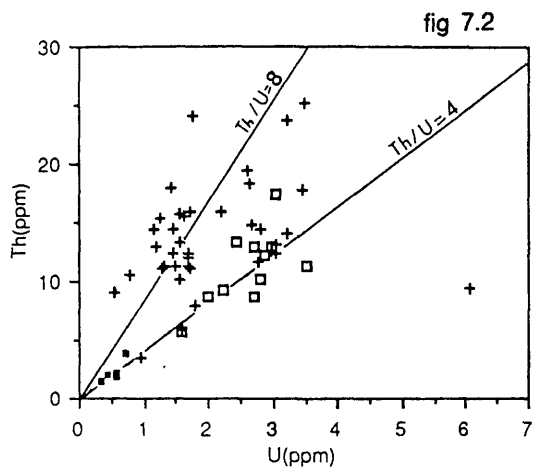


fig 7.8

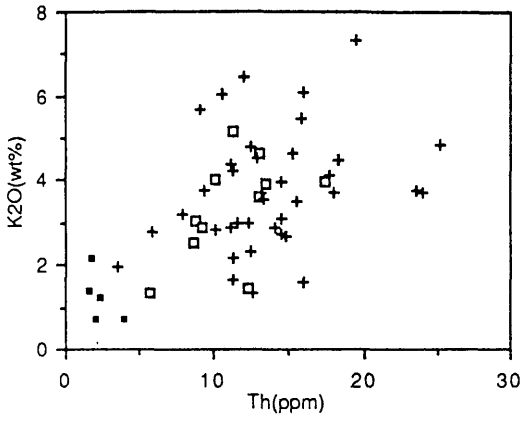


fig 7.9

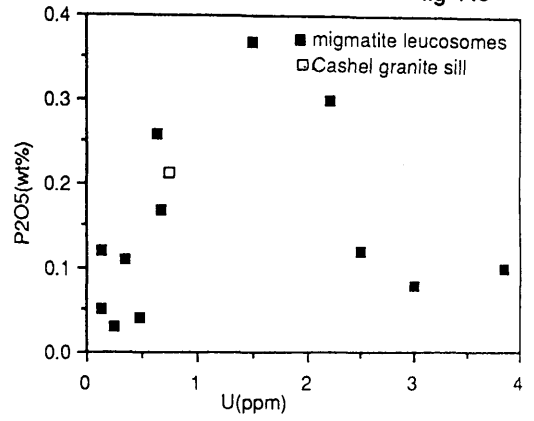


fig 7.10

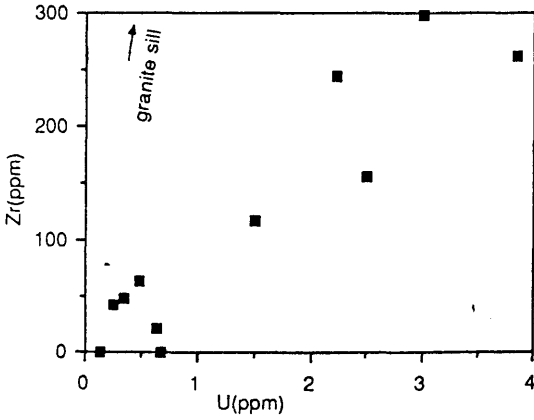


fig 7.11

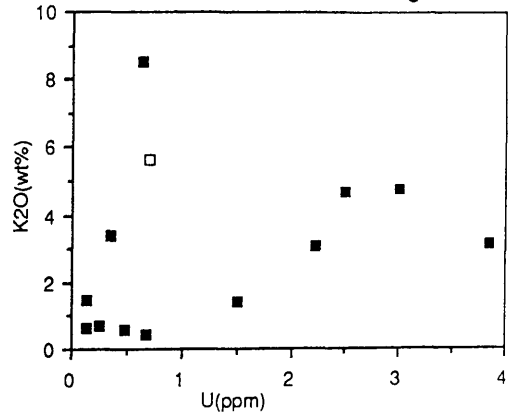


fig 7.12

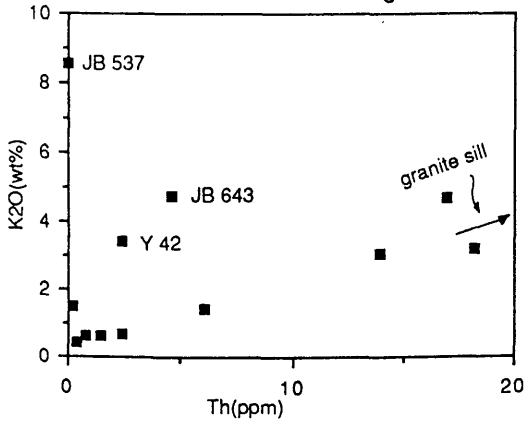


fig 7.13

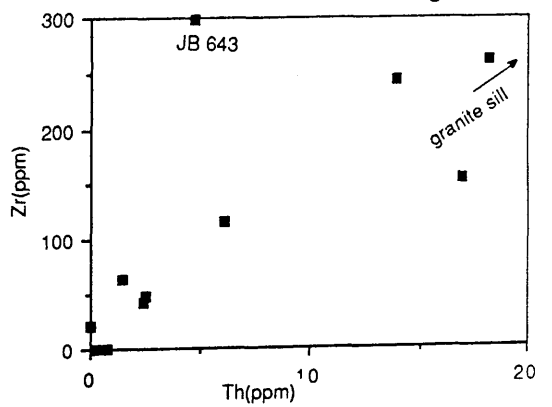
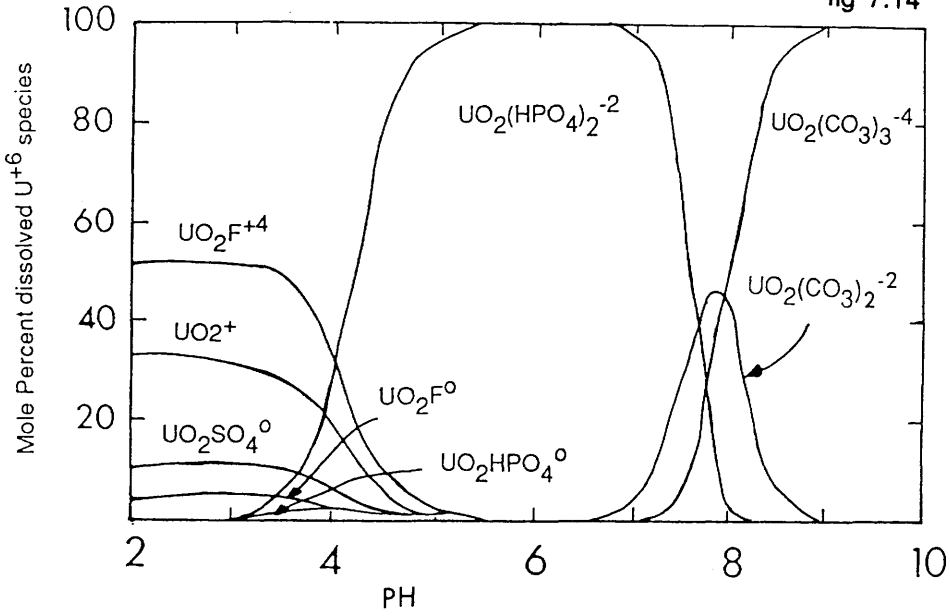


fig 7.14



Distribution of uranyl complexes vs pH for some typical ligand concentrations in ground waters of the Wind River Formation at 25°C. $P_{CO_2}=10^{-2.5}$ atm., $\Sigma F=0.3$ ppm, $\Sigma Cl=10$ ppm, $\Sigma SO_4=100$ ppm, $\Sigma PO_4=0.1$ ppm, $\Sigma Si=30$ ppm, after Lagmuir (1978).

fig 7.15

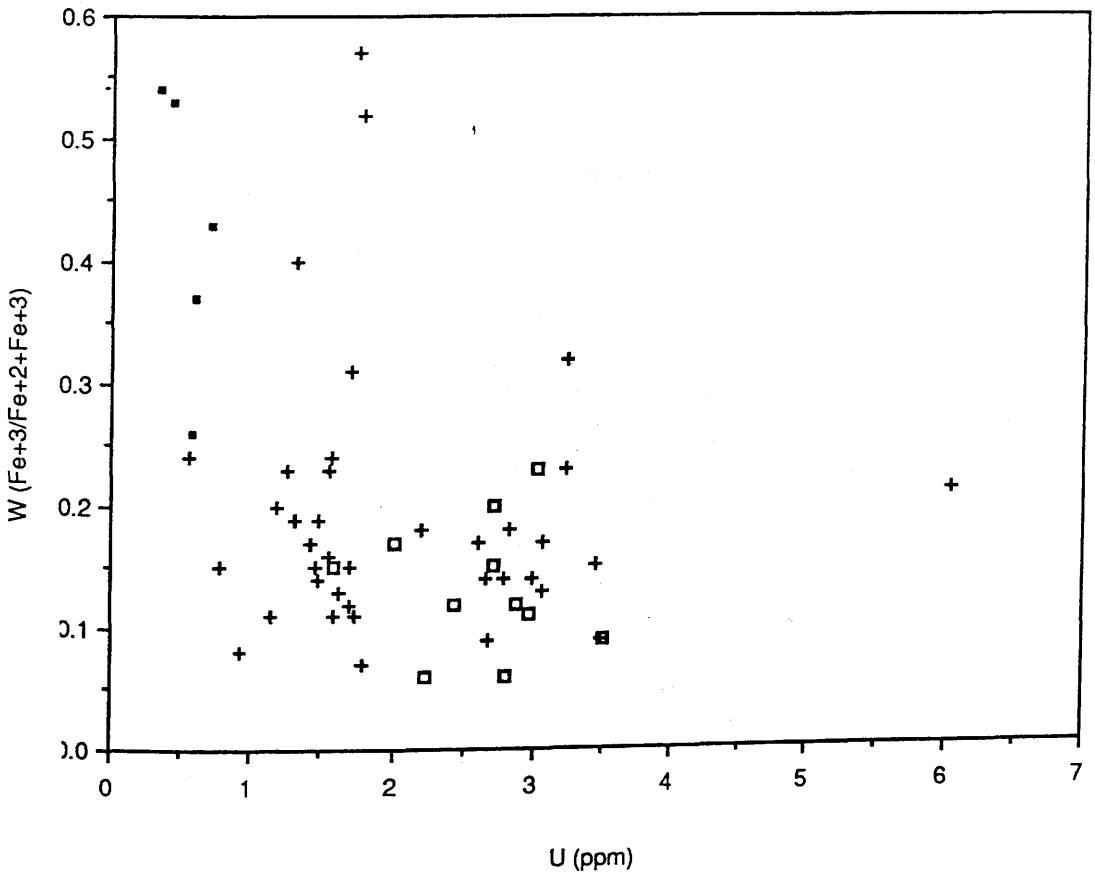


fig 7.16

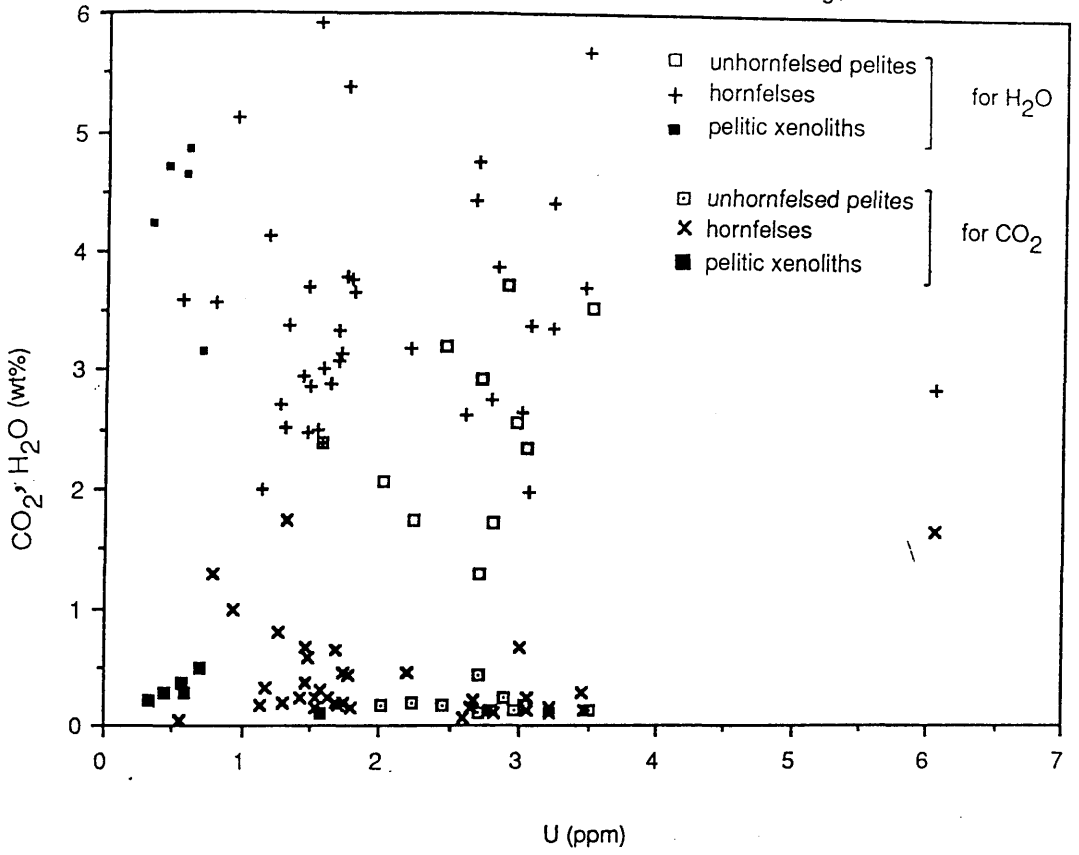
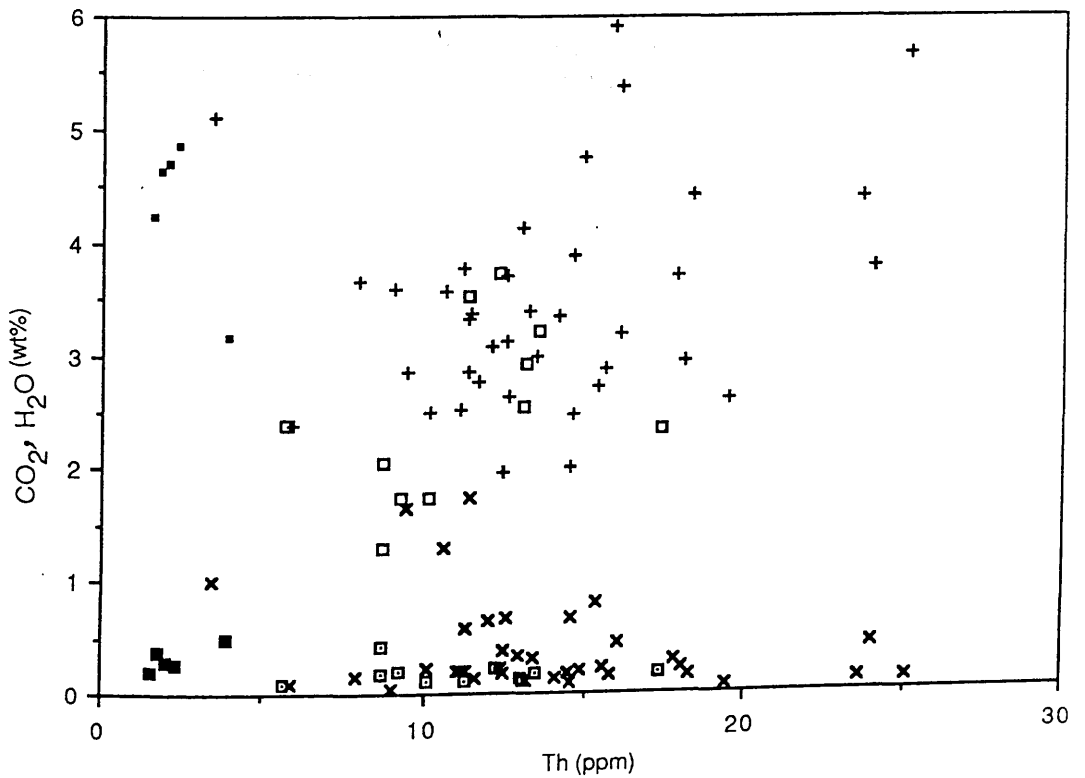
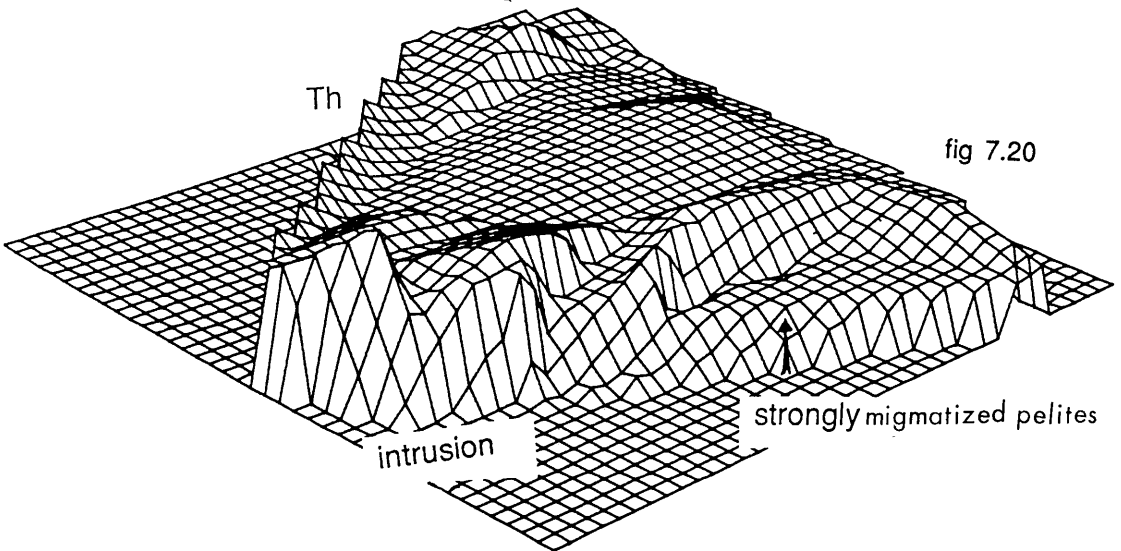
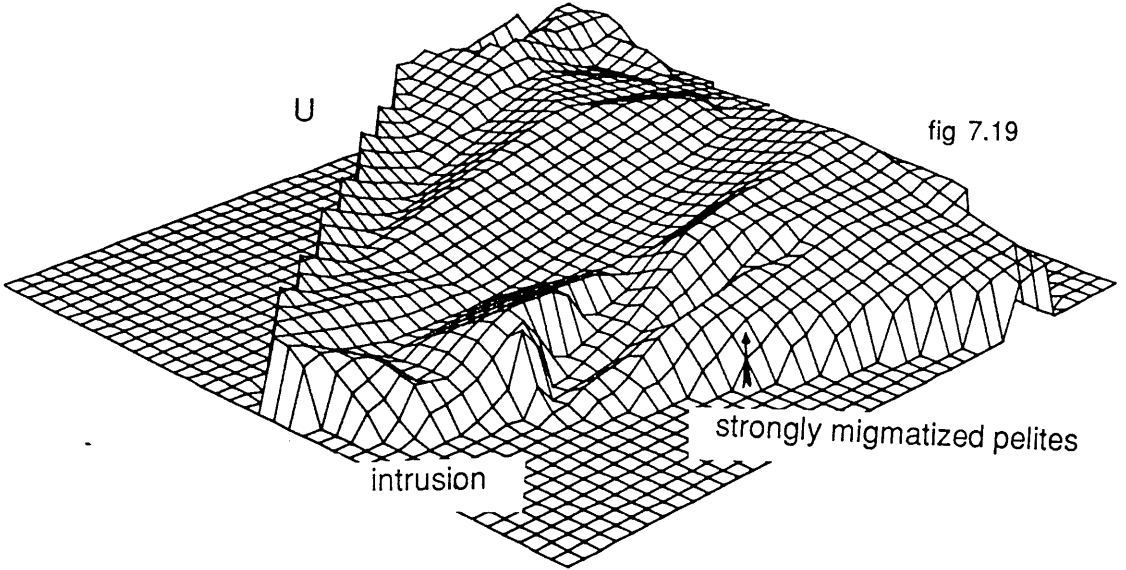
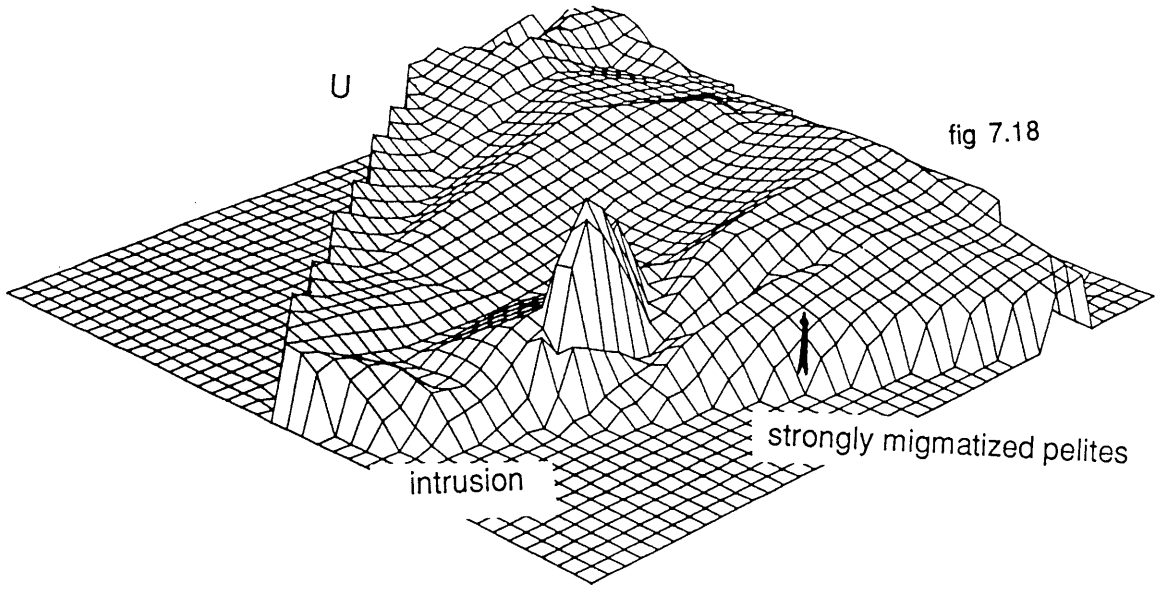


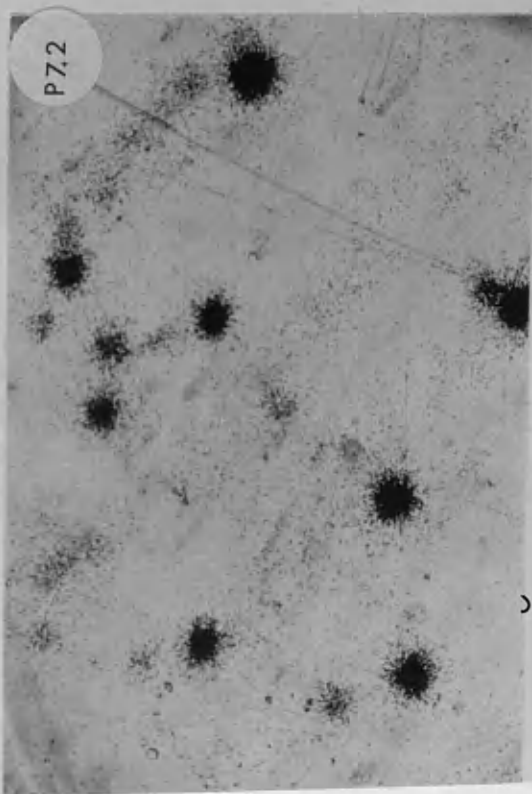
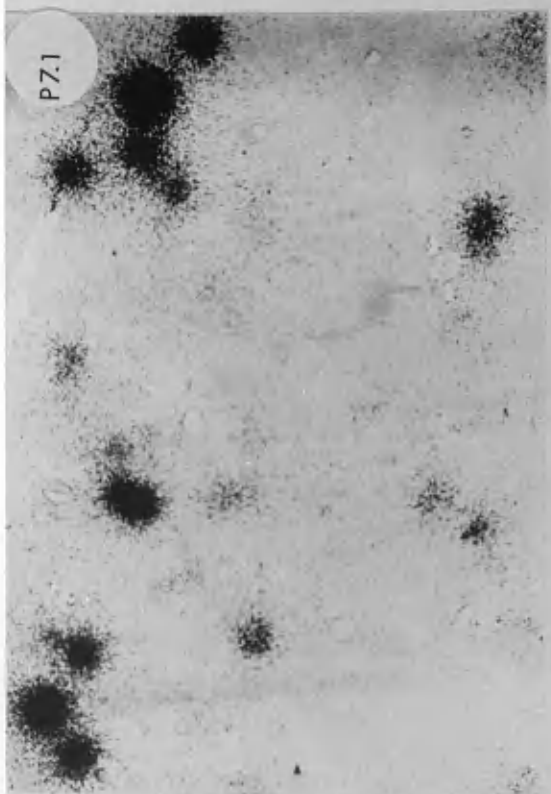
fig 7.17

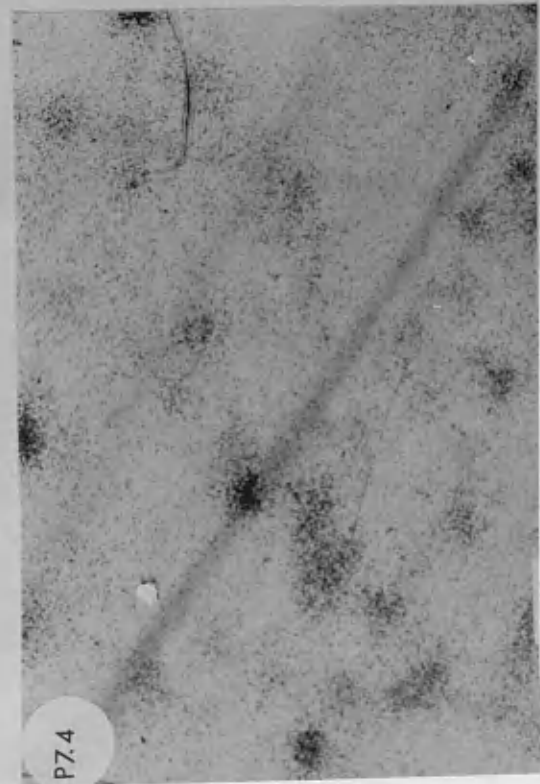
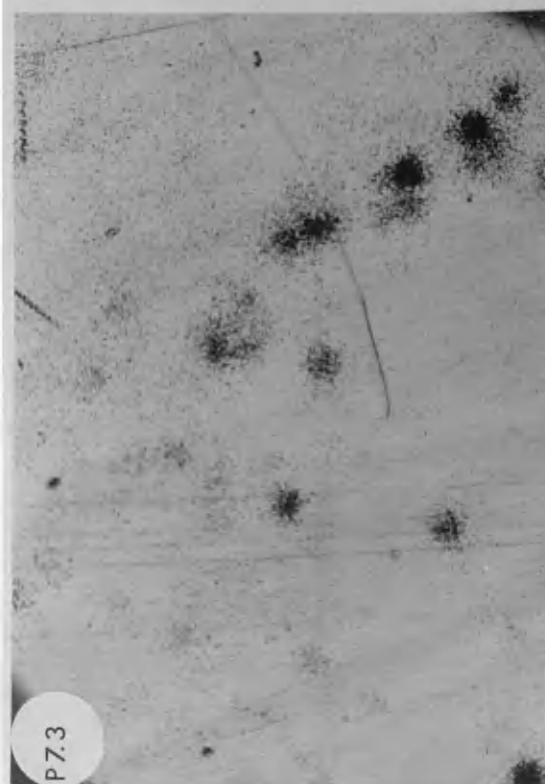
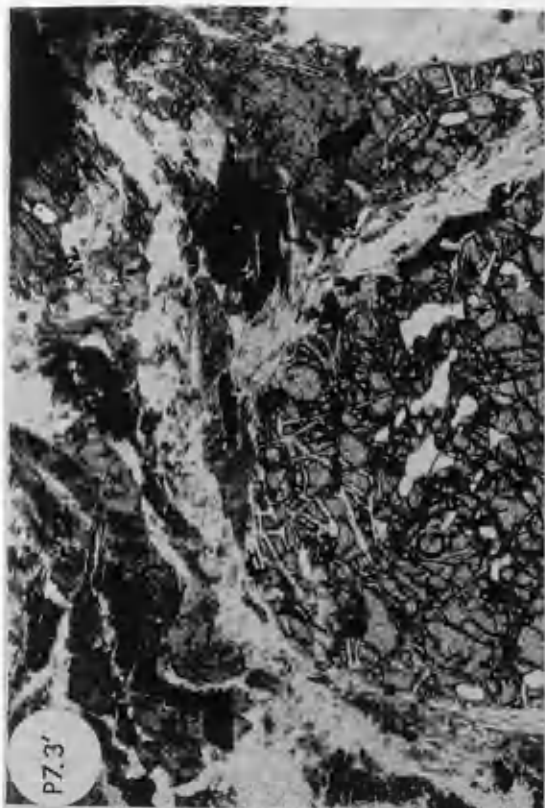


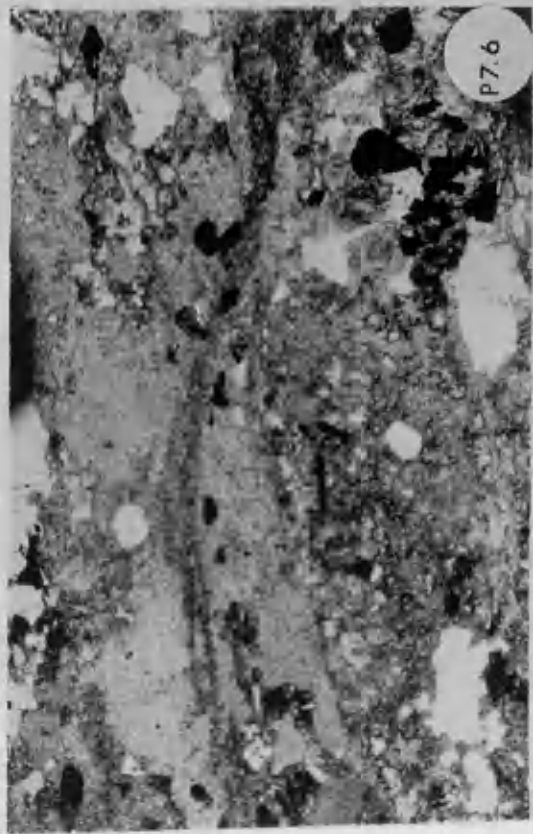
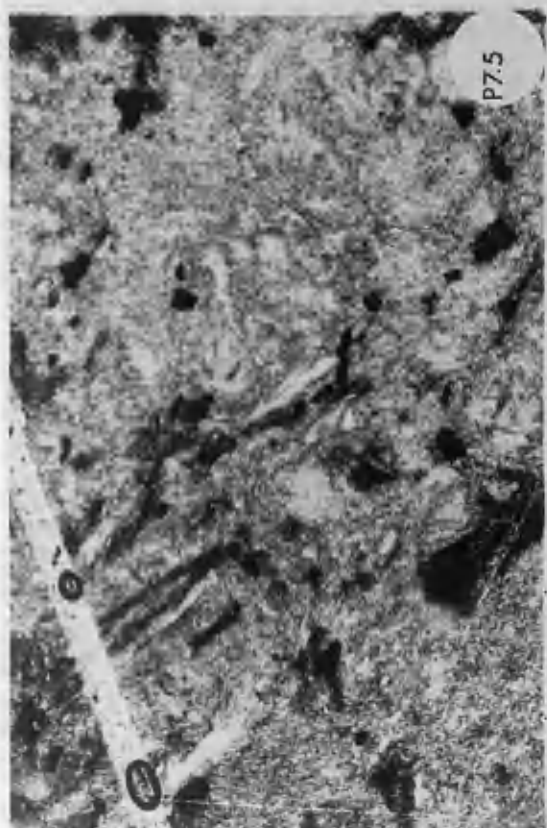
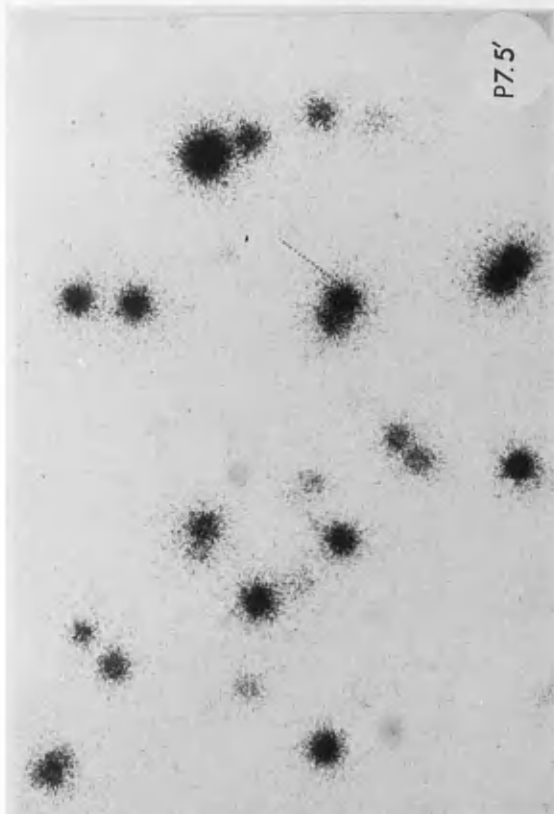


PLates 7.1-13 U distribution patterns in the Cashel pelites and some individual minerals. The corresponding whole rock sections are also shown.

- P7.1'-2' Typical whole rock U distribution patterns. Note the presence of rare scattered tracks over biotite (P 7.1') and over sericitized plagioclase (P 7.2'). the star-like tracks are formed over zircon.(X2.5, magn.30x)
- P7.3' U at the garnet-biotite boundaries and in sericitized biotite. Note the rarity of the tracks over garnet except over zircon therein. (X2.5, magn.30x)
- P7.4' U in sericitized biotite. (X2.5, magn.30X).
- P7.5' U in zircon within pinitized cordierite. (X2.5, magn.30X).
- P7.6' U in veins over secondary epidote. (X2.5, magn.30X)
- P7.7' U in apatite. Note the homogeneous distribution of U within the crystal and the absence of track over quartz (inside apatite) and partly sericitized plagioclase. (X6.3, magn. 75X)
- P7.8' U in zircon within a garnet poikiloblast. Note the presence of rare tracks over the cracks and the sericitized parts. (X10, magn. 120X)
- P7.9 U in a deep brown grain of zircon. (X40, magn. 480X)
- P7.10 U in an intermediate crystal of zircon. (X40, magn. 480X)
- P7.11 U in a pink crystal of zircon. (X40, magn. 480X)
- P7.12 Spontaneous fission track in apatite. (X40, 480X)
- P7.13 Spontaneous fission tracks in pink zircon. (X40, magn. 700X)



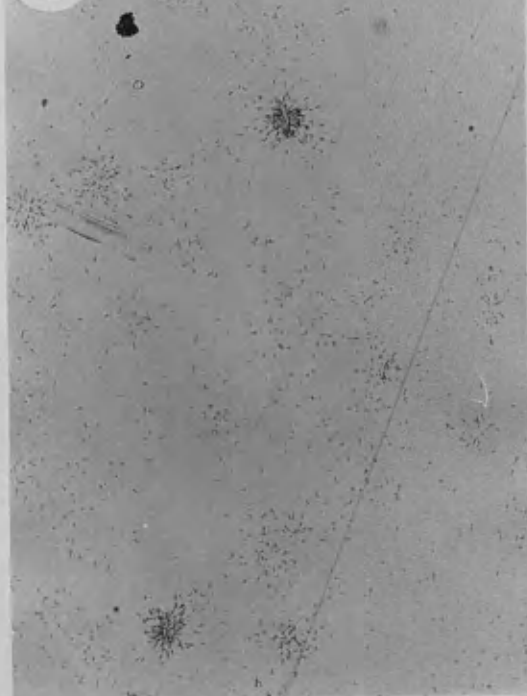




P7.7



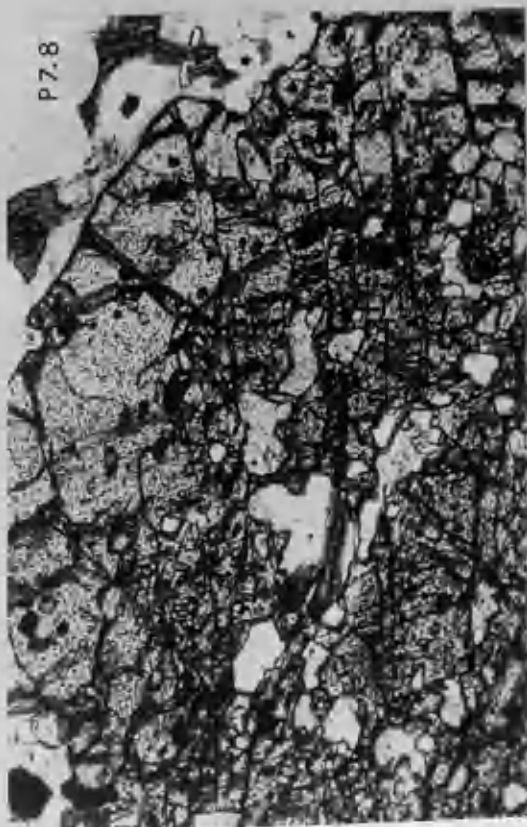
P7.8'

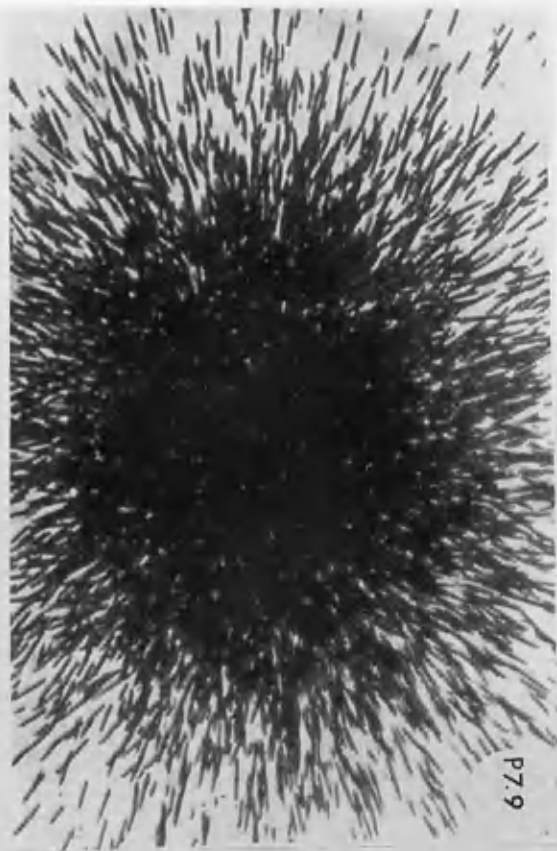


P7.7



P7.8





P7.9



P7.10

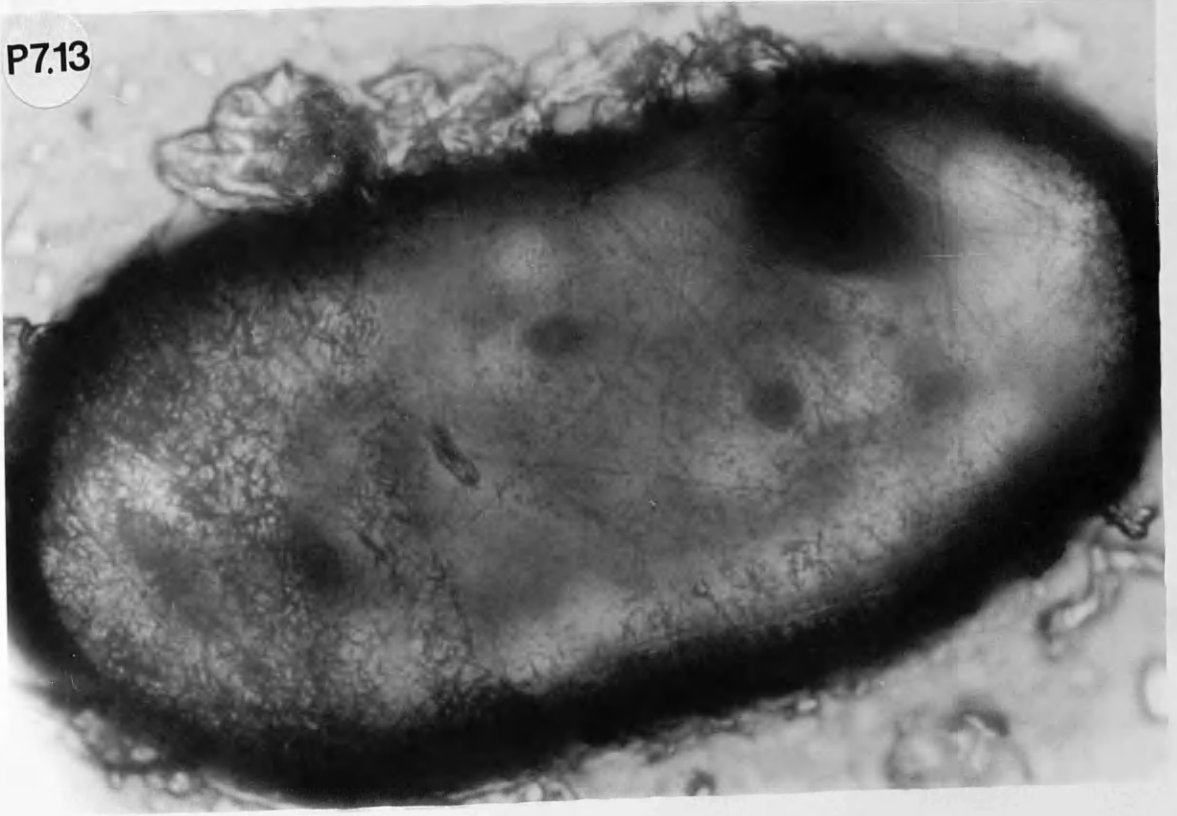


P7.11



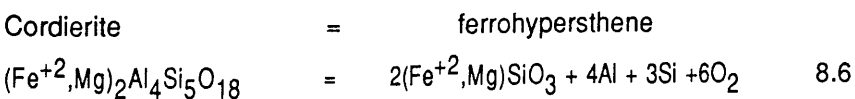
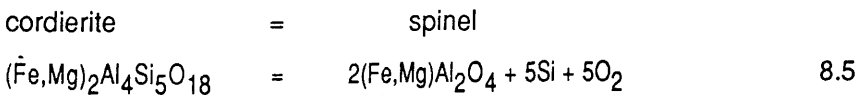
P7.12

P7.13



(Table 8.2) are due to higher X_{Mg} (ions Mg/(Fe+Mg)) and more importantly to higher Ti. This conclusion which is in excellent agreement with that reached from biotite analyses from the Cashel thermal aureole (Chapter 4) conclusively indicates that the red colour of biotite commonly found in thermal aureoles is due to an increase in the Ti and Mg contents rather than Fe and Ti as previously thought (e.g. Leake and Skirrow 1960).

Cordierite appears as small spongy unzoned grains replacing the biotite flakes either in the matrix or within the spots which suggests that the spots were formed by internal selective concentration of certain elements which preceded the formation of cordierite rather than to retrograde metamorphism as suggested by Mason (1978). The rocks are poorly exposed in many contact areas but some samples (e.g. Y50, Y51, Y87) contain coexisting biotite and cordierite but are corundum-, spinel-orthopyroxene-free which suggests that a separate cordierite zone exists. The cordierite and its repeated lamellae twinning increase rapidly inward resulting in a significantly coarser texture of the rocks but in the innermost parts of the aureole cordierite tends to decline, being dominantly replaced by spinel and orthopyroxene.

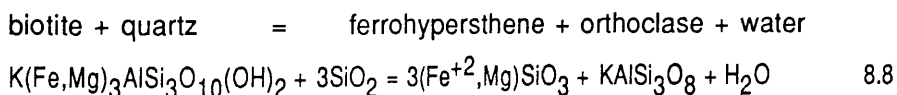
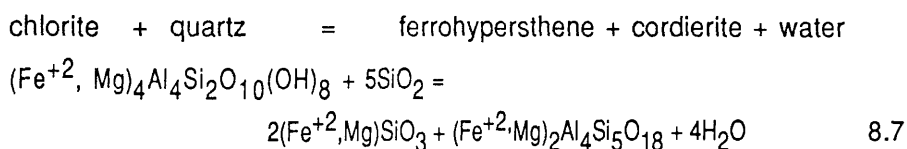


Spinel is first seen as green droplets inside magnetite and cordierite at about 60m from the contact then increases rapidly in size and volume in the most hornfelsed rocks (see Figures 8.2-4). 10 spinel analyses fall between the two analyses given in Table 8.2 which shows that the spinel is dominantly hercynite with Mg/Fe⁺² ratios well below unity (range from 0.11 to 0.43). In the most altered rocks, substitution of Mg for Fe⁺² took place but replacement of Fe⁺³ for Al was much less significant (Table 8.2). Cr, Ni and Co are often present in the spinel.

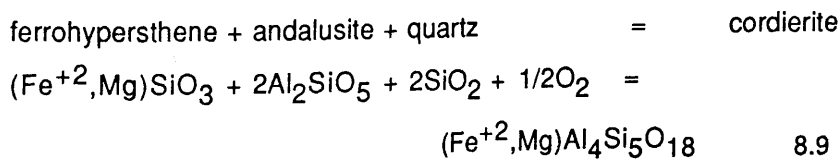
Corundum occurs as small colourless or slightly pleochroic crystal usually replacing biotite or set in cordierite. It commonly shows either

hexagonal or rectangular outlines and parting is very common. Rare blue crystals of corundum have also been noted.

Orthopyroxene (0.9mm average diameter) occurs as fresh, unzoned, strongly pleochroic crystals replacing biotite, as veins or more often set in a base of cordierite and K-feldspar (Plates 8.2-3). Four representative analyses given in Table 8.2 show that orthopyroxene is invariably ferrohypersthene, En_{38-40} . The presence of orthopyroxene as veins suggests that it has replaced chlorite along the cleavages of the slates following reaction 8.7 whereas its growing in the groundmass of cordierite and K-feldspar and replacing biotite suggests reactions 8.6 and 8.8.

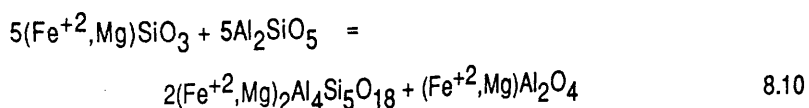


Andalusite has not been recorded in all studied samples but if present in the outer envelope but not found in the rocks studied it is absent from the inner aureole because it was completely consumed in the reactions given below :



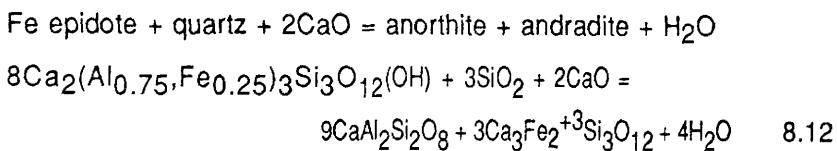
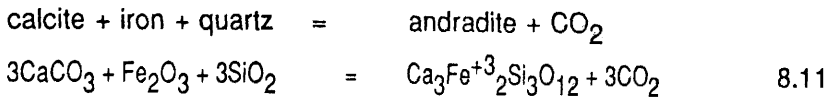
or if quartz is deficient

ferrohypersthene + andalusite = cordierite + spinel

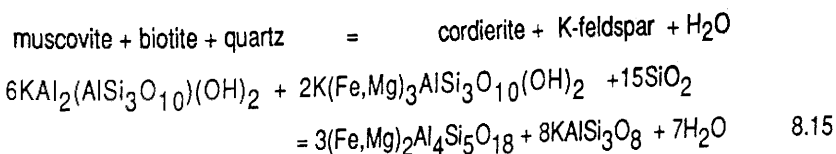
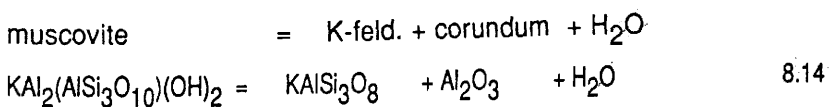
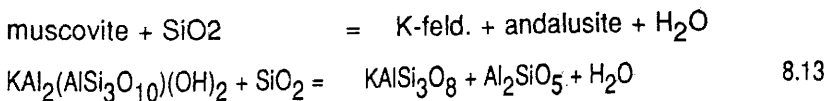


Cr, Ni and Co were not detected in any ferrohypersthene analysis.

Garnet, which is unzoned nearly pure andradite (Table 8.2), is extremely rare and only one poikiloblast is found in one sample (Y59). It was probably formed according to reaction 8.11 as reaction 8.12 is improbable because anorthite is totally absent from the contact samples which still contain epidote.



The regional chlorite, sericite and iron ore do not change in shape and abundance until the appearance of biotite where much of the chlorite, iron ore and some sericite were consumed in reactions like 8.1-2 whereas the remaining sericite was recrystallized into small ill-shaped muscovite. This was quickly broken down either to K-feldspar and andalusite (equation 8.13), K-feldspar and corundum (equation 8.14) or more probably to cordierite and K-feldspar (equation 8.15). However it is very probable that both dehydration reactions 8.13 and 8.14 took place and the absence of andalusite from the slates may be because it was consumed in other reactions such as 8.9 and 8.10.



Plagioclase does not change in shape, grain size and composition except in the innermost parts of the aureole (0-10m from the contact) where large euhedral crystals of albite (An_{0-10}) were crystallized in the hornfelses or alternatively the parent rocks were rich in albite.

Similarly, quartz does not change until in the most altered hornfelses where it is either absent or if present occurs as isolated microscopic pods and lenses. Rare K-feldspar crystals have also, but only occasionally, been noted within these quartzose lenses which suggests that partial melting and mobilization of low melting point minerals occurred.

8.4 Changes in the mineral chemistry

Biotite, which is always unzoned, does not change in composition until about 40m from the contact where X_{Mg} (ions $Mg/(Mg+Fe)$) rises reaching its highest value of 0.52 in sample Y70 about 30m from the contact (Figure 8.5). This rise in the Mg values is accompanied by a parallel decrease in the Fe contents. Much higher Ti values are also recorded in biotite from the more hornfelsed slates (Figure 8.5). As would be expected the Mg-richest biotites occur in sample Y70 with the Mg-richest cordierite. Biotite does not change in composition whatever the mineral(s) in contact which indicates that re-equilibration during cooling between biotite and other phases particularly cordierite did not take place.

Cordierite also underwent significant chemical changes in the more thermally affected slates (Figure 8.6). Mg increases but Fe decreases towards the intrusion reaching their highest and lowest values of 1.48 and 0.565 about 30m from the contact respectively. In the banded samples Mg and Fe tend to reverse either as a result of re-equilibration between the leucosomes (pink-orange bands) and the hornfelses (black bands) or the cordierites may have crystallized from different starting material.

There is not enough exposure for small scale sampling (i.e. within 60m from the contact) to study whether ferrohpersthenite and spinel change in composition with rising temperature but the available analyses suggest that they are homogeneous throughout the whole contact areas.

Plagioclase and K-feldspars analyses are plotted in Figure 8.7 but both phases have similar composition in all analysed samples.

8.5 Metamorphic thermal zones

The mineralogical changes described previously are progressive and although post hornfelsing folding and faulting occurred, the outcrops are not strongly disturbed. There are four thermal zones namely; spotted slates zone, biotite zone, cordierite zone and the cordierite-orthopyroxene-spinel - corundum zone (Figure 8.1A). The spotted slates zone was mapped in the field because the spots are not easily seen in thin sections cut perpendicular to the cleavages. The limits of all the zones are within 5-10m accuracy. The biotite zone is fairly well defined but the cordierite zone could be traced only near Craig More summit because of poor exposure elsewhere. In the cordierite zone, cordierite, biotite, chlorite and muscovite occur. The cordierite-orthopyroxene-spinel-corundum \pm sillimanite zone can be defined in the inner aureole only where the hornfelses are sericite-, chlorite and biotite-free. The presence of prismatic sillimanite indicates that the sillimanite zone is reached.

8.6 Conditions of metamorphism

It is unfortunate that the garnet poikiloblast is Mg-free (*i.e.* reactions 3.1-2 did not take place) as the calculations of the temperature and pressure within the aureole require the presence of Mg. The absence of andalusite from the studied samples for indirect evaluation of the conditions of metamorphism is also a disadvantage. However, assuming the temperature is similar at any given distance from the intrusion and that within the Ben Ledi Grits andalusite coexists with muscovite in the outer envelope and then disappears in the innermost parts of it (Tilley 1924a), both dehydration reactions 8.13 and 8.14 must therefore have occurred. The univariant curves for the breakdown of muscovite were determined under hydrothermal conditions (*i.e.* high H₂O activity) by Turner (1968) and this can be used to roughly limit the conditions of metamorphism in the study area. Within the aureole, the low grade of regional metamorphism coupled with the continuous driving of water from the rocks with rising degrees of hornfelsing indicate that the activity of water must have been very high and the curves shown in Figure 8.8 probably represent realistic temperature and pressure in the Comrie thermal aureole. If the pressure is set to 0.1 GPa (representing a depth of 3-4km) the

temperature in the inner aureole must therefore have exceeded 700°C. However, the presence of prismatic sillimanite within the strongly hornfelsed slates suggests that the temperature was somewhat higher (750-800°C) and a pressure of about 0.15 GPa.

It is unfortunate that the application of the physical model for estimating the contact temperature is uncertain because the presence of a separate aplitic intrusion inside the main granodiorite intrusion (Woodland 1979) and the large variety of intrusive rocks may be the result of successive magmatic injections. Further, the presence of late stage "sub-solidus" alterations at the contact between the black and pink-orange bands (see Chapter 9) indicates that heat was not transferred to the country rocks by conduction only and therefore invalidating Jaeger's model. However, if we assume that all the igneous rocks to have been intruded in a single phase and much of the heat was transferred by conduction, application of equation 3.4 using the same thermal constants for slates as for shales (see page 39 for definition of terms that follow and page 40 for the values given for shales) and $C_p = 0.25$, $K_1 = 0.0057$, $k_1 = 0.009$ for granodiorite, being values given for granite porphyry by Jaeger (1959), the contact temperatures in °C are given below for (T_m range 800 - 1000°C), $L(80-100 \text{ cal g}^{-1}$ except for $T_m = 800^\circ\text{C}$ where L must be low).

T_m	T_c (for $L=80$)	T_c (for $L=100$)
1000	773	800
900	695	720
800	650	-

Assuming the initial temperature of the country rock $T_0 = 100^\circ\text{C}$, the contact temperatures for $L=80 \text{ cal g}^{-1}$ therefore range from 750 to 873°C which indeed fall within the expected limits. This range not only suggests that the stability field of muscovite and probably andalusite were exceeded but it indicates that partial melting is very probable.

8.7 Summary

The thermal aureole within the Aberfoyle Slates is well defined and extends up to 580m from the main intrusion with four thermal zones : spotted, biotite, cordierite, and cordierite, orthopyroxene, spinel, corundum \pm biotite \pm sillimanite zones. Within the Comrie aureole the hornfels minerals appeared in the following way : spots, 580m; biotite, 200m; cordierite, 150m and spinel-corundum-orthopyroxene, \leq 60m from the contact.

The conditions of metamorphism as deduced from petrological evidence and the physical model suggest that the stability field of muscovite and andalusite were exceeded and melting temperatures in the range 700-820^o C and pressures of about 0.8-0.18 GPa were probably reached.

The possible partial melts will discussed in Chapter 9.

Table 8.1 : Summary statistics of modal analyses.

	R	SS	S*	SS	BB	SS	CC	SS
Chlorite	46.7	8.09	36.6	11.92	18.29	9.76	0	-
sericite	19.92	8.09	29.88	11.15	32.79	6.11	0	-
Quartz	18.98	3.81	13.19	4.42	20.74	3.09	5.67	9.04
Iron ore	5.60	3.50	5.77	4.89	2.32	3.18	0	-
Epidote	2.99	2.40	9.17	3.81	6.02	2.69	0.20	0.27
Plagio..	2.39	1.94	1.50	1.63	1.90	1.08	3.18	2.91
Opaque	2.73	2.13	2.39	1.56	6.06	9.05	9.64	3.90
K-feld..	acc	-	0.82	0.85	8.55	11.02	5.06	3.45
Biotite	0	-	0	-	2.65	4.64	23.38	14.58
Cordierite	0	-	0	-	0	-	33.38	16.71
Spinel	0	-	0	-	0	-	12.80	10.47
Corundum	0	-	0	-	0	-	3.58	5.22
Orthop.	0	-	0	-	0	-	0.37	0.32

R = average of 11 regional slates

S* = average of 6 spotted slates

B = average of biotite-bearing hornfelses

C = average of 5 contact hornfelses (cordierite-, ± spinel-, ± corundum-, ± orthopyroxene-, ± biotite-, ± garnet-, ± sillimanite-bearing hornfelses)

S = standard deviation

Plagio. = Plagioclase

Orthop. = Orthopyroxene

Table 8.2 : Results of mineral analyses . The number of minerals analyzed is given in brackets

Biotite

	Y37[4]	S	Y50[1]	Y53[5]	S	Y70[4]	S
SiO ₂	35.77	0.08	33.53	35.39	0.18	34.33	0.73
TiO ₂	5.08	0.07	3.19	4.12	0.11	4.29	0.45
Al ₂ O ₃	15.40	0.10	19.32	15.47	0.08	18.72	0.73
FeO	19.96	0.62	24.37	23.09	0.89	17.15	0.77
MgO	10.64	0.43	5.60	7.96	0.04	10.64	0.88
MnO	0	-	0.18	0	-	0.04	0.08
CaO	0.08	0.08	0	0	-	0	-
Na ₂ O	0	-	0	0.48	0.02	0	-
K ₂ O	9.61	0.03	9.20	8.91	0.27	9.51	0.16
Total	96.54		95.39	95.42		94.68	

Number of ions per formula unit computed on the basis of 22 oxygens.

Si	5.419	0.001	5.168	5.542	0.079	5.22	0.067
Al ⁺⁴	2.581		2.832	2.548		2.780	
Al ⁺⁶	0.169	0.010	0.778	0.347	0.018	0.575	0.150
Ti	0.579	0.010	0.381	0.476	0.011	0.490	0.051
Fe	2.562	0.083	3.231	2.969	0.112	2.182	0.119
Mg	2.401	0.091	1.323	1.825	0.006	2.407	0.183
Mn	0	-	0.18	0	-	0.04	0.08
Ca	0.08	0.08	0	0.48	0.02	0	-
Na	0	-	0	0.142	0.006	0	-
K	1.85	0.012	1.86	1.747	0.051	1.842	0.031
total	15.582		15.597	15.596		15.496	

ions Mg/(Fe+Mg)

0.484

0.290

0.380

0.524

contd

Table : 8.2 : Continued

	biotite			Garnet		Cordierite	
	Y83[1]	Y87[3]	S	Y59	Y59	Y37[3]	S
SiO ₂	33.16	33.36	0.23	35.042	34.70	45.83	0.92
TiO ₂	3.18	2.89	0.38	0	0	0	-
Al ₂ O ₃	18.74	20.36	0.72	0.25	0	32.21	0.07
FeO	24.84	23.58	0.92	31.99	31.83	11.60	2.13
MgO	5.50	5.56	0.16	b.d.l(0.07)		7.85	3.63
MnO	0	0	-	0.29	0.39	0	-
CaO	0.11	0	-	33.72	32.64	0	0
K ₂ O	9.11	8.77	0.44	0	0	0	0
Total	94.64	94.52		101.67	99.56	97.72	

ions on the basis of 22 oxygens for biotite, 24 for garnet.and 18 for cordierite.

Si	5.234	5.20	0.02	5.94	5.93	5.43	0.49
Al ⁺⁴	2.766	2.80	-	0	0	0.57	-
Al ⁺⁶	0.726	0.941	0.107	0	0	3.55	0.10
Ti	0.378	0.339	0.045	0	0	0	-
Fe	3.279	3.074	0.124	4.037	4.096	1.06	0.22
Mg	1.293	1.293	0.032	0	0	1.020	0.005
Ca	0	0	-	0	0	0	-
K	1.834	1.745	0.09	0	0	0	-
Total	15.538	15.392		16.03	16.00	11.65	

ion Mg/(Fe+Mg)

100% andradite

0.283 0.296

0.532

b.d.l = below detection limit(0.07 wt% for Mg)

Fe in garnet was recalculated as Fe₂O₃

contd

Table 8.2 : Continued

	Y50[2]	S	Y53[1]	Y70[1]	Y83[4]	S	Y87[4]	S
SiO ₂	44.26	0.11	46.65	47.89	46.26	0.22	46.26	0.19
TiO ₂	0.41	0.16	0	0	0.26	0.26	0	-
Al ₂ O ₃	31.15	0.29	32.35	33.04	31.58	1.03	32.31	0.24
FeO	13.88	0.35	11.35	6.53	11.97	0.69	12.78	0.36
MgO	5.74	0.66	6.23	9.61	6.23	0.53	5.54	0.12
MnO	0.33	0.01	0	0.23	0.30	0.05	0.23	0.07
Total	95.77		96.58	97.30	96.60		97.12	

Number of ions per formula unit computed on the basis of 18 oxygens

Si	4.83	0.04	4.954	4.949	4.915	0.005	4.937	0.009
Al ⁺⁴	1.17	-	1.046	1.051	1.085	-	1.063	-
Al ⁺⁶	2.835	0.005	3.004	2.973	2.87	0.105	2.994	0.03
Ti	0.035	0.015	0	0	0	-	0	-
Fe	1.265	0.015	1.0	0.565	1.06	0.07	1.138	0.024
Mg	0.935	0.095	0.986	1.48	0.985	0.07	0.881	0.01
Mn	0.031	0.001	0	0.02	0.025	0.005	0.021	0.006

ions Mg/(Fe+Mg)

0.575	0.496	0.723	0.481	0.436
-------	-------	-------	-------	-------

contd

Table 8.2 : Continued

			Spinel	
	Y79[2]	S	Y50[1]	Y70[1]
SiO ₂	46.08	0.19	0.39	0
TiO ₂	0	-	0	0
Al ₂ O ₃	32.24	0.19	56.05	59.83
FeO	10.0	0.47	39.96	32.41
MgO	7.19	0.48	2.25	7.31
MnO	0.25	0.04	0.15	0.18
Total	95.76		98.80	99.73

Ions basis of 18 oxygens for cordierite and 32 for spinel.

Si	4.912	0.011	0.09	0	
Al ⁺⁴	1.088		15.350	15.618	
Al ⁺⁶	2.965	0.024	0	0	
Ti	0	-	0	0	
Fe	0.891	0.04	0.560	0.460	Fe+3
Mg	1.141	0.08	7.20	5.54	F+2
Mn	0.009	0.007	0.77	2.34	Mg
			0.03	0.03	Mn
ions Mg/(Fe+Mg)					
	0.561		0.11	0.43	contd

Table 8.2 : Continued

Plagioclase							
	Y17[5]	S	Y50[1]	Y53[3]	S	Y70[1]	Y771
SiO ₂	64.95	4.37	62.50	65.36	0.25	65.52	63.62
Al ₂ O ₃	20.49	3.17	21.50	19.96	0.05	19.96	21.58
FeO	0.47	0.10	0.22	0.48	0.05	2.21	0.45
CaO	1.94	3.25	2.72	0.57	0.01	0.57	2.73
Na ₂ O	9.91	1.69	8.94	9.49	0.42	10.35	9.79
K ₂ O	0.04	0.05	1.12	2.01	1.21	0.39	0.56
Total	97.80		97.00	97.87		99.00	98.73

Number of ions per formula unit computed on the basis of 32 oxygens

Si	11.646	0.071	11.382	11.742	0.031	11.68	11.402
Al	4.338	0.704	4.616	4.228	0.003	4.19	4.560
Fe	0.07	0.016	0.033	0.072	0.008	0.33	0.068
Ca	0.376	0.633	0.530	0.109	0.003	0.11	0.525
Na	3.443	0.565	3.155	3.479	0.323	3.57	3.401
K	0.009	0.011	0.260	0.460	0.276	0.09	0.128

end member proportions

An	9.44	5.76	13.43	2.69	0.04	2.92	12.95
Ab	90.32	15.93	79.97	85.85	6.93	94.70	83.89
Or	0.236	0.41	6.69	11.46	6.97	2.38	3.16

contd

Table 8.2 : Continued

	K-Feldspar						
	Y79[1]	Y37[1]	Y50[2]	S	Y53[1]	Y59[2]	S
SiO ₂	66.54	63.62	62.41	0.33	65.38	63.32	0.22
Al ₂ O ₃	19.39	19.40	19.10	0.37	19.25	19.85	0.20
FeO	0	0.37	0.26	-	0	0.37	0.04
CaO	0.14	0.27	0.56	0.32	0.34	0.73	0.26
Na ₂ O	11.32	3.46	3.68	0.85	6.51	5.58	0.84
K ₂ O	0.19	11.81	10.48	1.56	6.25	8.05	1.22
Total	97.58	98.93	96.49		97.73	97.90	

Number of ions per formula unit computed on the basis of 32 oxygens

Si	11.921	11.75	11.773	0.046	11.924	11.67	0.034
Al	4.095	4.22	4.254	0.052	04.138	4.317	0.047
Fe	0	0.05	0.04	0	0	0.054	0
Ca	0.027	0.05	0.114	0.064	0.067	0.054	0.044
Na	3.931	1.24	1.341	0.301	2.303	1.994	0.301
K	0.044	2.78	2.525	0.395	1.455	1.894	0.285

end member proportions

An	0.69	1.23	2.875	1.625	1.75	3.39	1.08
Ab	98.22	30.47	15.25	10.68	60.21	49.43	6.68
Or	1.09	68.30	63.37	9.44	38.04	47.18	7.69

contd

Table 8.2 : Continued

	K-feldspar from the leucosomes						
	Y70[2]	S	Y79[1]	Y77[2]	S	Y79[2]	S
SiO ₂	62.06	1.10	61.78	64.83	0.08	64.80	0.30
Al ₂ O ₃	19.56	0.60	20.42	18.58	0.21	18.59	0.17
FeO	0.50	0.07	0.30	0	0	0.18	0.01
CaO	0.74	0.74	0.99	0.33	0.09	0.48	0.07
Na ₂ O	3.52	1.05	3.36	4.33	0.30	4.53	0.85
K ₂ O	10.66	2.36	10.11	9.96	0.51	9.44	1.23
Total	97.04		96.96	98.03		98.02	

Number of ions per formula unit computed on the basis of 32 oxygens

Si	11.64	0.175	11.52	11.961	0.034	11.935	0.045
Al	4.327	0.147	4.485	4.044	0.04	4.035	0.045
Fe	0.081	0.011	0.045	0	0	0.024	0.001
Ca	0.15	0.015	0.019	0.066	0.018	0.09	0.01
Na	1.282	0.382	1.21	1.547	0.104	1.615	0.305
K	2.55	0.56	2.41	2.346	0.125	2.215	0.285

end member proportions

An	3.79	3.79	5.2	1.68	0.47	2.30	0.23
Ab	32.26	9.87	32.01	39.08	2.66	41.14	7.47
Or	63.95	13.61	62.79	59.24	3.13	56.56	6.70

contd

Table 8.2 : Continued

Orthopyroxene

	Y56	Y59	Y77	Y78
SiO ₂	47.96	47.54	48.13	48.04
TiO ₂	0.34	0	0.25	0.40
Al ₂ O ₃	2.68	2.80	2.66	2.85
FeO	35.41	34.80	34.39	35.59
MnO	0.62	0.53	0.62	0.53
MgO	13.66	13.06	12.93	13.04
CaO	0.17	0.16	0	0.14
Total	100.87	98.89	98.98	100.59

Number of ions per unit formula computed on the basis of 6 oxygens

Si	1.880	1.901	1.925	1.893
Al ⁺⁴	0.120	0.099	0.075	0.107
Al ⁺⁶	0.030	0.030	0.050	0.025
Ti	0.010	0	0.007	0.011
Fe ⁺³	0.096	0.065	0.009	0.062
Fe ⁺²	1.064	1.098	1.140	1.110
Mg	0.798	0.778	0.770	0.766
Mn	0.020	0.018	0.021	0.017
Ca	0.007	0.007	0	0.059
%Fe	59.04	59.70	59.88	58.70
%Mg	40.61	39.94	40.12	38.35
%Ca	0.34	0.36	0	2.95

KEY TO FIGURE 8.2 - 8.8

Figure 8.1 Sample location map

Figure 8.1A Thermal metamorphic zone (cellophane film)

Figure 8.2 Mineralogical cross section AA'

Figure 8.3 Mineralogical cross section BB'

Figure 8.4 Mineralogical cross section CC'

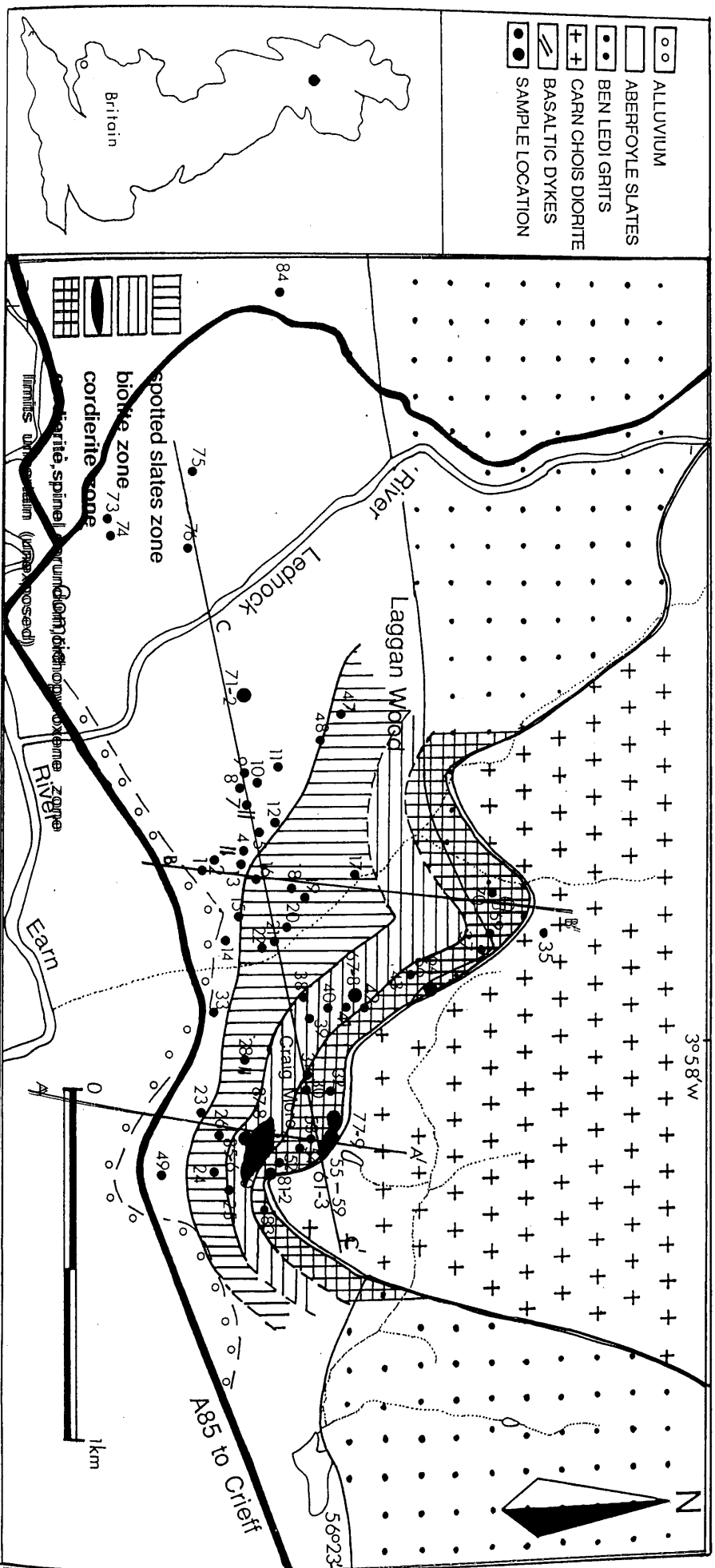
Figure 8.5 Traverse BB' showing the changes in the composition of biotite.

Figure 8.6 Traverse AA' showing the changes in the composition of cordierite.

Figure 8.7 Plot of Na₂O-K₂O-CaO for plagioclase and K-feldspar from the slates and hornfelses. Four K-feldspar analyses from the leucosomes are also shown.

Figure 8.8 P(GPa) vs (T°C) for estimating the conditions of metamorphism in the Cornie thermal aureole.

fig. 8.1 GEOLOGICAL SKETCH MAP SHOWING THE THERMAL ZONES, IN THE LABRINOR (BESOUAUSID)



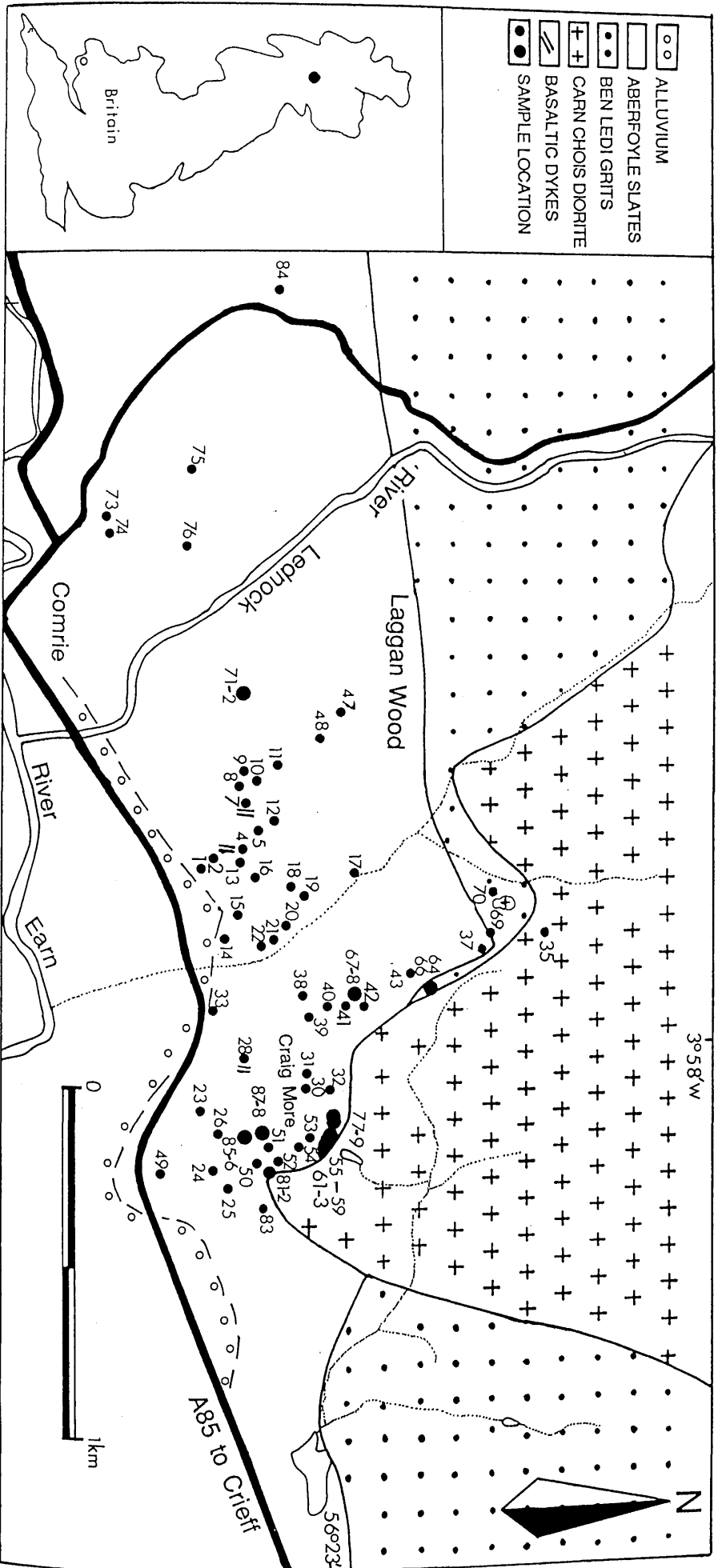


fig 8. 1 GEOLOGICAL SKETCH-MAP OF THE COMRIE AREA, PERTHSHIRE (SCOTLAND)

fig 8.2

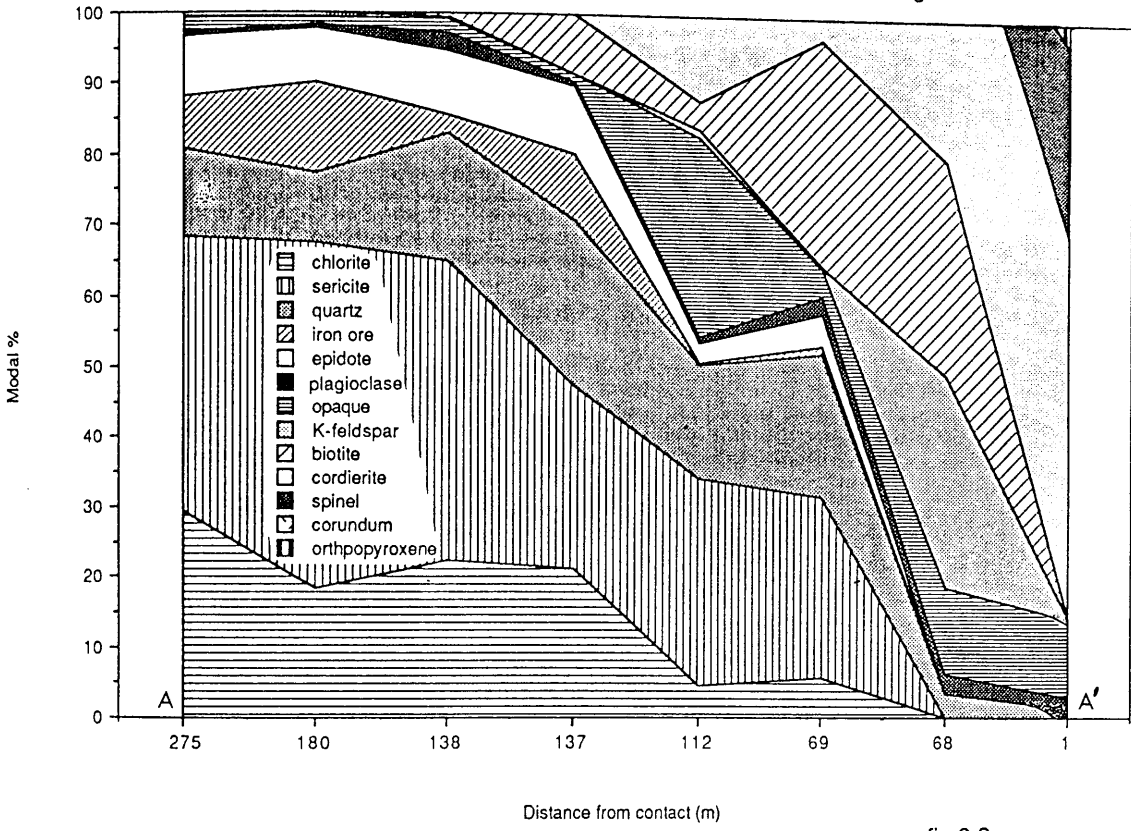


fig 8.3

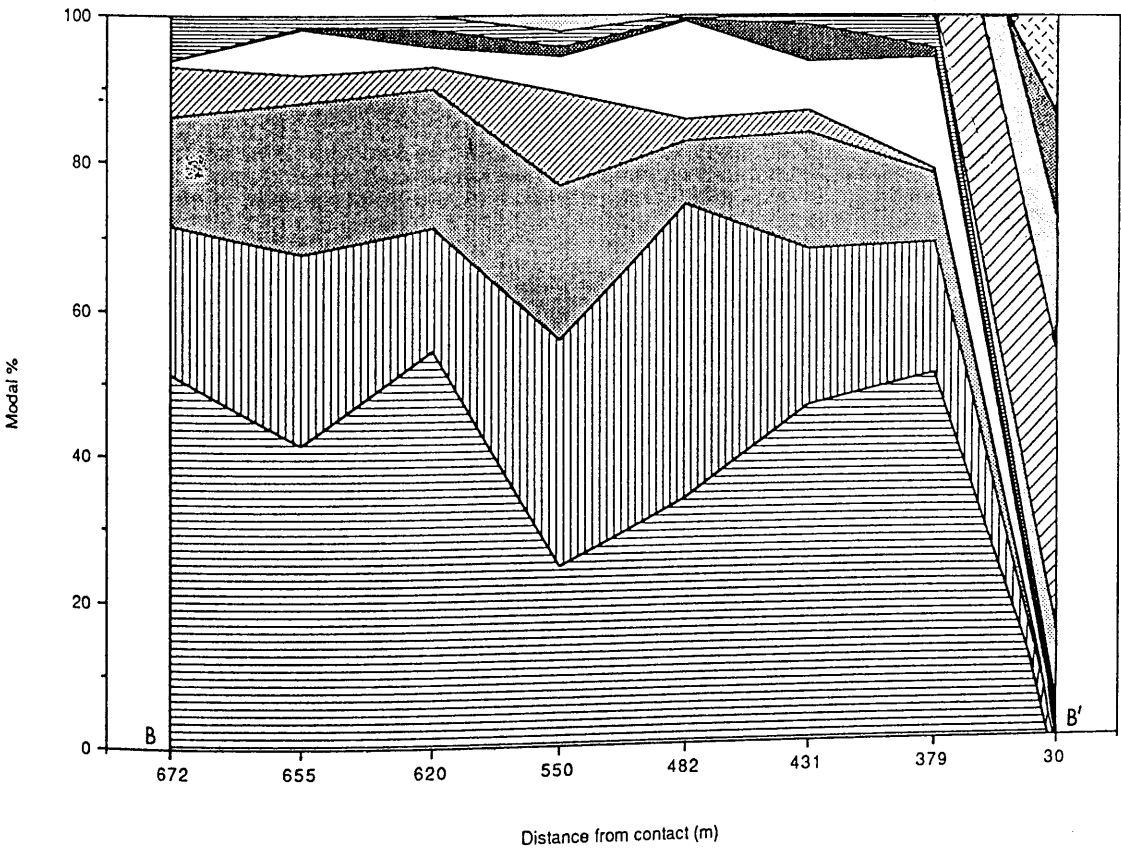


fig 8.4

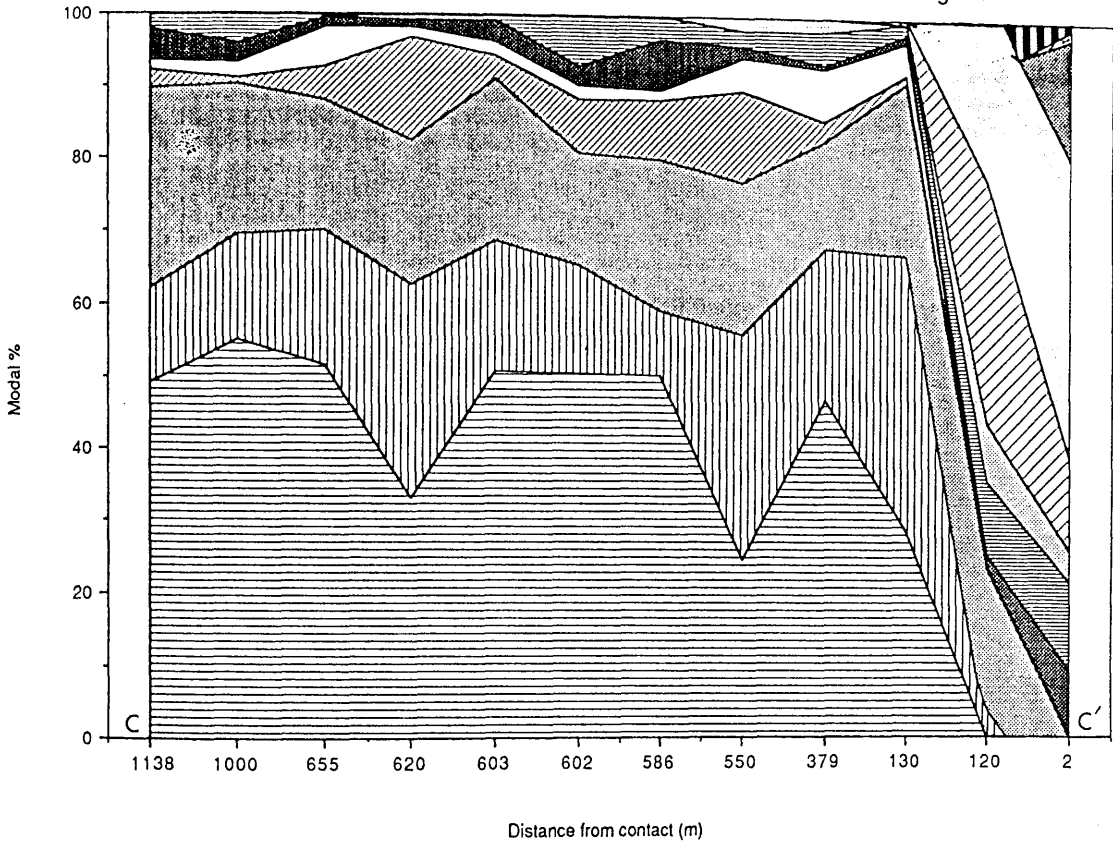


fig 8.5

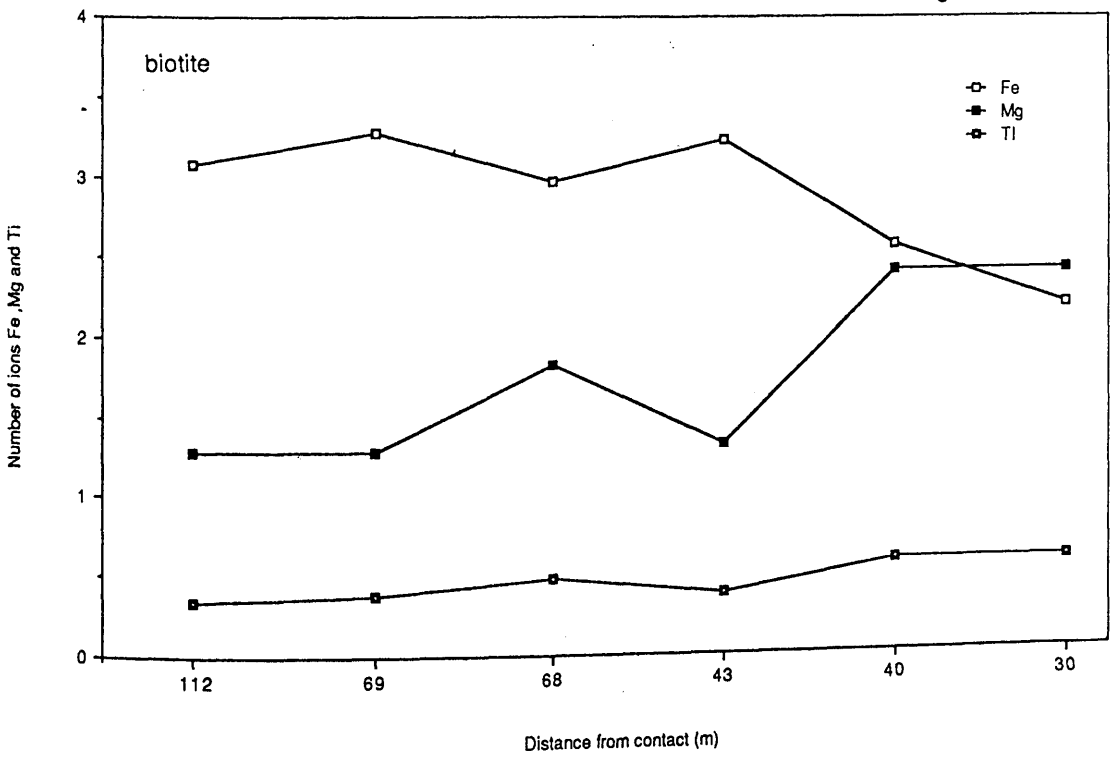


fig 8.6

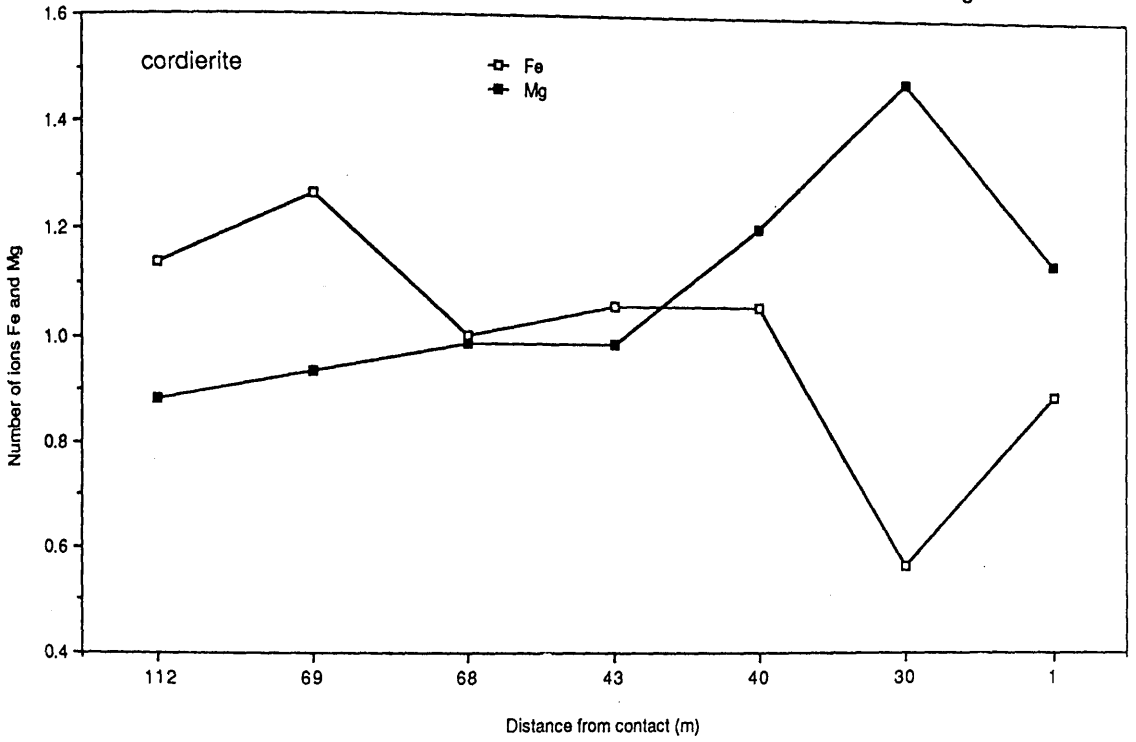
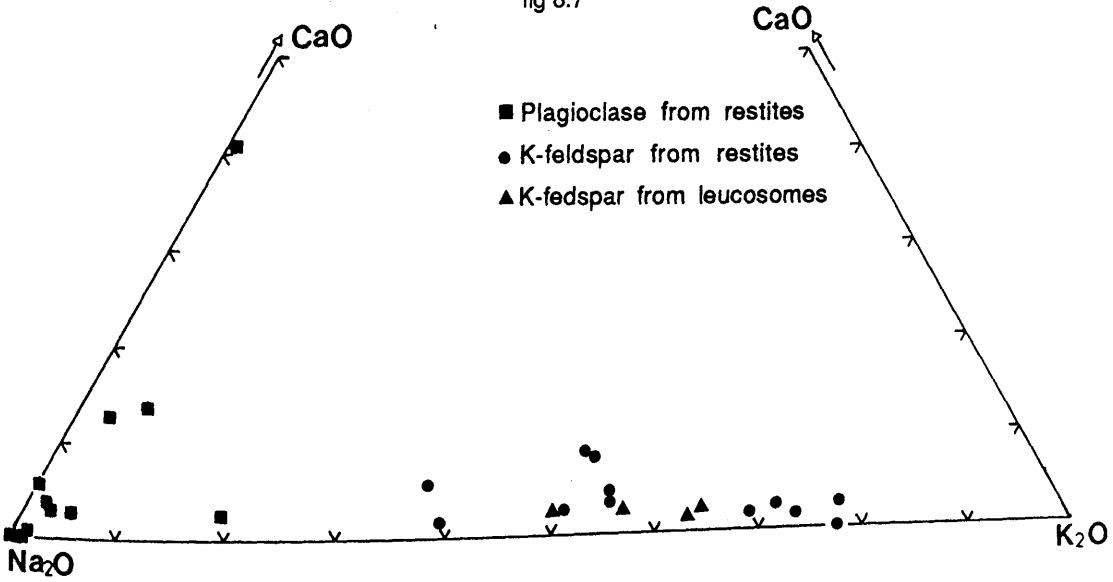


fig 8.7



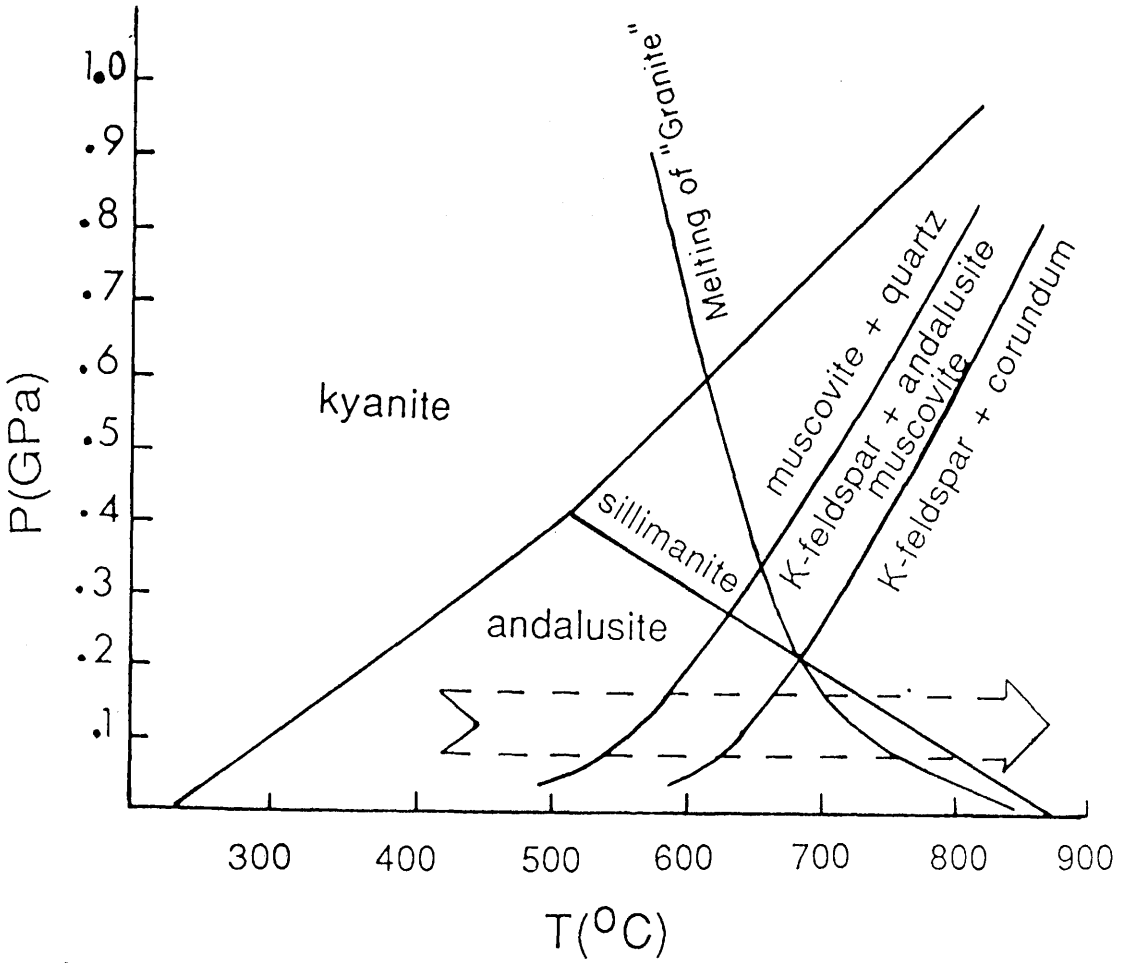
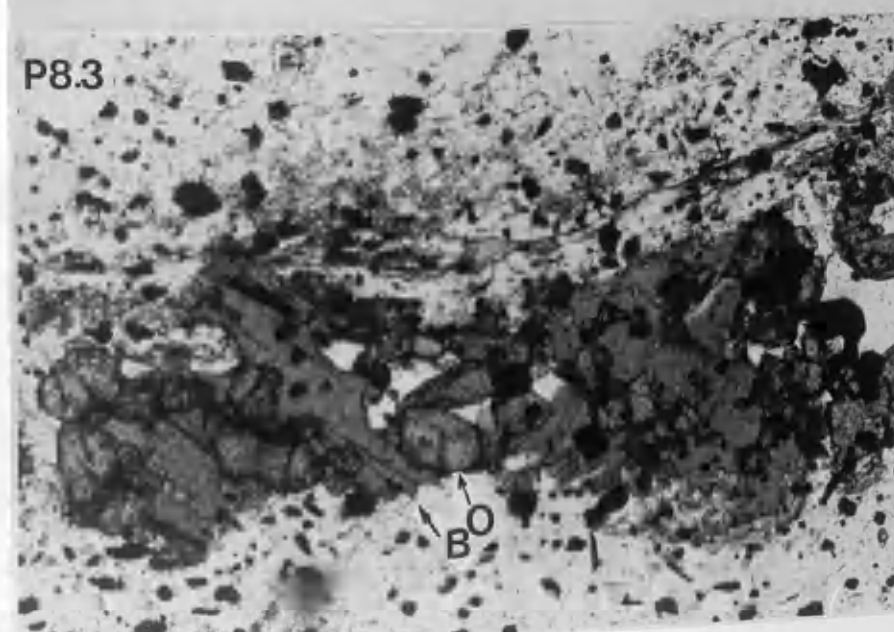
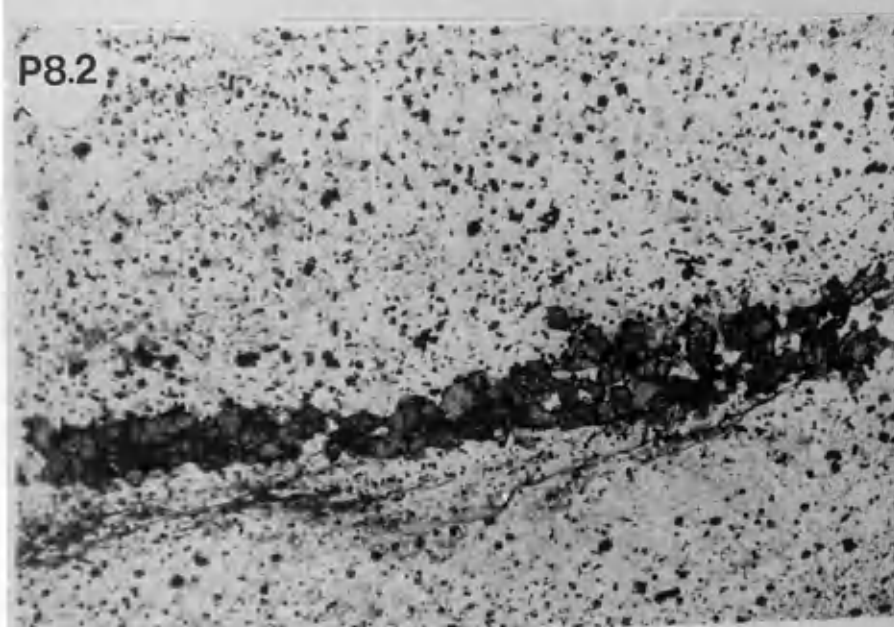


fig 8.8 superimposition of the univariant curves for the breakdown of muscovite from Turner (1968) and the stability field of Al_2SiO_5 minerals (Richardson *et al* 1969) to derive the likely PT conditions in the Comrie thermal aureole . The direction of the arrow indicates the direction of the reactions while its width is a suggestive range of pressure .

- P8.1 Typical banding pattern in the Comrie contact hornfels (hand specimen).
- P8.2 Veins of orthopyroxene from the inner Comrie aureole.(X2.5, magn. 30X)
- P8.3 Replacement of biotite (B) by orthopyroxene (O) in the Comrie inner aureole.(X2.5, magn. 60X)



CHAPTER NINE CHEMISTRY & ORIGIN OF THE LEUCOSOMES

9.1 Introduction

The general chemistry of the regional slates is first discussed and compared to many shale and pelite compositions from the literature and then the chemical changes experienced by the hornfelses are established and interpreted. U and Th are treated separately and the possible origin of eight pink-orange bands (hereafter called leucosomes) is finally discussed to decide whether are magmatic injections or else represent the melts derived from the country rocks or both.

9.2 General chemistry of the regional slates

9.2.1 Major and trace elements

Because no chemical differences have been noted between the regional and spotted slates their major and trace elements are grouped together and are given with four REE analyses in appendix 3 and summarized and compared to 55 southern Connemara pelites (SCP) and other shales in tables 9.1-2 (see table 6.1 for shale and pelite compositions from the literature).

The Aberfoyle slates generally compare well in their major elements with shale and pelite compositions from the literature although they tend to be richer and poorer in silica than SCP and T&M pelites respectively. The slates are also poorer in Ca but richer in Na compared to C, K and T&M (see foot of table 5.1 for definition of T&M, C T&W and K) and this is due to their predominantly albite-rich plagioclase.

Despite the large standard deviations of the trace elements the slates are strongly depleted in Sr and to lesser extent Rb and Ni compared to SCP, T&W, K and T&M. Ba in the slates also approaches the lower limits of its content in the SCP and this is not surprising in view of the dominance of chlorite in the slates and the scarcity of plagioclase and K-feldspar .

In terms of inter-element relationships, the picture clearly reflects the mineralogy in that Ba and Rb correlate excellently with K (figures 9.1-2) which indicates that both elements are coming in sericite and K-feldspar where present especially as neither elements is substantially held in plagioclase (figures 9.3-4). Sr does not correlate very well with Ca (figure 9.5)

which in turn correlates poorly with Na (figure 9.6) and this is because plagioclase is not the only control over Ca which is also coming in epidote, calcite, apatite and tourmaline . Ti is essentially held in rutile (figures 9.7-8, i.e. not dominantly held in magnetite and ilmenite) which must therefore be the control over, Co and Cr (only Ti versus Cr is shown in figure 9.9). Some Ti and probably also the trace Cr, Ni and Co are held in ilmenite but the presence of Fe essentially in iron ore and chlorite obscures the true picture of its relationships with Ti .

As shown by Senior and Leake (1978), the parameter Niggli al-alk provides a measure of Al in the original sediments contained in the clay minerals and micas rather than Al added in feldspar because al-alk in albite and K-feldspar is zero while detrital anorthite-rich plagioclase is absent from the slates (chapter. 8). Figures 9.10-17 therefore suggest that K, Rb, Ce, Ba, Ga and to lesser extent Y, Zn and Fe were added in clay minerals while Zr, Ti, Cr, Ni and P were controlled by detrital zircon, rutile (and ilmenite) and apatite respectively (none of the last listed elements correlate well with Niggli al-alk and hence are not shown).

9.2.2 REE

The arithmetic means and standard deviation of the REE from four Aberfoyle Slates and four hornfeses are compared in table 9.2 with four unhornfeses pelites from Connemara, Ireland and eventually with REE values for PAAS, NAMSC and ESC (see table 5.2).

The REE from The Aberfoyle Slates have negative Eu anomalies and compare reasonably well with those of the Connemara pelites except that the former generally exhibit steeper distribution patterns (figure 9.18) and this is not surprising in view of the scarcity of zircon and apatite in the slates compared to the pelites. Correspondingly, the slates are remarkably richer in REE than PAAS, NAMSC and ESC but all have similar Eu/Eu^* ratios (see tables 5.2 and 9.2). Sample Y76 is strongly depleted in Ce but rich in most LREE and MREE despite having very similar mineralogy and chemistry to Y75 and this depletion is probably a sedimentary feature .

which in turn correlates poorly with Na (figure 9.6) and this is because plagioclase is not the only control over Ca which is also coming in epidote, calcite, apatite and tourmaline. Ti is essentially held in rutile (figures 9.7-8, i.e. not dominantly held in magnetite and ilmenite) which must therefore be the control over, Co and Cr (only Ti versus Cr is shown in figure 9.9). Some Ti and probably also the trace Cr, Ni and Co are held in ilmenite but the presence of Fe essentially in iron ore and chlorite obscures the true picture of its relationships with Ti.

As shown by Senior and Leake (1978), the parameter Niggli al-alk provides a measure of Al in the original sediments contained in the clay minerals and micas rather than Al added in feldspar because al-alk in albite and K-feldspar is zero while detrital anorthite-rich plagioclase is absent from the slates (chapter. 8). Figures 9.10-17 therefore suggest that K, Rb, Ce, Ba, Ga and to lesser extent Y, Zn and Fe were added in clay minerals while Zr, Ti, Cr, Ni and P were controlled by detrital zircon, rutile (and ilmenite) and apatite respectively (none of the last listed elements correlate well with Niggli al-alk and hence are not shown).

9.2.2 REE

The arithmetic means and standard deviation of the REE from four Aberfoyle Slates and four hornfeses are compared in table 9.2 with four unhornfeses pelites from Connemara, Ireland and eventually with REE values for PAAS, NAMSC and ESC (see table 5.2).

The REE from The Aberfoyle Slates have negative Eu anomalies and compare reasonably well with those of the Connemara pelites except that the former generally exhibit steeper distribution patterns (figure 9.18) and this is not surprising in view of the scarcity of zircon and apatite in the slates compared to the pelites. Correspondingly, the slates are remarkably richer in REE than PAAS, NAMSC and ESC but all have similar Eu/Eu^* ratios (see tables 5.2 and 9.2). Sample Y76 is strongly depleted in Ce but rich in most LREE and MREE despite having very similar mineralogy and chemistry to Y75 and this depletion is probably a sedimentary feature.

9.3 Chemical changes

As a geochemical framework, the slates are grouped into three categories : regional slates, intermediate and contact hornfeses (table 9.1). The regional slates include both the country and spotted slates whereas the intermediate hornfeses are rocks always containing biotite \pm cordierite \pm spinel \pm corundum \pm orthopyroxene. The contact hornfeses, which all come from banded rocks, are practically biotite-free and represent the highest degree of hornfelsing. The chemical changes will be described as they appear and then a discussion will be given to study whether these changes are the result of hornfelsing only or sedimentary chemical variations between the remote slates and those occurring near the contact are complicating factors.

It is unfortunate that no published chemical analyses of the Aberfoyle Slates could be found and all interpretations have to rely on the rocks analysed in the present work which include 36 regional slates, 29 intermediate and eight contact hornfeses.

9.3.1 Fractionation of the major elements

Silica changes very little in the intermediate hornfeses but in the banded samples it decreases to an average of 48.38 ± 2.85 wt% compared to 58.64 ± 2.44 wt% in the country rocks.

The behaviour of alkalis is much less clear than that of silica in that Na tends to rise in the most altered contact samples while K rises in some e.g Y58 (5.38 wt% compared to 3.12 ± 0.69 average regional slates) but decline in others e.g Y61 (1.97 wt%), Y78 (1.87 wt%) which suggests that much K entered the melt compared to Na. The high K contents of some restites though may be due to contamination from the K-feldspar-rich leucosomes or a sedimentary enrichment is because some K-feldspar crystallized in the restites.

The early and relatively greater removal of K compared to Na suggests an aplitic liquid was derived from the slates. This is in agreement with findings by Winkler and von Platen (1960) who have shown that anatexis of pelitic rocks begins with the formation of quartz-K-feldspar (aplitic) melts followed with rising temperature by the solution of more calcic plagioclase. Ca is ambiguous because it is coming in other minerals but a slight increase can be

noted in the contact hornfelses which indicates that small amounts of Ca might have accompanied K.

Mn remains unchanged throughout the whole aureole though lower values are recorded in the banded samples but only if the standard deviations are ignored. Only very small amounts of Mn, if any, would have entered the melts.

P fluctuates in the intermediate hornfelses then rises in the contact rocks to 0.32 ± 0.06 wt% compared to 0.16 ± 0.09 in the country rocks. It is very likely that the increase of P and Zr (see below) is because of the removal of the aplitic melt (i.e. the melting temperatures were not high enough to melt zircon and apatite) although a sedimentary enrichment in apatite and zircon of the contact samples can be a very important cause.

Similarly, Ti, which averages 1.19 ± 0.2 wt% in the regional slates, increases insignificantly to 1.41 ± 0.23 wt% in the intermediate hornfelses followed by a pronounced rise in the banded samples (average 2.37 ± 0.23 wt%)

There is no apparent change in the contents of both Fe and Mg even in the contact hornfelses but Al rises to an average of 26.78 ± 2.19 wt% compared to 18.23 ± 1.27 wt% in the regional slates. Table 9.1 shows that Niggli mg changes insignificantly within the aureole (0.364 ± 0.01 in the slates compared to 0.343 ± 0.03 in the contact hornfelses) whereas Niggli fm decreases insignificantly from 40.51 ± 4.87 in the country rocks to 32.77 ± 4.12 in the contact samples. This trend is probably caused by the melting of Fe-rich biotite and in the most advanced stages cordierite (chapter 8) because there is no evidence which suggests the melting of ferrohypersthene. Fe and Mg will probably crystallize in the melts as magnetite, ilmenite and biotite.

Niggli al plots negatively with Niggli fm (figure 9.19) as if Fe and Mg were added to the hornfelses, Al was subtracted from them, both processes took place or it is mainly due to sedimentary variations. As just showed, Niggli fm tends to be lower in the contact hornfelses compared to the country rocks and consequently, the negative correlation can only be because Al was removed from the contact hornfelses in much greater amounts than Fe and Mg. Because Al was removed in smaller amounts than it was present in the original slates, the proportions of Al remaining in the residual hornfelses has increased. However, if the increase of Al is due to partial melting only then Mg and Fe

should increase in the restites which is not the case. This therefore indicates that the negative correlation between Niggli al and Niggli fm is due mainly to original sedimentary variations ; although partial melting is also an important factor (see subsection 9.3.4)

H₂O decreases from 3.56 ± 0.65 in the country slates to 1.23 ± 0.49 in the more desilicated hornfelses but CO₂ remains practically unchanged (table 9.1).

9.3.2 Fractionation of the trace elements

The trace elements generally mirror the behaviour of their major equivalents in that Cr, Co, Ga and to much lesser extent Ni increase in the contact samples whereas Rb tends to decrease. Zr, Ba and Sr also increase in the contact hornfelses.

Zr remains practically unchanged in the intermediate hornfelses (average 264 ± 71 ppm compared to 269 ± 52 ppm in the regional slates) then it rises sharply to 484 ± 45 ppm in the banded samples. This rise suggests that only minor amounts of Zr, if any, entered the melts.

Ga in the contact hornfelses is almost twice as high as in the regional slates, (table 9.1). The Ga:Al ratio remains almost unchanged within the whole aureole although the contact rocks have slightly higher ratios (table 9.1). This trend is in agreement with magmatic crystallization where the Ga:Al ratio remains the same or increases slightly, Wedepohl (1978).

The femic elements Cr and Co are always higher in the contact samples compared to the regional slates but Ni is only higher if the standard deviations are ignored. Cr and Co are probably enriched in spinel, rutile and ilmenite whereas some Ni is in biotite and the melting of this caused some Ni to enter the melts.

Pb, Zn and Cu, which are probably dominantly held in pyrite and chalcopyrite, do not change throughout the whole aureole and therefore are not considered further.

The Rb $\times 10^{-4}$:K ratio decreases from 0.00364 ± 0.0002 in the regional slates to 0.00308 ± 0.0003 in the banded samples thus agreeing with magmatic crystallization where the Rb:K ratio increases from mafic to acidic rocks.

Similarly, the Ba $\times 10^{-4}$:K ratio remains unchanged until in the contact

samples where it rises sharply to 0.00698 ± 0.003 compared to 0.01901 ± 0.003 in the regional slates. This behaviour agrees excellently with magmatic crystallization where Ba is enriched in early formed K-bearing minerals, although the exceptionally high ratio in the most altered contact hornfelses suggests that only very insignificant amounts of Ba have entered the melts.

The $Sr \times 10^{-4} : Ca$ ratio also tend to decreases from 0.027188 ± 0.0145 in the country slates to 0.016 ± 0.005 in the contact hornfelses which indicates that the Sr:Ca is much lower in the melts than in the residual plagioclase.

9.3.3 Fractionation of the REE

REE from four biotite-, cordierite-bearing hornfelses and two desilicated rocks are given in appendix 3 and plotted in figures 9.20-1. The average of individual elements for both groups of hornfelses are compared with those from the four analysed regional slates in table 9.2 and figure 9.22 respectively.

In the Comrie thermal aureole, the REE generally tend to have higher ΣREE and Eu/Eu^* but lower $(La/Lu)_{CN}$ ratios in the contact hornfelses compared to the regional slates. The ΣREE tend to rise from 274.2 ± 103.83 in the unhornfelled slates through 352.82 ± 45.04 to 354.27 ± 74.84 in the intermediate and contact hornfelses respectively, although the very large standard deviations makes the increase equivocal. However, while LREE and MREE (up to Sm) of the hornfelses fall well within those of the regional slates, the hornfelses are always richer in HREE compared to the country rocks thus giving low $(La/Lu)_{CN}$ ratios in the contact hornfelses (figure 9.22). This trend is caused by : a massive transfer of HREE or LREE from the magma into the hornfelses, by partial melting or a sedimentary origin. Contamination from the magma cannot be totally excluded because connecting pipes representing late stage hydrothermal alterations are present, although the strong control of zircon and apatite on HREE (figures 9.23-6) suggests that, if any, it is the LREE which were added to the restites rather than the HREE.

Melting of biotite and cordierite but not zircon and apatite could deplete the restites in LREE which thereby become rich in HREE but no depletion of LREE is found unless it was compensated from the magma. figure 9.41 shows

that both LREE and HREE are very similar in a granodiorite and two leucosomes suggesting insignificant transfer, if any, of LREE from the magma to the restites. The evidence therefore suggests a sedimentary origin for most of the differences discussed above although hornfelsing and partial melting of the slates might have had some minor influence.

In the Cashel thermal aureole it has been shown that the positive Eu anomalies in the more desilicated hornfelses and pelitic xenoliths is caused by partial melting of a granitic melt (chapter. 5). Therefore, if partial melting has taken place in the Comrie thermal aureole, then a positive Eu anomaly should be produced in the most hornfelsed rocks and indeed figure 9.21 shows that both contact hornfelses (Y59, Y 78) have the highest Eu/Eu* ratios with that of Y59 being above unity; although the size of the anomaly suggests that partial melting was insignificant.

Both Sr and Ca exhibit positive correlation with Eu (figures 9.27-8) which indicates that much of Eu is in the divalent state. However, in sample Y 59 in which a positive Eu anomaly is recorded, high Eu contents are accompanied by low Sr and Ca contents, thus excluding Eu being added in any Ca-rich magmatic plagioclase. The positive Eu anomaly could be due to partial melting.

The non-correlativity of Eu-Sr in the hornfelses showing positive Eu anomalies seems to prevail in thermal aureoles where partial melting has taken place because the same pattern was noted in the Cashel thermal aureole (see subsection 5.3.3). It is unfortunate that experimental work on the partitioning of Eu^{+2} and Eu^{+3} between plagioclase and granitic melts is not available to numerically assess the $\text{Eu}^{+2}/\text{Eu}^{+3}$ ratios and correspondingly the oxygen fugacities. However, the similar behaviour of Eu in both the Cashel and Comrie thermal aureoles suggests that high oxygen fugacities prevailed in both aureoles and possibly also in thermal aureoles where partial melting take place.

9.3.4 Discussion

Since one of the main aims of this chapter is to establish and interpret the changes in the chemical composition accompanying hornfelsing of the slates by the Carn Choix intrusion, it is important to determine whether the chemical

composition of the contact hornfelses is produced totally by metasomatism from the country rock slates, or whether the two rock types were originally chemically different or whether alternatives applied. It is very important however to note that the standard deviations of both the country rocks and contact hornfelses are generally small suggesting that the true compositions do not deviate appreciably from the averages given in table 9.1.

In the Cashel thermal aureole where partial melting was very significant, it has been shown that none of Cr, Co, Ni, Ti and Mg enter the melts until very high degrees of partial melting are reached (see subsection 5.4.1). therefore, the assumption that these elements would be zero in early formed partial melts as is probably the case in the Comrie aureole is adequate up to 30% partial melting. Consequently, the contents of these elements in the original unhornfelses slates can be estimated from their contents in the strongly hornfelses rocks with reasonable certainty. Applying equation 5.1, the results obtained for partial melting up to 30% given in fractions of five are shown in table 9.3.

Table 9.3 : Predicted contents in Ti, Mg, Cr, Co, and Ni in the parent country rocks of the contact hornfelses.

%Melt	0%	5%	10%	15%	20%	25%	30%
Ti	2.37	2.25	2.13	2.01	1.90	1.78	1.66
Mg	2.61	2.48	2.35	2.22	2.09	1.95	1.82
Cr	183	173	164	155	146	137	128
Co	38	36	34	32	30	28	26
Ni	60	57	54	51	48	45	42

It is clear from table 9.3 that even if 30% partial melting is assumed, the contents of Ti, Cr and to lesser extent Co in the original unhornfelses slates should be higher than the actual values of the regional slates given in table 9.1 whereas the contents of Mg and Ni should be much lower. Further, if 30% partial melting had occurred, the contact hornfelses should be much lower in silica and K than the present values. The evidence therefore suggests that the parent rocks of the contact hornfelses were originally lower in Fe, Mg and Ni but richer in Ti, Cr, Co and to lesser extent K and Na than the 36 slates given

in table 9.1

The contact hornfelses cannot have been grits because the average of eight contact hornfelses analysed is different from the three most common Ben Ledi Grit hornfelses given in Tilley (1924a) (table 9.1). Field evidence also exclude this possibility.

Contamination from the magma cannot be totally ruled out because some pipes connecting the pink orange bands (i.e cross cutting the black bands) are occasionally present together with late stage hydrothermal alterations (see subsection 9.4 and plates 9.7,9.9) although most often the contacts between the leucosomes and black bands are sharp and no mechanical introduction of material from the leucosomes into the restites has been noted. Further, if transfer of material from the magma had occurred and is responsible for high LREE contents in the contact hornfelses, it is still unable to provide the abnormally high contents of Ti, Cr, Zr and Ba of the restites and does not explain the high LREE contents of the hornfelses relatively remote from the contact.

The view that the original sediments were enriched in particular accessory mineral(s) which control many of the trace elements ^{cannot} answer all the facts. Sphene would be the most likely mineral to explain the abnormally high Ti, Sr and to some extent Cr in the hornfelses but the low Mg and Fe contents of the contact hornfelses than should be expected remain unexplained. Furthermore, the negative correlation between Niggli al and fm indicate that both Fe and Mg must have increased in the restites whereas table 9.1 shows otherwise.

The evidence therefore suggests that the parent rocks from which most of the contact hornfelses were derived were somewhat chemically different from the composition of the 36 slates analysed and therefore the absolute composition of the melts derived therefrom cannot be computed. Because the slates are underlain by mineralogically and chemically variable grits, the differences discussed above are probably a sedimentary feature although metasomatism and partial melting are probably significant factors. The original sediments that formed the slates probably included some components from the grits near the contact and/or material from different sources such as volcanic material. This is not considered further as it is beyond the scope of

the present work.

In summary, despite the above discussed complications, both mineralogical and chemical evidence show that strong hornfelsing had occurred and partial melting had also taken place although sedimentary variations have complicated the true behaviour of many elements and severely restricted the calculations of the melted out material from the hornfelses.

9.4 The behaviour of U and Th in the Comrie aureole

9.4.1 Spatial distribution of U

In the Aberfoyle Slates, U is always held in zircon, apatite, epidote and sericite. Chlorite, iron ore, plagioclase and K-feldspars must therefore be very low in U to produce any fission tracks. Typical whole rock U distribution patterns are shown in plates 9.1'-2'.

The fission tracks formed over zircon are always star-like, those over apatite are uniformly distributed whereas the smallness of epidote grains does not allow any typical U distribution patterns for this mineral to be made although the density of the tracks is between that of zircon and apatite. In sericite, U is revealed by single fission tracks scattered throughout the whole sections. The smallness of the grains of epidote and the aggregate nature of sericite did not allow any detailed fission track studies to be done on these minerals.

In the hornfelses, U is restricted to zircon, apatite and epidote. Biotite must be very low in U because only occasionally rare single fission tracks are seen over some flakes whereas cordierite, ferrohypersthene, spinel, corundum, plagioclase and K-feldspars are U-free. This therefore indicates that U was lost from the hornfelses during the breakdown of sericite into biotite (equations 8.1-2), sericite into K-feldspar and corundum and cordierite and K-feldspar (equations 8.14-15) and the breakdown of biotite into cordierite (equation 8.3), ferrohypersthene (equation 8.3') and sillimanite (equation 8.4), although the density of the tracks over sericite and occasionally biotite suggests that the loss of U from the whole rocks is not substantial.

The fission track density and distribution patterns over single zircon mounts are rather uniformly distributed throughout the whole crystals

although there is a tendency of the tracks to be relatively denser at the rims and two ends over many crystals (see plates 9.3-3'). These differences in the distribution patterns do not seem to be related to the shape, size and colour of the crystals and hence are believed to be the result of various uptake of U by zircons. There is no change in the distribution patterns and apparent contents of U in zircons as the contact of the intrusion is approached neither different types of zircon were found. This therefore suggests that if recrystallization of zircon with U loss has indeed take place as deduced from the chemistry (see below) this loss must have been insignificant although the uncountability of the fission tracks makes this deduction only approximate.

The fission tracks over the nine apatites examined show that this mineral contains very little U (range 1.36-14.2ppm, see table 9.4.A). The rarity of apatite in the slates (2-3 grains for 3-4 standard separations) did not allow systematic studies towards the contact of the intrusion although the evidence as deduced from the grains analysed and whole rock fission track sections do not suggest any variations in the contents of U. The paucity in U of all the apatites analysed suggests they are metamorphic.

9.4.2 Chemistry

The results of 43 rock analyses (20 country slates, 14 intermediate and 5 contact hornfelses, 3 leucosomes and 1 granodiorite) for U and Th are given in table 9.5 and summarized and compared in table 9.4 with other shales and pelites from the literature. The partition coefficients of both elements between three restite-leucosome pairs are also given in table 9.4.

The unhornfelsed slates average 2.37 ± 0.35 ppm U, 11.48 ± 1.97 ppm Th and 4.70 ± 0.80 Th/U ratios. These values compare reasonably well with the average of of 11 unhornfelsed Connemara pelites and 15 Moine schists, Scotland of 2.62 ± 0.50 ppm U, 10.80 ± 2.39 ppm Th, 4.25 ± 0.79 Th/U ratios and 2.4 ± 1.2 ppm U, 12.8 ± 9.8 ppm Th and 5.3 Th/U ratios respectively. However, the slates are poorer in U than the Mancos shales and North American Shales (NAS) but richer in Th than other Scottish Dalradian rocks (at 95% level) (see table 9.4). The Th/U ratios clearly reflect these differences ; the Dalradian rocks having the highest average of 7.73 ± 2.46 . The U, Th and Th/U ratios of the Aberfoyle Slates are considerably different

from 12 Dalradian rocks (calculations excluded rocks having CaO > 4 wt%) given in Wilson and Leake (1972) of 6.5 ± 1.8 ppm U, 8.6 ± 4.5 ppm Th and 1.5 ± 1.0 Th/U ratios. These remarkably high values of U are probably due to the inaccuracy of XRF for the determination of this element as shown in chapter two.

The differences reported between the Aberfoyle Slates and the other Scottish Dalradian rocks cannot be related to the degree of metamorphism because the rocks come from low to medium grades (chlorite to sillimanite zones), Atherton and Brotherton (1979) while the effects of metamorphism on U and Th are only significant under granulite facies of metamorphism, (Heier, 1979). Therefore, these difference can only be due to provenance and depositional differences particularly as figure 9.38 excludes any significant low temperature remobilization and removal of U from the slates.

9.4.2.1 Field relationships

As shown in table 9.4, the averages of both U and Th remain almost unchanged throughout the whole aureole. However, one biotite- cordierite- and ferrohypersthene-bearing intermediate hornfelses (Y64) and one contact hornfels (Y62R) are rich in Th but depleted in U thus giving exceptionally high Th/U ratios (figure 9.29). This suggests that at lower degrees of hornfelsing, remobilization and removal of U but not Th occurred. The significantly low contents of both U and Th in a strongly desilicated contact hornfels (Y79R) indicates that in the innermost parts of the aureole both elements partitioned into the outgoing melts; although a sedimentary depletion cannot be fully ruled out.

9.4.2.2 Relationships of U and Th with K, Zr,P and Ca

U correlates positively with P, Zr, K and to lesser extent Ca (figures 9.30-33) consistent with fission track analysis where U is held in apatite, zircon, sericite, epidote and biotite. Two contact hornfelses (Y62R, Y79R) are particularly rich in zircon and to a lesser extent in apatite but strongly depleted in U which indicates that, as in the Cashel aureole, recrystallization of zircon and apatite took place in the inner aureole releasing some U to the melts. The high Ca but low U contents of some hornfelses (e.g Y55, Y61R,

Y62R, Y79R) is because some of Ca is in U-free plagioclase.

Th exhibits a positive correlation with K but not P, Zr and Ca (figures 9.34-7) which indicates that much of the Th is held in sericite, biotite and possibly K-feldspar but only very little, if any, resides in zircon, apatite and epidote. The contact hornfelses Y61R, Y62R, Y78R are rich in Th but poor in K as if K-bearing minerals are not the only control over Th. These particular samples are rich in zircon but not apatite which suggests that recrystallized zircons are possibly richer in Th than those from the country slates. Original enrichment in Th of the contact hornfelses cannot be excluded particularly because of the original chemical differences between the remote slates and the contact hornfelses although the similar behaviour of Th in the Cashel thermal aureole where recrystallization of zircon is proved (see chapter. 7) indicates that recrystallization of zircon is probably a very important factor.

The partition coefficients of U and Th between the restites and leucosomes are inconclusive because the leucosomes do not represent only the partial melts but also magmatic injections (see subsection 9.5).

9.4.2.3 Discussion

The replacement of U-bearing sericite and biotite by U-free cordierite, ferrohypersthene, spinel, corundum, K-feldspar and sillimanite and the possible recrystallization of U-rich to U-poor zircons in the contact hornfelses indicate that U and possibly also Th should decrease in the most desilicated rocks but table 9.6 shows that only two out five analysed contact hornfelses have significantly lower U contents than the unhornfelled slates. Addition of U from the magma is excluded by the absence of U at the restite-leucosome contacts or along the pipes cross-cutting the hornfelses and therefore the country slates from which the majority of the contact hornfelses were derived must have been richer in U and possibly Th than the average given in table 9.5. However, individual hornfelses, e.g. Y62, Y79, are particularly low in U and to lesser extent Th even if the average 23 country slates given in table 9.5 is considered as the parent rocks of the contact samples which indicates that small amounts of U must have left the crystal fractions.

9.5 Possible origin of of the pink-orange bands

9.5.1 Mineralogy

The leucosomes consist of equal proportions of intergrown quartz and K-feldspar in typical granophyric and graphic textures (plates 9.5-6). Chloritized biotite, ilmenite and hornblende are sometimes also present but secondary sericite, apatite and zircon occur as accessories or are absent.

The contact between the leucosomes and the black bands is usually sharp and consists of almost continuous lines of ilmenite and magnetite (plate 9.7). However, some rare crystals of quartz and K-feldspar are not intergrown and tend to occur more often as isolated crystals near the contact with the restites and these crystals probably represent the material melted out of the slates.

In rare cases, hydrothermal alterations (\approx 1-2 mm thick) at the restite-leucosome interfaces and pipes connecting the leucosomes to one another have also been noted and are believed to represent late stage "subsolidus" water-rich alterations derived from the magma (plate 9.7, 9.9). In other cases, isolated crystals of ferrohypersthene of the same composition to those in the restites and very small xenoliths of relict slates consisting of ilmenite, magnetite and cordierite (\approx 1-2 mm average length, plate 9.8) are recorded inside the leucosomes which indicates that partial consumption of slaty material by the leucosomes has taken place. The temperatures were probably not high enough to substantially melt ferrohypersthene, ilmenite, magnetite or cordierite.

From the above discussion, it is therefore expected that the non contaminated leucosomes and igneous rocks should be metaluminous i.e. $A/CNK \leq 1$ whereas those strongly contaminated should be peraluminous i.e. $A/CNK \geq 1$. The A/CNK ratios of the eight leucosomes and three igneous rocks are given in table 9.6 as are the CIPW normative corundum and $Qz:Ab:Or$ ratios recalculated to 100. From this table and figure 9.39 it is clear that while all the igneous rocks have A/CNK ratios less than one, some leucosomes fall below unity i.e. I-type and others above unity i.e. S-type. The leucosomes are clearly more variable in terms of their $Qz:Ab:Or$ ratios and only one sample (Y57L) falls within the anatectic field of Winkler (1979); although it is very interesting to note that most of the leucosomes plot near Winkler's field (figure 9.40). This coupled with the high A/CNK ratios of some leucosomes

and the presence of normative corundum instead of normative diopside suggest that melting of the hornfelses has contributed substantially to the composition of the leucosomes.

The mechanism(s) of incorporation of slaty material into the leucosomes seems to have been operating in two ways: consumption of whole pieces of slates and migration of the melts generated into the pre-existing leucosome veins. The presence of small relicts of hornfelses and xenocrystic ferrohypersthene crystals inside the leucosomes and the tendency of non-intergrown quartz and K-feldspar to be present near the contact with the restites indicate that both mechanisms took place.

9.5.2 Chemistry

The eight leucosomes were analysed for major and trace elements (see appendix 3) and are summarized and compared to the three igneous rocks from the Carn Choix intrusion in table 9.2.

Among the two rock types (leucosomes and igneous rocks) Al, Mg, Ti, Ca and to lesser extent Fe decrease with increasing acidity (figures 9.42-6) but K increases with increasing SiO₂ (figure 9.47). Na and P are inconclusive probably because of contamination from the melting slates (figures 9.48-9).

Generally, the patterns exhibited by the trace elements is what would be predicted from major element geochemistry. The compatible elements viz: Cr, Co, Ni fall with rising SiO₂ whereas the opposite is true for incompatible elements viz: Rb, Zr and to lesser extent Ba (figures 9.50-55). These observations is what would be expected in magmatic differentiation thus indicating that the leucosomes are dominantly late stage magmatic injections although subsequent partial melting and incorporation of slaty material by the leucosomes have affected the behaviour of some elements.

The REE from two leucosomes (Y59L, Y78L) and one granodiorite (Y35) (appendix 3) are portrayed in figure 9.41. From this it can be seen that the only significant difference is the negative Eu anomaly recorded in the leucosomes compared to the granodiorite and this is in agreement with magmatic differentiation where Eu is enriched in early formed Ca-rich plagioclase although the anomaly may be partly produced by partial melting. The lack of Eu anomaly in Y35 indicates that the parent magma must have had a

high oxygen fugacity.

9.5.3 Conclusions

Mineralogical evidence particularly the fact that the leucosomes crosscut the bedding of the slates, the presence of sub-solidus hydrothermal alterations at the leucosome-restite contacts, the granophyric and graphic textures which are probably produced by the introduction of hot magmatic liquid into cold country rocks, the low A/CNK ratios (≤ 1) of some leucosomes coupled with field evidence indicate that much of the material forming the pink orange bands were derived from the magma. The chemistry also generally support this conclusion although partial melting and consumption of slaty material by the leucosomes complicated the behaviour of some elements. Further support to this interpretation is the high Mg of biotites from the leucosomes ($X_{Mg} \geq 0.56$) because partial melting is insignificant to provide such high amounts of Mg.

However, the presence of xenocrystic ferrohypersthene and small relicts of slates within the leucosomes, the high A/CNK ratios (> 1) of many leucosomes, the fact that most of these plot near Winkler's anatectic field with one sample plotting inside the field and the presence of large non intergrown quartz and K-feldspar crystals indicate that incorporation of slaty material both as partial melts and consumption of pieces of slates in the leucosomes is extremely probable.

9.6 Summary of the chemistry of the Comrie aureole

The Aberfoyle Slates compare reasonably well in their major and trace elements with Dalradian rocks from Connemara and other shales and pelites from the literature although there is^a tendency for the slates to be poorer in Ca, Sr, U and to lesser extent Ca and Rb. They are also poorer in Th than other Dalradian rocks from Scotland and this depletion is attributed to great sedimentary variations which are probably due to different provenance areas because the effects of metamorphism on U and Th are thought to be significant only under granulite facies metamorphism. The large similarities in the contents of most major, trace and rare earth elements of the Aberfoyle Slates in Scotland with the southern Connemara pelites from Ireland confirm the

growing consensus that the Dalradian rocks of Ireland are a geographical extension of those in Scotland.

During the hornfelsing of the slates by the Carn Chois intrusion, the behaviour of the major and trace elements was strongly affected by sedimentary variations within the slates and possible small scale contamination from the magma. This severely restricted the calculation of the composition of the melted out material and the order of fractionation of elements into these melts. Despite these complications some elements, viz: Si, K, Rb, U and to lesser extent Th tend to be lower in the restites, others, viz: Ti, Cr, Co, Ga, Zr tend to be higher while Al, and to lesser extent Ba and Sr are both enriched and depleted in the restites. This coupled with the excellent agreement of the Rb:K, Ba:K, Sr:Ca and Ga:Al ratios with magmatic crystallization suggest that fractional melting of the contact rocks was operative as the major process of melting; although the trends of Fe and Mg suggest that metasomatism was very insignificant if the remote slates are considered as the parent country rocks.

The HREE increase systematically as the contact of the intrusion is approached but the LREE remain unchanged. The increase of the Eu/Eu^* ratios as the degree of hornfelsing rises indicates that partial melting has taken place and some REE must have entered the outgoing melts. This coupled with the strong control of zircon and apatite on HREE indicate that the parent rocks of the contact hornfelses were LREE-rich (sericite-rich?) or some transfer of LREE from the magma into the adjacent hornfelses occurred although the behaviour of Fe and Mg in the hornfelses suggests that original sedimentary variations between the remote slates and the contact hornfelses were probably the controlling factors.

The evidence as deduced from the fission track and chemical analyses show that some U was lost from the most altered hornfelses possibly through three main mechanisms: recrystallization of minerals (U-rich sericite into U-poor (-free) biotite, U-poor biotite into U-free cordierite, ferrohypsthene, K-feldspa, sillimanite, recrystallization of U-rich zircon into U-poor ones and dehydration and partial melting with U preferentially fractionated into the melts by forming uranyl hydroxy complexes.

Field, mineralogical and chemical evidence indicate that the pink-orange

Table 9.1 : Summary statistics of the major and trace data in the Aberfoyle Slates and hornfelses. The average of 55 southern Connemara pelites is also given for comparison.

	R	S	I	S	C	S	SCP	S
Major elements(wt%)								
SiO ₂	58.64	2.44	55.59	4.29	48.38	2.85	53.85	5.13
TiO ₂	1.19	0.12	1.41	0.28	2.37	0.23	1.33	0.33
Al ₂ O ₃	18.23	1.27	20.46	2.77	26.78	2.19	20.26	3.06
Fe ₂ O ₃	1.81	0.88	2.42	1.80	2.26	0.77	2.29	1.22
FeO	6.67	1.54	6.94	1.86	6.88	1.40	7.21	2.36
MnO	0.11	0.06	0.11	0.03	0.09	0.04	0.21	0.12
MgO	2.66	0.37	2.71	0.62	2.61	0.31	3.34	0.88
CaO	0.44	0.36	0.78	0.78	1.64	0.84	1.80	1.06
Na ₂ O	2.83	0.68	2.79	0.86	4.06	0.91	2.12	0.78
K ₂ O	3.12	0.69	3.82	1.19	2.90	1.09	3.91	1.20
P ₂ O ₅	0.16	0.09	0.22	0.18	0.32	0.06	0.20	0.11
H ₂ O	3.56	0.65	2.67	1.13	1.23	0.49	-	-
CO ₂	0.23	0.11	0.24	0.13	0.32	0.29	-	-
Trace elements(ppm)								
Rb	114	27	136	42	88	29	168	59
Ba	594	136	707	239	1611	415	1147	633
Zr	269	52	264	71	484	45	284	75
Sr	94	40	119	57	239	62	258	137
Ga	27	24	30	5	43	4	29	5
Ni	53	9	57	9	60	9	76	26
Co	24	7	26	6	38	5	31	8
Cr	98	12	117	23	183	20	100	36
Pb	16	8	17	12	25	6	47	24
Zn	117	31	137	40	138	29	158	49
Cu	40	17	41	17	39	9	56	70
Rbx10 ⁻⁴ /K	0.00360	0.0002	0.00370	0.0008	0.0030	0.0003	-	-
Bax10 ⁻⁴ /K	0.01920	0.0268	0.01930	0.006	0.0698	0.003	-	-
Srx10 ⁻⁴ /K	0.02720	0.0145	0.02030	0.01	0.0164	0.005	-	-
Gax10 ⁻⁴ /Al	0.00015	0	0.00015	0	0.00016	0	-	-
Niggli mg	0.364	0.01	0.345	0.033	0.343	0.027	-	-
Niggli fm	40.51	4.87	39.14	4.36	32.77	4.12	-	-

Table 9.2 : Summary statistics of the REE in the Aberfoyle Slates, hornfelses, leucosomes and a granodiorite. The average of 4 southern Connemara pelites are also give for comparison.

	R	S	I	S	C	S	SCP	S	L	S	G
La	67.35	39.41	75.14	12.07	68.55	14.63	66.53	15.04	26.91	0.35	30.39
Ce	97.51	21.49	141.26	26.38	149.35	31.43	130.91	30.14	58.27	3.02	63.56
Pr	15.95	7.01	18.96	2.27	18.56	3.10	16.12	4.16	8.03	0.53	8.78
Nd	58.49	26.95	72.17	9.71	67.76	18.29	61.51	12.83	28.97	2.29	32.53
Sm	9.89	3.88	12.66	2.06	12.86	2.29	10.38	2.33	5.72	0.45	6.23
Eu	2.28	0.89	2.64	0.34	3.64	0.27	2.11	0.25	0.75	0.09	1.80
Gd	8.56	2.96	11.23	2.40	11.65	2.0	8.77	2.07	5.29	0.38	5.60
Dy	6.39	1.53	8.58	1.76	9.67	1.3	7.54	1.66	4.65	0.15	4.53
Hb	1.30	0.28	1.74	0.32	2.07	0.26	1.73	0.40	0.98	0.02	0.96
Er	3.15	0.55	4.14	0.63	4.78	0.58	4.86	1.17	2.37	0.03	2.25
Yb	2.86	0.23	3.72	0.41	4.68	0.59	4.23	0.99	2.48	0.07	2.14
Lu	0.44	0.03	0.55	0.04	0.69	0.09	0.61	0.14	0.36	0.01	0.32
Σ REE	274.20	103	352.82	45	354.27	74	315.3	38	144.8	6.98	159.09
Eu/Eu*	0.75	0.01	0.68	0.04	0.92	0.09	0.71	0.17	0.42	0.08	0.93
(La/Lu)CN	15.64	8.3	14.40	2.87	10.20	0.87	11.24	0.82	7.77	0.32	9.85

R = average of 4 country slates

I = average of 4 intermediate hornfelses

C = average of 2 contact hornfelses

SCP = average of 4 southern Connemara pelites

L = average of 2 leucosomes

G = one granodiorite (Y35)

S = standard deviations

Table 9.4 : Summary statistics for U, Th, their relative ratios in the Aberfoyle Slates and other shale and pelites from the literature and the partition coefficient between 3 restite-leucosome pairs.

	U	S	Th	S	Th/U	S	Th/K	S	U/K	S
R	2.37	0.35	11.48	1.97	4.70	0.80	3.58	0.73	0.75	0.18
I	2.86	0.75	13.72	2.96	4.99	1.37	3.19	0.54	0.67	0.20
C	2.53	1.00	13.80	4.62	6.22	3.60	5.82	2.84	1.09	0.67
L	1.81	1.02	5.51	2.42	3.87	1.51	1.27	0.31	0.38	0.16
SCP	2.62	0.50	10.80	2.39	4.25	0.79	3.73	1.60	0.87	0.39
MS	3.7	1.17	10.4	4.0	3.3	2.3	-	-	-	-
NAS	3.2	2.2	13.5	6.9	5.1	2.5	-	-	-	-
DR	2.18	0.85	15.82	7.32	7.73	2.46	-	-	-	-
MS*	2.4	1.2	12.8	9.8	5.3	1.2	-	-	-	-

Partition coefficients(restite/leucosome)

	U	Th
Y59	0.89	1.23
Y61	8.97	6.88
Y78	1.69	2.89

R= average of 23 country slates (20 from this work, 3 from Atherton and Brotherton(1979).

I= average of 14 intermediate hornfelses

C= average of 5 contact hornfelses.

L= average of 3 leucosomes.

SCP= average of 11 southern Connemara pelites (chapter 7)

MS= average of 102 Mancos shales (Pliler and Adams, 1962).

NAS= average of 50 North American Shales (Adams and Weaver, 1958).

DR= average of 62 Scottish Dalradian rocks for Th and Th/U ratios and 68 for U (Richardson and powell, 1976 and Atherton and Brotherton , 1979).

MS*= average of 15 Moine schists (Richardson and powell, 1976)

S = standard deviations.

- not determined and/or calculated.

Table 9.4A : Quantitative estimation of U in apatite. The samples are listed from top to bottom in decreasing distance toward the contact.

Sample number	tracks counted	U contents(ppm)
Y17	53	6.78
Y25	61	10.32
	64	11.91
	43	4.75
Y85	22	3.76
	5	1.36
	64	9.11
Y78	47	3.43
	112	14.20
Y35(ganodiorite)	102	20.09
	116	22.10
	252	18.71
	178	17.36

Table 9.5 : U, Th, K and their relative ratios in the Aberfoyle slates, hornfelses, leucosomes and a Carn Chois granodiorite.

Sample number	U(ppm)	Th(ppm)	K ₂ O(wt%)	Th/U	Th/K	U/K
Unhornfelsed slates						
Y2	2.54±0.04	11.96±0.03	3.47	4.70	3.44	0.73
Y8	2.55±0.04	13.60±0.05	4.37	5.34	3.11	0.58
Y10	2.55±0.04	11.51±0.04	4.02	4.51	2.86	0.63
Y12	2.03±0.05	8.81±0.06	2.74	4.33	3.21	0.74
Y16	1.94±0.02	8.54±0.03	3.27	4.40	2.61	0.60
Y17	2.37±0.04	12.01±0.04	2.93	5.06	4.09	0.80
Y21	2.83±0.04	12.21±0.03	2.45	4.31	4.98	1.15
Y23	2.89±0.03	15.33±0.02	3.65	5.30	4.20	0.79
Y24	2.68±0.03	12.74±0.03	3.46	4.75	3.68	0.77
Y26	2.33±0.03	12.92±0.03	4.48	5.54	2.88	0.52
Y28	2.56±0.04	11.02±0.03	2.94	4.30	3.74	0.87
Y33	2.61±0.03	13.11±0.02	2.60	5.02	5.04	1.00
Y48	2.83±0.04	11.98±0.04	3.68	4.23	3.25	0.76
Y49	2.62±0.03	11.76±0.02	3.29	4.49	3.57	0.79
Y72	2.33±0.05	11.53±0.05	2.92	4.94	3.95	0.80
Y73	3.11±0.03	11.70±0.03	3.03	3.76	3.86	1.02
Y74	2.47±0.03	8.24±0.04	2.20	3.33	3.74	1.12
Y75	2.17±0.04	9.28±0.04	3.07	4.27	3.02	0.70
Y76	2.05±0.04	9.45±0.04	2.96	4.60	3.19	0.69
Y84	1.82±0.04	8.82±0.05	2.94	4.84	3.00	0.62
Intermediate hornfelses						
Y31	2.60±0.04	12.85±0.03	3.76	4.94	3.41	0.69
Y32	2.37±0.04	10.48±0.03	3.02	4.42	3.47	0.78
Y37	3.41±0.03	15.25±0.02	5.93	4.47	2.57	0.57
Y38	3.04±0.02	11.97±0.02	3.55	3.93	3.37	0.85
Y39	2.32±0.04	9.73±0.04	4.12	4.19	2.36	0.56
Y50	4.30±0.02	15.76±0.02	3.55	3.66	4.44	1.21
Y55	1.78±0.04	8.56±0.03	2.90	4.80	2.95	0.61
Y64	1.69±0.02	15.81±0.02	4.60	9.35	3.43	0.36
Y70	3.58±0.03	19.51±0.02	7.65	5.44	2.55	0.46
Y81	3.35±0.02	15.68±0.01	4.19	4.68	3.74	0.80
Y83	4.01±0.02	16.02±0.03	6.27	3.99	2.55	0.64
Y85	2.45±0.02	11.73±0.01	3.80	4.78	3.08	0.64
Y86	2.70±0.02	12.50±0.02	3.51	4.62	3.56	0.76
Y87	2.51±0.02	16.35±0.01	4.97	6.51	3.29	0.50

Table 9.5 : Continued

Sample number	U(ppm)	Th(ppm)	K ₂ O(wt%)	Th/U	Th/K	U/K
Contact hornfelses						
Y59	2.53±0.06	10.81±0.05	3.30	4.27	3.27	0.77
Y61	3.59±0.04	16.51±0.03	1.97	4.59	8.38	1.82
Y62	1.39±0.06	18.67±0.02	2.79	13.43	6.69	0.49
Y78	3.71±0.03	16.83±0.03	1.87	4.53	9.00	1.98
Y79	1.43±0.06	6.19±0.06	3.50	4.32	1.76	0.40
Leucosomes						
Y59L	2.82±0.05	8.32±0.09	4.88	2.95	1.70	0.58
Y61L	0.40±0.18	2.40±0.13	2.14	6.0	1.12	0.19
Y78L	2.19±0.06	5.81±0.04	5.91	2.65	0.98	0.37
Granodiorite						
Y35	2.35±0.04	8.18±0.05	3.13	3.48	2.61	0.75

Table 9.6 : Molecular A/CNK ratios, normative corundum(C) and normative Qz:Ab:Or ratios of the comrie leucosomes and igneous rocks.

Leucosomes	Qz:Ab:Or	C	A/CNK
Y57L	39:23:38	1.74	1.11
Y58L	37:21:42	1.83	1.13
Y59L	30:39:31	0	0.94
Y61L	31:51:18	0	1.00
Y62L	47:28:25	2.87	1.30
Y63L	28:33:39	2.17	1.15
Y78L	27:35:38	0	0.96
Y79L	31:30:39	0	0.81
Igneous rocks			
Y35	12:58:30	0	0.94
Y60	4:78:18	0	0.83
Y82	14:57:29	0.84	0.95

A/CNK = mole Al₂O₃/(CaO+Na₂O+K₂O)

Figures 9.29 - 38 Scatter diagrams of U and Th in the unhornfelsed slates,
intermediate and contact hornfelses.

Figure 9.29 U vs Th

Figure 9.30 U vs P_2O_5

Figure 9.31 U vs Zr

Figure 9.32 U vs K_2O

Figure 9.33 U vs CaO

Figure 9.34 Th vs K_2O

Figure 9.35 Th vs P_2O_5

Figure 9.36 Th vs Zr

Figure 9.37 Th vs CaO

Figure 9.38 U vs $W(Fe^{+3}/(Fe^{+2} + Fe^{+3}))$

Figure 9.39 Mole ($Al_2O_3/(CaO + Na_2O + K_2O)$) vs SiO_2 for the
leucosomes and Carn Chois intrusive rocks.

Figure 9.40 Normative Qz:Ab:Or ratios of the leucosomes and igneous rocks
from the Carn Chois intrusion. The anatectic field of Winkler
(1979) is also shown.

Figure 9.41 REE distribution patterns in two leucosomes and one Carn
Chois intrusive rock.

Figures 9.42 - 55 Harker-type diagrams for the leucosomes and Carn
Chois intrusive rocks.

Figure 9.42 Al_2O_3 vs SiO_2

Figure 9.43 MgO vs SiO_2

Figure 9.44 TiO_2 vs SiO_2

Figure 9.45 CaO vs SiO_2

Figure 9.46 Fe_{tot} vs SiO_2

Figure 9.47 K_2O vs SiO_2

Figure 9.48 Na_2O vs SiO_2

Figure 9.49 P_2O_5 vs SiO_2

Figure 9.50 Co vs SiO_2

Figure 9.51 Ni vs SiO_2

Figure 9.52 Cr vs SiO_2

Figure 9.53 Rb vs SiO_2

Figure 9.54 Zr vs SiO_2

Figure 9.55 Ba vs SiO_2

KEY TO FIGURES 9.1 - 9.49

Figures 9.1 - 17 Scatter diagrams of the unhornfelsed slates

- Figure 9.1 Rb vs K_2O
- Figure 9.2 Ba vs K_2O
- Figure 9.3 Rb vs $CaO + Na_2O$
- Figure 9.4 Ba vs $CaO + Na_2O$
- Figure 9.5 Sr vs CaO
- Figure 9.6 Na_2O vs CaO
- Figure 9.7 FeO vs TiO_2
- Figure 9.8 Fe_2O_3 vs TiO_2
- Figure 9.9 Cr vs TiO_2
- Figure 9.10 K_2O vs Niggli al-alk
- Figure 9.11 Rb vs Niggli al-alk
- Figure 9.12 Ce vs Niggli al-alk
- Figure 9.13 Ba vs Niggli al-alk
- Figure 9.14 Ga vs Niggli al-alk
- Figure 9.15 Y vs Niggli al-alk
- Figure 9.16 Zn vs Niggli al-alk
- Figure 9.17 Fe_{tot} vs Niggli al-alk

Figure 9.18 REE distribution patterns in the unhornfelsed slates

Figure 9.19 Niggli al vs Niggli fm of the regional slates and hornfelses

Figure 9.20 REE distribution patterns in the intermediate hornfelses

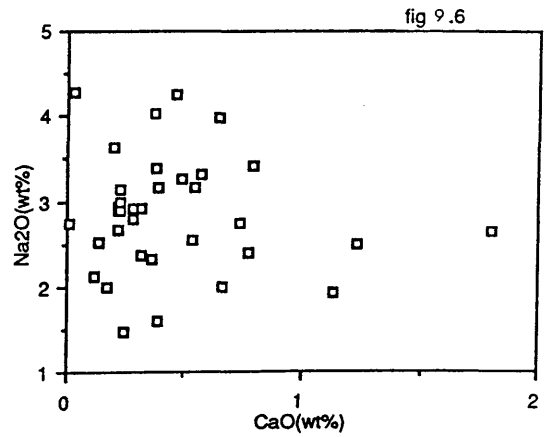
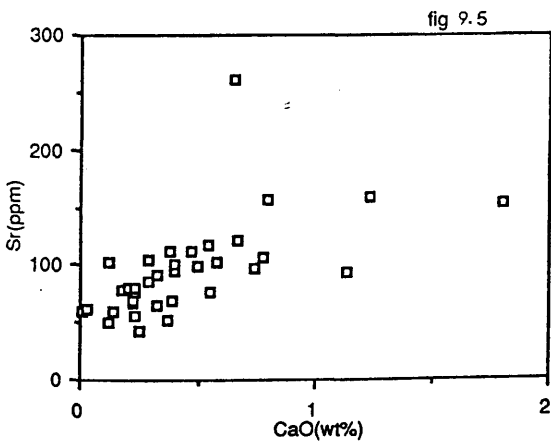
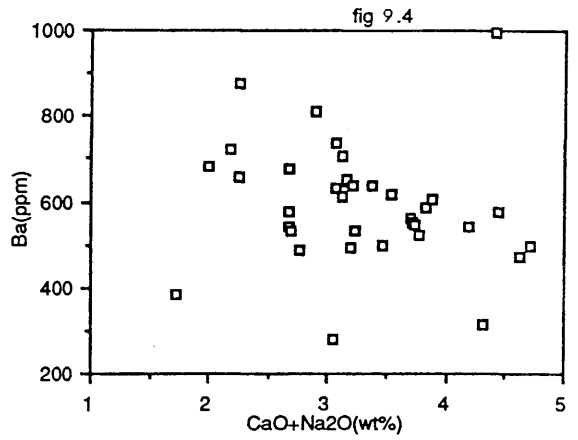
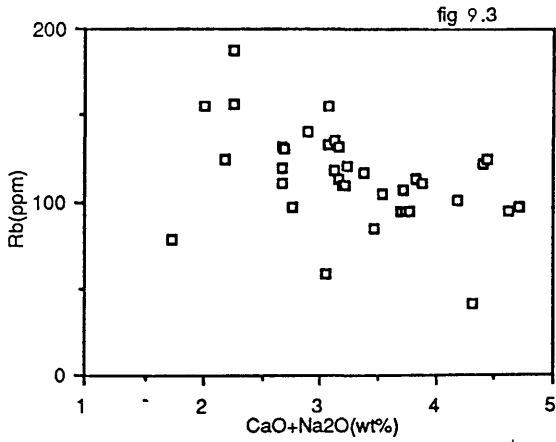
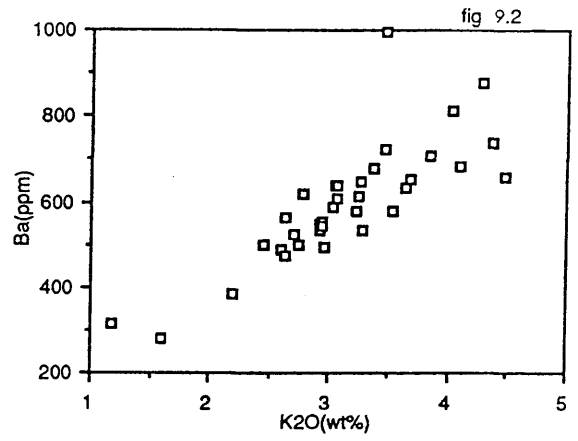
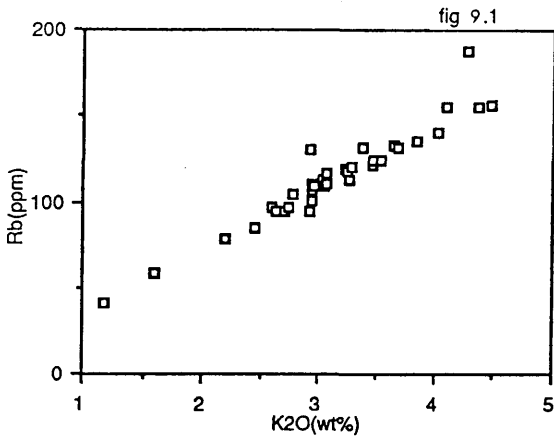
Figure 9.21 REE distribution patterns in the contact hornfelses

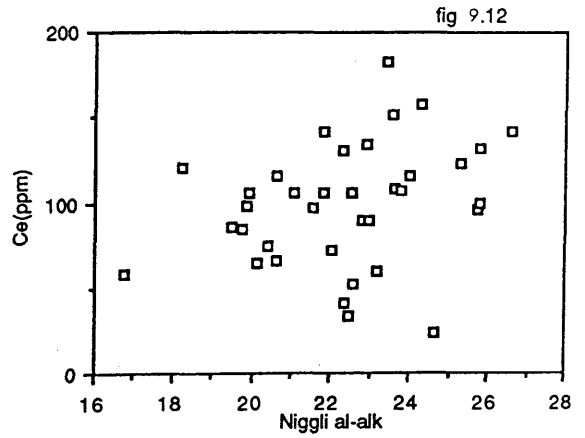
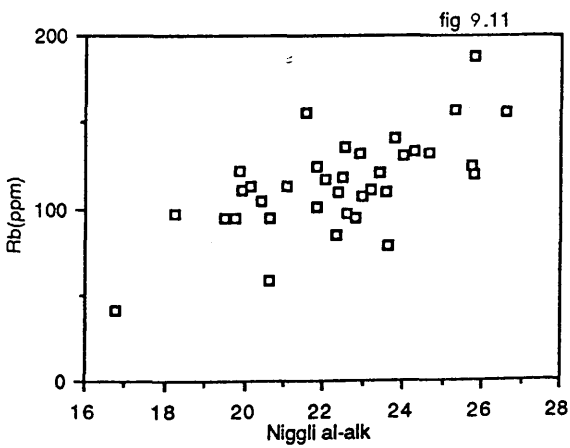
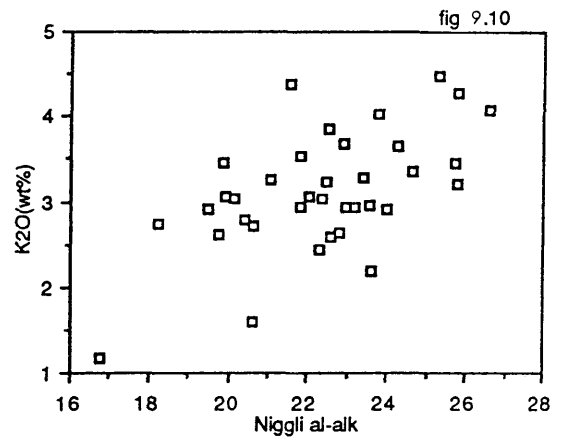
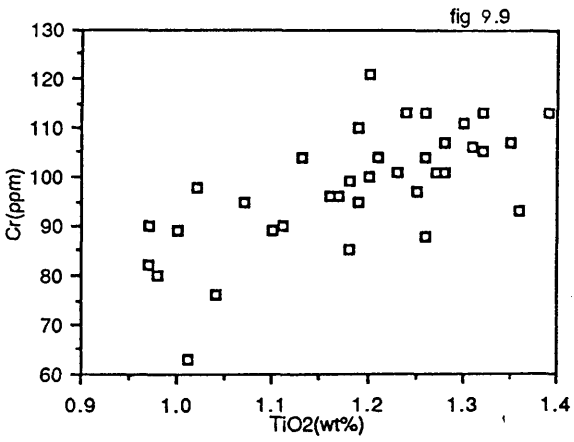
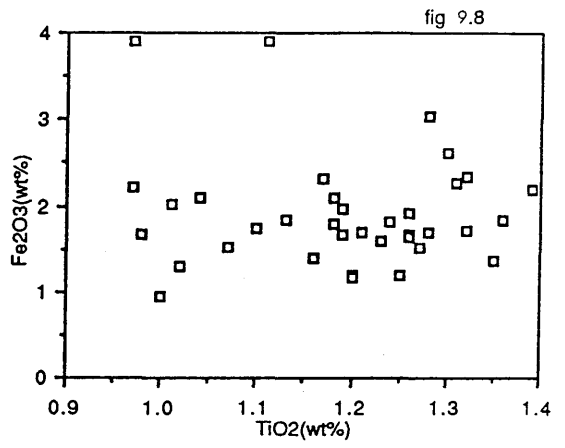
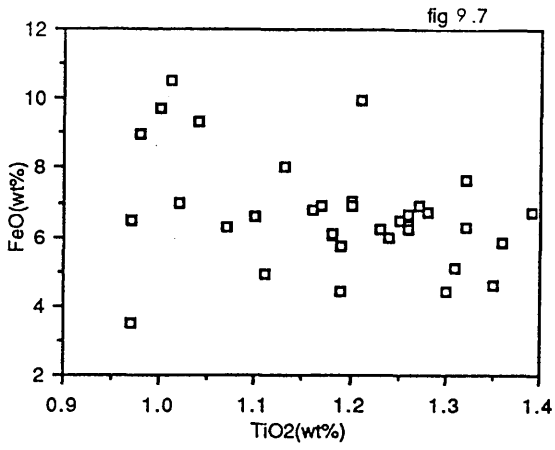
Figure 9.22 Summary of REE distribution patterns in the unhornfelsed slates, intermediate and contact hornfelses

Figures 9.23 - 28 Scatter diagrams of Lu, Yb and Eu versus Zr, P_2O_5 , CaO

and Sr

- Figure 9.23 Lu vs Zr
- Figure 9.24 Yb vs Zr
- Figure 9.25 Lu vs P_2O_5
- Figure 9.26 Yb vs P_2O_5
- Figure 9.27 Eu vs CaO
- Figure 9.28 Eu vs Sr





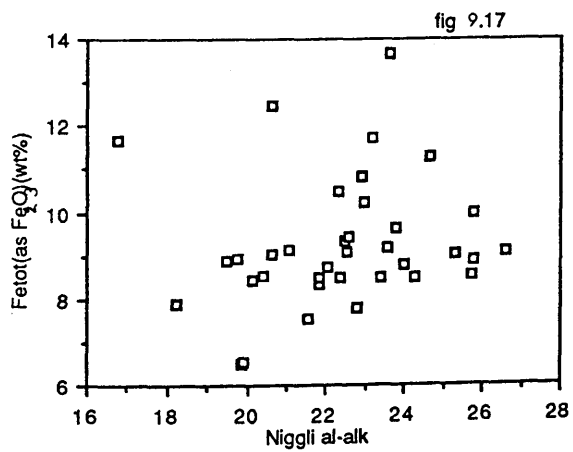
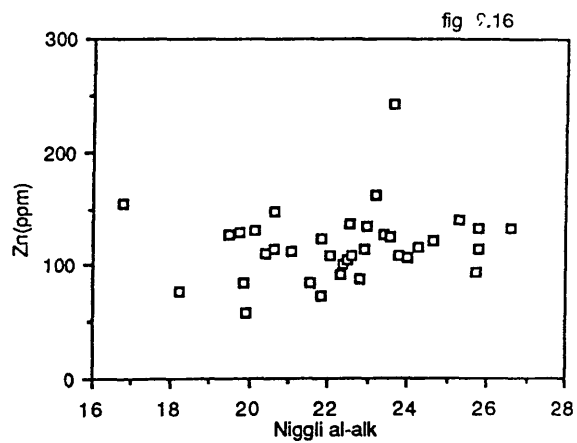
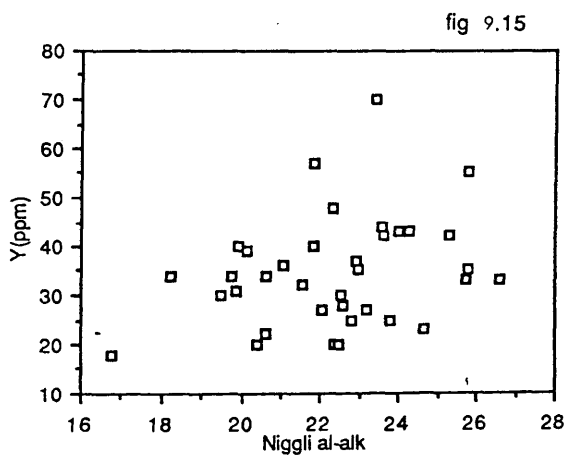
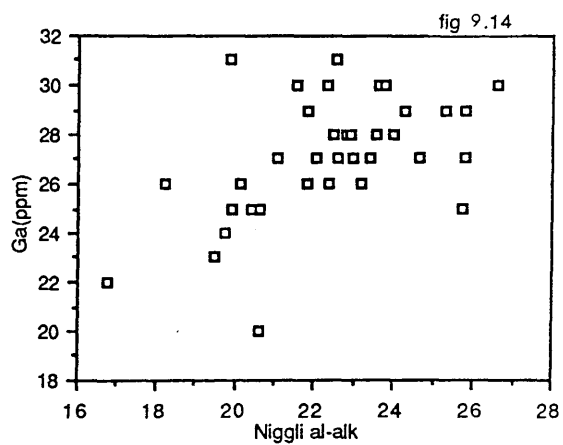
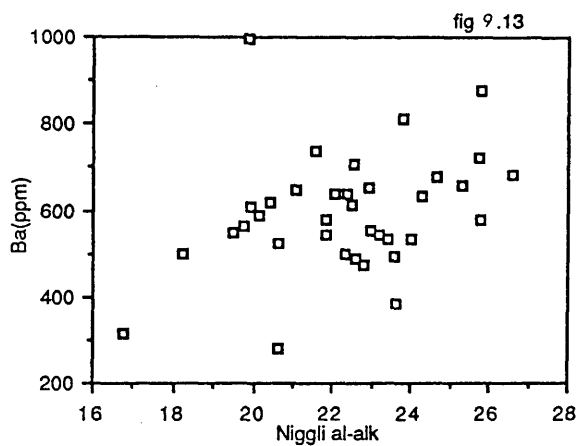


fig 9.18

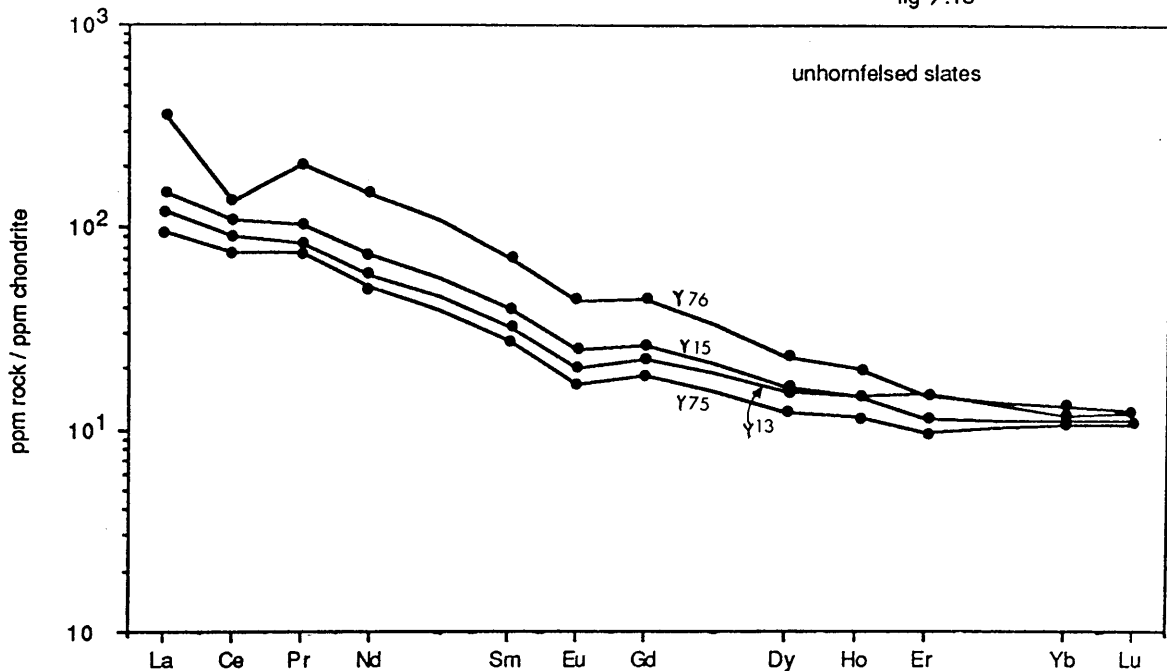


fig 9.19

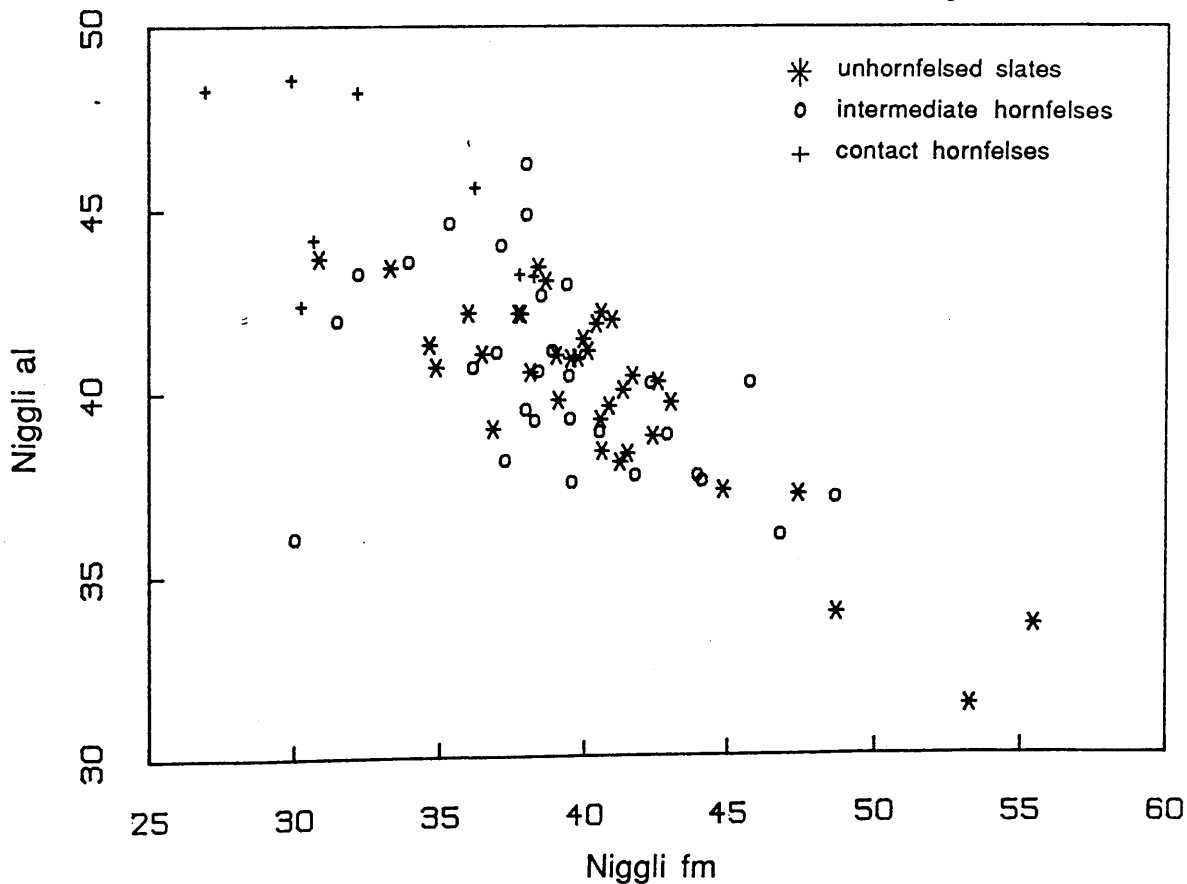


fig 9.20

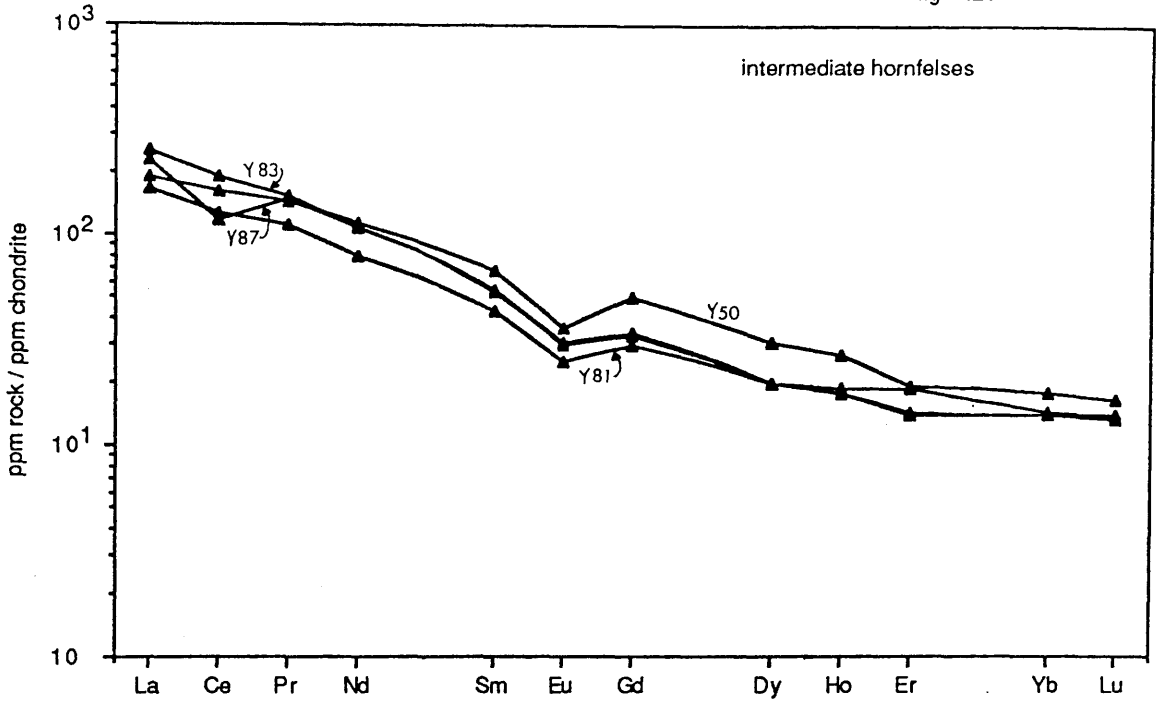


fig 9.21

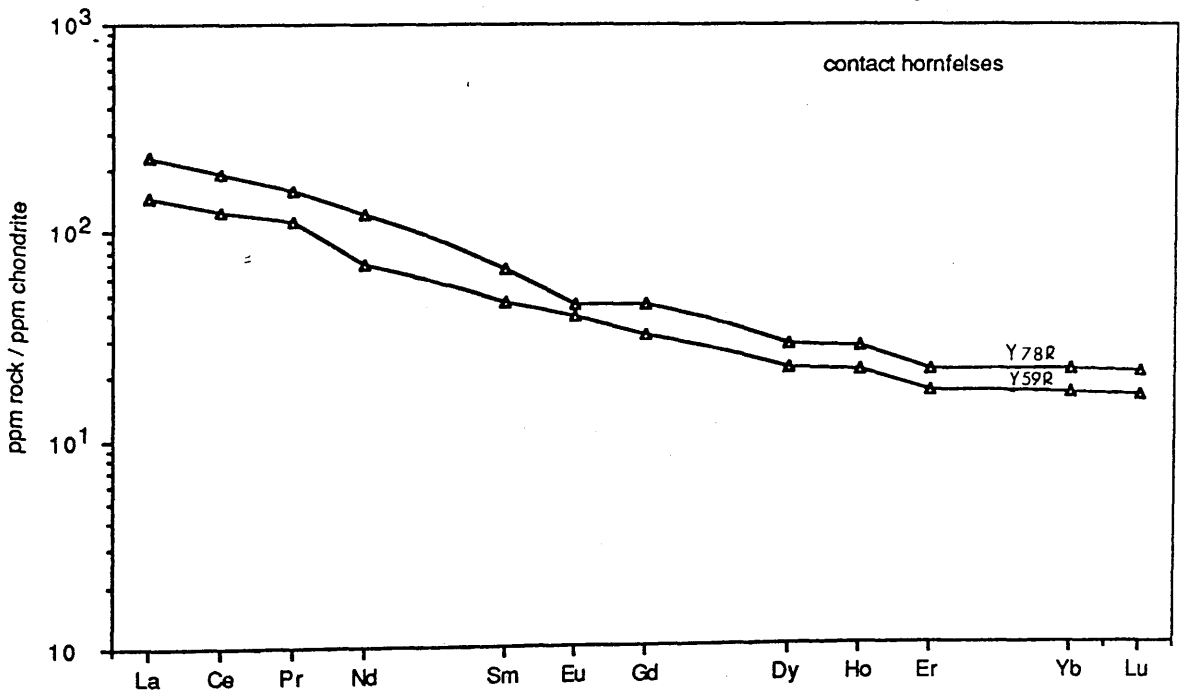
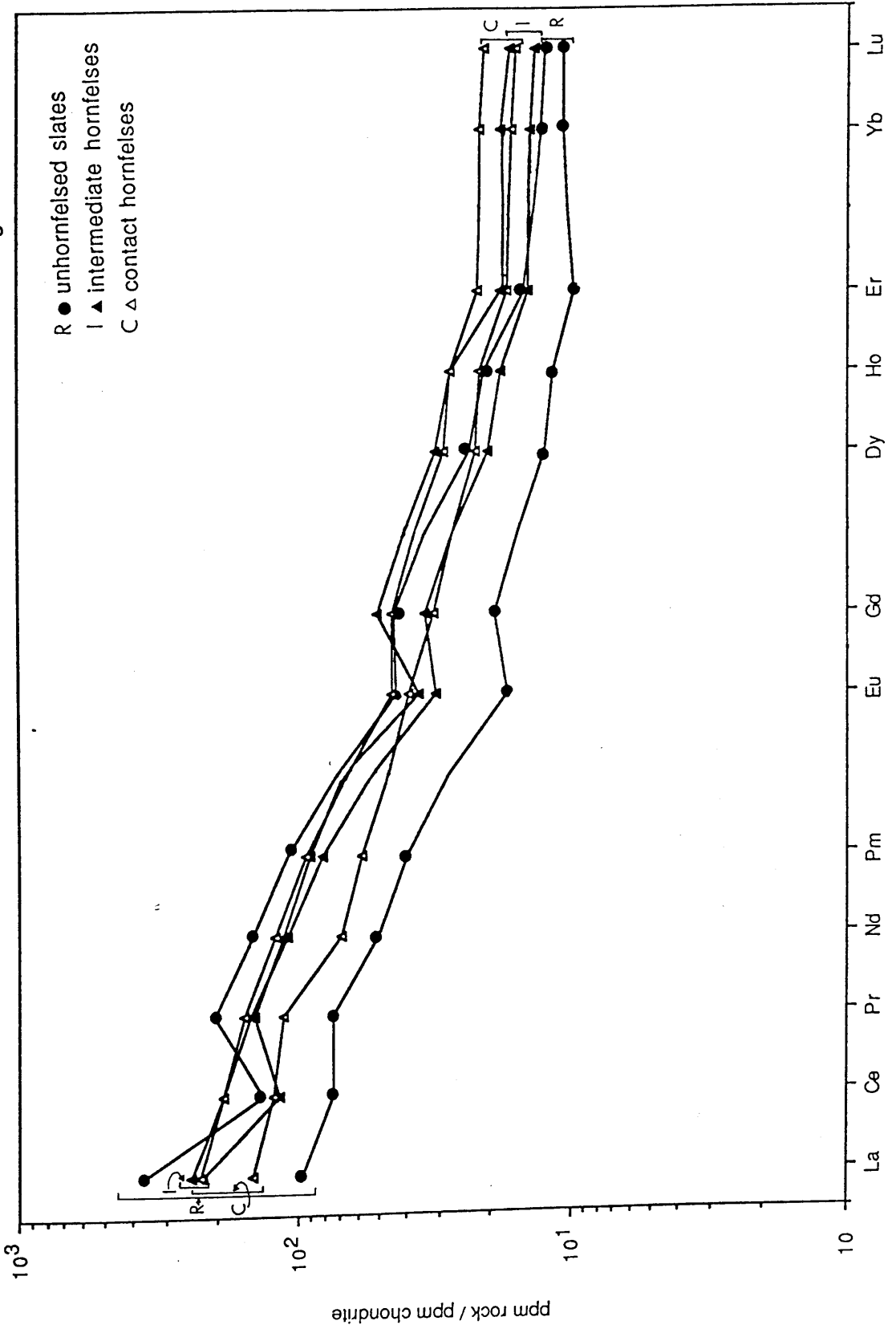
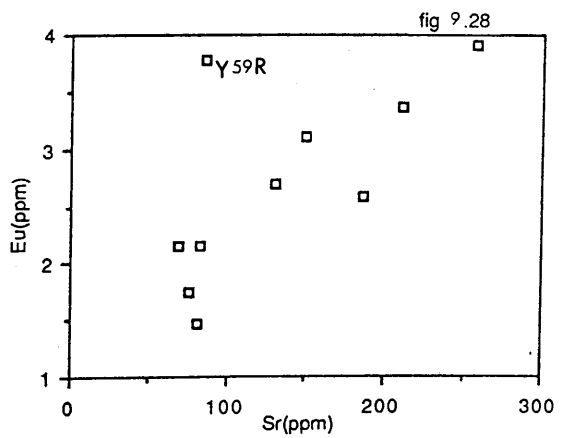
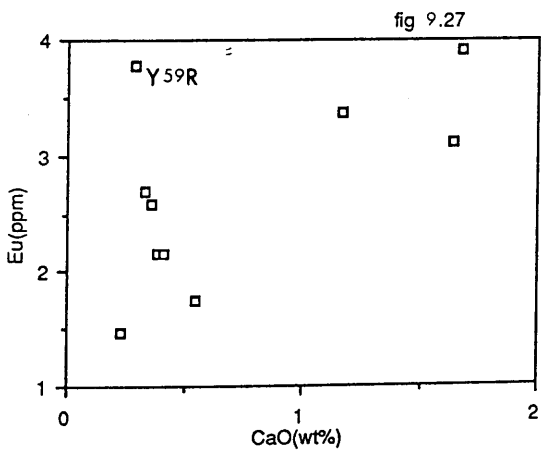
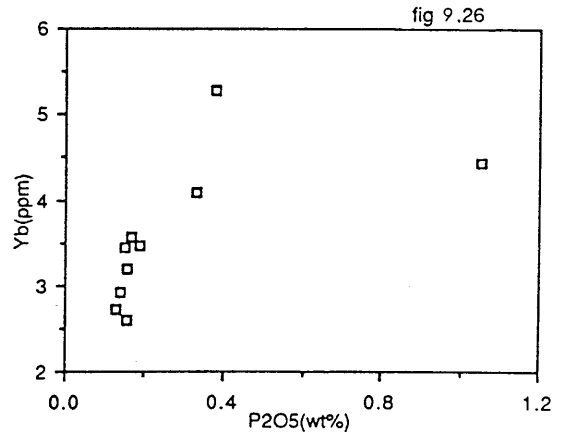
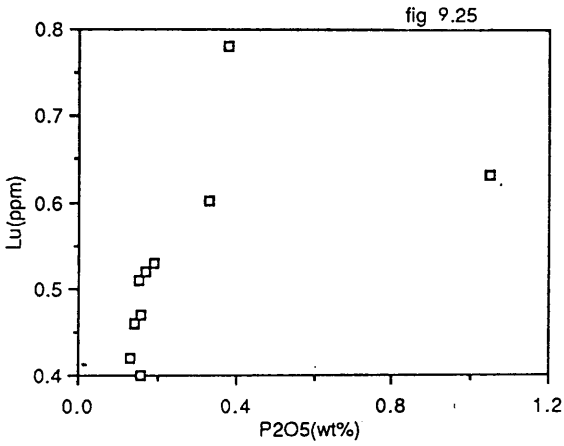
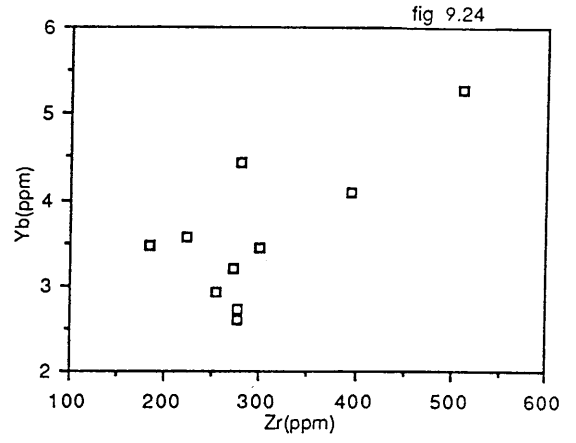
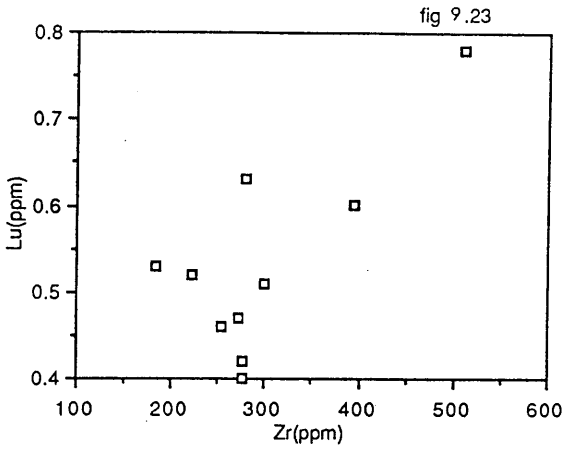
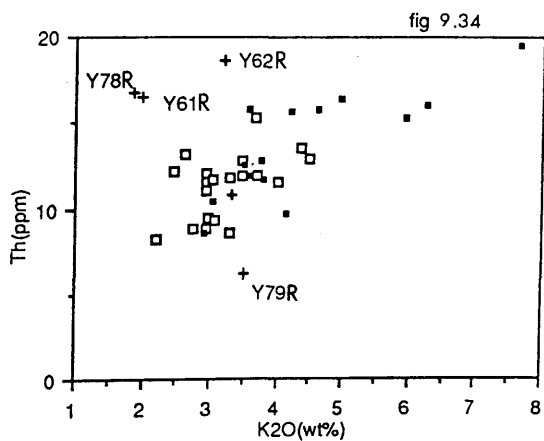
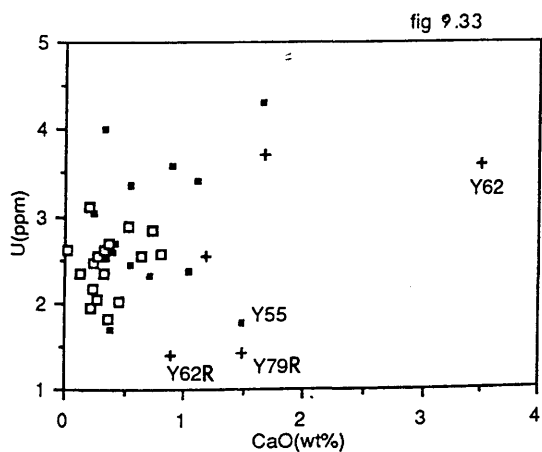
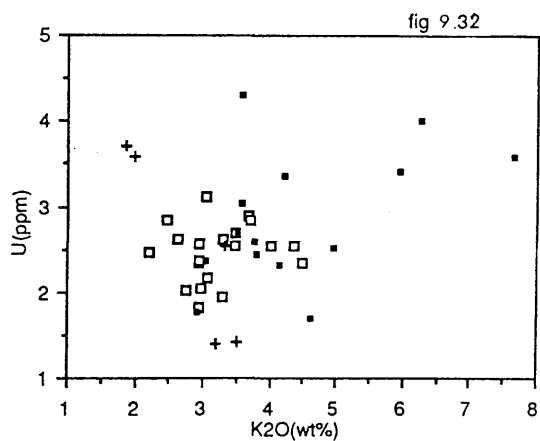
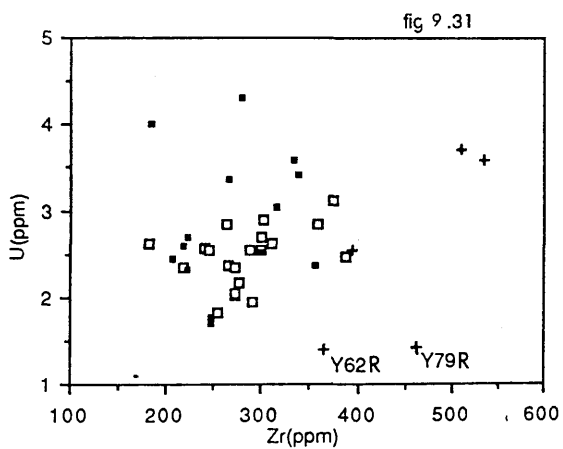
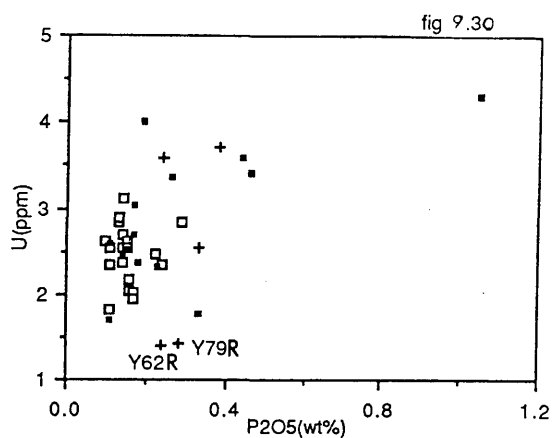
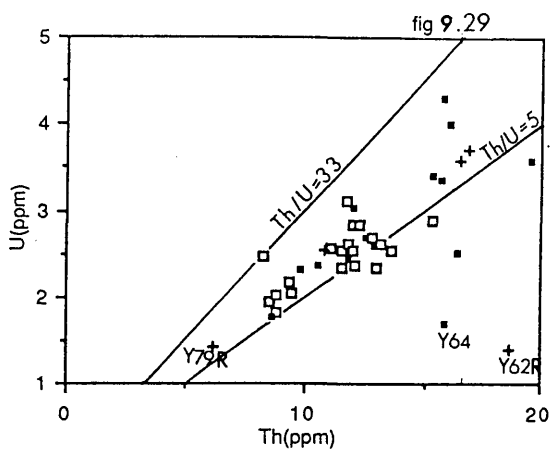
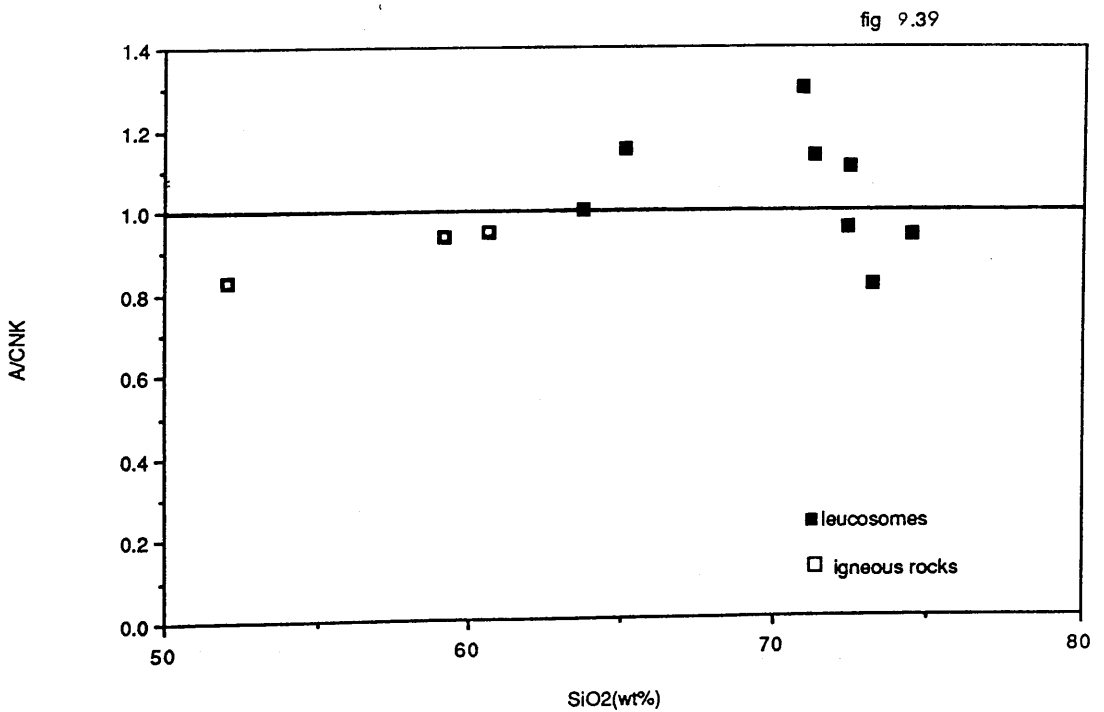
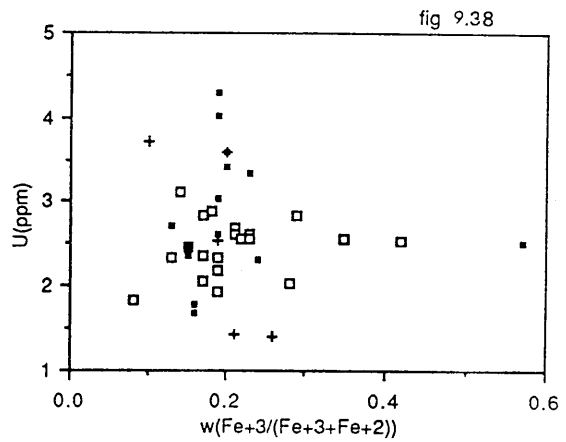
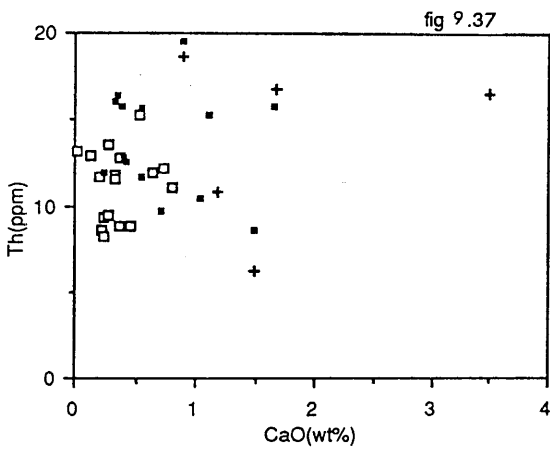
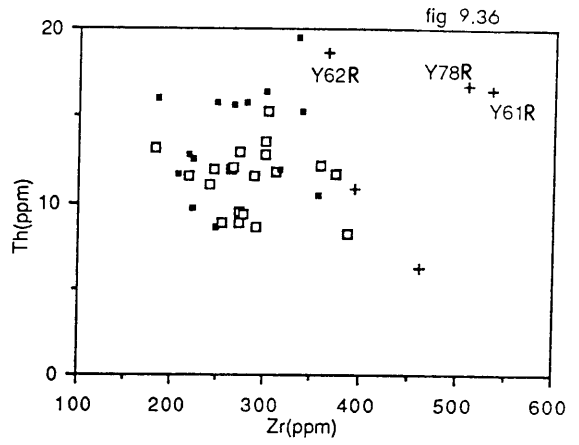
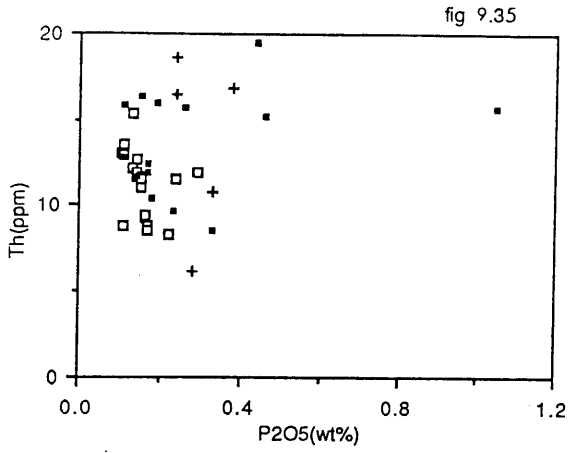


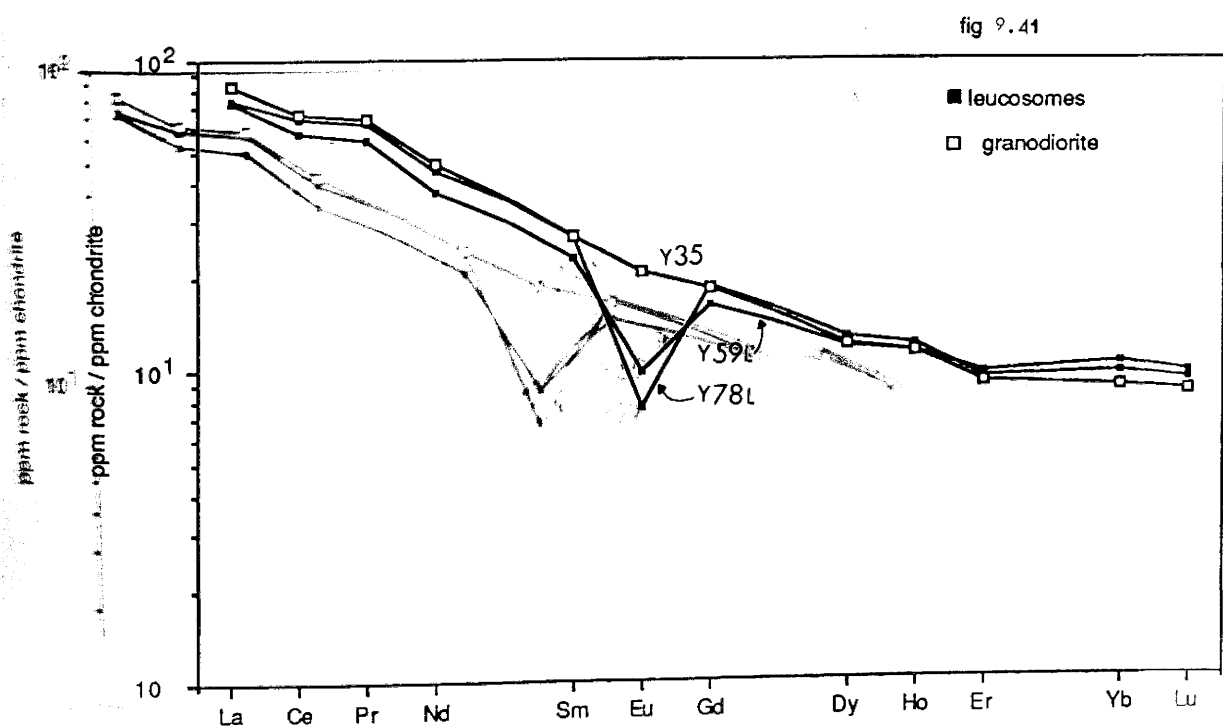
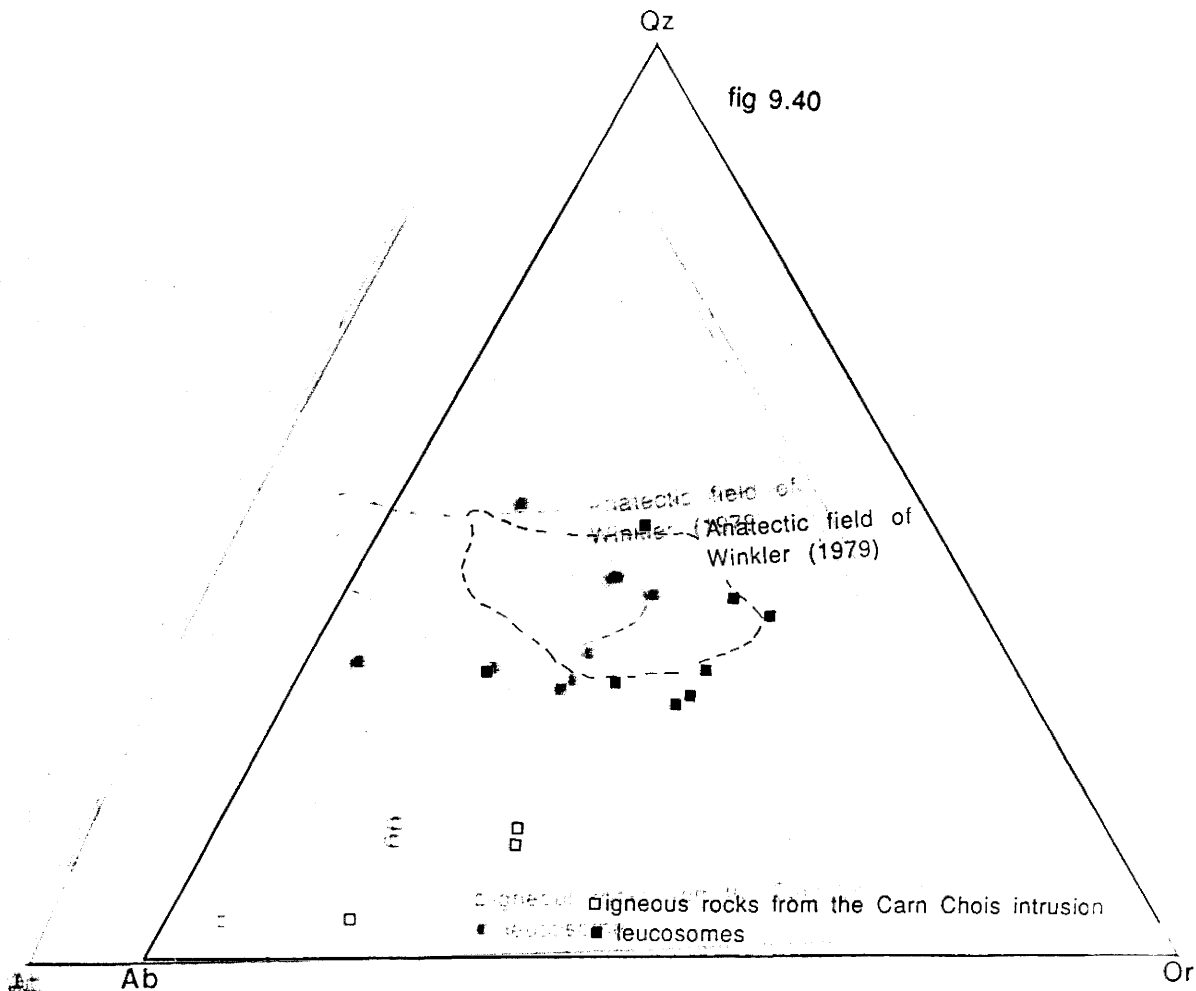
fig 9.22

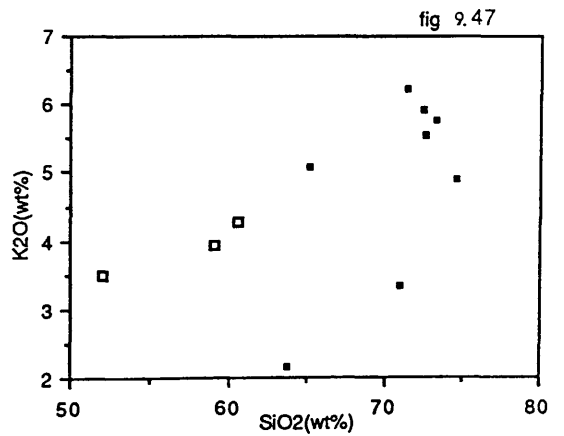
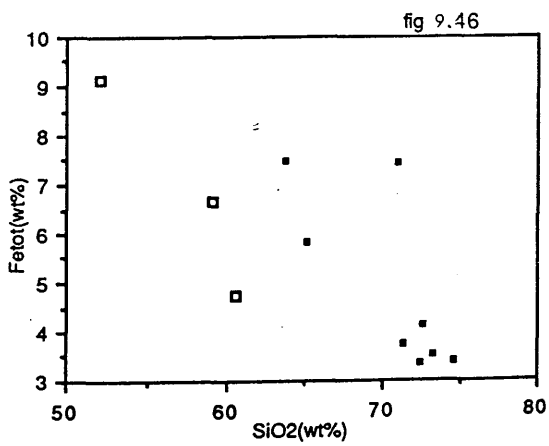
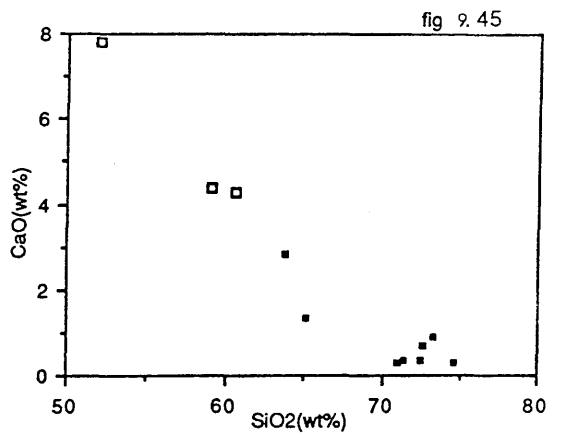
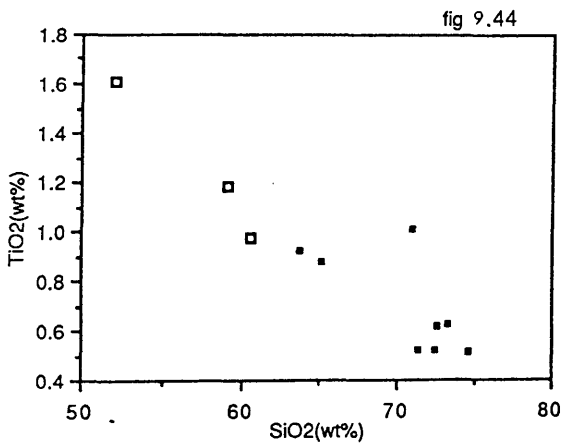
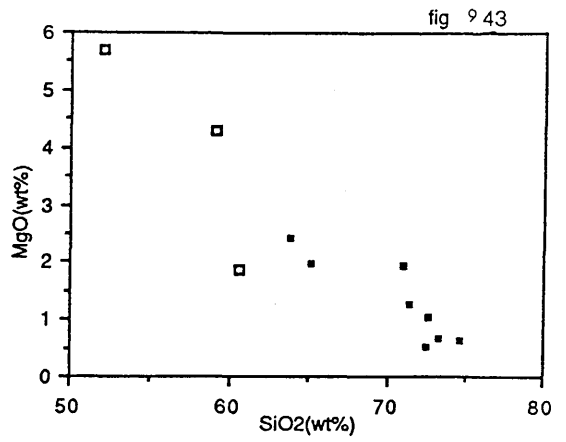
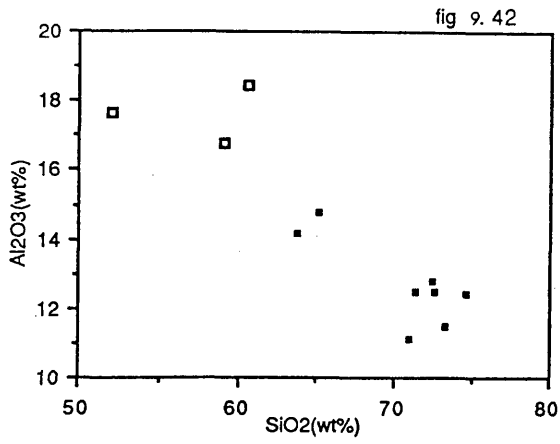


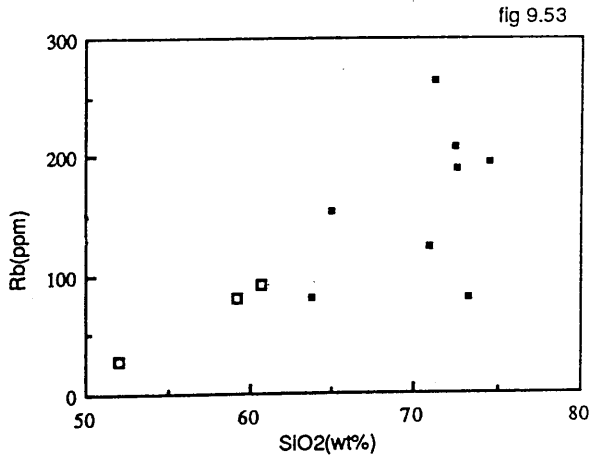
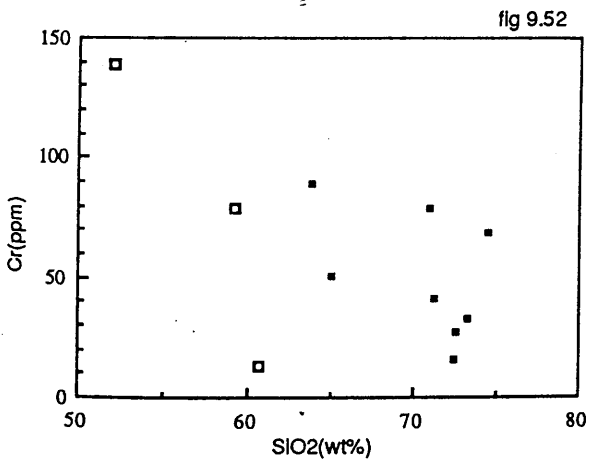
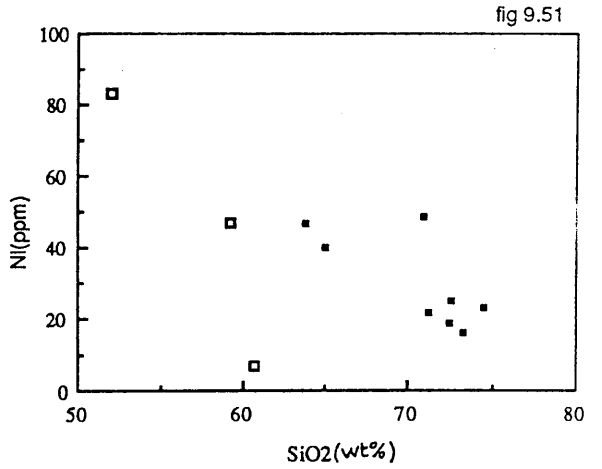
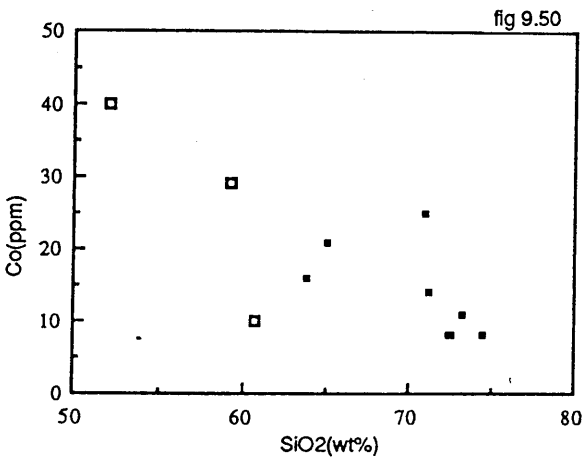
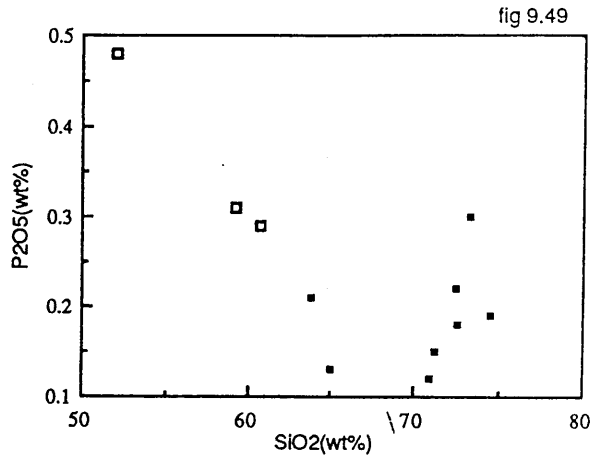
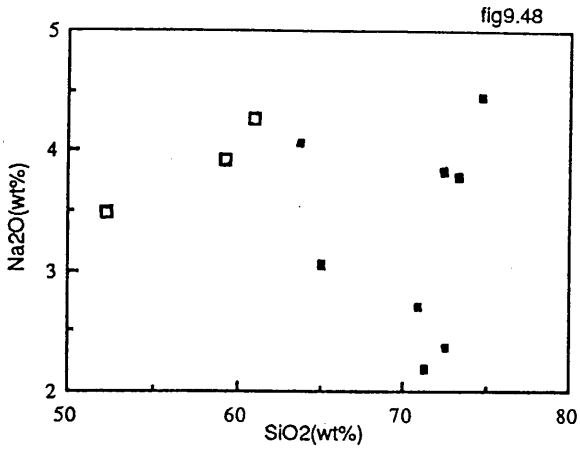


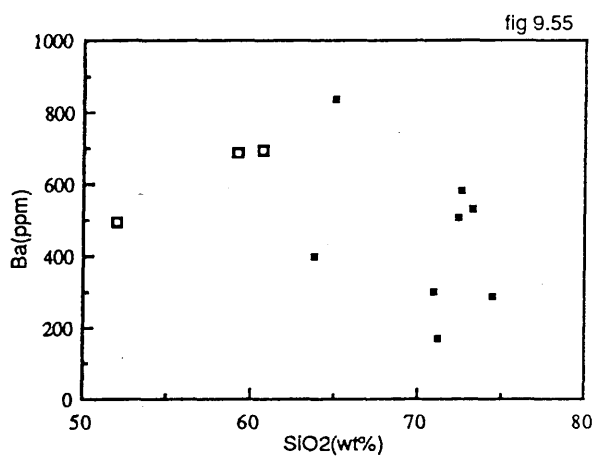
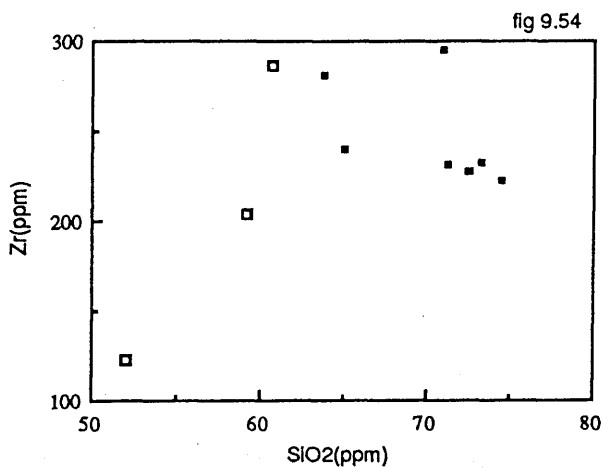












Plates 9.1-4A : U distribution patterns in the Aberfoyle Slates and some individual minerals. The corresponding whole rock sections are also shown.

9.1'-2' Typical whole rock U distribution patterns. Note the high track density over sericite (P9.2') compared to chlorite- and quartz-rich sample (P9.1'). The star-like tracks are formed over zircon. (X2.5, magn. 30)

9.3(A-E)-3'(A'-E') U in crystals of zircon from the country rocks and hornfelses. Note the similarities in both U contents and distribution patterns between zircons from the contact hornfelses (P9.3) and country rocks (P9.3'). (X40, magn. 480X)

9.4(A-B)-4'(A'-B') U in apatites from the slates and a granodiorite. Note the very low content in U of apatite from the slates (P9.4) compared to apatite from the granodiorite. (X40, magn. 480X)

Plates 9.5-9 : Characteristics of the leucosomes from the Comrie aureole.

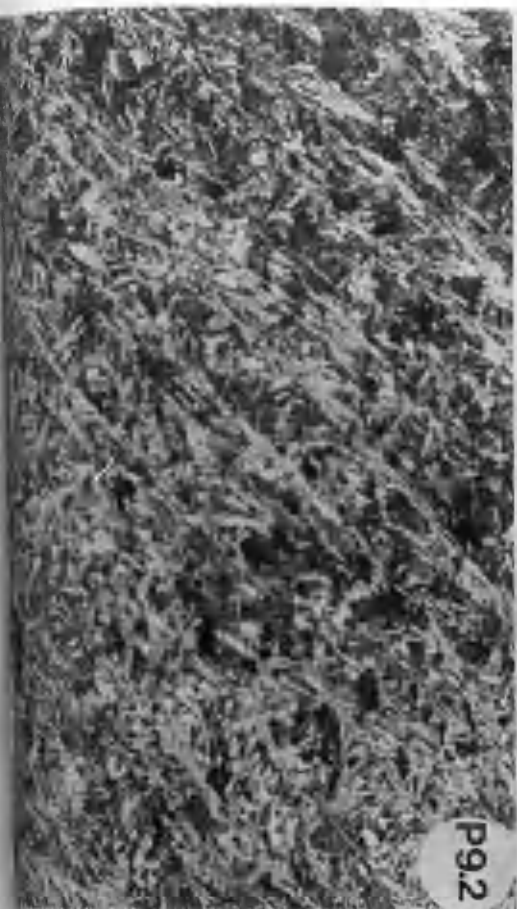
9.5 Typical granophyric texture. (crossed Nicols). White = quartz, black-grey = K-feldspar. (X10, magn. 120X)

9.6 Typical graphic texture (crossed Nicols). White = quartz, black-grey = K-feldspar. (X10, magn. 120X)

9.7 Water-rich pipes from the magma cross cutting the restites (R). Note the sharp contact between the restites (R) and the leucosomes (L) (Transmitted light). (X10, magn. 120X)

9.8 Water-rich "sub-solidus" alterations at the restite leucosome contact (crossed Nicols). (X10, magn. 120)

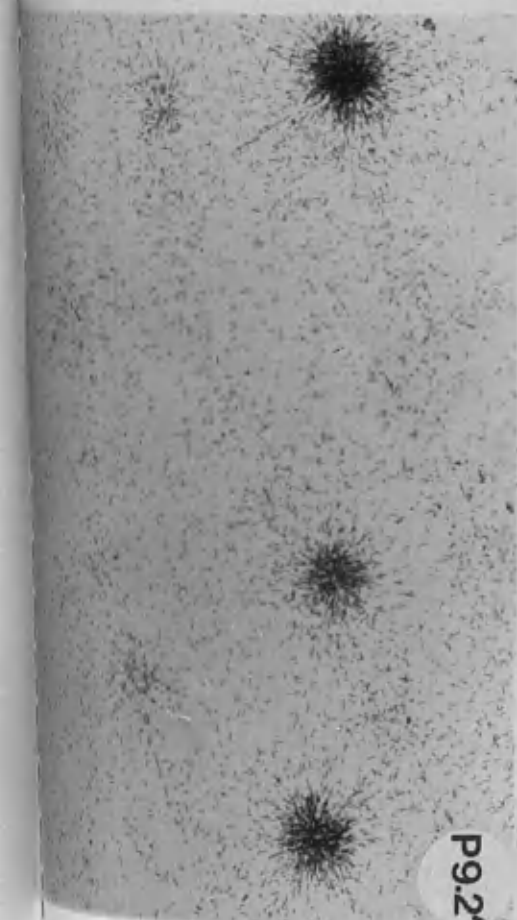
9.9 Relict of slate and xenocrystic orthopyroxene inside a leucosome (crossed Nicols). (X6.3, magn. 75)



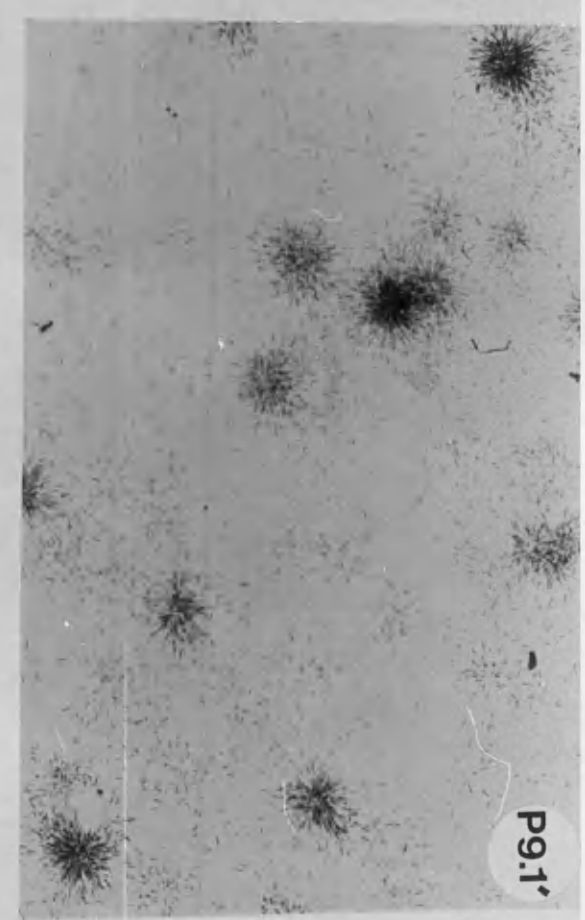
P9.2



P9.1

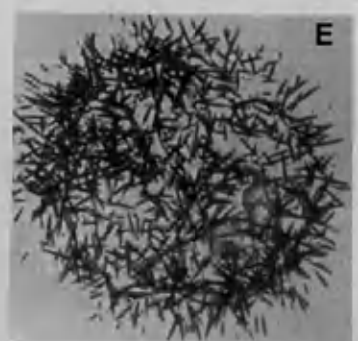
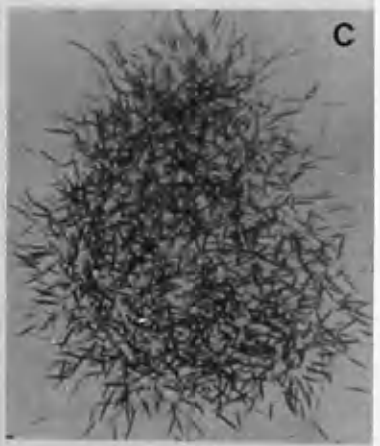
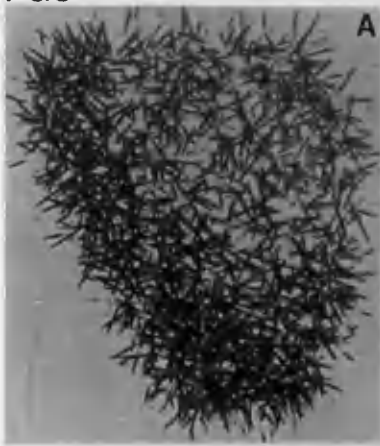


P9.2'

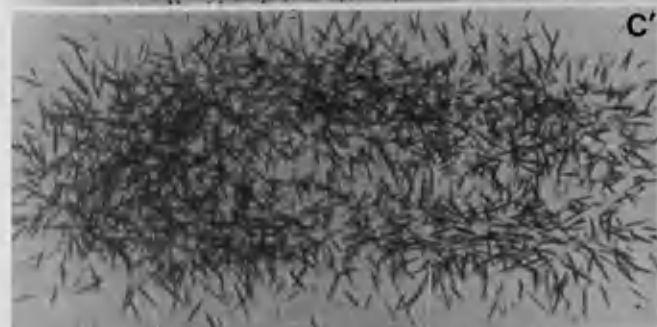
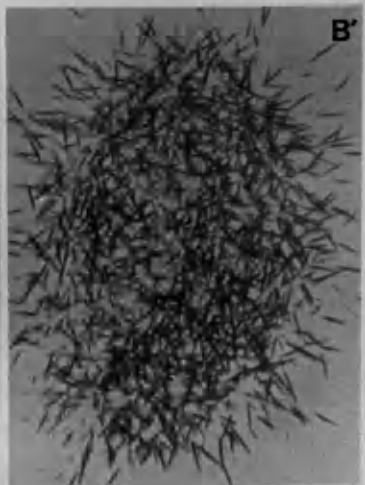


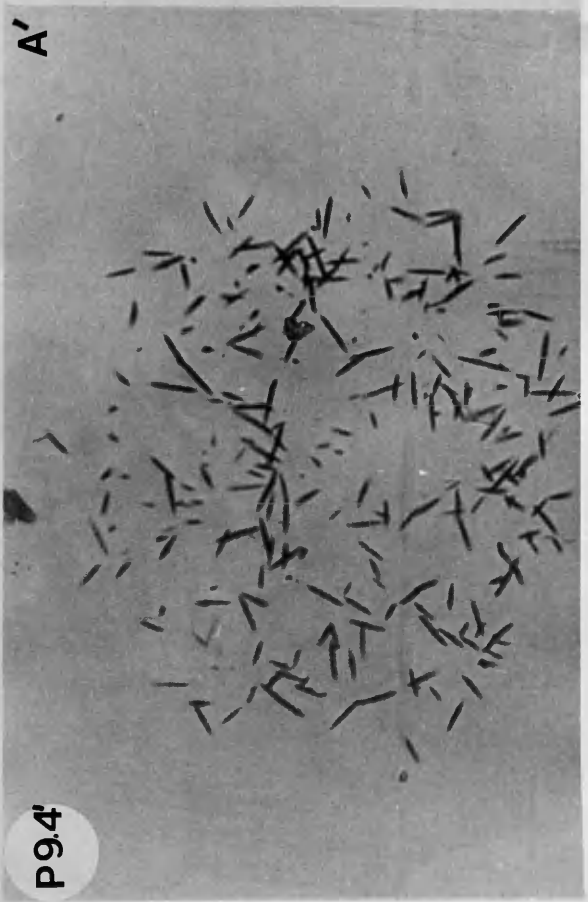
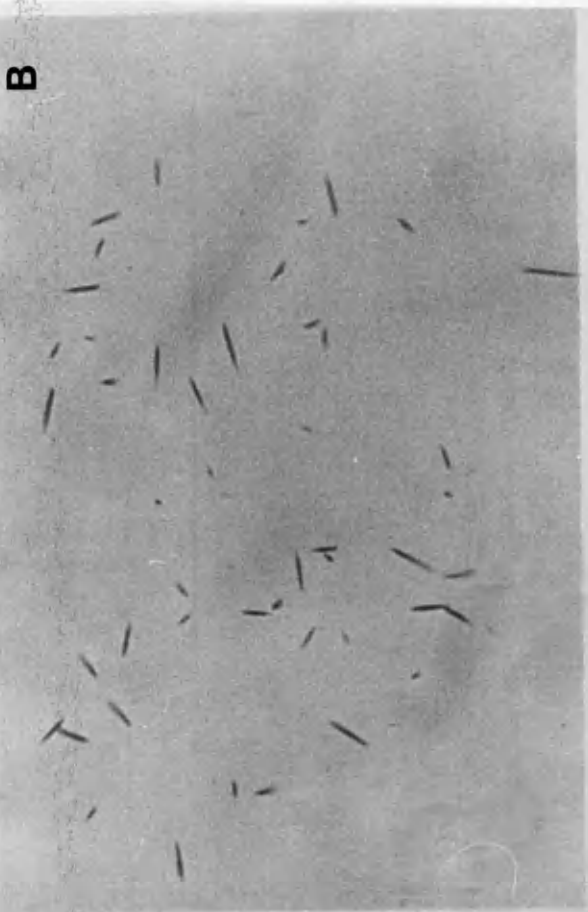
P9.1'

P9.3



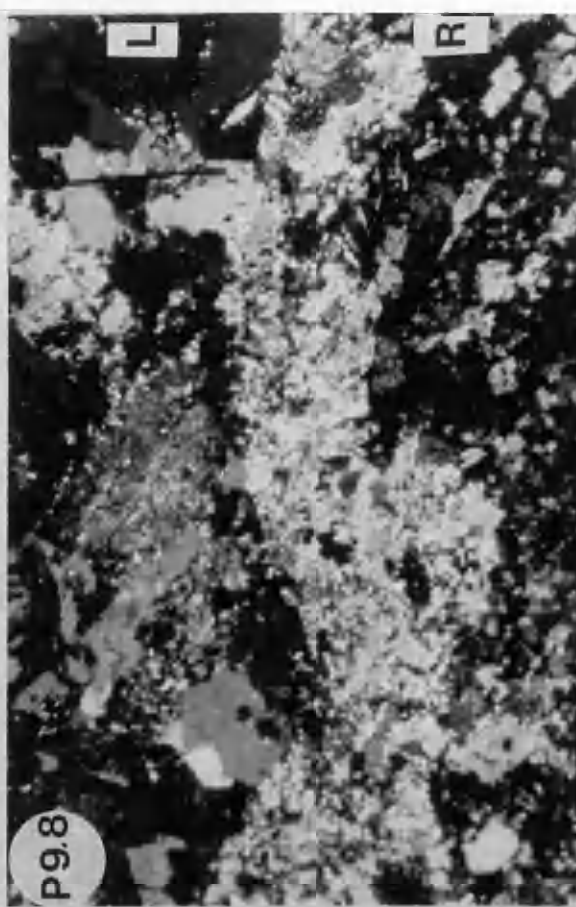
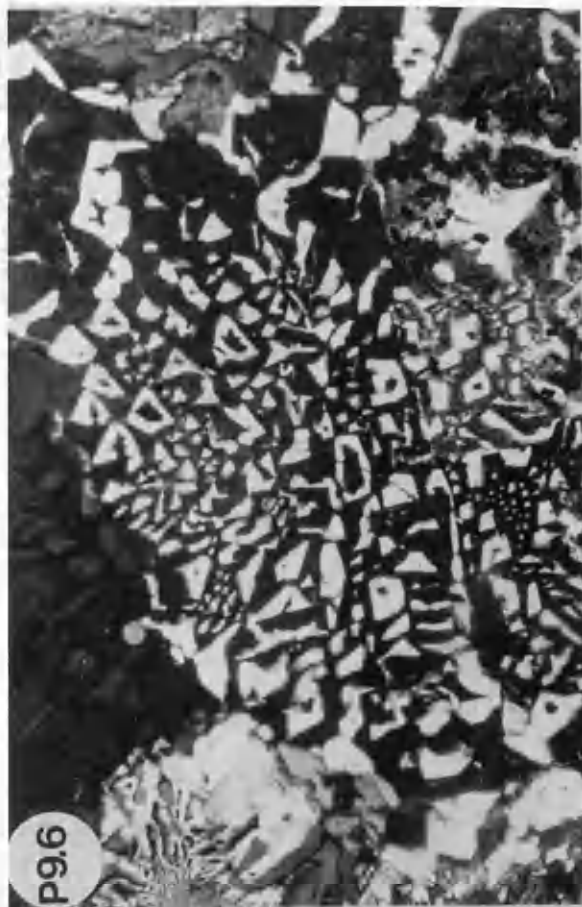
P9.3'



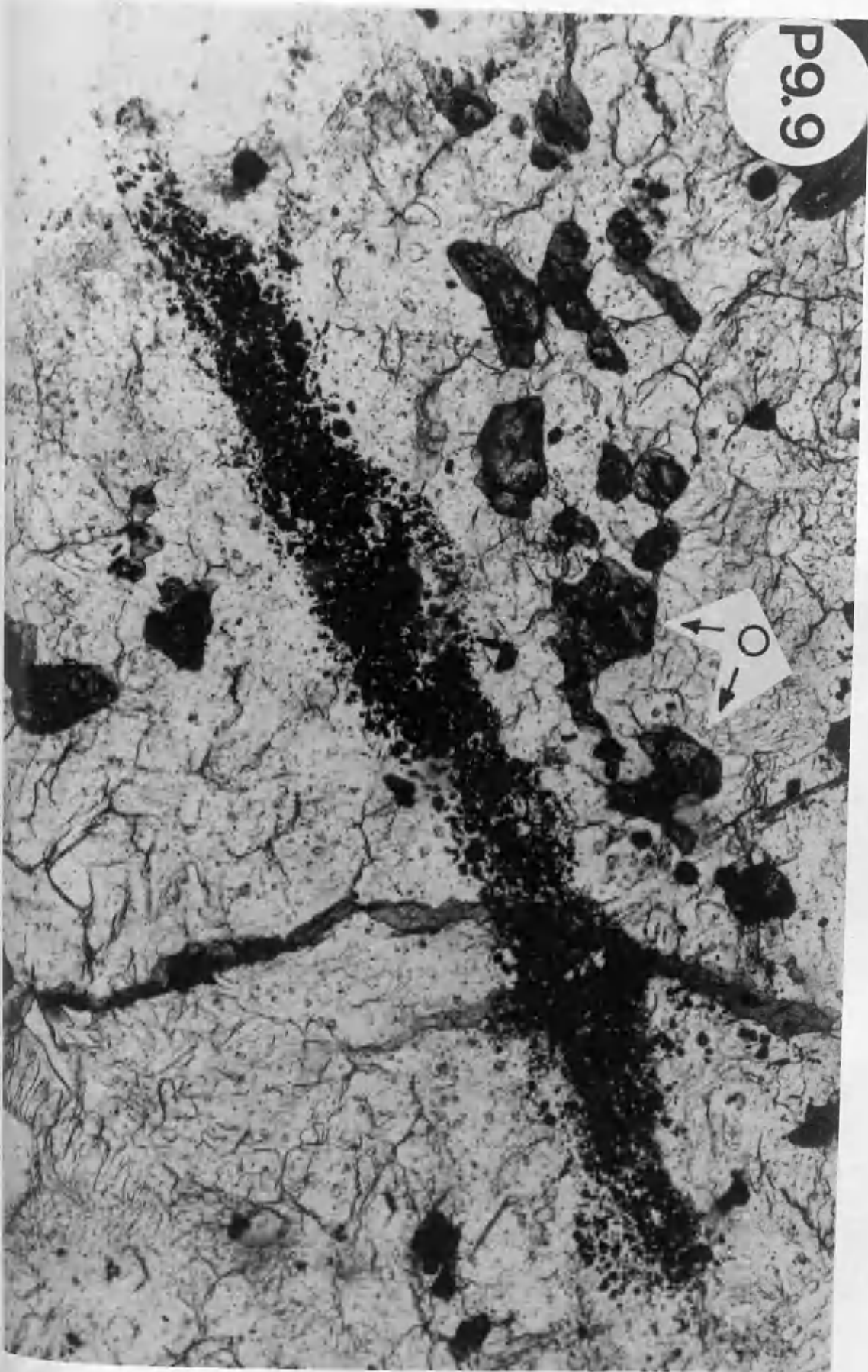


P9.4

P9.4'



P9.9



CHAPTER TEN : DISCUSSION AND CONCLUSIONS

Detailed studies of the Cashel-Lough Wheelaun and Comrie thermal aureoles show that generally similar systematic mineralogical changes occurred in both aureoles despite the differences in the intrusive and country rock types and the degree of regional metamorphism experienced by the country rocks. Original sedimentary variations within the Aberfoyle Slates have however severely obscured the chemical changes.

In terms of mineralogy, the unhornfelsed southern Connemara pelites consisting of biotite-acid andesine-quartz-fibrolite-almandine were altered to magnetite-spinel-cordierite \pm corundum \pm orthopyroxene hornfels in the pelitic xenoliths. Similarly, the regional Aberfoyle Slates which consist of chlorite-sericite-quartz-iron ore \pm opaque \pm epidote \pm plagioclase slates grade through biotite-cordierite quartz-sericite-chlorite-opaque \pm epidote \pm plagioclase hornfels to cordierite - magnetite (ilmenite) -spinel \pm corundum \pm orthopyroxene \pm prismatic sillimanite \pm K-feldspar \pm epidote \pm garnet in the contact hornfelses. This therefore suggests similar, but not identical, mineralogical changes have taken place in both thermal aureoles. The changes in the mineralogy established in the Cashel-Lough Wheelaun and Comrie thermal aureoles coupled with those around other intrusions; *eg* in Aberdeenshire, (Read, 1923, 1924, 1935; Gribble, 1966), Skiddaw, Cumbria, (Rastal, 1910) and the Cortlandt complex, New York (Friedman, 1952) indicate similar mineralogical changes take place in thermal aureoles produced in pelites and slates independently of the degree of regional metamorphism and the intrusive rock types provided sufficient heat is generated by the the intrusive magmas.

The chemistry is more sensitive than the mineralogy particularly as small scale sedimentary variations and/or contamination from the intrusive magmas complicate the trends of important elements particularly the strongly incompatible elements.

In the Cashel thermal aureole, the behaviour of the major and trace elements including the REE is the opposite to what would be expected in magmatic crystallization as deduced from experimental and theoretical work. The elements which are commonly enriched in basic magmas viz : Mg, Fe, Cr,

Ni, and Co largely remained in the crystal fractions, those enriched in the acidic magmas viz : Si, K, Na, P, Rb, Ba, U, Th and to lesser extent Zr strongly fractionated into the outgoing melts whereas those elements which are intermediate in character viz : Al, Ti, Ca, Ga, and Sr were both enriched and removed. The REE also exhibited systematic trends. The early loss of LREE did not seem to be shared by the HREE because the latter were strongly controlled by zircon and apatite. The recrystallization of these two minerals followed by their substantial melting in the pelitic xenoliths fractionated the HREE into the liquids dramatically whereas some of the LREE were probably retained in relict biotite. Eu fractionated into the melts only insignificantly relative to the other REE giving increasing positive Eu anomalies as the degree of hornfelsing and partial melting rise which indicate that partial melting and oxygen fugacity were the control over Eu.

In the Comrie thermal aureole, the relatively low degree of hornfelsing and partial melting compared to the Cashel aureole coupled with original sedimentary variations within the Aberfoyle Slates across the aureole as deduced from the chemistry (chapter.9) frustrated decisive conclusions concerning the movement of most of the elements. Despite these complications, the incompatible elements Si, K, Rb, U and to lesser extent Th tend to decrease in the contact hornfelses, the compatible Ti, Cr, Co and Ga increase whereas Al tends to be both enriched and depleted but Zr, Ba, and Sr are always higher in the contact hornfelses compared to the regional slates. However, the small variability of Mg and Fe in the restites as should be expected indicates that many of the changes described indeed reflect sedimentary variations between the remote slates and contact hornfelses although , at least partly, the decrease of Si, K, Rb and U and the increase of Cr, Co, Ti, Ga, Al and Zr coupled with the agreement of the Rb:K, Ba:K, Sr:Ca and Ga:Al ratios with magmatic crystallization are probably due to hornfelsing and partial melting. These sedimentary variations also strongly affected the behaviour of the REE although the increase in the Eu contents and Eu/Eu^* ratios -like in the Cashel aureole- as the degree of desilication rises indicate that REE were fractionated into the outgoing melts whereby the restites became enriched in Eu. Again, the increasing Eu/Eu^* ratios in the more altered hornfelses suggests the control of partial melting and oxygen fugacity on Eu.

Using Cr, Co and Ni as indicators of the absolute chemical composition of the material removed from the hornfelses and xenoliths from the Cashel thermal aureole, the melts were proved to be S-type granites and agree excellently with the composition of the Cashel granite sill and the migmatites leucosomes associated with the metasedimentary rocks. This coupled with field evidence and the high $^{87}\text{Sr}/^{86}\text{Sr}$ and $\delta^{34}\text{S}$, conclusively indicate that both the microgranite sill and the migmatite leucosomes are S-type granites derived from metasedimentary protoliths which are probably the Cashel metasediments.

Mass balance calculations also proved very useful in estimating the order of fractionation of elements into the melts which are found in the Cashel aureole to agree excellently with their order of fractionation during magmatic crystallization. Although these conclusions were reached from studies from Cashel Hill only for reasons stated in chapter one, the interaction between the basic and ultrabasic magma and the metasedimentary rocks is very complex and extends over 40 km along strike, generating regional hornfelsing and partial melting. Further east of the Cashel district, the Oughterard granite was also derived from metasedimentary protoliths (Barber, 1985; Laouar, 1987). The Cashel situation is therefore one of a "mid-crustal" interaction between the metasediments and the basic and ultrabasic intrusions highly relevant to one way in which the generation of S-type granites and other crustally contaminated magmas can take place within the crust.

The Comrie thermal aureole is much less complex than the Cashel aureole as the contact between the metasediments and Carn Chois intrusive rocks is simpler and the level of hornfelsing and partial melting is relatively higher. This coupled with the late stage "sub-solidus" magmatic injections and the original sedimentary variations discussed above did not allow mass balance and eventually the order of fractionation of elements into the melts to be calculated. However, mineralogical and chemical evidence coupled with A/CNK ratios indicate that the partially melted metasediments contributed to the composition of, at least, many leucosomes and the S-type granitic melts derived from the contact hornfelses were probably eutectic in composition.

The order of fractionation of elements in thermal aureoles as a whole; i.e. $\text{Si} > \text{K} > \text{Na} > \text{Ca} > \text{Mn} > \text{Al} > \text{Fe} > \text{Mg}$ and $\text{Rb} > \text{Ba} > \text{Sr} > \text{Ga} > \text{Cr}, \text{Ni}, \text{Co}$ as can be deduced from

the similar mineralogical changes from the Cashel, Comrie, Aberdeenshire, Skiddaw and Cortlandt thermal aureoles should be roughly similar if no original sedimentary variations between the remote rocks and those occurring near the intrusions are found and/or contamination from the intrusive magma did not take place. Under low degrees of hornfelsing and with no partial melting isochemical metamorphism is to be expected.

- ABBOT, R.N. and CLARKE, D.B. 1979. Hypothetical liquidus relationships in the subsystem Al_2O_3 -FeO-MgO projected from quartz, alkali feldspar and plagioclase for $a(H_2O) \leq 1$. Canadian Mineralogist 17, 549-560.
- ADAMS, J.A.S. and WEAVER, C.E. 1958. Thorium to uranium ratios as indicators of sedimentary processes; example of concept of geochemical facies. American Association of Petroleum Geologists Bulletin 42, 387-430.
- ADAMS, F. and DAMS, R. 1970. Applied Gamma-ray Spectrometry. Pergamon Press, Oxford (second edition) 753pp.
- ALBEE, A.L. 1965. Distribution of Fe, Mg and Mn between garnet and biotite in natural mineral assemblages. Journal of Geology 73, 155-164.
- ANDERSON, D.E. and BUCKLEY, G.R. 1973. Zoning in garnets - diffusion models. Contributions to Mineralogy and Petrology 40, 87-104.
- ASHWORTH, J.R. 1976. Petrogenesis of migmatites in the Huntly-Portsoy area, north-east Scotland. Mineralogical Magazine 40, 661-682.
- ASHWORTH, J.R. 1985. Introduction. In ASHWORTH, J. R. (ed.) Migmatites. Blackie, Glasgow and London, pp302.
- ATHERTON, M.P. 1968. The variation in garnet, biotite and chlorite composition in medium grade pelitic rocks from the Dalradian, Scotland, with particular reference to the zonation in garnet. Contributions to Mineralogy and Petrology 18, 347-371.
- ATHERTON, M.P. and BROTHERTON, M.S. 1979. Thorium and uranium in some pelitic rocks from the Dalradian, Scotland. Chemical Geology 27, 329-342.
- BADLEY, M.E. 1976. Stratigraphy, structure and metamorphism of Dalradian rocks of the Maumturk Mountains, Connemara, Ireland. Journal of the Geological Society London 132, 509-520.
- BARBER, J.P. 1985. High-grade metamorphism and melting in the Dalradian of eastern Connemara, Ireland. Ph.D. thesis, University of East Anglia (unpub.).
- BARBER, J.P. and YARDLEY, B.W.D. 1985. Conditions of high grade

- metamorphism in the Dalradian of Connemara, Ireland. Journal of the Geological Society London 142,87-96.
- BARROW,G.1912.On the geology of lower Dee-side and the Southern Highland border. Proceedings of the Geological Association 23, 274-290.
- BOHLEN,S.R. and ESSEN,E.J.1980. Evaluation of coexisting garnet-biotite, garnet-clinopyroxene, and other Mg-Fe exchange thermometers in Adirondack granulites: Summary. Bulletin of the Geological Society of America 91,107-109.
- BOWEN,N.L.1928.The Evolution of the Igneous Rocks. Princeton University Press, Princeton, New Jersey.
- BOWEN,N.L. and SCHAIRER,J.F.1935.The system MgO-FeO-SiO₂. American Journal of Science 29,151-217.
- BOYLE,R.W.1982.Geochemical prospecting for thorium and uranium deposits. In Developments in Economic Geology 16, 498pp, Elsevier, Amsterdam.
- BROWN,P.E.1983. Caledonian and earlier magmatism. In CRAIG,G.Y.(ed.) Geology of Scotland. Scottish Academic Press, Edinburgh (second edition). pp167-204.
- BRUNFELT,A.O. and STEINNES,E.1969. Instrumental activation analysis of silicate rocks with epithermal neutrons. Analytica Chimica Acta 48, 13-24.
- CALLAWAY,C.1887.On the alleged conversion of crystalline schists into igneous rocks in County Galway. Quarterly Journal of the Geological Society of London 43, 517-524.
- CARSLAW,H.S. and JAEGER,J.C.1947. Conduction of Heat in Solids. Oxford University Press, 386pp.
- CARSLAW,H.S. and JAEGER,J.C.1959.Conduction of Heat in Solids. Oxford University Press, (second edition) 510pp.
- CHAPPELL,B.W. and WHITE,A.J.R.1974. Two contrasting granite types. Pacific Geology 8, 173-174.
- CHAYES,F.1964.Variance-covariance relations in Harker diagrams of volcanic suites. Journal of Petrology 5, 219-237.
- CLARKE,F.W.1924.The data of geochemistry. Bulletin of the United States Geological Survey 770, 841pp.

- CLARKE,D.B.1981.The mineralogy of peraluminous granites: a review. Canadian Mineralogist 19, 3-17.
- CLEMENS,J.D. and WALL,V.J.1981.Origin and crystallization of some peraluminous (S-type) granitic magmas. Canadian Mineralogist 19, 111-131.
- CRONSHAW,H.B.1923.The Connemara serpentine rocks. Geological Magazine 60, 467-471.
- CRUSE,M.J.B. and LEAKE,B.E.1968.The Geology of Renvyle, Inishbofin and Inishark, north-west Connemara, Co. Galway. Proceedings of the Royal Irish Academy 67B, 1-36.
- DALLMEYER,R.D.1974.The role of crystal structure in controlling the partitioning of Mg and Fe⁺² between coexisting garnet and biotite. American Mineralogist 59, 201-203.
- DAS,N.1985.Geochemical Studies of Caithness Flags. Ph.D thesis, University of Glasgow (unpub.).
- DEER,W.A.,HOWIE,R.A. and ZUSSMAN,J.1966.An Introduction to the Rock Forming Minerals. Longman, pp.528.
- DEER,W.A.,HOWIE,R.A. and ZUSSMAN,J.1982.Orthosilicates. In: Rock Forming Minerals vol. 1A (second editions). Longman, pp.528.
- DRAKE,M.J.1975.The oxidation state of europium as an indicator of oxygen fugacity. Geochimica et Cosmochimica Acta 39, 55-64.
- DRURY,S.A.1978.REE distributions in a high grade Archaean gneiss complex in Scotland: Implications for the genesis of ancient sialic crust. PreCambrian Research 7, 237-257.
- EVANS,B.W.1964.Fractionation of elements in the pelitic hornfelses of the Cashel-Lough Wheelaun intrusion, Connemara, Eire. Geochimica et Cosmochimica Acta 28, 127-156.
- EVANS,B.W. and LEAKE,B.E.1960.The composition and origin of the striped amphibolites of Connemara, Ireland. Journal of Petrology 1, 337-363.
- EVANS,B.W. and LEAKE,B.E.1970.The geology of the Toombeola district, Connemara, Co.Galway. Proceedings of the Royal Irish Academy 70B, 105-139.
- FERRY,J.M. and SPEAR,F.S.1978.Experimental calibration of the

- partitioning of Fe and Mg between biotite and garnet. Contributions to Mineralogy and Petrology 66,113-117.
- FLEISCHER,R.L., PRICE,P.B. and WALKER,R.M.1965a. The ion explosion spike mechanism for formation of charged particle tracks in solids. Journal of Applied Physics 36,3645-3652.
- FLEISCHER,R.L., PRICE,P.B. and WALKER,R.M.1965b.Tracks of charged particles in solids. Science 149, 383-393.
- FLEISCHER,R.L., PRICE, P.B. and WALKER,R.M. 1965c. Effects of temperature, pressure, ionization on the formation and stability of fission tracks in minerals and glasses. Journal of Geophysical Research 70, 1497-1502.
- FLEISCHER,R.L., PRICE,P.B. and WALKER,R.M. 1975.Nuclear Tracks in Solids. Principles and Applications. Berkeley: University of California Press, pp.605.
- FLYNN,R.T. and BURNHAM,C.W.1978.An experimental determination of rare partition coefficients between a chloride containing vapor phase and silicate melts. Geochimica et Cosmochimica Acta 42, 685-701.
- FOSTER,M.D.1960.Interpretation of the composition of trioctahedral micas. United States Geological Survey (Professional Paper) 354-B, 11-49.
- FRASER,D.H.1975.Activities of trace elements in silicate melts. Geochimica et Cosmochimica Acta 39, 1525-1530.
- FRIEDLANDER,G., KENNEDY, J.W., MACIAS, E.S. and MILLER, J.M. 1981.Nuclear and Radiochemistry. John Wiley and Sons (3rd edition),pp.684.
- FRIEDMAN,G.M.1952.Sapphirine occurrence of Cortlandt, New York. American Mineralogist 37,244-249.
- FROST,M.J. 1962. Metamorphic grade and iron-magnesium distribution between co-existing garnet-biotite and garnet-hornblende. Geological Magazine 99, 427-438.
- GANGULY,J. and KENNEDY,G.C.1974.The energetics of natural garnet solid solution. 1.Mixing of the aliumino-silicate end-members. Contributions to Mineralogy and Petrology 48, 137-148.
- GANGULY,J. and SAXENA,S.K. 1984. Mixing properties of aluminosilicate

- garnets: constraints from natural and experimental data, and applications to geothermo-barometry. American Mineralogist 69, 88-97.
- GHENT, E.D. 1976. Plagioclase-garnet- Al_2SiO_5 -quartz: a potential geobarometer-geothermometer. American Mineralogist 61, 710-714.
- GHENT, E.D., ROBBINS, D.B. and STOUT, M.Z. 1979. Geothermometry, geobarometry, and fluid compositions of metamorphosed calc-silicates and pelites, Mica Creek, British Columbia. American Mineralogist 64, 874-885.
- GLEADOW, A.J.W, HURFORD, A.J. and QUAIFFE, R.D. 1976. Fission track dating of zircon: improved etching techniques. Earth and Planetary Science Letters 33, 273-276.
- GOLDSMITH, J.R. 1980. Melting and breakdown reactions of anorthite at high pressures and temperatures. American Mineralogist 65, 272-284.
- GRANT, J.A. and WEIBLEN, P.W. 1971. Retrograde zoning in garnet near the second sillimanite isograd. American Journal of Science 270, 281-296.
- GRAUERT, B., SEITZ, M.G., and SOPTRAJANOVA, G. 1974. Uranium and lead gain of detrital zircon studied by isotopic analyses and fission-track mapping. Earth and Planetary Science Letters 21, 389-399.
- GREEN, T.H. 1976. Experimental generation of cordierite - or garnet-bearing granitic liquids from a pelitic composition. Geology 4, 85-88.
- GRIBBLE, C.D. 1966. The thermal aureole of the Haddo House norite in Aberdeenshire. Scottish Journal of Geology 2, 306-313.
- HARVEY, P.K., TAYLOR, D.M., HENDRY, R.D. and BANCROFT, F.L. 1973. An accurate fusion method for the analysis of rocks and chemically related minerals by X-ray fluorescence spectrometry. X-Ray Spectrometry 2, 33-44.
- HASKIN, M.A. and HASKIN, L.A. 1966. Rare earths in European shales: a re-determination. Science 154, 507-509.
- HASKIN, L.A., HASKIN, M.A., FREY, F.A. and WILDEMAN, T.R. 1968. Relative and absolute terrestrial abundances of the rare earths. In AHRENS, L.H. (ed.) Origin and Distribution of the Elements. Pergamon

- Press, 889-912.
- HEDGE, C.E. 1972. Source of leucosomes of migmatites in the Front Range, Colorado. Memoirs of the Geological Society of America 135, 65-72.
- HEIER, K.S. 1979. The movement of uranium during higher grade metamorphic processes. Philosophical Transactions of the Royal Society of London 291A, 413-421.
- HEIER, K.S. and ADAMS, J.A.S. 1965. Concentration of radioactive elements in deep crustal material. Geochimica et Cosmochimica Acta 29, 53-61.
- HENDERSON, P. 1982. Inorganic Geochemistry. Pergamon, Oxford, pp353.
- HENDERSON, P. 1984. General geochemical properties and abundances of the rare earth elements. In HENDERSON, P. (ed.) Rare Earth Element Geochemistry. Developments in Geochemistry 2, 1-32, Elsevier.
- HINE, R., WILLIAMS, I.S., CHAPPELL, B.W. and WHITE, A.J.R. 1978. Contrast between I- and S-type granitoids of the Kosciusko Batholith. Journal of the Geological Society of Australia 25, 219-234.
- HODGES, K.V. and SPEAR, F.S. 1982. Geothermometry, geobarometry and the Al_2SiO_5 triple point at Mt. Moosilauke, New Hampshire. American Mineralogist 67, 1118-1134.
- HOLDAWAY, M.J. 1971. Stability of andalusite and the aluminium silicate phase diagram. American Journal of Science 271, 97-131.
- HOLDAWAY, M.J. and LEE, S.M. 1977. Cordierite stability in high-grade pelitic rocks based on experimental, theoretical and natural observations. Contributions to Mineralogy and Petrology 63, 175-198.
- HOLLISTER, L.S. 1966. Garnet zoning: an interpretation based on the Rayleigh fractionation model. Science 154, 1647-1651.
- HURFORD, A.J. and GREEN, P.F. 1982. A user's guide to fission track dating calibration. Earth and Planetary Science Letters 59, 343-354.
- HURFORD, A.J. and GREEN, P.F. 1983. The zeta age calibration of fission-track dating. Isotope Geoscience 1, 285-317.
- HURFORD, A.J., FITCH, F.J. and CLARKE, A. 1984. Resolution of the age structure of the detrital zircon populations of two Lower Cretaceous sandstones from the Weald of England by fission track dating. Geological Magazine 121, 269-396.
- INDARES, A. and MARTIGNOLE, J. 1985. Biotite-garnet geothermometry

- in the granulite facies: the influence of Ti and Al in biotite. American Mineralogist 70, 272-278.
- IRVING, A.J. 1978. A review of experimental studies of crystal/liquid trace element partitioning. Geochimica et Cosmochimica Acta 42, 743-770.
- JAEGER, J.C. 1957. The temperature in the neighborhood of a cooling intrusive sheet. American Journal of Science 255, 306-318.
- JAEGER, J.C. 1959. Temperatures outside a cooling intrusive sheet. American Journal of Science 257, 44-54.
- JAGGER, M.D. 1985. The Cashel district of Connemara, Co. Galway, Eire: An isotopic study. Ph.D. thesis, University of Glasgow (unpubl).
- JENKINS, R. and DE VRIES, J.L. 1967. Practical X-Ray Spectrometry. Centrex Eindhoven, pp.182.
- JOHSTONE, S.J. 1954. Minerals for the Chemical and Allied Industries. Chapman and Hall, pp.692.
- KEELING, B.E. 1981. The geochemistry of the Connemara gneiss complex, Co. Galway, Ireland. Ph.D. thesis, University of Glasgow (unpubl.).
- KENAH, C. and HOLLISTER, L.S. 1983. Anatexis in the central gneiss complex, British Columbia. In ATHERTON, M.P. and GRIBBLE, C.S. (eds). Migmatites, melting and metamorphism. Shiva, Orpington, 142-162.
- KEPEZHINSKAS, K.B. 1973. Pressure variability during medium-temperature metamorphism of meta-pelites. Lithos 6, 145-157.
- KILBURN, C., PITCHER, W.S. and SHACKLETON, R.M. 1965. The stratigraphy and origin of the Portaskaig boulder bed series (Dalradian). Geological Journal 4, 343-360.
- KLEEMAN, J.D. and LOVERING, J.F. 1967a. Uranium distribution in rocks by fission-track registration in lexan plastic. Science 156, 512-513.
- KOMAROV, A.N. and SKOVORODKIN, N.V. 1969. Investigation of the abundance and distribution of uranium in ultra-mafic and mafic rocks by fission track methods. Geochemistry International 6, 127-133.
- KOMAROV, A.N., SHIKOLYUKOV, Yu.A. and SKOVORODKIN, N.V. 1967. Investigation of the content and distribution of uranium in some rocks and minerals by neutron activation analysis by counting fission

- fragment tracks. Geochemistry International 4, 647-659.
- KRAUSKOPF, K.B. 1967. Introduction to Geochemistry. McGraw-Hill, pp721.
- KRETZ, R. 1959. Chemical study of garnet, biotite and hornblende from gneisses of southwestern Quebec, with emphasis on distribution of elements in coexisting minerals. Journal of Geology 67, 371-402.
- KRETZ, R. 1961. Some applications of thermodynamics to coexisting minerals of variable compositions. Examples: orthopyroxene-clinopyroxene and orthopyroxene-garnet. Journal of Geology 69, 361-387.
- LAOUAR, R. 1987. A sulphur isotope study of the Caledonian granites of Britain and Ireland. M.Sc. thesis, University of Glasgow (unpubl.).
- LANGMUIR, D. 1978. Uranium solution - mineral equilibria at low temperatures with applications to sedimentary ore deposits. Geochimica et Cosmochimica Acta 42, 547-569.
- LEAKE, B.E. 1958a. The Cashel-Lough Wheelaun intrusion, Co. Galway, Ireland. Proceedings of the Royal Irish Academy 59B, 155-203.
- LEAKE, B.E. 1958b. Composition of pelites from Connemara, Co. Galway, Ireland. Geological Magazine 95, 281-296.
- LEAKE, B.E. 1964. New light on the Dawros Peridotite, Connemara, Ireland. Geological Magazine 101, 63-75.
- LEAKE, B.E. 1967. Zoned garnets from the Galway granite and its aplites. Earth and Planetary Science Letters 3, 311-316.
- LEAKE, B.E. 1969. The origin of the Connemara migmatites of the Cashel district, Connemara, Ireland. Quarterly Journal of the Geological Society London 125, 219-276.
- LEAKE, B.E. 1970. The fragmentation of the Connemara basic and ultrabasic intrusions. In NEWALL, G. and RAST, N. (eds). Mechanisms of Igneous Intrusion. Geological Journal Special Issue 2, 103-122.
- LEAKE, B.E. 1972. Garnetiferous striped amphibolites from Connemara, western Ireland. Mineralogical Magazine 38, 649-665.
- LEAKE, B.E. and SKIRROW, G. 1960. The pelitic hornfelses of the Cashel-Lough Wheelaun intrusion, Co. Galway, Eire. Journal of Geology 68, 23-40.
- LEAKE, B.E., HENDRY, G.L., KEMP, A., PLANT, A.G., HARVEY, P.K., WILSON, I.R., COATS, J.S., AUCOTT, J.W., LUNEL, T. and HOWARTH, R.J. 1969. The chemical

- analysis of rock powders by automatic X-ray fluorescence. Chemical Geology 5, 7-86.
- LEAKE, B.E. *et al.* 1981. The Geology of Connemara. 1:63360 geological map. University of Glasgow.
- LEGGO, P.J., COMPSTON, W. and LEAKE, B.E. 1966. The geochronology of the Connemara granites and its bearing on the antiquity of the Dalradian series. Quarterly Journal of the Geological Society London 122, 91-118.
- LOOMIS, T.P. 1978. Multicomponent diffusion in garnet: I. Formation of isothermal models. American Journal of Science 278, 1099-1118.
- LOOMIS, T.P. 1978a. Multicomponent diffusion in garnet: II. Comparison of models with natural data. American Journal of Science 278, 1119-1137.
- LOPATKINA, A.P. 1964. Characteristics of migration of uranium in the natural waters of humid regions and their use in the determination of the geochemical background for uranium. Geochemistry International 4-6, 788-795.
- LOVERING, T.S. 1935. Theory of heat conduction applied to geological problems. Bulletin of the Geological Society of America 46, 69-94.
- LOVERING, T.S. 1936. Heat conduction in dissimilar rocks and the use of thermal models. Bulletin of the Geological Society of America 47, 87-100.
- LOVERING, T.S. 1955. Temperatures in and near intrusions. Economic Geology 50th anniversary volume, 249-281.
- LUTH, W.C. JAHNS, R.H. and TUTTLE, O.F. 1964. The granite system at pressures of 4 to 10 kbs. Journal of Geophysical Research 69, 759-773.
- LYONS, J.B. and MORSE, S.A. 1970. Mg/Fe partitioning in garnet and biotite from some granitic, pelitic and calcic rocks. American Mineralogist 55, 231-245.
- MACKENZIE, A.B., SCOTT, R.D. and SMELLIE, J.A.T. 1986. A comparison of neutron activation and alpha spectroscopy analyses of thorium in crystalline rocks. Journal of Radioanalysis and Nuclear Chemistry Letters 103, 321-330.

- MANNING,D.A.C.1981.The effect of fluorine on liquidus phase relationships in the system Qz:Ab:Or with excess water at 1kb. Contributions to Mineralogy and Petrology 76, 206-215.
- MANNING,D.A.C. and PICHAVANT,M.1983.The role of fluorine and boron in the generation of granitic melts. In ATHERTON,M.P. and GRIBBLE,C.D. (eds). Migmatites, melting and metamorphism. Shiva, Orpington 94-109.
- MASON,R.1978.Petrology of the Metamorphic Rocks (volume 3). George Allen and Unwin/Thomas Murby.
- MCCARTY,T.S. and KABLE,E.J.C.1978.On the behaviour of rare-earth elements during partial melting of granitic rocks. Chemical Geology 22, 21-29.
- MEAGHER,E.P.1982.Silicate garnets in orthosilicates. In RIBBE,P.H. (ed.) Reviews in Mineralogy 5, 25-66.
- MEHNERT,K.R. 1968. Migmatites and Origin of Granitic Rocks. Elsevier, Amsterdam, 393pp.
- MISCH,P.1968.Plagioclase compositions and non anatectic origin of migmatitic gneisses in northern Cascade Mountains of Washington State. Contributions to Mineralogy and Petrology 17, 1-70.
- MIYASHIRO,A. 1953. Calcium-poor garnet in relation to metamorphism. Geochimica et Cosmochimica Acta 4, 179-208.
- MOORBATH, S., BELL, K., LEAKE, B.E. and MCKERROW, W.S. 1968. Geochronological studies in Connemara and Murrisk, Western Ireland. In HAMILTON,E.I. and FARQUHAR,R.M. (eds). Radiometric Dating for Geologists. Wiley-Interscience, London, 259-298.
- MORRIS,R.V. and HASKIN,L.A.1974.EPR measurement of the effects of glass composition on the oxidation states of europium. Geochimica et Cosmochimica Acta 38, 1435-1445.
- MORTON,W.H.1964.The petrology and structure of the basic igneous complex at Roundstone, Co. Galway, Eire. Ph.D. thesis, University of Manchester (unpubl.).
- NANCE,W.B. and TAYLOR,S.R.1976.Rare earth element patterns and crustal evolution I: Australian Post-Archean sedimentary rocks. Geochimica et Cosmochimica Acta 40, 1539-1551.

- NEWTON,R.C. and HASELTON,H.T.1981.Thermodynamics of the garnet-plagioclase- Al_2SiO_5 -quartz geobarometer. In NEWTON,R.C., NAVROTSKY,A. and WOOD,B.J.(eds). Thermodynamics of Minerals and Melts. Springer-Verlag, New York, 131-147.
- NICOL,J.1866.On the geological structure of southern Grampians. Quarterly Journal of the Geological Society London 19, 180-209.
- NORRICH, K. and CHAPPELL, B.W. 1967. X-ray fluorescence spectrography. In ZUSSMANN,J. (ed.) Physical Methods in Determinative Mineralogy. Academic Press, London 161-214.
- OLSEN,S.N.1977.Origin of the Baltimore gneiss migmatites at Piney Creek, Maryland. Bulletin of the Geological Society of America 88, 1089-1101.
- OLSEN,S.N.1984.Mass-balance and mass-transfer in migmatites from the Colorado Front Range. Contributions to Mineralogy and Petrology 85, 30-44.
- ORVILLE,P.M.1972.Plagioclase cation exchange equilibria with aqueous chloride solution: results at 700°C and 2000 bars in the presence of quartz. American Journal of Science 272, 234-272.
- OSBERG,P.H. 1971. An equilibrium model for Buchan-type metamorphic rocks south-central Maine. American Mineralogist 56, 570-586.
- PHINNEY,W.C.1963.Phase equilibria in metamorphic rocks of St Paul Island and Cape North, Nova Scotia. Journal of Petrology 4, 90-130.
- PICHAVANT,M.1981.An experimental study of the effect of boron on a water saturated haplogranite at 1 kbar vapour pressure. Geological applications. Contributions to Mineralogy and Petrology 76, 430-439.
- PIGAGE, L.C. and GREENWOOD, H.J. 1982. Internally consistent estimates of pressure and temperature: the staurolite problem. American Journal of Science 282, 943-969.
- PITCHER,W.S. and BERGER,A.R.1972.The Geology of Donegal: a Study of Granite Emplacement and Unroofing. Wiley, London, 435pp.
- PLILER,R. and ADAMS,J.A.S 1962.The distribution of thorium, uranium and potassium in the Mancos shale. Geochimica et Cosmochimica Acta 26, 1115-1135.

- POUPEAU,G.1981.Precision, accuracy and meaning of fission track ages. Earth and Planetary Science Letters 90, 403-436.
- RASTAL,R.H. 1910. The Skiddaw granite and its metamorphism. Quarterly Journal of the Geological Society London 66, 116-141.
- READ,H.H.1923.The petrology of the Arnage district in Aberdeenshire: a study of assimilation. Quarterly Journal of the Geological Society London 79, 446-486.
- READ,H.H.1924.On certain xenoliths associated with the contaminated rocks of the Huntley mass, Aberdeenshire. Geological Magazine 61, 433-444.
- READ,H.H.1931.On corundum-spinel xenoliths in the gabbro of Haddo House, Aberdeenshire. Geological Magazine 68, 446-453.
- READ,H.H.1935.The gabbros and associated xenolithic complexes of the Haddo House district, Aberdeenshire. Quarterly Journal of the Geological Society London 91, 591-635.
- READ,H.H.1966.On orthonorite containing spinel xenoliths with late diaspore at Mill of Boddam, Inch, Aberdeenshire. Proceedings of the Geological Association 77, 65-77.
- READ,H.H. and WATSON,J.1962.Introduction to Geology, volume 1. Macmillan.
- RICH,R.A., HOLLAND, H.D. and PETERSON,U. 1977. Hydrothermal uranium deposits. In Developments in Economic Geology 6, Elsevier, 264pp.
- RICHARDSON,S.W. and POWELL,R. 1976. Thermal causes of the Dalradian metamorphism in the central highlands of Scotland. Scottish Journal of Geology 12, 237-268.
- RICHARDSON,S.W.,GILBERT,M.C. and BELL,P.M. 1969. Experimental determination of kyanite-andalusite and andalusite-sillimanite equilibria: the aluminium silicate triple point. American Journal of Science 267, 259-272.
- RILEY,J.P.1958.Simultaneous determination of water and carbon dioxide in rocks and minerals. Analyst 83, 42-49.
- ROGERS,N.W.1977.Granulite xenoliths from Lesotho Kimberlites and the lower continental crust. Nature 270, 681-684.
- ROTHSTEIN,A.T.V.1964. New light on the Dawros peridotite. Geological

Magazine 101, 283-285.

- SAXENA, S.K. 1969. Silicate solid solutions and geothermometry:3. Distribution of Fe and Mg between coexisting garnet and biotite. Contributions to Mineralogy and Petrology 22, 259-267.
- SEN, S.K. and CHAKRABORTY, K.R. 1968. Magnesium-iron exchange in garnet-biotite and metamorphic grade. Neues Jahrbuch Mineral Abh. 108, 181-207.
- SENIOR, A. and LEAKE, B.E. 1978. Regional metasomatism and the geochemistry of the Dalradian metasediments of Connemara, western Ireland. Journal of Petrology 19, 585-625.
- SERGEYEVA, E.I., NIKITIN, A.A., KHODAKOVSKIY, I.L. and NAUMOV, G.B. 1972. Experimental investigation of equilibria in the system $UO_3-CO_2-H_2O$ in 25-200°C temperature interval. Geochemistry International 9, 900-910.
- STORZER, D. and WAGNER, G.A. 1982. The application of fission track dating in stratigraphy: a critical review. In ODIN, G.S. (ed.) Numerical Dating in Stratigraphy. John Wiley and Sons.
- STUCKLESS, J.S. and NKOMO, I.T. 1978. Uranium-lead isotope systematics in uraniumiferous alkali-rich granites from the Granite Mountains, Wyoming: implications for uranium source rocks. Economic Geology 73, 427-441.
- STUCKLESS, J.S., NKOMO, I.T., WENNER, D.B. and VAN TRUMP, G. 1983. Geochemistry and uranium favourability of the postorogenic granites of the northwestern Arabian shield, Kingdom of Saudi Arabia. Bulletin of the Faculty of Earth Sciences, King Abdulaziz University 6, 195-209.
- STURT, B.A. 1962. The composition of garnets from pelitic schists in relation to the grade of regional metamorphism. Journal of Petrology 3, 181-191.
- SUN, C.O., WILLIAMS, R.J. and SUN, S.S. 1974. Distribution coefficients of Eu and Sr for plagioclase-liquid and clinopyroxene-liquid equilibria in oceanic ridge basalt: an experimental study. Geochimica et Cosmochimica Acta 38, 1415-1433.
- SZALAY, A. 1964. Cation exchange properties of humic acids and their

- importance in the geochemical enrichment of UO_2^{++} and other cations. Geochimica et Cosmochimica Acta 28, 1605-1614.
- SZALAY, A. and SAMSONI, Z. 1969. Investigation of the leaching of uranium from crushed magmatic rocks. Geochemistry International 6, 613-623.
- TANNER, P.W.G. and SHACKLETON, R.M. 1979. Structure and stratigraphy of the Dalradian rocks of the Bennabeola area, Connemara, Ireland. In HARRIS, A.L., HOLLAND, C.H. and LEAKE, B.E. (eds) The Caledonides of the British Isles-reviewed. Special Publications of the Geological Society London 8.
- TAYLOR, S.R. and MCLENNAN, S.M. 1985. The Continental Crust: its Composition and Evolution. Blackwell Scientific Publications, pp312.
- THOMPSON, A.B. 1976. Mineral reactions in pelitic rocks: II. Calculation of some P-T-X (Fe-Mg) phase relations. American Journal of Science 276, 425-454.
- THOMPSON, A.B. 1982. Dehydration melting of pelitic rocks and the generation of H_2O - undersaturated granitic liquids. American Journal of Science 282, 1567-1595.
- THOMPSON, A.B. and TRACY, R.J. 1979. Model systems for anatexis of pelitic rocks. II. Facies series melting and reactions in the system $\text{KAlO}_2\text{-NaAlO}_2\text{-Al}_2\text{O}_3\text{-SiO}_2\text{-H}_2\text{O}$. Contributions to Mineralogy and Petrology 70, 429-438.
- TILLEY, C.E. 1924. Contact-metamorphism in the Comrie area of the Perthshire Highlands. Quarterly Journal of the Geological Society London 80, 22-71.
- TOOLE, J. 1985. Marine chemistry of uranium: studies by particle track analysis and alpha spectrometry. Ph.D. thesis, University of Glasgow (unpubl.).
- TRACY, R.J. 1978. High grade metamorphic reactions and partial melting in pelitic schist, west-central Massachusetts. American Journal of Science 278, 150-178.
- TRACY, R.J. and ROBINSON, P. 1983. Acadian migmatite types in pelitic rocks of central Massachusetts. In ATHERTON, M.P. and GRIBBLE, C.D. (eds). Migmatites. Melting and Metamorphism. Shiva, Orpington, 163-173.

- TRACY, R.J., ROBINSON, P. and THOMPSON, A.B. 1976. Garnet composition and zoning in the determination of temperature and pressure of metamorphism, central Massachusetts. American Mineralogist 61, 762-775.
- TRELOAR, P.J. 1981. Garnet-biotite-cordierite thermometry and barometry in the Cashel thermal aureole, Connemara, Ireland. Mineralogical Magazine 44, 183-189.
- TRELOAR, P.J. 1985. Metamorphic conditions in central Connemara, Ireland. Journal of the Geological Society London 142, 183-189.
- TUREKIAN, K.K. and WEDEPOHL, K.H. 1961. Distribution of the elements in some major units of the earth's crust. Bulletin of the Geological Society of America 72, 175-192.
- TUREKIAN, K.K. and KULP, J.L. 1956. The geochemistry of strontium. Geochimica et Cosmochimica Acta 10, 245-296.
- TURNER, F.J. 1968. Metamorphic Petrology. New York: McGraw Hill, pp403.
- TUTTLE, O.F. and BOWEN, N.L. 1958. Origin of granite in the light of experimental studies in the system $\text{NaAlSi}_3\text{O}_8\text{-KAlSi}_3\text{O}_8\text{-SiO}_2\text{-H}_2\text{O}$. Memoirs of the Geological Society of America 74, 153pp.
- VAN BREEMAN, O., AFTALION, M., PANKHURST, R.J. and RICHARDSON, S.W. 1979. Age of the Glen Dessary syenite Inverness-shire: diachronous Paleozoic metamorphism across the Great Glen. Scottish Journal of Geology 15, 49-62.
- VAN DER PLAS, L. and TOBI, A.C. 1965. A chart for judging the reliability of point counting results. American Journal Science. 263, 87-90
- WAGER, L.R. 1932. The geology of the Roundstone district, Co. Galway. Proceedings of the Royal Irish Academy 41B, 46-72.
- WAGER, L.R. 1939. Outline of the geology of Connemara. Proceedings of the Geological Association London 50, 346-351.
- WAGNER, G.A. 1968. Fission track dating of apatites. Earth and Planetary Science Letters 4, 411-415.
- WAKAT, M.A. 1971. Nuclear Data Tables A., volume 8, pp.445.
- WALSH, J.N. 1980. The simultaneous determinations of the major minor and true constituents of silicate rocks using Inductively Coupled Plasma spectrometry. Spectrochimica Acta 35, 107-111.

- WALSH, J.N. 1982. Whole rock analysis by Inductively Coupled Plasma spectrometry in sampling and analysis for the mineral industry. Institute of Mining and Metallurgy 79-91.
- WALSH, J.N. 1985. The determination of boron levels in rocks by ICP spectrometry. Analyst (in press).
- WALSH, J.N. and HOWIE, R.A. 1980. An evaluation of the performance of an inductively coupled plasma source spectrometer for the determination of the major and trace constituents of silicate rocks and minerals. Mineralogical Magazine 43, 967-974.
- WALSH, J.N. and HOWIE, R.A. 1986. Recent developments in analytical methods: uses of inductively coupled plasma source spectrometry in applied geology and geochemistry. Applied Geochemistry 1, 161-171.
- WALSH, J.N., BUCKLEY, F. and BARKER, J. 1981. The simultaneous determination of the rare-earth elements in rocks using inductively coupled plasma source spectrometry. Chemical Geology 33, 141-153.
- WARD, C.D. 1987. Rare earth element distribution within the Dartmoor granite, SW England: the importance of accessory phases during petrogenesis and effects of secondary alteration. In preparation at Royal Holloway and Bedford College, Egham.
- WEDEPOHL, K.W. 1978. Handbook of Geochemistry. Springer-Verlag, Berlin. II-1(12); II-2(22,23); III-3(24,26,27,28,31) II-4 (37,38, 40,56); II-5(90,92).
- WELLS, P.R.A. and RICHARDSON, S.W. 1980. Thermal evolution of metamorphic rocks in the Central Highlands of Scotland. In HARRIS, A.L., HOLLAND, C.H. and LEAKE, B.E. (eds). The Caledonides of the British Isles - reviewed. Special Publications of the Geological Society of London 8, 339-344.
- WHITE, A.J.R. and CHAPPELL, B.W. 1977. Ultrametamorphism and granitoid genesis. Tectonophysics 43, 7-22.
- WHITE, A.J.R. and CHAPPELL, B.W. 1983. Granitoid types and their distributions in the Lachlan Fold Belt, Southeastern Australia. Memoirs of the Geological Society of America 159, 21-34.
- WHITTAKER, E.J.W. and MUNTUS, R. 1970. Ionic radii for use in

- geochemistry. Geochimica et Cosmochimica Acta 34, 945-956.
- WILSON, J.R. and LEAKE, B.E. 1972. The petrochemistry of the epidiorites of the Tayvallich Peninsula, north Knapdale, Argyllshire. Scottish Journal of Geology, 8 215-252.
- WINKLER, H.G.F. 1976. Petrogenesis of Metamorphic Rocks (4th edition). Springer-Verlag, New York, pp334.
- WINKLER, H.G.F. 1979. Petrogenesis of Metamorphic Rocks (fifth edition) Springer-Verlag, New York, 348pp.
- WINKLER, H.G.F. and VON PLATTEN, H. 1960. Experimentelle gesteinsmetamorphose - II Analektische Ultrametamorphose Kalkhaltiger tone. Geochimica et Cosmochimica Acta 18, 294-316.
- WINKLER, H.G.F. and BREITBARTH, R. 1978. New aspects of granitic magma. Neues Jahrb. Mineral. Mh. 1978, 463-480.
- WOODLAND, A.W. 1979. Geological map of the United Kingdom north (3rd edition). Institute of Geological Sciences.
- WOLLENBERG, H.A. 1972. Fission-track radiography of uranium and thorium radioactive minerals. In Geochemical Exploration, London. Institute of Mining and Metallurgy, 347-358.
- WYLLIE, B.K.N. and SCOTT, A. 1913. The plutonic rocks of Garabal Hill. Geological Magazine 50, 536-545.
- YARDLEY, B.W.D. 1975. On some quartz-plagioclase veins in the Connemara schists. Geological Magazine 112, 183-190.
- YARDLEY, B.W.D. 1976. Deformation and metamorphism of Dalradian rocks and the evolution of the Connemara cordillera. Journal of the Geological Society London 132, 521-542.
- YARDLEY, B.W.D. 1977c. An empirical study of diffusion in garnet. American Mineralogist 62, 793-800.
- YARDLEY, B.W.D. 1978. Gnesis of the Skagit Gneiss migmatites, Washington and the distinction between possible mechanisms of migmatization. Bulletin Geological Society of America 89, 941-951
- YARDLEY, B.W.D., LEAKE, B.E. and FARROW, C.M. 1980. The metamorphism of Fe-rich pelites from Connemara, Ireland. Journal of Petrology 21, 365-399.
- YARDLEY, B.W.D., SHEPHERD, T.J. and BARBER, J.P. 1983. Fluid inclusion

studies of high grade rocks from Connemara, Ireland. In
ATHERTON, M.P. and GRIBBLE, C.D. (eds) Migmatites, Melting and
Metamorphism. Shiva, Orpington, 110-126.

YARDLEY, B.W.D., BARBER, J.P. and GRAY, J.R. 1987. The metamorphism of
the Dalradian rocks of western Ireland and its relation to tectonic
setting. Philosophical Transactions of the Royal Society of London
321, 243-270.

ZIELINSKI, R.A., PETERMAN, Z.E., STUCKLESS, J.S., ROSHOLT, J.N. and
NKOMO, I.T. 1981. The chemical and isotopic record of rock-water
interaction in the Sherman Granite, Wyoming and Colorado.
Contributions to Mineralogy and Petrology. 78, 209-219

... ..

... ..

... ..

... ..

APPENDICES

... ..

... ..

... ..

where \dots

... ..

... ..

Appendix 1 : summary of the equations used in geothermometry and geobarometry

A- equations used in geothermometry.

1° = Garnet biotite geothermometry

$$T(^{\circ}\text{K}) = \frac{2740 + 0.023P(\text{bars})}{\text{Ln}K_D + 1.56} \pm 50^{\circ}\text{C} \quad \text{Thompson(1976)}$$

$$T(^{\circ}\text{K}) = \frac{6150 + 0.0246P(\text{bars})}{\text{RLn}K_D + 3.93} \pm 50^{\circ}\text{C} \quad \text{Holdaway and Lee(1971)}$$

$$T(^{\circ}\text{C}) = \frac{4151 + 0.019P(\text{bars})}{\text{RLn}K_D + 1.554} \pm 50^{\circ}\text{C} \quad \text{Ferry and Spear(1978)}$$

where

$$K_D = \frac{X_{\text{Fe}}^{\text{gt}} \cdot X_{\text{Mg}}^{\text{bio}}}{X_{\text{Mg}}^{\text{gt}} \cdot X_{\text{Fe}}^{\text{bio}}}$$

Correction of Hodges and Spear (1982, equation 9).

$$K_D = \left(\frac{X_{\text{Fe}}^{\text{gt}} \cdot X_{\text{Mg}}^{\text{bio}}}{X_{\text{Mg}}^{\text{gt}} \cdot X_{\text{Fe}}^{\text{bio}}} \right) \cdot \left(\frac{a_{\text{Fe}}^{\text{gt}}}{a_{\text{Mg}}^{\text{gt}}} \right)$$

where a = activity and

$$\text{Ln} \left(\frac{a_{\text{Fe}}^{\text{gt}}}{a_{\text{Mg}}^{\text{gt}}} \right) = - \left(\frac{[3300 - 1.5T(^{\circ}\text{C})](X_{\text{Ca}}^2 + X_{\text{Fe}}X_{\text{Ca}} + X_{\text{Mn}}X_{\text{Ca}}X_{\text{Mg}}X_{\text{Ca}})}{\text{RT} (^{\circ}\text{K})} \right) + \left(\frac{W_{\text{MgMn}}(X_{\text{Mn}}^2 + X_{\text{Ca}}X_{\text{Mn}} + X_{\text{Fe}}X_{\text{Mn}} + X_{\text{Mg}}X_{\text{Mn}})}{\text{RT} (^{\circ}\text{K})} \right)$$

where

W_{MgMn} is the Margule parameter for MgMn solid solutions in garnet. It was taken equal to zero as suggested by the authors.

Correction of Indares and Martignole(1985, equations 18 and 19).

Equation 18:

$$T(^{\circ}\text{C}) = \frac{4151 + 0.019P(\text{bars}) + (-4.54X_{\text{Al}}^{\text{bio}} - 6767X_{\text{Tl}}^{\text{bio}}) + (3300 - 1.5)X_{\text{Ca}}^{\text{gt}}}{R \ln K_D + 1.554}$$

Equation 19:

$$T(^{\circ}\text{C}) = \frac{4151 + 0.019P(\text{bars}) + (-1590X_{\text{Al}}^{\text{bio}} - 7451X_{\text{Tl}}^{\text{bio}}) + (3000(X_{\text{Ca}}^{\text{gt}} + X_{\text{Mn}}^{\text{gt}}))}{R \ln K_D + 1.554}$$

where
$$K_D = \frac{X_{\text{Fe}}^{\text{gt}} \cdot X_{\text{Mg}}^{\text{bio}}}{X_{\text{Mg}}^{\text{gt}} \cdot X_{\text{Fe}}^{\text{bio}}}$$

2^o) = Garnet-cordierite geothermometry

$$T(^{\circ}\text{C}) = \frac{2725 + 0.0155P(\text{bars})}{\ln K_{D1} + 0.896} \pm 75 \quad \text{Thompson (1976)}$$

$$T(^{\circ}\text{C}) = \frac{6150 + 0.0303P(\text{bars})}{R \ln K_{D1} + 2.69} \pm 75 \quad \text{Holdaway and Lee(1977)}$$

where
$$K_{D1} = \frac{X_{\text{Fe}}^{\text{gt}} \cdot X_{\text{Mg}}^{\text{bio}}}{X_{\text{Mg}}^{\text{gt}} \cdot X_{\text{Fe}}^{\text{bio}}}$$

B- Equations used in geobarometry

1^o) Garnet-plagioclase geobarometer

a) Ghent (9176)

$$11675 - 32.815T(^{\circ}\text{K}) + 1.301[P(\text{bars}) - 1] + RT(^{\circ}\text{K}) \ln K_{D3}$$

where
$$K_{D3} = \frac{X_{\text{Ca}}^{\text{plagio}}}{X_{\text{Ca}}^{\text{gt}}}$$

b) Newton and Haselton (1981)

$$\Delta G^0 = -RT \ln \left(\frac{a_{\text{Ca}^{\text{gt}}}}{a_{\text{Ca}^{\text{gt}}}} \right) + P(\text{bars}) \Delta \bar{V} = 0$$

where $\Delta G^0 = -P^0 \Delta V^0$

$P^0 = -1.17 + 0.0238T(^{\circ}\text{C})$ (for sillimanite)

$\Delta V^0 =$ end member volume change to be found for the specific garnet composition under study (see published calibration for detail).

$$a_{\text{Ca}^{\text{plagio}}} = \frac{X_{\text{Ca}^{\text{plagio}}}(1 + X_{\text{Ca}^{\text{plagio}}})^2}{4} \exp \left(\frac{(1 - X_{\text{Ca}^{\text{plagio}}})^2}{RT(^{\circ}\text{K})} (2050 + 9392X_{\text{Ca}^{\text{plagio}}}) \right)$$

$$a_{\text{Ca}^{\text{gt}}} = X_{\text{Ca}^{\text{gt}}} \exp \frac{(3300 - 1.5T(^{\circ}\text{K}))[X_{\text{Mg}}^2 + X_{\text{Mg}}X_{\text{Fe}}]}{RT(^{\circ}\text{K})}$$

$\Delta \bar{V}$ is the partial molal of the reaction and is given by

1) Pyrope-grossular volume

$$V_{\text{Ca}^{\text{gt}}} = A - C \cdot X_{\text{Mg}}^2 + D \left(1 + \frac{Z \cdot X_{\text{Mg}}}{F} \right) \exp \left(\frac{-Z^2}{2} \right)$$

where $Z = \frac{X_{\text{Mg}}^2 - E}{F}$

$A = 125.24; \quad B = -11.205; \quad C = -0.512; \quad D = -0.418; \quad E = 0.94$

$F = 0.083$

b) Almandine-grossular volume

$A = 125.24; \quad B = -8.293; \quad C = -1.482; \quad D = 0.480; \quad E = 0.914$

$F = 0.066$

20 Garnet-cordierite geobarometer

$$P = \frac{27808 - (15.103 - 6R \ln D_3)T(^{\circ}K)}{3.886} \pm 500(\text{bars}) \quad T(1976)$$

$$P = 7631 + (4.2877 \ln D_3 - 4.59)T(^{\circ}K) \pm 500(\text{bars}) \quad \text{H\&L}(1977)$$

$$P = \frac{1 + 13818 - (6.38 - 6 \ln KD_3)T(^{\circ}K)}{2.01609} \pm 400(\text{bars}) \quad \text{W\&R}(1980)$$

$$\text{where } KD_3 = \frac{X_{\text{Fe}}^{\text{gt}}}{X_{\text{Fe}}^{\text{cord}}}$$

T = Thompson(1976)

H&L = Holdaway and Lee(1977)

W&R = Wells and Richardson(1980)

Appendix 2 : results of modal analyses

CASHEL THERMAL AUREOLE

Unhornfelsesd pelites

	Y1	Y2	Y4	Y5'	Y6	Y7	Y8	Y9	Y53
Quartz	11.8	14.8	17.2	29.6	8.2	7.0	30.2	30.2	20.8
Plagio.	34.4	38.4	13.8	28.2	46.0	14.2	27.6	30.8	9.0
K-feld.	0.0	0.0	0.0	0.0	0.4	0.0	0.0	0.0	1.0
Biotite	46.4	44.6	55.0	36.8	40.0	59.6	34.4	31.8	35.0
Garnet	1.6	0.4	2.6	1.4	2.2	3.2	0.6	1.0	1.4
Sillim.	2.0	0.6	7.6	0.2	0.0	13.0	4.6	3.8	3.0
Sericite	3.0	0.0	2.4	2.2	1.0	1.4	1.8	0.4	7.2
Chlorite	0.0	0.4	0.0	0.0	0.0	0.2	0.2	1.4	0.0
Muscovite	0.2	0.0	0.0	0.0	0.0	0.0	0.0	0.0	22.4
Opaque	0.0	0.4	0.0	0.6	1.0	1.2	0.4	0.0	0.0
Zircon	0.0	0.2	0.2	0.2	0.4	0.0	0.0	0.0	0.2
Apatite	0.6	0.2	0.2	0.2	0.8	0.2	0.2	1.0	0.0

Intermediate hornfelses

	Y57	Y79	Y82	Y83	Y3	Y5	Y10	Y13
Quartz	25.6	18.2	21.2	7.4	26.8	15.7	22.8	16.2
Plagio.	25.0	21.4	24.2	25.4	28.2	28.7	33.8	18.4
K-feld.	0.0	0.0	0.0	1.0	0.0	0.0	0.0	2.8
Biotite	44.8	41.8	42.6	37.0	30.0	47.7	35.8	45.4
Garnet	1.8	2.6	4.8	0.0	0.0	2.2	1.6	1.4
Sillim.	0.4	11.8	0.2	2.2	0.4	0.5	1.2	4.2
Sericite	0.2	3.0	7.0	1.6	5.4	1.5	0.8	4.2
Chlorite	0.4	0.0	0.0	0.4	0.6	2.0	0.0	0.0
Muscovite	0.0	0.0	0.0	24.8	1.4	0.0	0.0	3.4
Opaque	0.8	0.6	0.0	0.2	1.0	1.7	0.8	0.0
Zircon	0.8	0.6	0.0	0.0	0.0	0.2	0.4	0.0
Apatite	0.4	0.0	0.0	0.0	0.0	0.5	0.4	0.0
Cordierite	0.0	0.0	0.0	0.0	6.2	1.0	2.4	4.0

Cashel thermal aureole : Continued

	Y23	Y25	Y34	Y36	Y37	Y47	Y49	Y50	Y51
Quartz	3.8	21.6	17.2	9.2	14.0	19.0	18.0	2.0	12.5
Plagio.	4.0	10.2	9.8	13.2	23.2	13.2	13.4	25.0	17.2
K-feld.	0.0	1.0	2.4	0.0	0.0	0.0	0.0	0.0	0.0
Biotite	56.0	27.8	38.8	40.6	35.7	48.8	52.0	43.6	29.1
Garnet	2.2	0.8	2.8	2.2	1.0	0.0	5.2	7.6	0.0
Sillim.	11.0	1.4	0.0	1.2	0.0	9.2	1.6	0.3	1.7
Sericite	6.4	5.4	4.4	12.6	4.0	3.0	2.6	10.0	22.3
Chlorite	0.0	18.2	2.0	2.6	0.0	0.0	0.0	2.3	5.4
Muscovite	14.2	0.0	19.0	1.2	0.0	1.3	0.0	0.0	0.0
Opaque	0.6	3.0	0.2	0.2	1.9	1.5	0.2	2.0	2.1
Zircon	0.8	0.0	0.4	0.2	0.0	0.0	1.2	0.0	0.0
Apatite	0.0	0.0	0.0	0.0	0.2	0.0	1.2	0.0	0.0
Cordierite	1.0	10.6	2.0	16.8	19.8	4.0	5.6	6.6	9.3

Contact hornfelses

	Y52	Y54	Y55	Y81	Y11	Y14	Y15	Y16
Quartz	5.2	30.4	22.2	17.6	10.6	22.4	1.6	9.0
Plagio.	5.6	24.6	21.4	38.6	17.6	8.2	2.0	27.2
K-feld.	0.0	0.0	0.6	0.0	0.0	0.0	0.0	0.0
Biotite	63.2	2.7	20.8	35.6	33.2	2.5	32.8	16.0
Garnet	6.0	0.0	10.2	3.6	12.6	7.5	2.4	16.8
Sillim.	7.8	2.2	0.0	0.0	17.8	0.0	0.0	0.0
Sericite	8.6	7.0	4.6	0.2	4.4	47.0	8.4	0.0
Chlorite	0.0	3.4	0.4	0.0	0.4	17.0	46.0	0.0
Muscovite	0.0	0.0	0.0	0.0	0.0	1.7	3.0	0.0
Opaque	1.2	0.0	0.0	1.0	0.6	1.0	2.4	0.4
Zircon	0.4	0.4	0.0	0.0	0.2	0.0	0.0	0.8
Apatite	0.0	0.0	0.0	1.8	0.0	0.0	0.0	0.4
Cordierite	2.0	4.0	19.8	1.0	2.0	24.2	4.4	29.1
Spinel	0.0	0.0	0.0	0.0	0.0	0.0	0.5	0.05

Cashel thermal aureole continued

	Y17	Y18	Y19	Y20	Y24	Y28	Y29	Y30	Y32
Quartz	7.2	7.6	6.4	11.9	26.0	5.6	1.8	6.8	13.6
Plagio.	38.0	1.6	16.2	17.1	0.8	11.5	31.6	13.8	9.4
K-feld.	0.0	0.0	0.0	0.0	0.0	0.0	0.0	0.0	0.0
Biotite	12.8	10.0	27.0	37.2	26.2	10.7	4.4	11.0	20.2
Garnet	3.8	5.0	7.4	2.3	0.0	6.6	1.0	4.6	13.2
Sillim.	0.0	0.0	0.0	0.7	0.0	0.7	0.0	0.2	0.8
Sericite	6.4	18.6	0.0	0.0	9.0	7.3	2.0	4.2	4.8
Chlorite	0.8	11.6	0.0	0.0	0.8	21.6	5.2	7.2	0.0
Muscovite	0.0	2.4	0.0	23.7	0.0	9.5	0.0	0.0	0.0
Opaque	4.3	2.0	0.4	0.7	6.6	0.9	11.8	5.4	4.4
Zircon	0.0	0.4	0.8	0.0	0.0	0.0	0.0	0.0	0.0
Apatite	0.0	0.2	0.4	0.0	0.2	0.2	0.0	0.0	0.0
Cordierite	15.6	40.6	41.4	6.0	28.4	25.0	41.8	47.2	33.6

	Y33	Y35	Y39	Y40	Y42	Y43	Y45	Y46	Y48
Quartz	5.4	14.0	20.0	18.2	5.6	10.5	28.8	15.0	0.8
Plagio.	0.6	12.6	1.0	1.6	2.6	1.8	5.0	5.6	0.2
K-feld.	0.0	0.0	0.0	0.0	0.0	0.0	1.2	0.0	0.0
Biotite	26.4	7.6	5.7	22.4	28.8	29.3	35.2	20.0	6.6
Garnet	6.2	17.3	0.0	0.0	4.4	6.2	0.0	0.0	3.8
Sillim.	24.6	3.0	3.7	0.4	0.0	4.7	0.8	0.0	0.2
Sericite	3.2	3.3	14.0	1.6	0.0	8.5	5.4	36.6	0.8
Chlorite	1.8	2.0	23.4	0.0	0.0	1.1	0.0	14.0	1.6
Muscovite	0.0	3.3	0.0	0.0	0.0	0.0	2.8	0.0	0.0
Opaque	2.8	2.6	1.7	0.4	0.4	0.0	0.0	0.6	4.8
Zircon	0.0	0.0	0.2	0.4	0.0	0.0	0.0	0.0	0.2
Apatite	0.0	0.0	0.0	0.0	0.0	0.0	0.0	0.0	0.0
Cordierite	28.8	33.6	27.0	55.0	58.2	38.6	20.2	8.0	80.8

Cashel thermal aureole : Continued

	Y60	Y65	Y65	Y68	Y69	Y70	Y71	Y72	Y78
Quartz	0.2	13.8	1.8	9.8	5.8	3.6	12.0	13.6	0.6
Plagio.	0.0	8.6	5.6	5.2	4.5	3.2	3.6	5.6	2.0
K-feld.	0.0	0.0	0.0	1.0	0.0	0.0	0.0	0.0	0.0
Biotite	21.5	27.4	5.2	40.4	32.3	31.2	47.8	20.4	37.2
Garnet	2.7	6.6	14.8	0.0	6.4	3.0	9.8	37.2	13.4
Sillim.	2.6	0.0	20.2	0.0	9.1	0.0	3.8	3.0	43.0
Sericite	13.0	1.0	1.4	1.4	26.0	1.6	4.8	0.0	2.6
Chlorite	8.7	1.4	1.2	0.0	0.4	0.0	2.0	0.0	0.0
Muscovite	0.5	0.0	0.0	2.0	0.0	0.6	12.2	0.0	0.0
Opaque	3.0	1.6	1.0	0.4	0.2	2.2	0.0	0.2	0.4
Zircon	0.2	0.0	0.0	0.4	0.4	0.0	0.6	0.6	0.0
Apatite	0.0	0.0	0.0	0.0	0.0	0.0	0.0	0.0	0.0
Cordierite	46.5	39.6	49.8	40.0	15.2	54.6	3.4	19.0	0.8
Spinel	0.0	0.0	0.5	0.0	0.0	0.0	0.0	0.4	0.0

Pelitic xenoliths

	Y62	Y73	Y80
Quartz	0.0	0.0	0.0
Plagio.	1.0	1.0	2.6
K-feld.	0.0	0.0	0.0
Biotite	12.8	23.8	7.2
Garnet	0.0	0.0	0.0
Sillim.	0.0	0.0	0.0
Sericite	1.6	34.6	32.0
Chlorite	0.0	4.6	0.0
Muscovite	0.0	0.8	0.8
Opaque	38.4	18.2	39.8
Zircon	0.0	0.0	0.0
Apatite	0.0	0.0	0.0
Cordierite	7.6	11.4	10.6
Spinel	2.8	0.5	5.8
Corundum	0.6	0.8	0.5
Orthopyr.	0.0	0.4	0.2
Tourmali.	25.0	3.7	0.00

KEY TO THE CASHEL AUREOLE

Plagio = Plagioclase

K-feld = K-feldspar

Sillim = Sillimanite

Orthopyr = Orthopyroxene

Tourmali = Tourmaline

Comrie thermal aureole : Continued

	Biotite-bearing hornfelses						Contact hornf.	
	Y31	Y38	Y51	Y85	Y86	Y87	Y30	Y53
Chlorite	28.7	27.5	5.7	22.4	21.1	4.3	0.0	0.0
Sericite	38.0	34.5	26.0	42.5	26.2	29.5	0.0	0.0
Quartz	23.7	23.5	20.5	18.0	23.2	15.2	23.57	3.5
Iron ore	1.0	0.2	1.0	2.5	9.2	0.0	0.2	0.0
Epidote	4.7	6.2	4.7	9.2	9.5	1.8	0	0
Plagio	1.0	3.7	2.5	2.5	0.7	1.0	1.70	1.60
Opaque	1.7	1.5	4.0	2.0	1.0	26.2	10.20	12.5
K-feld.	0.0	0.0	acc	acc	acc	1.0	8.0	2.0
Biotite	0.5	2.2	32.2	0.7	8.5	7.2	33.7	30.7
Cordieri	0.0	.0.0	3.2	0.0	0.0	12.7	16.7	45.0
Spinel	0.0	0.0	.0.0	0.0	0.0	0.0	0.8	0.5
Corundum	0.0	0.0	0.0	0.0	0.0	0.0	0.2	1.2
Orthopyr.	0.0	0.0	0.0	0.0	0.0	0.0	4.2	0.0
Other	0.70	0.70	0.20	0.20	0.60	0.80	0.73	0.40
accessories								

	Y61	Y70	Y78
Chlorite	0.0	0.0	0.0
Sericite	0.0	0.0	0.0
Quartz	0.0	0.0	1.3
Iron ore	0.0	0.0	0.0
Epidote	0.30	0.7	0.0
Plagio	9.0	2.0	1.6
Opaque	2.0	10.0	11.3
K-feld.	4.3	10.0	1.0
Biotite	13.2	39.3	0.0
Cordieri.	40.5	12.0	55.2
Spinel	16.1	20.0	26.6
Corundum	1.2	14.0	1.3
Orthopyr.	2.5	0	0
Other	0.70	0.0	1.7
accessories			

KEY TO THE COMRIE AUREOLE

K-feld = K-feldspar

Cordieri. = Cordierite

Orthopyr. = Orthopyroxene

acc = accessory

Appendix three : results of major, trace and RE elementsCASHEL-LOUGH WHEELAUN THERMAL AUREOLE

Unhornfelses pelites

	Y1	Y2	Y4	Y5'	Y6	Y7	Y8	Y9
Major elements(wt%)								
SiO ₂	52.44	54.38	52.99	59.36	54.01	51.06	62.90	63.49
TiO ₂	1.37	1.30	1.42	1.57	1.30	1.35	0.90	0.91
Al ₂ O ₃	20.79	17.43	20.96	16.88	20.06	20.15	17.47	15.97
Fe ₂ O ₃	1.23	1.09	1.24	1.27	1.22	2.84	0.44	1.15
FeO	8.46	8.72	8.74	6.72	8.14	8.58	6.06	5.13
MnO	0.15	0.19	0.17	0.14	0.20	0.22	0.12	0.08
MgO	2.99	3.36	2.80	2.20	2.81	3.12	2.04	2.10
CaO	1.98	2.07	1.34	2.76	2.83	1.52	0.81	1.76
Na ₂ O	3.56	3.54	2.16	3.82	4.06	2.31	1.91	3.59
K ₂ O	3.90	2.91	4.67	2.52	1.46	3.96	4.03	3.07
P ₂ O ₅	0.26	0.14	0.35	0.16	0.49	0.17	0.08	0.16
H ₂ O	3.21	2.73	2.55	1.29	3.72	2.34	1.73	2.06
CO ₂	0.18	0.62	0.13	0.43	0.23	0.17	0.12	0.18
Total	100.5	98.48	99.52	99.12	100.5	97.79	98.61	99.65

Trace elements(ppm)

Rb	115	96	176	99	58	147	116	109
Ba	721	727	1013	634	275	1384	706	829
Zr	272	226	297	343	269	343	254	262
Sr	273	247	158	310	328	299	237	237
Ga	28	25	31	22	32	28	24	19
Ni	36	59	58	39	59	59	44	31
Co	19	37	19	23	35	22	19	10
Cr	125	106	127	108	114	118	103	94
Pb	16	22	16	19	47	19	19	14
Zn	112	141	116	121	131	136	107	90
Cu	22	24	23	18	52	51	44	20

Niggli values

Si	160	175.9	169.4	211.4	170.7	158.4	261.8	253
al	37.39	33.24	39.49	35.44	37.37	36.84	42.85	37.61
fm	38.01	42.46	39.7	35.11	37.66	43.32	35.13	33.11
c	6.47	7.18	4.59	10.54	9.59	5.05	3.61	7.54
alk	18.12	17.11	16.22	18.92	15.39	14.79	18.41	21.74
ti	3.14	3.16	3.41	4.21	3.09	3.15	2.82	2.74
k	0.42	0.35	0.59	0.30	0.19	0.53	0.58	0.36
mg	0.36	0.38	0.34	0.33	0.35	0.33	0.36	0.38
w	0.12	0.10	0.11	0.15	0.12	0.23	0.06	0.17

Cashel thermal aureole : Continued

Interm. hornfel.

	Y53	Y57	Y79	Y82	Y83	Y3	Y5
Major elements(wt%)							
SiO ₂	55.68	62.57	56.52	56.54	53.22	62.64	52.71
TiO ₂	0.97	1.03	1.42	1.12	1.12	0.78	2.192
Al ₂ O ₃	20.18	15.65	21.81	17.99	24.19	15.90	20.01
Fe ₂ O ₃	1.27	1.18	2.11	0.53	0.68	1.60	1.24
FeO	7.43	6.22	7.76	7.0	5.95	4.83	8.03
MnO	0.10	0.17	0.15	0.22	0.10	0.12	0.13
MgO	3.71	1.88	2.79	3.49	2.49	3.40	2.75
CaO	0.41	2.53	1.22	3.50	1.26	1.62	3.02
Na ₂ O	1.02	3.35	2.14	3.09	2.68	2.68	4.18
K ₂ O	6.06	1.35	3.60	2.89	5.15	2.47	3.18
P ₂ O ₅	0.08	0.19	0.07	0.14	0.22	0.05	0.18
H ₂ O	2.66	2.38	2.93	1.74	3.52	2.64	2.03
CO ₂	0.31	0.10	0.11	0.20	0.12	0.28	0.34
Total	99.88	98.6	102.6	98.45	100.7	99.01	99.99

Trace elements(ppm)

Rb	196	54	129	119	117	103	121
Ba	1503	474	851	800	1673	773	689
Zr	206	319	258	300	198	190	390
Sr	84	236	213	260	266	215	347
Ca	29	22	36	28	35	25	30
Ni	58	34	66	46	43	59	60
Co	18	24	33	29	23	20	49
Cr	118	86	119	104	103	127	145
Pb	10	22	25	45	32	31	31
Zn	99	92	150	118	90	127	154
Cu	21	71	8	9	14	101	15

Niggli values

Si	186.3	251.3	183.7	184.5	173.4	244.7	162.4
al	39.8	36.99	41.78	34.6	46.45	36.62	35.89
fm	42.5	35.66	39.77	37.38	29.97	40.3	35.75
c	1.47	10.87	4.25	12.24	4.4	6.78	9.85
alk	16.24	16.48	14.21	15.8	19.17	16.31	18.51
ti	2.44	3.11	3.47	2.75	2.74	2.3	5.01
k	0.8	0.21	0.53	0.38	0.56	0.38	0.33
mg	0.44	0.32	0.34	0.45	0.40	0.49	0.35
w	0.13	0.15	0.20	0.06	0.09	0.23	0.12

Cashel thermal aureole : Continued

Interm. hornfel.

	Y53	Y57	Y79	Y82	Y83	Y3	Y5
Major elements(wt%)							
SiO ₂	55.68	62.57	56.52	56.54	53.22	62.64	52.71
TiO ₂	0.97	1.03	1.42	1.12	1.12	0.78	2.192
Al ₂ O ₃	20.18	15.65	21.81	17.99	24.19	15.90	20.01
Fe ₂ O ₃	1.27	1.18	2.11	0.53	0.68	1.60	1.24
FeO	7.43	6.22	7.76	7.0	5.95	4.83	8.03
MnO	0.10	0.17	0.15	0.22	0.10	0.12	0.13
MgO	3.71	1.88	2.79	3.49	2.49	3.40	2.75
CaO	0.41	2.53	1.22	3.50	1.26	1.62	3.02
Na ₂ O	1.02	3.35	2.14	3.09	2.68	2.68	4.18
K ₂ O	6.06	1.35	3.60	2.89	5.15	2.47	3.18
P ₂ O ₅	0.08	0.19	0.07	0.14	0.22	0.05	0.18
H ₂ O	2.66	2.38	2.93	1.74	3.52	2.64	2.03
CO ₂	0.31	0.10	0.11	0.20	0.12	0.28	0.34
Total	99.88	98.6	102.6	98.45	100.7	99.01	99.99

Trace elements(ppm)

Rb	196	54	129	119	117	103	121
Ba	1503	474	851	800	1673	773	689
Zr	206	319	258	300	198	190	390
Sr	84	236	213	260	266	215	347
Ga	29	22	36	28	35	25	30
Ni	58	34	66	46	43	59	60
Co	18	24	33	29	23	20	49
Cr	118	86	119	104	103	127	145
Pb	10	22	25	45	32	31	31
Zn	99	92	150	118	90	127	154
Cu	21	71	8	9	14	101	15

Niggli values

Si	186.3	251.3	183.7	184.5	173.4	244.7	162.4
al	39.8	36.99	41.78	34.6	46.45	36.62	35.89
fm	42.5	35.66	39.77	37.38	29.97	40.3	35.75
c	1.47	10.87	4.25	12.24	4.4	6.78	9.85
alk	16.24	16.48	14.21	15.8	19.17	16.31	18.51
ti	2.44	3.11	3.47	2.75	2.74	2.3	5.01
k	0.8	0.21	0.53	0.38	0.56	0.38	0.33
mg	0.44	0.32	0.34	0.45	0.40	0.49	0.35
w	0.13	0.15	0.20	0.06	0.09	0.23	0.12

Cashel thermal aureole : Continued

	Y10	Y13	Y23	Y25	Y34	Y36	Y37	Y47
Major elements(wt%)								
SiO ₂	57.61	50.72	45.14	57.93	58.64	54.20	53.77	56.49
TiO ₂	1.25	1.29	1.12	0.73	0.80	1.02	0.90	1.26
Al ₂ O ₃	17.99	20.35	25.32	17.32	18.22	19.9	20.1	19.34
Fe ₂ O ₃	1.56	2.06	1.81	1.55	0.91	1.51	1.55	1.12
FeO	6.9	8.21	8.07	5.76	6.97	7.44	6.93	6.91
MnO	0.11	0.28	0.12	0.17	0.34	0.27	0.23	0.07
MgO	2.95	4.19	4.08	3.17	3.29	3.74	4.15	3.36
CaO	2.15	1.00	0.31	1.71	1.88	0.5	2.09	1.53
Na ₂ O	3.75	1.54	1.19	1.26	1.44	0.96	1.82	3.02
K ₂ O	3.00	6.07	7.34	4.34	3.97	6.46	4.29	3.73
P ₂ O ₅	0.17	0.10	0.07	0.08	0.07	0.05	0.17	0.17
H ₂ O	1.97	3.19	3.62	3.25	2.00	3.08	3.58	3.38
CO ₂	0.23	0.45	0.06	1.75	0.18	0.64	0.66	0.12
Total	99.64	99.45	98.25	99.02	98.71	99.77	100.2	100.5

Trace elements(ppm)

Rb	123	140	224	145	133	198	163	140
Ba	592	1216	1575	1066	710	1026	1270	901
Zr	300	282	266	161	191	204	146	249
Sr	241	165	178	187	194	177	148	190
Ga	26	29	38	22	27	29	30	28
Ni	61	74	68	40	52	76	55	42
Co	18	20	23	21	26	34	31	18
Cr	121	136	137	94	105	128	150	127
Pb	23	34	15	14	19	40	23	19
Zn	154	161	161	113	135	172	147	130
Cu	40	15	5	70	10	26	39	13

Niggli values

Si	193.3	153.3	127.9	216.7	208.7	179.2	169.4	188.5
al	35.58	36.24	42.3	38.2	38.22	38.77	37.33	38.03
fm	38.06	44.31	40.22	40.05	40.63	42.75	41.43	38.8
c	7.73	3.24	0.94	6.85	7.17	1.77	7.06	5.47
alk	18.62	16.21	16.54	14.92	13.98	16.7	14.18	17.71
ti	3.16	2.93	2.39	2.05	2.14	2.54	2.13	3.16
k	0.38	0.72	0.80	0.69	0.64	0.82	0.61	0.45
mg	0.39	0.43	0.43	0.44	0.43	0.43	0.47	0.47
w	0.17	0.18	0.17	0.19	0.11	0.15	0.17	0.13

Cashel thermal aureole : Continued

	Y49	Y50	Y51	Y52	Y54	Y55	Y81
Major elements(wt%)							
SiO ₂	57.35	49.67	56.95	53.36	69.94	59.00	53.74
TiO ₂	1.29	1.80	0.98	1.35	0.84	0.79	1.15
Al ₂ O ₃	18.10	21.89	18.67	20.84	12.86	19.12	18.55
Fe ₂ O ₃	1.38	2.06	2.70	2.03	1.47	1.01	1.29
FeO	7.75	10.27	5.46	8.60	4.34	6.38	7.18
MnO	0.15	0.20	0.17	0.15	0.08	0.12	0.16
MgO	3.38	3.20	3.55	3.26	1.92	3.42	2.19
CaO	1.76	0.74	0.97	1.07	1.00	1.00	3.33
Na ₂ O	2.85	2.43	2.39	3.63	2.56	3.03	3.84
K ₂ O	2.99	4.12	4.81	3.08	2.83	2.18	1.32
P ₂ O ₅	0.19	0.17	0.09	0.16	0.07	0.08	0.49
H ₂ O	2.76	3.70	3.13	3.87	2.49	3.33	2.64
CO ₂	0.13	0.28	0.17	0.10	0.23	0.19	0.66
Total	100.08	100.5	100.04	101.5	100.6	99.65	96.54

Trace elements(ppm)

Rb	117	153	160	114	96	102	54
Ba	828	773	1183	988	759	769	263
Zr	278	153	217	270	334	155	242
Sr	213	140	131	186	145	255	353
Ga	26	31	28	30	17	24	28
Ni	75	76	56	65	31	46	46
Co	20	31	16	22	11	20	26
Cr	165	159	117	122	92	110	99
Pb	10	14	18	27	18	26	40
Zn	134	148	130	132	86	124	79
Cu	17	87	2	50	11	24	69

Niggli values

Si	192.6	147.9	194.2	164.2	340.6	211.8	183.4
al	35.82	38.41	37.53	37.8	36.91	40.45	37.31
fm	42.17	44.39	40.55	41.79	37.00	40.17	34.94
c	6.33	2.36	3.55	3.53	5.22	3.85	12.18
alk	15.68	14.84	18.37	16.88	20.88	15.54	15.58
ti	3.26	4.03	2.51	3.12	3.08	2.13	2.95
k	0.41	0.53	0.57	0.36	0.42	0.32	0.18
mg	0.40	0.32	0.45	0.36	0.38	0.46	0.32
w	0.14	0.15	0.31	0.18	0.23	0.12	0.14

Cashel thermal aureole : Continued				Contact hornfelses				
	Y11	Y14	Y15	Y16	Y17	Y18	Y19	Y20
Major elements(wt%)								
SiO ₂	49.06	66.39	43.81	48.97	47.17	55.06	51.13	53.84
TiO ₂	1.4	0.92	2.11	1.51	2.28	0.99	1.29	1.21
Al ₂ O ₃	22.84	15.34	18.4	21.57	17.1	19.49	21.14	20.00
Fe ₂ O ₃	2.53	2.31	1.53	1.65	3.33	1.42	1.94	6.05
FeO	9.24	4.32	11.23	9.43	13.2	7.54	8.73	4.04
MnO	0.34	0.13	0.22	0.15	0.22	0.22	0.21	0.12
MgO	2.96	2.17	5.41	3.85	5.51	4.02	4.17	3.46
CaO	1.09	0.52	2.25	2.40	3.02	1.20	1.10	0.67
Na ₂ O	1.91	0.93	3.11	2.73	2.74	1.18	1.38	1.59
K ₂ O	4.55	2.89	1.59	2.32	1.63	3.48	3.74	4.39
P ₂ O ₅	0.06	0.08	0.19	0.23	0.09	0.07	0.06	0.12
H ₂ O	4.13	3.35	5.38	3.70	2.86	3.92	2.94	3.78
CO ₂	0.33	0.14	0.45	0.37	0.58	0.48	0.23	0.20
Total	100.4	99.49	95.68	98.88	99.73	99.07	98.06	99.47

Trace elements(ppm)								
Rb	141	62	76	96	51	103	109	98
Ba	1307	981	919	509	560	765	1419	1792
Zr	280	314	541	327	312	206	304	324
Sr	125	72	198	240	312	198	178	152
Ga	38	20	31	34	31	30	31	27
Ni	57	35	93	69	110	60	79	67
Co	31	14	38	32	32	30	36	30
Cr	122	111	223	144	278	110	155	176
Pb	16	7	10	12	13	17	18	26
Zn	145	95	115	167	233	153	164	148
Cu	9	15	116	49	74	76	63	25

Niggli values								
Si	146.8	317.2	122.0	142.87	121.7	186.6	158.1	179.8
al	40.27	43.2	30.21	37.09	26.0	38.93	38.53	39.38
fm	42.01	41.02	51.84	43.37	56.12	45.3	46.31	43.72
c	3.48	2.66	6.72	7.50	8.35	4.36	3.64	2.40
alk	14.22	13.12	11.23	12.04	9.53	11.40	11.52	14.50
ti	3.15	3.31	4.42	3.31	4.42	2.52	3.00	3.04
k	0.61	.67	0.25	0.36	0.28	0.66	0.64	0.64
mg	0.31	0.38	0.43	0.39	0.38	0.45	0.41	0.39
w	0.20	0.32	0.11	0.14	0.19	0.14	0.17	0.57

Cashel thermal aureole continue

	Y22	Y24	Y28	Y29	Y30	Y32	Y33	Y35
Major elements(wt%)								
SiO ₂	63.41	62.18	50.15	47.02	52.93	51.81	40.6	57.56
TiO ₂	0.94	0.64	1.55	1.83	1.60	1.22	2.24	1.09
Al ₂ O ₃	17.27	14.50	22.56	20.34	20.4	20.62	27.89	20.32
Fe ₂ O ₃	3.16	1.52	1.14	8.49	2.72	2.95	2.62	1.11
FeO	4.32	5.20	9.90	7.14	8.18	7.19	12.61	6.72
MnO	0.17	0.13	0.16	0.26	0.09	0.22	0.14	0.11
MgO	1.75	3.72	3.21	2.65	3.21	4.62	5.32	2.39
CaO	1.38	0.59	1.53	1.76	1.34	1.95	0.08	0.80
Na ₂ O	1.07	0.71	2.33	2.32	1.41	0.99	0.24	0.93
K ₂ O	2.87	3.75	2.68	3.70	3.80	3.60	1.42	3.50
P ₂ O ₅	0.09	0.17	0.26	0.10	0.12	0.10	0.05	0.07
H ₂ O	2.52	2.86	4.76	3.77	3.85	3.15	3.49	2.88
CO ₂	0.19	1.66	0.21	0.42	0.94	1.44	0.04	0.23
Total	99.14	97.63	100.4	99.8	100.6	99.86	96.74	97.71

Trace elements(ppm)

Rb	93	150	104	90	97	116	74	81
Ba	910	499	868	1618	1057	958	641	1114
Zr	295	142	258	351	298	168	375	251
Sr	96	81	185	249	116	174	34	134
Ga	20	19	31	41	29	32	53	30
Ni	39	47	94	108	71	79	120	44
Co	10	13	28	55	34	34	48	22
Cr	104	90	150	140	132	164	234	98
Pb	11	11	13	17	37	17	8	14
Zn	82	150	145	146	153	176	264	128
Cu	37	49	910	13	118	61	60	30

Niggli values

Si	274.2	266.9	152.8	135.1	171.2	158.8	106.5	221.5
al	44.02	36.68	40.5	34.45	38.88	37.26	43.13	46.09
fm	37.19	47.38	42.41	46.88	44.22	46.35	53.65	38.55
c	6.39	2.71	4.99	5.42	4.64	6.41	0.22	3.30
alk	12.4	13.22	12.09	13.25	12.26	9.98	2.99	12.06
ti	3.06	2.07	3.55	3.96	3.89	2.81	4.42	3.15
k	0.64	0.78	0.43	0.51	0.64	0.71	0.80	0.71
mg	0.30	0.50	0.34	0.24	0.35	0.46	0.39	0.36
w	0.40	0.21	0.09	0.52	0.23	0.27	0.16	0.13

Cashel thermal aureole : Continued

	Y39	Y40	Y42	Y43	Y44	Y45	Y46	Y58
Major elements(wt%)								
SiO ₂	40.0	55.9	43.46	56.71	58.78	61.16	54.7	49.11
TiO ₂	1.20	0.99	1.56	0.94	0.74	0.80	1.02	1.53
Al ₂ O ₃	30.13	20.01	23.42	19.65	18.75	15.07	19.45	25.24
Fe ₂ O ₃	1.70	0.96	2.24	1.38	1.87	0.91	1.94	1.76
FeO	8.86	6.40	10.57	7.37	5.87	6.00	7.04	7.34
MnO	0.09	0.10	0.21	0.11	0.15	0.12	0.16	0.07
MgO	2.61	4.51	6.52	3.58	3.83	5.56	3.60	3.34
CaO	0.16	0.34	0.07	0.37	1.05	0.84	0.68	0.06
Na ₂ O	0.88	0.91	0.33	0.60	2.40	0.79	1.35	1.04
K ₂ O	7.57	4.68	5.45	4.51	4.33	3.55	3.97	5.43
P ₂ O ₅	0.07	0.04	0.04	0.08	0.11	0.12	0.06	0.11
H ₂ O	4.78	5.00	5.92	4.42	3.00	3.94	4.98	4.82
CO ₂	1.22	0.45	0.15	0.16	0.31	0.12	0.95	0.20
Total	99.27	100.3	99.94	99.98	101.2	98.98	99.9	100.0

Trace elements(ppm)

Rb	171	127	219	154	153	105	146	151
Ba	1547	884	1053	1416	627	1714	983	759
Zr	193	198	265	200	127	156	200	285
Sr	85	76	52	64	147	71	102	99
Ga	42	32	38	32	28	22	31	38
Ni	95	59	100	64	45	45	62	67
Co	39	36	48	32	26	30	28	29
Cr	204	122	191	109	105	88	111	131
Pb	19	24	12	14	20	6	13	16
Zn	142							
Cu	45	5	71	55	148	9	13	10

Niggli values

Si	110.5	193.9	114.6	203.3	200.7	228.2	190.2	154.2
al	49.07	4092	36.4	41.51	37.78	33.14	39.88	46.7
fm	34.76	44.4	53.4	44.67	41.05	52.2	44.23	39.06
c	0.47	1.26	0.20	1.42	3.84	3.36	2.53	0.20
alk	15.71	13.42	10.01	12.4	17.38	11.31	13.36	14.04
ti	2.49	2.58	3.09	2.53	1.90	2.24	2.67	3.61
k	0.85	0.77	0.92	0.83	0.54	0.75	0.66	0.77
mg	0.31	0.53	0.48	0.42	0.47	0.59	0.42	0.40
w	0.15	0.12	0.16	0.14	0.22	0.12	0.20	0.18

Cashel thermal aureole : Continued

	Y60	Y65	Y67	Y68	Y69	Y70	Y71	Y72
Major elements(wt%)								
SiO ₂	42.6	54.17	44.29	45.63	45.55	57.74	55.47	52.88
TiO ₂	2.17	1.04	1.46	1.61	1.94	0.88	1.02	1.28
Al ₂ O ₃	24.25	19.57	30.62	21.38	19.05	18.70	20.41	20.51
Fe ₂ O ₃	1.19	1.72	1.17	0.88	0.91	2.08	2.35	1.69
FeO	10.94	8.90	8.62	9.94	9.28	6.12	6.82	8.83
MnO	0.08	0.20	0.13	0.15	0.15	0.20	0.13	0.09
MgO	4.60	3.91	4.01	6.48	7.03	3.35	4.15	2.82
CaO	0.03	0.44	1.05	3.84	7.40	1.48	0.24	1.46
Na ₂ O	0.95	0.84	1.83	2.05	1.13	1.34	0.63	2.86
K ₂ O	4.83	6.06	2.77	3.19	1.96	4.66	5.67	2.91
P ₂ O ₅	0.12	0.05	0.05	0.06	0.02	0.06	0.05	0.08
H ₂ O	5.67	3.56	2.38	3.66	5.11	2.72	3.60	2.47
CO ₂	0.12	1.30	0.10	0.16	1.00	0.80	0.04	0.67
Total	97.55	101.76	98.48	99.03	99.53	100.13	100.58	98.55

Trace elements(ppm)

Rb	144	183	80	105	72	147	143	95
Ba	1226	1212	326	1682	1050	1011	1221	1103
Zr	376	199	282	186	346	178	174	235
Sr	85	97	183	475	278	210	168	231
Ga	41	31	52	36	31	28	31	37
Ni	77	69	95	88	85	60	72	62
Co	37	41	43	47	44	33	32	32
Cr	172	127	220	220	234	108	131	100
Pb	12	9	12	19	14	33	19	39
Zn	139	153	317	169	184	121	152	158
Cu	15	5	102	16	13	58	7	12

Niggli values

Si	120.9	173.3	120.4	115.9	110.2	202.2	183.9	169.8
al	40.57	36.91	49.07	32	27.77	38.6	39.87	38.82
fm	47.98	46.61	38.25	47.33	46.81	40.82	45.27	41.29
c	0.09	1.51	3.06	10.45	19.61	5.55	0.85	5.02
alk	11.36	14.98	9.63	10.22	5.80	14.96	14.01	14.87
ti	4.63	2.50	2.99	3.08	3.61	2.32	2.54	3.09
k	0.77	0.83	0.50	0.51	0.53	0.70	0.86	0.40
mg	0.41	0.40	0.42	0.52	0.55	0.43	0.45	0.33
w	0.09	0.15	0.11	0.07	0.08	0.23	0.24	0.15

Cashel thermal aureole : Continued		Pelitic xenoliths				BEL	
	Y78	Y26	Y62	Y73	Y80	1470	1586
Major elements(wt%)							
SiO ₂	35.98	34.63	20.74	30.85	24.76	19.11	20.14
TiO ₂	1.53	1.40	1.12	1.49	0.80	4.17	2.24
Al ₂ O ₃	34.93	26.80	37.98	29.17	33.66	30.91	37.36
Fe ₂ O ₃	3.97	8.15	11.96	3.96	10.91	14.23	7.01
FeO	11.73	12.63	9.51	10.17	8.50	16.65	17.10
MnO	0.30	0.13	0.18	0.12	0.10	0.20	0.18
MgO	3.00	7.43	6.48	4.39	6.19	11.47	7.16
CaO	0.15	1.23	4.00	8.72	8.18	0.49	1.02
Na ₂ O	0.39	1.37	1.95	2.07	2.70	0.19	0.93
K ₂ O	3.70	1.24	0.70	2.17	1.41	0.73	0.53
P ₂ O ₅	0.11	0.03	0.03	0.05	0.05	0.03	0.03
H ₂ O	4.40	4.86	4.70	4.65	4.23	3.17	6.20
CO ₂	0.11	0.27	0.29	0.37	0.21	0.49	0.08
Total	100.36	100.17	99.64	98.18	101.7	101.84	99.98
Trace elements(ppm)							
Rb	95	37	18	64	40	28	27
Ba	1485	653	637	857	883	618	300
Zr	206	148	66	132	65	151	162
Sr	83	931	502	882	966	99	198
Ga	59	49	106	66	83	70	68
Ni	109	99	225	110	173	248	186
Co	49	60	136	75	116	117	102
Cr	243	214	422	240	321	615	596
Pb	10	8	6	7	8	0	0
Zn	218	249	875	430	436	981	483
Cu	180	69	76	78	121	49	120
Niggli values							
Si	88.18	73.54	34.25	64.33	43.70	31.27	36.89
al	50.45	33.54	40.29	35.85	35.01	29.81	40.33
fm	42.44	59.16	47.36	37.59	43.32	68.27	55.20
c	0.39	2.80	7.82	19.48	15.47	0.86	2.0
alk	6.71	4.50	4.53	7.07	6.21	1.06	2.27
ti	2.82	2.24	1.57	2.34	1.06	5.13	3.09
k	0.86	0.37	0.19	0.41	0.26	0.72	0.27
mg	0.26	0.40	0.38	0.36	0.38	0.41	0.35
w	0.23	0.34	0.48	0.26	0.54	0.43	0.27

Cashel thermal aureole : Continued

Straumatic migmatite leucosomes.

	Y11L	Y12L	Y42L	Y44L	Y68L	Y69L	Y71L	Y72L
Major elements(wt%)								
SiO ₂	68.28	70.21	68.50	72.28	76.75	72.73	68.12	73.68
TiO ₂	0.46	0.21	0.23	0.04	0.14	0.09	0.49	0.40
Al ₂ O ₃	16.23	17.04	16.12	14.77	12.63	14.40	16.56	13.60
Fe ₂ O ₃	1.34	0.18	0.89	0.18	0.87	0.11	0.56	0.38
FeO	2.20	1.20	2.04	0.40	1.32	0.42	3.29	1.96
MnO	0.05	0.04	0.03	0.01	0.04	0.03	0.04	0.04
MgO	0.82	0.25	1.76	0.04	1.05	0.09	1.61	0.96
CaO	1.62	2.33	1.33	2.35	3.05	1.61	2.43	2.50
Na ₂ O	2.60	5.31	1.33	4.10	2.64	7.38	2.86	3.15
K ₂ O	2.23	1.30	3.42	1.70	0.60	0.46	2.03	1.55
P ₂ O ₅	0.08	0.26	0.11	0.13	0.04	0.17	0.10	0.06
L.O.W	3.29	2.32	3.04	4.19	1.91	2.71	2.61	1.52
Total	99.20	100.65	98.8	99.98	101.0	100.0	100.7	99.8

Trace elements(ppm)

Rb	68	40	124	57	16	14	70	40
Ba	400	277	641	314	496	183	500	200
Zr	30	51	49	0	67	0	120	20
Sr	210	362	149	384	444	489	170	140
Ga	20	16	16	15	17	13	31	13
Ni	8	6	13	2	12	0	17	9
Co	3	3	7	0	2	0	12	2
Cr	9	5	17	2	3	0	6	10
Pb	20	52	19	24	22	36	25	20
Zn	60	37	66	25	70	33	52	50
Cu	20	9	4	34	7	1	12	12
La	22	51	16	10	9	6	40	12
Ce	31	20	21	20	21	8	12	17
Y	31	12	5	9	9	4	38	18

Cashel thermal aureole : continued

Quartz-rich migmatite leucosomes except:(Y38PM = a strongly migmatitized rock; Y42PC = a cordierite phenocryst)

	Y5L	Y40L	Y43L	Y60L	Y65L	Y78L	Y38PM	Y42PC
Major elements(wt%)								
SiO ₂	86.44	78.18	88.55	89.75	93.55	89.22	50.81	42.23
TiO ₂	0.06	0.03	0.05	0.14	0.03	0.33	1.65	0.02
Al ₂ O ₃	6.88	11.40	6.24	5.10	2.26	5.15	21.93	29.78
Fe ₂ O ₃	0.07	0.18	0.43	0.44	0.07	0.31	1.88	2.14
FeO	0.20	0.40	1.56	0.90	0.24	1.00	9.09	3.24
MnO	0.02	0.03	0.03	0.02	0.02	0.01	0.16	0.13
MgO	0.0	0.31	0.80	0.15	0.0	0.18	3.41	5.90
CaO	1.44	1.55	0.24	0.0	1.26	0.46	1.70	0.0
Na ₂ O	2.14	3.19	0.47	1.44	0.61	0.49	1.79	0.36
K ₂ O	0.74	1.57	1.50	0.70	0.65	0.90	3.46	7.65
P ₂ O ₅	0.19	0.05	0.12	0.03	0.05	0.06	0.35	0.01
L.O.W	1.92	2.06	1.51	1.33	0.86	1.64	4.37	5.34
Total	100.1	98.95	101.5	100.0	99.6	99.75	100.6	99.80

Trace elements(ppm)

Rb	21	64	47	28	15	20	99	339
Ba	290	257	366	205	120	382	768	2480
Zr	0	0	0	42	0	287	263	0
Sr	205	242	32	65	48	56	210	81
Ga	7	11	7	8	3	6	28	34
Ni	0	0	7	10	0	1	48	12
Co	0	0	9	0	0	2	32	23
Cr	0	0	0	3	9	19	112	0
Pb	8	25	14	8	4	7	26	9
Zn	12	40	58	44	44	54	121	131
Cu	4	3	52	20	1	7	42	6
La	4	5	8	10	3	16	40	0
Ce	11	21	21	21	11	29	99	0
Y	12	0	6	7	0	7	58	0

Cashel thermal aureole : Continued. Results of REE.

Unhornfesesed rocks

Hornfelses

	Y4	Y7	Y79	Y82	Y36	Y17
La	71.38	87.33	61.50	45.94	47.75	58.19
Ce	144.84	172.06	114.13	92.62	91.51	107.55
Pr	15.67	22.96	13.93	11.92	10.11	13.12
Nd	70.07	75.66	58.17	42.15	41.65	44.82
Sm	12.92	12.28	9.17	7.17	6.51	6.42
Eu	1.87	2.47	2.04	2.06	1.39	1.88
Gd	11.40	10.14	7.24	6.30	5.50	5.18
Dy	9.46	8.76	6.72	5.24	5.32	3.85
Hb	2.06	2.14	1.60	1.12	1.24	0.85
Er	5.48	6.37	4.35	3.24	3.46	2.28
Yb	4.42	5.76	3.65	3.10	2.99	2.90
Lu	0.63	0.84	0.52	0.47	0.45	0.50
Σ REE	350.2	406.77	224.85	221.33	217.88	247.54
Eu/Eu*	0.47	0.67	0.76	0.94	0.71	0.99
(La/Lu)CN	11.76	10.79	12.28	10.15	11.01	12.08

xenoliths

	Y19	Y42	Y68	Y69	Y62	Y80
La	69.74	63.06	37.90	17.79	23.71	13.85
Ce	135.6	121.17	66.51	28.83	38.06	21.12
Pr	14.56	14.94	9.04	3.80	3.88	2.17
Nd	63.16	55.52	28.94	11.35	15.17	8.32
Sm	10.66	8.16	3.99	1.53	1.89	1.00
Eu	2.28	1.16	1.34	1.18	0.90	0.64
Gd	8.91	6.18	3.34	1.16	1.41	0.68
Dy	7.63	3.91	2.67	0.76	0.60	0.38
Hb	1.78	0.83	0.59	0.17	0.12	0.07
Er	4.98	2.51	1.89	0.57	0.39	0.39
Yb	4.45	2.51	1.87	0.70	0.19	0.23
Lu	0.67	0.42	0.30	0.14	0.03	0.03
Σ REE	324.42	280.37	158.38	67.98	86.08	48.88
Eu/Eu*	0.71	0.50	1.12	2.71	1.68	2.37
(La/Lu)CN	10.82	15.60	13.17	13.20	82.82	48.37

Cashel thermal aureole : Continued

	leucosomes			metagabbros	
	Y42L	Y68L	Y69L	XG J002	NXG GJ009
La	15.81	12.60	5.11	26.11	32.16
Ce	26.50	19.98	9.25	61.23	73.65
Pr	3.59	2.66	1.23	7.79	9.17
Nd	11.72	7.61	4.84	35.36	41.93
Sm	1.70	1.24	1.08	6.26	7.77
Eu	1.87	1.10	1.85	1.21	1.91
Gd	1.36	1.08	1.13	5.07	6.39
Dy	0.90	1.08	0.72	3.51	4.63
Hb	0.16	0.28	0.08	0.74	1.04
Er	0.56	0.86	0.34	2.08	2.73
Yb	0.47	0.88	0.13	1.48	2.10
Lu	0.08	0.14	0.02	0.21	0.30
Σ REE	64.72	49.51	25.78	151.05	183.78
Eu/Eu*	3.75	2.91	5.12	0.65	0.82
(La/Lu)CN	20.69	9.62	26.76	12.91	11.13

	Y21(graniets sill)	NF
La	45.61	0.367
Ce	99.05	0.957
Pr	10.80	0.137
Nd	45.04	0.711
Sm	7.08	0.231
Eu	1.52	0.087
Gd	5.22	0.306
Dy	2.86	0.381
Hb	0.58	0.0851
Er	1.64	0.249
Yb	1.06	0.248
Lu	0.18	0.0381

KEY TO THE CASHEL AUREOLE

B.E.L = B.E Leake

L = Leucosome

L.O.W = Lost on weight

NF = Normalizing factors

CN = Chondrite normalized

X.G = xenolithic gabbro

N.X.G = non xenolithic gabbro

Σ REE	220.64
Eu/Eu*	0.76
(La/Lu)CN	26.33

Comrie thermal aureole : Continued

	Y11r	Y12r	Y13r	Y14r	Y15r	Y16s	Y17s	Y18s
Major elements(wt%)								
SiO ₂	58.7	61.99	61.16	61.04	59.78	61.18	58.17	56.57
TiO ₂	1.32	1.31	1.16	1.04	1.20	1.28	1.32	1.20
Al ₂ O ₃	18.73	18.03	16.66	14.25	17.92	17.83	18.08	18.48
Fe ₂ O ₃	2.33	2.25	1.40	2.09	1.19	1.70	1.71	1.82
FeO	6.30	5.09	6.78	9.33	7.05	6.70	7.64	5.98
MnO	0.08	0.13	0.10	0.17	0.08	0.10	0.13	0.10
MgO	2.93	2.11	2.62	3.26	2.76	2.65	2.59	2.62
CaO	0.23	0.46	0.54	1.13	0.38	0.22	1.23	1.80
Na ₂ O	2.88	4.25	3.16	1.92	3.39	2.93	2.48	2.63
K ₂ O	3.24	2.74	2.62	1.60	2.71	3.27	2.93	3.53
P ₂ O ₅	0.22	0.17	0.14	0.11	0.13	0.17	0.14	0.65
H ₂ O	3.09	2.12	3.20	4.20	3.13	2.97	3.19	4.13
CO ₂	0.31	0.47	0.37	0.41	0.17	0.09	0.27	0.32
Total	100.3	101.1	99.91	100.5	99.89	100.1	99.88	99.83

Trace elements(ppm)

Rb	118	97	94	58	95	113	107	124
Ba	614	500	563	281	521	646	553	577
Zr	220	271	254	256	277	289	265	243
Sr	56	111	76	94	69	69	158	152
Ga	28	26	24	20	25	27	27	29
Ni	51	58	49	48	54	62	58	52
Co	16	31	28	31	25	28	25	31
Cr	105	106	96	76	100	107	113	113
Pb	28	22	9	8	10	12	15	21
Zn	29	77	128	147	114	112	135	123
Cu	51	39	40	26	40	41	35	58
Y	56	34	34	22	34	36	35	57
Ce	34	121	85	66	115	105	89	141

Niggli values

Si	213.2	237.7	237.4	228.4	222.3	193.11	209.4	202.8
al	40.09	40.74	38.11	31.42	39.28	39.65	38.35	39.04
fm	41.36	34.87	41.26	53.26	40.56	40.87	41.52	36.83
c	0.90	1.89	2.25	4.53	1.51	0.89	4.74	6.91
alk	17.65	22.50	18.38	10.78	18.65	18.59	15.38	17.21
ti	3.61	3.78	3.39	2.93	3.36	3.63	3.57	3.34
k	0.43	0.30	0.35	0.53	0.34	0.42	0.44	0.47
mg	0.38	0.35	0.37	0.34	0.38	0.36	0.33	0.38
w	0.25	0.28	0.16	0.17	0.13	0.19	0.17	0.21

Comrie thermal aureole : Continued

	Y19s	Y20s	Y21s	Y22s	Y23r	Y24s	Y25s	Y26s
Major elements(wt%)								
SiO ₂	57.28	57.33	57.77	61.04	58.63	59.45	56.91	57.01
TiO ₂	1.17	1.26	1.28	1.18	1.07	1.35	1.02	1.10
Al ₂ O ₃	18.81	20.0	17.74	17.23	19.11	19.00	19.08	20.21
Fe ₂ O ₃	2.30	1.91	3.04	2.08	1.51	1.37	1.29	1.73
FeO	6.92	6.25	6.70	6.12	6.28	4.62	6.99	6.58
MnO	0.12	0.06	0.07	0.11	0.12	0.42	0.12	0.14
MgO	2.81	2.51	3.13	2.72	2.48	2.02	2.68	2.60
CaO	0.66	0.12	0.73	0.49	0.53	0.37	0.39	0.12
Na ₂ O	2.00	2.13	2.73	3.25	2.53	4.03	1.60	2.13
K ₂ O	3.22	4.28	2.45	2.92	3.65	3.46	4.09	4.48
P ₂ O ₅	0.23	0.14	0.12	0.11	0.13	0.14	0.14	0.11
H ₂ O	3.78	3.98	3.49	2.98	3.97	2.87	4.32	2.97
CO ₂	0.20	0.17	0.57	0.31	0.08	0.25	0.27	0.15
Total	99.50	100.1	99.82	100.5	100.0	99.35	98.90	99.33

Trace elements(ppm)

Rb	119	188	84	95	133	122	155	156
Ba	579	876	498	548	633	995	682	655
Zr	231	427	359	254	302	299	245	273
Sr	121	102	97	98	118	111	100	51
Ga	27	29	30	23	29	31	30	29
Ni	60	46	55	51	45	31	55	53
Co	15	26	31	21	24	27	34	31
Cr	96	88	101	99	95	107	98	89
Pb	20	16	37	12	15	12	16	8
Zn	132	114	91	126	115	84	132	140
Cu	55	16	56	33	44	55	26	39
Y	35	55	48	30	43	31	33	42
Ce	100	132	131	86	158	98	141	123

Niggli values

Si	208.3	211.4	206.3	230.9	219.6	232.1	213.7	206.2
al	40.32	43.47	37.34	38.42	42.19	43.72	42.22	43.09
fm	42.58	38.37	44.84	40.62	37.78	30.86	40.59	38.64
c	2.57	0.47	2.79	1.99	2.13	1.55	1.57	0.47
alk	14.52	17.68	15.03	18.97	17.91	23.87	15.62	17.81
ti	3.20	3.49	3.44	3.36	3.01	3.96	2.88	2.99
k	0.51	0.57	0.37	0.37	0.49	0.36	0.63	0.58
mg	0.40	0.36	0.37	0.38	0.37	0.38	0.37	0.36
w	0.18	0.20	0.29	0.23	0.18	0.21	0.14	0.19

Comrie thermal aureole : Continued

	Y28s	Y33r	Y47s	Y48r	Y49r	Y71r	Y72r	Y73r
Major elements(wt%)								
SiO ₂	60.28	62.57	62.84	54.36	58.21	57.51	58.07	59.40
TiO ₂	1.36	0.97	1.19	1.13	1.18	1.21	1.20	1.25
Al ₂ O ₃	18.68	16.94	16.89	19.27	18.71	19.07	17.34	18.32
Fe ₂ O ₃	1.83	2.20	1.67	1.85	1.78	1.70	1.14	1.20
FeO	5.88	6.49	4.41	8.05	6.04	9.96	6.89	6.50
MnO	0.13	0.11	0.06	0.09	0.11	0.07	0.08	0.11
MgO	2.33	2.50	2.28	2.87	2.32	2.54	2.62	2.55
CaO	0.79	0.01	0.57	0.77	0.32	0.14	0.32	0.20
Na ₂ O	3.40	2.74	3.31	2.39	2.91	2.52	2.37	3.63
K ₂ O	2.94	2.60	3.07	3.68	3.28	3.37	2.92	3.03
P ₂ O ₅	0.15	0.10	0.15	0.29	0.15	0.12	0.24	0.14
H ₂ O	3.24	3.51	3.24	4.22	3.26	2.21	4.73	3.88
CO ₂	0.17	0.36	0.20	0.15	0.10	0.13	0.22	0.12
Total	101.2	101.1	99.88	99.12	98.37	100.5	98.14	100.3

Trace elements(ppm)

Rb	101	97	110	132	121	132	131	113
Ba	543	488	606	653	532	678	531	589
Zr	241	181	255	264	311	242	217	374
Sr	156	59	103	106	65	60	91	81
Ga	26	27	25	28	27	27	28	26
Ni	50	47	47	57	50	52	85	49
Co	27	19	31	24	26	29	42	18
Cr	93	82	110	104	85	104	121	97
Pb	26	4	31	13	10	14	26	19
Zn	72	108	58	114	127	121	106	131
Cu	53	37	77	99	48	21	65	32
Y	40	28	40	37	70	23	43	39
Ce	105	52	105	134	182	24	116	65

Niggli values

Si	225.0	249.1	261.0	185.8	222.7	214.4	230.0	223.3
al	41.09	39.75	41.35	38.83	42.20	41.91	40.48	40.59
fm	36.45	43.03	34.65	42.40	37.69	40.41	41.69	38.11
c	3.16	1.04	2.54	2.82	1.31	0.56	1.36	0.81
alk	19.30	17.18	21.46	15.95	18.80	17.13	16.48	20.49
ti	3.82	290	3.72	2.91	3.40	3.39	3.57	3.53
k	0.36	0.38	0.38	0.50	0.43	0.47	0.45	0.35
mg	0.36	0.34	0.41	0.34	0.35	0.35	0.37	0.37
w	0.22	0.23	0.25	0.17	0.21	0.18	0.19	0.14

Comrie thermal aureole : Continued

Interm. hornf.

	Y74r	Y75r	Y76r	Y84r	Y30c	Y31b	Y32c
Major elements(wt%)							
SiO ₂	56.86	58.94	58.30	55.85	61.26	57.71	60.08
TiO ₂	1.01	1.26	1.27	1.00	1.35	1.14	1.41
Al ₂ O ₃	16.17	18.33	18.68	18.47	18.23	20.23	18.36
Fe ₂ O ₃	2.01	1.63	1.52	0.95	1.75	1.74	1.34
FeO	10.49	6.37	6.88	9.70	6.93	6.54	7.04
MnO	0.17	0.08	0.11	0.13	0.07	0.12	0.09
MgO	3.64	2.49	2.57	3.37	2.73	2.19	2.45
CaO	0.24	0.23	0.28	0.36	0.16	0.40	1.04
Na ₂ O	1.48	3.14	2.91	2.31	3.97	2.29	3.20
K ₂ O	2.20	3.07	2.96	2.94	2.49	3.76	3.02
P ₂ O ₅	0.22	0.16	0.16	0.11	0.13	0.11	0.18
H ₂ O	4.71	3.52	4.06	4.52	1.27	3.62	1.64
CO ₂	0.05	0.18	0.16	0.22	0.09	0.38	0.27
Total	99.25	99.40	99.86	99.93	100.4	100.2	100.1

Trace elements(ppm)

Rb	78	117	109	111	85	126	113
Ba	382	636	492	543	459	648	693
Zr	387	277	271	253	254	218	356
Sr	43	81	85	52	72	99	136
Ga	30	27	28	26	24	29	27
Ni	62	54	58	52	64	53	52
Co	20	15	29	29	32	34	28
Cr	63	104	101	89	126	94	105
Pb	21	12	10	26	5	16	6
Zn	243	109	124	163	122	119	120
Cu	23	21	48	44	39	43	33
Y	42	27	44	27	32	29	38
Ce	108	72	151	60	95	101	80

Niggli values

Si	200.7	223.9	217.9	191.0	222.5	213.6	218.4
al	33.63	41.05	41.16	37.23	39.02	44.14	39.33
fm	55.44	39.01	40.11	47.37	40.61	37.18	38.34
c	0.91	0.94	1.12	1.32	0.62	1.59	4.05
alk	10.02	19.01	17.61	14.08	19.75	17.10	18.28
ti	2.68	3.60	3.57	2.57	3.69	3.17	3.85
k	0.49	0.39	0.40	0.46	0.29	0.52	0.38
mg	0.35	0.36	0.36	0.36	0.36	0.32	0.35
w	0.15	0.19	0.17	0.08	0.19	0.19	0.15

Comrie thermal aureole : Continued

	Y37c	Y38b	Y39b	Y40b	Y41b	Y42b	Y50b	Y51b
Major elements(wt%)								
SiO ₂	48.31	58.80	57.18	56.04	53.06	60.32	56.08	59.32
TiO ₂	1.69	1.34	1.47	1.45	1.54	1.20	1.35	1.11
Al ₂ O ₃	26.88	18.46	18.88	19.02	19.83	17.07	20.62	18.99
Fe ₂ O ₃	2.12	1.87	2.25	1.36	1.36	0.90	1.53	1.31
FeO	7.64	7.33	6.41	6.85	9.36	5.75	5.85	6.60
MnO	0.10	0.11	0.12	0.11	0.10	0.12	0.13	.10
MgO	3.05	2.61	2.77	2.58	3.19	1.94	2.06	2.30
CaO	1.11	0.24	0.71	1.07	0.69	4.34	1.64	0.52
Na ₂ O	2.12	2.19	2.64	2.76	2.66	3.28	3.70	3.55
K ₂ O	5.93	3.55	4.12	3.01	3.69	2.45	3.55	2.62
P ₂ O ₅	0.46	0.17	0.23	0.16	0.28	0.11	1.05	0.15
H ₂ O	0.95	4.61	4.00	4.47	3.78	1.80	1.52	3.03
CO ₂	0.26	0.17	0.12	0.21	0.27	0.83	0.26	0.21
Total	100.6	101.4	100.9	99.09	99.81	100.1	99.34	99.81

Trace elements(ppm)

Rb	206	115	130	98	116	110	126	134
Ba	1181	634	811	538	575	424	664	567
Zr	338	316	223	208	227	179	279	195
Sr	125	46	91	141	70	361	150	107
Ga	36	29	26	27	27	27	30	28
Ni	59	58	67	60	53	43	49	50
Co	30	29	24	20	16	19	39	20
Cr	153	114	119	120	111	105	118	93
Pb	10	12	13	22	22	12	64	7
Zn	120	84	93	122	144	95	110	109
Cu	46	50	61	44	14	38	67	43
Y	51	39	37	34	23	35	65	31
Ce	150	120	95	102	19	72	153	102

Niggli values

Si	136.5	218.1	202.3	203.4	171.7	216.7	194.2	216.2
al	44.75	40.37	39.38	40.69	37.82	36.15	42.09	40.8
fm	35.40	42.40	39.57	38.47	44.03	30.10	31.56	36.21
c	3.36	.95	2.69	4.16	2.13	16.71	6.09	2.03
alk	16.49	16.28	18.36	16.68	15.96	17.04	20.37	20.96
ti	3.59	3.74	3.91	3.96	3.75	3.24	3.52	3.04
k	0.65	0.52	0.51	0.42	0.48	0.33	0.39	0.40
mg	0.36	0.34	0.37	0.36	0.35	0.35	0.34	0.35
w	0.20	0.19	0.24	0.15	0.12	.012	0.19	0.15

Comrie thermal aureole : Continued

	Y52c	Y53c	Y54c	Y55c	Y56c	Y64c	Y66c	Y67b
Major elements(wt%)								
SiO ₂	53.30	52.79	54.44	59.89	55.73	54.78	51.03	54.01
TiO ₂	1.72	1.45	1.36	1.25	1.53	1.62	2.23	1.66
Al ₂ O ₃	23.35	21.56	19.26	16.40	20.20	22.80	23.05	20.28
Fe ₂ O ₃	1.52	3.00	2.14	1.45	3.02	1.66	3.37	1.23
FeO	7.47	8.90	9.50	6.94	7.68	7.56	8.83	8.01
MnO	0.14	0.14	0.17	0.10	0.15	0.10	0.11	0.08
MgO	2.62	3.46	3.56	2.20	2.98	3.05	3.69	2.70
CaO	0.18	0.51	0.41	1.48	1.26	0.38	0.50	0.67
Na ₂ O	2.80	3.20	1.76	2.47	2.30	2.61	2.15	2.57
K ₂ O	2.69	3.87	3.36	2.90	3.05	4.60	3.17	4.17
P ₂ O ₅	0.17	0.16	0.12	0.33	0.14	0.11	0.12	0.20
H ₂ O	3.29	1.37	2.97	2.65	2.06	0.82	1.57	3.42
CO ₂	0.37	0.11	0.27	0.30	0.12	0.28	0.11	0.31
Total	99.62	100.6	99.32	98.36	100.2	100.4	99.93	99.31

Trace elements(ppm)

Rb	182	155	152	128	115	91	93	166
Ba	911	560	518	525	722	1021	1124	518
Zr	467	360	307	246	303	246	364	207
Sr	65	70	82	125	148	134	147	108
Ga	40	36	33	25	31	36	38	30
Ni	57	60	65	41	56	65	74	60
Co	12	20	22	28	26	24	30	32
Cr	112	92	95	92	111	142	180	122
Pb	12	12	10	11	8	37	9	16
Zn	154	200	228	125	135	137	167	116
Cu	32	22	0	62	35	36	18	76
Y	54	32	33	40	37	31	26	32
Ce	202	125	133	100	98	119	163	125

Niggli values

Si	179.6	156.5	178.5	233.3	182.3	174.3	151.6	183.3
al	46.36	37.67	37.21	37.65	38.95	42.76	40.37	40.56
fm	38.06	44.19	48.72	39.63	42.98	38.56	45.83	39.53
c	0.65	1.62	1.44	6.18	4.42	1.30	1.59	2.44
alk	14.93	16.52	12.62	16.54	13.66	17.39	12.20	17.48
ti	4.36	3.23	3.35	3.66	3.76	3.88	4.98	4.24
k	0.39	0.44	0.56	0.44	0.47	0.54	0.49	0.52
mg	0.35	0.35	0.36	0.32	0.34	0.38	0.36	0.35
w	0.15	0.24	0.17	0.16	0.26	0.16	0.26	0.12

Comrie thermal aureole : Continued

	Y68b	Y69c	Y70c	Y77c	Y81c	Y83c	Y85b	Y86b
Major elements(wt%)								
SiO ₂	58.95	55.53	40.78	54.66	59.60	51.86	59.21	57.76
TiO ₂	1.59	1.09	1.73	1.74	1.30	1.07	1.09	1.29
Al ₂ O ₃	19.11	18.98	29.20	20.89	20.81	24.22	19.42	19.43
Fe ₂ O ₃	0.11	3.51	2.59	2.46	1.81	1.93	1.14	1.16
FeO	9.53	8.17	9.14	7.84	5.51	7.43	5.99	7.27
MnO	0.09	0.15	0.10	0.12	0.13	0.12	0.09	0.13
MgO	2.50	3.36	4.14	3.50	2.12	2.96	2.04	2.59
CaO	0.43	0.31	0.88	1.05	0.54	0.33	0.55	0.41
Na ₂ O	5.30	2.15	1.20	3.94	3.74	1.06	2.91	2.91
K ₂ O	2.50	4.43	7.65	2.61	4.19	6.27	3.80	3.51
P ₂ O ₅	0.20	0.11	0.44	0.11	0.26	0.19	0.14	0.17
H ₂ O	1.24	2.28	3.07	2.24	1.23	3.46	3.99	3.71
CO ₂	0.21	0.21	0.16	0.11	0.20	0.30	0.29	0.11
Total	101.7	100.3	101.1	101.2	101.4	101.2	100.6	100.4

Trace elements(ppm)

Rb	140	126	284	76	134	204	133	137
Ba	612	502	1490	818	665	785	796	603
Zr	210	252	334	380	265	183	207	222
Sr	100	88	107	153	136	136	91	83
Ga	25	27	47	32	30	35	28	27
Ni	65	47	80	75	42	61	48	52
Co	34	18	32	34	27	25	23	21
Cr	117	104	168	160	115	119	96	100
Pb	12	7	15	17	25	11	38	14
Zn	110	165	218	152	106	150	113	96
Cu	78	15	38	44	60	38	40	38
Y	28	20	44	29	46	40	33	31
Ce	120	92	166	106	121	154	99	116

Niggli values

Si	200.2	179.6	102.0	167.9	210.8	163.4	226.1	208.0
al	38.25	36.19	43.07	37.83	43.38	44.98	43.70	41.24
fm	37.32	46.85	39.45	41.86	32.29	38.06	34.02	38.95
c	1.56	1.07	2.36	3.46	2.05	1.11	2.25	1.58
alk	2.87	15.89	15.12	16.35	22.28	15.8	20.03	18.23
ti	4.06	2.65	3.26	4.02	3.46	2.54	3.13	3.49
k	0.24	0.58	0.81	0.30	0.42	0.80	0.46	0.44
mg	0.34	0.35	0.39	0.38	0.35	0.37	0.34	0.36
w	0.99	0.28	0.20	0.22	0.23	0.19	0.15	0.13

Comrie thermal aureole : Continued Contact hornfelses

	Y87b	Y88b	Y57x	Y58x	Y59x	Y61x	Y62x
Major elements(wt%)							
SiO ₂	52.24	57.39	47.44	47.64	52.97	45.41	53.16
TiO ₂	1.02	0.99	2.63	2.15	1.95	2.60	2.16
Al ₂ O ₃	19.71	18.17	28.90	27.64	24.12	26.78	23.07
Fe ₂ O ₃	6.24	4.99	2.38	3.68	1.62	2.14	2.70
FeO	5.30	4.34	3.73	5.06	6.04	7.70	6.80
MnO	0.05	0.03	0.12	0.07	0.08	0.14	0.00
MgO	1.44	1.94	2.62	2.60	2.41	2.15	2.78
CaO	0.35	0.61	2.12	0.56	1.17	3.50	0.88
Na ₂ O	2.67	2.93	3.90	2.66	4.86	5.32	3.35
K ₂ O	4.97	3.98	2.32	5.38	3.30	1.97	2.79
P ₂ O ₅	0.15	0.24	0.35	0.40	0.33	0.24	0.24
H ₂ O	4.15	3.21	0.92	1.03	1.56	2.25	0.75
CO ₂	0.29	0.17	0.26	0.16	0.18	0.35	0.25
Total	98.58	98.99	97.69	99.03	100.6	100.5	98.93

Trace elements(ppm)

Rb	159	162	65	159	111	59	99
Ba	703	642	2153	1499	1502	1969	1181
Zr	300	208	524	467	393	534	448
Sr	58	186	253	134	210	421	214
Ga	31	27	48	40	38	46	37
Ni	55	51	58	58	49	61	49
Co	22	33	30	30	31	43	31
Cr	109	91	202	173	145	206	158
Pb	31	8	65	159	18	33	99
Zn	240	145	120	109	106	203	135
Cu	45	32	35	49	35	48	18
Y	41	34	64	40	50	33	37
Ce	138	115	164	105	113	97	119

Niggli values

Si	185.3	212.4	135.3	141.0	164.8	122.0	169.1
al	41.21	39.64	48.59	32.20	44.22	42.42	43.26
fm	37.03	38.03	29.92	32.20	30.68	30.25	37.74
c	1.33	2.42	6.48	1.78	3.90	10.08	3.00
alk	20.43	19.91	15.01	17.80	21.10	17.24	16.00
ti	2.72	2.76	5.64	4.79	4.56	5.26	5.17
k	0.55	0.47	0.28	0.57	0.31	0.20	0.35
mg	0.21	0.28	0.37	0.36	0.36	0.28	0.35
w	0.57	0.51	0.27	0.40	0.19	0.20	0.26

Comrie thermal aureole : Continued

Leucosomes

	Y63x	Y78x	Y79x	Y57L	Y58L	Y59L	Y61L
Major elements(wt%)							
SiO ₂	45.51	46.75	48.17	72.54	71.26	74.51	63.72
TiO ₂	2.52	2.46	2.53	0.62	0.52	0.51	0.92
Al ₂ O ₃	25.55	28.81	29.37	12.48	12.47	12.43	14.17
Fe ₂ O ₃	2.62	1.21	1.74	1.75	1.83	1.49	2.58
FeO	9.21	9.56	5.99	2.16	1.73	1.72	4.40
MnO	0.13	0.12	0.09	0.07	0.07	0.05	0.11
MgO	3.01	3.06	2.24	1.06	1.28	0.62	2.43
CaO	1.79	1.67	1.49	0.70	0.37	0.30	2.81
Na ₂ O	3.30	3.89	5.20	2.37	2.19	4.45	4.06
K ₂ O	2.12	1.87	3.50	5.54	6.21	4.88	2.14
P ₂ O ₅	0.39	0.38	0.28	0.18	0.15	0.19	0.21
H ₂ O	1.57	1.10	0.70	0.96	0.64	0.96	1.39
CO ₂	1.07	0.25	0.07	0.27	0.14	0.23	0.21
Total	98.79	101.1	101.3	100.7	98.86	102.3	99.25

Trace elements(ppm)

Rb	63	86	190	265	195	80
Ba	1967	2108	581	170	286	397
Zr	510	461	228	231	223	281
Sr	256	238	114	97	74	298
Ga	47	44	15	12	16	18
Ni	85	60	25	22	23	47
Co	60	50	8	14	8	16
Cr	195	186	27	41	17	89
Pb	22	31	20	15	15	21
Zn	171	109	52	109	45	81
Cu	44	56	23	20	20	56
Y	61	66	33	30	29	27
Ce	168	153	83	78	68	69

Niggli values

Si	130.6	125.6	134.4
al	43.21	45.64	48.30
fm	38.23	36.20	26.95
c	5.50	4.81	4.45
alk	13.06	13.35	20.30
ti	5.44	4.97	5.31
k	0.30	0.24	0.31
mg	0.34	0.34	0.35
w	0.22	0.10	0.21

Comrie thermal aureole : Continued

					Igneous		
	Y62L	Y63L	Y78L	Y79L	Y35I	Y60I	Y82I
Major elements(wt%)							
SiO ₂	70.88	65.05	72.43	73.28	59.16	52.02	60.62
TiO ₂	1.01	0.88	0.52	0.63	1.18	1.61	0.97
Al ₂ O ₃	11.13	14.78	12.80	11.51	16.77	17.63	18.45
Fe ₂ O ₃	2.05	2.13	1.34	1.41	2.44	2.75	1.21
FeO	4.43	3.34	1.80	1.88	3.78	5.73	3.18
MnO	0.11	0.11	0.05	0.06	0.11	0.16	0.07
MgO	1.93	1.96	0.52	0.66	4.28	5.69	1.85
CaO	0.29	1.34	0.36	0.91	4.37	7.80	4.26
Na ₂ O	2.69	3.03	3.81	3.77	3.91	3.49	4.27
K ₂ O	3.32	5.08	5.91	5.77	3.13	1.23	3.28
P ₂ O ₅	0.12	0.13	0.22	0.30	0.31	0.48	0.29
H ₂ O	0.17	1.57	0.19	0.24	1.00	1.25	1.11
CO ₂	1.55	0.22	0.14	0.11	0.17	0.15	0.21
Total	99.68	99.62	100.1	100.5	100.6	99.98	99.77

Trace elements(ppm)

Rb	123	154	208	186	80	28	91
Ba	300	835	507	534	685	495	693
Zr	295	240	228	233	204	123	286
Sr	61	188	82	108	549	729	545
Ga	15	22	16	12	21	23	22
Ni	49	40	19	16	47	83	7
Co	25	21	8	11	29	40	10
Cr	79	51	16	33	79	139	13
Pb	21	26	23	24	16	12	60
Zn	118	158	37	35	81	78	67
Cu	31	35	13	21	48	45	20
Y	33	32	27	33	25	24	28
Ce	86	99	61	89	61	50	93

Comrie thermal aureole : Continued

Unhornfelses slates

	Y13	Y15	Y75	Y76	interm. hornf.	Y83
La	43.96	55.41	35.53	134.51	68.01	90.69
Ce	85.81	103.81	71.60	129.20	153.58	178.29
Pr	11.59	14.12	10.24	27.86	19.70	20.70
Nd	41.74	52.23	35.93	104.06	80.04	77.11
Sm	7.58	9.16	6.44	16.40	15.69	12.34
Eu	1.74	2.16	1.47	3.77	3.11	2.70
Gd	6.92	8.10	5.74	13.49	15.31	10.35
Dy	5.46	6.16	4.68	8.88	11.64	7.55
Hb	1.25	1.24	0.98	1.74	2.30	1.53
Er	3.74	2.83	2.42	3.64	4.85	3.55
Yb	2.92	2.72	2.60	3.20	4.44	3.46
Lu	0.46	0.42	0.40	0.47	0.63	0.53
Σ REE	213.57	258.0	178.03	447.22	379.3	408.8
Eu/Eu*	0.73	0.77	0.74	0.77	0.61	0.73
(La/Lu)CN	9.92	13.7	9.22	29.72	11.21	17.74

hornfelses.

leucosomes

	Y86	Y87	Y59	Y78	Y59L	Y78L
La	59.63	82.24	53.92	83.18	27.26	26.56
Ce	121.17	112.0	117.92	180.79	61.29	55.25
Pr	15.09	20.38	15.46	21.66	8.56	7.50
Nd	55.54	76.02	49.47	86.06	31.26	26.68
Sm	9.88	12.76	10.57	15.15	6.18	5.27
Eu	2.16	2.59	3.37	3.91	0.66	0.85
Gd	9.12	10.14	9.65	13.65	5.67	4.91
Dy	7.62	7.54	8.37	10.97	4.80	4.50
Hb	1.60	1.53	1.81	2.33	1.01	0.96
Er	4.70	3.46	4.20	5.37	2.34	2.41
Yb	3.56	3.45	4.09	5.27	2.41	2.56
Lu	0.52	0.51	0.60	0.78	0.35	0.37
Σ REE	290.59	332.62	279.43	429.12	151.79	137.82
Eu/Eu*	0.69	0.69	1.02	0.83	0.34	0.51
(La/Lu)CN	11.91	16.74	9.33	11.07	8.09	7.45

Comrie thermal aureole : Continued

Y35(granodiorite)

La	30.39
Ce	63.56
Pr	8.78
Nd	32.53
Sm	6.23
Eu	1.80
Gd	5.60
Dy	4.53
Hb	0.96
Er	2.25
Yb	2.14
Lu	0.32

Σ REE 159.09

Eu/Eu* 0.93

(La/Lu)CN 9.85

KEY TO THE COMRIE THERMAL AUREOLE

Regional slates(r+s) : r = not spotted slates; s = spotted

Intermediate hornfelses(b+c): b = biotite-bearing hornfelses but cordierite-, spinel-, orthopyroxene-, corundum-free c = hornfelses containing biotite and cordierite \pm spinel \pm orthopyroxene \pm corundum.

contact hornfelses : all rich in the hornfels minerals mentioned above but are practically biotite-free.

L = Leucosomes

